Arthritis & Rheumatology

An Official Journal of the American College of Rheumatology
www.arthritisrheum.org and wileyonlinelibrary.com

Editor
S. Louis Bridges, Jr., MD, PhD, *New York*

Deputy Editors
Karen H. Costenbader, MD, MPH, *Boston*
Mariana J. Kaplan, MD, *Bethesda*
Kenneth G. Saag, MD, MSc, *Birmingham*

Co-Editors
Edward M. Behrens, MD, *Philadelphia*
David T. Felson, MD, MPH, *Boston*
Richard F. Loeser Jr., MD, *Chapel Hill*

Editor-in-Chief Emeriti
Richard Bucala, MD, PhD, *New Haven*
Daniel H. Solomon, MD, MPH, *Boston*

Journal Publications Committee
Chair - Betty Tsao, PhD, *Charleston*

Member - ARP Liaison
Cynthia Crowson, PhD, *Stewartville*

Members
Elana Bernstein, MD, MSc, *New York*
Krati Chauhan, MD, PhD, *Burlington*
Himanshu Vashistha, PhD, MBA, *Great Neck*
Marwin Groener, MD, FIT Member, *Baltimore*
Mark Hwang, MD, MS, Member, *Houston*
Eric Roberts, MPH, PhD, ARP Member, *San Francisco*

Editorial Staff
Susan Case, *Vice President, Strategic Marketing, Communications and Publishing, Maryland*
Maggie Parry, *Director, Quality and Production, Georgia*
Brian T. Robinson, *Director, Digital Content, Pennsylvania*
Christy Austin, *Publishing Coordinator, Washington*
Laura Bolte, *Managing Editor, North Carolina*

Associate Editors
Rohit Aggarwal, MD, *Pittsburgh*
Ivona Aksentijevich, MD, PhD, *Bethesda*
Marta Alarcón-Riquelme, MD, PhD, *Stockholm, Sweden*
Elizabeth Arkema, ScD, *Stockholm*
Neil Basu, MD, PhD, *Scotland*
Ashira D. Blazer, MD, MSCI, *Baltimore*
Nunzio Bottini, MD, PhD, *Los Angeles*
John Carrino, MD, MPH, *New York*
Andrew Cope, MD, PhD, *London, UK*
Jeffrey Curtis, MD, MS, MPH, *Birmingham*
Nicola Dalbeth, MBChB, MD, FRCP, *Auckland, NZ*
Maria Danila, MD, MS, *Birmingham*
Christopher Denton, PhD, FRCP, *London, UK*
Doruk Erkan, MD, *New York*
Carol Feghali-Bostwick, PhD, *Charleston*
Richard A. Furie, MD, *Great Neck*
Hassan Ghomrawi, PhD, MPH, *Birmingham*
V. Michael Holers, MD, *Aurora*
J. Michelle Kahlenberg, MD, PhD, *Ann Arbor*
Wan-Uk Kim, MD, PhD, *Seoul, Korea*
Jason S. Knight, MD, PhD, *Ann Arbor*
Carl D. Langefeld, PhD, *Winston-Salem*
Katherine Liao, MD, MPH, *Boston*
Tony R. Merriman, PhD, *Birmingham*
Sara S. McCoy, MD, PhD, *Milwaukee*
Dennis McGonagle, FRCPI, PhD, *Leeds*
Rachel E. Miller, PhD, *Chicago*
Yukinori Okada, MD, PhD, *Osaka, Japan*
Karen B. Onel, MD, *New York*
Dana Orange, MD, MS, *New York*
Janet E. Pope, MD, MPH, FRCPC, *London, Ontario, Canada*
Lisa G. Rider, MD, *Bethesda*
Christopher T. Ritchlin, MD, MPH, *Rochester*
Amr Sawalha, MD, *Pittsburg*
Carla R. Scanzello, MD, PhD, *Philadelphia*
Georg Schett, MD, *Erlangen, Germany*
Gabriela Schmajuk, MD, *Palo Alto*
Raphaèle Seror, MD, PhD, *Becetre, France*
Jasvinder Singh, MD, MPH, *Houston*
Robert F. Spiera, MD, *New York*
Yoshiya Tanaka, MD, PhD, *Kitakyushu, Japan*
Ranjeny Thomas, MBBS, *Queensland*
Fei Wang, PhD, *New York*
Baohong Zhao, PhD, *New York*

Advisory Editors
Hannah C. Ainsworth, PhD, *Winston-Salem*
Matthew C. Baker, MD, MS, *Palo Alto*
Jamie Collins, PhD, *Boston*
Kelsey Collins, PhD, *San Francisco*
Kristen Demoruelle, MD, PhD, *Denver*
Anisha Dua, MD, MPH, *Chicago*
David Fernandez, MD, PhD, *New York*
Shivani Garg, MD, PhD, *New Haven*
Peter Grayson, MD, MSc, *Bethesda*
Lauren Henderson, MD, MMSc, *Boston*
Monique Hinchcliff, MD, MS, *New Haven*
Evelyn Hsieh, MD, PhD, *New Haven*
Deanna P. Jannat-Khah, MSPH, DrPH, *New York*
Vasileios Kyttaris, MD, *Boston*
Kimberly Lakin, MD, MS, *New York*
Lindsay S. Lally, MD, MS, *New York*
Susan MacLauchlan, PhD, *Boston*
Bella Mehta, MBBS, MS, MD, *New York*
Alicia Mueller, MD, PhD, *Stanford*
Julie Paik, MD, MHS, *Baltimore*
Michael Paley, MD, PhD, *St. Louis*
Misti L. Paudel, PhD, MPH, *Boston*
Grant Schulert, MD, PhD, *Cincinnati*
Andrew D Schweitzer, MD, *New York*
Jeffrey A. Sparks, MD, MMSc, *Boston*
Sara K. Tedeschi, MD, MPH, *Boston*
Gaëlle Varkas, MD, PhD, *Ghent*
Fan Zhang, PhD, *Aurora*

AMERICAN COLLEGE OF RHEUMATOLOGY

William Harvey, MD, MSc, *Boston*, **President**
Anne Bass, MD, *New York*, **President-Elect**
Angus Worthing, MD, *Washington, DC,* **Secretary**
Eric Ruderman, MD, *Chicago,* **Treasurer**
Bryce Binstadt, MD, PhD, *Minneapolis,* **Foundation President**
Becki Cleveland, PhD, *Chapel Hill*, **ARP President**
Steven Echard, IOM, CAE, *Atlanta*, **Executive Vice-President**

© 2026 American College of Rheumatology. All rights reserved, including rights for text and data mining and training of artificial technologies or similar technologies. No part of this publication may be reproduced, stored or transmitted in any form or by any means without the prior permission in writing from the copyright holder. Authorization to copy items for internal and personal use is granted by the copyright holder for libraries and other users registered with their local Reproduction Rights Organization (RRO), e.g. Copyright Clearance Center (CCC), 222 Rosewood Drive, Danvers, MA 01923, USA (www.copyright.com), provided the appropriate fee is paid directly to the RRO. This consent does not extend to other kinds of copying or use such as copying for general distribution, for advertising or promotional purposes, for creating new collective works, for resale, or for artificial intelligence tools or technologies. Special requests should be addressed to: permissions@wiley.com.

Access Policy: Subject to restrictions on certain backfiles, access to the online version of this issue is available to all registered Wiley Online Library users 12 months after publication. Subscribers and eligible users at subscribing institutions have immediate access in accordance with the relevant subscription type. Please go to onlinelibrary.wiley.com for details.

The views and recommendations expressed in articles, letters, and other communications published in Arthritis & Rheumatology are those of the authors and do not necessarily reflect the opinions of the editors, publisher, or American College of Rheumatology. The publisher and the American College of Rheumatology do not investigate the information contained in the classified advertisements in this journal and assume no responsibility concerning them. Further, the publisher and the American College of Rheumatology do not guarantee, warrant, or endorse any product or service advertised in this journal.

♾This journal is printed on acid-free paper.

Arthritis & Rheumatology

An Official Journal of the American College of Rheumatology
www.arthritisrheum.org and wileyonlinelibrary.com

VOLUME 78 • September 2026 • NO. 9

In This Issue A7

Journal Club A8

Clinical Connections A9

Special Article

Editorial: T Cells in Osteoarthritis: Drivers, Repairers, or Bystanders in Osteoarthritis?
Tonia L. Vincent and Andrew P. Cope 1813

Editorial: Somatic Variants in Immune Dysregulation: An Ongoing Challenge
Sofia Torreggiani and Ivona Aksentijevich 1816

Editorial: From Genome-Wide Association Study Signal to Mechanism in Rheumatoid Arthritis: Lessons From a Single Risk Locus
Ryuya Edahiro and Yukinori Okada 1819

Notes From the Field: When Blood Proteins Reveal What Transcripts Miss: Immune Cell Priming and the Road to Prognostic Biomarkers in Lupus
Ioannis Parodis 1823

Rheumatoid Arthritis

Baseline Interleukin-10 Levels as a Predictive Biomarker for Achieving Clinical Response With Abatacept in Patients Who Were Disease-Modifying Antirheumatic Drug Naive and Anti–Citrullinated Protein Antibody Positive With Early Rheumatoid Arthritis
Jinqi Liu, Yicong Li, Kai Fu, Chun Wu, Peter Schafer, Sean E. Connolly, Ian M. Catlett, Michael A. Maldonado, Robert Wong, Paul Emery, Yoshiya Tanaka, Vivian P. Bykerk, Clifton O. Bingham, Thomas W. J. Huizinga, and Roy Fleischmann 1826

Tissue Damage in Rheumatoid Arthritis Is Genetically Linked to Low Peptidylglycine Alpha-Amidating Monooxygenase Activity in Synovial Fibroblasts
Kevin J. Sheridan, Emma R. Dorris, Maria Inês Pimenta, Jemma Falkov, Matthew Fisher, Sam Pledger, Hector Devey, Munitta Muthana, Denis C. Shields, Richard E. Mains, Betty A. Eipper, Christopher D. Buckley, and Anthony G. Wilson 1837

Osteoarthritis

Tissue-Specific and Spatially Dependent Metabolic Signatures Perturbed by Injury in Male and Female Mice
Hope D. Welhaven, Avery H. Welfley, Priyanka P. Brahmachary, Mark Greenwood, Donald F. Smith, Brian Bothner, and Ronald K. June 1850

The Potential Role of Synovial T Cell Infiltration Following Knee Joint Injury in Symptoms and Progression to Osteoarthritis
Babak Moradi, Miriam T. Jackson, Cindy C. Shu, Susan M. Smith, Margaret M. Smith, Sanaa Zaki, Hadrian Platzer, Nils Rosshirt, David Giangreco, Carla R. Scanzello, and Christopher B. Little 1863

Systemic Lupus Erythematosus

Multi-Omic Profiling Reveals Immune Cell Priming Signature Linked to Lupus Prognosis
Michael A. Smith, Dominic Sinibaldi, Saifur Rahman, Chia-Chien Chiang, Anna M. Hansen, Jill Henault, Carlos P. Roca, Shu Wang, Kamelia Zerrouki, Rebecca Filippi, Christopher Groves, Zerai Manna, Jun Chu, Michael Davis, Sarthak Gupta, Christopher Morehouse, Melissa de los Reyes, Rachel Ettinger, Roland Kolbeck, Mariana J. Kaplan, Miguel A. Sanjuan, Richard M. Siegel, Sarfaraz A. Hasni, and Kerry A. Casey 1878

TWEAK/Fn14 Signaling Drives Oxidative Cardiac Injury in Systemic Lupus Erythematosus: Evidence From Patient Biomarker Studies, Lupus Mouse Models, and Cardiomyocyte Assays
Yale Liu, Zhu Yan, Xueting Peng, Meixuan Li, Juan Wang, Yan Zhang, Xiaoqian Hu, Mingzhu Zhou, Kaixuan Ren, Dan Zhang, Xingyi Guo, Yumin Xia, and Huanhuan Huo 1892

Single-Cell Level Characterization of B Cell Depletion and Repopulation Following Rituximab in Systemic Lupus Erythematosus
Haerin Jang, Norzawani Buang, Catherine Sutherland, Wanseon Lee, Lauren Overend, Tarran S. Rupall, Katie L. Burnham, Matthew C. Pickering, Marina Botto, and Emma E. Davenport 1907

Vasculitis

Prognosis and Long-Term Outcome of Stenotic Large Vessel Involvement in Giant Cell Arteritis
Georgina Maalouf, Bérangère Arnould, Olivier Espitia, Hubert Deboysson, Maxime Samson, Arnaud Hot, Eric Liozon, Simon Parreau, Christian Lavigne, Valentin Lacombe, Jean-Francois Alexandra, Thomas Thibault, Laurent Chiche, Julien Gaudric, Alban Redheuil, Matheus Vieira, Matthieu Groh, Cécile-Audrey Durel, Thibaud Chazal, Chloé Comarmond, Nadine Magy-Bertrand, Stéphane Vinzio, Lionel Martzolff, Pierre Lozac'h, Rodérau Outh, Jérémy Clément, Pierre Duffau, Anael Dumont, Sebastien Humbert, Constance Guillaud, Azeddine Dellal, Grégory Pugnet, Valérie Devauchelle-Pensec, Patrice Cacoub, Lucie Biard, and David Saadoun, on behalf of the GEFA (French Study Group for Large Vessel Vasculitis) 1920

Systemic Sclerosis

Long Noncoding RNA *H19* Mediates STAT3-Dependent Activation of Keratinocytes and Fibroblasts in Systemic Sclerosis Skin
Begoña Caballero-Ruiz, Christopher W. Wasson, Rebecca L. Ross, and Francesco Del Galdo 1929

Myositis

Investigating the Role of Type I Interferon Signaling on Muscle Disease Using Mouse Models
Rita Spathis, Sabrina Narvesen, Deeva Robles Kuriplach, Karen Huang, Teja Sundar, Elizabeth Bagley, Joanna Parkes, Xinyu Jia, Nandhana Sudhan, Alfredo Guzman, Kanneboyina Nagaraju, and Melissa Morales 1942

Improved Detection of Myositis-Specific Autoantibodies Using Luciferase Immunoprecipitation Systems Assay: Comparison With Line Blot and Conventional Immunoprecipitation
Peter D. Burbelo, Iago Pinal-Fernandez, Maria Casal-Dominguez, Xin Tian, Shijinqiu Gao, Neha Gupta, Eric W. Robbins, John A. Chiorini, Christopher A. Mecoli, Lisa Christopher-Stine, Livia Casciola-Rosen, Andrew L. Mammen, Sonye K. Danoff, Anthony F. Suffredini, and Julio A. Huapaya 1952

Autoinflammatory Disease

A Multifaceted Interplay Among Hemophagocytosis, Interleukin-18, and Type I Interferon Distinguishes Still Disease From Other Autoinflammatory Diseases
Yvonne M. Mueller, Charlotte Girard, Harmen J. G. van de Werken, Stefan J. Erkeland, Dwin G. B. Grashof, Laurie Vaillant, Renske J. H. den Dekker, Iris van Zuijen, Sharon Veenbergen, Fanny Coffin, Eric Bindels, Yvan Jamilloux, Katerina Laskari, Vassili Soumelis, Bruno Fautrel, Cem Gabay, and Peter D. Katsikis 1961

Landscape of Somatic Mutations in a Large Cohort of Chinese Patients With Immune Dysregulations
Jinjian Fu, Qiong Fu, Jun Wang, Qintao Wang, Liang Zhang, Huihui Chi, Lei Zhang, Li Sun, Ying Huang, Tingyan He, Yuhao Yao, Xu Han, Shuangyue Ma, Chenlu Liu, Lin Liu, Xiang Chen, Shihao Wang, Hong Jiang, Wenjie Zheng, Shaoling Zheng, Qiao Ye, Yue Du, Li Guo, Jing Zhu, Guomin Li, Changming Zhang, Zhimiao Lin, Xiuli Ju, Yongmei Han, Weiqian Chen, Jin Lin, Jing Xue, Hao Cheng, Caiqing Xu, Lin Huang, Longyan Qin, Jiashun Zeng, Yifang Mei, Tingting Yan, Qianying Lv, Yaoyao Shangguan, Cuifang Zheng, Xiaoliang He, Hongfei Liu, Xiaoli Chen, Hua Xie, Xue Li, Ying Jin, Jiahui Peng, Bo Lin, Yao Huang, Xiuli Wang, Xiaoxi Yang, Nan Jiang, Wei Wang, Tong Wu, Dongze Wu, Yun Zhu, Yakai Fu, Jie Chen, Ran Wang, Xiaojun Liu, Dongbin Jiang, Huijie Xiao, Baige Su, Benshan Zhang, Fengqi Wu, Qiongyi Hu, Chengde Yang, Meiping Lu, Shuang Ye, Min Shen, Hongmei Song, Jianghua Chen, Jun Yang, Zhihong Liu, Xiaomin Yu, and Qing Zhou 1975

Pediatric Rheumatology

Inosine-Triphosphate-Pyrophosphatase Activity as a Potential Predictor of Methotrexate Remission in Juvenile Idiopathic Arthritis
Sofia Sindici Forgiarini, Marianna Lucafò, Debora Curci, Davide Selvestrel, Valentina Moressa, Sofia Pagarin, Barbara Bellich, Martina Franzin, Alberto Tommasini, Mara L. Becker, Laura B. Ramsey, Susan D. Thompson, Carl D. Langefeld, Federica Corba, Edoardo Marrani, Gabriele Simonini, Gabriele Stocco, Giuliana Decorti, Andrea Taddio, and Serena Pastore 1989

Clinical Image

Clinical Images: Complete Distal Phalanx Resorption in Systemic Sclerosis
Ken Yoshida 2000

Clinical Images: Skeletal Fluorosis Presenting With Diffuse Periostitis and Polyarticular Synovitis
Mitali Sen 2001

Letter

How Do Interleukin-33 and Neutrophil Extracellular Traps Cooperate to Induce Epithelial-Mesenchymal Transition in Alveolar Epithelial Cells?: Comment on the Article by Yang et al
Jiaxin Cai and Zaixing Yang 2002

Reply
Jumei Yang, Jiarui Zhu, Wenjun Li, Xi Cui, Hui Chai, Qiyan Su, Yingyue Feng, and Sigong Zhang 2002

Clarifying the Clinical Implications of Clonal Hematopoiesis in Late-Onset Seropositive Rheumatoid Arthritis: Comment on the Article by Zhao et al
Weiqi Hu, Xun Zhou, Luxue Wang, and Changfeng Hu 2003

Reply
Kun Zhao, Yash Pershad, Alexander G. Bick, and Robert W. Corty 2004

Cover image: The image on the cover (from Caballero-Ruiz et al; pages 1929–1941) shows an in situ hybridization (RNAscope) of long noncoding RNA H19 (pink) costained with collagen 1 (brown) and nuclear counterstain with hematoxylin (blue) in a representative systemic sclerosis skin sample. High H19 levels were detectable in the epidermal layer, and high levels of collagen 1 were detectable within the dermis.

In this Issue

Highlights from this issue of *A&R* | By Lara C. Pullen, PhD

TWEAK Drives Cardiac Injury in Systemic Lupus Erythematosus

Oxidative stress drives the pathogenesis of systemic lupus erythematosus (SLE) and subsequent organ damage, including cardiac injury. Cardiovascular complications resulting from the convergence of chronic immune activation and oxidative stress–mediated tissue damage remain a leading cause of morbidity and mortality in SLE. Echocardiographic abnormalities in SLE span a broad spectrum of structural and functional changes that often precede overt symptoms.

p. 1892

Researchers have identified tumor necrosis factor–like weak inducer of apoptosis (TWEAK) as playing a critical role in both oxidative injury and additional cardiopathogenic processes, such as maladaptive calcium handling, hypertrophic signaling, and adverse remodeling following myocardial injury. **In this issue, Liu et al. (p. 1892)** report that TWEAK/fibroblast growth factor–inducible 14 (Fn14) signaling drives oxidative stress–mediated cardiomyocyte injury in SLE. Their data also reveal that mitochondrial dysfunction is a key mechanistic link between TWEAK/Fn14 signaling and cardiomyocyte injury.

The investigators performed cross-sectional clinical analyses of 242 patients with SLE and 66 age- and sex-matched controls. Serum TWEAK levels were significantly elevated in patients with SLE and were highest in those with cardiac abnormalities compared with healthy controls. TWEAK also correlated positively with malondialdehyde, 8-hydroxy-2'-deoxyguanosine, disease activity, and inflammatory cytokines and inversely with superoxide dismutase. The researchers found that elevated baseline TWEAK predicted new cardiac abnormalities during follow-up and that TWEAK levels declined with clinical improvement.

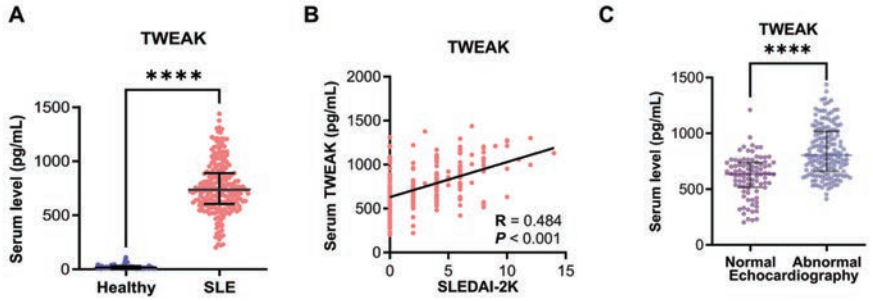

Figure 1A-C. (A) Serum TWEAK levels are elevated in patients with systemic lupus erythematosus (SLE; n = 242) compared with healthy controls (n = 66) and (B) are positively correlated with SLE Disease Activity Index 2000 scores. (C) In patients with SLE stratified by echocardiography, serum TWEAK levels are highest in those with cardiac abnormalities. ****P < 0.0001

In a mouse model of lupus, *Fn14* deficiency reduced accumulation of reactive oxygen species in the heart, restored Nrf2/HO-1 antioxidant signaling, attenuated histopathological injury, and preserved cardiac function. In vitro, TWEAK induced mitochondrial superoxide production, suppressed Nrf2 signaling, and promoted apoptosis in lupus-prone cardiomyocytes. Taken together, the data point to serum TWEAK as both a clinically relevant biomarker and a mechanistic driver of cardiac injury in SLE, positioning it as a promising biomarker and therapeutic target for lupus-associated cardiac damage.

ITPA Activity May Predict MTX Remission in JIA

In previous research, patients with juvenile idiopathic arthritis (JIA) with low inosine triphosphate pyrophosphatase (ITPA) activity showed a lower probability of reaching clinical remission than those with higher ITPA activity. **In this issue, Sindici Forgiarini et al. (p. 1989)** confirm that ITPA activity is a promising predictive biomarker for methotrexate (MTX) response in JIA, outperforming genotyping of the *ITPA* rs1127354 SNP, a nonsynonymous variant previously associated with reduced enzymatic activity. Among 195 patients with JIA treated with MTX, ITPA activity was significantly associated with likelihood of achieving clinical remission. This predictive value was evident at treatment initiation, supporting ITPA's potential use for personalized treatment.

p. 1989

The investigators also used in vitro studies in immortalized human hepatic cells to explore the molecular mechanisms associated with ITPA activity. ITPA-overexpressing cells exhibited increased cytotoxicity to MTX. The authors propose that higher ITPA activity may enhance MTX efficacy through the adenosine/inosine-$ADORA_{2A}$ pathway. $ADORA_{2A}$-mediated signaling increases intracellular cyclic AMP and protein kinase A, which can modulate inflammatory responses via effects on nuclear factor-κB (NF-κB).

The study suggests ITPA activity level might serve as a tool for personalizing JIA treatment. Measurement could guide the choice of upfront biologic or targeted therapy at baseline and prompt an early switch during treatment, with the aim of optimizing treatment response and reducing the risk of disease progression and permanent joint damage.

Multiomic Analysis of Still Disease and Other Autoinflammatory Diseases

Rheumatologists successfully use recombinant human interleukin-18 binding protein (r-hIL-18BP) to treat patients with Still disease (SD), which suggests that IL-18 plays an important role in the pathophysiology of SD. Moreover, IL-18 levels can provide key information about disease trajectory, with IL-18:IL-6 ratios used to classify patients with SD as macrophage activation syndrome (MAS) or arthritis-dominated. p. 1961 **In this issue, Mueller et al. (p. 1961)** report the results of their analysis of a large omics dataset from systemic autoinflammatory diseases (SAIDs) to identify SD-specific biomarkers and pathophysiologic pathways that could distinguish SD from other SAIDs.

The investigators evaluated data from 372 patients with SAIDs from the European Union–funded Immunome project consortium for Autoinflammatory Disorders (ImmunAID). Using RNA sequencing (RNA-Seq) of blood monocytes, they found that, although proinflammatory cytokines and C-reactive protein did not distinguish SD from other SAIDs, IL-18 and heme oxygenase 1 were markedly elevated and predicted SD. Patients with SD could also be characterized by complex interactions among hemophagocytosis, IL-18, and type I interferon (IFN) signaling.

The researchers then performed an integrated, unbiased analysis of these datasets and stratified patients with SD into two distinct subgroups based on hemophagocytic activity rather than disease activity or general inflammation. Although the origin of high IL-18 in SD is unknown, the authors explain that type I IFN may contribute to its increased expression. They conclude by suggesting that the large proteomics and RNA-Seq datasets generated in the study can serve as an invaluable resource for further investigation of SD and other SAIDs.

Journal Club

A monthly feature designed to facilitate discussion on research methods in rheumatology.

Improved Detection of Myositis-Specific Autoantibodies Using Luciferase Immunoprecipitation Systems Assay

Burbelo et al. *Arthritis Rheumatol*. 2026;78:1952–1960.

Myositis-specific autoantibodies are essential for diagnosing and classifying idiopathic inflammatory myopathies and for identifying patients at risk for distinct clinical phenotypes, including interstitial lung disease. However, commonly used commercial line blot assays vary in accuracy, and low-to-intermediate positive results can be difficult to interpret, especially for less common antisynthetase antibodies. In this study, we evaluated whether the luciferase immunoprecipitation systems (LIPS) assay could improve detection of myositis-specific autoantibodies compared with line blot and how each assay performed relative to the current gold standard, conventional immunoprecipitation.

We analyzed 279 sera with line blot results from the Johns Hopkins Myositis Center. Line blot results were assessed using standard thresholds, including ≥36 and ≥71 arbitrary units, and were compared with LIPS results for anti–Jo-1, anti–PL-7, anti–PL-12, anti-MDA5, and anti-EJ antibodies. Assay performance was evaluated against conventional immunoprecipitation in a subset of 141 samples. LIPS provides quantitative antibody levels and may detect antibodies directed against both linear and discontinuous epitopes. These features may help clarify line blot results that are indeterminate or not confirmed by conventional immunoprecipitation.

Overall, LIPS showed strong agreement with conventional immunoprecipitation and performed better than line blot, particularly for clarifying low-to-intermediate positive line blot results that may otherwise lead to misclassification. Because treatment decisions, prognosis, and research classification often depend on the specific autoantibody identified, these findings support a more antibody-specific approach to interpreting line blot signal strength, particularly when results are low positive or clinically unexpected. Although LIPS is not yet routinely available, the study reinforces the need to interpret line blot results cautiously and in the context of the specific autoantibody and clinical phenotype.

Questions

1. **What are the clinical and research consequences of inaccurate myositis-specific autoantibody testing?**
2. **How should clinicians interpret low-to-intermediate positive line blot results, especially for less common antisynthetase antibodies such as PL-7 and PL-12?**
3. **What are the strengths and limitations of using conventional immunoprecipitation as the reference comparator in this study?**

Multiomic Analysis of Still Disease and Other Autoinflammatory Diseases

Rheumatologists successfully use recombinant human interleukin-18 binding protein (r-hIL-18BP) to treat patients with Still disease (SD), which suggests that IL-18 plays an important role in the pathophysiology of SD. Moreover, IL-18 levels can provide key information about disease trajectory, with IL-18:IL-6 ratios used to classify patients with SD as macrophage activation syndrome (MAS) or arthritis-dominated. p. 1961 **In this issue, Mueller et al. (p. 1961)** report the results of their analysis of a large omics dataset from systemic autoinflammatory diseases (SAIDs) to identify SD-specific biomarkers and pathophysiologic pathways that could distinguish SD from other SAIDs.

The investigators evaluated data from 372 patients with SAIDs from the European Union–funded Immunome project consortium for Autoinflammatory Disorders (ImmunAID). Using RNA sequencing (RNA-Seq) of blood monocytes, they found that, although proinflammatory cytokines and C-reactive protein did not distinguish SD from other SAIDs, IL-18 and heme oxygenase 1 were markedly elevated and predicted SD. Patients with SD could also be characterized by complex interactions among hemophagocytosis, IL-18, and type I interferon (IFN) signaling.

The researchers then performed an integrated, unbiased analysis of these datasets and stratified patients with SD into two distinct subgroups based on hemophagocytic activity rather than disease activity or general inflammation. Although the origin of high IL-18 in SD is unknown, the authors explain that type I IFN may contribute to its increased expression. They conclude by suggesting that the large proteomics and RNA-Seq datasets generated in the study can serve as an invaluable resource for further investigation of SD and other SAIDs.

Journal Club

A monthly feature designed to facilitate discussion on research methods in rheumatology.

Improved Detection of Myositis-Specific Autoantibodies Using Luciferase Immunoprecipitation Systems Assay

Burbelo et al. *Arthritis Rheumatol*. 2026;78:1952–1960.

Myositis-specific autoantibodies are essential for diagnosing and classifying idiopathic inflammatory myopathies and for identifying patients at risk for distinct clinical phenotypes, including interstitial lung disease. However, commonly used commercial line blot assays vary in accuracy, and low-to-intermediate positive results can be difficult to interpret, especially for less common antisynthetase antibodies. In this study, we evaluated whether the luciferase immunoprecipitation systems (LIPS) assay could improve detection of myositis-specific autoantibodies compared with line blot and how each assay performed relative to the current gold standard, conventional immunoprecipitation.

We analyzed 279 sera with line blot results from the Johns Hopkins Myositis Center. Line blot results were assessed using standard thresholds, including ≥36 and ≥71 arbitrary units, and were compared with LIPS results for anti–Jo-1, anti–PL-7, anti–PL-12, anti-MDA5, and anti-EJ antibodies. Assay performance was evaluated against conventional immunoprecipitation in a subset of 141 samples. LIPS provides quantitative antibody levels and may detect antibodies directed against both linear and discontinuous epitopes. These features may help clarify line blot results that are indeterminate or not confirmed by conventional immunoprecipitation.

Overall, LIPS showed strong agreement with conventional immunoprecipitation and performed better than line blot, particularly for clarifying low-to-intermediate positive line blot results that may otherwise lead to misclassification. Because treatment decisions, prognosis, and research classification often depend on the specific autoantibody identified, these findings support a more antibody-specific approach to interpreting line blot signal strength, particularly when results are low positive or clinically unexpected. Although LIPS is not yet routinely available, the study reinforces the need to interpret line blot results cautiously and in the context of the specific autoantibody and clinical phenotype.

Questions

1. **What are the clinical and research consequences of inaccurate myositis-specific autoantibody testing?**
2. **How should clinicians interpret low-to-intermediate positive line blot results, especially for less common antisynthetase antibodies such as PL-7 and PL-12?**
3. **What are the strengths and limitations of using conventional immunoprecipitation as the reference comparator in this study?**

Clinical Connections

Multi-Omic Profiling Reveals Immune Cell Priming Signature in Lupus

Smith et al. *Arthritis Rheumatol.* 2026;78:1878–1891.

CORRESPONDENCE
Dominic Sinibaldi, PhD: nsinibaldi@gmail.com

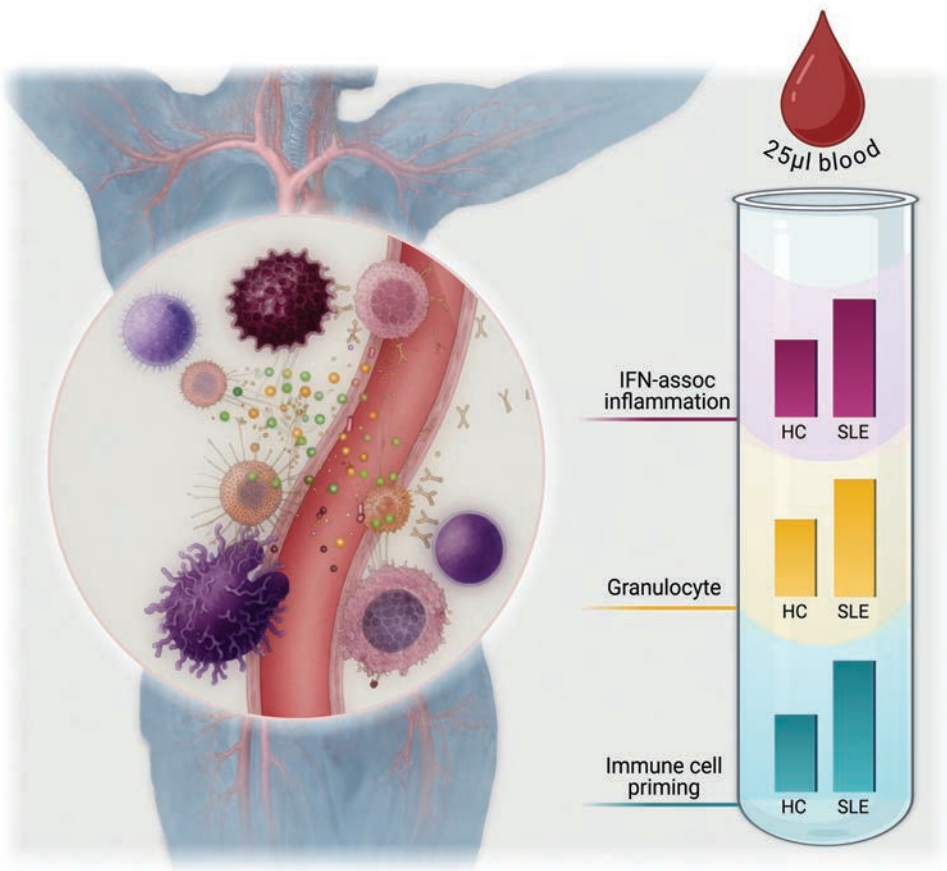

KEY POINTS

- Proteins released from inflamed tissues could be detected in the blood of patients with lupus.
- Multidimensional analysis of integrated immune cell, protein, and transcriptome data identified three protein immune patterns.
- A newly discovered blood protein signature that detects tissue immune activity was linked to future organ damage risk.
- These findings may improve disease monitoring and support personalized treatment approaches.

SUMMARY

Systemic lupus erythematosus is an autoimmune disease in which the immune system attacks healthy tissues and organs, causing inflammation and damage throughout the body. Immune cell interactions in tissues such as the kidneys, skin, and joints contribute to the inflammatory milieu, releasing proteins that can egress into the bloodstream.

Smith et al. studied blood samples from 87 people with lupus, combining protein, immune cell, and gene activity information to identify three immune patterns linked to different types of disease activity and organ involvement. In addition to type I interferon and granulocyte pathways, the study uncovered a new immune cell priming protein signature linked to a higher risk of future organ damage, which performed better than standard clinical tests at predicting risk of disease worsening. These findings could support earlier identification of high-risk patients and timely intervention to prevent irreversible organ damage.

Somatic Mutations in a Large Cohort of Chinese Patients With Immune Dysregulation

Fu et al. *Arthritis Rheumatol.* 2026;78:1975–1988.

CORRESPONDENCE
Qing Zhou, PhD: zhouqingnwu@gmail.com

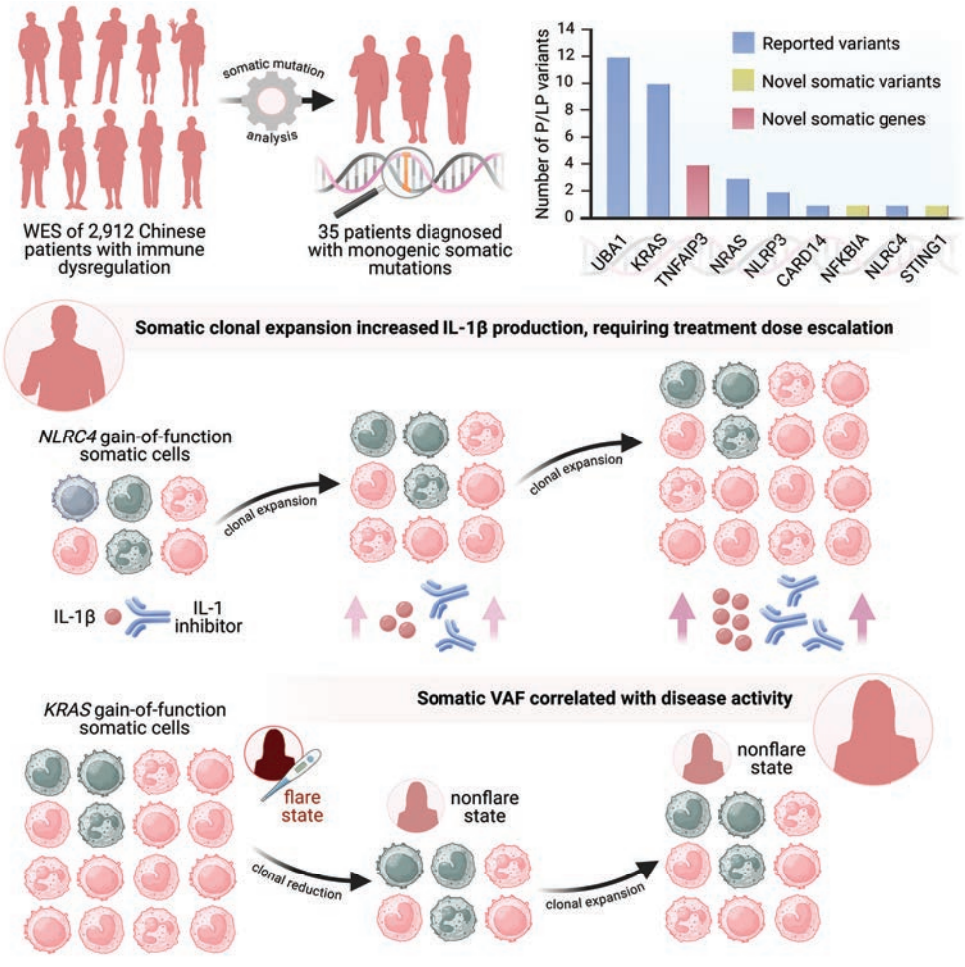

KEY POINTS

- This study delineated the genetic landscape of pathogenic somatic mutations underlying immune dysregulation diseases.
- Findings expand the genetic diagnostic landscape and highlight the importance of considering somatic mutations in germline-negative patients.
- Novel somatic pathogenic genes and variants add to the diagnostic spectrum and support improved diagnosis and targeted treatment.
- Longitudinal monitoring of somatic mutation ratio may improve precision medicine.

SUMMARY

Clinically, a large number of patients with immune dysregulation have negative genetic diagnoses, suggesting overlooked mutation types. Fu et al. reanalyzed whole-exome sequencing data from 2,912 patients with immune dysregulation disorders who previously tested negative for germline pathogenic variants. Through systematic somatic mutation analysis, they identified 35 patients carrying disease-causing monogenic somatic mutations, involving genes such as *UBA1*, *KRAS*, *TNFAIP3*, *NRAS*, and *NLRP3*.

In addition, the authors monitored longitudinal changes in somatic mutations. In a patient with a somatic *NLRC4* mutation, canakinumab initially controlled disease, but became insufficient over time. Variant allele fraction (VAF) increased from 1.73% to 19.49%, and disease control was restored after dose escalation. In another patient with a somatic *KRAS* mutation, VAF was 26.16% during flare and decreased to 1.32% and 7.6% during nonflare periods, paralleling disease activity.

Arthritis & Rheumatology
Vol. 78, No. 9, September 2026, pp 1813–1815
DOI 10.1002/art.70135
© 2026 American College of Rheumatology

American College of Rheumatology
Empowering Rheumatology Professionals

EDITORIAL

T Cells in Osteoarthritis: Drivers, Repairers, or Bystanders in Osteoarthritis?

Tonia L. Vincent, MD, PhD[1] and Andrew P. Cope, MD, PhD[2]

The involvement of the immune system in osteoarthritis (OA) is undisputed but the specific role of lymphoid cells in its pathogenesis has continued to fuel debate. In this issue of *Arthritis & Rheumatology*, the study by Moradi et al[1] revisits the role of T cells in OA and persuades us that they contribute to OA pathogenesis. Historically, there is a body of evidence that suggests a possible causal role for T cells in OA. This includes the identification of increased numbers of memory T cells in the OA synovium, some which show early activation markers and evidence of oligoclonality; the presence of ectopic lymphoid tissue in up to 30% of OA synovial biopsy samples; the association of HLA genotypes with OA risk from genetic linkage studies; evidence of specific autoantigens, for example, to type II collagen; and increased levels of T cell cytokines in OA synovial fluid.[2,3] More recent observations include reports of individuals with OA being nearly eight times more likely to develop inflammatory arthritis after checkpoint inhibitor treatment for cancer than patients without a history of OA.[4] Some of the evidence for an association has not stood the test of time; for instance, large-scale genome-wide association studies, largely superseding linkage studies, have not confirmed that HLA alleles contribute to OA genetic risk.[5]

In the study by Moradi et al, they first perform a detailed longitudinal characterization of immune cell profiles in a well-validated surgical joint destabilization model in mice. The authors demonstrate a cyclical increase in T cells in the synovium starting immediately after surgery that is more evident in the destabilized joint (OA) compared with sham-operated control and surgery-naïve groups. These cells have increased ratios of Th1/2- and Th17-associated cytokines, suggesting a proinflammatory rather than pro-resolving function. The regulation of T cell numbers appears dominant over myeloid cells, and although a cyclical pattern is also demonstrated for monocyte/macrophage numbers (out of phase with the T cells), there is no significant difference in their levels over time comparing OA and sham-operated joints. Lymphocyte subsets have not been phenotyped in depth, and so it is difficult to determine whether these subsets have arisen from resident memory T cells (eg, $CD8^+CD69^+CD103^+$), whether they have differentiated in situ to bona fide T helper cell subsets expressing their master transcription factor and associated chemokine receptors, or whether these cells have migrated into the joint as a consequence of the injury perturbation. Indeed, injury or inflammation would induce a leaky synovial joint with infiltration of a wide repertoire of CD4 or CD8 T cells because these cells are intrinsically migratory and have the habit of being retained in the tissue beyond the period of the traumatic or inflammatory "insult."[6]

The big question is whether T cells truly contribute to disease outcomes and, if so, whether targeted therapies would benefit patients. Moradi et al demonstrate a correlation between patient-reported pain and T cell numbers in synovial biopsies of patients with early posttraumatic or established OA. However, because all pathologies within the OA joint correlate weakly with pain and generally correlate with one another, it is difficult to use this as evidence for causality. The authors also show evidence in vitro that T cells are capable of making matrix metalloproteinases, which they suggest could be contributing to degradation of the articular cartilage, a primary feature of OA. Based on single-cell data from OA synovium,[7] other cell types, principally fibroblasts and macrophages, appear to be making a much bigger contribution to this when considering the whole tissue.

Mechanical joint stress is a primary factor in OA pathogenesis,[8] and pathologic changes in the joint, as well as inflammatory gene regulation from whole-joint extracts, are abrogated when the joint is immobilized after surgical joint destabilization in mice, either by prolonged anesthesia or sciatic/femoral neurectomy.[9] Both immune cells and stromal cells of the cartilage and synovium are responsible for mechanosensitive regulation of inflammatory genes through a variety of described mechanisms.[10] Sterile tissue injury responses in other organs also activate a myriad of other classical innate immune processes,

[1]Centre for Osteoarthritis Pathogenesis, Kennedy Institute of Rheumatology, University of Oxford, Oxford, United Kingdom; [2]Centre for Rheumatic Diseases, King's College London, London, United Kingdom.

Author disclosures are available at https://onlinelibrary.wiley.com/doi/10.1002/art.70135.

Address correspondence via email to Tonia L. Vincent, MD, PhD, at tonia.vincent@kennedy.ox.ac.uk.

Submitted for publication February 20, 2026; accepted in revised form February 24, 2026.

including activation of clotting cascades and the complement pathway, that contribute to innate immune cell (neutrophils, monocytes, innate lymphoid cells) recruitment and activation and pave the way for repair. T cells (and B cells) enter the joint later, ensure sterility of the wound, and also contribute to wound resolution and repair in a non–antigen-dependent manner.[11]

A dominant role for the innate immune response in OA is supported by STEpUP OA, a large-scale proteomic analysis of the synovial fluid in over 1,300 individuals with early- and late-stage radiographic OA.[12] Core pathways identified in this analysis that predicted having more severe radiographic disease include "epithelial to mesenchymal transition," "complement," and "coagulation." Targeting of both complement and coagulation pathways are shown to be disease modifying in surgically induced OA in mice.[13,14] There are no published reports of joint protection when OA is induced in Rag1$^{-/-}$ and Rag2$^{-/-}$ mice, in which T and B cells are absent, or in severe combined immunodeficient mice, although we are aware of unpublished studies from our own laboratory and others in which no OA protection is seen in these strains. Moradi et al failed to see robust protection in mice in which depleting anti-CD3 antibodies were given either at the time of surgery or once disease was established, although these experiments are somewhat problematic and hard to interpret because the anti-CD3 clone 145.2C11 is a potent agonistic monoclonal antibody, so any depletion (reported here in the spleen but not synovial tissue) may arise through activation-induced cell death. Further studies and alternative approaches would help to clarify this.

Rheumatologists are familiar with the classic immune-mediated diseases of the joint that have strong T cell dependence. As trainees, we are taught to distinguish inflammatory arthritis from OA by examining the cell type and number within the synovial fluid. OA joint fluid is typically paucicellular and mainly monocytic. Diseases such as rheumatoid arthritis (RA) demonstrate compelling evidence for T cell dependence, including highly cellular synovial fluid (often >50% neutrophils); strong genetic associations with HLA alleles and T cell receptor modulator genes; diagnostic and prognostic autoantibodies such as those against citrullinated peptides; and clinical response to immunomodulation, including specific T cell–targeted therapies such as abatacept. The latter acts as an agonist at CTLA-4 and is efficacious in active RA as well as suppressing development of RA when given to at-risk but asymptomatic individuals.[15] Repurposing of disease-modifying antirheumatic drugs in OA has been generally disappointing, either failing to meet primary study end points when targeting cytokines such as interleukin-1 (IL-1), tumor necrosis factor, and IL-6, or by using general immunosuppressive treatments such as hydroxychloroquine. Modest changes of questionable clinical significance are seen with methotrexate across knee and hand OA.[16] Intra-articular glucocorticoid injection is superior to placebo in reducing pain, but it is short lived (<12 weeks), and repeated injections has been shown to accelerate structural disease.[17]

Taken together, the evidence suggests that T cells are unlikely primary drivers of OA and targeting their activity is unlikely to deliver beneficial clinical outcomes. Their presence in the joint is not questioned, and there may be aspects of disease that lymphocytes contribute to, but the relative importance of these to effector or even regulatory pathways in OA may be modest. T cell–dependent autoantibody production is not a feature of OA nor animal models thereof. Very little is understood about "inflammatory flares" in OA, which are often unpredictable but can occur with increased mechanical stress or intercurrent illness. It is tempting to speculate that the adaptive immune cells have a greater contribution to such episodes, but at present these remain poorly characterized.

AUTHOR CONTRIBUTIONS

Both authors contributed to at least one of the following manuscript preparation roles: conceptualization AND/OR methodology, software, investigation, formal analysis, data curation, visualization, and validation AND drafting or reviewing/editing the final draft. As corresponding author, Dr Vincent confirms that all authors have provided the final approval of the version to be published and takes responsibility for the affirmations regarding article submission (eg, not under consideration by another journal), the integrity of the data presented, and the statements regarding compliance with institutional review board/Declaration of Helsinki requirements.

REFERENCES

1. Moradi B, Jackson MT, Shu CC, et al. The potential role of synovial T cell infiltration following knee joint injury in symptoms and progression to osteoarthritis. Arthritis Rheumatol 2026;78(9):1863–1877. doi: https://doi.org/10.1002/art.70157
2. Sakkas LI, Platsoucas CD. The role of T cells in the pathogenesis of osteoarthritis. Arthritis Rheum 2007;56(2):409–424. doi:https://doi.org/10.1002/art.22369
3. Zhang X, Cao M, Fu BS, et al. Adaptive immunity in osteoarthritis: mechanisms and opportunities for regulatory T-cell-targeted therapy. Pharmacol Res 2025;222:108041. doi:https://doi.org/10.1016/j.phrs.2025.108041
4. Portnoy DM, Paiola M, Tymm C, et al. Understanding the inflammatory aspect of osteoarthritis: lessons from immune checkpoint inhibitors. J Clin Med 2026;15(2):658. doi:https://doi.org/10.3390/jcm15020658
5. Hatzikotoulas K, Southam L, Stefansdottir L, et al; arcOGEN Consortium; ARGO Consortium; DBDS Genomic Consortium; Estonian Biobank Research Team; FinnGen; Genes & Health Research Team; HUNT All-In Pain; Million Veteran Program; Regeneron Genetics Center. Translational genomics of osteoarthritis in 1,962,069 individuals. Nature 2025;641(8065):1217–1224. doi:https://doi.org/10.1038/s41586-025-08771-z
6. Prendergast CT, Patakas A, Al-Khabouri S, et al. Visualising the interaction of CD4 T cells and DCs in the evolution of inflammatory arthritis. Ann Rheum Dis 2018;77(4):579–588. doi:https://doi.org/10.1136/annrheumdis-2017-212279
7. Chou CH, Jain V, Gibson J, et al. Synovial cell cross-talk with cartilage plays a major role in the pathogenesis of osteoarthritis. Sci Rep 2020;10(1):10868. doi:https://doi.org/10.1038/s41598-020-67730-y
8. Brandt KD, Dieppe P, Radin EL. Commentary: is it useful to subset "primary" osteoarthritis? A critique based on evidence regarding the

etiopathogenesis of osteoarthritis. Semin Arthritis Rheum 2009;39(2):81–95. doi:https://doi.org/10.1016/j.semarthrit.2009.06.001

9. Burleigh A, Chanalaris A, Gardiner MD, et al. Joint immobilization prevents murine osteoarthritis and reveals the highly mechanosensitive nature of protease expression in vivo. Arthritis Rheum 2012;64(7):2278–2288. doi:https://doi.org/10.1002/art.34420
10. Vincent TL. A unified mechanobiological model for osteoarthritis across joint tissues - a perspective. Ann Anat 2026;265:152772. doi:https://doi.org/10.1016/j.aanat.2025.152772
11. Wang X, Balaji S, Steen EH, et al. T lymphocytes attenuate dermal scarring by regulating inflammation, neovascularization, and extracellular matrix remodeling. Adv Wound Care (New Rochelle) 2019;8(11):527–537. doi:https://doi.org/10.1089/wound.2019.0981
12. Perry TA, Deng Y, Hulley P, et al. Deconvoluting synovial fluid molecular endotypes in knee osteoarthritis: primary results from the STEpUP OA Consortium. medRxiv Preprint posted online June 6, 2024. doi:https://doi.org/10.1101/2024.06.05.24308485
13. Wang Q, Rozelle AL, Lepus CM, et al. Identification of a central role for complement in osteoarthritis. Nat Med 2011;17(12):1674–1679. doi:https://doi.org/10.1038/nm.2543
14. Wang Q, Shao G, Zhao X, et al. Dysregulated fibrinolysis and plasmin activation promote the pathogenesis of osteoarthritis. JCI Insight 2024;9(8):e173603. doi:https://doi.org/10.1172/jci.insight.173603
15. Cope AP, Jasenecova M, Vasconcelos JC, et al; APIPPRA study investigators. Abatacept in individuals at high risk of rheumatoid arthritis (APIPPRA): a randomised, double-blind, multicentre, parallel, placebo-controlled, phase 2b clinical trial. Lancet 2024;403(10429):838–849. doi:https://doi.org/10.1016/S0140-6736(23)02649-1
16. Kuswanto W, Baker MC. Repurposing drugs for the treatment of osteoarthritis. Osteoarthritis Cartilage 2024;32(8):886–895. doi:https://doi.org/10.1016/j.joca.2024.05.008
17. McAlindon TE, LaValley MP, Harvey WF, et al. Effect of intra-articular triamcinolone vs saline on knee cartilage volume and pain in patients with knee osteoarthritis: a randomized clinical trial. JAMA 2017;317(19):1967–1975. doi:https://doi.org/10.1001/jama.2017.5283

American College of Rheumatology
Empowering Rheumatology Professionals

Arthritis & Rheumatology
Vol. 78, No. 9, September 2026, pp 1816–1818
DOI 10.1002/art.70179
© 2026 American College of Rheumatology

EDITORIAL

Somatic Variants in Immune Dysregulation: An Ongoing Challenge

Sofia Torreggiani, MD and Ivona Aksentijevich, MD

Over the past three decades, the genetic investigation of disorders of immune dysregulation has undergone a notable transformation. The identification of monogenic causes of inborn errors of immunity (IEIs), including autoinflammatory and autoimmune disorders, has reshaped disease classification and increasingly informed clinical management.[1] However, despite the widespread implementation of next-generation sequencing, the diagnostic yield of molecular analysis in patients with suspected monogenic immunologic disorders has remained limited, typically averaging 30% to 40% in outbred populations.[2]

In the early 2000s, a subset of germline-negative patients with a phenotype highly suggestive for autoimmune lymphoproliferative syndrome and cryopyrin-associated autoinflammatory syndrome were found to carry somatic variants in *FAS* and *NLRP3*, respectively.[3,4] In the following years, additional discoveries expanded the list of mosaic errors of immunity (MEIs)[5]—conditions in which only a fraction of the cells in the organism carries the pathogenic variant—although often involving only a limited number of patients.

The discovery of Vacuoles, E1 enzyme, X-linked, autoinflammatory, somatic (VEXAS) syndrome in 2020 based on whole-exome sequencing (WES) brought a change in perspective.[6] The identification of somatic variants in *UBA1*, a gene not previously implicated in immunologic disease, as the cause of a relatively common, severe, adult-onset autoinflammatory syndrome showed that postzygotic mutations could drive monogenic systemic immune disease in more than just a few patients and across diverse phenotypes. However, more than 5 years after this discovery, it remains unclear how frequently somatic mutations are disease-causing in patients with immune dysregulation. An early study, based on targeted amplicon sequencing of six known MEI-associated genes in 30 symptomatic patients at higher risk of mosaicism based on predefined criteria, identified a pathogenic postzygotic variant in 18 individuals.[7] Another study based on targeted sequencing of five systemic autoinflammatory disease–associated genes in 158 less stringently selected patients had a much lower yield of 1.9%.[8]

In this context, the recent larger-scale study by Fu et al,[9] in this issue of *Arthritis & Rheumatology*, exploring a broader set of genes, has brought some clarity on the potential benefits of reanalyzing exome data to detect somatic variants that may have been missed by standard germline variant calling. Using bulk DNA exome sequencing with an in silico gene panel, investigators analyzed a cohort of 2,912 pediatric (39%) and adult (61%) individuals with autoinflammatory and autoimmune disorders in whom no germline cause had been identified. After orthogonal validation, including deep amplicon sequencing and multitissue sampling, to confirm the candidate somatic variants, the study identified MEIs in only 1.35% of adults and 0.97% of children. Although these findings confirm the contribution of somatic mutations to immune dysregulation, they also temper earlier expectations of a rapid increase in diagnostic yield from WES-based somatic variant analysis.

Several methodological considerations are critical to contextualize these findings. First, the study focused on a predefined panel of 157 genes already implicated in disorders of immune regulation. Although this approach is pragmatic and clinically oriented, it may limit the potential for new discovery. The 35 pathogenic or likely pathogenic somatic variants identified occurred only in nine genes. *TNFAIP3* variants, which were recently reported to be MEI-causing,[10] were detected in four families with seven patients, with a variant allele fraction (VAF) between 5% and 20%. Interestingly, three of these patients had gonosomal mosaicism (ie, a condition in which the postzygotic variant is present in a combination of somatic and germinal cells), as evidenced by their transmission of the variant to their offspring,

This research was supported by the Intramural Research Program of the NIH. The contributions of the NIH authors are considered works of the United States Government. The findings and conclusions presented in this paper are those of the authors and do not necessarily reflect the views of the NIH or the US Department of Health and Human Services.

Inflammatory Disease Section, National Human Genome Research Institute, National Institutes of Health, Bethesda, Maryland.

Author disclosures are available at https://onlinelibrary.wiley.com/doi/10.1002/art.70179.

Address correspondence via email to Ivona Aksentijevich, MD, at aksentii@mail.nih.gov.

Submitted for publication February 23, 2026; accepted in revised form March 19, 2026.

who displayed a more severe phenotype associated with their germline status. The other genes identified (*CARD14*, *KRAS*, *NFKBIA*, *NLRC4*, *NLRP3*, *NRAS*, *STING*, and *UBA1*) had previously been shown to be associated with MEI. This observation suggests that, at least with current methods targeting genes already associated with IEIs, detection of somatic mutations largely converges on established pathogenic pathways rather than revealing new genetic architectures.

Second, the reliance on bulk WES with a mean depth of 98× imposes some sensitivity constraints, as identification of low-level mosaicism may be limited. Thus, pathogenic somatic variants present at low VAFs, particularly those confined to specific cell subsets, may remain undetected. In this context, negative results from standard-depth WES-based testing cannot be interpreted as definitive evidence against a somatic contribution. Whole-genome sequencing is even less preferred for identifying somatic mutations because of lower read depth across the genome, resulting in lower detecting efficiency. A targeted high-depth gene sequencing panel with an average read depth of >1,000× can significantly increase the diagnostic yield.[10]

Cellular context is likely to be a decisive factor in the pathogenesis of MEI. For instance, in autoimmune disease, if a specific lymphocyte subpopulation is driving the pathogenesis, sequencing unsorted peripheral blood-derived DNA may dilute the signal of causative variants. Approaches incorporating sequencing of sorted cell populations, particularly when guided by disease pathogenesis, have shown improved sensitivity.[3,11,12] However, such strategies are more costly and may not be applicable to large cohorts. Although selecting populations with a higher risk of carrying somatic variants, such as individuals with late-onset disease or evidence of clonal hematopoiesis (CH), may provide some advantage, it should be noted that MEIs can also present early, typically with postzygotic variants detectable in tissues derived from multiple germ layers.[13] Currently, there are no established criteria to reliably select patients for a more in-depth somatic variant analysis.

The study by Fu et al, like most existing studies on somatic mutations in immune dysregulation, focused primarily on single-nucleotide variants and small insertions or deletions. Other forms of somatic variation may also contribute to disease pathogenesis but remain comparatively understudied. Mosaic chromosomal abnormalities could disrupt immune regulation through gene dosage effects or gene fusions. To date, such abnormalities have been examined mainly in the context of neoplasia or CH, with only limited exploration in immune-mediated disease. A few notable exceptions, such as mosaic trisomy 8,[14] illustrate that somatic chromosomal alterations can have immunologic consequences without myelodysplastic features, but systematic data are lacking.

A further challenge lies in functional validation. Demonstrating the pathogenicity of somatic variants, particularly those presenting at low VAF and in novel genes, is inherently difficult. Traditional bulk functional assays may obscure cell-specific effects, and animal models are often impractical for mosaic conditions. In this context, emerging single-cell technologies offer considerable promise. Single-cell DNA and RNA sequencing, coupled with immune profiling, may allow direct linkage of somatic variants to transcriptional programs, cellular phenotypes, and functional outcomes, as has been suggested for germline variants.[15] As these approaches mature and become more accessible, they are likely to play a pivotal role in clarifying the contribution of somatic mutations to immune dysregulation.

Interestingly, Fu et al noticed a possible correlation between disease manifestations and longitudinal changes in the VAF, underlying the need for serial genetic analysis at multiple time points. Further prospective studies are needed to better clarify the factors that influence clonal dynamics and explore the therapeutic potential of approaches that limit or reduce clonal expansion.

Fu et al also curated CH based on a list of 11 genes, identifying 36 adult patients with CH-associated variants, of whom 72% presented with an autoinflammatory phenotype. Only one of these patients, carrying a *DNMT3A* variant, also carried a pathogenic somatic variant in *UBA1*. Although initial efforts have begun to characterize the landscape of CH in VEXAS syndrome,[16] further studies are needed to better explore the relationship between CH and pathogenic variants in other MEI-associated genes. CH-driver variants are increasingly detected in aging populations and are well-established risk factors for hematologic malignancy and cardiovascular disease. Whether, and to what extent, such driver variants can contribute to immune dysregulation when coexisting with potentially impactful passenger variants in immune-related genes still needs to be fully elucidated.[17]

More broadly, it remains difficult to estimate what proportion of genetically unexplained immune dysregulation is attributable to somatic variation. Although the low yield observed in large, unselected cohorts may suggest that somatic mutations are unlikely to account for most unresolved cases, it has to be noted that their contribution may be underestimated by current methodologies. Resolving this uncertainty will require harmonized approaches that integrate immunologic phenotyping, the implementation of tailored next-generation sequencing technologies, and the development of targeted variant-calling algorithms designed for non-neoplastic tissues.

Although several outstanding questions remain unanswered, the study by Fu et al confirms that somatic mutations can contribute to immune dysregulation, although their detectable impact, using current bulk exome sequencing approaches, still appears limited in broadly defined populations. The conceptual advance introduced by the MEI framework remains highly influential, yet translating this insight into widespread diagnostic gains will require more refined strategies.

Future progress will depend on analysis of specific cell subsets, deeper and error-corrected sequencing, systematic assessment of multiple classes of somatic variation, and integration of single-cell functional approaches. Finally, although a modest

diagnostic yield of the current broadly accessible strategies for somatic variant analysis may suggest that mosaicism is not likely the missing explanation for most unresolved cases, for a small but meaningful subset of patients, it still may represent a critical and clinically actionable piece of the diagnostic puzzle that is worth identifying.

AUTHOR CONTRIBUTIONS

All authors contributed to at least one of the following manuscript preparation roles: conceptualization AND/OR methodology, software, investigation, formal analysis, data curation, visualization, and validation AND drafting or reviewing/editing the final draft. As corresponding author, Dr Aksentijevich confirms that all authors have provided the final approval of the version to be published and takes responsibility for the affirmations regarding article submission (eg, not under consideration by another journal), the integrity of the data presented, and the statements regarding compliance with institutional review board/Declaration of Helsinki requirements.

REFERENCES

1. Poli MC, Aksentijevich I, Bousfiha AA, et al. Human inborn errors of immunity: 2024 update on the classification from the International Union of Immunological Societies Expert Committee. J Hum Immun 2025;1(1):e20250003. PubMed doi:10.70962/jhi.20250003
2. Chen Y, Li D, Yin J, et al. Diagnostic yield of next-generation sequencing in suspect primary immunodeficiencies diseases: a systematic review and meta-analysis. Clin Exp Med 2024;24(1):131. PubMed doi:10.1007/s10238-024-01392-2
3. Holzelova E, Vonarbourg C, Stolzenberg MC, et al. Autoimmune lymphoproliferative syndrome with somatic Fas mutations. N Engl J Med 2004;351(14):1409–1418. PubMed doi:10.1056/NEJMoa040036
4. Saito M, Fujisawa A, Nishikomori R, et al. Somatic mosaicism of CIAS1 in a patient with chronic infantile neurologic, cutaneous, articular syndrome. Arthritis Rheum 2005;52(11):3579–3585. PubMed doi:10.1002/art.21404
5. Roosens W, Demeulemeester J, Legius E, et al. Emerging insights into mosaic errors of immunity. Trends Immunol 2026;47(2):130–146. PubMed doi:10.1016/j.it.2025.09.003
6. Beck DB, Ferrada MA, Sikora KA, et al. Somatic mutations in *UBA1* and severe adult-onset autoinflammatory disease. N Engl J Med 2020;383(27):2628–2638. PubMed doi:10.1056/NEJMoa2026834
7. Mensa-Vilaró A, Bravo García-Morato M, de la Calle-Martin O, et al. Unexpected relevant role of gene mosaicism in patients with primary immunodeficiency diseases. J Allergy Clin Immunol 2019;143(1):359–368. PubMed doi:10.1016/j.jaci.2018.09.009
8. Kant B, Carbo EC, Kokmeijer I, et al. Gene mosaicism screening using single-molecule molecular inversion probes in routine diagnostics for systemic autoinflammatory diseases. J Mol Diagn 2019;21(6):943–950. PubMed doi:10.1016/j.jmoldx.2019.06.009
9. Fu J, Fu Q, Wang J, et al. Landscape of somatic mutations in a large cohort of Chinese patients with immune dysregulations. Arthritis Rheumatol 2026;78(9):1975–1988. doi:10.1002/art.70126
10. Schmitz EG, Paul AJ, Ghosh R, et al. Targeted deep sequencing identifies mosaicism in patients with immune dysregulation. J Allergy Clin Immunol Published online February 5, 2026. PubMed doi:10.1016/j.jaci.2026.01.023
11. Saito M, Nishikomori R, Kambe N, et al. Disease-associated CIAS1 mutations induce monocyte death, revealing low-level mosaicism in mutation-negative cryopyrin-associated periodic syndrome patients. Blood 2008;111(4):2132–2141. PubMed doi:10.1182/blood-2007-06-094201
12. Nicola PA, Lawson ARJ, Tidd A, et al. Polyclonal selection of immune checkpoint mutations in thyroid autoimmunity. Nature 2026. doi:10.1182/blood-2007-06-094201
13. Torreggiani S, Castellan FS, Aksentijevich I, et al. Somatic mutations in autoinflammatory and autoimmune disease. Nat Rev Rheumatol 2024;20(11):683–698. PubMed doi:10.1038/s41584-024-01168-8
14. Pan FY, Fan HZ, Zhuang SH, et al. Severe inflammatory disorder in trisomy 8 without myelodysplastic syndrome and response to methylprednisolone: a case report. World J Clin Cases 2023;11(26):6206–6212. PubMed doi:10.12998/wjcc.v11.i26.6206
15. Novotny S, Yoo N, Chen J, et al. Association of clinical manifestations and immune alterations with genetic variants of uncertain significance in patients concerned for inborn errors of immunity. Clin Immunol 2025;277:110513. PubMed doi:10.1016/j.clim.2025.110513
16. Gutierrez-Rodrigues F, Kusne Y, Fernandez J, et al. Spectrum of clonal hematopoiesis in VEXAS syndrome. Blood 2023;142(3):244–259. PubMed doi:10.1182/blood.2022018774
17. De Langhe E, Van Loo S, Malengier-Devlies B, et al. *TET2*-driver and *NLRC4*-passenger variants in adult-onset autoinflammation. N Engl J Med 2023;388(17):1626–1629. PubMed doi:10.1056/NEJMc2212928

Arthritis & Rheumatology
Vol. 78, No. 9, September 2026, pp 1819–1822
DOI 10.1002/art.70182
© 2026 American College of Rheumatology

American College of Rheumatology
Empowering Rheumatology Professionals

EDITORIAL

From Genome-Wide Association Study Signal to Mechanism in Rheumatoid Arthritis: Lessons From a Single Risk Locus

Ryuya Edahiro, MD, PhD[1,2,3] and Yukinori Okada, MD, PhD[1,3,4,5,6]

Large-scale genome-wide association studies (GWASs) have identified over 100 genetic loci associated with rheumatoid arthritis (RA),[1–3] underscoring the strong genetic contribution to disease susceptibility. RA also provided early evidence that GWAS findings can directly inform the prioritization of existing and potential therapeutic targets for complex traits.[1] Even as GWAS data sets continue to expand in scale and diversity, translating genetic association signals into locus-level mechanism—and ultimately therapeutic hypotheses—remains challenging. In this issue of *Arthritis & Rheumatology*, Sheridan et al address this gap by tracing a long-standing RA risk variant from its expression quantitative trait locus (eQTL) effect to enzymatic consequences in synovial fibroblasts with secondary effects on local immune phenotypes.[4] Beyond elucidating a single locus, this study raises broader questions about how genetic risk is interpreted and translated into therapeutic strategy.

Most RA risk variants—and, more broadly, autoimmune disease–associated variants identified through GWASs—reside in noncoding regions of the genome,[5] complicating the identification of their functional mechanisms. Statistical association between genotype and phenotype alone does not define which gene or protein is functionally perturbed, in which a cell-type or cell-state variant exerts its effect, or how such genetic regulatory changes are ultimately translated into pathogenic processes. To decipher the function of genetic variants and nominate candidate genes and proteins at GWAS loci, molecular QTL (mol-QTL) analyses, most prominently eQTL, have become a central component of post-GWAS analyses[6] (Figure 1). Early efforts were largely based on bulk transcriptomic data sets, exemplified by the Genotype-Tissue Expression (GTEx) project,[7] which have provided foundational insight into genetically regulated gene expression across tissues. More recently, these frameworks have expanded to incorporate single-cell transcriptomic data, enabling cell-type– and cell-state–resolved analyses of genetically regulated expression.[8,9] In parallel, protein QTL (pQTL) resources have been increasingly developed to capture genetic effects on the protein level.[10,11] However, the expansion of mol-QTL resources across tissues, cell types, and molecular layers remains incomplete, limiting our ability to fully resolve the underlying genetic regulatory mechanisms at individual GWAS loci.

Sheridan et al address this mechanistic gap from variant to function through a careful and stepwise functional dissection of rs26232 (5q21), a well-established RA susceptibility and severity variant located within the first intron of *MACIR*.[4] Despite its intronic position, eQTL analysis across the surrounding genomic region in RA synovial fibroblasts (RASFs) demonstrates that the regulatory effect of this locus extends beyond its annotated host gene, instead implicating *PAM* as the true functional target. This finding underscores the importance of rigorous locus-level regulatory mapping to assign variants to their true functional targets rather than relying on genomic proximity alone.

Beyond accurate gene assignment, the study also prompts reconsideration of the tissue and cell-type contexts through which genetic risk exerts its effects. Interpretation of RA genetics has largely been shaped by immune-cell–derived data sets,[8] reflecting both the autoimmune nature of the disease and the

Dr Edahiro's work was supported by the Japan Society for the Promotion of Science (JSPS) KAKENHI (grant 25K18835), Japan Agency for Medical Research and Development (AMED; grants JP25tm0424233, JP25gm7110002, JP25gm2010008, JP25kk0305029, JP24gm1810012, and JP24ek0210207), and a Japan Foundation for Applied Enzymology grant. Dr Okada's work was supported by the JSPS KAKENHI (grant 25H01057); AMED (grants JP24km0405217, JP24ek0109594, JP24ek0410113, JP24kk0305022, JP223fa627001, JP223fa627002, JP223fa627010, JP223fa627011, JP22zf0127008, JP24tm0524002, JP24wm0625504, and JP24gm1810011); Japan Science and Technology Agency (JST) Moonshot R&D (grants JPMJMS2021 and JPMJMS2024); Ono Pharmaceutical Foundation for Oncology, Immunology, and Neurology; CiDER and CAMaD, Osaka University; and RIKEN TRIP Initiative (AGIS).

[1]Graduate School of Medicine, Department of Statistical Genetics, University of Osaka, Suita, Japan; [2]Graduate School of Medicine, Department of Respiratory Medicine and Clinical Immunology, University of Osaka, Suita, Japan; [3]Laboratory for Systems Genetics, RIKEN Center for Integrative Medical Sciences, Yokohama, Japan; [4]Graduate School of Medicine, Department of Genome Informatics, University of Tokyo, Tokyo, Japan; [5]Laboratory of Statistical Immunology, Immunology Frontier Research Center, University of Osaka, Suita, Japan; [6]Premium Research Institute for Human Metaverse Medicine, University of Osaka, Suita, Japan.

Author disclosures are available at https://onlinelibrary.wiley.com/doi/10.1002/art.70182.

Address correspondence via email to Ryuya Edahiro, MD, PhD, at r.edahiro@imed3.med.osaka-u.ac.jp; or Yukinori Okada, MD, PhD, at yuki-okada@m.u-tokyo.ac.jp.

Submitted for publication March 3, 2026; accepted in revised form March 9, 2026.

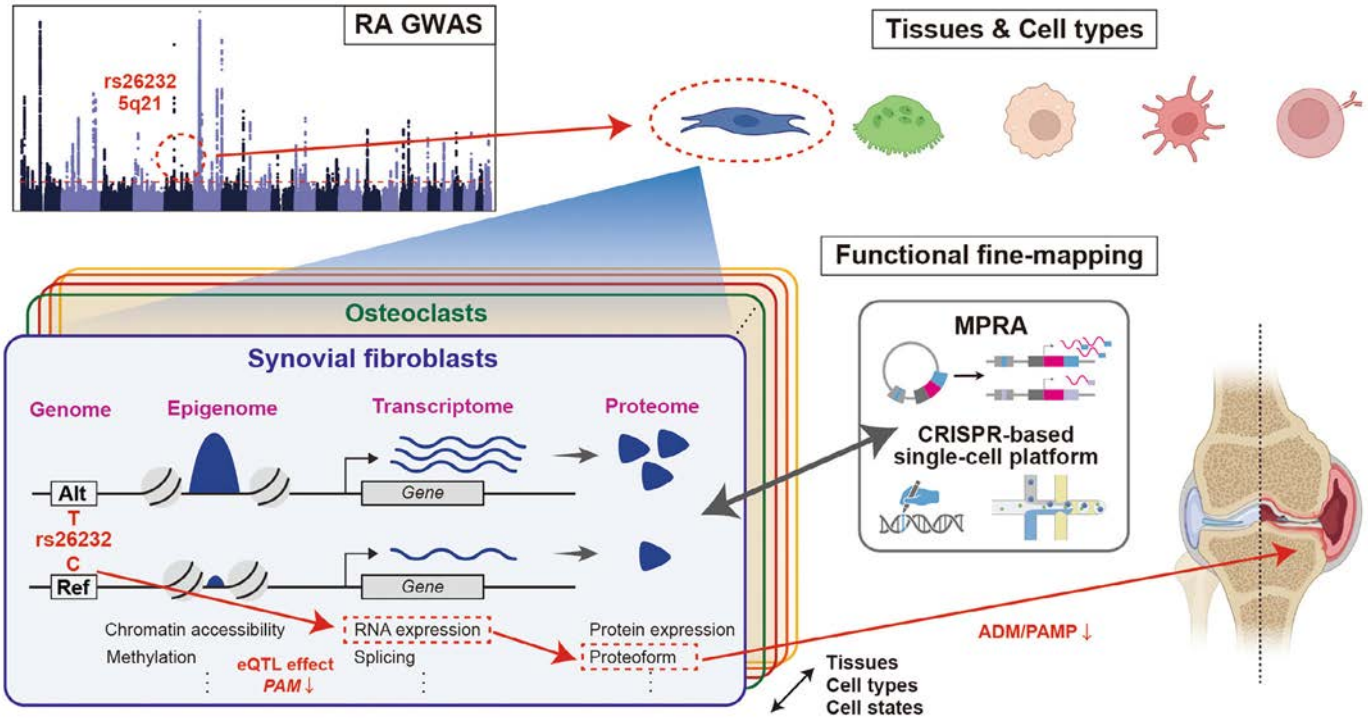

Figure 1. A conceptual framework for resolving genetic risk across tissues, cell types, and molecular layers. The schematic diagram outlines a general strategy for translating genome-wide association study (GWAS) signals into mechanistic and therapeutic insight by integrating tissue- and cell-type–specific molecular quantitative trait locus (QTL) mapping with multilayer molecular profiling and functional fine-mapping. In this framework, genetic variants are examined across epigenome, transcriptome, and proteome to identify regulatory effects and downstream biochemical consequences. The rs26232 locus on 5q21 is shown as an illustrative example, in which an expression QTL (eQTL) effect on *PAM* in synovial fibroblasts leads to diminished peptide amidation and subsequent tissue damage. Some graphical elements were created with BioRender.com. ADM, adrenomedullin; Alt, alternative allele; MPRA, massively parallel reporter assay; PAMP, pro-ADM N-terminal peptide; RA, rheumatoid arthritis; Ref, reference allele.

scale of available blood-based mol-QTL resources. Sheridan et al demonstrate the eQTL effect of rs26232-C on *PAM* expression in RASFs, wherein expression levels are markedly higher than in endothelial or immune cells within RA synovial tissue.[12] Although GTEx data indicate that rs26232 exhibits eQTL effects across multiple tissues, its relevance to RA pathogenesis appears most pronounced within synovial fibroblasts. This observation highlights the need for expanded mol-QTL resources within disease-associated tissues, particularly the synovium for RA. Integrative post-GWAS analyses leveraging mol-QTL data sets across diverse tissues and cell types will be essential to refine causal inference and resolve context-dependent genetic mechanisms.[7–9] In RA, in which synovial fibroblasts actively shape inflammatory amplification, extracellular matrix remodeling, and joint destruction, resolving genetic effects within the stromal compartment provides a more complete view of pathogenic circuitry without diminishing the central role of immune processes.

Defining the relevant cellular context is an essential first step toward understanding how genetic variation contributes to disease. Although mol-QTL mapping clarifies where genetic risk manifests, it does not necessarily explain how regulatory effects are translated into pathogenic mechanisms. Such mechanistic resolution may require interrogation beyond steady state RNA and total protein abundance. Although eQTL and pQTL frameworks have greatly advanced post-GWAS gene prioritization, they primarily capture quantitative variation and do not inherently establish its functional biochemical consequences.

Sheridan et al make this distinction clear by mapping rs26232 from its eQTL effect to downstream enzymatic function, directly linking quantitative variation to biochemical consequence.[4] Although rs26232 acts as an eQTL for *PAM* in synovial fibroblasts, the pathogenic mechanism does not reside solely in altered expression levels. *PAM* encodes an enzyme responsible for C-terminal peptide amidation, a posttranslational modification critical for the stability and bioactivity of multiple signaling peptides. Genetically determined reduction in *PAM* expression leads to diminished peptide amidation, altering the maturation and functional potency of downstream mediators. Thus, although the variant exerts its primary genetic effect through reduced *PAM* expression, the pathogenic consequence of this eQTL effect ultimately manifests at the level of enzymatic activity and peptide maturation. Capturing such effects requires molecular measurement technologies that extend beyond conventional transcript- and protein-level quantification. In the present study,

complementary mass spectrometry analyses directly resolved peptide amidation status, providing biochemical evidence consistent with reduced *PAM* enzymatic activity.

The findings by Sheridan et al highlight an important limitation of the conventional analytical pipeline for genomics-driven drug discovery. Recent integrative frameworks leveraging pQTL and transcriptome-wide association studies (TWASs) derived from eQTL have provided powerful strategies for prioritizing candidate genes at GWAS loci.[1,13] However, genes nominated through eQTL or TWAS do not necessarily represent the most effective therapeutic targets. Rather, the actionable points of intervention may reside within downstream pathways or molecular processes shaped by their regulatory effects. In parallel with the expansion of eQTL resources, pQTL catalogs have grown rapidly. However, most large-scale pQTL studies rely on affinity-based platforms that quantify total protein levels.[10,11] Although these platforms have enabled scalable, population-level quantification of protein abundance, such approaches are generally not designed to resolve distinct biochemical states of proteins or peptides, including posttranslational modification, proteolytic processing, or activation status. Consequently, regulatory layers operating at the level of protein function rather than abundance may remain obscured within conventional pQTL frameworks. Incorporating molecular measurement strategies capable of resolving functional molecular states may therefore provide additional mechanistic insight in contexts in which disease risk is mediated through altered protein or peptide activity rather than changes in total abundance. Affinity-based platforms may be susceptible to binding effects from coding variants that alter epitope or aptamer recognition, warranting careful interpretation of pQTL signals and potentially complicating fine-mapping efforts because apparent abundance differences may reflect altered binding rather than true protein levels.[11]

Although this study focuses on a single RA-associated locus,[4] its mechanistic depth yields broader insights for the interpretation of genetic risk in complex disease. First, genetic effects relevant to disease may reside within nonimmune stromal compartments rather than immune cells alone. Second, eQTL effects at GWAS loci may manifest at posttranscriptional and biochemical levels that are not readily captured by conventional mol-QTL frameworks. Finally, genes nominated through eQTL-based prioritization may not themselves represent optimal therapeutic targets; instead, actionable intervention points may reside within downstream pathways shaped by their regulatory effects.

Taken together, these observations illustrate how deeply resolving a single GWAS signal can refine our understanding of disease architecture and therapeutic opportunity. The detailed functional analyses in this study position synovial fibroblasts as causal nodes within inflammatory circuits, with surrounding immune phenotypes shaped by genetically perturbed stromal programs.[4] This finding suggests that, in some cases, immune activation may represent a downstream consequence of genetically encoded tissue-resident mechanisms. This reframing of immune activation has therapeutic implications. Although immune suppression remains central to RA management, deeper genomic resolution raises the possibility that targeting genetically defined stromal or downstream molecular pathways may complement existing strategies. In this way, functional interpretation of GWAS signals may expand the spectrum of therapeutic hypotheses beyond conventional immune-centric approaches.

As RA GWASs continue to expand in scale and diversity, a subset of identified loci may harbor similarly multilayered genetic mechanisms. The detailed functional dissection of the rs26232 locus serves as a paradigm for rigorous functional dissection, illustrating that resolving causal mechanisms may, in some cases, require regulatory and biochemical depth. Human genetic evidence has been associated with an increased probability of therapeutic success,[14] underscoring the translational value of robust genetic evidence. Yet, the impact of expanding GWAS data sets will depend not only on the number of variants discovered but on the depth at which their functional consequences are resolved. Fully leveraging these insights will require the expansion and integration of mol-QTL resources across tissues, cell types, and molecular layers, enabling more precise dissection of disease-relevant mechanisms. Beyond mol-QTL mapping, perturbation-based functional fine-mapping will be essential to experimentally validate candidate variants and establish causality, particularly for noncoding GWAS signals. Approaches such as massively parallel reporter assays[11] and CRISPR-based multimodal single-cell platforms like CRISPR by ADT, flow cytometry and transcriptome sequencing (CRAFTseq)[15] enable direct testing of regulatory variants and linkage of edited alleles to downstream molecular phenotypes. Together, the integration of expanded mol-QTL resources with experimental fine-mapping strategies holds the potential to substantially accelerate genomics-driven drug discovery. No data were used in this article.

AUTHOR CONTRIBUTIONS

Both authors contributed to at least one of the following manuscript preparation roles: conceptualization AND/OR methodology, software, investigation, formal analysis, data curation, visualization, and validation AND drafting or reviewing/editing the final draft. As corresponding authors, Drs Edahiro and Okada confirm that they both have provided the final approval of the version to be published, and take responsibility for the affirmations regarding article submission (eg, not under consideration by another journal), the integrity of the data presented, and the statements regarding compliance with institutional review board/Declaration of Helsinki requirements. Both authors contributed to the investigation, formal analysis of the data, and writing, reviewing, and editing of the manuscript.

REFERENCES

1. Okada Y, Wu D, Trynka G, et al; RACI consortium; GARNET consortium. Genetics of rheumatoid arthritis contributes to biology and drug discovery. Nature 2014;506(7488):376–381. doi:https://doi.org/10.1038/nature12873

2. Okada Y, Eyre S, Suzuki A, et al. Genetics of rheumatoid arthritis: 2018 status. Ann Rheum Dis 2019;78(4):446–453. doi:https://doi.org/10.1136/annrheumdis-2018-213678
3. Ishigaki K, Sakaue S, Terao C, et al; BioBank Japan Project. Multi-ancestry genome-wide association analyses identify novel genetic mechanisms in rheumatoid arthritis. Nat Genet 2022;54(11):1640–1651. doi:https://doi.org/10.1038/s41588-022-01213-w
4. Sheridan KJ, Dorris ER, Pimenta MI, et al. Tissue damage in rheumatoid arthritis is genetically linked to low peptidylglycine alpha-amidating monooxygenase activity in synovial fibroblasts. Arthritis Rheumatol 2026;78(9):1837–1849. doi:https://doi.org/10.1002/art.70123
5. Farh KKH, Marson A, Zhu J, et al. Genetic and epigenetic fine mapping of causal autoimmune disease variants. Nature 2015;518(7539):337–343. doi:https://doi.org/10.1038/nature13835
6. Aguet F, Alasoo K, Li YI, et al. Molecular quantitative trait loci. Nat Rev Methods Primers 2023;3:4. doi:https://doi.org/10.1038/s43586-023-00196-0
7. Aguet F, Anand S, Ardlie KG, et al; GTEx Consortium. The GTEx Consortium atlas of genetic regulatory effects across human tissues. Science 2020;369(6509):1318–1330. doi:https://doi.org/10.1126/science.aaz1776
8. Edahiro R, Sato G, Naito T, et al; Japan COVID-19 Task Force. Deciphering state-dependent immune features from multi-layer omics data at single-cell resolution. Nat Genet 2025;57(8):1905–1921. doi:https://doi.org/10.1038/s41588-025-02266-3
9. Perez RK, Gordon MG, Subramaniam M, et al. Single-cell RNA-seq reveals cell type-specific molecular and genetic associations to lupus. Science. 2022;376(6589):eabf1970. doi:10.1126/science.abf1970 Erratum in: *Science* 2024;385:eadr4064.
10. Sun BB, Chiou J, Traylor M, et al; Alnylam Human Genetics; AstraZeneca Genomics Initiative; Biogen Biobank Team; Bristol Myers Squibb; Genentech Human Genetics; GlaxoSmithKline Genomic Sciences; Pfizer Integrative Biology; Population Analytics of Janssen Data Sciences; Regeneron Genetics Center. Plasma proteomic associations with genetics and health in the UK Biobank. Nature 2023;622(7982):329–338. doi:https://doi.org/10.1038/s41586-023-06592-6
11. Wang QS, Hasegawa T, Namkoong H, et al; Japan COVID-19 Task Force. Statistically and functionally fine-mapped blood eQTLs and pQTLs from 1,405 humans reveal distinct regulation patterns and disease relevance. Nat Genet 2024;56(10):2054–2067. doi:10.1038/s41588-024-01896-3 Erratum in: *Nat Genet* 2024;56:2281.
12. Zhang F, Jonsson AH, Nathan A, et al; Accelerating Medicines Partnership: RA/SLE Network. Deconstruction of rheumatoid arthritis synovium defines inflammatory subtypes. Nature 2023;623(7987):616–624. doi:https://doi.org/10.1038/s41586-023-06708-y
13. Namba S, Konuma T, Wu KH, et al; Global Biobank Meta-analysis Initiative. A practical guideline of genomics-driven drug discovery in the era of global biobank meta-analysis. Cell Genom 2022;2(10):100190. doi:https://doi.org/10.1016/j.xgen.2022.100190
14. Ochoa D, Karim M, Ghoussaini M, et al. Human genetics evidence supports two-thirds of the 2021 FDA-approved drugs. Nat Rev Drug Discov 2022;21(8):551. doi:https://doi.org/10.1038/d41573-022-00120-3
15. Baglaenko Y, Mu Z, Curtis M, et al. Precisely defining disease variant effects in CRISPR-edited single cells. Nature 2025;646(8083):117–125. doi:https://doi.org/10.1038/s41586-025-09313-3

Arthritis & Rheumatology
Vol. 78, No. 9, September 2026, pp 1823–1825
DOI 10.1002/art.70065
© 2026 The Author(s). *Arthritis & Rheumatology* published by Wiley Periodicals LLC on behalf of American College of Rheumatology.
This is an open access article under the terms of the Creative Commons Attribution License, which permits use, distribution and reproduction in any medium, provided the original work is properly cited.

AMERICAN COLLEGE of RHEUMATOLOGY
Empowering Rheumatology Professionals

NOTES FROM THE FIELD

When Blood Proteins Reveal What Transcripts Miss: Immune Cell Priming and the Road to Prognostic Biomarkers in Lupus

Ioannis Parodis, MD, PhD

Introduction

Systemic lupus erythematosus (SLE) remains a disease in which we can often describe immune dysregulation with impressive molecular detail yet still struggle to predict what matters most to patients and clinicians, ie, who will accrue irreversible organ damage and when.[1] Whole-blood transcriptomic profiling has long provided a detailed and structured view of immune dysregulation in SLE, including modular frameworks for interpreting blood genomic data.[2] In this issue of *Arthritis & Rheumatology*, Smith and colleagues report an integrated multi-omic analysis in SLE that argues convincingly that serum proteomics may have the ability to illuminate clinically meaningful biology not captured by whole-blood transcriptomics alone.[3]

Summary of the article

Using a clinically well-annotated National Institutes of Health (NIH) cohort of 87 patients with predominantly mild-to-moderate SLE and 48 healthy controls, the authors integrated high-throughput aptamer-based serum proteomics supported by orthogonal antibody-based measurements, transcriptomics, immunophenotyping, and autoantibody profiling to identify patterns linked to disease activity and, importantly, long-term damage accrual. Three protein signatures emerged from correlation structure and factor-based scoring: (1) the interferon-associated inflammation (IAI) signature, reflecting canonical interferon-driven biology and correlating with established interferon gene signatures (IFNGS); (2) the granulocyte-related (GRN) signature, capturing granulocyte activation across multiple granulocyte subsets; and (3) the immune cell priming (ICP) signature, a more unexpected constellation, enriched for molecules suggestive of enhanced costimulatory and cytokine-mediated crosstalk between antigen-presenting cells and effector lymphocytes, alongside markers of tissue injury, including kidney injury molecule 1[4] and cystatin C, and immune-related proteins such as β_2-microglobulin, CD40, inducible T cell 27 costimulator, interleukin 12 subunit 40, and matrix metalloproteinase 7.

Using a threshold of two SDs above the healthy control mean, almost all patients were positive for at least one protein signature, highlighting that under this operational definition, signature positivity was common in the cohort. These signatures, their key clinical associations, and the key validation steps required for translation are summarized in Table 1.

Two observations are particularly noteworthy. First, although multiple platforms detected associations with interferon activity and anti–double-stranded DNA autoantibodies, whole-blood transcriptomic alterations were not associated with organ-specific activity measures, consistent with observations in a European SLE cohort,[5] whereas proteins and other modalities were, most strongly with reduced glomerular filtration rate. Second, and strikingly, the ICP signature was associated with kidney involvement and with subsequent organ damage progression over approximately six years, adding prognostic information beyond conventional markers in the authors' models. Notably, disease activity and damage indices increased with the number of protein signatures present, suggesting that cumulative "signature burden" may capture a broader immune perturbation state rather than a single pathway in isolation. The authors also report validation in an independent NIH cohort comprising 43 patients with mild-to-moderate SLE from 2016 to 2017, with matched controls, supporting reproducibility of signature loadings and showing consistent directionality for the prognostic association, albeit with limited power.

Dr Parodis's work was supported by grants from the Swedish Rheumatism Association (R-995882), King Gustaf V's 80-Year Foundation (FAI-2023-1055), the Swedish Society of Medicine (SLS-974449), Nyckelfonden (OLL-1000881), the Professor Nanna Svartz Foundation (2021-00436), the Ulla and Roland Gustafsson Foundation (2024-43), Region Stockholm (FoUI-1004114), and Karolinska Institutet.

[1]Division of Rheumatology, Department of Medicine, Solna and Center for Molecular Medicine, Karolinska Institutet and Karolinska University Hospital, Stockholm, Sweden; [2]Department of Rheumatology, Faculty of Medicine and Health, Örebro University, Örebro, Sweden.

Author disclosures are available at https://onlinelibrary.wiley.com/doi/10.1002/art.70065.

Address correspondence via email to Ioannis Parodis, MD, PhD, at ioannis.parodis@ki.se.

Submitted for publication December 27, 2025; accepted in revised form January 7, 2026.

Table 1. Interpreting serum protein signatures in SLE: biologic framing, clinical associations, and required validation steps*

Signature	Putative biology	Key associations	Required validation steps
IAI	IFN-associated inflammatory response	IFN biology; serologies; rash signal differences vs IFNGS	Added value over transcript-based IFNGS; response tracking with IFN-targeted therapy
GRN	Granulocyte activation across granulocyte subsets	Arthritis; pyuria; class IV LN; less confounding by some therapies	Relationship to NETosis/vascular injury; links to treatment response and flare prediction
ICP	ICP and tissue injury spill-over	Kidney involvement; risk of long-term damage accrual; limited blood gene/cell correlates	Prospective prognostic validation; paired blood and kidney tissue studies; deployable panel development

* GRN, granulocyte-related; IAI, interferon-associated inflammation; ICP, immune cell priming; IFN, interferon; IFNGS, interferon gene signature; LN, lupus nephritis; NETosis, neutrophil extracellular trap formation; SLE, systemic lupus erythematosus.

Critical appraisal

A central tension in lupus biomarker research is the gap between statistical association and actionable biologic insight. The ICP signal is compelling precisely because it is not mirrored by strong circulating gene-expression or cell-count correlates, raising the possibility that it reflects processes occurring outside peripheral blood, with "spill-over" into serum. The authors explore this by interrogating public kidney transcriptomic data sets, showing increased expression of several ICP-linked genes in glomerular and tubulointerstitial compartments in patients with lupus nephritis compared with controls, and they further link a dendritic-cell signature in kidney tissue to renal dysfunction across kidney diseases.

The mechanistic inference that ICP reflects intrarenal processes, or similar processes in other highly vascularized organs, and represents ICP within tissue is plausible but not proven. Bulk transcriptomic comparisons in archived data sets are a useful starting point, yet they cannot replace direct evidence from, for example, paired tissue and blood proteomics, spatial transcriptomics and proteomics, or functional studies.[6,7] Importantly, the study by Smith et al acknowledges the need for prospective validation and paired biopsies to establish clinical correlates and tissue relationships, which appropriately tempers overinterpretation.[3]

A second caution concerns effect size and event rates. Although the longitudinal association with damage accrual is clinically meaningful, the number of high-damage progression events is modest, and the validation cohort is small, limitations that are common and understandable in deep multi-omic studies but nonetheless constrain immediate clinical translation. The way forward is not to dismiss the signal but to stress test it in large and well-characterized multicenter cohorts, ideally ethnically diverse, which would also address generalizability.

Contextualization

The IAI signature mirrors interferon-driven biology and correlates strongly with established IFNGS. That concordance is reassuring, and the authors note an association with rash that may differ from transcript-based IFNGS performance in their data set.

Yet from a translational standpoint, the key question is what a protein-based interferon signature adds beyond transcript-based IFNGS in routine practice.[8] The more distinctive contribution of this article may therefore be less about relabeling interferon biology and more about demonstrating a general principle: proteins can capture clinically relevant biology, as well as potentially tissue-derived pathology, that is not readily captured by whole-blood transcriptomics.[9] Moreover, protein assays may be more readily translated into clinical workflows, provided that rigorous analytical validation and standardization steps are undertaken and clinically meaningful thresholds are established.

Similarly, the GRN signature usefully broadens what we mean by "neutrophil biology" in SLE by correlating with multiple granulocyte subsets and showing clinical associations with, for example, arthritis, pyuria, and class IV lupus nephritis, while appearing less confounded by certain standard therapies in this cohort. This is concordant with transcriptomic evidence of lupus nephritis–specific enrichment of neutrophil degranulation pathways when comparing active renal SLE with active nonrenal SLE in patients with no prior kidney involvement[10] and with converging urine proteomic and blood transcriptomic data sets, as well as cross-species transcriptomic analyses, that implicate neutrophil degranulation and neutrophil activation signatures in lupus nephritis.[11–13] Table 1 summarizes how these signatures might be viewed as candidate biologically informed risk states, alongside the key steps needed before clinical implementation.

Beyond signatures, a major contribution of the study is the interactive SLE Immune Atlas portal, designed to allow exploration of linked clinical and multi-omic readouts. Resources like this can accelerate the field if they (1) make cohort composition and metadata transparent, (2) support reproducible reanalysis, and (3) allow meaningful hypothesis generation across endotypes rather than only "signature look-up." The portal is therefore best viewed not as a clinical tool today but as a community substrate, ie, a reference data set that can be queried to help interpret future cohorts, support replication, and inform the design of prospective studies.

Implications

To move ICP and related signatures from discovery to practice, three steps would be particularly important: first, analytical

translation, which would entail moving from high-dimensional discovery platforms to a deployable assay, eg, a small targeted protein panel, with stable calibration and prespecified thresholds; second, clinical validation, ie, demonstration of incremental prognostic value over standard-of-care variables, such as disease duration, baseline organ damage, proteinuria, kidney function, serologies, and treatment exposure, in larger cohorts; and third, biologic anchoring, which would connect the serum signal to tissue pathology and actionable mechanisms, especially in lupus nephritis. This would require paired sampling and spatially resolved technologies, enabling biomarkers to be related to intrarenal activity or chronicity features and response trajectories.

If successful, such an approach could shift prognostication in SLE away from single markers and toward biologically informed risk states, eg, interferon-driven inflammation, granulocyte activation, and tissue-linked immune priming and injury. Even if individual signatures are imperfect, their combinations may reflect the disease heterogeneity and guide enrichment strategies for clinical trials.[14,15]

Conclusions

Smith and colleagues provide a timely reminder that in SLE, where disease occurs matters as much as what we measure in blood. Their work supports the view that serum proteomics can capture a dimension of lupus biology, potentially tissue-linked immune priming and injury, that is not faithfully represented by whole-blood transcriptomics.

The ICP signature is best interpreted as a promising, hypothesis-generating prognostic signal that merits careful prospective validation and deeper tissue anchoring before it can be considered clinically actionable. Done well, that next phase could bring us closer to risk-stratified, mechanism-informed monitoring, an outcome that people living with SLE have waited a long time to see.

AUTHOR CONTRIBUTIONS

Dr Parodis contributed to at least one of the following manuscript preparation roles: conceptualization AND/OR methodology, software, investigation, formal analysis, data curation, visualization, and validation AND drafting or reviewing/editing the final draft. As corresponding author, Dr Parodis confirms that he has provided the final approval of the version to be published and takes responsibility for the affirmations regarding article submission (eg, not under consideration by another journal), the integrity of the data presented, and the statements regarding compliance with institutional review board/Declaration of Helsinki requirements.

REFERENCES

1. Bruce IN, O'Keeffe AG, Farewell V, et al. Factors associated with damage accrual in patients with systemic lupus erythematosus: results from the Systemic Lupus International Collaborating Clinics (SLICC) inception cohort. Ann Rheum Dis 2015;74(9):1706–1713. doi:10.1136/annrheumdis-2013-205171
2. Chaussabel D, Quinn C, Shen J, et al. A modular analysis framework for blood genomics studies: application to systemic lupus erythematosus. Immunity 2008;29(1):150–164. doi:10.1016/j.immuni.2008.05.012
3. Smith MA, Sinibaldi D, Rahman S, et al. Multi-omic profiling reveals immune cell priming signature linked to lupus prognosis. Arthritis Rheumatol 2026;78(9):1878–1891. doi:10.1002/art.70105
4. Han WK, Bailly V, Abichandani R, et al. Kidney injury molecule-1 (KIM-1): a novel biomarker for human renal proximal tubule injury. Kidney Int 2002;62(1):237–244. doi:10.1046/j.1523-1755.2002.00433.x
5. Lindblom J, Toro-Domínguez D, Carnero-Montoro E, et al; PRECISESADS Clinical Consortium. Distinct gene dysregulation patterns herald precision medicine potentiality in systemic lupus erythematosus. J Autoimmun 2023;136:103025. doi:10.1016/j.jaut.2023.103025
6. Arazi A, Rao DA, Berthier CC, et al; Accelerating Medicines Partnership in SLE network. The immune cell landscape in kidneys of patients with lupus nephritis. Nat Immunol 2019;20(7):902–914. doi:10.1038/s41590-019-0398-x
7. Louis Sam Titus ASC, Tan Y, Tran P, et al. Molecular architecture of proliferative lupus nephritis as elucidated using 50-plex imaging mass cytometry proteomics. Clin Immunol 2023;254:109713. doi:10.1016/j.clim.2023.109713
8. Kennedy WP, Maciuca R, Wolslegel K, et al. Association of the interferon signature metric with serological disease manifestations but not global activity scores in multiple cohorts of patients with SLE. Lupus Sci Med 2015;2(1):e000080. doi:10.1136/lupus-2014-000080
9. Vogel C, Marcotte EM. Insights into the regulation of protein abundance from proteomic and transcriptomic analyses. Nat Rev Genet 2012;13(4):227–232. doi:10.1038/nrg3185
10. Parodis I, Lindblom J, Toro-Domínguez D, et al; PRECISESADS Clinical Consortium. Interferon and B-cell signatures inform precision medicine in lupus nephritis. Kidney Int Rep 2024;9(6):1817–1835. doi:10.1016/j.ekir.2024.03.014
11. Fava A, Buyon J, Magder L, et al; Accelerating Medicines Partnership in RA/SLE network. Urine proteomic signatures of histological class, activity, chronicity, and treatment response in lupus nephritis. JCI Insight 2024;9(2):e172569. doi:10.1172/jci.insight.172569
12. Jourde-Chiche N, Whalen E, Gondouin B, et al. Modular transcriptional repertoire analyses identify a blood neutrophil signature as a candidate biomarker for lupus nephritis. Rheumatology (Oxford) 2017;56(3):477–487. doi:10.1093/rheumatology/kew439
13. Frangou E, Garantziotis P, Grigoriou M, et al. Cross-species transcriptome analysis for early detection and specific therapeutic targeting of human lupus nephritis. Ann Rheum Dis 2022;81(10):1409–1419. doi:10.1136/annrheumdis-2021-222069
14. Parodis I. Molecular signature-based decision making in the era of targeted therapies for systemic lupus erythematosus. Lancet Rheumatol 2023;5(1):e4–e6. doi:10.1016/S2665-9913(22)00358-7
15. Banchereau R, Hong S, Cantarel B, et al. Personalized immunomonitoring uncovers molecular networks that stratify lupus patients. Cell 2016;165(3):551–565. doi:10.1016/j.cell.2016.03.008

American College of Rheumatology
Empowering Rheumatology Professionals

Arthritis & Rheumatology
Vol. 78, No. 9, September 2026, pp 1826–1836
DOI 10.1002/art.70106
© 2026 American College of Rheumatology

Baseline Interleukin-10 Levels as a Predictive Biomarker for Achieving Clinical Response With Abatacept in Patients Who Were Disease-Modifying Antirheumatic Drug Naive and Anti–Citrullinated Protein Antibody Positive With Early Rheumatoid Arthritis

Jinqi Liu, PhD,[1] Yicong Li, PhD,[2] Kai Fu, PhD,[1] Chun Wu, PhD,[1] Peter Schafer, PhD,[1] Sean E. Connolly, PhD,[1] Ian M. Catlett, PhD,[1] Michael A. Maldonado, MD,[1] Robert Wong, MD,[1] Paul Emery, FMedSci,[3] Yoshiya Tanaka, MD,[4] Vivian P. Bykerk, MD,[5] Clifton O. Bingham, MD,[6] Thomas W. J. Huizinga, MD, PhD,[7] and Roy Fleischmann, MD[8]

Objective. Predictive biomarkers for patients with early rheumatoid arthritis (RA) are needed. This exploratory post hoc analysis investigated inflammatory biomarkers associated with baseline disease activity and biomarkers predictive of treatment response in patients who were seropositive with early RA from a phase 3 study.

Methods. The AVERT-2 study (NCT02504268) included patients who were disease-modifying antirheumatic drug naive and anti–citrullinated protein antibody positive randomized to abatacept and methotrexate (MTX) or placebo and MTX for 56 weeks. Correlations were assessed among biomarkers and disease activity, pharmacodynamic (PD) changes on disease-associated biomarkers in response to treatment, and baseline biomarkers to predict treatment response at week 52.

Results. In the analysis, 446 patients received abatacept and MTX and 300 received placebo and MTX. Of 103 biomarkers, 47 demonstrated a significant reduction in PD changes with abatacept and MTX versus placebo and MTX, with 18 out of 47 biomarkers showing correlations with baseline disease activity. High baseline interleukin-10 (IL-10) levels were associated with greater probability of achieving efficacy measures by week 52 in patients receiving abatacept and MTX versus placebo and MTX, consistent with a significant reduction in disease activity with abatacept and MTX ($P < 0.03$ to $P < 0.0007$). Higher baseline IL-10 levels were associated with lower bone erosive development with abatacept and MTX compared with placebo and MTX.

Conclusion. Treatment with abatacept and MTX resulted in significantly greater reduction of biomarkers relevant to RA, and high baseline IL-10 levels predicted better treatment response with abatacept and MTX versus placebo and MTX across clinical outcomes. Findings suggest a well-suited mechanism of action for abatacept and MTX in patients with early RA and high baseline IL-10 levels.

INTRODUCTION

Rheumatoid arthritis (RA) is a systemic autoimmune disease characterized by the production of both pathogenic autoantibodies and proinflammatory cytokines, causing systemic inflammation and leading to the resorption of cartilage and bone, the development of bone erosions, and long-term destruction of synovial joints.[1–4] RA affects approximately 0.5% to 1% of the

ClinicalTrials.gov identifier: NCT02504268.

Data were previously presented at the American College of Rheumatology Convergence, November 10–15, 2023, in San Diego, California (oral presentation 2539), and at the European Alliance of Association for Rheumatology, June 12–15, 2024, in Vienna, Austria (poster 0611). Permission for reuse was obtained.

Supported by Bristol Myers Squibb.

[1]Bristol Myers Squibb, Princeton, New Jersey; [2]Parexel International, Durham, North Carolina; [3]Leeds Institute of Rheumatic and Musculoskeletal Medicine, University of Leeds and Leeds NIHR Biomedical Research Centre, Leeds, United Kingdom; [4]First Department of Internal Medicine, University of Occupational and Environmental Health, Kitakyushu, Japan; [5]Department of Rheumatology, Hospital for Special Surgery, New York, New York; [6]Division of Rheumatology, Department of Medicine, Johns Hopkins University, Baltimore, Maryland; [7]Department of Rheumatology, Leiden University Medical Center, Leiden, the Netherlands; [8]Division of Rheumatology, University of Texas Southwestern Medical Center, Metroplex Clinical Research Center, Dallas.

Additional supplementary information cited in this article can be found online in the Supporting Information section (https://acrjournals.onlinelibrary.wiley.com/doi/10.1002/art.70106).

global population,[5] and patients with anti–citrullinated protein antibody (ACPA)-positive RA have a poorer prognosis because they are more likely to develop severe erosive disease than patients with ACPA-negative disease.[6,7] Treatment guidelines from both the American College of Rheumatology (ACR) and EULAR recommend a treat-to-target approach for RA management, using biologic and targeted synthetic disease-modifying antirheumatic drugs (DMARDs) when conventional synthetic DMARDs fail to achieve the treat-to-target goal within three to six months.[8,9]

Segmentation of populations with RA based on patients' responses to different interventions is not yet possible,[10] and predicting response to treatment has been one of the main challenges in RA management. Further investigation is needed to understand the interaction between distinct immune pathways and disease progression in patients with RA.[2] Currently, immune-based therapeutics are used across the stages of RA without considering the dominant immune pathotypes at a given disease stage. Investigating and identifying clinically applicable peripheral blood biomarkers associated with disease-relevant immune pathotypes could support individualized treatment options, enabling patients to achieve optimal clinical outcomes. The identification of potential predictive biomarkers for RA in response to a given therapy is challenging because RA is a heterogeneous disease in terms of its clinical characteristics and pathologic processes. Multiple therapeutic agents are available with distinct mechanisms of action that have the potential to be linked to the pathobiology and response to treatment of individual patients, suggesting that clinical remission is an achievable goal for patients.[11] However, a significant unmet need in RA is for clinically meaningful predictive biomarkers of treatment response to aid in clinical decision-making for appropriate individualized targeted therapies.

Abatacept, a selective T cell costimulation modulator, effectively treats patients with RA, including those with very early RA.[12,13] Identifying a window of therapeutic opportunity is needed to improve long-term outcomes for patients with early RA.[14,15] The phase 3b AVERT-2 study (NCT02504268) evaluated the efficacy of subcutaneous (SC) abatacept and methotrexate (MTX) versus placebo and MTX in treating patients who were MTX naive with early, active, seropositive RA. Although the primary study endpoint, Simplified Disease Activity Index (SDAI) remission (≤3.3) at week 24, did not meet statistical significance, more patients achieved SDAI remission with abatacept and MTX than placebo and MTX at week 52.[16] Moreover, abatacept and MTX resulted in a significantly higher proportion of radiographic nonprogressors at week 52.[16] In addition, an analysis of AVERT-2 data suggested that cross-linked carboxy-terminal telopeptide of type I collagen, a biomarker reflecting active bone remodeling, was a predictor of treatment response with abatacept and MTX versus placebo and MTX.[17] This exploratory post hoc analysis used data from the AVERT-2 study to identify a wide range of inflammatory serum biomarkers for prediction of treatment response by assessing the correlations between baseline serum biomarker levels and disease activity while also exploring the utility in predicting clinical response in patients with early RA treated with abatacept and MTX or placebo and MTX.

METHODS

Study design. The AVERT-2 study (NCT02504268) was a phase 3b, 132-week study of patients with active, early RA who were ACPA positive. This two-part study consisted of a 56-week, double-blind, randomized, placebo-controlled induction period followed by a 48-week treatment de-escalation period. Full details of the study design have been reported previously.[16,18] At the start of the induction period, patients were randomized (3:2) to weekly 125 mg SC abatacept and MTX (starting dose 7.5–15 mg/wk titrated to ≥15 mg within eight weeks) or placebo and MTX for 56 weeks. The primary endpoint was the proportion of patients in SDAI remission (≤3.3) at week 24 of the induction period. Other efficacy endpoints included the proportions of patients in SDAI remission at week 52, with Disease Activity Score in 28 joints (DAS28) using C-reactive protein (CRP) <2.6, in Boolean remission, or who achieved 20% improvement in ACR criteria response (ACR20)/ACR50/ACR70 at weeks 24 and 52.[19] Race and ethnicity were self-reported from a fixed set of categories.

Patient population. The AVERT-2 study included adult patients (aged ≥18 years) with RA (defined by ACR/EULAR 2010 criteria) of six months or fewer in duration who were ACPA positive and DMARD naive.[8,9,20] Eligible patients had SDAI scores >11, ≥3 tender joints and ≥3 swollen joints, and high-sensitivity CRP >3 mg/L or erythrocyte sedimentation rate ≥28 mm/hr at baseline. Cohort 1 (the intent-to-treat [ITT] population) included all randomized patients who received at least one dose of the study drug during the 56-week induction period.[16] This study was an exploratory post hoc analysis that included a subgroup of patients from cohort 1 with available serum samples for biomarker analysis. Of the 752 patients in cohort 1, a total of 446 from the arm that received abatacept and MTX and 300 from the arm that received placebo and MTX were included in the biomarker analyses. The AVERT-2 study was conducted in accordance with the Declaration of Helsinki and the International Conference on Harmonisation Guidelines for Good Clinical Practice. The protocol and patient-informed consent received institutional review board

Author disclosures are available at https://onlinelibrary.wiley.com/doi/10.1002/art.70106.

Address correspondence via email to Jinqi Liu, PhD, at jinqi.liu@bms.com.

Submitted for publication May 30, 2025; accepted in revised form December 15, 2025.

(IRB)/independent ethics committee approval before study initiation. The study was governed by both a central IRB (New England IRB) and local and university-based IRBs if required at individual sites. All patients provided written informed consent before enrollment.

Collection of serum samples. Patient blood samples were collected in standard serum separation tubes and prepared into aliquots. Serum samples were stored at ≤−70°C and shipped frozen on dry ice to the vendors Olink and Rules-Based Medicine (RBM) for biomarker assessment.

Assessment of serum biomarkers, bone erosion, and disease activity. A total of 103 inflammatory and immune response-related proteins from Olink Target 96 multiplex immunoassay inflammation panel and selected panels from RBM were analyzed, with three proteins overlapping across the two panels (Supplementary Table 1), to study their correlation with baseline disease activity, pharmacodynamic (PD) changes over treatment course, and their value for predicting achievement of ACR response and SDAI remission by week 52. Biomarkers were selected based on their role in mediating inflammation relevant in RA disease and were tested for suitability as predictive biomarkers based on baseline levels using the following formula:

$$E(Y|Trt, BM) = \beta_0 + \beta_{Trt} Trt + \boldsymbol{\beta_{BM} BM} + \beta_{IX} Trt \times BM + \beta_{cov} Covariates$$

When $\beta_{IX} \neq 0$, the marker is predictive. Baseline disease activity measures assessed were SDAI (key clinical outcome), DAS28 (CRP), and Health Assessment Questionnaire Disability Index (HAQ-DI). Bone erosion was assessed by mean change in erosion score via x-ray and modified total Sharp score and was analyzed by baseline interleukin-10 (IL-10; cutoff: median value of 4.26 normalized protein expression [NPX]) levels in patients who were treated with abatacept and MTX or placebo and MTX. Disease activity over the treatment course was stratified by baseline IL-10 level tertiles, categorized as low (3.20–4.04 NPX), intermediate (4.05–4.54 NPX), or high (4.55–12.66 NPX).

Statistical analysis. Spearman's *rho* was employed to assess correlations between biomarkers and disease activity measures at baseline and posttreatment visits. Logistic regression was used to estimate predictive values of baseline biomarkers on clinical efficacy, with adjustments made for baseline demographics and disease activities, including age, SDAI, pain (measured via Visual Analog Scale), and ACPA positivity. A linear mixed-effects model was used to examine PD changes in biomarker levels over time in response to treatment. The treatment difference in adjusted mean change from baseline (least squares mean, converted to percent change from baseline) between abatacept and MTX versus placebo and MTX at posttreatment time points, along with corresponding 95% confidence interval and *P* values, were reported. Data are available on request from the authors. Bristol Myers Squibb policy on data sharing may be found at https://www.bms.com/researchers-and-partners/independent-research/data-sharing-request-process.html.

RESULTS

Patients. Cohort 1 (ITT population) in the AVERT-2 study included 752 patients who were randomized to receive abatacept and MTX (n = 451) or placebo and MTX (n = 301; Supplementary Figure 1).[16] Serum samples were available from 446 patients treated with abatacept and MTX and 300 treated with placebo and MTX for biomarker studies and included in the present analysis (Table 1). Demographics and baseline characteristics were similar between the overall ITT population and the biomarker subgroup and across treatment arms in these two populations (Table 1; Supplementary Table 2). There were no significant differences between treatment arms in baseline levels of all tested biomarkers (Supplementary Table 2).

Correlation between serum biomarkers and disease activity at baseline. Inflammatory biomarkers (n = 103) were tested for their correlation with baseline disease activity measures, including SDAI, DAS28 (CRP), and HAQ-DI. Of these, 18 biomarkers, including IL-6, methyl-accepting chemotaxis protein–3 (MCP-3), IL-2RA, CXCL13, S100A12, matrix metalloproteinase 3 (MMP3), signaling lymphocytic activation molecule family 1 (SLAMF1), IL-10, CXCL10, MMP1, tumor necrosis factor α (TNFα), CXCL9, LAP TGFβ, CCL19, IL-15RA, PD-L1, CCL23, and TNF receptor subfamily 9 (TNFRSF9), had correlation with significant *P* values ($P \leq 0.05$; Figure 1A). Further analyses were conducted to investigate the correlation between change from baseline of these biomarkers and change from baseline of disease activity by weeks 24 and 52 after treatment with abatacept and MTX or placebo and MTX. The same 18 biomarkers that had a reduction from baseline were associated with a decrease from baseline in disease activity, independent of treatment (Supplementary Figure 2).

PD changes in biomarkers after treatment. PD changes in all 103 biomarkers were assessed during the induction period. Of these, 47 biomarkers demonstrated significant reduction with abatacept and MTX than placebo and MTX. The most prominent 21 biomarkers are shown in Figure 1B (9 biomarkers) and Supplementary Figure 3 (12 biomarkers), consistent with the observed superior and sustained clinical outcome observed with abatacept and MTX versus placebo and MTX.[16,18]

Prediction of treatment response by baseline IL-10 levels. A total of 47 proteins showed significant PD changes, including 18 biomarkers associated with disease activity, that were further analyzed for prediction of differential treatment

Table 1. Baseline demographics and disease characteristics*

Characteristic	Abatacept and MTX (n = 446)	Placebo and MTX (n = 300)	*P* value
Age, y	49 (±13)	49 (±14)	0.64
Female, n (%)	346 (78)	242 (81)	0.36
Race, n (%)			
White	313 (70)	208 (69)	0.31
Japanese	62 (14)	41 (14)	–
Other	38 (9)	22 (7)	–
Black/African American	18 (4)	15 (5)	–
Asian other	10 (2)	6 (2)	–
Chinese	3 (1)	5 (2)	–
Asian Indian	2 (0.5)	0	–
American Indian/Alaska Native	0	3 (1)	–
Disease duration, mo	1.2 (±1.4)	1.2 (±1.4)	0.68
SDAI	38 (±14)	39 (±14)	0.20
ACPA level, U/mL	827 (±1,400)	778 (±1,500)	0.39
Tender joint count (68 joints)	21 (±13)	22 (±13)	0.42
HAQ-DI	1.6 (±1)	1.6 (±1)	0.84

* Values given are mean (±SD) unless otherwise stated. ACPA, anti–citrullinated protein antibody; HAQ-DI, Health Assessment Questionnaire Disability Index; MTX, methotrexate; SDAI, Simplified Disease Activity Index.

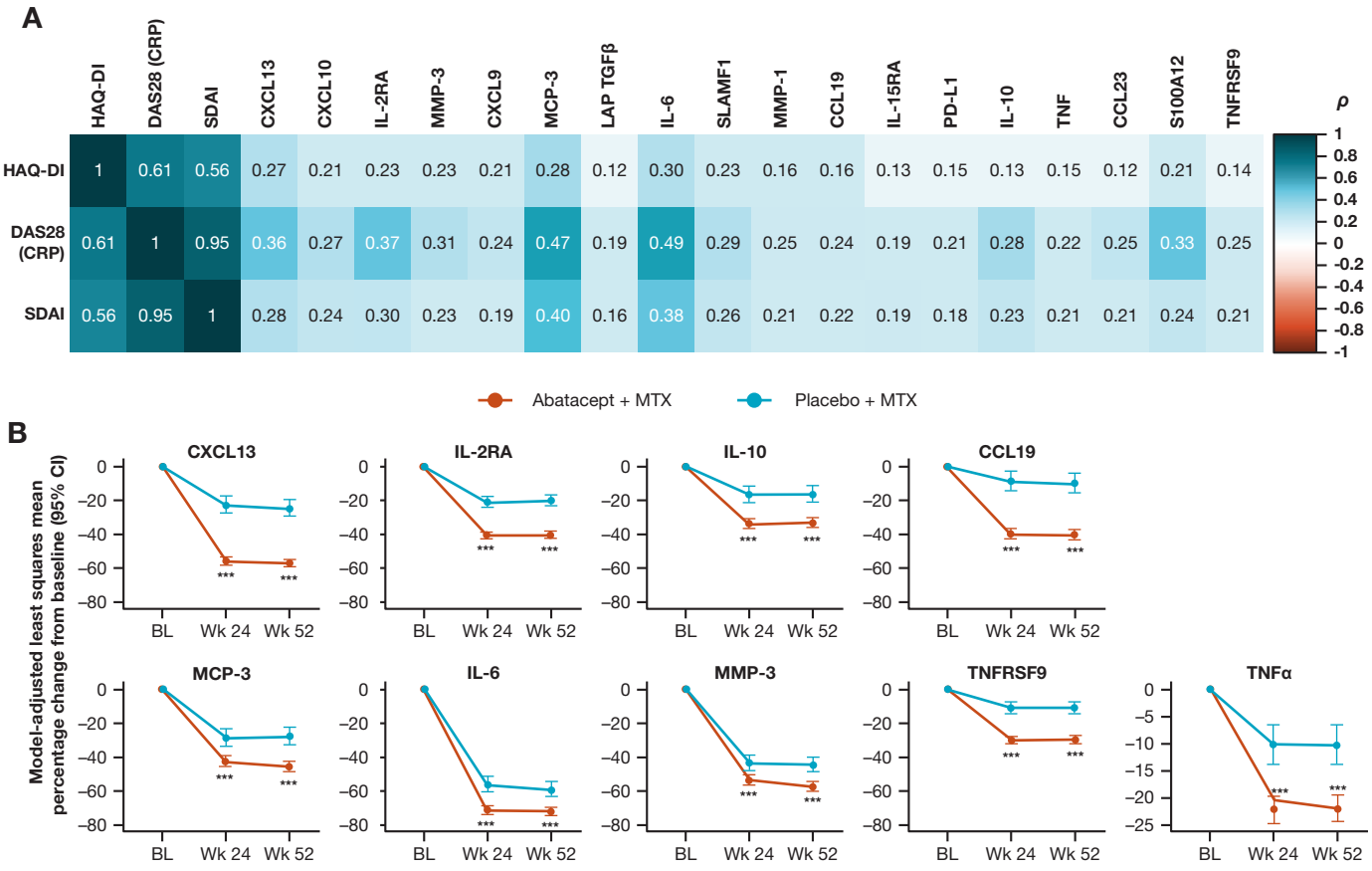

Figure 1. (A) Correlation of BL biomarkers and disease activity and (B) significant PD changes observed with abatacept and MTX versus placebo and MTX (adapted from Liu et al).[21] ***$P < 0.001$. BL, baseline; CCL, CC chemokine ligand; CI, confidence interval; CXCL, chemokine (C-X-C motif) ligand; DAS28 (CRP), Disease Activity Score in 28 joints using C-reactive protein; HAQ-DI, Health Assessment Questionnaire Disability Index; IL, interleukin; IL-2RA, interleukin-2 receptor alpha; IL-15RA, interleukin-15 receptor alpha; LAP TGFβ, tumor growth factor–beta latency-associated peptide; MCP, methyl-accepting chemotaxis protein; MMP, matrix metalloproteinase; MTX, methotrexate; PD, pharmacodynamic; PD-L1, programmed death ligand 1; S100A12, S100 calcium-binding protein A12; SDAI, Simplified Disease Activity Index; SLAMF, signaling lymphocytic activation molecule family; TNF, tumor necrosis factor; TNFRS, TNF receptor subfamily; Wk, week.

outcomes between abatacept and MTX versus placebo and MTX. IL-10 was identified as the only biomarker to predict the treatment response across multiple outcome measures. At lower levels of baseline IL-10, there was similar treatment efficacy between the two treatment arms. However, a worse treatment response was observed in patients treated with placebo and MTX with increasing baseline IL-10 levels. However, adding abatacept to MTX significantly reversed the poor outcome with MTX monotherapy as demonstrated across multiple efficacy measures, including ACR50, ACR70, DAS28 (CRP) <2.6, and SDAI remission (Figure 2).

Greater reduction of disease activity with abatacept and MTX at high levels of baseline IL-10. With baseline IL-10 identified as a significant predictive biomarker, we next investigated the attenuation of disease activity over the treatment course by IL-10 tertile. In the low IL-10 tertile, a similar reduction of disease activity was observed with abatacept and MTX and with placebo and MTX. However, a significantly greater reduction of disease activity was observed in patients with intermediate and high baseline IL-10 levels who were treated with abatacept and MTX. Similar results were obtained when assessing treatment response by DAS28 (CRP) or SDAI (Figure 3).

Greater erosion and modified total Sharp scores for patients with high baseline IL-10 after MTX treatment. We next assessed whether high baseline IL-10 levels were associated with differential worsening of bone erosions in patients treated with placebo and MTX who had worse clinical outcomes. Higher baseline IL-10 levels were associated with lower erosive development with abatacept and MTX compared with placebo and MTX (Figure 4). Significant worsening of joint damage was

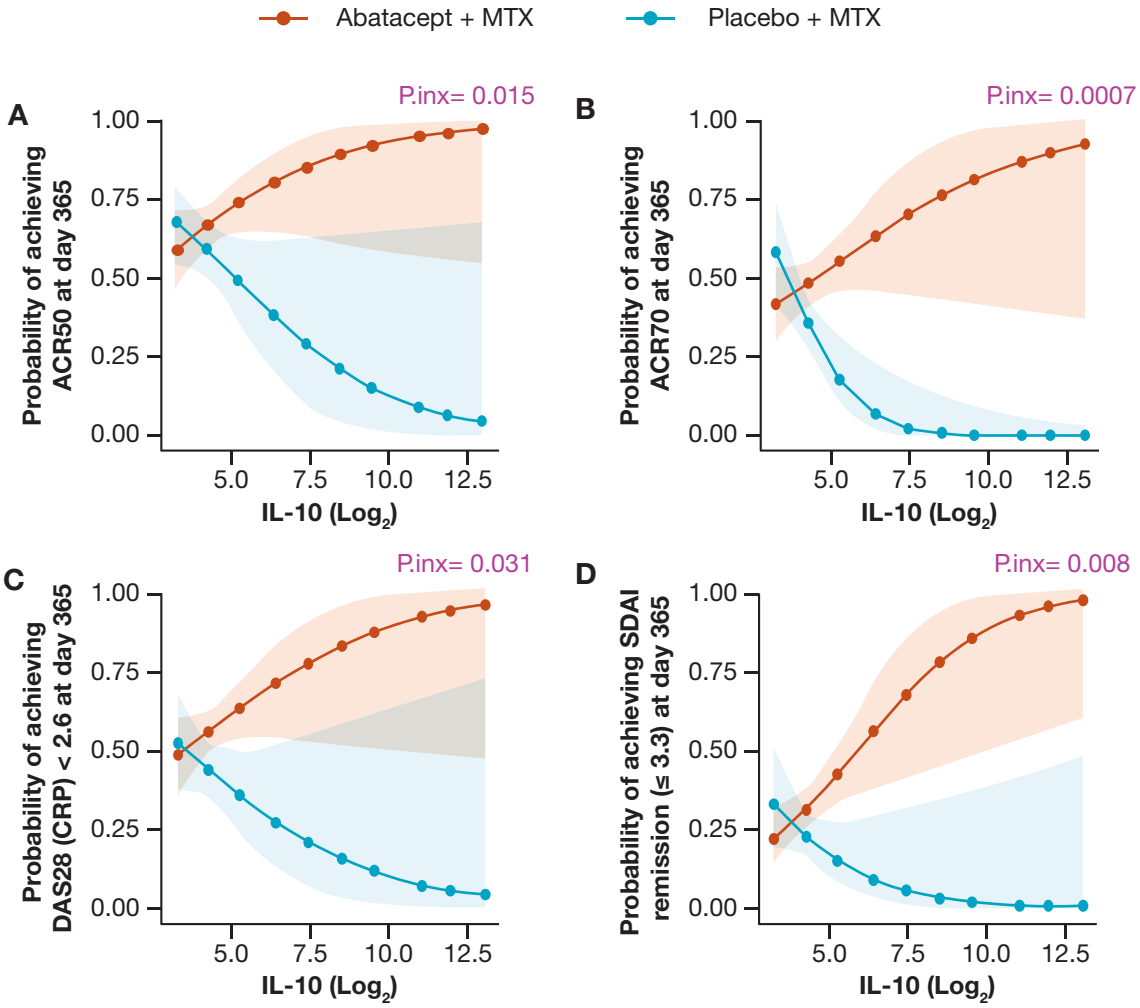

Figure 2. Probability of achieving (A) ACR50, (B) ACR70, (C) DAS28 (CRP) <2.6, and (D) SDAI remission ≤3.3 at day 365 by baseline IL-10 level in patients treated with abatacept and MTX or placebo and MTX (adapted from Liu et al).[21] Interaction *p*-value is the significance level of the interaction term ($\beta IX\ Trt \times BM$). Shaded areas show 95% confidence intervals. ACR50, 50% improvement in American College of Rheumatology criteria; DAS28 (CRP), Disease Activity Score in 28 joints using C-reactive protein; IL-10, interleukin-10; MTX, methotrexate; SDAI, Simplified Disease Activity Index.

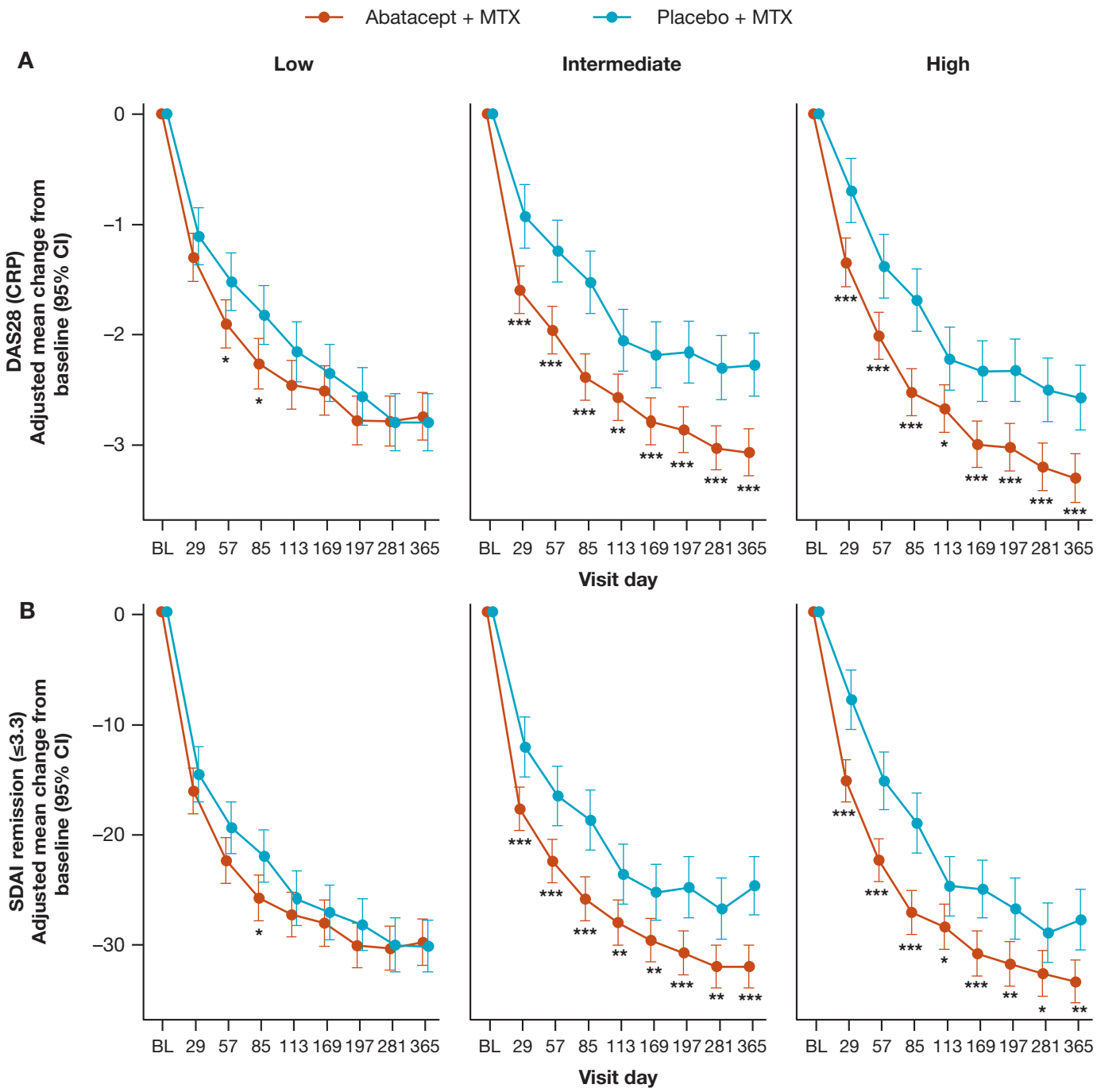

Figure 3. Mean change from baseline in (A) DAS28 (CRP) and (B) SDAI in patients treated with abatacept and MTX versus placebo and MTX, stratified by baseline IL-10 levels (adapted from Liu et al).[21] Baseline IL-10 levels were categorized as low, 3.20 to4.04; intermediate, 4.05 to 4.54; and high, 4.54 to 12.66. *$P < 0.05$; **$P < 0.01$; ***$P < 0.001$. BL, baseline; CI, confidence interval; DAS28 (CRP), Disease Activity Score in 28 joints using C-reactive protein; IL-10, interleukin-10; MTX, methotrexate; SDAI, Simplified Disease Activity Index.

shown in patients treated with placebo and MTX with high versus low baseline IL-10 (Figure 4).

DISCUSSION

In this study of patients with early, DMARD-naive, ACPA-positive RA, we identified biomarkers significantly correlated with baseline RA disease activity and PD changes with abatacept and MTX compared with placebo and MTX treatment. Notably, high baseline IL-10 predicted improved clinical responses with abatacept and MTX compared with placebo and MTX across multiple measures at week 52. High baseline IL-10 levels were also associated with the greatest risk of radiographic progression in patients who received placebo and MTX, not seen in those

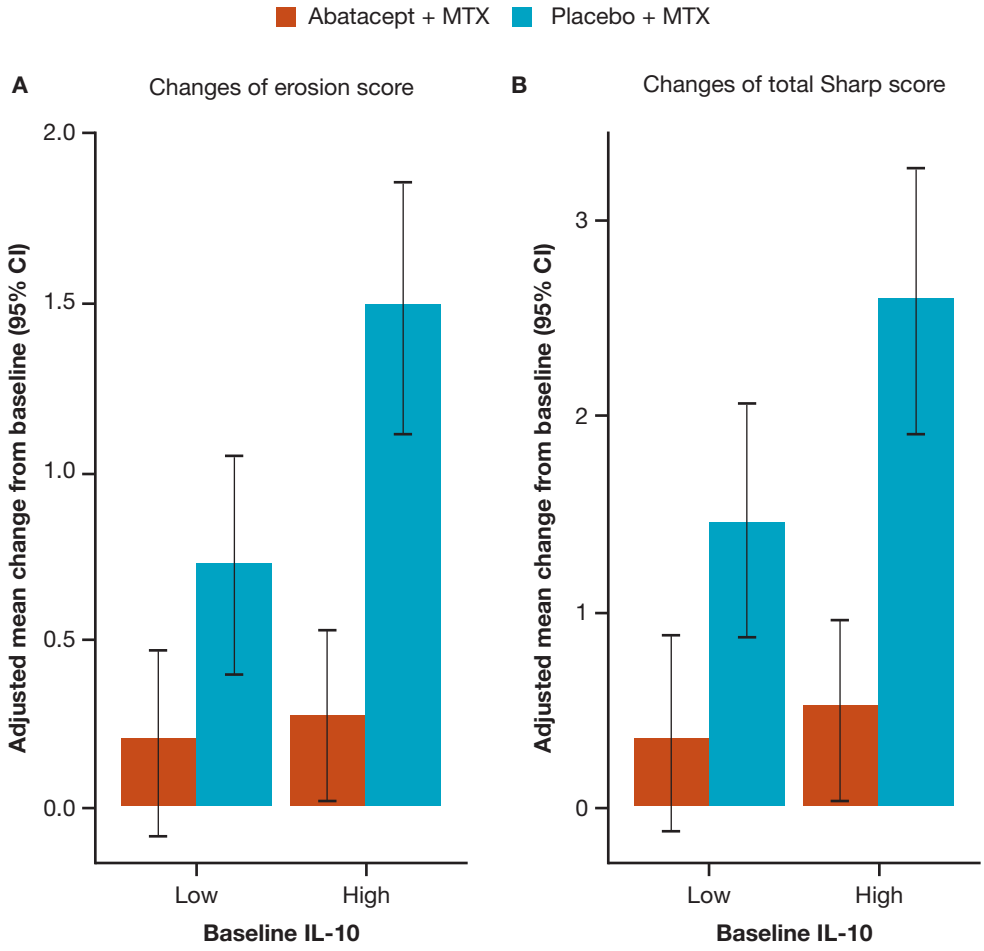

Figure 4. Change from baseline in (A) erosion score and (B) modified total Sharp score in patients treated with abatacept and MTX compared with placebo and MTX, stratified by baseline IL-10 levels (adapted from Liu et al).[21] The IL-10 cutoff for bone erosion and modified total Sharp score was the median (4.26). CI, confidence interval; IL-10, interleukin-10; MTX, methotrexate.

treated with abatacept and MTX. These findings suggest that patients with high baseline IL-10 levels may represent a distinct RA immune pathotype well suited for abatacept and MTX treatment.

A total of 18 biomarkers that significantly correlated with RA disease activity were identified in our study. Reductions from baseline in these biomarkers (IL-6, MCP-3, IL-2RA, CXCL13, S100A12, MMP3, SLAMF1, CXCL10, MMP1, IL-10, TNFα, CXCL9, LAP TGFβ, CCL19, IL-15RA, PD-L1, CCL23, and TNFRSF9) were correlated with improvement of disease activity. Abatacept and MTX treatment demonstrated a more profound reduction of these biomarkers compared with placebo and MTX; however, IL-10 was the only biomarker identified at baseline that predicted treatment response to abatacept. Further studies are needed to confirm the predictive value of IL-10. Elevation of IL-10 levels in patients with early RA have been previously observed[22]; IL-10 levels have been reported to be lower in healthy volunteers than in patients with RA; one study found mean IL-10 levels in healthy women to be 13 pg/mL versus 34 pg/mL in women with RA.[23] IL-10 is a pivotal proinflammatory cytokine that supports ongoing inflammation and erosion in the affected joints.[23–27] This observation was further supported by a study that demonstrated changes in the single-nucleotide polymorphism (SNP) at G-2849A in the IL-10 promoter was associated with IL-10 overproduction.[23,27] Patients with RA carrying –2849 G displayed higher levels of both rheumatoid factor (RF) and anti-cyclic citrullinated peptide (CCP) autoantibody titers and a higher rate of joint destruction compared with patients with RA who were non-G carriers, a finding consistent with our observation. A recent analysis of genetic data from genome-wide association studies found that among other inflammatory cytokines and metabolites, IL-10 was associated with a significantly increased risk of RA.[28] Our findings offer a comprehensive description of IL-10 levels in patients with RA and its correlation with disease activity, response to therapy, and erosive damage progression. Arguably, the anti- or proinflammatory role of IL-10 may be context dependent. Previous studies have found IL-10 to be an enhancer of both IgM RF and IgG anti-CCP autoantibody

production by B cells in patients with RA.[29,30] Increased IL-10 levels may represent an immune pathotype with augmented follicular activity and enhanced interaction of T and B cells in the extrafollicular compartment, leading to impaired B cell tolerance. Moreover, these changes may lead to defects in B cell tolerance and elevated autoreactive B cells with increased polyreactivity and autoimmunity,[31] which may reflect resistance to MTX monotherapy.

We report positive outcomes with abatacept and MTX treatment in patients with higher baseline levels of IL-10. Others have reported clinical responses to the TNF inhibitor etanercept based on genotyping the IL-10 promoter SNPs. A strong association was seen for a favorable outcome following treatment with etanercept with the SNP that was associated with constitutively low IL-10 production.[32] The association of high baseline IL-10 levels with treatment response and clinical efficacy for other RA therapies such as rituximab (anti-CD20), tocilizumab (anti–IL-6R), or JAK inhibitors remains to be determined. At present, baseline IL-10 levels appear to predict response differentially to therapy for abatacept and etanercept. Future studies are needed to dissect the relationship between baseline IL-10 levels and the cellular and molecular signatures identified for the responders and nonresponders of RA therapies. As such, we have proposed a model to explain our findings (Figure 5). Because IL-10 is a pleiotropic immunoregulatory cytokine, greater IL-10 levels may represent an early seropositive RA immunopathotype with greater B cell activation and more reactive germinal center activity, as seen in other studies in RA and infection.[22,33,34] In our study, baseline IL-10 levels were associated with CXCL13 levels, a chemokine critically involved in mediating the activity of germinal centers. In addition, extrafollicular T and B cell interactions may be strengthened by high levels of IL-10, resulting in increasing levels of autoantibodies, as has been found in our study and reported by others.[35] Abatacept and MTX inhibits the dysregulated germinal centers and extrafollicular T cell/B cell interactions (Figure 5), which suggests an effective treatment option for patients with RA and high baseline IL-10 levels compared with MTX alone.

Our findings regarding baseline IL-10 levels and differential accumulation of radiographic damage are notable. Patients with higher baseline IL-10 may represent a patient subset with faster progression and more difficult-to-treat bone damage, consistent with the lack of effectiveness with MTX monotherapy, whereas adding abatacept attenuated the progression of structural damage. On the other hand, abatacept and MTX was effective in treating patients with lower baseline IL-10, a population with less difficult-to-treat disease. A previous post hoc analysis of AVERT-2 showed that abatacept and MTX resulted in significant reductions in bone remodeling-related biomarkers, including RANKL and collagen degradation biomarkers, compared with MTX monotherapy.[17] This was consistent for the entire study patient population that had a wide spectrum of baseline IL-10 levels, supporting that abatacept and MTX treatment attenuated

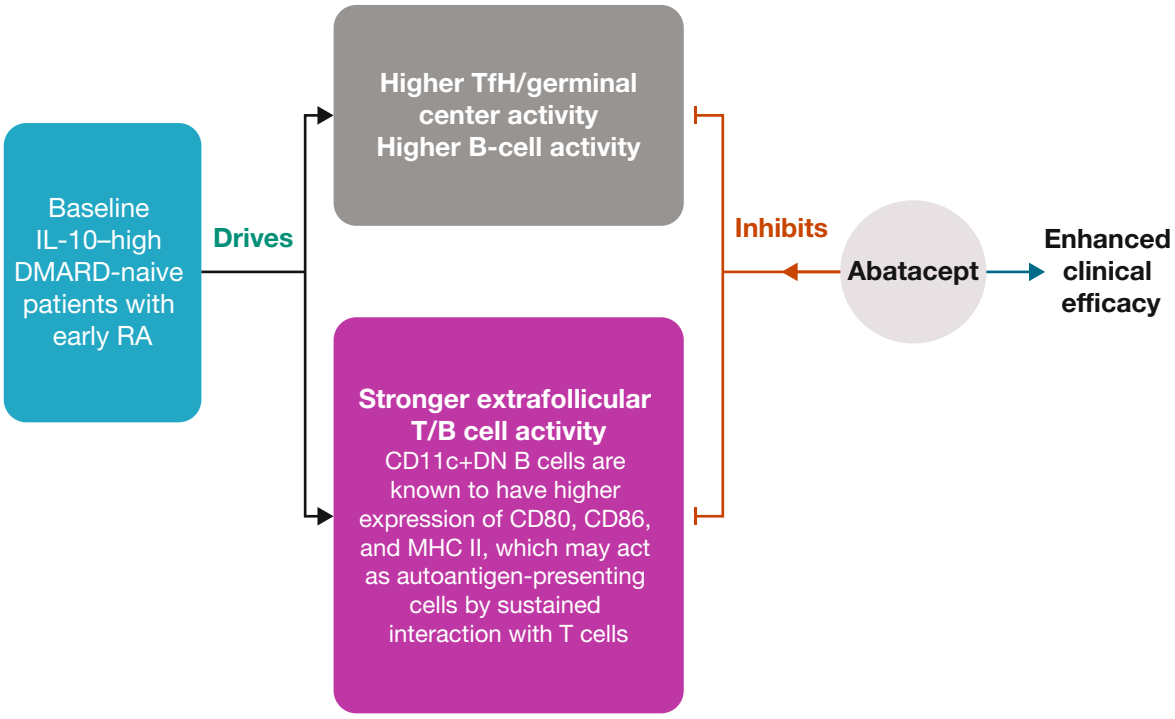

Figure 5. Current working model of IL-10 levels in patients who were DMARD naive with early RA (adapted from Liu et al).[21] DMARD, disease-modifying antirheumatic drug; DN, double negative; IL-10, interleukin-10; MHC, major histocompatibility complex; RA, rheumatoid arthritis; TfH, T follicular helper. Color figure can be viewed in the online issue, which is available at http://onlinelibrary.wiley.com/doi/10.1002/art.70106/abstract.

radiographic progression and bone absorption biomarkers in all treated patients; however, the effectiveness of abatacept and MTX was more pronounced in patients with fast-progression with higher baseline IL-10 compared with MTX. These patients at high risk may achieve better clinical outcomes if treated earlier with abatacept and MTX. Overall, treatment with abatacept and MTX not only resulted in the best outcomes at a group level, but as identified by IL-10 levels, it had the greatest impact on the subgroup at highest risk of progression. Together, these analyses suggest that abatacept has an important impact on bone remodeling and inflammation, but additional, more in-depth cellular and molecular analyses are required to understand fully the mechanism of IL-10 as a predictive biomarker of treatment response in patients with very early RA.

The need for clinical response predictors that can help identify which DMARD may have the greatest clinical utility for an individual patient is a widely shared position.[11] We have conducted similar analyses from other controlled trials to design confirmatory studies.[36–40] As our understanding of RA disease pathophysiology continues to expand and the technologies available to characterize patients evolve, treatment development programs should emphasize identification of response predictors linked to novel therapies.

There are several limitations of this study. This is a retrospective, exploratory analysis in a subset of patients from the ITT population of the AVERT-2 clinical study; additional validation studies are needed for clinical applications of the findings. Our data suggest the predictive value of IL-10 and a potential correlation of high baseline IL-10 levels with an enrichment of pathogenic interaction of T cells/B cells. However, an in-depth cellular and molecular analysis of patients with a range of IL-10 levels is necessary to understand better the mechanism of IL-10 as a predictive biomarker of treatment response given the limited availability of such data in the AVERT-2 study. The patient population used for this analysis was relatively small; therefore, further analyses with larger patient populations should be completed to confirm our findings. Clinical differences between patients with low versus high baseline IL-10 levels were not examined; however, we observed a positive correlation between IL-10 and RA disease activity and levels of anti-CCP and RF in our study. It is plausible that patients with higher baseline IL-10 may represent a patient population with greater clinical disease activity and other molecular features more suitable for the abatacept mechanism of action. In addition, the Olink platform used in this study produces outputs using NPX relative units when reporting IL-10 levels. We have seen a very high correlation between NPX relative units and absolute quantitation as demonstrated by the three overlapped proteins we tested in the Olink and RBM panels and in other studies we conducted (data not shown). Further quantification of IL-10 levels is needed to confirm these observations, though we expect the conclusions to be consistent. Moreover, given the well-accepted heterogeneity of RA, it is plausible that a more powerful predictive algorithm is needed to identify additional biomarkers representing distinct aspects of the disease pathology, such as bone metabolism, immune phenotypes, or other clinical features.

We have identified high baseline IL-10 levels as a biomarker of treatment response in patients who were MTX naive and ACPA positive with early RA. Results suggest that patients with high baseline IL-10 represent an immunopathotype indicative of a strong interaction between T and B cells that can be targeted by abatacept's mechanism of action. Early combination of abatacept with MTX may represent a more optimal treatment option for this subset of patients who are DMARD naive with early RA and high baseline IL-10 levels.

ACKNOWLEDGMENTS

We gratefully acknowledge the patients who participated in this study and their families. We thank the clinical research staff and caregivers at all participating sites. Professional medical writing and editorial assistance were provided by Alexus Shirk, PhD, of Caudex, an IPG Health Company, funded by Bristol Myers Squibb.

AUTHOR CONTRIBUTIONS

All authors contributed to at least one of the following manuscript preparation roles: conceptualization AND/OR methodology, software, investigation, formal analysis, data curation, visualization, and validation. All authors contributed to writing, reviewing, and editing of the manuscript. As corresponding author, Dr Liu confirms that all authors have provided the final approval of the version to be published, and takes responsibility for the affirmations regarding article submission (eg, not under consideration by another journal), the integrity of the data presented, and the statements regarding compliance with institutional review board/Declaration of Helsinki requirements.

ROLE OF THE STUDY SPONSOR

Bristol Myers Squib had a role in the study design or in the collection, analysis, or interpretation of the data, the writing of the manuscript, or the decision to submit the manuscript. Publication of this article was contingent upon approval by authors employed by Bristol Myers Squib.

REFERENCES

1. Aletaha D, Smolen JS. Diagnosis and management of rheumatoid arthritis: a review. JAMA 2018;320(13):1360–1372. doi:https://doi.org/10.1001/jama.2018.13103
2. McInnes IB, Buckley CD, Isaacs JD. Cytokines in rheumatoid arthritis - shaping the immunological landscape. Nat Rev Rheumatol 2016;12(1):63–68. doi:https://doi.org/10.1038/nrrheum.2015.171
3. McInnes IB, Schett G. The pathogenesis of rheumatoid arthritis. N Engl J Med 2011;365(23):2205–2219. doi:https://doi.org/10.1056/NEJMra1004965
4. Smolen JS, Aletaha D, Barton A, et al. Rheumatoid arthritis. Nat Rev Dis Primers 2018;4(1):18001. doi:https://doi.org/10.1038/nrdp.2018.1
5. Xu Y, Wu Q. Prevalence trend and disparities in rheumatoid arthritis among US adults, 2005-2018. J Clin Med 2021;10(15):3289. doi:https://doi.org/10.3390/jcm10153289
6. Hecht C, Englbrecht M, Rech J, et al. Additive effect of anti-citrullinated protein antibodies and rheumatoid factor on bone

erosions in patients with RA. Ann Rheum Dis 2015;74(12):2151–2156. doi:https://doi.org/10.1136/annrheumdis-2014-205428

7. van der Helm-van Mil AHM, Verpoort KN, Breedveld FC, et al. Antibodies to citrullinated proteins and differences in clinical progression of rheumatoid arthritis. Arthritis Res Ther 2005;7(5):R949–R958. doi:https://doi.org/10.1186/ar1767
8. Smolen JS, Landewé RBM, Bergstra SA, et al. EULAR recommendations for the management of rheumatoid arthritis with synthetic and biological disease-modifying antirheumatic drugs: 2022 update. *Ann Rheum Dis* 2023;82(1):3–18. doi:10.1136/ard-2022-223356 Erratum in: Ann Rheum Dis 2023;82:e76.
9. Fraenkel L, Bathon JM, England BR, et al. 2021 American College of Rheumatology guideline for the treatment of rheumatoid arthritis. Arthritis Rheumatol 2021;73(7):1108–1123. doi:https://doi.org/10.1002/art.41752
10. Firestein GS. The disease formerly known as rheumatoid arthritis. Arthritis Res Ther 2014;16(3):114. doi:https://doi.org/10.1186/ar4593
11. Gravallese EM, Firestein GS. Rheumatoid arthritis - common origins, divergent mechanisms. N Engl J Med 2023;388(6):529–542. doi:https://doi.org/10.1056/NEJMra2103726
12. Bathon J, Robles M, Ximenes AC, et al. Sustained disease remission and inhibition of radiographic progression in methotrexate-naive patients with rheumatoid arthritis and poor prognostic factors treated with abatacept: 2-year outcomes. Ann Rheum Dis 2011;70(11):1949–1956. doi:https://doi.org/10.1136/ard.2010.145268
13. Emery P, Burmester GR, Bykerk VP, et al. Evaluating drug-free remission with abatacept in early rheumatoid arthritis: results from the phase 3b, multicentre, randomised, active-controlled AVERT study of 24 months, with a 12-month, double-blind treatment period. Ann Rheum Dis 2015;74(1):19–26. doi:https://doi.org/10.1136/annrheumdis-2014-206106
14. Harrold LR, Litman HJ, Connolly SE, et al. A window of opportunity for abatacept in RA: is disease duration an independent predictor of low disease activity/remission in clinical practice? Clin Rheumatol 2017;36(6):1215–1220. doi:https://doi.org/10.1007/s10067-017-3588-7
15. Raza K, Filer A. The therapeutic window of opportunity in rheumatoid arthritis: does it ever close? Ann Rheum Dis 2015;74(5):793–794. doi:https://doi.org/10.1136/annrheumdis-2014-206993
16. Emery P, Tanaka Y, Bykerk VP, et al. Sustained remission and outcomes with abatacept plus methotrexate following stepwise dose de-escalation in patients with early rheumatoid arthritis. Rheumatol Ther 2023;10(3):707–727. doi:https://doi.org/10.1007/s40744-022-00519-9
17. Wu C, Hu Y, Schafer P, et al. Baseline serum levels of cross-linked carboxy-terminal telopeptide of type I collagen predict abatacept treatment response in methotrexate-naive, anticitrullinated protein antibody-positive patients with early rheumatoid arthritis. RMD Open 2022;8(2):e002683. doi:https://doi.org/10.1136/rmdopen-2022-002683
18. Emery P, Tanaka Y, Bykerk VP, et al. The trajectory of clinical responses in patients with early rheumatoid arthritis who achieve sustained remission in response to abatacept: subanalysis of AVERT-2, a randomized phase IIIb study. Arthritis Res Ther 2023;25(1):67. doi:https://doi.org/10.1186/s13075-023-03038-2
19. American College of Rheumatology Committee to Reevaluate Improvement Criteria. A proposed revision to the ACR20: the hybrid measure of American College of Rheumatology response. Arthritis Rheum 2007;57:193–202. Erratum in: *Arthritis Rheum* 2007;57:1574.
20. Aletaha D, Neogi T, Silman AJ, et al. 2010 Rheumatoid arthritis classification criteria: an American College of Rheumatology/European League Against Rheumatism collaborative initiative. Arthritis Rheum 2010;62:2569–2581.
21. Liu J, Li Y, Fu K, et al. POS0611 baseline IL-10 levels as a predictive biomarker for achieving clinical response with abatacept in ACPA+ patients with early RA. Ann Rheum Dis 2024;83:750–751. doi:https://doi.org/10.1136/annrheumdis-2024-eular.118
22. Cush JJ, Splawski JB, Thomas R, et al. Elevated interleukin-10 levels in patients with rheumatoid arthritis. Arthritis Rheum 1995;38(1):96–104. doi:https://doi.org/10.1002/art.1780380115
23. Vasilev G, Ivanova M, Stanilov I, et al. Influence of *IL10* and *TGFB1* promoter polymorphisms on serum cytokine levels in development and severity of RA. Int J Mol Sci 2022;23(19):11955. doi:https://doi.org/10.3390/ijms231911955
24. Perez L, Orte J, Brieva JA. Terminal differentiation of spontaneous rheumatoid factor-secreting B cells from rheumatoid arthritis patients depends on endogenous interleukin-10. Arthritis Rheum 1995;38(12):1771–1776. doi:https://doi.org/10.1002/art.1780381210
25. Reparon-Schuijt CC, van Esch WJ, van Kooten C, et al. Functional analysis of rheumatoid factor-producing B cells from the synovial fluid of rheumatoid arthritis patients. Arthritis Rheum 1998;41(12):2211–2220. doi:https://doi.org/10.1002/1529-0131(199812)41:12<2211:AID-ART17>3.0.CO;2-O
26. Reparon-Schuijt CC, van Esch WJ, van Kooten C, et al. Secretion of anti-citrulline-containing peptide antibody by B lymphocytes in rheumatoid arthritis. Arthritis Rheum 2001;44(1):41–47. doi:https://doi.org/10.1002/1529-0131(200101)44:1<41:AID-ANR6>3.0.CO;2-0
27. Bucht A, Larsson P, Weisbrot L, et al. Expression of interferon-gamma (IFN-gamma), IL-10, IL-12 and transforming growth factor-beta (TGF-beta) mRNA in synovial fluid cells from patients in the early and late phases of rheumatoid arthritis (RA). Clin Exp Immunol 1996;103(3):357–367. doi:https://doi.org/10.1111/j.1365-2249.1996.tb08288.x
28. Peilin Z, Wenqiang W, Yongzhen L, et al. Inflammatory cytokines, metabolites, and rheumatoid arthritis. Postgrad Med J 2025;101(1194):313–320. doi:https://doi.org/10.1093/postmj/qgae146
29. Nemec P, Goldbergova MP, Gatterova J, et al. Association of polymorphisms in interleukin-10 gene promoter with autoantibody production in patients with rheumatoid arthritis. Ann N Y Acad Sci 2009;1173(1):501–508. doi:https://doi.org/10.1111/j.1749-6632.2009.04625.x
30. Laurent L, Anquetil F, Clavel C, et al. IgM rheumatoid factor amplifies the inflammatory response of macrophages induced by the rheumatoid arthritis-specific immune complexes containing anticitrullinated protein antibodies. Ann Rheum Dis 2015;74(7):1425–1431. doi:https://doi.org/10.1136/annrheumdis-2013-204543
31. Wang Y, Lloyd KA, Melas I, et al. Rheumatoid arthritis patients display B-cell dysregulation already in the naïve repertoire consistent with defects in B-cell tolerance. Sci Rep 2019;9(1):19995. doi:https://doi.org/10.1038/s41598-019-56279-0
32. Schotte H, Schlüter B, Schmidt H, et al. Putative IL-10 low producer genotypes are associated with a favourable etanercept response in patients with rheumatoid arthritis. PLoS One 2015;10(6):e0130907. doi:https://doi.org/10.1371/journal.pone.0130907
33. Guthmiller JJ, Graham AC, Zander RA, et al. Cutting edge: IL-10 is essential for the generation of germinal center B cell responses and anti-plasmodium humoral immunity. J Immunol 2017;198(2):617–622. doi:https://doi.org/10.4049/jimmunol.1601762
34. Laidlaw BJ, Lu Y, Amezquita RA, et al. Interleukin-10 from $CD4^+$ follicular regulatory T cells promotes the germinal center response. Sci Immunol 2017;2(16):eaan4767. doi:https://doi.org/10.1126/sciimmunol.aan4767
35. Lard LR, van Gaalen FA, Schonkeren JJ, et al. Association of the -2849 interleukin-10 promoter polymorphism with autoantibody production and joint destruction in rheumatoid arthritis. Arthritis Rheum 2003;48(7):1841–1848. doi:https://doi.org/10.1002/art.11160

36. Rigby W, Buckner JH, Louis Bridges S Jr, et al. HLA-DRB1 risk alleles for RA are associated with differential clinical responsiveness to abatacept and adalimumab: data from a head-to-head, randomized, single-blind study in autoantibody-positive early RA. Arthritis Res Ther 2021;23(1):245. doi:https://doi.org/10.1186/s13075-021-02607-7
37. Verstappen M, Matthijssen XME, Connolly SE, et al. ACPA-negative and ACPA-positive RA patients achieving disease resolution demonstrate distinct patterns of MRI-detected joint-inflammation. Rheumatology (Oxford) 2022;62(1):124–134. doi:https://doi.org/10.1093/rheumatology/keac294
38. Jabado O, Maldonado MA, Schiff M, et al. Differential changes in ACPA fine specificity and gene expression in a randomized trial of abatacept and adalimumab in rheumatoid arthritis. Rheumatol Ther 2022;9(2):391–409. doi:https://doi.org/10.1007/s40744-021-00404-x
39. Fleischmann R, Weinblatt M, Ahmad H, et al. Efficacy of abatacept and adalimumab in patients with early rheumatoid arthritis with multiple poor prognostic factors: post hoc analysis of a randomized controlled clinical trial (AMPLE). Rheumatol Ther 2019;6(4):559–571. doi:https://doi.org/10.1007/s40744-019-00174-7
40. Sokolove J, Schiff M, Fleischmann R, et al. Impact of baseline anti-cyclic citrullinated peptide-2 antibody concentration on efficacy outcomes following treatment with subcutaneous abatacept or adalimumab: 2-year results from the AMPLE trial. Ann Rheum Dis 2016;75(4):709–714. doi:https://doi.org/10.1136/annrheumdis-2015-207942

Arthritis & Rheumatology
Vol. 78, No. 9, September 2026, pp 1837–1849
DOI 10.1002/art.70123
© 2026 The Author(s). *Arthritis & Rheumatology* published by Wiley Periodicals LLC on behalf of American College of Rheumatology.
This is an open access article under the terms of the Creative Commons Attribution-NonCommercial License, which permits use, distribution and reproduction in any medium, provided the original work is properly cited and is not used for commercial purposes.

American College of Rheumatology
Empowering Rheumatology Professionals

Tissue Damage in Rheumatoid Arthritis Is Genetically Linked to Low Peptidylglycine Alpha-Amidating Monooxygenase Activity in Synovial Fibroblasts

Kevin J. Sheridan, PhD,[1] Emma R. Dorris, PhD,[1] Maria Inês Pimenta, MSc,[1] Jemma Falkov, MSc,[1] Matthew Fisher, BSc,[2] Sam Pledger, MSc,[3] Hector Devey, MSc,[3] Munitta Muthana, PhD,[2] Denis C. Shields, PhD,[1] Richard E. Mains, PhD,[4] Betty A. Eipper, PhD,[4] Christopher D. Buckley, MB, PhD,[3] and Anthony G. Wilson, MB, PhD[1]

Objective. Both susceptibility to, and severity of, rheumatoid arthritis (RA) is associated with the rs26232 C allele. Our primary aim was to identify the biologic mechanism underlying this association.

Methods. Expression of surrounding genes was compared among rs26232 genotypes. Publicly available databases were used to correlate expression with RA inflammation and single-cell synovial distribution. Inhibition of gene expression and activity was achieved using small interfering RNA and a pharmacology agent and effects on RA synovial fibroblasts (RASFs) characteristics in vitro were assayed. The amidated secretome of synovial fibroblasts were characterized by mass spectrometry and enzyme-linked immunosorbent assay. Effects of amidated peptides on macrophage polarity were determined using an RASF–macrophage coculture module.

Results. rs26232 C is associated with low expression of peptidylglycine alpha-amidating monooxygenase (*PAM*) in multiple tissues including RASFs. Synovial *PAM* is highly expressed in RASFs but not immune cells, and levels are inversely correlated with synovial and systemic levels of inflammation. Inhibition of *PAM* in RASFs increased tissue-damaging activities such as invasiveness in vitro. The most abundant amidated peptides secreted by RASFs were adrenomedullin (ADM) and pro-ADM N-terminal peptide (PAMP). Incubation of RASFs with either peptide inhibited interleukin-6 (IL-6) and IL-8, increased transforming growth factor β production, and reduced invasiveness in vitro. Inhibition of amidation in an RASF–macrophage coculture model skewed the macrophages to proinflammatory MerTK$^-$ phenotypes.

Conclusion. Genetically determined low *PAM* reduces the anti-inflammatory and tissue-damaging activities of ADM and PAMP mediated by macrophages and RASFs, explaining the association of rs26232 C with RA severity.

INTRODUCTION

Rheumatoid arthritis (RA) is a chronic autoimmune disease characterized by inflammation in synovial joints that, if prolonged, results in cartilage and bone damage with resultant stiffness, pain, and reduced functional abilities. Pathogenesis involves both genetic and environmental risk factors. The severity of tissue damage in RA varies widely but has significant genetic input.[1] Of the more than 100 RA risk alleles identified in a genome-wide association study (GWAS), there is significant enrichment within immune-cell enhancers resulting in expression quantitative trait loci (eQTL).[2]

It has also been established that 24% of RA genetic risk arises from variants affecting gene expression in nonimmune cells such as RA synovial fibroblasts (RASFs).[3] These stromal cells are central mediators of inflammation and tissue damage in RA.[4] The

Supported by the Health Research Board (grant ILP-POR-2022-014). The Genotype-Tissue Expression Project was supported by the Common Fund of the Office of the Director of the NIH (commonfund.nih.gov/GTEx) and by National Cancer Institute, NIH; National Human Genome Research Institute, NIH; National Heart, Lung, and Blood Institute, NIH; National Institute on Drug Abuse, NIH; National Institute of Mental Health, NIH; and National Institute of Neurological Disorders and Stroke, NIH.

[1]University College Dublin Centre for Arthritis Research, Conway Institute, University College Dublin, Dublin, Ireland; [2]Department of Oncology and Metabolism, University of Sheffield, Sheffield, United Kingdom; [3]Kennedy Institute of Rheumatology, University of Oxford, Oxford, United Kingdom; [4]Department of Neuroscience, University of Connecticut Health Center, Farmington.

Additional supplementary information cited in this article can be found online in the Supporting Information section (https://acrjournals.onlinelibrary.wiley.com/doi/10.1002/art.70123).

Author disclosures are available at https://onlinelibrary.wiley.com/doi/10.1002/art.70123.

Address correspondence via email to Kevin J. Sheridan, PhD, at kevin.sheridan1@ucd.ie.

Submitted for publication September 1, 2025; accepted in revised form February 5, 2026.

invasive activities of RASFs in vitro are predictive of the rate of progression of joint damage.[5] The C allele of the single-nucleotide variant rs26232 is associated with both susceptibility to, and severity of, RA. The minor T allele is protective and occurs at a frequency of approximately 30%.[6–8] Cultured RASFs of this genotype are more invasive and produce higher levels of inflammatory cytokines and adhesion molecules compared with the CT genotype; although rs26232 is located within the first intron of *MACIR*, which has been shown to be involved in RASF-mediated tissue damage[9] and macrophage-directed inflammation,[10] the variant is not an eQTL for this gene.[11] This suggests that the link between rs26232 and RA may be related to the activity of another nearby gene.

Here, we show that rs26232 is an eQTL for the enzyme peptidylglycine alpha-amidating monooxygenase (PAM) that catalyzes the amidation of many secreted peptides, with low levels being associated with the RA risk C allele. Amidation replaces the carboxyl group at the C-terminal of a peptide with another amine group and is important for optimal activity of hormones and messenger molecules. In RA synovial tissue, *PAM* expression is predominantly restricted to RASFs. Inhibition of *PAM* results in greater tissue damage in vivo and in vitro, as well as shifting macrophages toward a proinflammatory phenotype. Lower amidation of two related secreted peptides, adrenomedullin (ADM) and pro-ADM N-terminal peptide (PAMP), is a mechanism underlying the association of rs26232 C allele with RA severity.

MATERIALS AND METHODS

Cell culture. RASFs were purchased from Sigma-Aldrich and maintained in RPMI medium, supplemented with 10% fetal bovine serum (FBS), penicillin (100 units/mL), and streptomycin (100 units/mL). The RNA for the 33 samples was taken from RASFs collected from patients in Ireland. RASFs were used between passages 3 and 8. For proteomic experiments, cells were grown in RPMI media without phenol red, supplemented with ascorbic acid (100 μM), $CuSO_4$ (50 μM), and insulin, transferrin, and selenium (Gibco, 41400-04). Peripheral blood mononuclear cells were isolated and macrophages differentiated as previously described.[11]

Recombinant amidated ADM (ADM-NH_2), glycine-extended ADM (ADM-Gly) and amidated PAMP (PAMP-NH_2) peptides were acquired from Phoenix Europe GmbH. Glycine-extended PAMP (PAMP-Gly) was custom ordered from GenScript Biotech. All peptides were used at concentration of 50 nM. 4-Phenyl-3-butenoic acid (PBA; Sigma, 155322) was used at a concentration of 1 μM. Tumor necrosis factor α (TNFα) was used at a concentration of 50 ng/mL. Lipopolysaccharide (LPS) was used at a concentration of 100 ng/mL. Hypoxia work was conducted at 3% O_2 using an Invivo$_2$ 400 workstation (Baker Ruskinn).

Flow cytometry. Fibroblast–macrophage coculture was seeded in RPMI at 2 × 10^5 cells/well per cell type and 4 × 10^5 cells/well for macrophage-only cultures. All media were treated with ascorbic acid and incubated at 3% O_2. Media was changed at 24 hours, and 1 μM PBA was added to the treatment wells in addition to ascorbic acid in both treatment (n = 3) and control (n = 3) wells. At 48 hours, cells were harvested for flow cytometry staining. Cells were washed in phosphate buffered saline (PBS) and incubated for 20 minutes in Live Dead (1:1,000) and Fc block (1:100) at 4°C. Samples were stained using the cell surface markers CD45, CD48, CD86, MerTK, and CD206 (1:100). Samples were centrifuged and washed with fluorescence-activated cell sorting (FACS) buffer (10% FBS in PBS). Samples were then fixed in 4% paraformaldehyde (PFA) for 20 minutes in the dark at room temperature and centrifuged, and the pellet was resuspended in 300 μL FACS buffer before being run on the BD Fortessa X20. Data were analyzed using FlowJo version 10.

Small interfering RNA knockdown in cell culture. Small interfering RNA (siRNA) targeting *PAM* (Dharmacon siGENOME SmartPool) or a nontargeting control siRNA (siNTC; Dharmacon siGENOME nontargeting pool 2) were transfected into RASFs at 30 nM using lipofectamine 2000 (Thermo Fisher) for 120 hours. siRNA targeting *PRG4* (siPRG4; Dharmacon siGENOME SmartPool) or siNTC (as above) were transfected into RASFs at 5 nM using lipofectamine 2000 for 72 hours. Knockdowns were confirmed using Western blot, and knockdown efficiency was calculated using densitometry.

Quantitative polymerase chain reaction. Messenger RNA (mRNA) was extracted from RASFs using Macherey-Nagel nucleospin mRNA kit (740955.50) and reverse-transcribed using Multiscribe reverse-transcriptase (Thermo Fisher, 4311235). Real-time polymerase chain reaction (PCR) was conducted on a Roche Lightcycler using Roche SYBR Green. Relative levels of total RNA for target genes (*PAM*, *GIN1*, *PPIP5K2*, and *MACIR*) were calculated using ΔΔCt method, with *HPRT1* used as a housekeeping gene. Primers used as listed in Supplementary Data Table 1.

Protein extraction and Western blotting. Cells were washed in cold PBS, then resuspended in N-PER Neuronal Protein Extraction Reagent (Thermo, 87792) containing protease inhibitor cocktail (Roche, 04693116001). Samples were placed on ice for 10 minutes, and the supernatant was collected after centrifugation (13,000 revolutions per minute for 10 minutes at 4°C). Total cellular protein was determined by means of the Bio-Rad DC protein assay (5000111). Protein samples were subjected to sodium dodecyl sulfate–polyacrylamide gel electrophoresis and then transblotted onto PVDF membranes. Membranes were blocked in 5% bovine serum albumin (BSA) or milk before overnight incubation at 4°C in primary antibody, then washed in

Tris buffered saline–Tween and incubated with the appropriate horseradish peroxidase-conjugated secondary antibodies for one hour at room temperature. Western blots were imaged on Vilber Fusion Fx 7 Edge. Antibody details are listed in Supplementary Data Table 2.

Invasion assay. RASFs were harvested, and 2×10^4 cells were resuspended in 500 μL of serum-free RPMI medium in the upper compartment of the Matrigel-coated inserts (Corning, 354480). The lower compartment was filled with complete media and incubated at 37°C for 24 hours. The upper surface of the insert was cleaned and then stained with 0.1% crystal violet. Five fields of invading cells were counted.

Apoptosis assay. Apoptosis was measured using CellEvent Caspase-3/7 Detection Reagent (Thermo Fisher, C10423). RASFs were seeded in triplicate in a 96-well plate at a density of 1,000 cells/well and incubated at 37°C overnight. Medium was then removed, and the cells were incubated in 2 μM CellEvent Caspase-3/7 Detection Reagent diluted in 5% FBS in PBS for 30 minutes at 37°C. Apoptosis was measured with an excitation/emission of 502/530 nm using a BMG FLUOstar Omega Platereader.

Proliferation assay. Proliferation was measured using bromodeoxyuridine (BrdU) proliferation enzyme-linked immunosorbent assay (ELISA; Roche, NC0947823). RASFs were seeded in triplicate in a 96-well plate at a density of 1,000 cells/well and incubated at 37°C overnight. BrdU labeling reagent was added to the cell media, and the plate was incubated at 37°C overnight. Cells were then fixed, incubated with peroxidase-conjugated anti-BrdU antibody, and substrate solution was added. Absorbance was measured at 370 nm using a BMG FLUOstar Omega Platereader.

Migration assay. RASFs were seeded into a 12-well plate at a density of 3×10^6 cells/well and incubated at 37°C overnight. Using a micropipette tip, a scratch was made in the cell monolayer. Medium was then removed, cells were washed with PBS, and fresh media was added. An image at zero hours was then captured, and the area of the wound was calculated using EPview software. The plate was then incubated at 37°C for 24 hours. A 24-hour image was then captured, and area of the wound was calculated as before. The percentage of wound closure was then calculated using the difference between the 0- and 24-hour wound areas.

Fluorescent microscopy. RASFs were seeded at a density of 1×10^6 cells/mL into a Millicell EZ Slide eight-well glass microscopy slide (Millipore, PEZGS0816) and incubated at 37°C overnight. Medium was removed, and cells were fixed with 4% PFA. Cells were permeabilized with 0.1% Triton X-100 and blocked with 2% BSA in PBS. Primary antibodies were incubated with cells at room temperature for two hours, followed by three washes with PBS. Fluorescent secondary antibodies and DAPI (1 μg/mL; Thermo Fisher, 62248) were incubated with cells at room temperature for one hour in the dark and washed as before. A glass coverslip was adhered to the cells with mounting medium. Images were captured using Zeiss LSM 800 Airy microscope using a 63× objective. Antibody details are listed in Supplementary Data Table 2.

Database searches. The GTEx Portal (https://www.gtexportal.org/home/) was used to compare mRNA expression in relation to rs26232 genotype. Correlation between PAM expression and clinical markers of inflammation was gathered from the Pathobiology of Early Arthritis Cohort database (https://peac.hpc.qmul.ac.uk/).[12] Single-cell RNA sequencing (RNAseq) data for the RA synovium were acquired from the Accelerating Medicines Partnership phase II (AMP2) RA project (https://immunogenomics.io/ampra2/).[13]

RNAseq. RASFs (n = 7) were transfected as previously described with siRNA targeting *PAM* (siPAM) or siNTC. mRNA was extracted from cultured cells using Macherey-Nagel nucleospin mRNA kit (740955.50). Reverse transcription and RNAseq were conducted externally by Eurofins Scientific. The differential expression analysis of the RNAseq data was performed using edgeR package.[14]

ELISAs. Human ADM (EK-010-01) and PAMP (EK-010-05) ELISA kits were purchased from Phoenix Europe GmbH, and samples were analyzed as per the kit protocol. Transforming growth factor β1 (TGFβ1; DY240-05), interleukin-6 (IL-6; DY206-05), IL-8 (DY208-05), and TNFα (DY210) ELISA kits were purchased from R&D Systems, and samples were analyzed as per the kit protocol. ELISA plates were analyzed using BMG FLUOstar Omega plate reader.

Half-life analysis. ADM-NH_2 and ADM-Gly were added to RPMI media (supplemented with 10% FBS) at a concentration of 50 ng/μL and incubated at 37°C for 1, 2, 4, 8, or 24 hours and then stored at –20°C. The samples were then separated in a 15% polyacrylamide gel and analyzed via Western blot and densitometry. Half-life was determined by plotting the relative density of the ADM-NH_2 and ADM-Gly time courses and using a best-fit line to determine the time at which density reached 50%.

Collagen-induced arthritis mice. Eight-week-old male DBA/1 mice (Harlan) were maintained under conventional animal housing conditions in a specific pathogen–free setting in accordance with the UK Animals (Scientific Procedures) Act, 1986. Mice were immunized intradermally into the base of the tail with 50 μg/50 μL immunization Grade Bovine Type II collagen solution

(Amsbio) previously emulsified in complete Freund's adjuvant (Merck). On day 21 after the initial collagen immunization, the mice were intradermally boosted with 50 μg/50 μL bovine type II collagen emulsified in Freund's incomplete adjuvant. Severity of disease was graded by using a scale of 0 to 2. Scoring was based on amount and severity of joint swelling, mobility, skin condition, general appearance, bodyweight, body condition, and grimace score. siRNA targeting murine *Pam* (Ambion In Vivo siRNA, assay ID s224168) and nontargeting control (Ambion In Vivo Negative Control 1) were purchased from Thermo Fisher. siPAM efficiency was tested in N2A (mouse neuroblastoma) cells before commencing the experiment (Supplementary Data Figure 1). Mice were treated with 1 mg/kg siRNA against murine PAM (n = 8), siNTC (n = 8), or the vehicle control (n = 8). Three intravenous injections were given on days 20, 22, and 24. Seven mice were given dexamethasone administered intraperitoneal (0.5 mg/kg). The drug was given daily from day 20 until day 49. Three DBA/1 mice were not induced to have arthritis and were not treated.

Mass spectrometry. Supernatant from RASFs was collected following a four-hour incubation. Peptides were isolated and concentrated from the supernatant using PTMScan Peptide Purification Kit (Cell Signaling Technology, 35741) and eluate dried down in a speed vacuum concentrator, resuspended in 2M urea and reduced and alkylated using dithiothreitol and iodoacetamide, then digested with trypsin overnight at 37°C. Resultant peptide mixtures were analyzed via a Thermo Fisher Q-Exactive mass spectrometer coupled to a Dionex RSLCnano. Protein identification was performed with Maxquant (version 2.4.2) using a custom modification to detect the 58-Da loss ($-H_2C_2O_2$) resulting from the amidation of glycine.

Statistical analysis. Statistical analyses were conducted using SPSS version 29. Anderson–Darling and Shapiro–Wilk tests for normality were performed for all variables. For parametric data, two-tailed paired Student's *t*-test was used for paired samples and unpaired Student's *t*-test was used to compare independent groups. Nonparametric data were analyzed using a Kruskal–Wallis test. Linear regression (of log-transformed data) was used to determine $t_{1/2}$. All experiments were performed at least three times unless otherwise stated. All hypothesis testing assumes an α level of 0.05. Data will be shared upon request.

RESULTS

Genetically determined low PAM expression in RASFs is inversely correlated with inflammatory activity in RA. We measured expression of genes within 300 kilobases of rs26232 in RASFs by quantitative PCR (Figure 1A) based on the regional block of strong linkage disequilibrium (LD) between *MACIR* and *PAM*. The C allele was associated with lower *PAM* mRNA levels but was not linked with expression of *MACIR*, *PPIP5K2*, or *GIN1* (Figure 1B). Interrogation of the online Genotype-Tissue Expression database (https://www.gtexportal.org/home/) revealed similar associations in multiple human tissues (Figure 1C). Although we did not find rs26232 to be a cis-eQTL for any other nearby genes in RASFs, multiple such associations were detected in the GTEx database (Supplementary Data Table 3). Analysis of the Pathobiology of Early Arthritis database (https://peac.hpc.qmul.ac.uk/) showed highest *PAM* mRNA expression in the fibroblast-rich compared with either the lymphoid- or myeloid-rich synovial pathotypes (Figure 1D); furthermore, levels were inversely correlated with both systemic markers of inflammation, including C-reactive protein (Figure 1E), erythrocyte sedimentation rate (Figure 1F), ultrasound-assessed joint inflammation including synovial thickness (Figure 1G), and power Doppler vascular signal (Figure 1H). Single-cell RNAseq of RA synovial tissue from the AMP2 (https://immunogenomics.io/ampra2/) revealed the highest expression in all RASF subtypes, low levels in endothelium, and minimal expression in leucocyte subsets (Figure 1I; Supplementary Data Figure 2).[13] Fluorescent microscopy analysis demonstrated PAM localized to the Golgi apparatus in RASFs but not the cilia (Supplementary Data Figure 3). These data suggest that genetically associated low *PAM* expression in RASFs is linked with RA.

Inhibition of PAM expression increases tissue-damaging activities of RASFs and inflammation in the collagen-induced arthritis model. To explore the biologic roles of PAM, we used siRNA to target expression in nine RASF lines (Figure 2A). This resulted in increased invasiveness (+18%, P = 0.001; Figure 2B) and proliferation (+37%, P = 0.002; Figure 2C) and reduced apoptosis (–24%, P = 0.0003; Figure 2D); compared to siNTC-treated cells, migration was unaffected (Figure 2E). To determine whether the effects of PAM inhibition were mediated directly by amidation, we used the PAM enzymatic domain inhibitor PBA.[15] Incubation of RASFs with PBA resulted in similar effects to siRNA-mediated inhibition of invasiveness in matched samples, confirming amidation as the underlying mechanism (Figure 2F).

Having determined that PAM is an inhibitor of the pathologic activities of RASFs in vitro, we hypothesized that inhibition would result in greater disease activity in vivo. The collagen-induced arthritis model was used to test this concept in *Pam*-knockdown mice. Deletion of *Pam* is embryonically lethal in mice, so an siRNA strategy to knock down *Pam* was employed to overcome this.[16] Mice were injected with collagen at 0 and 21 days and with siRNA (NTC or *Pam*) at 20, 22, and 24 days. At four and five weeks post-immunization, the mean clinical score was significantly more severe in the mice deficient of *Pam* compared with mice treated with siNTC (P = 0.004; Figure 2G).

In RASFs inhibition of *PAM* expression resulted in increased levels of 1,242 transcripts, whereas 1,253 were decreased compared with siNTC-treated cells (Figure 2H), including genes linked

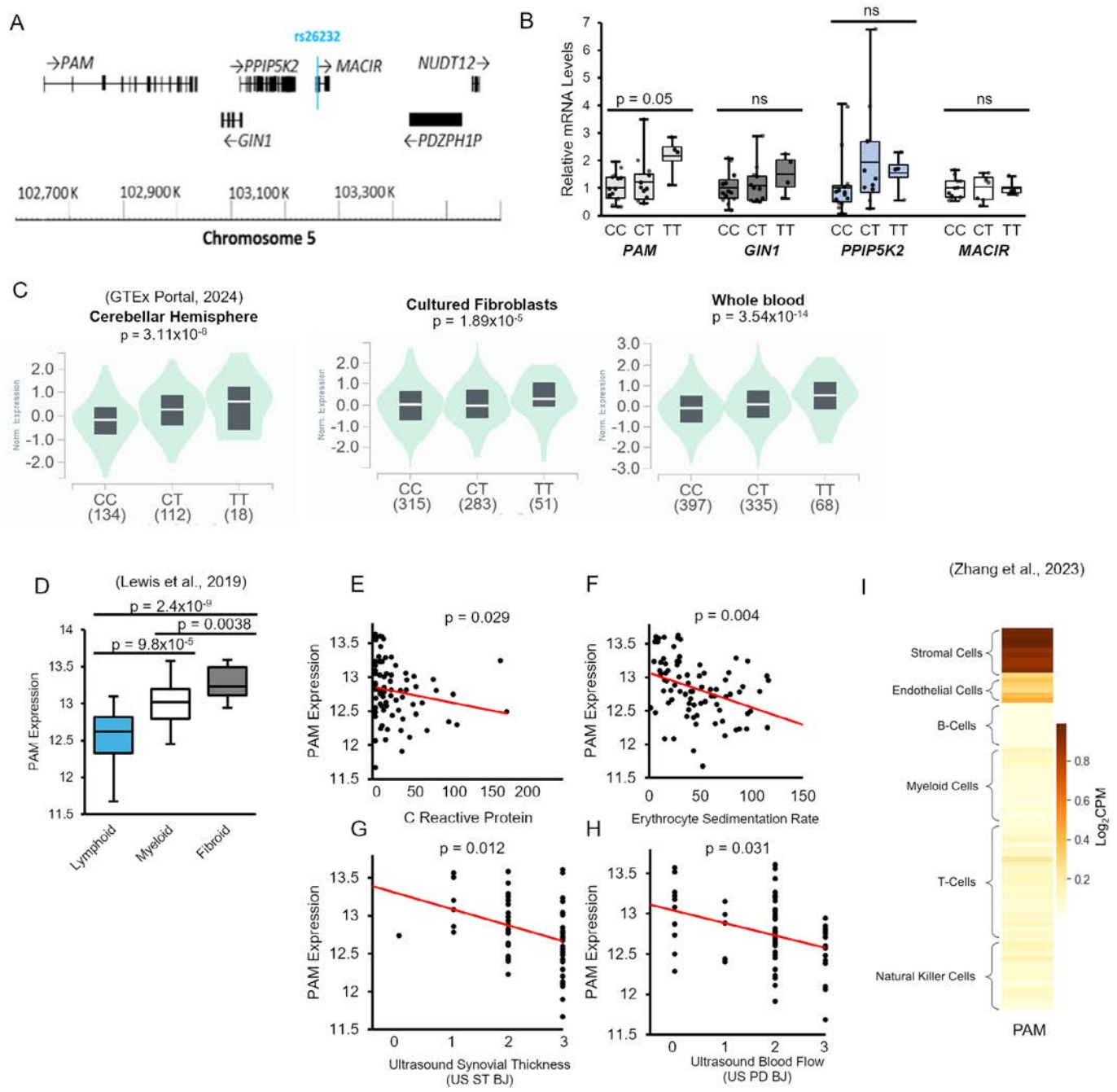

Figure 1. Relationship among rs26232 genotype, peptidylglycine alpha-amidating monooxygenase (PAM) expression, and rheumatoid arthritis (RA). (A) Annotation of genes in the locality of rs26232 (located within the first intron of *MACIR*). (B) Relative expression levels of *MACIR*, *PAM*, *GIN1*, and *PPIP5K2* in RA synovial fibroblasts (n = 33) by rs26232 genotype (CC, CT or TT). Kruskal–Wallis test was performed. (C) Association of rs26232 genotypes with PAM messenger RNA (mRNA) levels in human dermal fibroblasts, cerebellum, and whole blood in GTEx data. Rheumatoid synovial PAM mRNA levels and clinical activity in the Pathobiology of Early Arthritis study data (D) levels correlate with pathotype and inversely with measures of systemic inflammation, (E) C-reactive protein, (F) erythrocyte sedimentation rate, and ultrasound (US)-assessed synovitis including (G) synovial thickness (ST) and (H) blood flow. (I) Single-cell RNA sequencing in Accelerating Medicines Partnership phase II data showing subsets for cell lineages within the synovium. This reveals high level expression in all fibroblast subtypes with lower levels in endothelial cells and minimal expression in leucocytes. BJ, biopsy joint; CPM, counts per million; ns, not significant; PD, Power Doppler.

with proliferation, apoptosis, and invasion (Figure 2I). Of note was the reduced expression of *PRG4* (lubricin; $\log_2$ fold change –3.01, false discovery rate [FDR] $P = 1.06 \times 10^{-71}$; Figure 3F; Supplementary Data Table 4). PRG4 is a major constituent of synovial fluid, ensuring low frictional resistance in joints,[17] and has anti-inflammatory actions including reducing inflammatory cytokine–induced RASF proliferation.[18] PRG4 also regulates the balance of synovial macrophage subtypes, promoting a higher ratio of

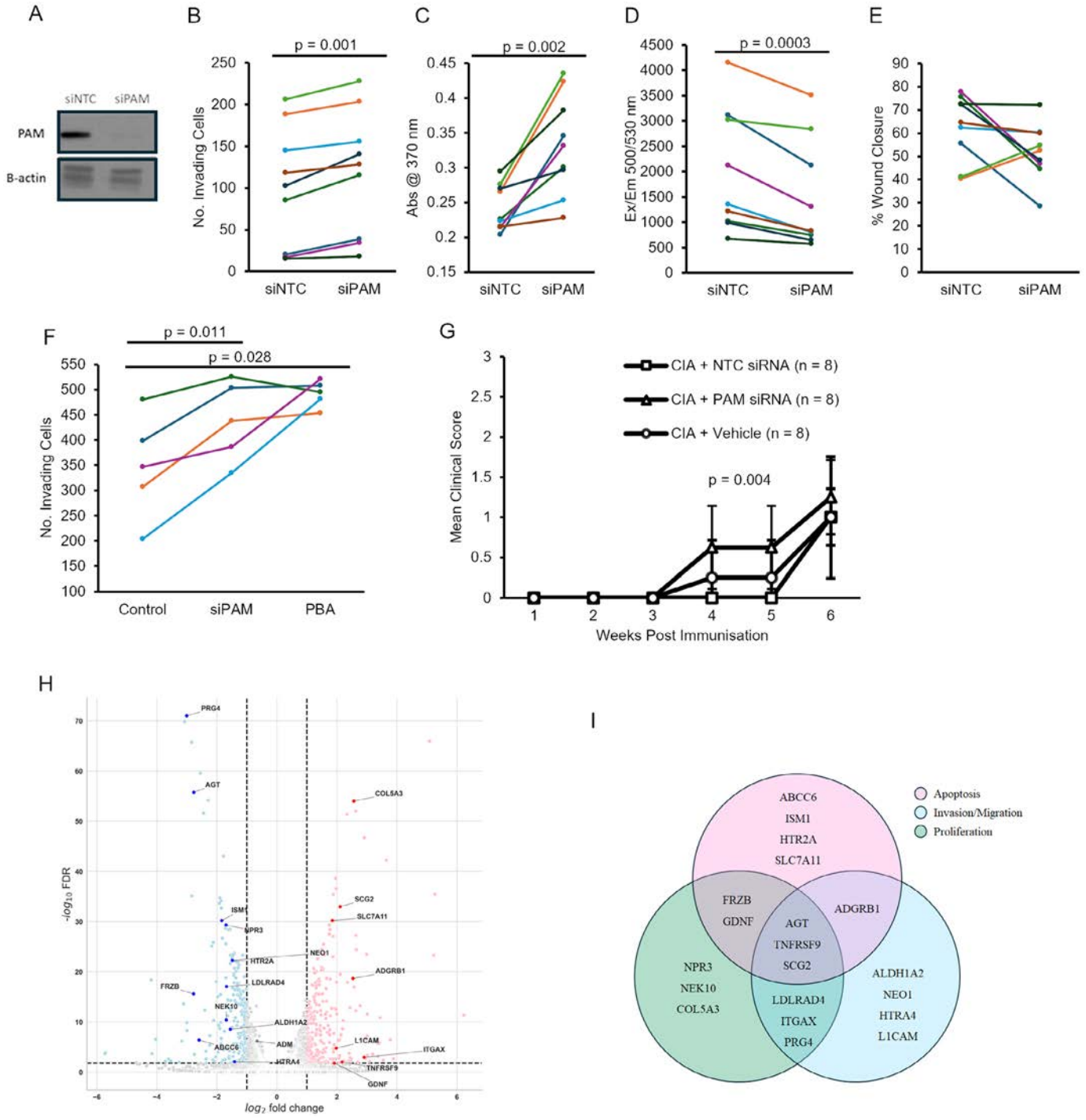

Figure 2. Effects of peptidylglycine alpha-amidating monooxygenase (PAM) inhibition on rheumatoid arthritis synovial fibroblast (RASF) biology. (A) Western blot demonstrating 92% reduction of PAM in RASFs following small interfering RNA targeting PAM (siPAM) treatment compared to nontargeting control small interfering RNA (siNTC). RASFs treated with siPAM showed significantly higher (B) proliferation, (C) invasion, and (D) lower apoptosis compared to RASFs treated with siNTC in n = 9 cell lines. (E) Migration rate was unaffected. (F) Inhibition of PAM enzymatic activity increased invasiveness in n = 5 cell lines, similar to treatment with siPAM. (G) Small interfering RNA (siRNA) knockdown of PAM in the collagen-induced arthritis (CIA) model increased clinical activity score at weeks 4 and 5 compared to mice treated with NTC (n = 8 each). (H) Volcano plot of RNA sequencing data from RASFs after siPAM treatment revealed differential expression of genes involved in (I) proliferation, invasion, and apoptosis pathways compared with siNTC. FDR, false discovery rate; No., number; PBA, 4-phenyl-3-butenoic acid. Color figure can be viewed in the online issue, which is available at http://onlinelibrary.wiley.com/doi/10.1002/art.70123/abstract.

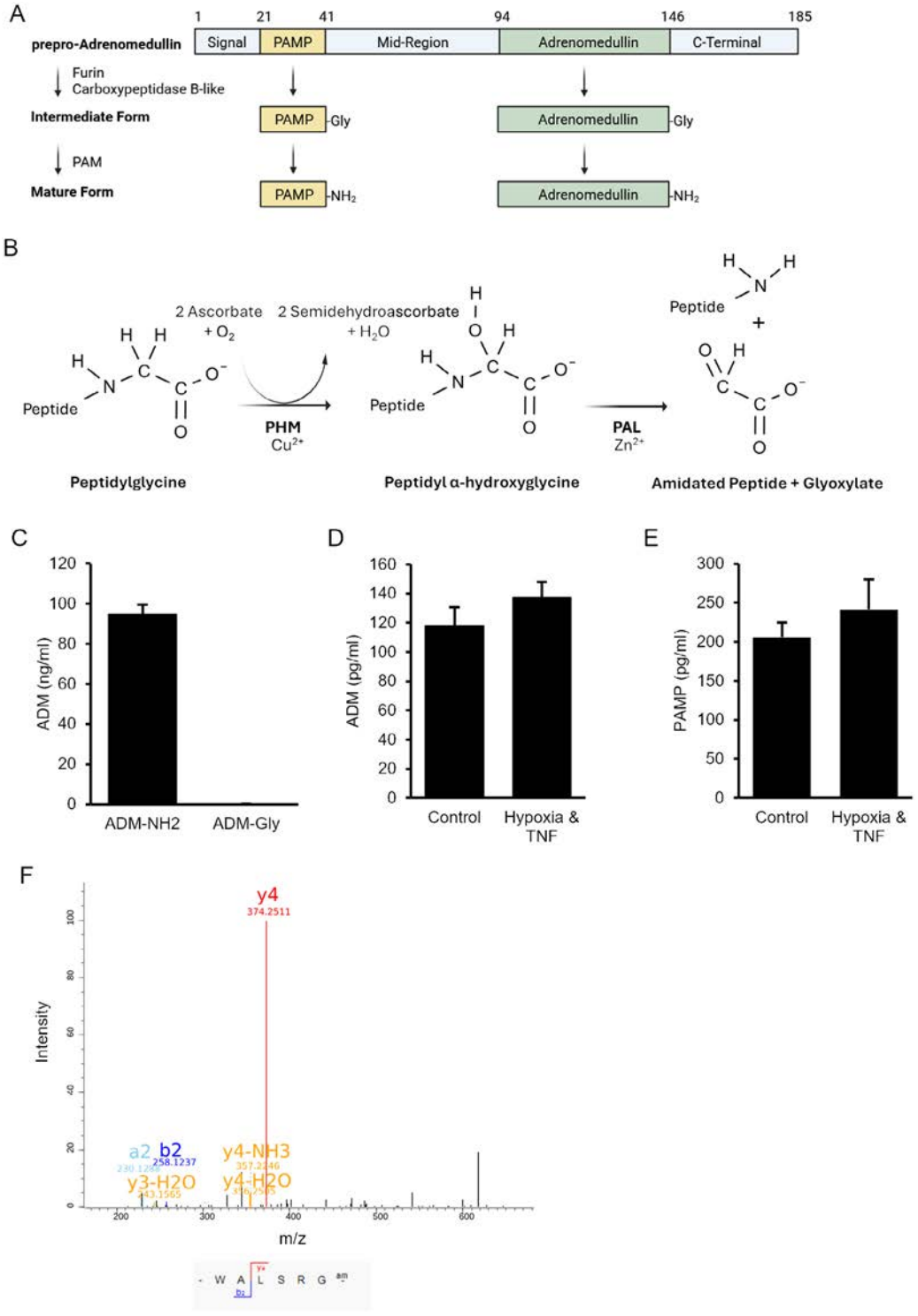

Figure 3. Identification of amidated peptides in rheumatoid arthritis synovial fibroblast (RASF) secretome. (A) Processing of preproadrenomedullin (ADM) into amidated ADM (ADM-NH_2) and amidated pro-ADM N-terminal peptide (PAMP-NH_2). (B) Amidation of peptidylglycine substrates by peptidylglycine alpha-amidating monooxygenase (PAM). (C) ADM enzyme-linked immunosorbent assay (ELISA) is specific for ADM-NH_2 using ADM-NH_2 and glycine-extended ADM (ADM-Gly) peptides. (D) Detection of ADM-NH_2 in RASF supernatants (n = 3) via ELISA in control and hypoxia/tumor necrosis factor (TNF) conditions. (E) Detection of total PAMP in RASF supernatants (n = 3) via ELISA in control and hypoxia/TNF conditions. (F) Mass spectrometry/mass spectrometry spectra of PAMP-NH_2 detected in RASF supernatant. PAL, peptidylglycine amidoglycolate lyase; PAMP-Gly, glycine-extended PAMP; PHM, peptidyl alpha-hydroxylating monooxygenase. Color figure can be viewed in the online issue, which is available at http://onlinelibrary.wiley.com/doi/10.1002/art.70123/abstract.

$CD86^-/CD206^+$ (M2) to $CD86^+/CD206^-$ (M1).[3] Loss-of-function mutations in *PRG4* cause an autosomal recessive condition that includes synovial hyperplasia, joint swelling, and damage.[19]

RASFs secrete amidated peptides, including ADM and PAMP. Because amidation is an underlying mechanism regulating RASF invasiveness, it was important to identify the amidated proteome of RASFs. Transcriptomic analysis revealed several preprohormone peptides that are expressed in RASFs (Supplementary Data Table 5). The highest expressed was *ADM*, which encodes two peptides that are both amidated: ADM and PAMP. *ADM* was significantly down-regulated in siPAM-treated RASFs compared to siNTC (FDR $P = 6.63^{-7}$).

Prepro-ADM is processed posttranslationally by the prohormone convertase furin and a carboxypeptidase B-type enzyme to produce ADM and PAMP[20] (Figure 3A). PAM then carries out amidation by conversion of the penultimate residue of the peptidylglycine substrate into an alpha amide. The peptidyl alpha-hydroxylating monooxygenase domain catalyzes the hydroxylation of the alpha carbon, followed by the peptidylglycine amidoglycolate lyase domain cleaving the N-C-alpha bond to produce an alpha-amidated peptide and glyoxylate[21] (Figure 3B). Amidation is oxygen dependent, and PAM is induced by hypoxia (Supplementary Data Figure 4A and B), which allows PAM to function in the low-oxygen environment of the RA joint. This is demonstrated by the detection of ADM-NH_2 in the RASF secretome under hypoxic conditions (Supplementary Data Figure 4C).

Specificity of the ADM ELISA for ADM-NH_2 was confirmed by using peptides, which demonstrate detection of ADM-NH_2 only (Figure 3C). ADM-NH_2 secretion from RASFs was confirmed by ELISA and was not influenced by either hypoxia or TNFα (Figure 3D). Total PAMP secretion was measured by ELISA, with hypoxia and TNFα having no effect (Figure 3E). PAMP-NH_2 secretion was confirmed using mass spectroscopy (Figure 3F).

ADM-NH_2 and PAMP-NH_2 inhibit RASF inflammatory cytokine production and invasiveness. ADM is a signaling peptide with anti-inflammatory effects on an RA animal model[22] and has shown efficacy in early-stage therapeutic trials of inflammatory bowel diseases.[23] Little is known about the biologic activities of PAMP in inflammation. Peptide amidation has been shown to increase half-life and receptor affinity.[24] We used an in vitro assay to measure half-life; this revealed ADM-NH_2 to have a significantly longer half-life than ADM-Gly; 21 versus 10.9 hours, respectively (Figure 4A and B). Additionally, ADM-NH_2 has been reported to bind its cognate receptor with 40-fold greater affinity compared with ADM-Gly.[25] Amidation of ADM therefore results in greater bioactivity.

We next compared the effects of amidated and non–ADM-NH_2 and PAMP-NH_2 on TNFα-induced inflammatory cytokine production by RASFs; incubation with both forms of PAMP inhibited IL-6 production, with PAMP-NH_2 being more potent (–30%, $P = 0.047$); ADM variants did not have an effect (Figure 4C). Similarly, both versions of PAMP inhibited IL-8 production, with PAMP-NH_2 having a greater effect (–23%, $P = 0.02$; Figure 4D). The invasiveness of RASFs was reduced upon incubation with ADM-NH_2 (–19%, $P = 0.03$) and PAMP-NH_2 (–30%, $P = 0.036$) compared to their glycine-extended precursors; culture with both peptides resulted in greater reduction than either alone (–38%, $P = 0.043$; Figure 4E).

ADM-NH_2 induces expression of PRG4 via TGFβ reducing RASF tissue–damaging activities. The reduction of *PRG4* expression following PAM inhibition was intriguing given the formers critical role in joint homeostasis[26] and inflammation.[3] The therapeutic benefits of ADM-NH_2 administration to models of RA[27] and inflammatory bowel diseases[28,29] have been linked with up-regulation of TGFβ production. *PRG4* expression is up-regulated by TGFβ and inhibited by IL-1 and TNFα.[30] We hypothesized that ADM-NH_2 may induce higher *PRG4* via TFGβ, resulting in altered RASF-associated tissue-damaging activities. Incubation of RASFs with ADM-NH_2 and PAMP-NH_2 resulted in significantly greater TGFβ than culture with glycine-extended versions (ADM-NH_2 +86%, $P = 0.023$; PAMP-NH_2 +38%, $P = 0.037$; Figure 5A). We next determined the effect of PRG4 on RASF activities using siRNA (Figure 5B). RASFs transfected with siPRG4 (n = 5) displayed greater invasiveness (+118%, $P = 0.003$) (Figure 5C) and proliferation (+7%, $P = 0.03$; Figure 5D), whereas apoptosis was reduced (–13%, $P = 0.048$; Figure 5D) compared to siNTC-exposed cells; migration was not significantly changed (Figure 5F). These results are broadly similar to those resulting from *PAM* inhibition (Figure 2B–E).

Inhibition of amidation shifts macrophages toward a proinflammatory state. Signals from RASFs can modulate synovial macrophage polarization and disease activity.[31] To determine the role of amidation in mediating macrophage polarity, we used an RASF–macrophage coculture model and PBA. Inhibition of amidation increased M1 macrophages ($MerTK^-CD48^+$ [+29%, $P = 0.001$] and $MerTK^-CD86^+$ [+31%, $P = 0.001$]; Figure 6A and B, respectively) and decreased M2 macrophages ($MerTK^+CD86^-$ [–32%, $P = 0.004$], $MerTK^+CD48^+$ [–12%, $P = 0.001$], and $MerTK^+CD86^+$ [–11%, $P = 0.002$] compared to control; Figure 6C–E). Incubation of macrophages alone with PBA had no effect on polarization (Supplementary Data Figure 5), indicating that the effect is mediated by a secreted amidated product of RASFs.

We next determined whether ADM and PAMP had effects on the release of proinflammatory cytokines by LPS-induced macrophages (Figure 6F and G). Compared to control, ADM-NH_2 reduced secretion of IL-8 (–55%, $P = 0.011$) and TNFα

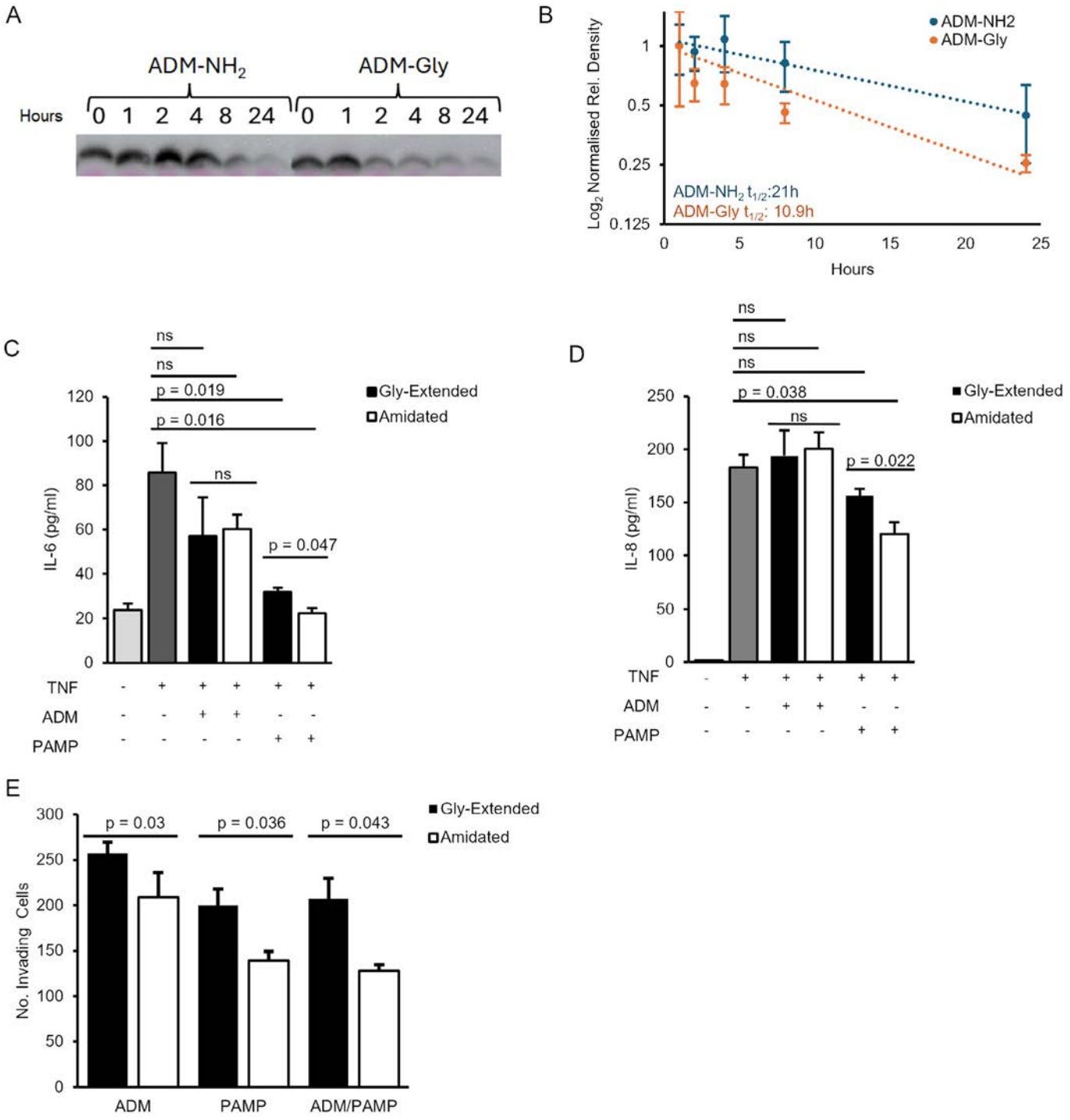

Figure 4. Amidated adrenomedullin (ADM-NH_2) and amidated pro-ADM N-terminal peptide (PAMP-NH_2) inhibit rheumatoid arthritis synovial fibroblast (RASF) inflammatory cytokine production and invasiveness. (A) Western blot and (B) ADM-NH_2 and glycine-extended ADM (ADM-Gly) degradation time course, ADM-NH_2 half-life is 21 hours (h), ADM-Gly half-life is 10.9 h. RASFs were incubated with tumor necrosis factor (TNF) and ADM or PAMP peptides. (C) Interleukin-6 (IL-6) production was reduced by PAMP-NH_2 and glycine-extended PAMP (PAMP-Gly), with the former having a greater effect. (D) IL-8 production was not altered by either form of ADM, only PAMP-NH_2 had a significant effect. (E) Amidated peptides had greater suppressive effects on RASF invasiveness compared with glycine-extended peptides. No., number; ns, not significant; Rel., relative. Color figure can be viewed in the online issue, which is available at http://onlinelibrary.wiley.com/doi/10.1002/art.70123/abstract.

(–47%, P = 0.002), whereas ADM-Gly had no significant impact for either cytokine compared to control. ADM-NH_2 reduced IL-8 (–42%, P = 0.032) and TNFα (–43%, P = 0.024) compared to ADM-Gly. Both PAMP-NH_2 (–37%, P = 0.04) and PAMP-Gly (–42%, P = 0.032) reduced IL-8 secretion compared to control, whereas only PAMP-Gly (–27%, P = 0.015) reduced TNFα

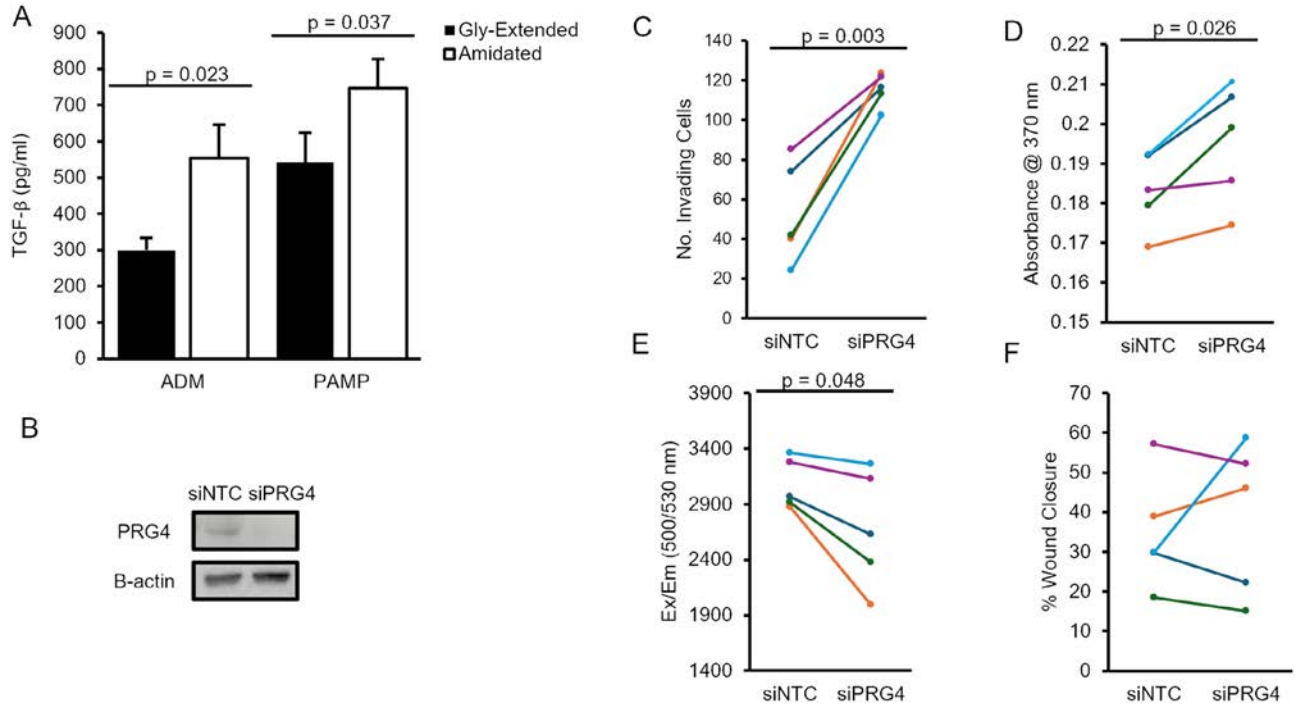

Figure 5. Amidated adrenomedullin (ADM-NH_2) and amidated pro-ADM N-terminal peptide (PAMP-NH_2) induce expression PRG4 via transforming growth factor β (TGFβ), resulting in reduced rheumatoid arthritis synovial fibroblast (RASF) tissue–damaging activities. (A) TGFβ secretion is higher in tumor necrosis factor–stimulated RASFs exposed to ADM-NH_2 or PAMP-NH_2 compared with glycine (Gly)-extended peptides. (B) RASF PRG4 protein levels are reduced by small interfering RNA targeting PRG4 (siPRG4) treatment compared to nontargeting control small interfering RNA (siNTC). Inhibition of PRG4 leads to significantly greater (C) proliferation, (D) invasion, (E) lower apoptosis, and (F) no significant difference in migration compared to RASFs treated with siNTC in n = 5 cell lines. Ex/Em, excitation/emission; No., number. Color figure can be viewed in the online issue, which is available at http://onlinelibrary.wiley.com/doi/10.1002/art.70123/abstract.

secretion compared to control. There was no significant difference observed between PAMP-NH_2 and PAMP-Gly on IL-8 or TNFα secretion.

DISCUSSION

Our data reveal the RA susceptibility and severity associated variant rs26232 to be an eQTL for *PAM*, with the risk C allele linked with low expression in RASFs. The resultant reduced levels of ADM-NH_2 and PAMP-NH_2 increase the inflammatory and tissue damage activities of RASFs and drive macrophages to proinflammatory subtypes. We show that the downstream effect on RASFs is influenced by TGFβ-induced PRG4 activity.

PAM has critical functions in the posttranslational modification of inactive peptidylglycine precursors to bioactive alpha-amidated peptides and is mainly present in the secretory pathway.[32] Ablation of *PAM* is embryonically lethal; heterozygote knockout mice have behavioral and metabolic defects.[16] It has roles in cytoskeletal organization as a secretagogue and in modulating gene expression.[33] Expression of *PAM* has similar sensitivity to hypoxia as hypoxia-inducible factor hydroxylases, whereas the activity of the PHL domain of PAM is oxygen dependent and falls linearly from 10% to 0% O_2.[34] Despite the RA synovium being hypoxic with O_2 of 3%,[35] we detected peptide amidation occurring in RASFs cultured in these conditions.

The invasive activities of RASFs in vitro are positively correlated with the rate of radiologically assessed joint damage over subsequent years.[5] The rs26232 C variant is associated with greater radiologic damage, and RASFs of this genotype are more invasive and express higher levels of chemokines and adhesion molecules.[11] Our data are consistent with a model in which lower amidation of ADM and PAMP results in increased inflammatory cytokine production and invasiveness of RASFs, and this is related to lower TGFβ-induced *PRG4* production. PRG4 is a key regulator of synovial joint homeostasis, having both important mechanical and anti-inflammatory effects.[26]

AMP2 data demonstrate that PAM expression is significantly higher in RASFs compared to all other cell types in the synovium. This suggests that RASFs are the most important source of amidated peptides in the RA synovium, though the study of other synovial cell types, particularly endothelial, is warranted. Although *PAM* is not expressed in immune cells, by using an RASF–macrophage coculture model, we found that pharmacological inhibition with PBA increased polarization toward proinflammatory $MerTK^-CD48^+$ and $MerTK^-CD86^+$ macrophages and reduced anti-inflammatory $MerTK^+CD48^+$, $MerTK^+CD86^+$, and $MerTK^+CD86^-$ macrophages. $MerTK^+$ macrophages are

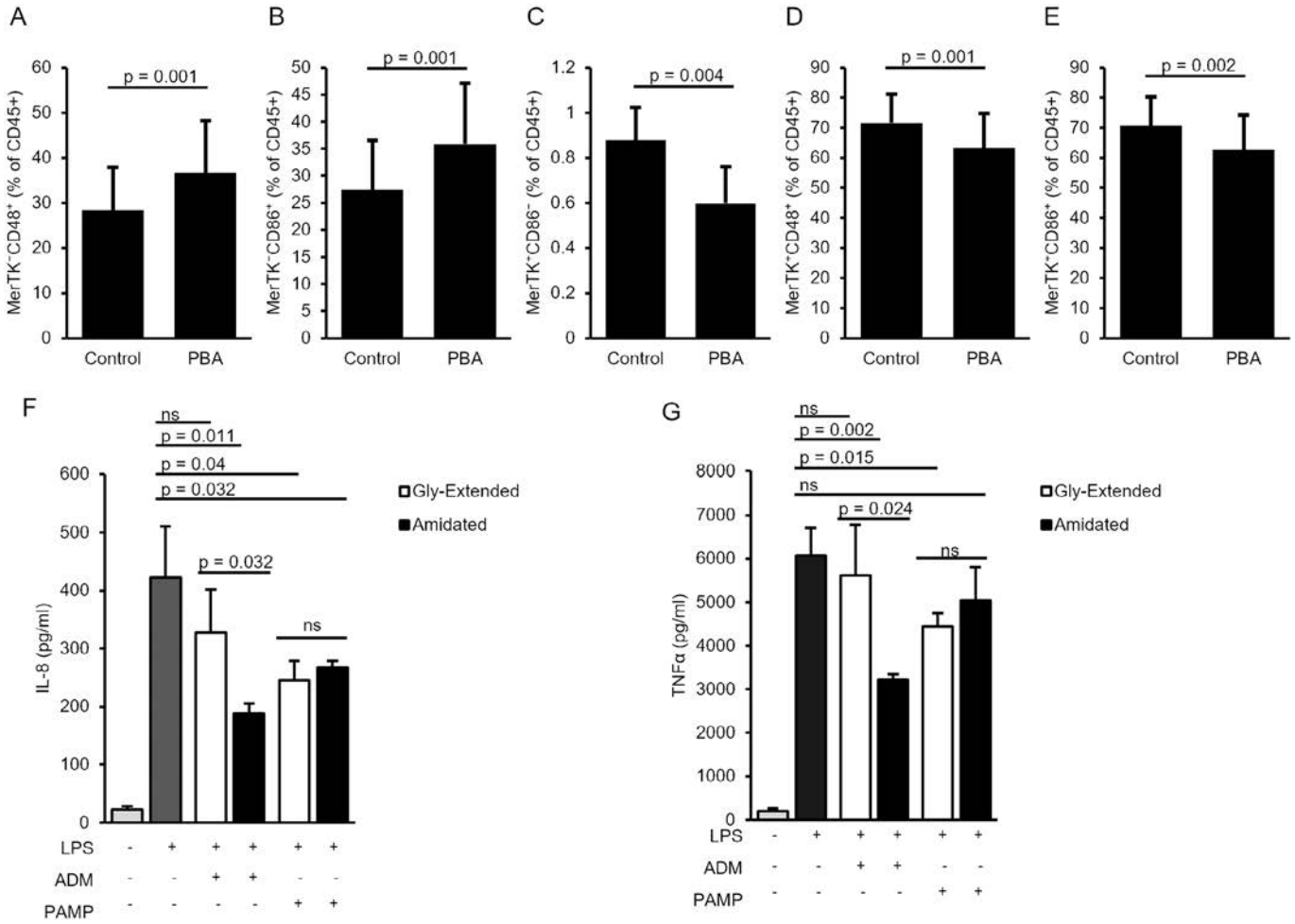

Figure 6. Inhibition of amidation in rheumatoid arthritis synovial fibroblasts (RASFs) results in a shift from M2 to M1 macrophages. Flow cytometry data demonstrating an increase in (A) MerTK$^-$CD48$^+$ and (B) MerTK$^-$CD86$^+$ macrophages and decrease in (C) MerTK$^+$CD86$^-$, (D) MerTK$^+$CD48$^+$, and (E) MerTK$^+$CD86$^+$ macrophages in RASF–macrophage cocultures incubated with 4-phenyl-3-butenoic acid (PBA). Macrophages were incubated with lipopolysaccharide (LPS) and adrenomedullin (ADM) or pro-ADM N-terminal peptide (PAMP) peptides. (F) Interleukin-8 (IL-8) production was reduced by amidated ADM (ADM-NH_2), but not glycine (Gly)-extended ADM, and by amidated PAMP and Gly-extended PAMP (PAMP-Gly). (G) Tumor necrosis factor (TNF) production was reduced by ADM-NH_2 and PAMP-Gly only. ns, not significant.

enriched in healthy controls/RA remission and are associated with lower disease activity and inflammation markers. MerTK$^-$ macrophages are enriched in patients with active RA and are associated with higher disease activity and inflammation markers.[31] In this way, genetically determined decreased levels of *PAM* can shift macrophages toward a proinflammatory population, which increases inflammation and disease severity. In the RASF secretome, ADM is the most highly expressed amidated peptide. These data are consistent with data showing that administration of ADM to an animal model of uveitis resulted in decreased inflammation, greater TGFβ expression, and a shift to M2 macrophages.[36]

Our data complement GWAS in several other common human diseases; susceptibility to Parkinson disease (PD) is associated with rs26431 C allele,[37] which is in LD with rs26232 C (D' = 0.73, r^2 = 0.53 in 1,000 genomes european cohort), and primary biliary cirrhosis (PBC) is associated with the rs526231 C allele,[38] which is also in LD with rs26232 C (D' = 0.92, r^2 = 0.84 in 1,000 genomes european cohort). GTEx data reveal *PAM* to be highly expressed in the brain but minimally in the liver, perhaps implicating a low-frequency cell type in the pathogenesis of PBC or the effect of an amidated peptide produced extrahepatically. Low-frequency nonsynonymous *PAM* variants have been associated with risk of type 2 diabetes, which is attributed to reduced amidation of chromogranin A, leading to lower insulin secretion by pancreatic β cells.[39] Characterizing the amidated proteome of disease-relevant tissues in PD and PBC may reveal the mechanisms by which low PAM activity contributes to the pathogenesis of these conditions.

Our data reveal an important new mechanism regulating fibroblast-mediated tissue damage in RA, representing the first known role for PAM in both RA and fibroblast biology. We also

demonstrate the impact of amidated peptides on macrophages, showing that PAM has an effect beyond fibroblasts in RA. Most of the recent advances in RA treatment have targeted immune cells; although highly clinically effective, the resulting immunosuppression increases the risk of infection.[40] This risk is believed to be lower using treatments centered on fibroblasts. Therapies based on systemic administration of amidated proteins, such as ADM and PAMP, may be effective in RA with the added potential of using rs26232 genotype to preidentify patients most likely to benefit from such agents.

ACKNOWLEDGMENTS

We are grateful to our late colleague Professor Douglas Veale for access to synovial biopsy samples. We thank our patient and public Research Advisory Panel for input throughout the study. We would like to thank Dr Alison Gartland (University of Sheffield) because the animal component was conducted on her Home Office project license.

AUTHOR CONTRIBUTIONS

All authors contributed to at least one of the following manuscript preparation roles: conceptualization AND/OR methodology, software, investigation, formal analysis, data curation, visualization, and validation AND drafting or reviewing/editing the final draft. As corresponding author, Dr Sheridan confirms that all authors have provided the final approval of the version to be published, and takes responsibility for the affirmations regarding article submission (eg, not under consideration by another journal), the integrity of the data presented, and the statements regarding compliance with institutional review board/Declaration of Helsinki requirements. All authors contributed to the investigation, formal analysis of the data, and writing, reviewing, and editing of the manuscript.

REFERENCES

1. Knevel R, Gröndal G, Huizinga TW, et al. Genetic predisposition of the severity of joint destruction in rheumatoid arthritis: a population-based study. Ann Rheum Dis 2012;71(5):707–709. doi:https://doi.org/10.1136/annrheumdis-2011-200627
2. Walsh AM, Whitaker JW, Huang CC, et al. Integrative genomic deconvolution of rheumatoid arthritis GWAS loci into gene and cell type associations. Genome Biol 2016;17(1):79. doi:https://doi.org/10.1186/s13059-016-0948-6
3. Qadri M, Jay GD, Zhang LX, et al. Proteoglycan-4 is an essential regulator of synovial macrophage polarization and inflammatory macrophage joint infiltration. Arthritis Res Ther 2021;23(1):241. doi:https://doi.org/10.1186/s13075-021-02621-9 Erratum in: Arthritis Res Ther 2021;23:276.
4. Lefèvre S, Knedla A, Tennie C, et al. Synovial fibroblasts spread rheumatoid arthritis to unaffected joints. Nat Med 2009;15(12):1414–1420. doi:https://doi.org/10.1038/nm.2050
5. Tolboom TC, van der Helm-Van Mil AH, Nelissen RG, et al. Invasiveness of fibroblast-like synoviocytes is an individual patient characteristic associated with the rate of joint destruction in patients with rheumatoid arthritis. Arthritis Rheum 2005;52(7):1999–2002. doi:https://doi.org/10.1002/art.21118
6. Stahl EA, Raychaudhuri S, Remmers EF, et al; BIRAC Consortium; YEAR Consortium. Genome-wide association study meta-analysis identifies seven new rheumatoid arthritis risk loci. Nat Genet 2010;42(6):508–514. doi:https://doi.org/10.1038/ng.582
7. Viatte S, Plant D, Bowes J, et al. Genetic markers of rheumatoid arthritis susceptibility in anti-citrullinated peptide antibody negative patients. Ann Rheum Dis 2012;71(12):1984–1990. doi:https://doi.org/10.1136/annrheumdis-2011-201225
8. Teare MD, Knevel R, Morgan MD, et al. Allele-dose association of the C5orf30 rs26232 variant with joint damage in rheumatoid arthritis. Arthritis Rheum 2013;65(10):2555–2561. doi:https://doi.org/10.1002/art.38064
9. Muthana M, Hawtree S, Wilshaw A, et al. C5orf30 is a negative regulator of tissue damage in rheumatoid arthritis. Proc Natl Acad Sci U S A 2015;112(37):11618–11623. doi:https://doi.org/10.1073/pnas.1501947112
10. Dorris ER, Tazzyman SJ, Moylett J, et al. The autoimmune susceptibility gene *C5orf30* regulates macrophage-mediated resolution of inflammation. J Immunol 2019;202(4):1069–1078. doi:https://doi.org/10.4049/jimmunol.1801155
11. Dorris ER, Linehan E, Trenkmann M, et al. Association of the rheumatoid arthritis severity variant rs26232 with the invasive activity of synovial fibroblasts. Cells 2019;8(10):1300. doi:https://doi.org/10.3390/cells8101300
12. Lewis MJ, Barnes MR, Blighe K, et al. Molecular portraits of early rheumatoid arthritis identify clinical and treatment response phenotypes. Cell Reports 2017;28(9): 2455-2470.e5. https://doi.org/10.1016/j.celrep.2019.07.091
13. Zhang F, Jonsson AH, Nathan A, et al; Accelerating Medicines Partnership: RA/SLE Network. Deconstruction of rheumatoid arthritis synovium defines inflammatory subtypes. Nature 2023;623(7987):616–624. doi:https://doi.org/10.1038/s41586-023-06708-y
14. Robinson MD, McCarthy DJ, Smyth GK. edgeR: a Bioconductor package for differential expression analysis of digital gene expression data. Bioinformatics 2010;26(1):139–140. doi:https://doi.org/10.1093/bioinformatics/btp616
15. Mueller GP, Driscoll WJ, Eipper BA. In vivo inhibition of peptidylglycine-alpha-hydroxylating monooxygenase by 4-phenyl-3-butenoic acid. J Pharmacol Exp Ther 1999;290(3):1331–1336. doi:https://doi.org/10.1016/S0022-3565(24)35039-6
16. Gaier ED, Eipper BA, Mains RE. Pam heterozygous mice reveal essential role for Cu in amygdalar behavioral and synaptic function. Ann N Y Acad Sci 2014;1314(1):15–23. doi:https://doi.org/10.1111/nyas.12378
17. Coles JM, Zhang L, Blum JJ, et al. Loss of cartilage structure, stiffness, and frictional properties in mice lacking PRG4. Arthritis Rheum 2010;62(6):1666–1674. doi:https://doi.org/10.1002/art.27436
18. Al-Sharif A, Jamal M, Zhang LX, et al. Lubricin/proteoglycan 4 binding to CD44 receptor: a mechanism of the suppression of proinflammatory cytokine-induced synoviocyte proliferation by lubricin. Arthritis Rheumatol 2015;67(6):1503–1513. doi:https://doi.org/10.1002/art.39087
19. Marcelino J, Carpten JD, Suwairi WM, et al. CACP, encoding a secreted proteoglycan, is mutated in camptodactyly-arthropathy-coxa vara-pericarditis syndrome. Nat Genet 1999;23(3):319–322. doi:https://doi.org/10.1038/15496
20. Kim W, Essalmani R, Szumska D, et al. Loss of endothelial furin leads to cardiac malformation and early postnatal death. Mol Cell Biol 2012;32(17):3382–3391. doi:https://doi.org/10.1128/MCB.06331-11
21. Prigge ST, Kolhekar AS, Eipper BA, et al. Amidation of bioactive peptides: the structure of peptidylglycine alpha-hydroxylating monooxygenase. Science 1997;278(5341):1300–1305. doi:https://doi.org/10.1126/science.278.5341.1300
22. Ah Kioon M-D, Asensio C, Ea H-K, et al. Adrenomedullin(22-52) combats inflammation and prevents systemic bone loss in murine collagen-induced arthritis. Arthritis Rheum 2012;64(4):1069–1081. doi:https://doi.org/10.1002/art.33426

23. Kita T, Ashizuka S, Takeda T, et al. Adrenomedullin for biologic-resistant Crohn's disease: a randomized, double-blind, placebo-controlled phase 2a clinical trial. J Gastroenterol Hepatol 2022; 37(11):2051–2059. doi:https://doi.org/10.1111/jgh.15945
24. Wettergren A, Pridal L, Wøjdemann M, et al. Amidated and non-amidated glucagon-like peptide-1 (GLP-1): non-pancreatic effects (cephalic phase acid secretion) and stability in plasma in humans. Regul Pept 1998;77(1-3):83–87. doi:https://doi.org/10.1016/S0167-0115(98)00044-5
25. Eguchi S, Hirata Y, Iwasaki H, et al. Structure-activity relationship of adrenomedullin, a novel vasodilatory peptide, in cultured rat vascular smooth muscle cells. Endocrinology 1994;135(6):2454–2458. doi: https://doi.org/10.1210/endo.135.6.7988431
26. Maenohara Y, Chijimatsu R, Tachibana N, et al. Lubricin contributes to homeostasis of articular cartilage by modulating differentiation of superficial zone cells. J Bone Miner Res 2021;36(4):792–802. doi: https://doi.org/10.1002/jbmr.4226
27. Gonzalez-Rey E, Chorny A, O'Valle F, et al. Adrenomedullin protects from experimental arthritis by down-regulating inflammation and Th1 response and inducing regulatory T cells. Am J Pathol 2007;170(1): 263–271. doi:https://doi.org/10.2353/ajpath.2007.060596
28. Ashizuka S, Inagaki-Ohara K, Kuwasako K, et al. Adrenomedullin treatment reduces intestinal inflammation and maintains epithelial barrier function in mice administered dextran sulphate sodium. Microbiol Immunol 2009;53(10):573–581. doi:https://doi.org/10.1111/j.1348-0421.2009.00159.x
29. Gonzalez-Rey E, Chorny A, Varela N, et al. Urocortin and adrenomedullin prevent lethal endotoxemia by down-regulating the inflammatory response. Am J Pathol 2006;168(6):1921–1930. doi:https://doi.org/10.2353/ajpath.2006.051104
30. Jones AR, Flannery CR. Bioregulation of lubricin expression by growth factors and cytokines. Eur Cell Mater 2007;13:40–45. doi: https://doi.org/10.22203/eCM.v013a04
31. Alivernini S, MacDonald L, Elmesmari A, et al. Distinct synovial tissue macrophage subsets regulate inflammation and remission in rheumatoid arthritis. Nat Med 2020;26(8):1295–1306. doi:https://doi.org/10.1038/s41591-020-0939-8
32. Lindberg I, Glembotski CC. Physiological signaling in the absence of amidated peptides. Proc Natl Acad Sci U S A 2019;116(40):19774–19776. doi:https://doi.org/10.1073/pnas.1914001116
33. Francone VP, Ifrim MF, Rajagopal C, et al. Signaling from the secretory granule to the nucleus: Uhmk1 and PAM. Mol Endocrinol 2010;24(8): 1543–1558. doi:https://doi.org/10.1210/me.2009-0381
34. Simpson PD, Eipper BA, Katz MJ, et al. Striking oxygen sensitivity of the peptidylglycine α-amidating monooxygenase (PAM) in neuroendocrine cells. J Biol Chem 2015;290(41):24891–24901. doi:https://doi.org/10.1074/jbc.M115.667246
35. Ng CT, Biniecka M, Kennedy A, et al. Synovial tissue hypoxia and inflammation in vivo. Ann Rheum Dis 2010;69(7):1389–1395. doi: https://doi.org/10.1136/ard.2009.119776
36. Matsuda Y, Tanaka M, Zhao Y, et al. Adrenomedullin-RAMP2 system modulates inflammation and tissue repair in experimental autoimmune uveitis via T-cell and M2 macrophage regulation. Invest Ophthalmol Vis Sci 2025;66(6):12. doi:https://doi.org/10.1167/iovs.66.6.12
37. Nalls MA, Blauwendraat C, Vallerga CL, et al; 23andMe Research Team; System Genomics of Parkinson's Disease Consortium; International Parkinson's Disease Genomics Consortium. Identification of novel risk loci, causal insights, and heritable risk for Parkinson's disease: a meta-analysis of genome-wide association studies. Lancet Neurol 2019;18(12):1091–1102. doi:https://doi.org/10.1016/S1474-4422(19)30320-5
38. Cordell HJ, Han Y, Mells GF, et al; Canadian-US PBC Consortium; Italian PBC Genetics Study Group; UK-PBC Consortium. International genome-wide meta-analysis identifies new primary biliary cirrhosis risk loci and targetable pathogenic pathways. Nat Commun 2015; 6(1):8019. doi:https://doi.org/10.1038/ncomms9019
39. Thomsen SK, Raimondo A, Hastoy B, et al. Type 2 diabetes risk alleles in PAM impact insulin release from human pancreatic β-cells. Nat Genet 2018;50(8):1122–1131. doi:https://doi.org/10.1038/s41588-018-0173-1
40. Jones DS, Jenney AP, Swantek JL, et al. Profiling drugs for rheumatoid arthritis that inhibit synovial fibroblast activation. Nat Chem Biol 2017;13(1):38–45. doi:https://doi.org/10.1038/nchembio.2211

Arthritis & Rheumatology
Vol. 78, No. 9, September 2026, pp 1850–1862
DOI 10.1002/art.70098
© 2026 The Author(s). *Arthritis & Rheumatology* published by Wiley Periodicals LLC on behalf of American College of Rheumatology.
This is an open access article under the terms of the Creative Commons Attribution-NonCommercial-NoDerivs License, which permits use and distribution in any medium, provided the original work is properly cited, the use is non-commercial and no modifications or adaptations are made.

American College of Rheumatology
Empowering Rheumatology Professionals

Tissue-Specific and Spatially Dependent Metabolic Signatures Perturbed by Injury in Male and Female Mice

Hope D. Welhaven, PhD,[1] Avery H. Welfley, BS,[2] Priyanka P. Brahmachary, PhD,[2] Mark Greenwood, PhD,[3] Donald F. Smith, PhD,[1] Brian Bothner, PhD,[1] and Ronald K. June, PhD[2]

Objective. Osteoarthritis, the leading cause of disability worldwide, disproportionately affects women, yet sex remains an overlooked determinant. This disparity stems from sex-specific differences in injury susceptibility—a major risk factor for disease. Using a non-invasive injury model, we demonstrate that injury drives local and systemic metabolic alterations and that these responses differ by sex.

Methods. Male and female mice were subjected to non-invasive joint injury. Eight days after injury, serum, synovial fluid, and whole joints were collected for metabolomics. Additionally, whole joints were harvested for matrix-assisted laser desorption ionization–mass spectrometry imaging (MALDI-MSI) to capture the spatial distribution of molecular species and identify osteochondral regions perturbed by injury.

Results. Comparative analyses among injured, contralateral, and naive mice revealed metabolomic alterations across sample types. Data indicate that injury influences metabolic profiles in whole joints, synovial fluid, and serum, with consistent dysregulation of amino acid, purine, and pyrimidine metabolism, indicating a systemic effect of localized injury. Additionally, sex-dependent differences emerged across tissues, highlighting sexually dimorphic pathways following injury. MALDI-MSI generated 2D ion images of bone, the joint interface, and bone marrow, identifying region-specific metabolic changes following injury.

Conclusion. Joint injury induces coordinated metabolic responses locally and systemically that extend beyond the injured joint and are influenced by sex. Integrating metabolomic and spatial analyses reveals how injury modulates joint pathophysiology across tissues and reveals sex-specific patterns relevant to post-traumatic osteoarthritis (PTOA) risk. These findings improve preclinical PTOA models and deepen our understanding of the complex role of injury and sex in osteoarthritis pathogenesis, laying the foundation for targeted therapeutic strategies.

INTRODUCTION

Post-traumatic osteoarthritis (PTOA) accounts for 12% of OA cases, resulting in at least 5.6 million cases annually.[1] The most prevalent risk factors for PTOA are joint injury and sex. A total of 250,000 anterior cruciate ligament (ACL) injuries occur annually, commonly in young individuals aged 16 to 24 years. Upwards of 50% of patients will develop PTOA within 10 to 20 years of injury.[2,3] Female sex is a risk factor for joint injury: young female athletes are two to eight times more likely to sustain a traumatic knee injury requiring surgical repair compared with male athletes.[4] Women are also more likely to develop OA and typically experience greater symptom severity.[5] Sexual dimorphism in PTOA development may partially result from hormonal and anatomic differences where women have wider pelvises, smaller femurs and ACLs, and different muscle angles.[6,7] Despite these differences, many studies fail to include both men and women.

Although injury and sex are well-known PTOA risk factors, underlying mechanisms and changes in joint metabolism and microarchitecture postinjury remain incompletely understood.

Funding for the Montana State Mass Spectrometry Facility (RRID: SCR_012482) used in this publication was supported in part by the MJ Murdock Charitable Trust, the National Institute of General Medical Sciences, NIH (award numbers P20-GM-103474 and S10-OD-28650), and the Montana State University Office of Research and Economic Development. Supported by the NIH (award numbers R01-AR-073964 and R01-AR-081489 [to Dr June]) and the National Science Foundation (award number CMMI 1554708 [to Dr June]).

[1]Department of Chemistry & Biochemistry, Montana State University, Bozeman; [2]Department of Mechanical & Industrial Engineering, Montana State University, Bozeman; [3]Department of Mathematical Sciences, Montana State University, Bozeman.

Additional supplementary information cited in this article can be found online in the Supporting Information section (https://acrjournals.onlinelibrary.wiley.com/doi/10.1002/art.70098).

Author disclosures and graphical abstract are available at https://onlinelibrary.wiley.com/doi/10.1002/art.70098.

Address correspondence via email to Ronald K. June, PhD, at rjune@montana.edu.

Submitted for publication April 4, 2025; accepted in revised form January 6, 2026.

Metabolomics—the study of small molecule intermediates called metabolites—captures the physiologic and metabolic status of the joint. Although synovial fluid (SF) and serum are assessed postinjury in human and mouse models, metabolomics can also be applied to whole joint tissue to characterize metabolic changes occurring in bone and cartilage.[8–10] This approach examines the complex tissue system of the joint and when combined with spatial imaging through matrix-assisted laser desorption ionization–mass spectrometry imaging (MALDI-MSI) provides critical spatial context of osteochondral tissues at the metabolite level. Few studies report spatial data involving musculoskeletal tissues such as cartilage[11,12] and synovium.[13] However, no study to date has used MALDI-MSI to characterize molecular changes at the metabolite level postinjury.

Therefore, the first objective of this study was to characterize metabolomic differences within and across whole joints, SF, and serum from injured and naive male and female mice using liquid chromatography–mass spectrometry (LC-MS) metabolomics. Investigating differences in metabolism in different tissues and among injured, contralateral, and naive limbs is important to shed light on both local and systemic metabolic responses post-injury. The second objective was to spatially locate and identify osteochondral metabolites using MALDI-MSI. By applying untargeted metabolomic profiling combined with MALDI-MSI we can probe the response to injury metabolically across various compartments and spatially within the joint. These data offer novel insight into the mechanistic origins of metabolic and pathologic shifts post-injury, which is essential for improving patient outcomes.

MATERIALS AND METHODS

Animals. C57Bl/6J mice were purchased from Charles River Laboratories (material 701C57BL/6) at age 18 weeks and acclimated to the Montana State University (MSU) Animal Research Center for 3 weeks. Mice were housed in cages of three to five animals and fed standard chow ad libitum (PicoLab Rodent Diet 20, 20% protein). All animal procedures were approved by the MSU Institutional Animal Care and Use Committee.

Joint injury model and experimental design. Mice aged 21 weeks (N = 20) were randomly assigned to have half of each sex of mice in the injured and half in the naive group ($n_{naive\ female}$ = 5, $n_{naive\ male}$ = 5, $n_{injured\ female}$ = 5, $n_{injured\ male}$ = 5) (Figure 1; Supplementary Table S1). The injury group were subjected to a non-invasive compressive overload model where the ACL is ruptured similar to human ACL tears—an injury associated with degeneration of bone and cartilage (target force = 12 N, loading rate = 130 mm/s).[14] Both injury order and injured side (right or left) were randomized, and injury was confirmed by laxity tests. After 8 days, mice were euthanized in random order, and both rear whole joints, SF from both knees, and serum via cardiac puncture were harvested.[10] SF was recovered and extracted using established protocols,[15] with some modifications where Whatman paper (Sigma, WHA1441042) was used to absorb SF. Surrounding muscle fiber, ligaments, and tendons were removed from whole joints and were trimmed at the midshafts of the femur and tibia to include the whole joint, growth plate, and remaining joint capsule. Whole joints for MALDI-MSI were stored intact at –80°C whereas those for LC-MS were disarticulated to separate the tibia and femur to remove bone marrow via centrifugation. Naive mice served as the control group, with one SF and joint sample used per mouse to avoid pseudoreplicates (Figure 1).

Metabolomics. *Metabolite extraction and MS instrumentation.* Whole joints ($n_{LCMSJoints}$ = 24 and $n_{MALDIJoints}$ = 6), SF (n_{SF} = 30), and serum (n_{Serum} = 20) were extracted and analyzed using validated protocols with slight modifications.[16] Samples were randomized and blinded during the extraction process. Whole joints (disarticulated) were homogenized in 1 mL of 80:20 methanol:H_2O (1200 GenoLyte, Fischer Scientific). This same extraction solvent was added to serum and SF, followed by vortexing. All samples were chilled overnight at –20°C. The next day, samples were removed from –20°C, centrifuged, and the supernatant was dried via vacuum concentration. Dried extracts were resuspended with 250 uL of 1:1 acetonitrile:H_2O, vortexed, chilled at –20°C for 30 minutes, and centrifuged again. Supernatant was dried once more, and extracts were prepped for LC-MS using 100 uL of 1:1 acetonitrile:H_2O. Sample pooling was used for identification as it enables simultaneous LC-MS/MS analysis of metabolites combined from multiple samples. For each tissue type, pools were generated by combining small aliquots from four randomly selected samples. Pooled samples from each tissue type were also included in a "super pool" for additional identification purposes. All solvents used were LC-MS grade (Fischer Scientific). Extracted samples and pools were injected in a random sequence and analyzed via LC-MS as previously described.[16]

Metabolite profiling and identification. All LC-MS data—mass-to-charge ratios (m/z), relative metabolite abundance, and retention time—were processed using MSConvert and Progenesis QI (Supplementary Table S1). Statistical and pathway analyses were performed in MetaboAnalyst (version 6.0)[17] using a fold change >2.0 and false discovery rate–corrected $P < 0.05$ as significance thresholds. Injured and contralateral limbs were analyzed as separate groups, given the lack of direct injury to the contralateral limbs. For naive mice, one whole joint and SF sample was randomly selected per animal to ensure consistent representation and avoid pseudoreplication. LC-MS/MS data derived from pooled samples were analyzed within Progenesis QI where acquired fragmentation patterns were matched against theoretical spectra to identify metabolites.[16] Identified whole joint–derived metabolites were matched against populations distinguished by MALDI-MSI. To minimize false identifications when comparing

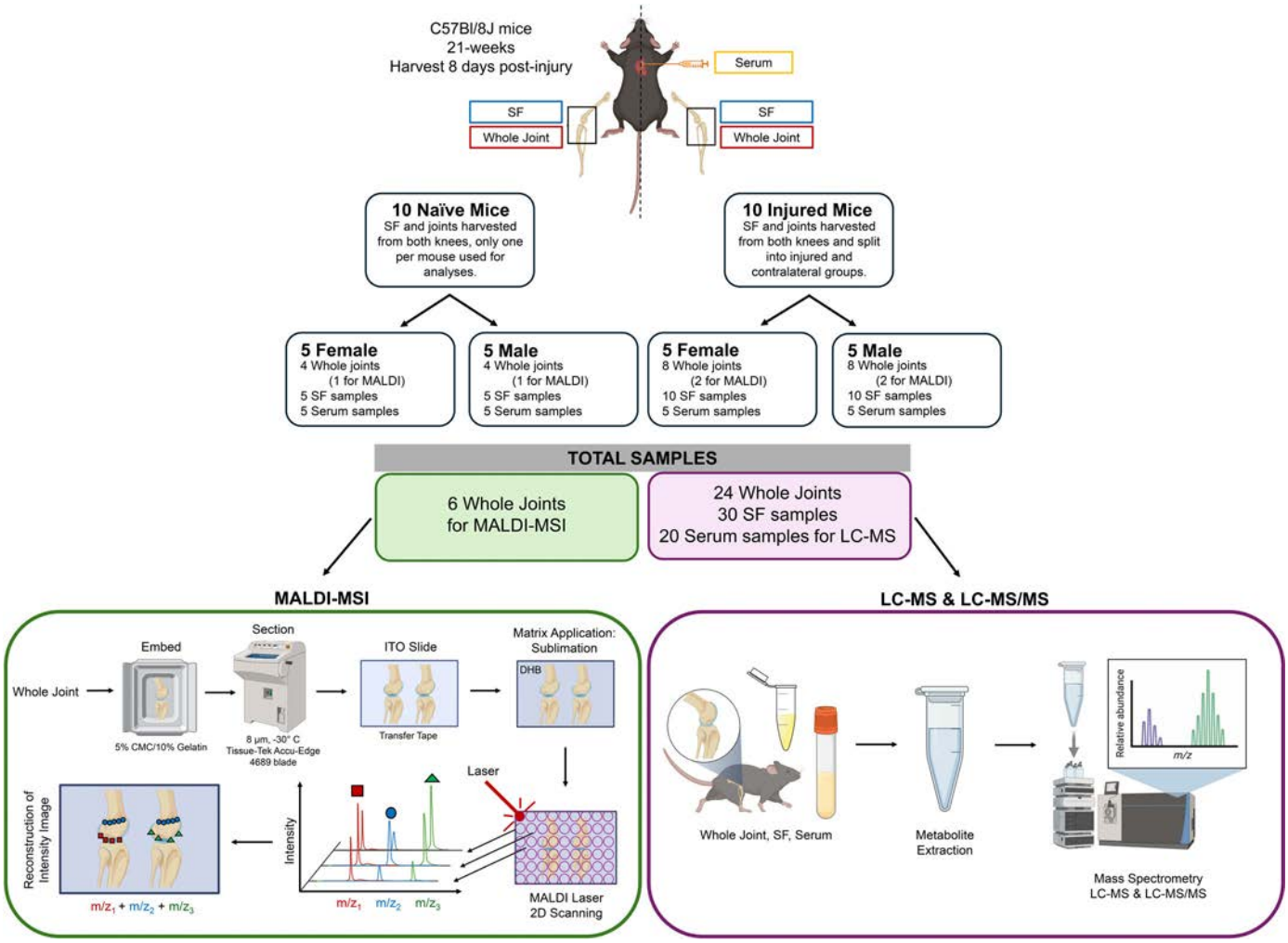

Figure 1. Experimental schematic and LC-MS/MS and MALDI-MSI workflow. Whole joints, SF, and serum samples were harvested from C57Bl6/J mice (N = 20; n = 10 naive and n = 10 injured) 8 days after non-invasive anterior cruciate ligament rupture. Both contralateral and injured limbs were included from injured mice, whereas one randomly selected limb was included from naive mice. Whole joints sent for MALDI-MSI were embedded in 5% CMC/10% gelatin, sectioned (8 µm), transferred to ITO slides, and sublimed with 2,5-dihydroxybenzoic acid matrix. Data were then acquired using 2D laser scanning followed by reconstruction of intensity images representing m/z values and intensity. Whole joints, SF, and serum samples for LC-MS and LC-MS/MS were processed for metabolite extraction using previously established protocols—including lipid and protein precipitation—and analyzed on a Waters Synapt XS. Data were then processed using MSConvert and Progenesis QI, and MetaboAnalyst was used for statistical and pathway analyses. Created using BioRender. CMC, carboxymethylcellulose; DHB, dihydroxybenzoic acid; ITO, indium tin oxide; LC-MS, liquid chromatography–mass spectrometry; m/z, mass-to-charge ratio; MALDI-MSI, matrix-assisted laser desorption ionization–mass spectrometry imaging; SF, synovial fluid. Color figure can be viewed in the online issue, which is available at http://onlinelibrary.wiley.com/doi/10.1002/art.70098/abstract.

MALDI-MSI and LC-MS/MS m/z values, a matching tolerance of 10 parts per million was applied.

MALDI imaging. *Sample preparation.* Whole joints selected for MALDI-MSI ($n_{MALDIJoints}$ = 6) were removed from –80°C and prepared according to the novel protocol developed for whole joint sectioning and imaging (Figure 1). Whole joints were embedded using warm 5% carboxymethylcellulose sodium salt (ThermoFischer, A18105-36) and 10% gelatin (Thermo Scientific, AC611995000)[18,19] as optimal cutting temperature media is incompatible with MS analysis as it contains polyethylene glycol, a major ion suppressor.

Medial and lateral aspects of the joint were sectioned sagittally at 8 µm thickness in a cryostat set to –30°C (OTF5000 Cryostat, Bright Instrument Co Ltd, Tissue-Tek Accu-Edge 4689 blade). Because whole joints did not undergo formalin fixation or paraffin embedding, Cryofilm 3C 16 UF (SECTION-LAB) was used to help transfer sections to indium tin oxide (ITO) slides (Delta Technologies, CB-401N, 4–10 Ω/sq, 25 × 50 mm).[20] Sections were adhered to ITO slides using double-stick tape and then directly stored at –80°C until matrix application.

Matrix application. A sublimation apparatus (Chemglass Life Sciences, CG-3038) was used for matrix application (Supplementary Figure S1). Sublimation was chosen over matrix

spraying as it forms smaller, more homogenous matrix crystals and lacks liquid—reducing the risk of molecule migration and microcracks in marrow and bone.[19] A total of 300 mg of 2,5-dihydroxybenzoic acid (Alfa Aesar, 490-79-9) was uniformly dispersed in the base of the sublimation apparatus, ITO slides were affixed to the flat bottom condenser, and the condenser was filled with tap water (22°C). The two glass compartments of the sublimator were assembled using an O-ring seal and connected to a vacuum pump. Tissue sections on ITO slides were sublimated at 50°C for 3 minutes under 68 millitorr vacuum, resulting in a uniform matrix layer (0.05 mg/cm^2) that was then recrystallized in a hydration chamber with 300 uL of 5% methanol 0.1% formic acid spotted onto Whatman paper. The chamber was heated in a 37°C oven for 1 minute, then ITO slides were sealed in the chamber and heated at 37°C for 1 minute.

MALDI image acquisition and analysis. A Bruker AutoFlex III MALDI time-of-flight (TOF) mass spectrometer (Bruker Daltonics) equipped with an MTP Slide Adapater II Imaging Plate (Bruker Daltonics) was used for image acquisition. Because of the size of the sublimator and ITO slides (25 × 50 mm), two small aluminum slide trays were milled to fit ITO slides into the imaging plate. Using a Smartbeam Nd:YAG laser (355 nm) and Bruker FlexImaging, images were collected in positive ionization and TOF modes in the 50 to 1,000 m/z mass range averaging 200 laser shots per pixel with a 100-um lateral resolution (laser power = 30%, range = 90%, and offset = 10%). Ion images were analyzed and generated using Bruker SCiLS Lab. All data are available in the main text and the supplementary materials. Raw metabolomics data are available in Supplementary Table S2.

RESULTS

Metabolomic profiling of naive whole joints, SF, and serum reveals local and systemic effects induced by injury. In total, 2,769 metabolite features were detected across all samples ($n_{LCMSJoints}$ = 24, n_{SF} = 30, and n_{serum} = 20). Whole joints, SF, and serum were assessed among all samples and within injured samples using analysis of variance and principal component analysis (PCA)—visualized in three equal dimensions (isometric) to capture and illustrate group separation in an unbiased and unsupervised manner—revealing distinct metabolomic profiles (Supplementary Figure S2A–D).

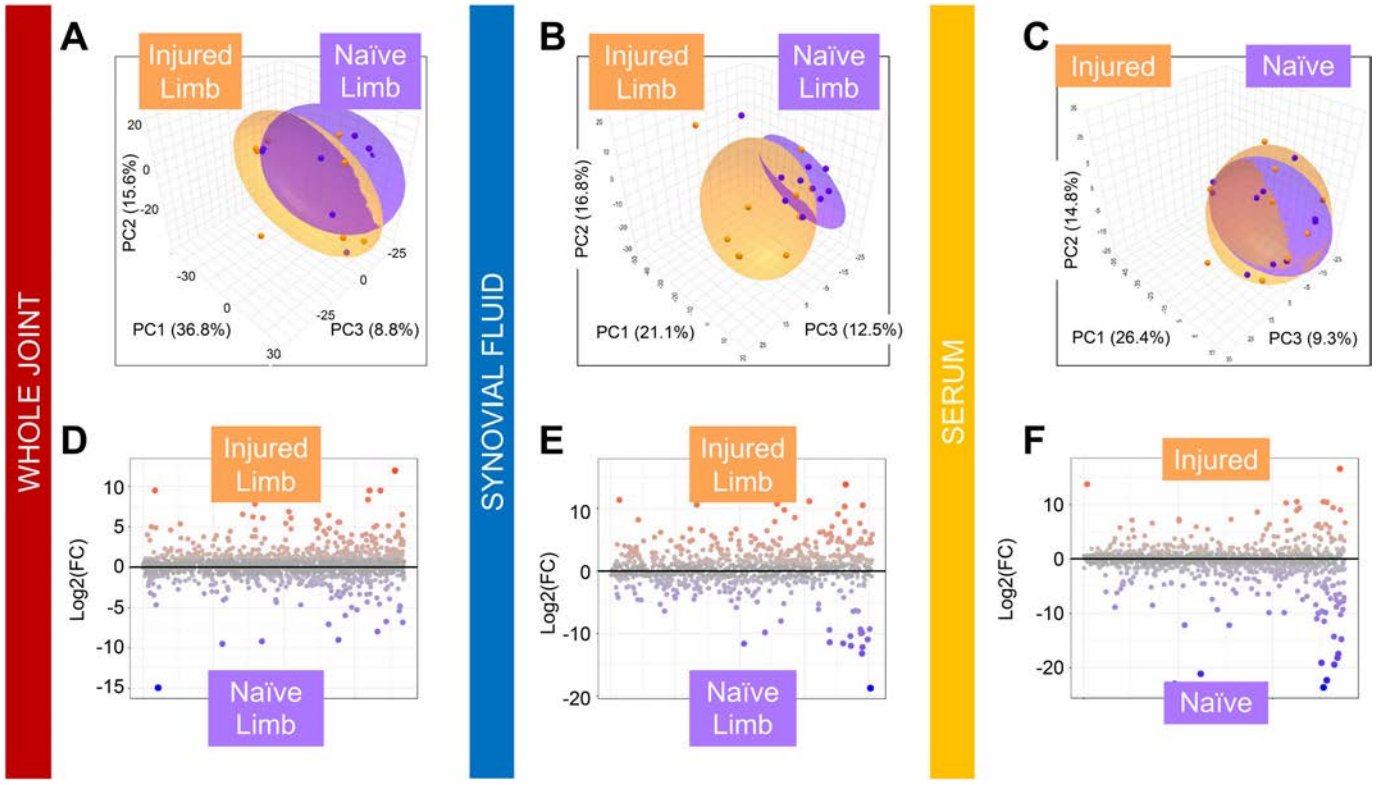

Figure 2. Global metabolomic profiles of whole joints, synovial fluid, and serum are driven by injury status. (A–C) PCA shows overlap between injured and naive limbs in all three tissues. (D–F) FC analysis distinguishes populations of metabolite features that are differentially regulated between injured and naive (D) whole joint, (E) synovial fluid, and (F) serum samples. Specifically, (D) 408 and 210 metabolite features were highest in injured and naive whole joints, respectively. (E) A total of 334 and 207 metabolite features were highest in injured and naive synovial fluid, respectively. (F) A total of 386 and 195 features were highest in injured and naive serum, respectively. For pathways associated with FC features, see Supplementary Table S3. The colors in A–F correspond to the following: purple = naive and orange = injured; sample types, red = whole joint, blue = synovial fluid, and yellow = serum. FC, fold change; PCA, principal component analysis. Color figure can be viewed in the online issue, which is available at http://onlinelibrary.wiley.com/doi/10.1002/art.70098/abstract.

Next, we assessed how injury influenced the metabolomic profiles within each sample type. PCA revealed considerable overlap in the whole joint and serum comparisons, with more distinct clustering shown in SF (Figure 2A–C). Metabolite features with a fold change >2.0 were subjected to pathway analysis (Figure 2D–F). Comparing injured and naive whole joints, 17 pathways were dysregulated, where numerous amino acid pathways—valine, leucine, isoleucine, alanine, aspartate, glutamate, histidine, tyrosine, glycine, and serine—butanoate metabolism, and sphingolipid metabolism were highest in injured whole joints (Supplementary Table S3A). In SF, 26 pathways were dysregulated: arginine and proline metabolism, lysine degradation, glutathione metabolism, and others were highest in injured SF (Supplementary Table S3B). In serum, 16 pathways were dysregulated between injured and naive animals, with amino acid pathways—including arginine and proline metabolism— alongside nucleotide, vitamin, and glutathione metabolism being highest in injured animals (Supplementary Table S3C). Metabolic indicators of injury were assessed using volcano plot analyses to identify features differentially regulated between injured and naive samples (Supplementary Figure S3A–C).

To investigate the systemic effects of injury, metabolic differences associated with injured, contralateral, and naive whole joints and SF were examined. PCA plots of the top three principal components were generated to capture and interpret trends in group separation, and although overlap between whole joint and SF samples were observed, 3D visualization helps reveal underlying structure in the data (Figure 3A and C). Differentially and coregulated

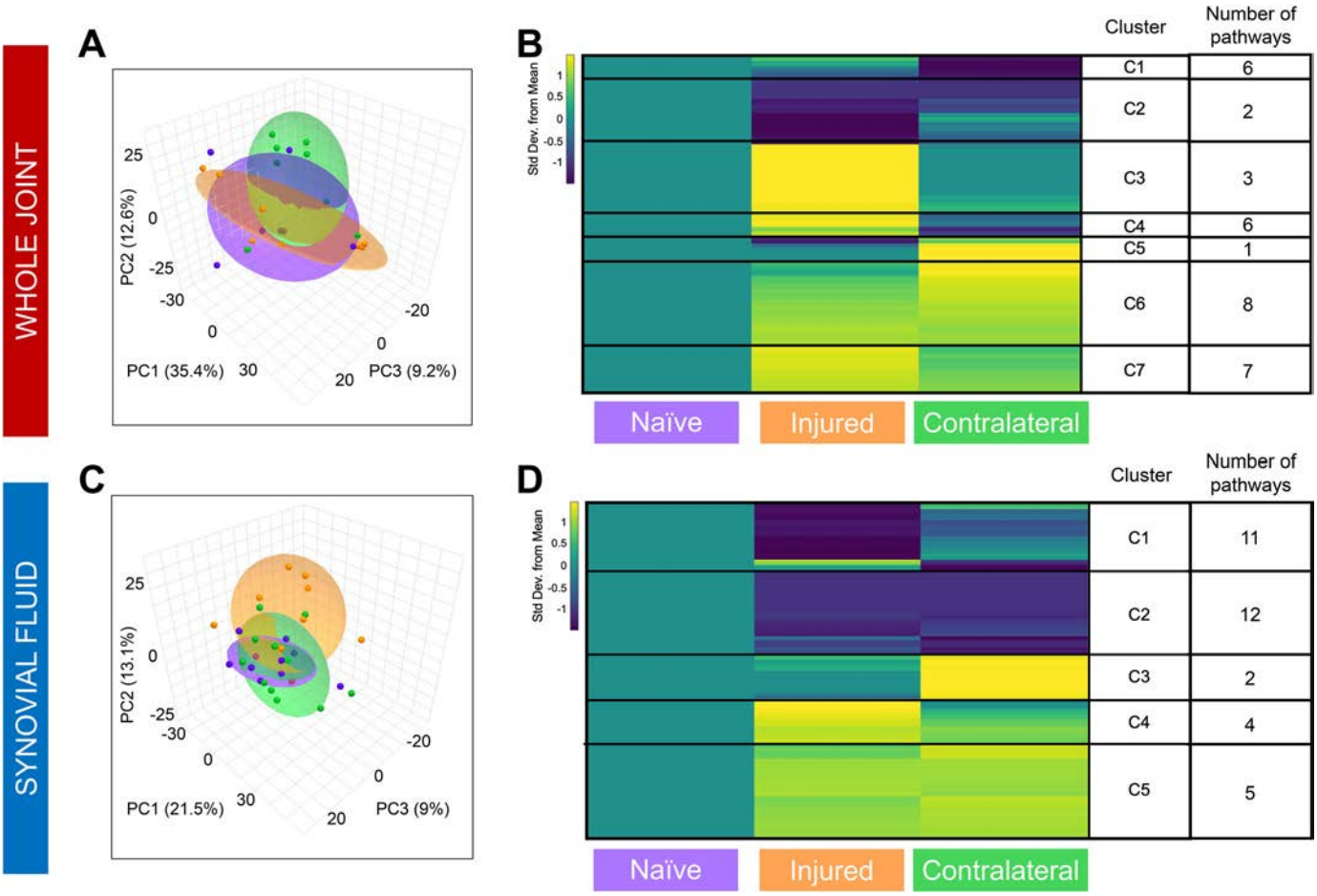

Figure 3. Whole joint and synovial fluid metabolic profiles are distinct among naive, injured, and contralateral limbs. PCA shows overlap among injured, contralateral, and naive groups in (A) whole joint samples with more distinct profiles shown in (C) synovial fluid. To pinpoint pathways driving metabolomic differences among limbs, median intensity heatmap analyses were performed, in which injured and contralateral limbs were normalized to naive limbs. Clusters of coregulated metabolite features within (B) whole joint and (D) synovial fluid samples were subjected to pathway analyses to identify biologic pathways that differ in regulation across limbs in both whole joint and synovial fluid samples. Pathways associated with clusters in parts B and D primarily associated with amino acid, lipid, and energy metabolisms. A breakdown of corresponding pathways can be found in Table 1. Combined, the data provide strong evidence of distinct metabolomic regulation associated with injury status. Heatmap columns represent limbs (naive, injured, and contralateral) and rows represent metabolite features. Cooler and warmer colors indicate lower and higher metabolite abundance relative to the mean, respectively. The colors in A–F correspond to the following: purple = naive, orange = injured, and green = contralateral whole joint; sample types, red = whole joint, blue = synovial fluid, and yellow = serum. PCA, principal component analysis. Color figure can be viewed in the online issue, which is available at http://onlinelibrary.wiley.com/doi/10.1002/art.70098/abstract.

metabolite features expressed across whole joints and SF were clustered using heatmaps of median metabolite feature intensities and subjected to pathway analyses (Figure 3B and D). Comparative analysis of injured, contralateral, and naive whole joints revealed differential enrichment of 22 pathways and 24 pathways altered in SF (Table 1). Several pathways overlapped across joint and fluid compartments, highlighting shared metabolic responses to injury. Of these, amino acid pathways—alanine, aspartate, glutamate, arginine, proline metabolism, lysine—were higher in injured and contralateral whole joints and lower in these same groups in SF, compared with naive controls. Glutathione metabolism was consistently highest in injured whole joints and SF compared with contralateral and naive. Purine and pyrimidine metabolic pathways also displayed a similar result, where these pathways were highest

Table 1. Median intensity heatmap pathways*

Cluster	Pathway	FDR *P* value
Pathways associated with whole joints: median intensity heatmap (Figure 3B)		
1	Nitrogen metabolism	0.039
3	Glycerophospholipid metabolism	0.027
4	Glutathione metabolism	0.038
4	Purine metabolism	0.039
5	Lysine degradation	0.030
6	Tyrosine metabolism	0.021
6	Phenylalanine, tyrosine, and tryptophan biosynthesis	0.022
6	Drug metabolism: cytochrome P450	0.025
6	Ubiquinone and other terpenoid-quinone biosynthesis	0.032
6	Biosynthesis of unsaturated fatty acids	0.041
7	Glycine, serine, and threonine metabolism	0.027
7	Porphyrin metabolism	0.043
7	Selenocompound metabolism	0.047
1, 3	Alanine, aspartate, and glutamate metabolism	0.030
1, 4	Pyrimidine metabolism	0.028
1, 4	Arginine biosynthesis	0.033
1, 4, 7	Arginine and proline metabolism	0.042
1, 7	D-amino acid metabolism	0.045
2, 6	Phenylalanine metabolism	0.030
2, 6, 7	Valine, leucine, and isoleucine biosynthesis	0.026
3, 4	Histidine metabolism	0.025
6, 7	Valine, leucine, and isoleucine degradation	0.034
Pathways associated with synovial fluid: median intensity heatmap (Figure 3D)		
1	Fructose and mannose metabolism	0.046
1	Cysteine and methionine metabolism	0.046
1	Taurine and hypotaurine metabolism	0.048
1	Pyruvate metabolism	0.048
2	Tryptophan metabolism	0.016
2	Purine metabolism	0.016
2	Alanine, aspartate, and glutamate metabolism	0.016
2	D-amino acid metabolism	0.019
2	Arginine biosynthesis	0.044
3	Sphingolipid metabolism	0.020
3	Biosynthesis of unsaturated fatty acids	0.028
4	β-alanine metabolism	0.042
4	Glutathione metabolism	0.045
5	Pyrimidine metabolism	0.015
5	Terpenoid backbone biosynthesis	0.021
1, 2	Phenylalanine metabolism	0.014
1, 2	Lysine degradation	0.015
1, 2	Arginine and proline metabolism	0.017
1, 2	Drug metabolism: cytochrome P450	0.019
1, 2	Phenylalanine, tyrosine, and tryptophan biosynthesis	0.020
1, 2	Tyrosine metabolism	0.038
1, 4, 5	Valine, leucine, and isoleucine degradation	0.030
2, 5	Histidine metabolism	0.040
4, 5	Valine, leucine, and isoleucine biosynthesis	0.049

* Metabolic pathways associated with injured, contralateral, and naive whole joints and synovial fluid identified by median metabolite intensity heatmap analysis. All pathways listed were FDR-corrected using the Benjamini-Hochberg method (see Figure 3B and D). FDR, false discovery rate.

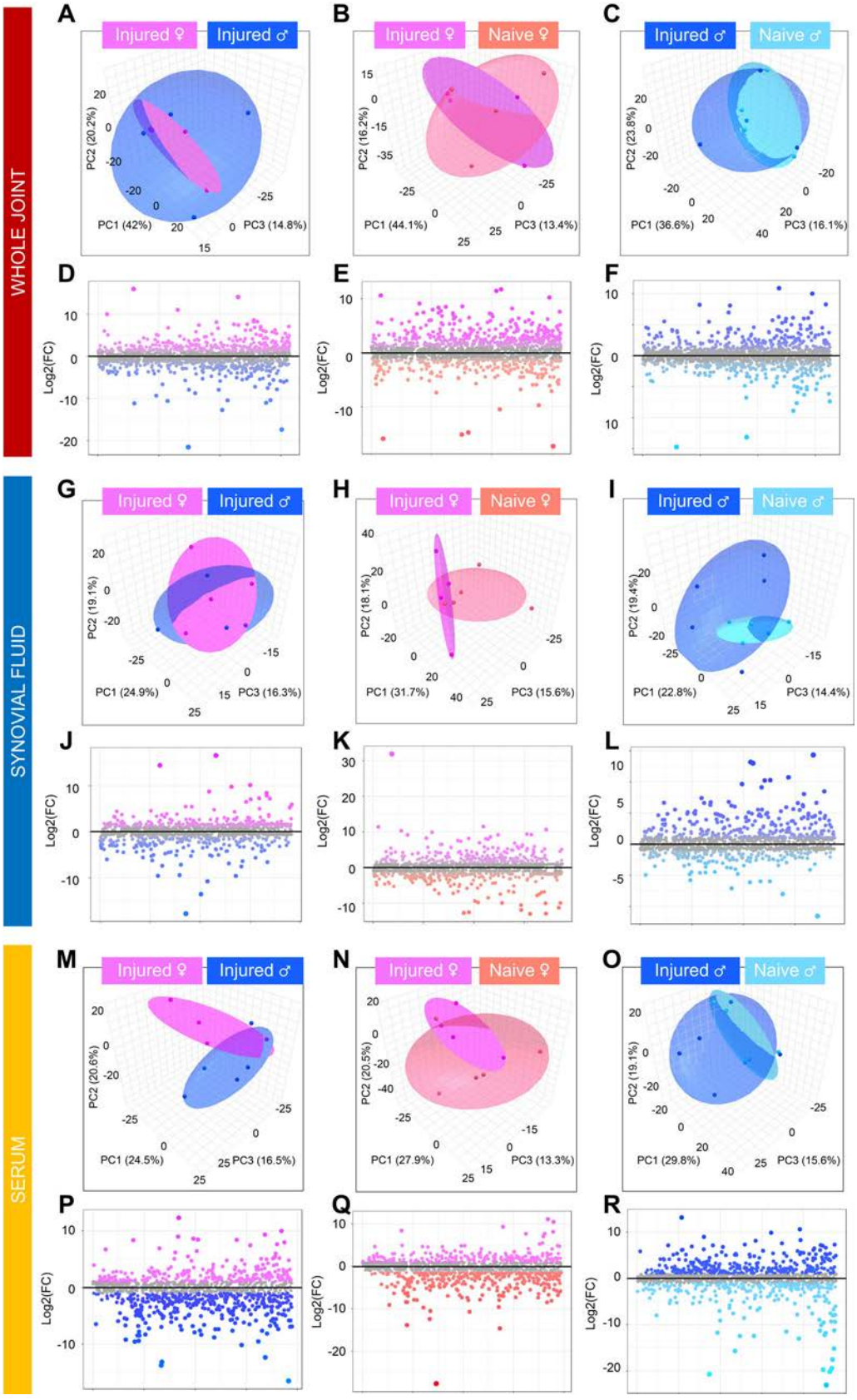

Figure 4. Legend on next page.

in injured whole joints and SF. Additional comparisons across limbs to evaluate systemic injury-induced effects in whole joints and SF are presented in the Supplementary Results (Supplementary Figure S4; Supplementary Tables S4 and S5). These results suggest unloaded contralateral limbs display their own unique metabolic profile from naive and injured limbs and that injury perturbs tissues beyond the local site of injury.

Sex influences metabolomic profiles across tissues and fluids of injured and naive mice. General and injury-associated sex differences were examined in whole joints (Supplementary Figure S5), revealing sex-dependent metabolomic profiles. PCA displays overlap between whole joints of injured and naive male and female mice, with less overlap among injured male and female mice (Figure 4A–C). PCA results were comparable between groups in SF (Figure 4G–I) and serum (Figure 4M–O) from both male and female mice. Across sample types, more overlap was observed when comparing injured and naive male mice. Fold change analysis identified populations of metabolite features from whole joints, SF, and serum that show distinct injury- and sex-specific pathways with many conserved across all three sample types (Figure 4D and E, J–L, and P–R; Supplementary Tables S6–S8). Alanine, aspartate, and glutamate metabolism were highest in the whole joints of injured males and were also enriched in the SF and serum of both injured male and female mice. Cysteine and methionine metabolism was enriched in both whole joint and SF in injured female mice. Similarly, lysine degradation was consistently enriched across all three sample types in injured male and female mice. Pyrimidine metabolism was consistently enriched across all three sample types in injured female mice. Volcano plot analysis was performed comparing whole joints, SF, and serum from injured and naive male and female mice, where metabolites with sex- and injury-specific differences were identified (Supplementary Figure S6). These molecular-level findings demonstrate that sex-specific differences emerge post-injury and contribute to the mounting evidence indicating the role of sex in PTOA development.

MALDI-MSI contextualizes osteochondral metabolites and their differences in the spatial plane. To complement metabolomic analyses, exploratory spatial profiling using MALDI-MSI was performed to characterize tissue-specific metabolites within the spatial plane. Although the sample size is small, these data provide preliminary insights into the spatial localization of metabolic changes post-injury. We developed a novel protocol for sample preparation, matrix application, and instrumentation to examine spatial changes across tissues with varying stiffness and cell compositions. Using unsupervised segmentation, discriminating features from different spatial areas of the joint were clustered together. When comparing spatial distributions of ions belonging to the bone and joint interface against bone marrow, 37 features had area under the receiver operating characteristic curve (AUC) values >0.6 and 21 were >0.8, demonstrating tissue-dependent metabolite signatures. Using LC-MS/MS–derived metabolite identifications from whole joint samples, metabolites with unique spatial patterns were putatively identified. Those with notable spatial patterns in bone included alpha-carboxy-delta-decalactone (215.20 m/z, AUC = 0.838), hydroxyprolyl-isoleucine (245.11 m/z, AUC = 0.859), and $C_{36}H_{38}O_7$ (629.61 m/z, AUC = 0.829) (Figure 5A; Supplementary Figure S7A; Supplementary Table S9A). Metabolites with notable patterns among bone marrow included carnitine (162.29 m/z, AUC = 0.821) and various phosphatidylcholine lipid species (34 carbons, two double bonds – 758.57 m/z, AUC = 0.731; 34 carbons bonds, three double bonds – 778.59 m/z, AUC = 0.856; and 39 carbons, six double bonds – 820.41 m/z, AUC = 0.866) (Figure 5A; Supplementary Figure S7B; Supplementary Table S2A). Many metabolites displayed unique spatial patterns among bone, the joint interface, and bone marrow but were unable to be identified. However, many were within the common lipid m/z range (400–800 m/z) (Supplementary Figure S8; Supplementary Table S9B).

To investigate injury-associated spatial patterns, ion images from medial and lateral aspects of both injured and contralateral mouse joints were examined. In an injured joint, the metabolite feature 544.41 m/z and the putatively identified metabolite—a phosphatidylcholine with 36 carbons and six double bonds 878.54 m/z—display notable injury-associated patterns between medial and lateral sagittal sections where they are more abundant in the injured joint compared with the contralateral joint (Figure 5B). Sex-associated patterns were not examined because of the limited number of joints allocated for MALDI-MSI.

Figure 4. Metabolomic profiles of whole joint, synovial fluid, and serum show sexual dimorphism across injured and naive mice. PCA reveals (A) considerable overlap of injured whole joints from male and female mice, as well as in (B) female and (C) male injured and naive mice. (D–F) FC analysis distinguished populations of whole joint metabolite features driving separation of metabolomic profiles. (G–I) PCA reveals (G) moderate overlap of injured SF from male and female mice as well as in (H) female and (I) male injured and naive mice. (J–L) FC analysis identified populations of synovial fluid metabolite features attributed to sex and injury differences. (M–O) A similar pattern is observed in the serum, where moderate overlap of injured SF from male and female mice, as well as in females alone, and considerable overlap in male injured and naive mice is observed. (P–R) FC analysis identified populations of serum metabolite features driving metabolomic profile separation. See Supplementary Tables S6–S8 for pathways. The colors in A–R correspond to the following: pink = injured female mice, peach = naive female mice, royal blue = injured male mice, and light blue = naive male mice; sample types, red = whole joint, blue = synovial fluid, and yellow = serum. FC, fold change; PCA, principal component analysis. Color figure can be viewed in the online issue, which is available at http://onlinelibrary.wiley.com/doi/10.1002/art.70098/abstract.

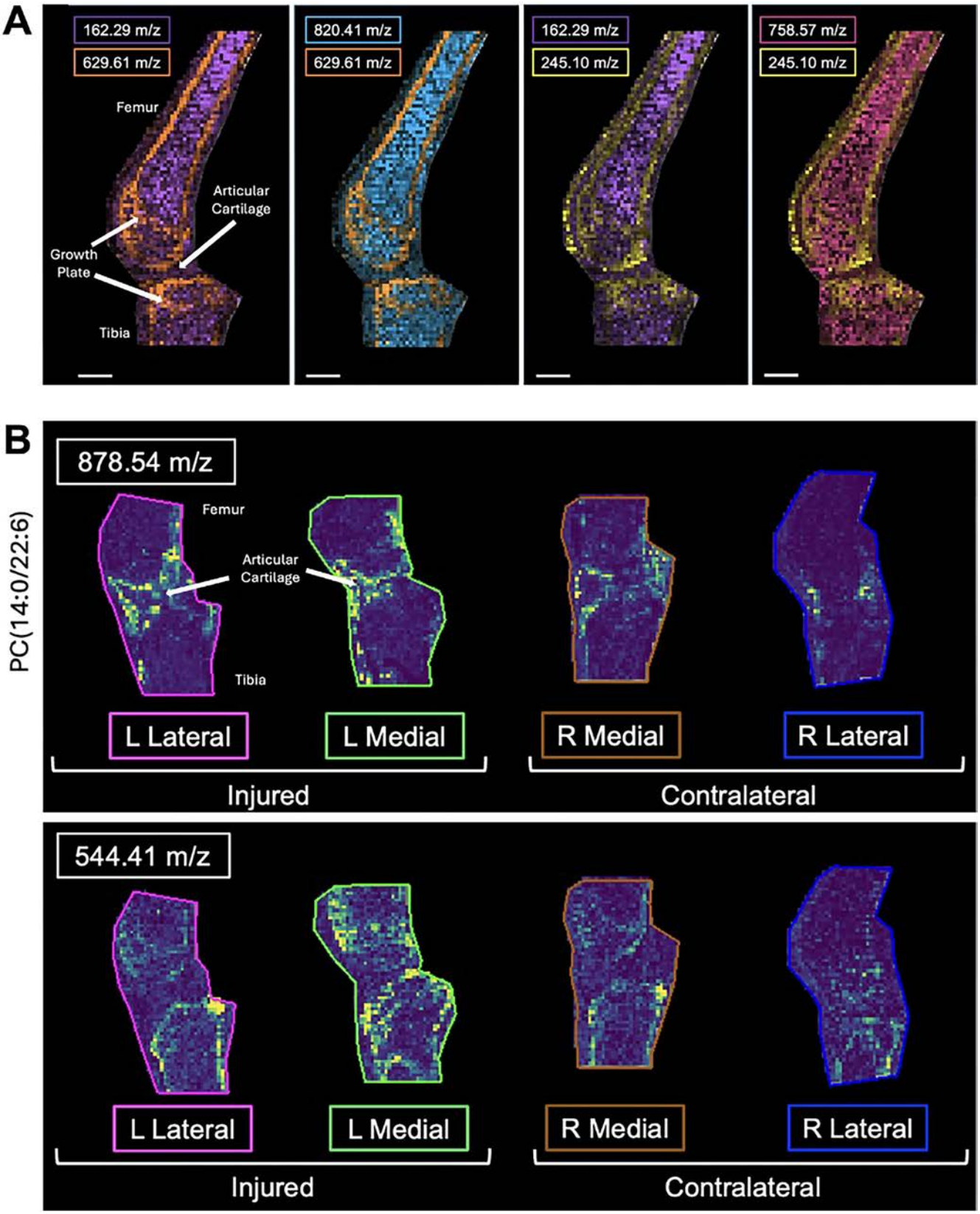

Figure 5. Legend on next page.

DISCUSSION

To our knowledge, this is the first study to comprehensively examine metabolic and spatially resolved responses following injury, both locally (whole joints and SF) and systemically (serum) across male and female mice using LC-MS metabolomic profiling and MALDI-MSI. Our findings reveal significant metabolic and pathologic shifts following joint injury, with discernible sex-specific associations. By uncovering novel metabolic differences linked to these key PTOA risk factors across multiple sample types and biologic scales, our study advances the understanding of post-injury responses beyond the joint. These insights provide critical, and previously unknown, context on the joint-specific metabolic and systemic changes that shape disease progression. These tools and developed framework can be leveraged for other injury models to underpin molecular mechanisms driving disease. Importantly, these findings help fill current gaps in knowledge regarding sex in disease development and underscore the need for improved understanding to overcome the translational challenge of sexual dimorphism in PTOA.

Distinct metabolomic profiles of whole joints, SF, and serum reveal acute changes in response to injury, with the greatest distinctions at the serum level. Various amino acid pathways exhibit differential regulation across all sample types, with many overlapping. Lysine degradation was differentially regulated across injured, contralateral, and naive whole joints while being downregulated in SF contralateral and injured limbs (vs naive). This may relate to collagen, where hydroxylation of lysine residues is crucial for structural integrity crosslinking.[21] In bone, collagen is a major component of the structural organic matrix. Alteration of lysyl hydroxylase in osteoblasts yields defective crosslinking, fibrillogenesis, and matrix mineralization,[21–23] underscoring the importance of lysine hydroxylation in bone quality. In SF, lysine metabolism decreases as OA progresses,[24] suggesting this pathway could represent acute joint changes following injury that could be monitored in the clinical setting to oversee disease progression.

Arginine and proline metabolism was upregulated in injured SF and serum. Like lysine, proline can strengthen collagen crosslinks through hydroxyproline modification. Arginine has anti-inflammatory effects and decreases as OA develops.[25,26] Arginine and proline metabolism increase in rabbit SF post-ACL injury,[27] in human SF after knee injuries,[16] and in mouse serum 1 day after ACL injury.[28] Combined, these suggest a short-term protective mechanism or cascade of pathways to enhance collagen production post-injury and could be further examined as a potential therapeutic option to administer in the acute phase following injury.

Phenylalanine, tyrosine, and tryptophan biosynthesis exhibited differential regulation among injured, contralateral, and naive limbs in whole joint samples and SF. Although higher in injured and contralateral whole joints (vs naive), these pathways showed the opposite trend in SF. Calcium-sensing receptors preferentially bind these aromatic amino acids, leading to a rise in intracellular calcium and modulation of bone turnover.[29,30] Phenylalanine and tyrosine metabolism are associated with the sclerosis of subchondral bone in OA.[31] In a non-invasive mouse injury model, tryptophan metabolism was higher in mouse SF 7 days post-injury compared with naive controls. Tryptophan has been noted as a promising OA biomarker with decreases as disease progresses.[32,33] Our detection of this pathway in both injured and contralateral whole joints is novel, suggesting a systemic response in both injured and contralateral whole joints. These results hold promise as amino acids play a role in the response to acute injury,[34] are detected post-injury across mammalian models,[27,28,35] and change concentration with disease progression.

Considering injury and sex, purine and pyrimidine metabolism—used for nucleotide synthesis—were dysregulated. Purine metabolism was consistently highest in injured male mice, with the strongest pattern in serum, likely reflecting increased levels of uric acid—an end product of purine metabolism—in male mice[36] because female hormones decrease uric acid levels.[37] Conversely, pyrimidine metabolism was dominant in tissues from injured female mice, necessitating further research to understand its sexual dimorphic regulation.

Following injury, glycine, serine, and threonine metabolism were altered in serum and SF from male and female mice. This pathway was perturbed among female sheep after ACL injury, with serine suggested as a biomarker for early degenerative changes.[38] Serine, a glucogenic amino acid, influences AMP kinase (AMPK), which acts as a key "energy sensor" that maintains energy homeostasis and promotes ATP synthesis via serine/threonine phosphorylation.[39] Enzymes like AMPK are differentially influenced by circulating sex hormones like estrogen, which can bind to estrogen receptor β, triggering downstream metabolic cascades to generate ATP.[40] The influence of circulating sex hormones, like estrogen, on AMPK activity may affect energy metabolism postinjury, warranting further investigation into

Figure 5. Matrix-assisted laser desorption ionization–mass spectrometry imaging combined ion images from sagittal whole joint sections and injury-associated spatial distribution patterns. (A) Putatively identified molecular species across various tissue structures in naive mouse joints. Spatial resolution = 100 μm. Scale bar = 1 mm. Interval width = 0.35 Da. (B) Putatively identified PC (14:0/22:6) (878.54 m/z) and 544.41 m/z display notable injury-associated patterns between medial and lateral sagittal sections from an injured and contralateral joint. Colors in panel A from left to right are as follows: L-carnitine (162.29 m/z, purple), $C_{36}H_{38}O_7$ (629.61 m/z, orange), (820.41m/z, blue), hydroxyprolyl-isoleucine (245.10 m/z, yellow), and lipid species 18:2/16:0 (758.57 m/z, pink). In panel B from left to right left lateral, left medial, right medial, and right lateral. Spatial resolution = 100 μm. Scale bar = 1 mm. Interval width = 0.35 Da. Da, Daltons; m/z, mass-to-charge ratio; PC, phosphatidylcholine

sexual dimorphic patterns to identify translation intervention opportunities.

Injured female mice exhibited dysregulated cysteine and methionine metabolism within whole joints and SF, whereas injured male mice showed similar metabolic changes in serum. Histidine metabolism was most dysregulated in injured male mice in serum and whole joints and in the SF of injured female mice. These three amino acids relate to matrix metalloproteinase (MMP) regulation of tissue remodeling and degradation of extracellular matrix proteins, cell proliferation, and immune responses.[41] MMP activation is modulated by a cysteine switch, and the catalytic domain of MMPs is regulated by these amino acids because zinc binds to histidines with assistance from conserved methionine sequences.[41,42] MMP activity is influenced by hormones,[43] like estrogen and progesterone, particularly in chondrocytes. Postmenopausal OA chondrocytes cultured with 17β-estradiol found that physiologic levels of estrogen suppressed the expression of MMP-1 and that hormone replacements might benefit female patients with OA in the early stages of disease.[44] Differential regulation of AMPK- and MMP-associated amino acids between male and female mice post-injury suggests reliance on different metabolic pools, mechanisms, and biofuels to meet energy demands and maintain matrix properties following joint injury.

To our knowledge, this is the first study to provide critical unknown spatial context of osteochondral tissues at the metabolite level and after joint injury. We developed an innovative protocol to spatially characterize osteochondral metabolites from whole joints—composed of different sample types with varying stiffness and cell types—of injured and naive mice using MALDI-MSI. Few studies have employed MALDI-MSI in musculoskeletal tissues to visualize the spatial distribution of proteins and peptides.[11–13] Traditionally, histologic sectioning and imaging of whole joints—and bone samples in general—require formalin fixation and paraffin embedding to preserve and demineralize the bone; however, this results in removal, crosslinking, and/or delocalization of molecular species, especially lipids,[19] leading us to develop this novel protocol to examine spatial metabolite distributions within this complex joint system.

Lipid metabolism is increasingly recognized in the development of PTOA and OA. Proteomic and metabolomic studies demonstrate an important relationship between OA and lipid metabolism in samples of SF, cartilage, bone, and circulatory fluids from both humans and mice.[11,24,45–48] Employing MALDI-MSI to target small molecules (50–1,500 m/z) provides novel insight into joint composition and changes post-injury. We successfully mapped differences in injury-related osteochondral metabolites, where many were lipids. These findings align with metabolomic assessments finding lipid-associated pathways—such as glycerophospholipid metabolism—higher in injured joints compared with naive and contralateral joints. Consistent with our previous analysis of metabolic endotypes of early PTOA in SF[8,16,24,49] and in OA cartilage,[48,50] dysregulated lipid metabolism is linked to both early-stage PTOA and end-stage OA, suggesting that comparable metabolic alterations arise throughout joint tissues and can be spatially resolved. This underscores the need for further research into lipid metabolism's role in both local and systemic changes following injury and during early PTOA. This two-pronged approach using LC-MS–based metabolomics and MALDI-MSI sheds light on the importance of lipids in joint metabolism, both systemically and intra-articularly. Moving forward, MALDI-MSI across proteins and metabolites can be leveraged and integrated with existing techniques to not only deepen our understanding of the joint's post-injury response across multiple tissues but also serve as a powerful framework for investigating complex tissue systems and diseases where spatially resolved molecular insights are critical.

Our study has limitations. First, we focused on the early response to joint injury, with mice euthanized 8 days post-injury. Additional time points within and beyond 7 days may shed light on the trajectory of structural and metabolic changes across serum, SF, and whole joints. Second, the number of joints allocated for MALDI-MSI limits the statistical power of this portion of the study, highlighting the need for further investigation with a larger sample size, which would also allow exploration of sex differences at the spatial level. Lastly, although this study reveals tissue- and sex-specific metabolic alterations, targeted quantification or validation of specific metabolites was not performed. Nonetheless, these results establish a compelling foundation for future work focused on mechanistic understanding and validation in human samples—critical steps toward translating these insights into potential therapeutics or diagnostics.

The findings of our study, integrating LC-MS–based metabolomics and MALDI-MSI, underscore important metabolic and pathologic shifts following joint injury, with discernible sex-specific associations. By uncovering novel injury and sex-related differences across whole joints, SF, and serum, we expand the current understanding of the post-injury response both locally and systemically. Our results demonstrate that injury drives whole joint pathophysiology across multiple tissues, and systemic responses extend beyond the injured joint to the contralateral joint. Comprehensive investigation into spatial- and sex-dependent molecular changes driven by injury, at the systemic, joint, and SF levels, is imperative for unraveling the complexities of injury-induced pathology. Broadly, this approach and its techniques mark a major advancement in the field, establishing a robust framework for advancing preclinical PTOA models, ultimately shaping the future of precision medicine in musculoskeletal research and beyond.

AUTHOR CONTRIBUTIONS

All authors contributed to at least one of the following manuscript preparation roles: conceptualization AND/OR methodology, software, investigation, formal analysis, data curation, visualization, and validation AND drafting or reviewing/editing the final draft. As corresponding

author, Dr June confirms that all authors have provided the final approval of the version to be published and takes responsibility for the affirmations regarding article submission (eg, not under consideration by another journal), the integrity of the data presented, and the statements regarding compliance with institutional review board/Declaration of Helsinki requirements.

REFERENCES

1. Brown TD, Johnston RC, Saltzman CL, et al. Posttraumatic osteoarthritis: a first estimate of incidence, prevalence, and burden of disease. J Orthop Trauma 2006;20(10):739–744. doi:https://doi.org/10.1097/01.bot.0000246468.80635.ef
2. Giugliano DN, Solomon JL. ACL tears in female athletes. Phys Med Rehabil Clin N Am 2007;18(3):417–438, viii. doi:https://doi.org/10.1016/j.pmr.2007.05.002
3. Lohmander LS, Englund PM, Dahl LL, et al. The long-term consequence of anterior cruciate ligament and meniscus injuries: osteoarthritis. Am J Sports Med 2007;35(10):1756–1769. doi:https://doi.org/10.1177/0363546507307396
4. Bruder AM, Culvenor AG, King MG, et al. Let's talk about sex (and gender) after ACL injury: a systematic review and meta-analysis of self-reported activity and knee-related outcomes. Br J Sports Med 2023;57(10):602–610. doi:https://doi.org/10.1136/bjsports-2022-106099
5. Srikanth VK, Fryer JL, Zhai G, et al. A meta-analysis of sex differences prevalence, incidence and severity of osteoarthritis. Osteoarthritis Cartilage 2005;13(9):769–781. doi:https://doi.org/10.1016/j.joca.2005.04.014
6. Faber SC, Eckstein F, Lukasz S, et al. Gender differences in knee joint cartilage thickness, volume and articular surface areas: assessment with quantitative three-dimensional MR imaging. Skeletal Radiol 2001;30(3):144–150. doi:https://doi.org/10.1007/s002560000320
7. Hitt K, Shurman JR II, Greene K, et al. Anthropometric measurements of the human knee: correlation to the sizing of current knee arthroplasty systems. J Bone Joint Surg Am 2003;85-A(suppl 4):115–122. doi:https://doi.org/10.2106/00004623-200300004-00015
8. Hahn AK, Wallace CW, Welhaven HD, et al. The microbiome mediates epiphyseal bone loss and metabolomic changes after acute joint trauma in mice. Osteoarthritis Cartilage 2021;29(6):882–893. doi:https://doi.org/10.1016/j.joca.2021.01.012
9. Hislop BD, Devine C, June RK, et al. Subchondral bone structure and synovial fluid metabolism are altered in injured and contralateral limbs 7 days after non-invasive joint injury in skeletally-mature C57BL/6 mice. Osteoarthritis Cartilage 2022;30(12):1593–1605. doi:https://doi.org/10.1016/j.joca.2022.09.002
10. Wallace CW, Hislop B, Hahn AK, et al. Correlations between metabolites in the synovial fluid and serum: a mouse injury study. J Orthop Res 2022;40(12):2792–2802. doi:https://doi.org/10.1002/jor.25310
11. Cillero-Pastor B, Eijkel G, Kiss A, et al. Time-of-flight secondary ion mass spectrometry-based molecular distribution distinguishing healthy and osteoarthritic human cartilage. Anal Chem 2012;84(21):8909–8916. doi:https://doi.org/10.1021/ac301853q
12. Peffers MJ, Cillero-Pastor B, Eijkel GB, et al. Matrix assisted laser desorption ionization mass spectrometry imaging identifies markers of ageing and osteoarthritic cartilage. Arthritis Res Ther 2014;16(3):R110. doi:https://doi.org/10.1186/ar4560
13. Cillero-Pastor B, Eijkel GB, Blanco FJ, et al. Protein classification and distribution in osteoarthritic human synovial tissue by matrix-assisted laser desorption ionization mass spectrometry imaging. Anal Bioanal Chem 2015;407(8):2213–2222. doi:https://doi.org/10.1007/s00216-014-8342-2
14. Christiansen BA, Guilak F, Lockwood KA, et al. Non-invasive mouse models of post-traumatic osteoarthritis. Osteoarthritis Cartilage 2015;23(10):1627–1638. doi:https://doi.org/10.1016/j.joca.2015.05.009
15. Seifer DR, Furman BD, Guilak F, et al. Novel synovial fluid recovery method allows for quantification of a marker of arthritis in mice. Osteoarthritis Cartilage 2008;16(12):1532–1538. doi:https://doi.org/10.1016/j.joca.2008.04.013
16. Welhaven HD, Welfley AH, Pershad P, et al. Metabolic phenotypes reflect patient sex and injury status: a cross-sectional analysis of human synovial fluid. Osteoarthritis Cartilage 2024;32(9):1074–1083. doi:https://doi.org/10.1016/j.joca.2023.09.004
17. Pang Z, Zhou G, Ewald J, et al. Using MetaboAnalyst 5.0 for LC-HRMS spectra processing, multi-omics integration and covariate adjustment of global metabolomics data. Nat Protoc 2022;17(8):1735–1761. doi:https://doi.org/10.1038/s41596-022-00710-w
18. Nelson KA, Daniels GJ, Fournie JW, et al. Optimization of whole-body zebrafish sectioning methods for mass spectrometry imaging. J Biomol Tech 2013;24(3):119–127. doi:https://doi.org/10.7171/jbt.13-2403-002
19. Good CJ, Neumann EK, Butrico CE, et al. High spatial resolution MALDI imaging mass spectrometry of fresh-frozen bone. Anal Chem 2022;94(7):3165–3172. doi:https://doi.org/10.1021/acs.analchem.1c04604
20. Kawamoto T, Kawamoto K. Preparation of thin frozen sections from nonfixed and undecalcified hard tissues using Kawamot's film method (2012). Methods Mol Biol 2014;1130:149–164. doi:https://doi.org/10.1007/978-1-62703-989-5_11
21. Yamauchi M, Terajima M, Shiiba M. Lysine hydroxylation and cross-linking of collagen. Methods Mol Biol 2019;1934:309–324. doi:https://doi.org/10.1007/978-1-4939-9055-9_19
22. Pornprasertsuk S, Duarte WR, Mochida Y, et al. Overexpression of lysyl hydroxylase-2b leads to defective collagen fibrillogenesis and matrix mineralization. J Bone Miner Res 2005;20(1):81–87. doi:https://doi.org/10.1359/JBMR.041026
23. Saito M, Marumo K. Collagen cross-links as a determinant of bone quality: a possible explanation for bone fragility in aging, osteoporosis, and diabetes mellitus. Osteoporos Int 2010;21(2):195–214. doi:https://doi.org/10.1007/s00198-009-1066-z
24. Carlson AK, Rawle RA, Wallace CW, et al. Characterization of synovial fluid metabolomic phenotypes of cartilage morphological changes associated with osteoarthritis. Osteoarthritis Cartilage 2019;27(8):1174–1184. doi:https://doi.org/10.1016/j.joca.2019.04.007
25. Tootsi K, Vilba K, Märtson A, et al. Metabolomic signature of amino acids, biogenic amines and lipids in blood serum of patients with severe osteoarthritis. Metabolites 2020;10(8):323. doi:https://doi.org/10.3390/metabo10080323
26. Ohnishi A, Osaki T, Matahira Y, et al. Correlation of plasma amino acid concentrations and chondroprotective effects of glucosamine and fish collagen peptide on the development of osteoarthritis. J Vet Med Sci 2013;75(4):497–502. doi:https://doi.org/10.1292/jvms.12-0241
27. Hu Y, Wu Q, Qiao Y, et al. Disturbances in metabolic pathways and the identification of a potential biomarker panel for early cartilage degeneration in a rabbit anterior cruciate ligament transection model. Cartilage 2021;13(2_suppl)(suppl):1376S–1387S. doi:10.1177/1947603520921434
28. Wallace CW, Hislop B, Hahn AK, et al. Correlations between metabolites in the synovial fluid and serum: a mouse injury study. J Orthop Res 2022;40(12):2792–2802. doi:https://doi.org/10.1002/jor.25310
29. Ding KH, Cain M, Davis M, et al. Amino acids as signaling molecules modulating bone turnover. Bone 2018;115:15–24. doi:https://doi.org/10.1016/j.bone.2018.02.028
30. Conigrave AD, Brown EM, Rizzoli R. Dietary protein and bone health: roles of amino acid-sensing receptors in the control of calcium

metabolism and bone homeostasis. Annu Rev Nutr 2008;28(1):131–155. doi:https://doi.org/10.1146/annurev.nutr.28.061807.155328

31. Yang G, Zhang H, Chen T, et al. Metabolic analysis of osteoarthritis subchondral bone based on UPLC/Q-TOF-MS. Anal Bioanal Chem 2016;408(16):4275–4286. doi:https://doi.org/10.1007/s00216-016-9524-x
32. Igari T, Tsuchizawa M, Shimamura T. Alteration of tryptophan metabolism in the synovial fluid of patients with rheumatoid arthritis and osteoarthritis. Tohoku J Exp Med 1987;153(2):79–86. doi:https://doi.org/10.1620/tjem.153.79
33. Kang KY, Lee SH, Jung SM, et al. Downregulation of tryptophan-related metabolomic profile in rheumatoid arthritis synovial fluid. J Rheumatol 2015;42(11):2003–2011. doi:https://doi.org/10.3899/jrheum.141505
34. Leimer EM, Tanenbaum LM, Nettles DL, et al. Amino acid profile of synovial fluid following intra-articular ankle fracture. Foot Ankle Int 2018;39(10):1169–1177. doi:https://doi.org/10.1177/1071100718786163
35. Welhaven HD, Welfley AH, Pershad P, et al. Metabolic phenotypes reflect patient sex and injury status: A cross-sectional analysis of human synovial fluid. Osteoarthritis Cartilage 2024;32(9):1074–1083. doi:https://doi.org/10.1016/j.joca.2023.09.004
36. Akasaka H, Yoshida H, Takizawa H, et al; BOREAS-CKD1 Investigators. The impact of elevation of serum uric acid level on the natural history of glomerular filtration rate (GFR) and its sex difference. Nephrol Dial Transplant 2014;29(10):1932–1939. doi:https://doi.org/10.1093/ndt/gfu197
37. Mumford SL, Dasharathy SS, Pollack AZ, et al. Serum uric acid in relation to endogenous reproductive hormones during the menstrual cycle: findings from the BioCycle study. Hum Reprod 2013;28(7):1853–1862. doi:https://doi.org/10.1093/humrep/det085
38. Mickiewicz B, Heard BJ, Chau JK, et al. Metabolic profiling of synovial fluid in a unilateral ovine model of anterior cruciate ligament reconstruction of the knee suggests biomarkers for early osteoarthritis. J Orthop Res 2015;33(1):71–77. doi:https://doi.org/10.1002/jor.22743
39. Yi D, Yu H, Lu K, et al. AMPK signaling in energy control, cartilage biology, and osteoarthritis. Front Cell Dev Biol 2021;9:696602. doi:https://doi.org/10.3389/fcell.2021.696602
40. Yang S, Wang J. Estrogen activates AMP-activated protein kinase in human endothelial cells via ERβ/Ca(2+)/calmodulin-dependent protein kinase kinase β pathway. Cell Biochem Biophys 2015;72(3):701–707. doi:https://doi.org/10.1007/s12013-015-0521-z
41. Cui N, Hu M, Khalil RA. Biochemical and biological attributes of matrix metalloproteinases. Prog Mol Biol Transl Sci 2017;147:1–73. doi:https://doi.org/10.1016/bs.pmbts.2017.02.005
42. Visse R, Nagase H. Matrix metalloproteinases and tissue inhibitors of metalloproteinases: structure, function, and biochemistry. Circ Res 2003;92(8):827–839. doi:https://doi.org/10.1161/01.RES.0000070112.80711.3D
43. Verma RP, Hansch C. Matrix metalloproteinases (MMPs): chemical-biological functions and (Q)SARs. Bioorg Med Chem 2007;15(6):2223–2268. doi:https://doi.org/10.1016/j.bmc.2007.01.011
44. Lee YJ, Lee EB, Kwon YE, et al. Effect of estrogen on the expression of matrix metalloproteinase (MMP)-1, MMP-3, and MMP-13 and tissue inhibitor of metalloproternase-1 in osteoarthritis chondrocytes. Rheumatol Int 2003;23(6):282–288. doi:https://doi.org/10.1007/s00296-003-0312-5
45. Eveque-Mourroux MR, Emans PJ, Boonen A, et al. Heterogeneity of lipid and protein cartilage profiles associated with human osteoarthritis with or without type 2 diabetes mellitus. J Proteome Res 2021;20(5):2973–2982. doi:https://doi.org/10.1021/acs.jproteome.1c00186
46. Pousinis P, Gowler PRW, Burston JJ, et al. Lipidomic identification of plasma lipids associated with pain behaviour and pathology in a mouse model of osteoarthritis. Metabolomics 2020;16(3):32. doi:https://doi.org/10.1007/s11306-020-01652-8
47. Carlson AK, Rawle RA, Wallace CW, et al. Global metabolomic profiling of human synovial fluid for rheumatoid arthritis biomarkers. Clin Exp Rheumatol 2019;37(3):393–399.
48. Welhaven HD, Viles E, Starke J, et al. Metabolomic profiles of cartilage and bone reflect tissue type, radiography-confirmed osteoarthritis, and spatial location within the joint. Biochem Biophys Res Commun 2024;703:149683. doi:https://doi.org/10.1016/j.bbrc.2024.149683
49. Carlson AK, Rawle RA, Adams E, et al. Application of global metabolomic profiling of synovial fluid for osteoarthritis biomarkers. Biochem Biophys Res Commun 2018;499(2):182–188. doi:https://doi.org/10.1016/j.bbrc.2018.03.117
50. Welhaven HD, Welfley AH, Brahmachary P, et al. Metabolomic profiles and pathways in osteoarthritic human cartilage: a comparative analysis with healthy cartilage. Metabolites 2024;14(4):183. doi:https://doi.org/10.3390/metabo14040183

Arthritis & Rheumatology
Vol. 78, No. 9, September 2026, pp 1863–1877
DOI 10.1002/art.70157
© 2026 The Author(s). *Arthritis & Rheumatology* published by Wiley Periodicals LLC on behalf of American College of Rheumatology.
This is an open access article under the terms of the Creative Commons Attribution-NonCommercial License, which permits use, distribution and reproduction in any medium, provided the original work is properly cited and is not used for commercial purposes.

American College of Rheumatology
Empowering Rheumatology Professionals

The Potential Role of Synovial T Cell Infiltration Following Knee Joint Injury in Symptoms and Progression to Osteoarthritis

Babak Moradi, MD,[1,2,3] Miriam T. Jackson, PhD,[1] Cindy C. Shu, PhD,[1] Susan M. Smith, BSc,[1] Margaret M. Smith, PhD,[1] Sanaa Zaki, BVSc, PhD,[1,4] Hadrian Platzer, MD,[1,2,3] Nils Rosshirt, MD,[2,3] David Giangreco, MD,[5] Carla R. Scanzello, MD, PhD,[5,6,7] and Christopher B. Little, BVMS, PhD[1]

Objective. Identification of osteoarthritis (OA)–specific synovial inflammatory pathways and their temporal relevance is critical for therapeutic targeting. We compared mononuclear inflammatory/immune cell responses following joint injury that does or does not lead to OA to define bona fide OA-associated cellular events.

Methods. We undertook detailed temporal flow cytometric and messenger RNA (mRNA) expression analysis in mice after sham or destabilization of the medial meniscus (DMM) surgery. This was compared with patients with meniscal injury and OA, evaluating the role of synovial monocytes/macrophages versus lymphocytes in catabolic metalloproteinase secretion in vitro. We determined the effect of transient or delayed systemic T cell depletion on DMM-induced OA pathology.

Results. OA-inducing/DMM and non–OA-inducing/sham surgery had an identical synovial monocyte/macrophage number, activation, and polarization. The number and activation of synovial (not splenic or peripheral blood) $CD4^+$ and $CD8^+$ lymphocytes were increased from one day after DMM versus sham and showed a persistent cyclical elevation throughout OA onset and progression. There was a temporal imbalance in synovial Th17/Treg and Th1/Th2 lymphocytes during DMM-induced OA initiation and progression. We confirmed early postinjury and late OA CD3/CD8 T cell responses in synovial tissues from patients, identified an association between CD8 and early postinjury symptoms, and defined a significant role for $CD3^+$ T cells in synovial metalloproteinase secretion. Anti-CD3 cell depletion studies in mice provided an initial approach to testing this hypothesis, offering preliminary evidence that early postinjury T cell responses may be associated with long-term OA pathology.

Conclusion. We identify a hitherto unappreciated pathophysiologic role of acute T cell activation after joint injury in long-term posttraumatic OA risk, providing a novel diagnostic and therapeutic target.

INTRODUCTION

Osteoarthritis (OA) affects 12% to 15% of the population, causing enormous individual and socioeconomic burden, with no treatments to halt disease onset or progression.[1] Studies in patients and preclinical models have implicated OA-associated synovitis as a potential disease-modifying target.[2,3] Synovial inflammatory mediators are more elevated in early OA,[4–6] and patients with synovitis/joint effusion have faster progression and more incident OA.[7,8] That inflammation impacts disease initiation is supported by animal studies in which synovitis precedes structural hip OA in at-risk dogs, and modulation of specific

Supported by the Australian National Health and Medical Research Council (project grant APP1045890), the Hillcrest Foundation through Perpetual Philanthropies, and Arthritis Australia. Dr Moradi's work was supported by a Research Scholarship of the German Research Foundation (Deutsche Forschungsgemeinschaft Project 199129044 and 277277765).

[1]Raymond Purves Bone and Joint Research Laboratories, Kolling Institute of Medical Research, University of Sydney at Royal North Shore Hospital, St Leonards, New South Wales, Australia; [2]Orthopedic Research Center, Kiel University, Kiel, Germany; [3]Department of Orthopedics and Trauma Surgery, University Medical Center Schleswig-Holstein, Campus Kiel, Kiel, Germany; [4]Sydney School of Veterinary Science, Faculty of Science, University of Sydney, Camperdown, New South Wales, Australia; [5]Division of Rheumatology, Rush University Medical Center, Chicago, Illinois; [6]VA CREATE Motion Center and Translational Musculoskeletal Research Center, Corporal Michael J. Crescenz VA Medical Center, Philadelphia, Pennsylvania; [7]Division of Rheumatology, University of Pennsylvania Perelman School of Medicine, Philadelphia.

Drs Moradi and Jackson contributed equally to this work.

Additional supplementary information cited in this article can be found online in the Supporting Information section (https://acrjournals.onlinelibrary.wiley.com/doi/10.1002/art.70157).

Author disclosures are available at https://onlinelibrary.wiley.com/doi/10.1002/art.70157.

Address correspondence via email to Babak Moradi, MD, at Babak.Moradi@uksh.de; or to Christopher B. Little, BVMS, PhD, at christopher.little@sydney.edu.au.

Submitted for publication August 24, 2025; accepted in revised form January 23, 2026.

inflammatory molecules/pathways reduces posttraumatic OA (ptOA) onset as well as progression in mice.[9] Better understanding of OA-specific inflammation may lead to much needed disease-modifying therapeutics.

Numerous inflammatory effectors have been identified in OA,[2,10–14] but detailed knowledge of their temporal regulation and association with pathology is lacking, particularly for innate and adaptive immune-cellular responses.[6,15,16] Macrophages[13,14,17] and lymphocytes[15,16,18] have been implicated in structural and symptomatic disease because they are present in synovium of patients with OA. However, restricted access to preclinical patient samples means the inflammatory cell events occurring during disease initiation are poorly defined. Occurring after known injury, ptOA offers the potential to study the earliest phases of synovial inflammation,[19] but comparison with "non–OA-inducing" joint injury has not been possible in clinical studies.[20]

Surgical destabilization of the medial meniscus (DMM) in mice is a widely used preclinical model for investigating ptOA pathobiology and treatment.[21] A key role for specific inflammatory pathways in initiation and progression of DMM-induced ptOA has been demonstrated using genetically modified mice.[9] This study aimed to analyze the temporal dynamics of synovial T cell infiltration relative to macrophage accumulation, examine their association with disease-related symptoms, and evaluate the effects of immune cell depletion strategies on OA pathology.

MATERIALS AND METHODS

DMM model. Studies were approved by the institutional ethics committee (protocol 1106-012A). Male 10- to 11-week-old C57BL6 mice were sourced and housed, and DMM surgery was performed in one knee and sham surgery was performed in the other as described.[22,23] Mice received no postoperative medication, had unrestricted cage activity, and were killed at days 1, 3, 7, 14, 21, 28, 35, 42, 49, 56, 72, 84, 98, and 112 post surgery (n = 16–22/time). At selected times, age- and sex-matched naïve mice were killed as nonoperated controls (NOC; n = 16–22/time). Additional mice had bilateral sham or DMM surgery and were killed at days 14, 42, 84, and 112 post surgery (n = 16/time/group) to evaluate changes in peripheral blood mononuclear cells (PBMCs) and spleen mononuclear cells (SpMCs). Another cohort of mice (n = 20/treatment/time) received a single 20-μg intraperitoneal injection of anti-CD3 (145-2C11; BioLegend) or isotype control (Armenian-Hamster IgG; BioLegend) one week before or three weeks after unilateral DMM and were killed at days 14, 28, 56, and 112 post surgery. Eight mice per treatment group had tactile allodynia measured before and at specified times post DMM.[24] Anti-CD3 dosing and timing were selected based on prior published studies and informed by our temporal analyses, and animals were monitored throughout the study for potential adverse effects, including changes in body weight, changes in general activity, and signs of infection, with no differences observed compared with isotype-treated controls.

Joint sample preparation. Immediately after death, synovial tissue (ST) consisting of infrapatellar fat pad, joint capsule, and synovial lining, was microdissected en bloc.[22] ST from six NOC, sham, and DMM joints at days 7, 14, 35, 49, and 112 was used for quantitative reverse transcriptase–polymerase chain reaction (qRT-PCR)[22,23] to quantify messenger RNA (mRNA) expression of *Cd3*, *Cd4*, *Cd8*, *Il1*, *Il6*, and *Tnf* relative to *Gapdh* (mouse-specific primers; Supplementary Table 1). ST from 16 animals/group was used for flow cytometry (4 "biologic replicates"/time point consisting of pooled ST from 4 mice). After ST removal, remaining joint tissues were processed, and sagittal sections every 80 μm through the medial femorotibial joint were stained with toluidine blue/fast green for histopathology scoring.[22,23]

Flow cytometry. For flow cytometry analysis, samples from mice were pooled to generate an adequate number of cells. Surface marker staining included a pool of four mice for each data point. For intracellular staining, samples from six mice were pooled. PBMCs, SpMCs, and ST mononuclear cells (STMCs) were isolated, live cells were counted, and subtypes were quantified using cell surface markers.[22] A total of 10^5 events were collected (four-color flow cytometer; Becton-Dickinson), and population analysis was performed (FlowJo, Treestar). Isolated synovial cells were gated using the forward scatter profile and 7-aminoactinomycin D–negative staining to exclude debris and dead cells. Cutoffs were established using isotype control antibodies. Viable $CD45^+$ MCs were gated on forward/side scatter as monocytic ($CD11b^+$) or lymphocytic ($CD3^+$), followed by $CD11b^+F4/80^-Ly6c^+$ resident monocytes, $CD11b^+F4/80^+Ly6c^{high}$ inflammatory monocytes, $CD11b^+F4/80^+Ly6c^{low}$ activated macrophages (M1 [$F4/80^+CD11c^+$] or M2 [$F4/80^+CD206^+$]), $CD3^+CD4^+CD8^-$ T helper cells, and $CD3^+CD4^-CD8^+$ cytotoxic T cells. For intracellular staining, cells were stimulated (5 hours, 50 ng/mL phorbol myristate acetate, 1 μg/mL ionomycin; BD Biosciences) before the addition of brefeldin A (5 μg/mL, 5 hours; Sigma-Aldrich). By surface marker staining, $CD45^+CD3^+CD4^+CD8^-$ T cell subsets were defined. Cells were fixed, permeabilized, and stained for their specific cytokines and transcription factors with BV-421–labeled anti-IFNγ ("Th1"), APC-labeled anti–IL-4 ("Th2"), PE-labeled anti–IL-17A ("Th17"), or Alexa Fluor 488–labeled anti-FoxP3 ("Treg"). For data evaluation, the mean value ± SEM was calculated. There was no difference in the synovial cell numbers in NOC over time, so a mean value (shown as a solid line ± SEM represented by gray shading in relevant figures) was calculated and used for comparison with sham (circle with dotted line) and DMM (square with dashed line) at each time point.

Human samples. Suprapatellar ST collected in the course of previous studies from three patient cohorts (Supplementary Information) was analyzed: 16 with advanced knee OA,[25] 19 with meniscal tear/early OA,[25] and 13 with meniscal tear/no OA.[20,26] Aliquots of RNA from deidentified patients were provided with clinical data (Supplementary Table 2), and *CD3*, *CD4*, and *CD8* were quantified by qRT-PCR (human-specific primers; Supplementary Table 1).

ST from 12 patients with OA undergoing unicompartmental or total knee replacement (University Hospital Heidelberg; ethics #S-156/2014; Supplementary Table 3) was digested (collagenase B [Roche], 6.7 µg/mg, 37°C, 2 hours), and MCs were isolated by centrifugation. Selective and efficient depletion of $CD3^+$, $CD4^+$, $CD8^+$, and $CD14^+$ cells in isolates from human OA synovium was achieved with magnetic-activated cell sorting according to the manufacturer's instructions (Miltenyi Biotec). Native and depleted samples were cultured (24 hours, RPMI/10% FCS/1% penicillin/streptomycin; 10^6 cells/mL), and the concentrations of MMP-1 (Sigma-RAB0361-1KT), MMP-3 (Sigma-RAB0367-1KT), MMP-9 (Sigma-RAB0372-1KT), and ADAMTS-5 (LOXO-6SEK205HU) in conditioned media were quantified by enzyme-linked immunosorbent assay.

Statistical analysis. The minimum number of animals and/or biologic replicates to detect differences with >80% power (two-sided, $\alpha = 0.05$) was determined a priori using previous data[22,23] (n = 5/group for histopathology, n = 4/group for surface fluorescence-activated cell sorting (FACS) [each a pool of 4 mice]/time/surgery; n = 4/group for intracellular FACS [each a pool of 6 mice]/time/surgery; n = 6/group for gene expression, and n = 8/group for mechanical allodynia). Animals were randomly assigned to groups, and investigators were blinded to these during data acquisition. Data from all animals and human participants were used for analysis (no outlier removal), with the number of replicates provided in the Materials and methods section, figure legends, and table. Except for the behavioral (von Frey) experiments, all mouse data were analyzed cross-sectionally: independent cohorts of animals were killed at each time point, and statistical comparisons were performed between groups (DMM, sham, NOC, and treatment groups) within each time point.

Following QQ plots and Shapiro–Wilk tests, normally distributed data were analyzed by analysis of variance (ANOVA) with Bonferroni and Tukey correction, whereas nonparametric outcomes were evaluated using Kruskal–Wallis and Friedman tests (Prism, GraphPad). Von Frey testing represents longitudinal measurements in the same animals over time and was analyzed using repeated-measures ANOVA with Bonferroni post hoc tests. Spearman correlations between clinical outcomes and mRNA expression were calculated using SPSS (IBM Inc). For all analyses, $P \leq 0.05$ was considered statistically significant. The exact statistical test and post hoc procedure used for each figure and panel are summarized in Supplementary Table 4.

RESULTS

OA histopathology. Progressively worsening medial femorotibial OA pathology, including significantly greater cartilage proteoglycan loss and structural damage, subchondral bone sclerosis, and osteophyte formation, was seen in DMM versus NOC (from day 7) and sham (from day 14) (Figure 1).

STMC number. The number of STMCs in NOC did not change over time ($P = 0.84$). STMCs increased markedly one day following sham and DMM, with cyclical decreases (days 3, 28, 56, and 84) and increases (days 14, 35, and 70) thereafter (Figure 2A). Resolution phases were of greater magnitude and increases were of less magnitude in sham, such that numbers returned to NOC levels after day 21, while remaining elevated in DMM versus NOC (days 1–70) and sham (days 3–49). Together, these data indicate an acute postinjury peak followed by recurrent resolution and reactivation phases, with DMM showing a more persistent and pronounced cyclical STMC response than sham.

Monocytes/macrophages. Frequencies of systemic $CD11b^+$ monocytes/macrophages were similar in NOC, sham, and DMM (mean ± SD 41.6% ± 27.1%, 35% ± 17.5%, and 30.6% ± 12.9% of PBMCs, respectively; 6.9% ± 0.6%, 9.8% ± 1.5%, and 5.8% ± 0.6% of SpMCs, respectively; no temporal differences within any group). This also applied to systemic $CD11b^+$ subtypes ($Ly6c^+$ resident monocytes mean ± SD: NOC 43.7% ± 11%, sham 49% ± 13%, DMM 44% ± 10%; $F4/80^+Ly6c^{high}$ inflammatory monocytes mean ± SD: NOC 26.6% ± 3%, sham 30.4% ± 6%, DMM 29.1% ± 3.5%; and $F4/80^+Ly6c^{low}$ activated macrophages mean ± SD: NOC 19.8% ± 7.8%, sham 17.5% ± 6.8%, DMM 23.1% ± 6.3%). In contrast, $CD11b^+$ STMCs increased immediately post surgery, followed by diminishing cyclical peaks (days 3, 28, 56, and 112), but with no difference between sham and DMM (Figure 2). Resident monocytes made up 60% to 80% of $CD11b^+$ STMCs in NOC at all times but decreased acutely in sham and DMM (<20% by day 3) before returning to NOC levels (days 28–35; Figure 2D). Inflammatory monocyte levels were elevated immediately post surgery before returning to NOC levels at day 35 (Figure 2E). Activated macrophages peaked three to seven days post surgery before returning to NOC levels at day 21 (Figure 2F). There was no difference between sham and DMM in any subtype at any time.

Polarization of ST macrophages into M1 and M2 subtypes showed distinct temporal patterns in NOC versus DMM and sham, but there was no difference between surgeries (Figure 2G). In NOC, the majority of ST macrophages expressed neither marker up to day 56 (M0: 57%–74%), with 17% to 26% expressing M1, 8% to 14% positive for both (M1/2), and only 0.1% to 2.5% expressing M2. With aging (day 112), increases in M1 (36%) and M1/2 (39%) occurred in NOCs. In both DMM and sham, there was a marked increase in M1 at day 1 (72%–76%),

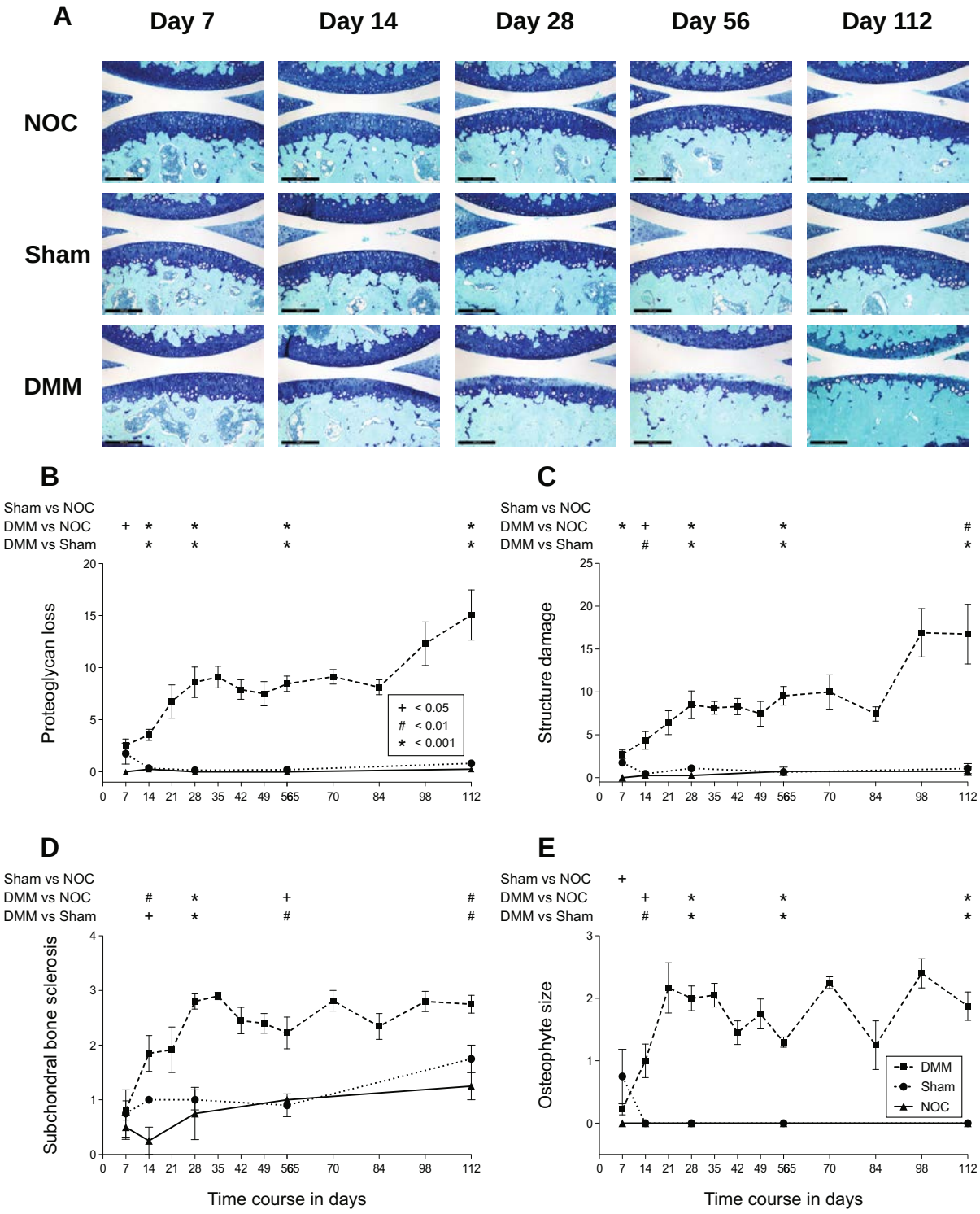

Figure 1. Progressive osteoarthritis structural pathology occurs after destabilization of the medial meniscus (DMM) but not sham surgery. (A) Representative images of toluidine blue/fast green–stained sections of medial femorotibial joints of mice 7 to 112 days after sham or DMM surgery compared with age-matched nonoperated controls (NOC; scalebar = 200 μm). Progressive loss of cartilage proteoglycan staining followed by noncalcified cartilage erosion only occurs in DMM and is accompanied by increased subchondral bone sclerosis and loss of epiphyseal marrow. Two observers blinded to injury and time scored the tibial (B) cartilage proteoglycan loss, (C) cartilage structural damage, (D) subchondral bone sclerosis, and (E) osteophyte size. Data are shown as the mean ± SEM. NOC is represented by the triangle and solid line, sham is represented by the circle and dotted line, and DMM is represented by the square and dashed line. Statistical comparison was performed for those time points in which scores for all three groups were available, with significant differences at each time shown above each graph. n = 10 for DMM and sham, and n = 4 for NOC: $^{*}P \leq 0.05$; $^{+}P \leq 0.01$; $^{\#}P \leq 0.001$.

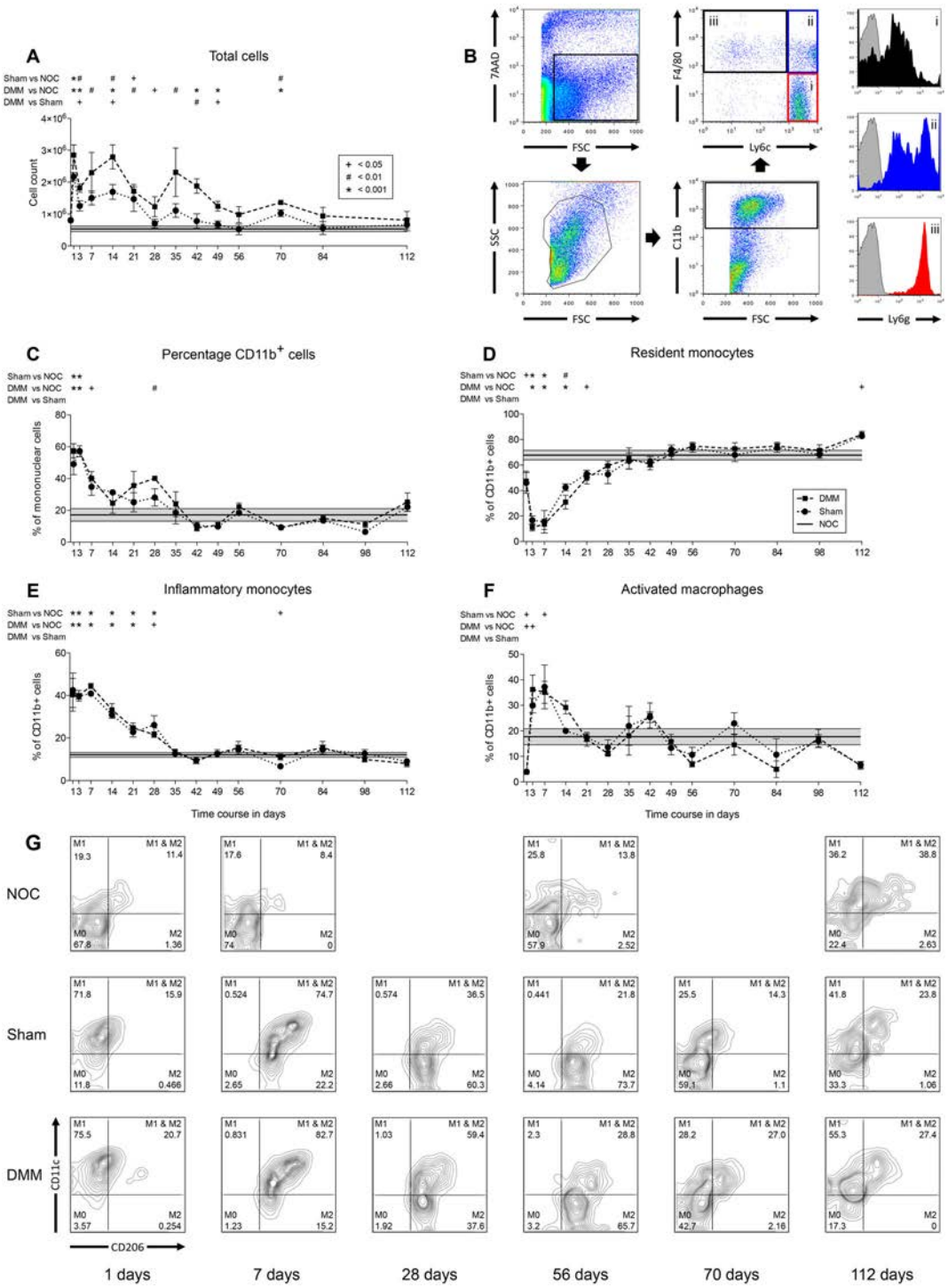

Figure 2. Destabilization of the medial meniscus (DMM) results in greater cyclical synovial mononuclear cell influx than sham surgery but no difference in monocyte/macrophage activation or polarization. (A) Both sham and DMM surgery resulted in a cyclical increase in the mononuclear cell number in the synovial tissue compared with nonoperated controls (NOC); however the effect was more pronounced and persistent with DMM. (B) Monocyte/macrophage cell populations were defined as (i) resident monocytes ($CD11b^+F4/80^-Ly6c^+$), (ii) inflammatory monocytes ($CD11b^+F4/80^+Ly6c^{high}$), and (iii) activated macrophages ($CD11b^+F4/80^+Ly6c^{low}$), which were further distinguished by their relative expression of Ly6g (right panel; colors according to gate i, ii, or iii). The frequency of (C) synovial $CD11b^+$ cells, (D) resident monocytes, (E) inflammatory monocytes, and (F) activated macrophages showed distinct temporal changes after surgery compared with NOC but with no significant difference between sham and DMM. (G) Activated macrophages ($CD11b^+F4/80^+Ly6c^{low}$) in sham and DMM showed a very similar temporal pattern of polarization from M0 ($CD11c^-/CD206^-$) to M1 ($CD11c^+/CD206^-$), M1/2 ($CD11c^+/CD206^+$), and finally M2 ($CD11c^-/CD206^+$). Statistically significant differences between sham and NOC, DMM and NOC and DMM and sham at each time point are indicated above each graph (n = 4 [each a pool of 4 mice]/time/surgery): $^*P \leq 0.05$; $^+P \leq 0.01$; $^\#P \leq 0.001$. Color figure can be viewed in the online issue, which is available at http://onlinelibrary.wiley.com/doi/10.1002/art.70157/abstract.

followed by a temporal transition to M1/2 (75%–83% at day 7), M2 (66%–73% by day 56), and thereafter to day 112 NOC levels. Overall, synovial monocyte/macrophage influx and polarization in both surgeries followed a wound-healing pattern with early M1 and later M2 predominance, which resolved over time and did not distinguish OA-inducing from non–OA-inducing injury.

Lymphocytes. There was a cyclic increase in ST lymphocytes after surgery (Figure 3): peaks at days 7, 35, and 98. The percentage of ST $CD3^+$ lymphocytes did not differ between sham and NOC at any time but was greater in DMM than NOC (days 1–98) and sham (days 1–14; Figure 3C). As a percentage of the $CD3^+$ lymphocytes, $CD4^+$ T cells were increased in DMM compared with NOC and sham from day 1 to 112 (Figure 3E). While showing similar cyclic fluctuation, the percentage of $CD8^+$ T cells did not differ between DMM and sham (Figure 3G). However, $CD3^+$, $CD4^+$, and $CD8^+$ T cell numbers (rather than percentage) were greater in DMM versus sham from day 1 to day 84 (Figure 3D, F, and H). Thus, in contrast to macrophages, OA-inducing DMM is characterized by an immediate (day 1) and recurrent T cell–dominated response that remains elevated through OA onset and progression and clearly distinguishes DMM from sham.

Splenic and ST T helper cells were further categorized post DMM as Th1 (IFN^+), Th2 ($IL\text{-}4^+$), Th17 ($IL\text{-}17^+$), or Treg cells ($FoxP3^+$) (Figure 4A). The percentage of all subtypes was almost always lower in the spleen, and when this was not the case, anti-inflammatory cell types predominated (Table 1). There was little change in splenic $CD4^+$ subtypes over time (all <5%; Figure 4B), and proinflammatory imbalances (Th1/Th2, Th17/Treg cells) were generally less than two-fold (Supplementary Table 4). In the ST, however, large temporally distinct changes in T helper subtypes occurred (Figure 4B, Table 1). Th17 cells predominated at day 7 post DMM (19%), with levels remaining >10% thereafter, whereas Treg cells were least common at day 7 (1.4%), increasing to 25% by day 35, then decreasing to <5% by days 84 to 112. Th1 cells showed the most dramatic post-DMM increase reaching >70% of $CD4^+$ T cells at day 70 before returning to ∼20% at day 112, and although the pattern was broadly similar, Th2 cell changes were smaller (peaking at ∼33% at day 70). Unlike the spleen, there was a marked proinflammatory imbalance in ST $CD4^+$ T cell subtypes post DMM: Th1 cell levels were significantly greater than Th2 cell levels at days 35, 56, 70, and 98; Th17 cell levels were significantly greater than Treg cell levels at days 1, 70, 84, and 98 (Figure 4B; Supplementary Table 5). Taken together, this reveals a phase-specific pattern in synovial $CD4^+$ T cell subsets, with an early postinjury Th17/Treg cell imbalance and a predominant Th1/Th2 cell imbalance during the progression of structural ptOA, which then diminishes again in late disease.

ST lymphocyte marker expression. Expression of *Cd4* and *Cd8* was markedly increased at day 7 in both sham and DMM (Figure 4C), decreasing by days 14 to 35 before increasing again, particularly in DMM, such that by day 112, expression was higher than in sham, reflecting flow cytometry data (Figure 3). Expression of *CD3*, *CD4*, and *CD8* mRNA was therefore measured in ST from patients after meniscal injury with no (New England Babtist Hospital cohort (NEBH)) or early (Rush University Medical Center cohort (RUSH)) OA, as well as with advanced OA. *CD3* and *CD4* were detected in 95% to 100% of all patients (no difference between groups), whereas the percentage of *CD8*-positive patients with advanced OA (100%) was greater than the percentage with meniscal injury (NEBH 77%, Rush 63%). There was no between-group difference in mean *CD3*, *CD4*, or *CD8* expression; however, *CD3* and *CD8* levels were higher with shorter time post injury (Figure 4D). Lymphocyte marker expression was significantly correlated with preoperative symptoms: NEBH patients *CD3* and Lysholm score; Rush patients *CD8* and Knee Injury and Osteoarthritis Outcome Score (KOOS) pain, KOOS activities of daily living, KOOS sport/recreation, and KOOS quality of life scores (Figure 4E; Supplementary Table 6). These findings support the mouse data by indicating an early $CD3^+/CD8^+$ synovial T cell response after meniscal injury that is linked to worse symptoms, whereas later-stage disease is dominated by more chronic T cell activation.

Impact of lymphocyte depletion. Magnetic-activated cell sorting selectively depleted $CD14^+$ and $CD3^+$ cells, including $CD4^+$ T helper cells and $CD8^+$ cytotoxic T cells from human OA ST (Figure 5A). Although removing $CD14^+$ monocytes/macrophages lead to the greatest reduction, depletion of $CD3^+$ cells and isolated $CD4^+$ or $CD8^+$ lymphocyte depletion significantly decreased MMP-1, MMP-3, and MMP-9 secretion (Figure 5B). In light of these in vitro data, we conducted pilot studies to evaluate whether $CD3^+$ lymphocyte depletion would modify DMM-induced ptOA and compared targeting the immediate postinjury influx versus that occurring later: pre-DMM versus three weeks post-DMM anti-CD3. Systemic anti-CD3 administered either one week before or three weeks after DMM significantly depleted splenic $CD3^+$ and $CD4^+$ T cells for two weeks post treatment and $CD8^+$ T cells for eight (before DMM treatment) or five weeks (after DMM treatment) compared with a control antibody. With pre-DMM treatment, the $CD4^+$ T cells rebounded and were increased compared with a control antibody at week 16. Despite effects on splenic T cells, there was no change in $CD4^+$ or $CD8^+$ T cells in the ST following systemic anti-CD3 administered either one week before or three weeks after DMM (Figure 5D).

Neither treatment protocol altered subchondral bone remodeling or osteophyte size, but osteophyte maturation from cartilage to bone was delayed: week 2 and week 8 after pre- and post-DMM treatment, respectively (Figure 5E). There was no effect of post-DMM anti-CD3 on cartilage structural pathology; however, targeting the initial T cell response reduced 2-week proteoglycan loss compared with IgG, slowed progressive 8- to 16-week

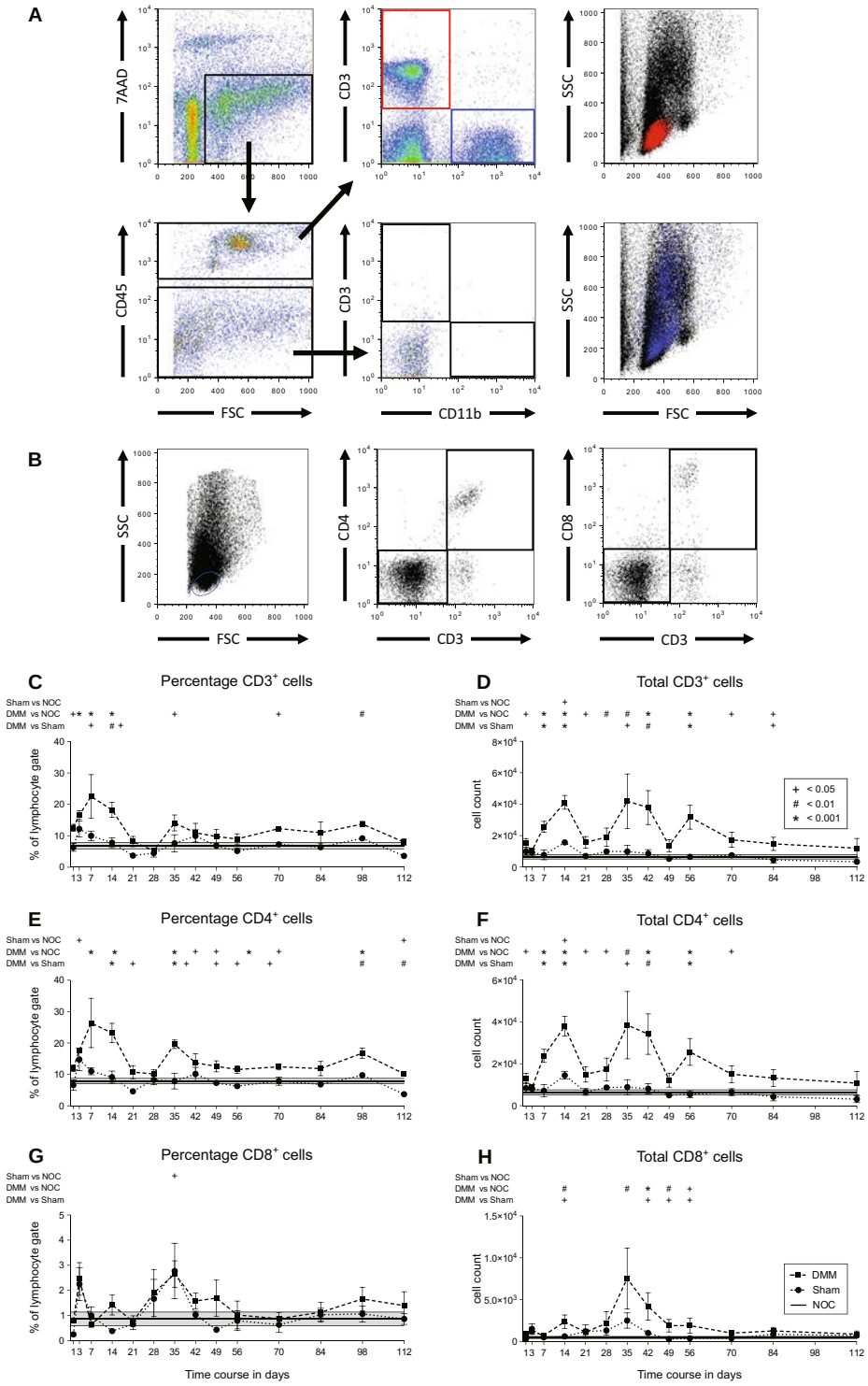

Figure 3. Destabilization of the medial meniscus (DMM) results in significantly greater cyclical synovial T cell influx than sham surgery. (A) Viable mononuclear cells were gated based on the negative 7-aminoactinomycin D (7-AAD) staining and further through the CD45 marker. CD3 and CD11b were used as broad markers for lymphocytes and monocytes/macrophages, respectively. These two distinct cell populations showed no overlap and were all $CD45^+$, with little or no CD3 or CD11b staining in the $CD45^-$ population. The right column shows the cell size and granularity of $CD3^+$ (red) and $CD11b^+$ (blue) cells. (B) Cells in the "lymphocyte gate" based on forward and side scatter were further defined as $CD3^+CD4^+CD8^-$ T helper cells and $CD3^+CD4^-CD8^+$ cytotoxic T cells. The (C, E, and G) frequency and (D, F, and H) absolute number of (C and D) synovial $CD3^+$ lymphocytes, (E and F) $CD4^+$ T helper cells, and (G and H) $CD8^+$ cytotoxic T cells showed distinct temporal changes after surgery compared with nonoperated controls (NOC), with significantly greater numbers at multiple time points in DMM compared with sham. Significant significant differences between sham and NOC, DMM and NOC, and DMM and sham at each timepoint are indicated above each graph (n = 4 [each a pool of 4 mice]/time/surgery): $^*P \leq 0.05$; $^+P \leq 0.01$; $^\#P \leq 0.001$. Color figure can be viewed in the online issue, which is available at http://onlinelibrary.wiley.com/doi/10.1002/art.70157/abstract.

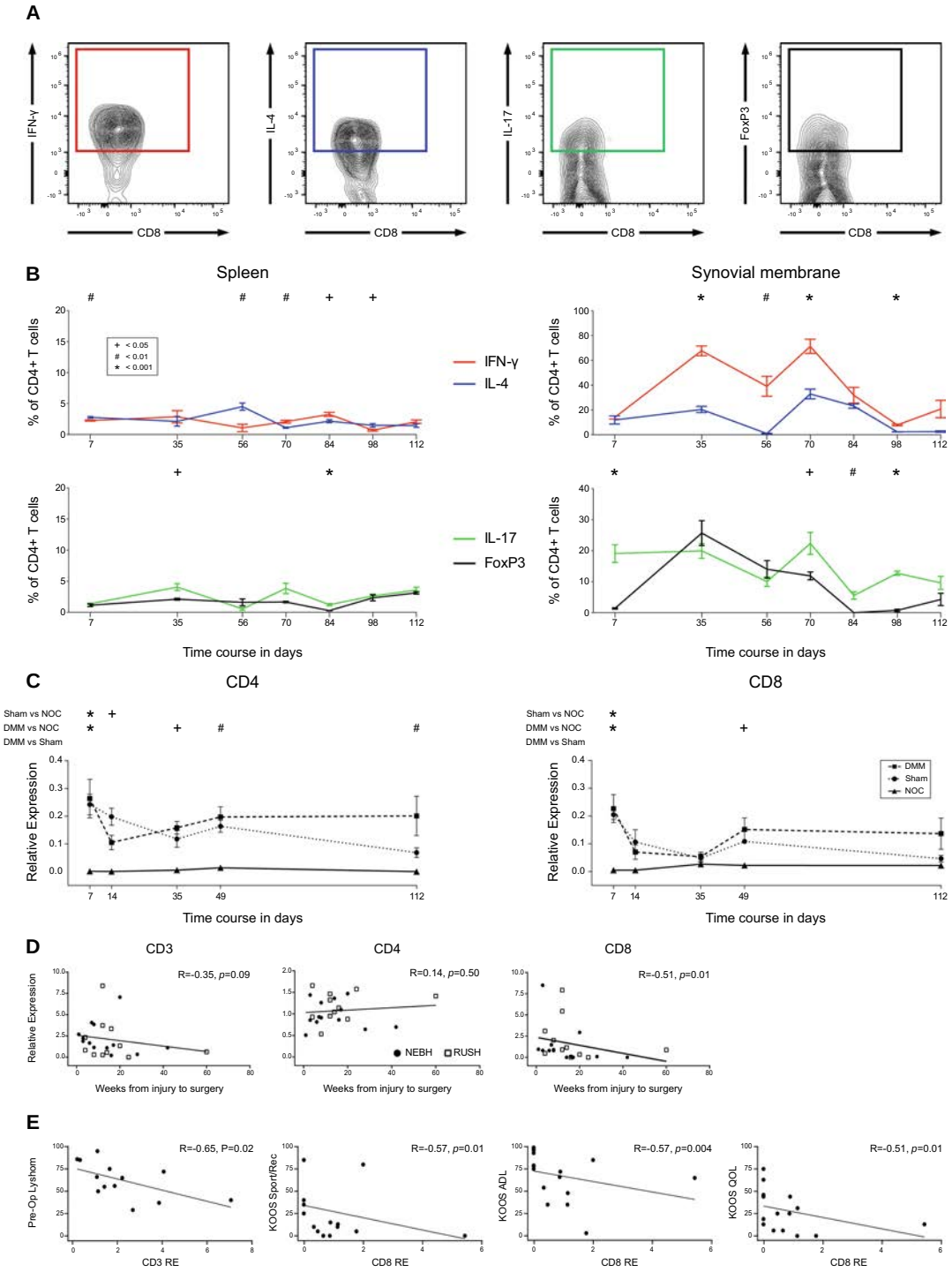

Figure 4. T cell changes in posttraumatic osteoarthritis (ptOA) are localized to the joint, show temporally distinct Th1/Th2 and Th17/Treg cell imbalance, and are associated with worse clinical symptoms in patients. (A) Th1 IFNγ$^+$, Th2 IL-4$^+$, Th17 IL-17a$^+$, and Treg FoxP3$^+$. (B) Destabilization of the medial meniscus (DMM) surgery resulted in little temporal change in these CD4$^+$ T cell subsets in the spleen but proinflammatory imbalances in Th17/Treg cells acutely after injury and in late disease, whereas a Th1/Th2 cell imbalance predominated during the progression of ptOA structural damage. Data are shown as the mean ± SEM (n = 4 replicates [each a pool of 6 mice]/time/surgery), with differences between Th17/Treg and Th1/Th2 cells analyzed at each time: $^*P \leq 0.05$; $^+P \leq 0.01$; $^\#P \leq 0.001$. (C) Analysis of synovial *Cd4* and *Cd8* messenger RNA expression in mice showed a cyclic pattern (similar to that seen with flow cytometry), with more persistent elevation in DMM than sham. (D) Expression of *CD3* and *CD8* (but not *CD4*) in synovial tissue collected at the time of arthroscopic partial meniscectomy in patients without or with early OA (New England Baptist Hospital (NEBH) and Rush University Medical Centrer (RUSH) cohorts, respectively) showed higher levels with a shorter time after injury. (E) Higher *CD3* (NEBH patients) and *CD8* (Rush patients) levels were significantly correlated with worse preoperative symptoms (lower Lysholm score or Knee Injury and Osteoarthritis Outcome Score [KOOS]). ADL, activities of daily living; QOL, quality of life.

Table 1. Comparison of the different CD4 T cell subtypes in the spleen versus synovium in mice at different time points*

Cell type and time post DMM	Spleen, mean ± SD (range), %	Synovium, mean ± SD (range), %	Mean difference	95% CI
Th1 (IFNγ$^+$), day 7	2.3 ± 0.3 (2.0 to 2.7)	13.9 ± 3.6 (9.0 to 18.6)	**−11.6**	**−14.6 to −8.6**
Th1 (IFNγ$^+$), day 35	2.9 ± 2.0 (1.7 to 5.8)	67.7 ± 7.9 (60.8 to 79.0)	**−64.8**	**−74.8 to −54.8**
Th1 (IFNγ$^+$), day 56	1.1 ± 1.2 (0.4 to 2.8)	39.0 ± 16.0 (19.1 to 58.3)	**−38.0**	**−57.6 to −18.3**
Th1 (IFNγ$^+$), day 70	2.1 ± 0.4 (1.5 to 2.5)	71.3 ± 11.4 (57.6 to 83.3)	**−69.2**	**−87.4 to −51.1**
Th1 (IFNγ$^+$), day 84	3.3 ± 0.9 (2.3 to 4.4)	31.8 ± 17.9 (15.0 to 60.4)	**−28.6**	**−43.6 to −13.6**
Th1 (IFNγ$^+$), day 98	0.7 ± 0.4 (0.1 to 1.2)	7.9 ± 1.9 (5.1 to 9.9)	**−7.2**	**−8.8 to −5.6**
Th1 (IFNγ$^+$), day 112	2.1 ± 0.9 (0.8 to 3.9)	20.7 ± 14.0 (7.5 to 38.4)	−18.6	−40.9 to −3.7
Th2 (IL-4$^+$), day 7	2.8 ± 0.4 (2.3 to 3.5)	11.9 ± 9.1 (4.3 to 26.3)	**−9.1**	**−16.7 to −1.5**
Th2 (IL-4$^+$), day 35	2.1 ± 1.5 (1.1 to 4.4)	20.4 ± 5.0 (16.1 to 27.5)	**−18.2**	**−24.7 to −11.8**
Th2 (IL-4$^+$), day 56	4.5 ± 1.2 (3.5 to 6.2)	0.9 ± 0.4 (0.3 to 1.3)	**3.6**	**2.0 to 5.1**
Th2 (IL-4$^+$), day 70	1.1 ± 0.2 (0.9 to 1.3)	32.9 ± 7.9 (24.1 to 40.2)	**−31.8**	**−44.3 to −19.3**
Th2 (IL-4$^+$), day 84	2.2 ± 0.7 (1.2 to 3.5)	23.1 ± 5.0 (18.3 to 28.6)	**−20.9**	**−25.1 to −16.8**
Th2 (IL-4$^+$), day 98	1.5 ± 0.8 (0.6 to 2.8)	2.4 ± 0.4 (2.0 to 3.0)	**−0.9**	**−1.6 to −0.1**
Th2 (IL-4$^+$), day 112	1.5 ± 0.9 (0.5 to 3.6)	2.5 ± 1.2 (1.3 to 4.0)	−1.1	−2.3 to 0.2
Th17 (IL-17$^+$), day 7	1.4 ± 0.3 (1.0 to 1.9)	19.1 ± 8.1 (12.7 to 32.3)	**−17.7**	**−24.4 to 11.0**
Th17 (IL-17$^+$), day 35	4.1 ± 1.1 (2.8 to 5.5)	20.0 ± 4.8 (13.7 to 24.5)	**−15.9**	**−23.3 to −8.5**
Th17 (IL-17$^+$), day 56	0.6 ± 0.5 (0.0 to 1.1)	10.0 ± 3.1 (6.3 to 13.4)	**−9.5**	**−14.3 to −4.7**
Th17 (IL-17$^+$), day 70	3.8 ± 1.7 (2.7 to 6.3)	22.4 ± 7.1 (14.2 to 31.5)	**−18.5**	**−27.4 to −9.6**
Th17 (IL-17$^+$), day 84	1.2 ± 0.5 (0.5 to 2.1)	5.6 ± 3.4 (2.7 to 10.5)	**−4.3**	**−7.2 to −1.5**
Th17 (IL-17$^+$), day 98	2.6 ± 0.9 (1.0 to 3.6)	12.7 ± 1.9 (9.8 to 14.5)	**−10.1**	**−11.7 to −8.5**
Th17 (IL-17$^+$), day 112	3.6 ± 1.5 (1.6 to 6.2)	9.6 ± 4.3 (3.3 to 12.3)	−6.1	−12.7 to 0.5
Treg (FoxP3$^+$), day 7	1.1 ± 0.6 (0.8 to 2.6)	1.4 ± 0.6 (0.4 to 2.1)	−0.2	−0.9 to −0.4
Treg (FoxP3$^+$), day 35	2.1 ± 0.3 (1.7 to 2.4)	25.7 ± 8.0 (19.3 to 37.1)	**−23.6**	**−33.4 to −13.8**
Treg (FoxP3$^+$), day 56	1.6 ± 1.1 (0.8 to 3.2)	14.0 ± 5.7 (8.8 to 21.9)	**−12.4**	**−19.5 to −5.4**
Treg (FoxP3$^+$), day 70	1.7 ± 0.2 (1.4 to 1.9)	11.9 ± 2.5 (8.7 to 14.1)	**−10.2**	**−14.3 to −6.2**
Treg (FoxP3$^+$), day 84	0.3 ± 0.1 (0.2 to 0.4)	0.0016 ± 0.0016 (0.0001 to 0.005)	**0.3**	**0.2 to 0.3**
Treg (FoxP3$^+$), day 98	2.3 ± 1.4 (0.9 to 5.1)	0.7 ± 1.1 (0.0 to 2.4)	**1.6**	**0.3 to 2.9**
Treg (FoxP3$^+$), day 112	3.1 ± 0.6 (2.2 to 4.4)	4.3 ± 4.0 (1.0 to 10.0)	−1.1	−7.4 to 5.2

* Comparison of the percentage of different CD4 T cell subtypes (Th1 [IFNγ$^+$], Th2 [IL-4$^+$], Th17 [IL-17$^+$], Treg [FoxP3$^+$]) in the spleen vs synovium in mice at different times (days 7, 35, 56, 70, 84, 98, and 112) post DMM surgery. Data show the mean ± SD (range) of the percentage of each cell type (n = 4–8 for each tissue at each time). Mean difference (spleen − synovium) and 95% CIs are shown; negative values indicate higher percentages in synovium. Bold values indicate differences between spleen and synovium that are statistically significant. CI, confidence interval; DMM, destabilization of the medial meniscus.

proteoglycan loss and cartilage structural damage (Figure 5G), and reduced late-stage (16-week) cartilage damage.

DISCUSSION

Burgeoning evidence implicates synovial inflammation not just in OA symptoms but also in structural disease pathophysiology.[2,3,11–14] Post hoc exploratory analysis reported that IL-1β inhibition was associated with reduced rates of hip or knee replacement and improved OA-related symptoms over 3.7 years. Although exploratory, these findings suggest that inflammation may represent a viable therapeutic target for modifying symptomatic and structural OA progression.[27] Failure of nonspecific anti-inflammatory approaches (nonsteroidal anti-inflammatory drugs, glucocorticoids) to modify OA pathology, together with experience from rheumatoid arthritis,[28] suggests that disease modification will require mechanism-based targeting of specific inflammatory pathways. Moreover, the disease specificity of these pathways and knowledge of when in the clinical course they are active are critical for therapeutic utility. Directly comparing mononuclear inflammatory/immune cell responses following significant joint injury that does (DMM surgery) and does not (sham surgery) lead to OA allowed us to define bona fide OA-associated events. Despite equivalent surgical joint insult and acute histologically graded inflammation,[22] flow cytometry revealed a more profound and distinct STMC influx in DMM compared with sham within the first three days post injury, well before OA histopathologic change.

The prevailing paradigm suggests that joint injury–induced inflammation follows a classical wound-healing response, initiated by tissue trauma and innate immune activation, including complement activation and sequential neutrophil and monocyte/macrophage infiltration.[5,19] Non–OA-inducing injury represents a resolving wound, whereas OA-inducing injury is proposed to involve persistent DAMP-driven innate immune activation that may promote adaptive immune responses, analogous to chronic wounds.[29,30] However, in the absence of direct in vivo evidence for antigen presentation or T cell activation, this mechanism remains speculative. In our study, OA-inducing injury (DMM surgery) showed ST monocyte/macrophage influx and polarization

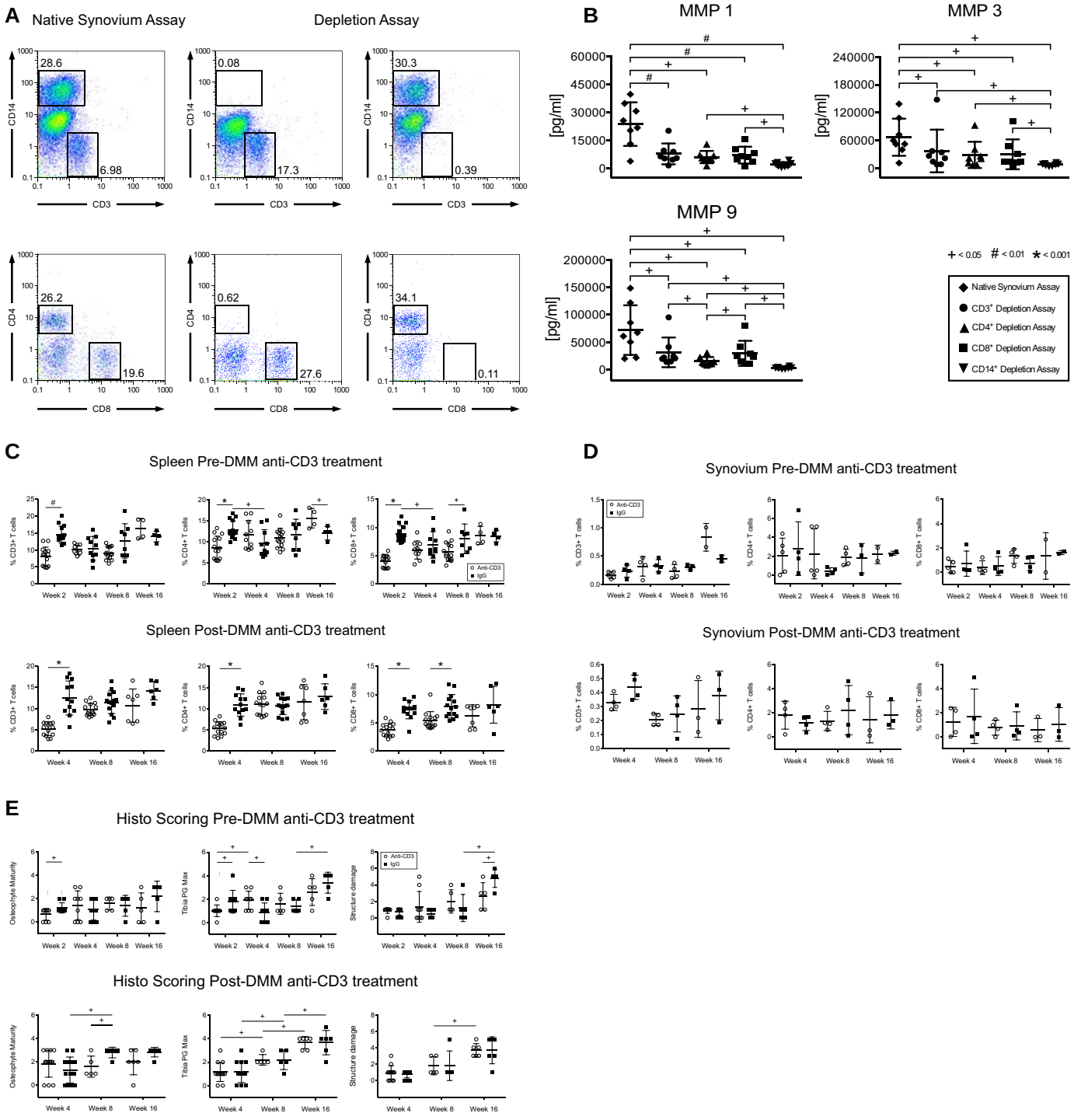

Figure 5. Depletion of T cells significantly reduces osteoarthritic synovial cell metalloproteinase secretion and late-stage progression and severity of destabilization of the medial meniscus (DMM)–induced posttraumatic osteoarthritis (OA). (A) Depletion assays of monocytes/macrophages ($CD14^+$) and lymphocytes ($CD3^+$) as well as $CD4^+$ T helper cells and $CD8^+$ cytotoxic T cells in isolates from human OA synovium and (B) their effect on MMP secretion are shown. Data show all individual patients as well as mean ± SEM (n = 12 group). $^*P \leq 0.05$; $^{**}P \leq 0.01$; $^{***}P \leq 0.001$. (C) Systemic anti-CD3 administration either one week before or three weeks after DMM and the effect on splenic $CD3^+$ and $CD4^+$ T cells and $CD8^+$-T cells are shown. Data show all individual replicates as well as mean ± SEM (n = 4–12 individual mouse spleens/time/treatment). $^*P \leq 0.05$; $^+P \leq 0.01$; $^\#P \leq 0.001$. (D) Despite effects on splenic T cells, there was no change in $CD4^+$ or $CD8^+$ T cells in the synovial tissues following systemic anti-CD3 administered either one week before or three weeks after DMM (n = 2–5 replicates [each a pool of 4 mice]/time/treatment). (E) Impact of anti-CD3 administration one week before and three weeks after DMM on histologic scoring is shown. Histology data show all individual mice as well as mean ± SEM (n = 5–8 mice/time/treatment). $^*P \leq 0.05$; $^+P \leq 0.01$. Color figure can be viewed in the online issue, which is available at http://onlinelibrary.wiley.com/doi/10.1002/art.70157/abstract.

patterns indistinguishable from sham surgery, characterized by an acute M1 response (days 3–7), followed by progressive M2 polarization over four to five weeks and a return to age-matched naïve levels. In contrast, there was a rapid (day 1) and chronic cyclical elevation of ST lymphocytes that, unlike the innate immune response, differentiated OA-inducing/DMM from resolving/sham injury. This implicates a more important role for the adaptive immune system in ptOA risk following joint injury, which occurs much earlier than previously suspected.[31]

Rather than a unimodal "insult inflammation resolution" model,[30] there were cyclical increases and decreases in STMCs after joint injury that were accentuated in DMM and particularly for lymphocytes. Although the observed cyclic T cell infiltration is consistent with immune involvement in OA progression, whether this represents an antigen-specific adaptive immune response or a nonspecific inflammatory recruitment following joint injury remains to be further studied. The slight lag between monocyte/macrophage and lymphocyte peaks (Figures 2 and 3) is consistent with the former secreting chemokines that attract the latter in a coordinated injury response.[30] However, despite an equivalent monocyte/macrophage number, activation/polarization, and associated *Il1* and *Il6* expression (Supplementary Figure 1A) in the immediate postinjury period, there was significantly greater acute ST lymphocyte influx in DMM versus sham. This could be associated with specific DAMP/antigen release from tissues only injured in DMM (meniscotibial ligament, destabilized meniscus[32]) and/or chemokines being secreted from mechanically injured chondrocytes, which occurs before histomorphologic pathology.[33] A limitation of the present study is the absence of direct evidence for an antigen-mediated response; however, published reports of clonal T cell expansion raise the possibility of antigen specificity, potentially involving cartilage-derived or damage-associated neoepitopes.[34–37] Synovial microdissection of the fat pad, capsule, and lining in murine joints is inherently variable due to the small joint size and close anatomic proximity of these structures. Although standardized protocols and experienced operators were used, minor differences in tissue composition between samples could influence absolute immune cell counts and contribute to dispersion in synovial cell readouts. However, cell numbers and distribution were highly consistent across time in NOCs using the same tissue microdissection technique, suggesting results in operated joints reflect bone fide injury/OA-associated temporal changes.

Analysis of PBMCs and SpMCs indicated a local rather than systemic response to DMM, even with bilateral knee injury, and that OA-associated adaptive immune response in one joint does not lead to widespread change, unlike rheumatoid arthritis.[38] Our data contrast with spontaneous OA in the STR/Ort mouse, in which macrophage and T cell ST infiltration is accompanied or preceded by systemic increases.[39] Joint pathology in STR/Ort mice is partly driven by metabolic dysfunction, including hyperlipidemia, insulin resistance, and systemic inflammation.[39] Such metabolic comorbidities are established OA risk factors and may explain the absence of systemic inflammation and differences in ST monocyte/macrophage populations in our nonobese C57BL/6 model. Although activated ST macrophages are increased in patients with late-stage OA[16–18] and show procatabolic effects, obesity and metabolic syndrome themselves promote macrophage-driven inflammation.[40] Although metabolic syndrome exacerbates ptOA and macrophage depletion can reduce pathology in obese mice, results in nonobese ptOA models are inconsistent and limited.[40–43] In our nonobese mice, both DMM and sham surgery induced comparable, self-resolving ST monocyte/macrophage responses, independent of OA development. This suggests that ST macrophage accumulation in patients with OA and STR/Ort mice may be associated more with their meta-inflammatory comorbidity than the OA per se.[44]

In contrast to macrophages, we showed major differences between DMM and sham in ST lymphocytes. Our data in advanced ptOA (day 112) are in accordance with patients with end-stage OA, showing the presence and activated phenotype of ST $CD4^+$ T cells.[15,16,18] We now report that increased ST lymphocytes, particularly $CD4^+$, occurs almost immediately following OA-inducing joint injury, consistent with the limited available data in patients with early versus late OA. The number of ST $CD8^+$ T cells was also increased in DMM compared with NOC and sham up to eight weeks post surgery, but there was less difference immediately post surgery or in late-stage OA. There is some suggestion in patients that ST $CD8^+$ T cells increase with knee OA severity,[45] and we found more patients with late OA had detectable *CD8* mRNA in their ST. There may be confounding effects as both age and obesity/metabolic syndrome increase $CD8^+$ T cell numbers and activation in blood and peripheral tissues,[46,47] and lack of systemic lymphocyte change or an increase in late-stage ST $CD8^+$ T cells in our study may be associated with use of young nonobese mice.

Previous studies have demonstrated a preponderance of Th1-activated ST $CD4^+$ T cells in late-stage human OA, with lower percentages of Treg, Th2, and Th17 cells.[15] Our mouse data show that ST Th1/Th2 cell imbalance occurs particularly during early and progressive OA and then diminishes before becoming apparent again in late-stage disease. In contrast, ST Th17/Treg cell imbalance predominated acutely post injury, was lost in early disease, and then re-emerged later due to a decrease in Treg cells. Increased ST Th17 cells has been reported in patients with OA,[37] but rather than being decreased, Treg cells were found in higher numbers in ST than in blood and with more advanced radiographic disease.[15,48] Again, differences in Th17/Treg cell balance in late-stage OA in DMM mice versus patients is likely associated with confounding effects of obesity and aging in the latter.[47] Importantly, the current mouse studies suggest that beyond early- versus late-stage OA differences, recurrent increases and decreases in synovial immune cell numbers occur over time. This implicates cyclical biologic dynamics following joint

injury and particularly with OA progression. Pooling strategies, limited sample sizes, and variability in synovial microdissection could contribute to these apparent cyclical patterns, and the current results should be confirmed in future studies.

Lymphocyte cell surface marker mRNA expression can provide a surrogate for flow cytometric cell counting.[4] That expression of classic monocyte/macrophage cytokines *Il1* and *Il6* in ST was not higher in DMM compared to sham and returned to naïve levels by five weeks post surgery (Supplementary Figure 1A) was consistent with the lack of OA-specific innate immune cell response (Figure 2). ST mRNA expression of *Cd4*, *Cd8*, and the Th1 cytokine *Tnf* (Supplementary Figure 1B) showed cyclic changes post surgery and was increased in DMM, similar to flow cytometry, supporting use of ST mRNA for analysis of archival human ST samples. Although mean mRNA levels of lymphocyte markers were not different between patient cohorts as in a previous analysis,[4] the temporal pattern in the meniscal injury groups was consistent with the mouse data, showing an early $CD3^+CD8^+$ response. Of interest was the positive association of ST *CD8* but not *CD4* expression with pain/symptoms in patients with meniscal injury. Generalized synovitis is associated with worse symptoms in patients with established OA[3] and meniscal injury.[20,26] In patients with late-stage OA, the percentage of ST $CD4^+$ T cells, but not $CD8^+$ T cells or macrophages, has been associated with pain even after adjusting for body mass index.[18] Although $CD4^+$ T cells have been strongly implicated in chronic neuropathic pain pathophysiology, the role of $CD8^+$ T cells is less clear with both proalgesic and analgesic effects reported.[49] Our association data in patients suggest a novel role for synovial $CD8^+$ T cells in the early clinical symptoms following meniscal injury, but pre- or post-DMM anti-CD3 failed to modify pain sensitization in mice (Supplementary Figure 1C). This could be associated with sex differences because T cells may play a more important role in chronic pain hypersensitivity in females[50] or because systemic anti-CD3 failed to modify lymphocyte numbers in the ST, where they may play a more direct proalgesic role. Finally, our broad anti-CD3 depletion strategy may have affected both proalgesic and analgesic T cells, and a more targeted approach may be needed.

Synovitis increases the risk of incident structural OA in population-based studies[7] and progression of cartilage damage in patients with meniscal injuries.[51] Our patient ST cell depletion studies demonstrate that $CD3^+$ lymphocytes play a role in upregulation of pathophysiologically relevant MMPs, consistent with previous reports.[4] Whether this is through inhibiting synthesis of metalloproteinases by lymphocytes or modulation of their costimulation of macrophage MMP synthesis is unclear.[52,53] Although T cell depletion significantly reduced ST cell MMP production in vitro, the relative contribution of T cells compared with the more abundant stromal cell populations and monocytes/macrophages in the joint remains uncertain and may also vary with temporal cyclical changes in number. However, $CD4^+$ T cell and macrophage activation in OA synovial fluid are positively associated,[17] and compared with PBMCs, T cells in late-stage OA ST show increased activation and secretion of inflammatory cytokines and chemokines.[15,18,37,54] This suggests that factors in the local joint environment drive T cell cytokine secretion, which in turn may modulate the effects of activated $CD4^+$ T cells in increasing chondrocyte and stromal cell MMP expression.[54]

Agnostic genetic and experimental evidence does not support a dominant, classic T cell–driven mechanism in OA structural pathology, as large genome-wide association studies have not identified immune or T cell pathways as major contributors.[55,56] Nevertheless, emerging genetic, epidemiologic, and interventional data suggest that immune pathways may modulate OA pathology risk or progression in specific contexts, indicating a more nuanced or indirect role rather than a primary adaptive immune–driven disease process.[57]

Direct evidence for T cells in OA pathophysiology comes from mice deficient in CD4[58] or CD8,[55] which both have reduced ptOA cartilage damage, and despite constitutive depletion, only protection in late-stage ptOA was seen. This is in line with our anti-CD3 data, but by using a transient depletion strategy, we show that although the immediate and four-week post-DMM T cell responses contribute to osteophyte development, the earliest T cell response may be key to late-stage ptOA cartilage damage. This is consistent with the presence and severity of the initial synovitis following meniscal injury, even if it subsequently resolves, being associated with risk of progressive cartilage damage in patients.[51] Although there was no change in the PBMC or SpMC T cell number or activation in DMM-induced ptOA, the anti-CD3 treatment outcomes implicate systemic T cells in progressive cartilage damage. The partial systemic T cell depletion achieved in vivo, without evident depletion in synovial tissues, represents a limitation of the current approach and suggests that alternative targeting or delivery strategies may be required to fully assess therapeutic efficacy. The absence of a clear effect on OA histopathology over time may reflect both biologic heterogeneity and incomplete in vivo depletion and, together with limited sample sizes, represents a limitation of these depletion experiments. That systemic T cell depletion was not mirrored in the ST raises the question of where the ST cells originate. In addition to influx and polarization of circulating cells, activation and proliferation of resident populations could contribute to both the innate and adaptive immune response. The majority of $CD45^+$ cells in normal ST are of $CD11b^+$ monocyte lineage, and our current and previous data[4,40] indicate that ~20% of these are macrophages that could participate immediately post injury. The predominant resident monocyte population could then be activated by mechanical, cellular, or soluble stimuli.[5,29,44] Because the number of resident T cells in normal ST is very low, the immediate postinjury increase more likely arises through influx rather than local replication. Analysis of patients with late-stage OA indicates $CD8^+$ clonality, but whether this occurs through selective migration/influx or local clonal selection/expansion is unclear.[37]

In conclusion our comprehensive temporal quantitative comparison of ST inflammatory cell influx after OA-inducing versus non–OA-inducing joint injury has enabled us to define the important role of the adaptive immune response. Increases in the number and activation of ST T cells in joints at risk of OA occurred within the first three days of injury, and although it recurs cyclically through subsequent disease onset, depletion studies suggest this initial influx may be important for long-term ptOA risk. There are a number of differences between our preclinical animal and patient populations that highlight key research questions for further study. Thus, the precise local environmental cues in the OA joint that stimulate and maintain the adaptive immune response, the specific T cell subsets involved in symptomatic and structural disease, and modification by systemic factors such as age, sex, and obesity/metabolic syndrome remain to be defined. Nevertheless, the present results implicate a hitherto unappreciated pathophysiologic role of acute T cell activation after joint injury in ptOA risk, opening new diagnostic, prognostic, and therapeutic avenues. The limitations of this study include the focus on a posttraumatic mice model. It would be of great interest to see how these data transfer to spontaneous OA models. Although we included analysis of human samples, further studies are needed to determine how the mouse data translate to human OA, which progresses over decades.

ACKNOWLEDGMENTS

We thank Craig Della Valle, Charles Bush-Joseph, and Nikhil Verma (Rush University Medical Center, Department of Orthopedics, Chicago, IL) and Brian McKeon and Anthony Albert (New England Baptist Hospital, Department of Orthopedics, Boston, MA) for the collection of the human synovial tissue biopsy samples. Open access publishing facilitated by The University of Sydney, as part of the Wiley - The University of Sydney agreement via the Council of Australasian University Librarians

AUTHOR CONTRIBUTIONS

All authors contributed to at least one of the following manuscript preparation roles: conceptualization AND/OR methodology, software, investigation, formal analysis, data curation, visualization, and validation AND drafting or reviewing/editing the final draft. As corresponding authors, Drs Moradi and Little confirm that all authors have provided the final approval of the version to be published and take responsibility for the affirmations regarding article submission (eg, not under consideration by another journal), the integrity of the data presented, and the statements regarding compliance with institutional review board/Declaration of Helsinki requirements.

REFERENCES

1. Menon J, Mishra P. Health care resource use, health care expenditures and absenteeism costs associated with osteoarthritis in US healthcare system. Osteoarthritis Cartilage 2018;26(4):480–484. doi:10.1016/j.joca.2017.12.007
2. Scanzello CR. Role of low-grade inflammation in osteoarthritis. Curr Opin Rheumatol 2017;29(1):79–85. doi:10.1097/BOR.0000000000000353
3. Wang X, Hunter DJ, Jin X, et al. The importance of synovial inflammation in osteoarthritis: current evidence from imaging assessments and clinical trials. Osteoarthritis Cartilage 2018;26(2):165–174. doi:10.1016/j.joca.2017.11.015
4. Scanzello CR, Umoh E, Pessler F, et al. Local cytokine profiles in knee osteoarthritis: elevated synovial fluid interleukin-15 differentiates early from end-stage disease. Osteoarthritis Cartilage 2009;17(8):1040–1048. doi:10.1016/j.joca.2009.02.011
5. Wang Q, Rozelle AL, Lepus CM, et al. Identification of a central role for complement in osteoarthritis. Nat Med 2011;17(12):1674–1679. doi:10.1038/nm.2543
6. Rosshirt N, Trauth R, Platzer H, et al. Proinflammatory T cell polarization is already present in patients with early knee osteoarthritis. Arthritis Res Ther 2021;23(1):37. doi:10.1186/s13075-020-02410-w
7. Atukorala I, Kwoh CK, Guermazi A, et al. Synovitis in knee osteoarthritis: a precursor of disease? Ann Rheum Dis 2016;75(2):390–395. doi:10.1136/annrheumdis-2014-205894
8. Ramezanpour S, Kanthawang T, Lynch J, et al. Impact of sustained synovitis on knee joint structural degeneration: 4-year MRI data from the osteoarthritis initiative. J Magn Reson Imaging 2023;57(1):153–164. doi:10.1002/jmri.28223
9. Little CB, Hunter DJ. Post-traumatic osteoarthritis: from mouse models to clinical trials. Nat Rev Rheumatol 2013;9(8):485–497. doi:10.1038/nrrheum.2013.72
10. Binvignat M, Dubois J, Marco Salvador M, et al. Immunological profiling suggests an association between Treg cell dysfunction and pain in knee osteoarthritis. Arthritis Rheumatol 2026;78(4):848–860. doi:10.1002/art.43437
11. Mathiessen A, Conaghan PG. Synovitis in osteoarthritis: current understanding with therapeutic implications. Arthritis Res Ther 2017;19(1):18. doi:10.1186/s13075-017-1229-9
12. Raut RD, Chakraborty AK, Neogi T, et al. A multi-tissue human knee single-cell atlas identifies that osteoarthritis reduces regenerative tissue stem cells while increasing inflammatory pain macrophages. Commun Biol 2025;8(1):1146. doi:10.1038/s42003-025-08586-8
13. Lee HR, Lee S, Yoo IS, et al. CD14+ monocytes and soluble CD14 of synovial fluid are associated with osteoarthritis progression. Arch Rheumatol 2022;37(3):335–343. doi:10.46497/ArchRheumatol.2022.9078
14. Mikulkova Z, Gallo J, Manukyan G, et al. Complexity of synovial fluid-derived monocyte-macrophage-lineage cells in knee osteoarthritis. Cell Rep 2024;43(12):115011. doi:10.1016/j.celrep.2024.115011
15. Rosshirt N, Hagmann S, Tripel E, et al. A predominant Th1 polarization is present in synovial fluid of end-stage osteoarthritic knee joints: analysis of peripheral blood, synovial fluid and synovial membrane. Clin Exp Immunol 2019;195(3):395–406. doi:10.1111/cei.13230
16. Moradi B, Rosshirt N, Tripel E, et al. Unicompartmental and bicompartmental knee osteoarthritis show different patterns of mononuclear cell infiltration and cytokine release in the affected joints. Clin Exp Immunol 2015;180(1):143–154. doi:10.1111/cei.12486
17. Gómez-Aristizábal A, Gandhi R, Mahomed NN, et al. Synovial fluid monocyte/macrophage subsets and their correlation to patient-reported outcomes in osteoarthritic patients: a cohort study. Arthritis Res Ther 2019;21(1):26. doi:10.1186/s13075-018-1798-2
18. Klein-Wieringa IR, de Lange-Brokaar BJ, Yusuf E, et al. Inflammatory cells in patients with endstage knee osteoarthritis: a comparison between the synovium and the infrapatellar fat pad. J Rheumatol 2016;43(4):771–778. doi:10.3899/jrheum.151068
19. Lieberthal J, Sambamurthy N, Scanzello CR. Inflammation in joint injury and post-traumatic osteoarthritis. Osteoarthritis Cartilage 2015;23(11):1825–1834. doi:10.1016/j.joca.2015.08.015
20. Scanzello CR, Albert AS, DiCarlo E, et al. The influence of synovial inflammation and hyperplasia on symptomatic outcomes up to 2 years

post-operatively in patients undergoing partial meniscectomy. Osteoarthritis Cartilage 2013;21(9):1392–1399. doi:10.1016/j.joca.2013.05.011

21. Malfait AM, Little CB. On the predictive utility of animal models of osteoarthritis. Arthritis Res Ther 2015;17(1):225. doi:10.1186/s13075-015-0747-6
22. Jackson MT, Moradi B, Zaki S, et al. Depletion of protease-activated receptor 2 but not protease-activated receptor 1 may confer protection against osteoarthritis in mice through extracartilaginous mechanisms. Arthritis Rheumatol 2014;66(12):3337–3348. doi:10.1002/art.38876
23. Shu CC, Jackson MT, Smith MM, et al. Ablation of perlecan domain 1 heparan sulfate reduces progressive cartilage degradation, synovitis, and osteophyte size in a preclinical model of posttraumatic osteoarthritis. Arthritis Rheumatol 2016;68(4):868–879. doi:10.1002/art.39529
24. Chaplan SR, Bach FW, Pogrel JW, et al. Quantitative assessment of tactile allodynia in the rat paw. J Neurosci Methods 1994;53(1):55–63. doi:10.1016/0165-0270(94)90144-9
25. Nair A, Gan J, Bush-Joseph C, et al. Synovial chemokine expression and relationship with knee symptoms in patients with meniscal tears. Osteoarthritis Cartilage 2015;23(7):1158–1164. doi:10.1016/j.joca.2015.02.016
26. Scanzello CR, McKeon B, Swaim BH, et al. Synovial inflammation in patients undergoing arthroscopic meniscectomy: molecular characterization and relationship to symptoms. Arthritis Rheum 2011;63(2):391–400. doi:10.1002/art.30137
27. Schieker M, Conaghan PG, Mindeholm L, et al. Effects of interleukin-1beta inhibition on incident hip and knee replacement: exploratory analyses from a randomized, double-blind, placebo-controlled trial. Ann Intern Med 2020;173(7):509–515. doi:10.7326/M20-0527
28. Smolen JS, Breedveld FC, Burmester GR, et al. Treating rheumatoid arthritis to target: 2014 update of the recommendations of an international task force. Ann Rheum Dis 2016;75(1):3–15. doi:10.1136/annrheumdis-2015-207524
29. Scanzello CR, Plaas A, Crow MK. Innate immune system activation in osteoarthritis: is osteoarthritis a chronic wound? Curr Opin Rheumatol 2008;20(5):565–572. doi:10.1097/BOR.0b013e32830aba34
30. Larouche J, Sheoran S, Maruyama K, et al. Immune regulation of skin wound healing: mechanisms and novel therapeutic targets. Adv Wound Care (New Rochelle) 2018;7(7):209–231. doi:10.1089/wound.2017.0761
31. Li YS, Luo W, Zhu SA, et al. T cells in osteoarthritis: alterations and beyond. Front Immunol 2017;8:356. doi:10.3389/fimmu.2017.00356
32. Brophy RH, Tycksen ED, Sandell LJ, et al. Changes in transcriptome-wide gene expression of anterior cruciate ligament tears based on time from injury. Am J Sports Med 2016;44(8):2064–2075. doi:10.1177/0363546516643810
33. Burleigh A, Chanalaris A, Gardiner MD, et al. Joint immobilization prevents murine osteoarthritis and reveals the highly mechanosensitive nature of protease expression in vivo. Arthritis Rheum 2012;64(7):2278–2288. doi:10.1002/art.34420
34. Marco-Salvador M, Binvignat M, Stys P, et al. T-cell receptor repertoire and HLA in osteoarthritis: a systematic literature review. Osteoarthritis Cartilage 2026;34(2):221–231. doi:10.1016/j.joca.2025.08.018
35. de Groot R, Folgado PB, Yamamoto K, et al. Cleavage of Cartilage Oligomeric Matrix Protein (COMP) by ADAMTS4 generates a neoepitope associated with osteoarthritis and other forms of degenerative joint disease. Matrix Biol 2025;135:106–124. doi:10.1016/j.matbio.2024.12.005
36. Zack MD, Arner EC, Anglin CP, et al. Identification of fibronectin neoepitopes present in human osteoarthritic cartilage. Arthritis Rheum 2006;54(9):2912–2922. doi:10.1002/art.22045
37. Sae-jung T, Sengprasert P, Apinun J, et al. Functional and t cell receptor repertoire analyses of peripheral blood and infrapatellar fat pad t cells in knee osteoarthritis. J Rheumatol 2019;46(3):309–317. doi:10.3899/jrheum.170775
38. Lefèvre S, Knedla A, Tennie C, et al. Synovial fibroblasts spread rheumatoid arthritis to unaffected joints. Nat Med 2009;15(12):1414–1420. doi:10.1038/nm.2050
39. Uchida K, Naruse K, Satoh M, et al. Increase of circulating $CD11b^{+}Gr1^{+}$ cells and recruitment into the synovium in osteoarthritic mice with hyperlipidemia. Exp Anim 2013;62(3):255–265. doi:10.1538/expanim.62.255
40. Sun AR, Wu X, Liu B, et al. Pro-resolving lipid mediator ameliorates obesity induced osteoarthritis by regulating synovial macrophage polarisation. Sci Rep 2019;9(1):426. doi:10.1038/s41598-018-36909-9
41. Guss JD, Ziemian SN, Luna M, et al. The effects of metabolic syndrome, obesity, and the gut microbiome on load-induced osteoarthritis. Osteoarthritis Cartilage 2019;27(1):129–139. doi:10.1016/j.joca.2018.07.020
42. Wu CL, McNeill J, Goon K, et al. Conditional macrophage depletion increases inflammation and does not inhibit the development of osteoarthritis in obese macrophage Fas-induced apoptosis-transgenic mice. Arthritis Rheumatol 2017;69(9):1772–1783. doi:10.1002/art.40161
43. Geraghty T, Ishihara S, Obeidat AM, et al. Acute systemic macrophage depletion in osteoarthritic mice alleviates pain-related behaviors and does not affect joint damage. Arthritis Res Ther 2024;26(1):224. doi:10.1186/s13075-024-03457-9
44. Li C, Xu MM, Wang K, et al. Macrophage polarization and meta-inflammation. Transl Res 2018;191:29–44. doi:10.1016/j.trsl.2017.10.004
45. Apinun J, Sengprasert P, Yuktanandana P, et al. Immune mediators in osteoarthritis: infrapatellar fat pad-infiltrating CD8+ T cells are increased in osteoarthritic patients with higher clinical radiographic grading. Int J Rheumatol 2016;2016:9525724. doi:10.1155/2016/9525724
46. Ponchel F, Burska AN, Hensor EM, et al. Changes in peripheral blood immune cell composition in osteoarthritis. Osteoarthritis Cartilage 2015;23(11):1870–1878. doi:10.1016/j.joca.2015.06.018
47. Kalathookunnel Antony A, Lian Z, Wu H. T cells in adipose tissue in aging. Front Immunol 2018;9:2945. doi:10.3389/fimmu.2018.02945
48. Moradi B, Schnatzer P, Hagmann S, et al. $CD4^{+}CD25^{+/high}CD127^{low/-}$ regulatory T cells are enriched in rheumatoid arthritis and osteoarthritis joints—analysis of frequency and phenotype in synovial membrane, synovial fluid and peripheral blood. Arthritis Res Ther 2014;16(2):R97. doi:10.1186/ar4545
49. Yang M, Peyret C, Shi XQ, et al. Evidence from human and animal studies: pathological roles of CD8+ T cells in autoimmune peripheral neuropathies. Front Immunol 2015;6:532. doi:10.3389/fimmu.2015.00532
50. Sorge RE, Mapplebeck JC, Rosen S, et al. Different immune cells mediate mechanical pain hypersensitivity in male and female mice. Nat Neurosci 2015;18(8):1081–1083. doi:10.1038/nn.4053
51. MacFarlane LA, Yang H, Collins JE, et al; MeTeOR Investigator Group. Association of changes in effusion-synovitis with progression of cartilage damage over eighteen months in patients with osteoarthritis and meniscal tear. Arthritis Rheumatol 2019;71(1):73–81. doi:10.1002/art.40660
52. Bar-Or A, Nuttall RK, Duddy M, et al. Analyses of all matrix metalloproteinase members in leukocytes emphasize monocytes as major inflammatory mediators in multiple sclerosis. Brain 2003;126(12):2738–2749. doi:10.1093/brain/awg285
53. Clark RT, Nance JP, Noor S, et al. T-cell production of matrix metalloproteinases and inhibition of parasite clearance by TIMP-1 during

chronic Toxoplasma infection in the brain. ASN Neuro 2011;3(1). doi:10.1042/AN20100027

54. Scotece M, Pérez T, Conde J, et al. Adipokines induce pro-inflammatory factors in activated Cd4+ T cells from osteoarthritis patient. J Orthop Res 2017;35(6):1299–1303. doi:10.1002/jor.23377
55. Hsieh JL, Shiau AL, Lee CH, et al. CD8+ T cell-induced expression of tissue inhibitor of metalloproteinses-1 exacerbated osteoarthritis. Int J Mol Sci 2013;14(10):19951–19970. doi:10.3390/ijms141019951
56. Hatzikotoulas K, Southam L, Stefansdottir L, et al; arcOGEN Consortium; ARGO Consortium; DBDS Genomic Consortium; Estonian Biobank Research Team; FinnGen; Genes & Health Research Team; HUNT All-In Pain; Million Veteran Program; Regeneron Genetics Center. Translational genomics of osteoarthritis in 1,962,069 individuals. Nature 2025;641(8065):1217–1224. doi:10.1038/s41586-025-08771-z
57. Teng M, Wang J, Su X, et al. Associations between immune cells signatures and osteoarthritis: an integrated analysis of bidirectional Mendelian randomization and Bayesian colocalization. Cytokine 2024;179:156633. doi:10.1016/j.cyto.2024.156633
58. Shen PC, Wu CL, Jou IM, et al. T helper cells promote disease progression of osteoarthritis by inducing macrophage inflammatory protein-1γ. Osteoarthritis Cartilage 2011;19(6):728–736. doi:10.1016/j.joca.2011.02.014

Arthritis & Rheumatology
Vol. 78, No. 9, September 2026, pp 1878–1891
DOI 10.1002/art.70105
© 2026 The Author(s). *Arthritis & Rheumatology* published by Wiley Periodicals LLC on behalf of American College of Rheumatology.
This is an open access article under the terms of the Creative Commons Attribution-NonCommercial-NoDerivs License, which permits use and distribution in any medium, provided the original work is properly cited, the use is non-commercial and no modifications or adaptations are made.

American College of Rheumatology
Empowering Rheumatology Professionals

Multi-Omic Profiling Reveals Immune Cell Priming Signature Linked to Lupus Prognosis

Michael A. Smith, PhD,[1] Dominic Sinibaldi, PhD,[2] Saifur Rahman, PhD, MBA,[1] Chia-Chien Chiang, PhD,[2] Anna M. Hansen, PhD,[1] Jill Henault, PhD,[1] Carlos P. Roca, PhD,[3] Shu Wang, BS,[1] Kamelia Zerrouki, MS,[1] Rebecca Filippi, MS,[1] Christopher Groves, BA,[1] Zerai Manna, MS,[4] Jun Chu, MSN, CRNP,[4] Michael Davis, MSN, CRNP,[4] Sarthak Gupta, MD,[4] Christopher Morehouse, MS,[1] Melissa de los Reyes, MS,[1] Rachel Ettinger, PhD,[1] Roland Kolbeck, PhD,[1] Mariana J. Kaplan, MD,[4,5] Miguel A. Sanjuan, PhD,[1] Richard M. Siegel, MD, PhD,[6] Sarfaraz A. Hasni, MD, MSc,[4] and Kerry A. Casey, PhD[1]

Objective. Systemic lupus erythematosus (SLE) is a multiorgan disease with widespread immune dysregulation and significant unmet clinical need. Blood-based gene expression studies have advanced our understanding of SLE pathogenesis but may overlook critical tissue-specific mechanisms that drive disease heterogeneity and progression. We posited that integrated multidimensional profiling could reveal novel molecular patterns underlying distinct SLE pathologies.

Methods. Here, we integrated immune cell, protein, and transcriptome data sets with disease activity and damage indices across 87 patients with SLE to reveal three independent protein signatures corresponding to discrete organ pathologies and immune perturbations.

Results. Alongside type I interferon and granulocyte pathways, our multidimensional analyses identified a previously uncharacterized immune cell priming protein signature that was enriched in patients with renal involvement and was indicative of elevated risk of six-year organ damage accrual. This minimally invasive signature outperformed conventional assessments and was only found in the serum proteomics data. Collectively, the protein signatures demonstrated a combined prevalence of 94%, reflecting their broad relevance to SLE.

Conclusion. Together, these results reveal parallel immune mechanisms in SLE and provide a framework to identify new therapeutic targets. Clinical and immune data are available for public exploration through the interactive SLE Immune Atlas.

INTRODUCTION

Systemic lupus erythematosus (SLE) is a complex autoimmune syndrome in which organ involvement and disease severity are heterogeneous and clinical course is unpredictable. Current SLE disease activity assessments do not capture the full spectrum of disease burden impacting patient quality of life, for example, cardiovascular disease.[1] Patients with SLE present

The contributions of the NIH authors were made as part of their official duties as NIH federal employees, are in compliance with agency policy requirements, and are considered works of the US Government. However, the findings and conclusions presented in this article are those of the author and do not necessarily reflect the views of the NIH or the US Department of Health and Human Services.

Supported by AstraZeneca. This research was supported in part by the Intramural Research Program of the National Institute of Arthritis and Musculoskeletal and Skin Diseases, NIH.

[1]BioPharmaceuticals R&D, AstraZeneca, Gaithersburg, Maryland; [2]Data Science and AI, AstraZeneca, Gaithersburg, Maryland; [3]Data Science and AI, AstraZeneca, Cambridge, United Kingdom; [4]Lupus Clinical Trials Unit, National Institute of Arthritis and Musculoskeletal and Skin Diseases, NIH, Bethesda, Maryland; [5]Systemic Autoimmunity Branch, National Institute of Arthritis and Musculoskeletal and Skin Diseases, NIH, Bethesda, Maryland; [6]Office of the Clinical Director, National Institute of Arthritis and Musculoskeletal and Skin Diseases, NIH, Bethesda, Maryland. Authors Smith, Wang, and Zerrouki's current address is Horizon Therapeutics, Rockville, Maryland. Dr Rahman's current address is Sanofi US, Cambridge, Massachusetts. Dr Chiang's current address is Discovery IO, LLC, Rockville, Maryland. Dr Henault's current address is Bristol Myers Squibb, Cambridge, Massachusetts. Author Filippi's current address is Oncology R&D, AstraZeneca, Gaithersburg, Maryland. Dr Groves's current address is Q2 Solutions, Durham, North Carolina. Dr Ettinger's current address is Kensington, Maryland. Dr Kolbeck's current address is Spirovant Sciences, Inc, Philadelphia, Pennsylvania. Dr Sanjuan's current addresses are Sanofi US, Cambridge, Massachusetts, and Paulex Bio, La Jolla, California. Dr Siegel's current address is Novartis Institutes of BioMedical Research, Basel, Switzerland. Dr Casey's current address is Regeneron Pharmaceuticals, Tarrytown, New York.

Authors Smith and Sinibaldi are co-first authors and contributed equally to this work. Drs Siegel, Hasni, and Casey are co-senior authors and contributed equally to this work.

Additional supplementary information cited in this article can be found online in the Supporting Information section (https://acrjournals.onlinelibrary.wiley.com/doi/10.1002/art.70105).

Author disclosures are available at https://onlinelibrary.wiley.com/doi/10.1002/art.70105.

Address correspondence via email to Dominic Sinibaldi, PhD, at nsinibaldi@gmail.com; or to Kerry A. Casey, PhD, at findingimmunity@gmail.com.

Submitted for publication May 29, 2025; accepted in revised form December 9, 2025.

with constellations of symptoms affecting multiple organ systems, including the skin, joints, kidney, and central nervous system.[2] Accrual of irreversible organ damage is a major contributor to morbidity and mortality.[3] Consequently, there is a pressing need for new approaches to unravel the molecular pathways responsible for the different SLE manifestations and to identify patients who are at the greatest risk of disease progression.

Much of our understanding of SLE immunopathogenesis is derived from gene profiling studies, in which core pathways such as neutrophil dysregulation and uncontrolled type I interferon (IFN) production by plasmacytoid dendritic cells (pDCs) and other cell types have been identified.[4–6] Up to 80% of patients with SLE display elevated expression of type I IFN-inducible genes[7,8] as determined by the presence of type I IFN gene signatures (IFNGS). The role of type I IFN in the pathogenesis of SLE is supported by a seminal study that identified associations between type I IFN levels and serologic disease markers, global disease activity scores, and cutaneous SLE disease activity.[9] Type I IFN receptor blockade with anifrolumab rapidly reduces IFNGS and SLE disease activity[10–12] while improving inflammatory disease markers.[13,14]

However, gene signatures found in whole blood may not reflect gene expression in tissues, potentially overlooking key local drivers of disease activity and pathogenesis.[15] Local inflammatory milieus likely contribute to the development of organ-specific disease manifestations. As such, immune cells and proteins from affected tissues may offer complementary insight into SLE-related pathologies. Recruitment of immune cells, such as pDCs, and downstream inflammatory processes may contribute to organ damage in patients with SLE.[16,17]

Although gene expression is commonly used as a proxy for protein abundance, significant discordance exists between transcript and protein levels.[18,19] Given that proteins are the predominant mediators of biologic processes, a comprehensive understanding of disease characteristics and activity requires proteomic assessments. Although there is great potential for proteomics data to identify molecular heterogeneity underlying SLE pathologies, relatively few protein signatures have been identified to date.[14,20,21]

In this study, we aimed to uncover unique pathologic features of SLE that go beyond gene expression data, investigating the heterogeneous patient phenotypes encountered in clinical practice. Through a multidimensional analysis of the relationships between blood cells, proteins, and transcripts, we sought to identify the biologic pathways preceding advanced disease. The clinically annotated immune profiling data supporting this work have been made available via the interactive SLE Immune Atlas portal (https://astrazeneca-bka.shinyapps.io/sle-immune-atlas/). This online resource will enable translation of our multi-omics reference data set into meaningful connections with future endotypes of interest,[22,23] supporting exploration of their links to immunologic features, disease activity, and clinical outcomes.

MATERIALS AND METHODS

Discovery and validation cohorts. Deidentified peripheral human whole-blood samples from 87 patients with predominantly mild to moderate SLE enrolled in the Lupus Natural History Cohort at the National Institutes of Arthritis and Musculoskeletal and Skin Diseases (NIAMS), National Institutes of Health (NIH), in Bethesda, Maryland (NIH-SLE 2013–2014 cohort), were shipped to MedImmune in Gaithersburg, Maryland, on a weekly basis throughout 2014 under clinical protocol NIH 94-AR-0066, approved by the NIAMS and National Institute of Diabetes and Digestive and Kidney Diseases Institutional Review Boards (IRBs). A total of 48 whole-blood samples from healthy controls were also obtained on a weekly basis under the internal donor program, approved by the MedImmune IRB, and processed and stored simultaneously with SLE samples arriving from the NIH. Because the demographics of patients with SLE were not known in advance, samples were matched in time to control for preanalytic variables known to confound multibatch proteomic and flow cytometry data sets.

To ensure the robustness of the protein signatures, an independent validation cohort of 43 patients with predominantly mild to moderate SLE (NIH-SLE 2016–2017 cohort) and 52 healthy controls were also collected from the NIH and MedImmune, respectively, under the same protocols. All patients gave signed informed consent. Clinical characteristics of the patients with SLE and healthy controls are listed in Supplementary Table S1.

Blood collection and processing. Blood samples were collected concurrently in sodium heparin, serum, and PAXgene Blood RNA (PAXr) tubes (Qiagen) as outlined in Supplementary Table S2. Whereas the sodium heparin and serum tubes were processed the same day for isolating peripheral blood mononuclear cells (PBMCs) and serum, respectively, the PAXr tubes were frozen. Blood samples collected in sodium heparin tubes were used for flow cytometry staining of whole blood and PBMCs. Additionally, a complete blood cell count (Sysmex) was also performed using the same blood sample as per the manufacturer's instructions.

For PBMC isolation, whole blood was transferred from sodium heparin tubes to cell preparation tubes (BD Biosciences) and then processed by density centrifugation as per the manufacturer's instructions. Briefly, the tubes were centrifuged at 1,700*g* (relative

centrifugal force [rcf]) for 25 minutes at 20 °C with brakes set at 6. Thereafter, the buffy coat was collected and washed once in 1X phosphate buffered saline (PBS) (pH 7.2) at 400*g* for 10 minutes. The PBMCs were finally counted using ViCell (Beckman Coulter) as per the manufacturer's instructions and resuspended in 1X PBS.

For serum isolation, the serum-separating tubes (BD Biosciences) were inverted five times to mix sample and processed as per the manufacturer's instructions. Briefly, the tubes were spun down at 1,200*g* for 10 minutes at 20 °C. The supernatant serum was aliquoted, stored at –30°C overnight and transferred to –80°C the following day.

Serum protein measurements. In the NIH-SLE 2013–2014 data set, 1,129 proteins were measured in serum from each sample using affinity-purified, modified DNA aptamer probes, which were subsequently quantified with a custom Agilent hybridization chip as described using the SOMAscan Assay v3.2 SLE-mitigated protocol (SomaLogic).[24,25] Protein measurements from the NIH-SLE 2016–2017 data set were used to validate the reproducibility of the protein scores. A total of 179 proteins were also measured in the NIH-SLE 2013–2014 cohort serum samples by Rules-Based Medicine (RBM) HumanMAP immunoassay using the Human DiscoveryMAP 175+ v1.0 (Myriad RBM).

Gene expression microarray and calculation of IFN 21 gene signature. Whole-blood gene expression microarray measurements were performed using the Affymetrix Human Genome U133 Plus 2.0 GeneChip array platform (Thermo Fisher Scientific). Sample processing and array hybridization were performed by Asuragen, and the continuous IFN 21 gene signature (21-IFNGS) was calculated as described previously.[26] Briefly, the mean signal across all healthy controls for each of the 21 probe sets was calculated. The fold change between healthy controls and SLE samples was then calculated for each probe set: log2 (probe set for sample) – log2 (probe set healthy control mean). The median fold change across all 21 probe sets represented the signature score for each sample. A median of 2 (log2, which is four-fold of healthy controls) was the cutoff for a positive versus negative score.

Gene expression measurements from microdissected glomeruli of patients with lupus nephritis (LN) and healthy controls were used for analysis as previously published under GEO accession no. GSE32591 and GSE99339. In GSE32591, RNA was isolated using the RNAeasy Mini Kit (Qiagen) and hybridized to Human Genome U133A gene chips (Affymetrix, Inc).[27] In GSE99339, microdissected glomerular biopsy samples from patients with chronic kidney disease were hybridized on Affymetrix HGU133A and HGU133 Plus 2 arrays.[28]

Flow cytometry surface and intracellular staining. Supplementary Table S2 lists all antibodies used for surface and intracellular staining. One million freshly isolated PBMCs from healthy control and SLE blood samples were used for flow cytometry. Fc receptor blocking (TrueStain FcX, Biolegend) was performed in PBMCs for 15 minutes in staining media (Dulbecco's phosphate buffered saline with 1% bovine serum albumin and 0.1% sodium azide) on ice. Cells were washed once (400*g* for 5 minutes at 4 °C) and then stained with antibody cocktail mixes for 30 minutes at 4 °C. The cells were then washed twice with staining media and fixed in freshly prepared 4% paraformaldehyde.

For whole-blood staining, 15-mL conical tubes containing 200 μL (for DC panel) and 1 mL (granulocyte panel) of whole blood were filled with 10 mL of 1X PBS (pH 7.2) for wash. The tubes were centrifuged at 400*g* (rcf) for 10 minutes at 20 °C. After discarding the supernatant, the pellet was resuspended in 1 mL of staining media. To this, 200 μL of DC and granulocyte antibody cocktails was added to the sample tubes and left for 30 minutes at 4 °C. Freshly prepared 1X fluorescence-activated cell-sorting lyse buffer (BD Biosciences) was added to all samples and left in the dark for 15 minutes at room temperature. The tubes were centrifuged at 400*g* for 10 minutes at 20 °C, the supernatant was discarded, and the pellet was resuspended in staining media. Intracellular staining was performed using permeabilization buffer as per the manufacturer's instructions (eBioscience).

The fixed cells were then acquired on a multicolor flow cytometry instrument (BD LSRFortessa, BD Biosciences), and data were analyzed using FlowJo software (BD Biosciences). Cell number calculations as well as lymphocyte and granulocyte population enumerations were performed using a complete blood cell count hematology analyzer (Sysmex).

Signature score calculation. SOMAscan measurements from the NIH-SLE 2013–2014 cohort were first filtered to those altered in SLE versus healthy control samples based on a 10% false discovery rate cutoff using *P* values from a Mann–Whitney U test. Correlations between proteins were visualized in the correlation matrixes using average linkage clustering with 1 – Spearman R^2 as a distance metric and were visualized in a heatmap using the *ggplot* package. Signature loadings were generated by first performing principal components analysis on the protein measurements using the prcomp method then performing a promax rotation using the *psych* package. To determine the appropriate number of signatures to extract from factor analysis before rotation, we employed parallel analysis.[29] We generated 50 randomized data sets by permuting the original data and compared the variance using scree plots. The components in the real data accounted for a greater proportion of variance than expected under randomized conditions, supporting their biologic relevance. Factors were subsequently retained for promax rotation to enhance the interpretability and reproducibility of factor loadings across data sets.

Reproducibility of signature scores across platforms was assessed by applying identical scoring methods to the NIH-SLE

2013–2014 SOMAscan and RBM HumanMAP data sets and verifying that patients were ranked similarly. Consistency of factor loadings was further evaluated by confirming that individual protein measurements contributed comparably within each signature across the NIH-SLE 2013–2014 and 2016–2017 SOMAscan and RBM HumanMAP data sets (Supplementary Figure S1A–C). Patient scores were validated by verifying similar patient classification when derived from independent proteomic platforms (SOMAscan and RBM HumanMAP) applied to the same sample set within the NIH-SLE 2013–2014 discovery cohort (Supplementary Figure S1D).

Kidney transcriptomic analysis. Using data from the European Renal cDNA Bank of laser-capture microdissected glomeruli and microarray profiling, we investigated internally derived DC signatures for patients with chronic kidney disease as well as SLE or nonlupus inflammatory nephropathies.

Statistical analysis. All statistical analyses were conducted in R 3.5.1. Pairwise comparisons were performed using the Mann–Whitney U test. Area under the curve (AUC) values were calculated and reported using the *pROC* package. Correlation tests were performed using the Spearman rank correlation test. False discovery rate was estimated using the Benjamini and Hochberg method. Principal components analysis was applied using the *prcomp* function. The correlation matrixes were generated using average linkage clustering with 1 – Spearman R^2 as a distance metric and were visualized using the *gplot* package.

RESULTS

Multidimensional blood profiling reveals associations of blood analytes with SLE disease activity measures. To understand whether circulating effectors of the immune system (proteins, cells, and autoantibodies) underlie SLE pathologies that are undetectable in transcripts found in whole-blood samples, we created the SLE Immune Atlas, which integrates multimodal immune measures with clinical features of the disease. Blood proteomics; eight-hour immunophenotyping; IgG, IgM, and IgA autoantibodies; and gene expression were assessed in a cross-sectional cohort of 87 patients with predominantly mild to moderate SLE and 48 healthy controls, matched by age and sex (https://astrazeneca-bka.shinyapps.io/sle-immune-atlas/; Figure 1). Patient and healthy control demographics and clinical characteristics are summarized in Supplementary Table S1.

All platforms identified hits that were significantly associated with the presence of type I IFN activity (21-IFNGS) and increased anti–double-stranded DNA (dsDNA) antibody levels. None of the 13,421 transcriptional alterations were associated with organ-specific disease activity, whereas protein, cell, and autoantibody-based measures were found to be associated with different combinations of markers for organ involvement (decreased glomerular filtration rate [GFR], active nephritis, history of cardiovascular disease, arthritis, and malar rash). Proportionally, the strongest association identified among the organ involvement markers was between serum proteins and decreased GFR.

Identification of three distinct protein signatures that are elevated in patients with SLE. To capture temporally regulated protein signals, we used an aptamer-based proteomic platform[30] to identify features of the immune system that are dysregulated in SLE and associated with disease activity or accrual of organ damage. Cross-correlation analysis of proteins up-regulated in SLE identified three distinct clusters of highly correlated proteins associated with clinical disease measures (Figure 2A). These clusters were classified based on their biologic context into an IFN-associated inflammation (IAI) signature, a granulocyte-related (GRN) signature, and an immune cell priming (ICP) signature, the latter marked by molecules secreted or shed by antigen-presenting cells (APCs) and effector cells and proteins related to tissue injury. Notably, the IAI and GRN clusters aligned with well-established pathways previously linked to SLE pathogenesis; these protein associations are listed in the Supplementary Excel Table.

To interrogate immunologic feature associations at the patient level, a protein signature score was generated for each of the three clusters using factor analysis. Protein loadings for these signatures were highly reproducible across independent cohorts of patients with SLE and were recapitulated using a dual antibody-based proteomics platform (RBM) (Supplementary Figure S1A–C). In addition, patient scores derived from independent proteomic platforms (RBM and SOMAscan) applied to the discovery cohort sample set were found to be significantly concordant, thus demonstrating robustness of the signature scores (Supplementary Figure S1D).

Nearly all patients with SLE (94.3%) were positive for one or more of the identified protein signatures or the 21-IFNGS (Figure 2B), defined by a score that is 2 SDs from the healthy control mean score. The IAI, GRN, and ICP signatures were present in 52.9%, 35.6%, and 42.5% of patients, respectively, whereas the 21-IFNGS was present in 69.0% of patients (Figure 2B; Supplementary Figure S2). All three protein signatures were significantly elevated compared with healthy controls in both IFNGS-high and IFNGS-low patients with SLE (GRN: healthy controls and 21-IFNGS-high patients, $P = 0.0017$; all others, $P < 0.001$; Figure 2C). The ICP protein signature did not differ between 21-IFNGS-high and 21-IFNGS-low patients (Figure 2C).

To elucidate the biologic drivers of the three protein signatures, we examined the association of the strongest protein correlates of the signature with other analytes. The IAI and GRN signatures correlated with transcripts (n = 61 and n = 18, respectively) (Supplementary Figure S3A) and circulating cell populations (both n = 5) (Supplementary Figure S3B). In contrast, we found no strong gene or cell correlates of the ICP signature (|Spearman R|

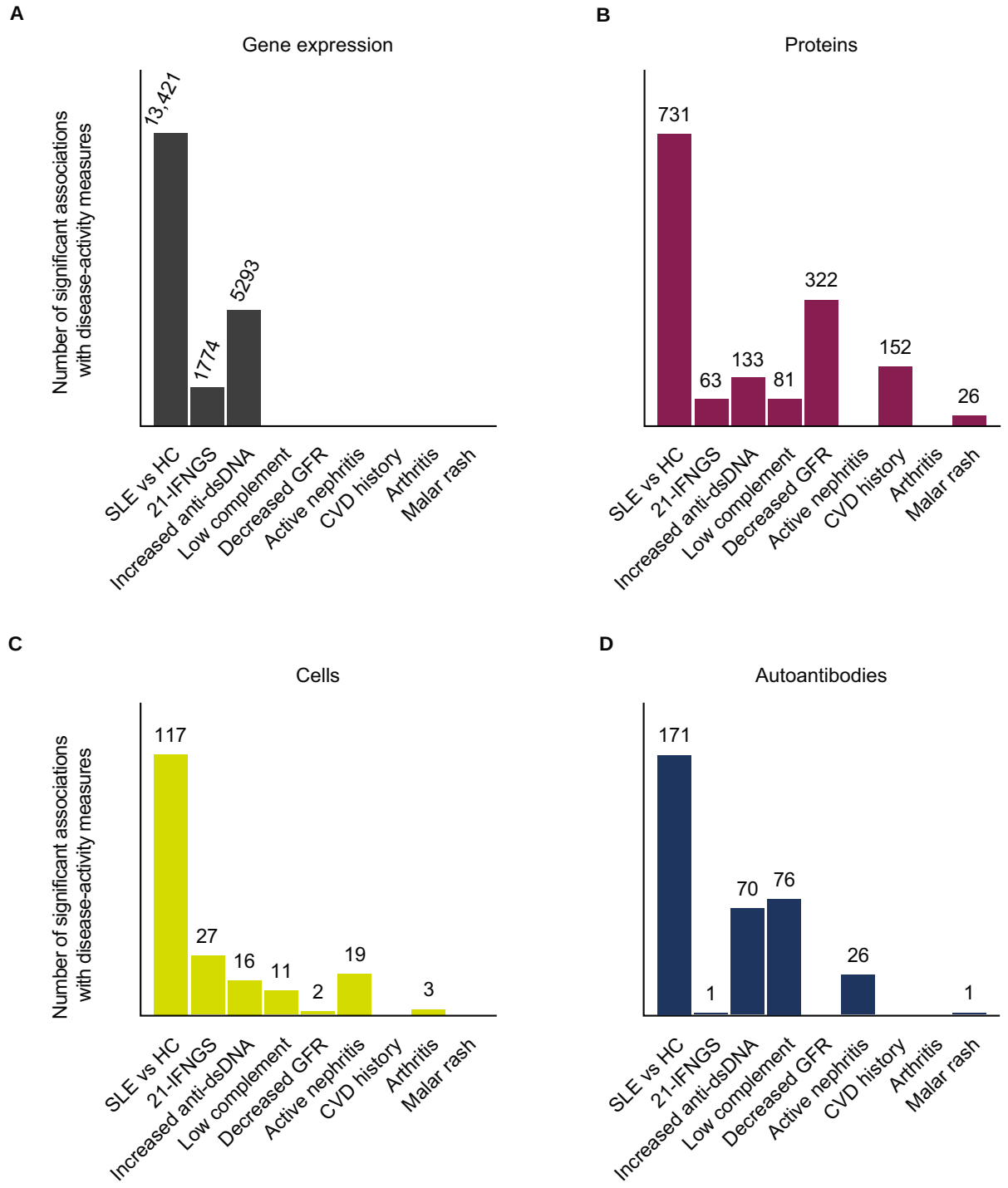

Figure 1. Multidimensional blood profiles reveal biologic links to SLE pathology that would not be detected in WB gene expression profiles alone. (A) HG U-133 Plus 2.0 Affymetrix Gene Expression microarray. (B) SOMAscan 1.1K Array and RBM HumanMAP 175+. (C) Multicolor flow cytometry. (D) UTSW autoantibody array. All protein, cellular, autoantibody, and gene expression measurements that met quality control criteria were compared between patients with predominantly mild to moderate SLE (n = 87) and HC (n = 48), matched by age and sex. Bar charts display the number of significant associations with different disease activity measures for each platform. 21-IFNGS, interferon 21 gene signature; anti-dsDNA, anti–double-stranded DNA; CVD, cardiovascular disease; GFR, glomerular filtration rate; HC, healthy controls; HG, human genome; RBM, Rules-Based Medicine; SLE, systemic lupus erythematosus; UTSW, University of Texas Southwestern; WB, whole blood.

> 0.5) in blood (Supplementary Figure S3). This may be due to protein changes that remain after the transcriptional program has been shut off or due to the signature being driven by cells outside of the blood.

The IAI protein signature and IFNGS are concordant and are associated with similar biology. The IAI signature featured canonical IFN-inducible proteins (eg, IP-10, I-TAC, MIP-3β, TIM-3; Supplementary Excel Table) known to be up-regulated

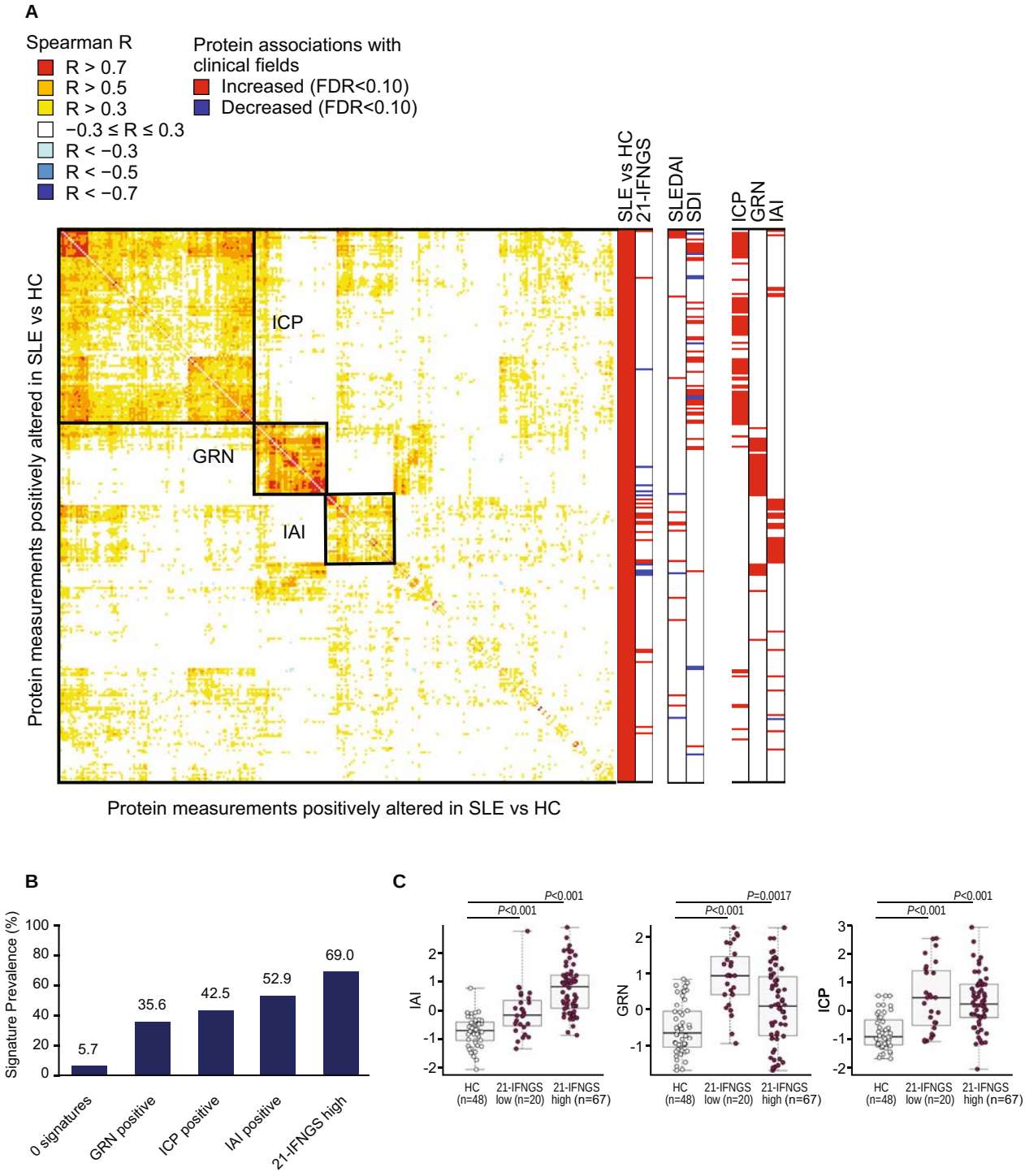

Figure 2. Protein signatures elevated in patients with SLE. (A) Correlation matrix displaying intercorrelation of SOMAScan 1.1K array protein measurements positively altered in patients with SLE versus HC (Mann–Whitney adjusted $P < 0.10$, AUC > 0.5). The directions of protein levels in SLE versus HC, 21-IFNGS-high patients, severe patients as determined by SELENA-SLEDAI or SDI, and protein signature–positive participants are displayed in the color bar on the right. (B) Bar chart displaying proportion of cohort negative for all four signatures (5/87 patients, 5.7%) or positive for at least one signature (2 SDs from HC mean used as threshold; 82/87 patients, 94.3%). (C) Scatter box plots displaying elevation of protein signatures in IFNGS-high and IFNGS-low patients with SLE versus HC. The Mann–Whitney U test was used to measure significance of differences between groups. 21-IFNGS, interferon 21 gene signature; AUC, area under the curve; FDR, false discovery rate; GRN, granulocyte; HC, healthy controls; IAI, interferon-associated inflammation; ICP, immune cell priming; SDI, Systemic Lupus International Collaborating Clinics/American College of Rheumatology Damage Index; SLE, systemic lupus erythematosus; SELENA-SLEDAI, Safety of Estrogens in Lupus Erythematosus National Assessment version of the Systemic Lupus Erythematosus Disease Activity Index.

during an inflammatory response.[31–34] Comparison of the IAI signature with established type I IFNGS (21-IFNGS, IFN signature metric, IFNGS, and modules M5.12, M1.2, and M3.4)[31,35,36] demonstrated concordance among all six IFNGS (Supplementary Figure S4A). Moreover, the IAI signature and 21-IFNGS correlated comparably with key discriminatory proteins, immune cell subsets, gene signatures, and clinical measures of disease activity and damage (Supplementary Figure S4B). Notably, the presence of rash, a disease manifestation highly responsive to type I IFN–targeted therapies,[37] was more strongly associated with the IAI signature than 21-IFNGS (IAI: AUC = 0.75; 21-IFNGS: AUC = 0.33; Supplementary Figure S4C).

The GRN protein signature reflects granulocyte activation across all granulocyte subsets and is associated with multiple SLE clinical measures. The GRN signature featured proteins such as cathepsin G, azurocidin, and LOX-1, known to play important roles in neutrophil, low-density granulocyte (LDG), and other granulocyte biology[38–40] (Supplementary Excel Table). Although the GRN signature correlated with protein granulocyte markers (Supplementary Figure S5A), it did not correlate significantly with M5.15 (R = 0.15), an established neutrophil gene expression module (Supplementary Figure S5B).

We found that, in contrast to the M5.15 neutrophil gene signature, the GRN protein signature correlated with all tested granulocyte populations (neutrophils: R = 0.60, $P = 1.9 \times 10^{-7}$; intermediate neutrophils: R = 0.39, $P = 0.0076$; mature neutrophils: R = 0.45, $P = 0.0018$; basophils: R = 0.33, $P = 0.0085$; eosinophils: R = 0.53, $P = 7.9 \times 10^{-6}$; and LDGs: R = 0.33, $P = 0.026$) (Supplementary Figure S5C). There was a moderate correlation between the M4.13 inflammation signature and intermediate neutrophils (R > 0.3). Overall, the GRN signature had stronger correlations with eosinophils and LDGs than the gene signatures commonly used to track neutrophil biology.

We next examined the association of the GRN signatures and granulocyte cell populations with clinical features of SLE. We found that the GRN signature was associated with arthritis (AUC = 0.75), pyuria (AUC = 0.59), and class IV LN (AUC = 0.65) (Supplementary Figure S5D). Similar trends were reflected by neutrophil, basophil, eosinophil, and LDG counts; LDG counts were positively associated with increased anti-dsDNA autoantibody levels. Additionally, the GRN signature was not significantly associated with therapeutic treatment with cyclophosphamide or oral glucocorticoids (Supplementary Figure S5E), suggesting this signature is not confounded by cyclophosphamide or oral glucocorticoid use in this cohort of patients.

ICP signature correlates with markers of renal dysfunction in patients with SLE. The ICP signature featured proteins such as KIM-1 and cystatin C, both classic markers of renal damage,[41,42] and secreted and cleavage proteins preferentially expressed by APCs (β_2m, CD40, ICOS, IL-12p40, and MMP-7) that were correlated with the ICP signature score (Supplementary Excel Table and Figure 3A), suggesting that this signature may be associated with immune responses between APCs and effector cells of the immune system.

To understand whether the ICP signature was correlated with any tissue-specific aspects of SLE disease activity, we next assessed the correlation between the ICP signature and SLE organ damage and disease activity as measured by the Systemic Lupus International Collaborating Clinics/American College of Rheumatology Damage Index (SDI) and the Safety of Estrogens in Lupus Erythematosus National Assessment version of the Systemic Lupus Erythematosus Disease Activity Index (SELENA-SLEDAI), respectively. Based on SDI analysis, the ICP signature score increased with greater renal impairment, whereas worsened renal function was not correlated with the IAI or GRN signatures (Figure 3B). We further identified significant associations between the ICP signature and SELENA-SLEDAI proteinuria ($P = 1.1 \times 10^{-3}$), decreased GFR ($P = 5.0 \times 10^{-7}$), and active nephritis ($P = 0.044$) (Figure 3C). Although we identified these associations between the ICP signature score and renal disease, we did not observe any significant relationship between the ICP signature score and the serologic markers of SLE disease activity (low complement level, increased DNA binding). Therefore, evaluation of the ICP signature score may be a more sensitive approach to disease assessment than current methods.

The correlation of the ICP signature with renal disease in patients with SLE, which was not detected in gene expression or flow cytometry using whole-blood samples, led us to investigate whether APC gene transcripts for proteins in the ICP signature were differentially expressed in renal biopsy samples of patients with LN. Using a publicly available data set from a study that included biopsy sample collection,[43,44] we identified expression of multiple ICP signature genes (*MMP7*, *B2M*, and *CD40*) that were more highly expressed in the tubulointerstitium of patients with LN than in healthy controls (Figure 4A). Patients with LN also had significantly higher levels of expression of multiple ICP signature genes (*TNFRSF21*, *TNFRSF1B*, *B2M*, *THBD*, *IL12A*, and *CD40*) in the glomeruli compared with healthy controls (Figure 4). These data provided evidence that protein correlates of the ICP signature score found in whole blood may also be produced within damaged kidneys of patients with SLE.

Using data from the European Renal cDNA Bank of laser-capture microdissected glomeruli and microarray profiling, we investigated internally derived DC signatures for patients with chronic kidney disease as well as SLE or nonlupus inflammatory nephropathies. We found elevated DC signatures in patients with diabetic nephropathy, SLE, IgA nephropathy, and hypersensitive nephropathy compared with healthy donor controls (Supplementary Figure S6) and found that the DC signature correlated with decreasing kidney function (r = –0.43). Together, these

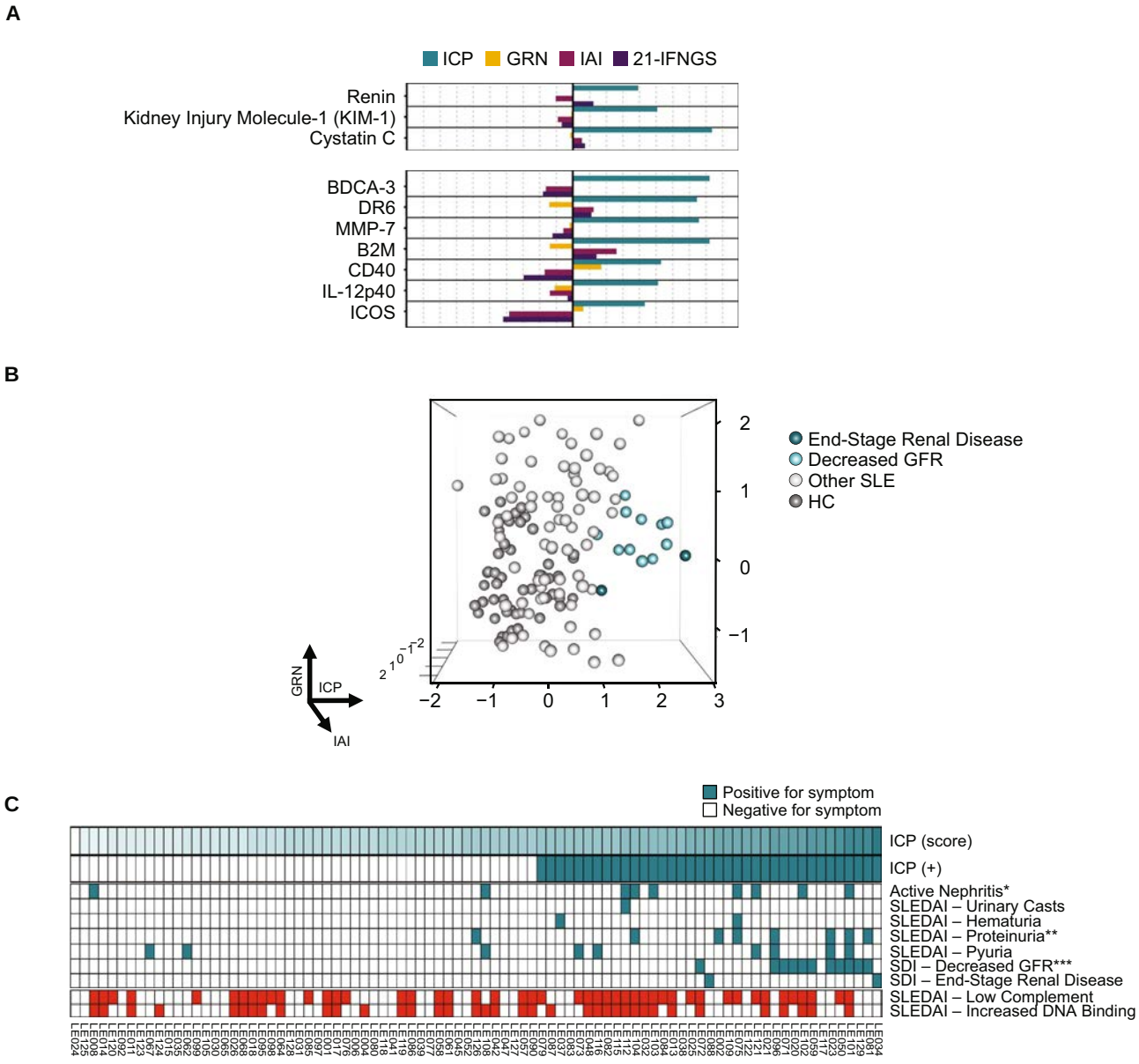

Figure 3. ICP signature correlates with markers of renal dysfunction. (A) Bar plot displaying select correlations between protein measurements and the ICP signature. (B) Scatterplot displaying association between IAI, GRN, and ICP signature scores and decreased GFR as determined by SDI. (C) Heatmap displaying prevalence of renal pathologies in the SLE cohort as ICP signature score increases. ICP positive designated at 2 SD from HC mean. The ICP signature score was compared between patients positive versus negative for each renal pathology, SELENA-SLEDAI serology components (red), and Mann–Whitney U test. *$P < 0.05$; **$P < 0.01$; ***$P < 0.001$. 21-IFNGS, interferon 21 gene signature; GFR, glomerular filtration rate; GRN, granulocyte; HC, healthy control; IAI, interferon-associated inflammation; ICP, immune cell priming; SDI, Systemic Lupus International Collaborating Clinics/American College of Rheumatology Damage Index; SLE, systemic lupus erythematosus; SELENA-SLEDAI; Safety of Estrogens in Lupus Erythematosus National Assessment version of the Systemic Lupus Erythematosus Disease Activity Index.

experiments place a cell type that contributes to the ICP signature in the nephrotic tissue and establish a linkage between the ICP signature and organ damage across multiple diseases.

ICP signature identifies patients with SLE with an increased rate of disease worsening. The majority of patients had at least one protein signature (Supplementary Figure S2). We examined the association between the number of protein signatures and disease activity and organ damage in patients with SLE. We found that patients with increased numbers of protein signatures had greater global disease activity, as measured by SELENA-SLEDAI, and organ damage scores, as assessed by SDI (Figure 5). Moreover, the ICP signature was predictive of increased SDI worsening over a six-year follow-up of the SLE cohort (Figure 6). A numerically greater proportion of ICP-positive patients had at least a 3-point increase in SDI scores than did ICP-negative patients (14% [5/36] vs 4% [2/48], respectively) (Figure 6A). Although the SDI score increased over time

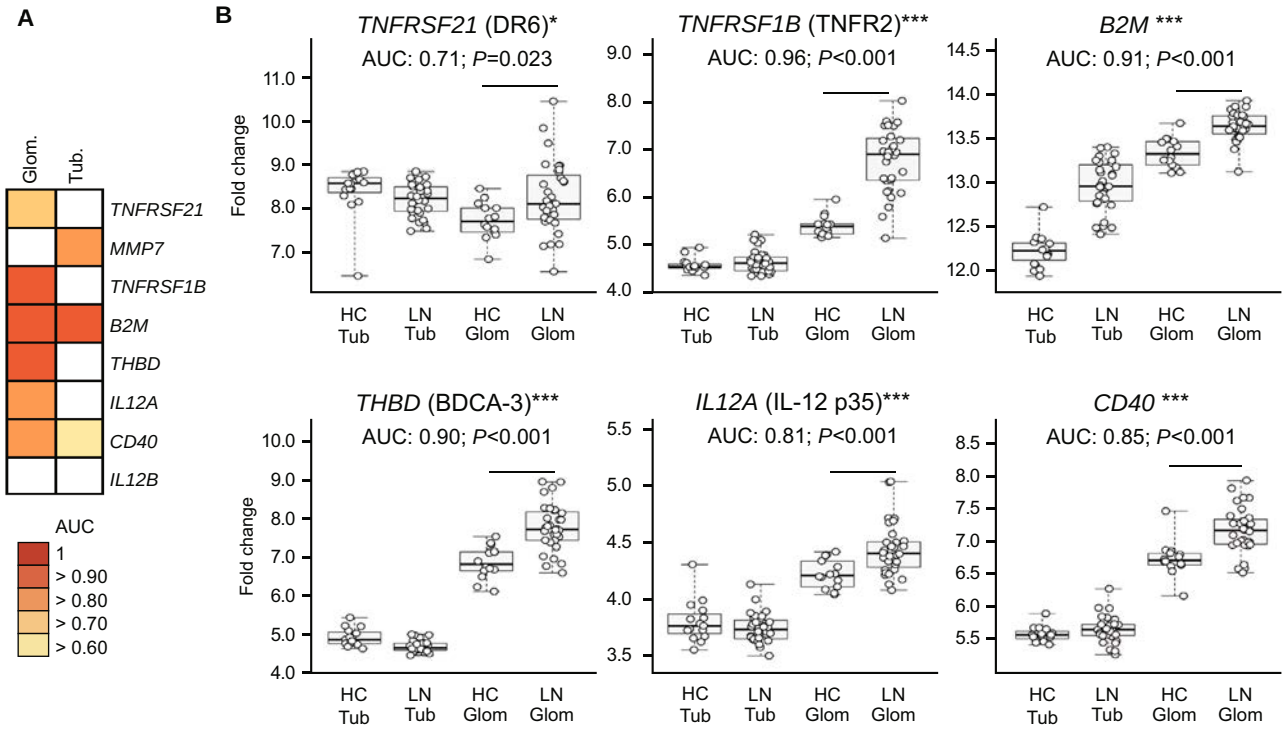

Figure 4. ICP markers are elevated in kidney biopsy samples from patients with LN. (A) Heatmap displaying relative expression of genes in LN Glom and Tub versus HC, colored by AUC (Mann–Whitney U test $P < 0.05$), in GSE32591. (B) Boxplots displaying elevation of gene expression of specific markers in LN Glom (n = 32) and Tub (n = 32) versus HC Glom (n = 14) and Tub (n = 15) in GSE32591 (Mann–Whitney U test). *$P < 0.05$; **$P < 0.01$; ***$P < 0.001$. AUC, area under the curve; Glom, glomeruli; HC, healthy control; ICP, immune cell priming; LN, lupus nephritis; Tub, tubulointerstitium.

across the cohort, the rate of disease progression was greater in ICP-positive patients (Figure 6B). Multiyear clinical follow-up data from the 2016 to 2017 validation cohort (n = 43) support the association between ICP and SDI disease worsening (Supplementary Figure S7A).

When evaluating the different domains that contribute to a patient's SDI score, ICP-positive patients were more likely to exhibit worsening in the ocular, renal, pulmonary, and skin domains compared with ICP-negative patients (Figure 4C). The association between the ICP signature status and SDI worsening remained significant ($P = 0.001$) after adjusting for disease duration and other covariates, including oral glucocorticoid use, by multivariate analysis (Supplementary Table S3 and Supplementary Figure S8).

ICP-positive patients had nearly twice the rate of damage accrual than did ICP-negative patients (rate ratio [RR] 1.92, 95% confidence interval [CI] 1.41–2.67, $P = 6.5 \times 10^{-5}$) (Figure 6D). Damage accrual was associated with the GRN signature to a lesser extent (RR 1.41, 95% CI 1.01–2.00, $P = 0.046$), and no significant association was found between damage accrual and the IAI signature (RR 1.06, 95% CI 0.76–1.49, $P = 0.71$). In the 2016 to 2017 validation cohort, ICP showed the highest RR, though significance was not achieved due to small sample sizes (RR 1.82, 95% CI 1.00–3.53, $P = 0.086$) (Supplementary Figure S7B).

DISCUSSION

The type I IFN pathway plays a critical role in SLE pathogenesis[10,43]; however, the mechanisms driving organ-specific damage remain elusive. The immense clinical and molecular heterogeneity of SLE and the paucity of data sets evaluating affected tissues over time have been key challenges for the field.[44,45] In addition, current disease activity assessments only partially capture the total disease burden.

We hypothesized that multidimensional blood profiling could identify new biology and reveal key molecular patterns that underlie distinct SLE pathologies. To this end, we profiled blood proteins, genes, cellular phenotypes, and autoantibodies to generate an assimilated overview of the SLE disease state, and we have made this available via the SLE Immune Atlas portal. This data set provides a valuable resource for bridging new biologic discoveries with clinically relevant patient populations and disease mechanisms through a precision medicine approach. Revealing these connections has the potential to expand treatment options

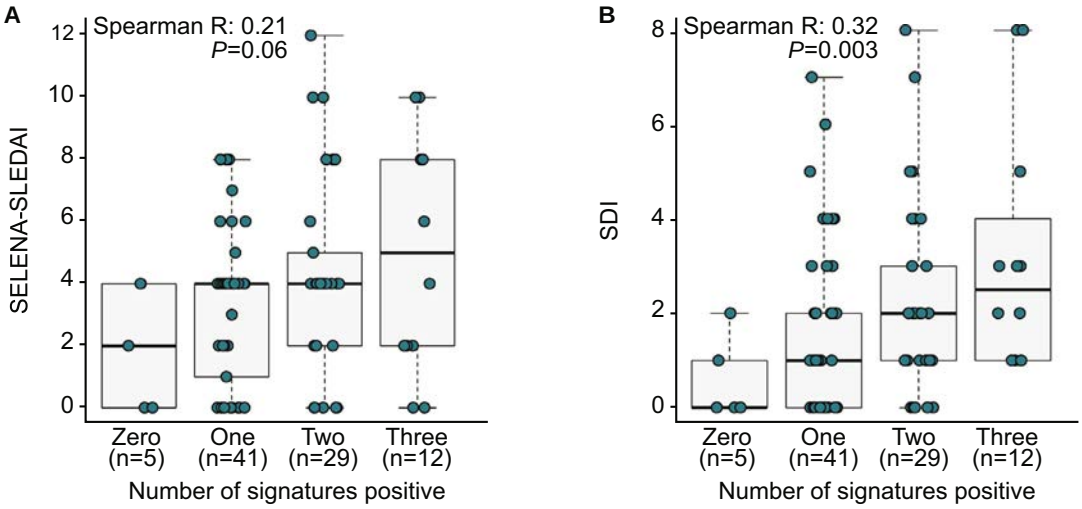

Figure 5. Protein signatures are associated with increased rate of disease worsening. Boxplots displaying (A) SELENA-SLEDAI and (B) SDI scores versus the number of protein signatures in each patient with SLE. SDI, Systemic Lupus International Collaborating Clinics/American College of Rheumatology Damage Index; SELENA-SLEDAI, Safety of Estrogens in Lupus Erythematosus National Assessment version of the Systemic Lupus Erythematosus Disease Activity Index; SLE, systemic lupus erythematosus.

for the diverse manifestations of SLE and redefine treatment landscapes.

Type I IFN signaling is commonly dysregulated in SLE, and many patients go on to develop heterogenous and diverse organ-specific pathologies.[10,43] This suggests that additional factors beyond type I IFN are driving disease manifestations in specific tissues. Here, we identified three protein signatures relating to IFN activity, granulocyte activation, and ICP that are significantly associated with SLE disease status and unique organ-specific manifestations in patients with SLE. Although increased circulating protein levels in patients with SLE may not inherently reflect immunopathogenicity, the correlation of each signature with specific clinical activity measures underscores their potential biologic significance. Overall, 94% of patients with SLE in the NIH cohort possessed at least one of the three protein signatures (IAI, GRN, and/or ICP) or 21-IFNGS. In addition, patients with an increased number of protein signatures were more likely to have greater disease activity and organ damage accrual compared with those with fewer signatures.

Although roles for the type I IFN pathway and neutrophil activation in SLE pathogenesis have been previously reported,[9,11–14,46] our multi-omics approach enabled identification of new biologic contributors that are independent from these axes. This approach revealed a previously uncharacterized ICP signature that was enriched in patients with renal involvement and was predictive of disease worsening independent from patient demographics, disease duration, established biomarkers, or the other protein signatures.

Unlike the IAI and GRN signatures, the ICP signature was not detectable by gene expression profiling alone. We hypothesized that the ICP signature signal may originate from a highly vascularized tissue compartment and that this was likely to be the kidneys. In support of this hypothesis, transcripts corresponding to APC-associated proteins found within the ICP signature were significantly elevated in kidneys of patients with LN.[43,44] Furthermore, we found a distinctive gene signature associated with DCs within kidney tissue in an independent cohort, and this signature correlated with estimated GFR (eGFR). Infiltration of classical DCs and pDCs in SLE kidney biopsy samples was previously shown to increase during active disease.[17] These findings collectively highlight the significance of local DCs and their involvement in ICP as potential contributors to the immunopathologic processes observed in LN.

Renal involvement in SLE has been associated with increased risk of death compared with the general population,[47] with an estimated 10% to 20% of patients with SLE developing end-stage renal disease.[48] Although the therapeutic management of renal disease has improved, there is still a need to better define biomarkers that predict prognosis and response to treatment to have more favorable renal outcomes.[49] Because it can be monitored in the periphery, the ICP signature is of specific interest for its potential utility in understanding renal disease progression over time in patients with SLE.

Here, we observed a differential outcome for patients by ICP signature within six years of disease onset, representing an important opportunity for early intervention to avoid disease progression and organ damage. The ICP signature predicted an increased rate of organ damage progression in two independent cohorts independent of common covariates, such as glucocorticoid use, the level of damage at baseline, or disease duration. Our findings indicate that patients with relatively high levels of damage at baseline who are ICP positive are likely to continue to

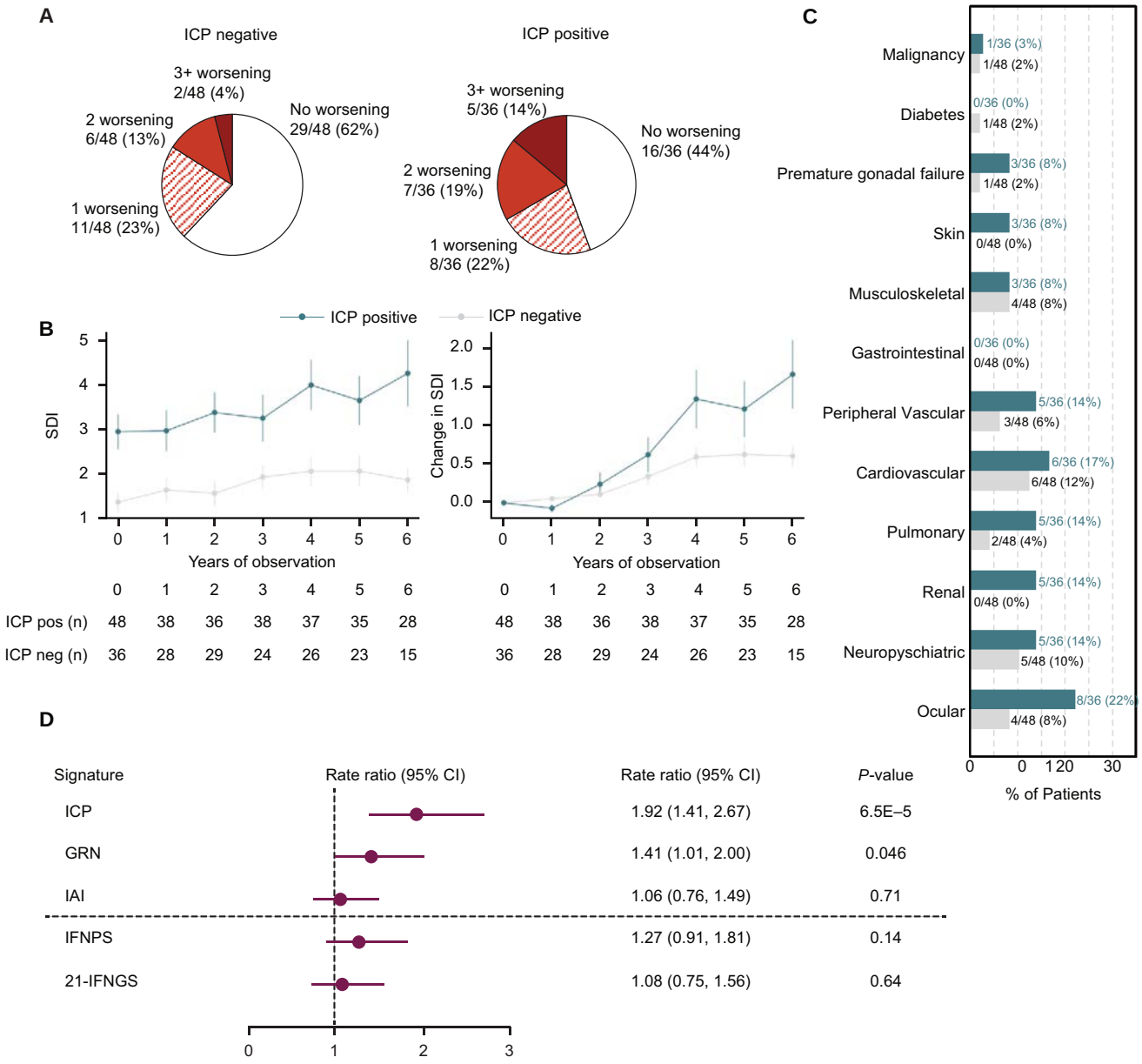

Figure 6. ICP signature predicts increased rate of disease worsening over time. (A) Pie charts displaying percentages of patients with longitudinal worsening in one, two, or three or more SDI domains among ICP-positive and ICP-negative patients. (B) Line charts displaying mean SDI and mean (±SEM) change in SDI per year of follow-up in ICP-positive (teal) and ICP-negative (gray) patients. (C) Bar plot displaying percentages of patients with worsening of domains of SDI in ICP-positive (teal) and ICP-negative (gray) patients. (D) Univariate association between each signature and SDI progression as measured by negative binomial regression. 21-IFNGS, interferon 21 gene signature; CI, confidence interval; GRN, granulocyte; IAI, interferon-associated inflammation; ICP, immune cell priming; IFNPS, interferon protein signature; neg, negative; pos, positive; SDI, Systemic Lupus International Collaborating Clinics/American College of Rheumatology Damage Index.

accrue organ damage. In contrast, after adjusting for the impact of covariates, neither the established serologic markers of SLE disease activity (C3, C4, and anti-dsDNA IgG) nor eGFR (a biomarker for kidney disease) was associated with organ damage progression. Thus, the ICP may provide complementary insight into established biomarkers. Despite small group sizes, ICP-positive patients were more likely to accumulate damage in organ domains associated with high levels of vascularization (eg, renal and pulmonary systems), which may provide preferential access for immune cells that contribute to organ damage while allowing protein efflux from tissue into blood.

Our immunophenotyping results are also consistent with a generalized model of effector immune populations moving out of the blood and into tissues. We observed associations between change in SDI over time and baseline levels of monocytes, DCs ($CD1c^{-}CD141^{+}$myeloid cells), proliferating CD4 T cells, platelets,

and natural killer (NK) cells. Monocytes and CD4 T cells were among the cell types that explained the most within-transcriptome variation in renal involvement in overall disease activity among patients with SLE,[50] and NK cells have previously been linked to disease activity and nephritis.[51]

In addition to the ICP signature, we identified the IAI signature, which was the most prevalent of the three signatures identified in this patient cohort. We demonstrated concordance between the IAI signature and the 21-IFNGS and showed that the IAI signature strongly correlated with canonical SLE pathologies that are observed with high frequency in patients with SLE, including elevated anti-dsDNA antibody levels, low complement levels, and malar rash.[52]

We also identified a GRN signature and multiple granulocyte subtypes associated with key SLE pathologies, supporting previous literature.[6,53–55] Patients who were positive for the GRN signature were more likely to exhibit arthritis, pyuria, and class IV LN. The GRN signature correlated to a similar extent with overall prevalence of all granulocyte populations tested in our study, whereas the established M5.15 gene signature did not correlate with basophils, eosinophils, or LDGs, which may explain the lack of correlation between the GRN and M5.15 signatures. Our results indicate that the GRN signature is a robust granulocyte signature that was not confounded by use of standard therapies (cyclophosphamides and oral glucocorticoids). Thus, an elevated GRN signature can serve as a marker for granulocyte dysfunction in a subset of patients with SLE who have distinct clinical features.

With this study, we set out to perform multi-omics characterization of patients with predominantly mild to moderate SLE to examine the biological pathways preceding advanced disease. As such, our findings reflect only a subset of the overall SLE patient population. Additionally, sample collection was optimized to reduce the impact of preanalytic variables known to confound multibatch proteomic and flow cytometry data sets. Although we used clinically validated measures of disease activity and damage, these measures do not fully capture all SLE pathologies and disease burden. Validation of the ICP signature will require prospective studies in larger patient cohorts, including those with severe kidney disease, to confirm its ability to identify individuals at highest risk of disease progression and to establish clinical correlates. Incorporation of paired biopsies would further enable evaluation of the ICP signature in both the kidney and blood, with direct comparison to activity and chronicity indices. Signatures that noninvasively predict organ-specific manifestations and/or greater levels of organ damage could represent important prognostic biomarkers that impact SLE disease management and identify patients more likely to develop progressive disease.

The protein signatures described here reveal key mediators of SLE, support patient stratification by disease features, and may help identify individuals at risk for organ involvement and clinical progression. Together with the immunophenotyping data, they offer a resource to advance understanding of immune mechanisms in SLE. These results reveal parallel immune mechanisms in SLE and provide a framework for the development of personalized management approaches. With the fully explorable, clinically annotated biomarker and long-term outcomes data accessible via the SLE Immune Atlas portal, this work provides a platform for connecting elegant academic findings using a multi-omics approach to clinically pursuable strategies.

ACKNOWLEDGMENTS

The authors would like to acknowledge the patients and healthy volunteers who participated in these studies and thank Bhargavi Rajan, Isharat Yusuf, Brandon Higgs, and Tomas Mustelin for their contributions to the Autoimmunity Molecular Medicine Team.

AUTHOR CONTRIBUTIONS

All authors contributed to at least one of the following manuscript preparation roles: conceptualization AND/OR methodology, software, investigation, formal analysis, data curation, visualization, and validation AND drafting or reviewing/editing the final draft. As corresponding authors, Drs Sinibaldi and Casey confirm that all authors have provided the final approval of the version to be published and take responsibility for the affirmations regarding article submission (eg, not under consideration by another journal), the integrity of the data presented, and the statements regarding compliance with institutional review board/Declaration of Helsinki requirements.

ROLE OF THE STUDY SPONSOR

Scientists at AstraZeneca and the National Institutes of Health contributed to the study design or in the collection, analysis, or interpretation of the data as well as the decision to submit the manuscript for publication. The authors thank Victoria Alikhan, PhD, of JK Associates Inc, part of Avalere Health, for medical writing support. This support was funded by AstraZeneca in accordance with Good Publication Practice (GPP3) guidelines (https://www.ismpp.org/gpp3).

ADDITIONAL DISCLOSURES

Authors Smith, Wang, and Zerrouki are currently employees of Horizon Therapeutics but were employed by AstraZeneca during the time the study was conducted. Author Rahman is currently an employee of Sanofi US but was employed by AstraZeneca during the time the study was conducted. Author Chiang is currently an employee of Discovery IO, LLC, but was employed by AstraZeneca during the time the study was conducted. Author Henault is currently an employee of Bristol Myers Squibb but was employed by AstraZeneca during the time the study was conducted. Author Filippi is an employee of AstraZeneca. Author Groves is currently an employee of Q2 Solutions but was employed by AstraZeneca during the time the study was conducted. Author Ettinger was employed by AstraZeneca during the time the study was conducted. Author Kolbeck is currently an employee of Spirovant Sciences, Inc, but was employed by AstraZeneca during the time the study was conducted. Author Sanjuan is currently an employee of Sanofi US and Paulex Bio but was employed by AstraZeneca during the time the study was conducted. Author Siegel is currently an employee of Novartis Institutes of BioMedical Research but was employed by the NIH during the time the study was conducted. Author Casey is currently an employee of Regeneron Pharmaceuticals but was employed by AstraZeneca during the time the study was conducted. The contributions of the NIH authors were made as part of their official duties as NIH federal employees, are in compliance with agency policy requirements, and are

considered Works of the United States Government. However, the findings and conclusions presented in this paper are those of the author and do not necessarily reflect the views of the NIH or the US Department of Health and Human Services.

REFERENCES

1. Nossent J, Cikes N, Kiss E, et al. Current causes of death in systemic lupus erythematosus in Europe, 2000--2004: relation to disease activity and damage accrual. Lupus 2007;16(5):309–317. doi:10.1177/0961203307077987
2. Tsokos GC. Systemic lupus erythematosus. N Engl J Med 2011;365(22):2110–2121. doi:10.1056/NEJMra1100359
3. Bruce IN, O'Keeffe AG, Farewell V, et al. Factors associated with damage accrual in patients with systemic lupus erythematosus: results from the Systemic Lupus International Collaborating Clinics (SLICC) Inception Cohort. Ann Rheum Dis 2015;74(9):1706–1713. doi:10.1136/annrheumdis-2013-205171
4. Banchereau J, Pascual V. Type I interferon in systemic lupus erythematosus and other autoimmune diseases. Immunity 2006;25(3):383–392. doi:10.1016/j.immuni.2006.08.010
5. Rönnblom L, Alm GV. A pivotal role for the natural interferon α-producing cells (plasmacytoid dendritic cells) in the pathogenesis of lupus. J Exp Med 2001;194(12):F59–F64. doi:10.1084/jem.194.12.f59
6. Denny MF, Yalavarthi S, Zhao W, et al. A distinct subset of proinflammatory neutrophils isolated from patients with systemic lupus erythematosus induces vascular damage and synthesizes type I IFNs. J Immunol 2010;184(6):3284–3297. doi:10.4049/jimmunol.0902199
7. Banchereau R, Hong S, Cantarel B, et al. Personalized immunomonitoring uncovers molecular networks that stratify lupus patients. Cell 2016;165(3):551–565. doi:10.1016/j.cell.2016.03.008
8. Crow MK. Type I interferon in the pathogenesis of lupus. J Immunol 2014;192(12):5459–5468. doi:10.4049/jimmunol.1002795
9. Dall'Era MC, Cardarelli PM, Preston BT, et al. Type I interferon correlates with serological and clinical manifestations of SLE. Ann Rheum Dis 2005;64(12):1692–1697. doi:10.1136/ard.2004.033753
10. Rönnblom L, Leonard D. Interferon pathway in SLE: one key to unlocking the mystery of the disease. Lupus Sci Med 2019;6(1):e000270. doi:10.1136/lupus-2018-000270
11. Furie R, Khamashta M, Merrill JT, et al; CD1013 Study Investigators. Anifrolumab, an anti-interferon-α receptor monoclonal antibody, in moderate-to-severe systemic lupus erythematosus. Arthritis Rheumatol 2017;69(2):376–386. doi:10.1002/art.39962
12. Morand EF, Furie R, Tanaka Y, et al; TULIP-2 Trial Investigators. Trial of anifrolumab in active systemic lupus erythematosus. N Engl J Med 2020;382(3):211–221. doi:10.1056/NEJMoa1912196
13. Casey KA, Guo X, Smith MA, et al. Type I interferon receptor blockade with anifrolumab corrects innate and adaptive immune perturbations of SLE. Lupus Sci Med 2018;5(1):e000286. doi:10.1136/lupus-2018-000286
14. Smith MA, Chiang C-C, Zerrouki K, et al. Using the circulating proteome to assess type I interferon activity in systemic lupus erythematosus. Sci Rep 2020;10(1):4462. doi:10.1038/s41598-020-60563-9
15. Catalina MD, Bachali P, Geraci NS, et al. Gene expression analysis delineates the potential roles of multiple interferons in systemic lupus erythematosus. Commun Biol 2019;2(1):140. doi:10.1038/s42003-019-0382-x
16. Wardowska A, Komorniczak M, Bułło-Piontecka B, et al. Transcriptomic and epigenetic alterations in dendritic cells correspond with chronic kidney disease in lupus nephritis. Front Immunol 2019;10:2026. doi:10.3389/fimmu.2019.02026
17. Fiore N, Castellano G, Blasi A, et al. Immature myeloid and plasmacytoid dendritic cells infiltrate renal tubulointerstitium in patients with lupus nephritis. Mol Immunol 2008;45(1):259–265. doi:10.1016/j.molimm.2007.04.029
18. de Sousa Abreu R, Penalva LO, Marcotte EM, et al. Global signatures of protein and mRNA expression levels. Mol Biosyst 2009;5(12):1512–1526. doi:10.1039/B908315D
19. Vogel C, Marcotte EM. Insights into the regulation of protein abundance from proteomic and transcriptomic analyses. Nat Rev Genet 2012;13(4):227–232. doi:10.1038/nrg3185
20. Nicolaou O, Kousios A, Hadjisavvas A, et al. Biomarkers of systemic lupus erythematosus identified using mass spectrometry-based proteomics: a systematic review. J Cell Mol Med 2017;21(5):993–1012. doi:10.1111/jcmm.13031
21. Bashant KR, Aponte AM, Randazzo D, et al. Proteomic, biomechanical and functional analyses define neutrophil heterogeneity in systemic lupus erythematosus. Ann Rheum Dis 2021;80(2):209–218. doi:10.1136/annrheumdis-2020-218338
22. Hubbard EL, Bachali P, Kingsmore KM, et al. Analysis of transcriptomic features reveals molecular endotypes of SLE with clinical implications. Genome Med 2023;15(1):84. doi:10.1186/s13073-023-01237-9
23. Toro-Domínguez D, Martorell-Marugán J, Martinez-Bueno M, et al. Scoring personalized molecular portraits identify systemic lupus erythematosus subtypes and predict individualized drug responses, symptomatology and disease progression. Brief Bioinform 2022;23(5):bbac332. doi:10.1093/bib/bbac332
24. Gold L, Ayers D, Bertino J, et al. Aptamer-based multiplexed proteomic technology for biomarker discovery. PLoS One 2010;5(12):e15004. doi:10.1371/journal.pone.0015004
25. Gold L, Walker JJ, Wilcox SK, et al. Advances in human proteomics at high scale with the SOMAscan proteomics platform. N Biotechnol 2012;29(5):543–549. doi:10.1016/j.nbt.2011.11.016
26. Yao Y, Higgs BW, Morehouse C, et al. Development of potential pharmacodynamic and diagnostic markers for anti-IFN-α monoclonal antibody trials in systemic lupus erythematosus. Hum Genomics Proteomics 2009;2009:34312.
27. Berthier CC, Bethunaickan R, Gonzalez-Rivera T, et al. Cross-species transcriptional network analysis defines shared inflammatory responses in murine and human lupus nephritis. J Immunol 2012;189(2):988–1001. doi:10.4049/jimmunol.1103031
28. Shved N, Warsow G, Eichinger F, et al. Transcriptome-based network analysis reveals renal cell type-specific dysregulation of hypoxia-associated transcripts. Sci Rep 2017;7(1):8576. doi:10.1038/s41598-017-08492-y
29. Revelle W. psych: Procedures for Psychological, Psychometric, and Personality Research. R package version 2.5.6. Northwestern University; 2025. https://cran.r-project.org/web/packages/psych/index.html
30. Smith MA, Henault J, Karnell JL, et al. SLE plasma profiling identifies unique signatures of lupus nephritis and discoid lupus. Sci Rep 2019;9(1):14433. doi:10.1038/s41598-019-50231-y
31. Cole KE, Strick CA, Paradis TJ, et al. Interferon-inducible T cell alpha chemoattractant (I-TAC): a novel non-ELR CXC chemokine with potent activity on activated T cells through selective high affinity binding to CXCR3. J Exp Med 1998;187(12):2009–2021. doi:10.1084/jem.187.12.2009
32. Liu M, Guo S, Hibbert JM, et al. CXCL10/IP-10 in infectious diseases pathogenesis and potential therapeutic implications. Cytokine Growth Factor Rev 2011;22(3):121–130. doi:10.1016/j.cytogfr.2011.06.001
33. Anderson AC, Joller N, Kuchroo VK. Lag-3, Tim-3, and TIGIT: co-inhibitory receptors with specialized functions in immune regulation. Immunity 2016;44(5):989–1004. doi:10.1016/j.immuni.2016.05.001

34. Parlato S, Santini SM, Lapenta C, et al. Expression of CCR-7, MIP-3β, and Th-1 chemokines in type I IFN-induced monocyte-derived dendritic cells: importance for the rapid acquisition of potent migratory and functional activities. Blood 2001;98(10):3022–3029. doi:10.1182/blood.V98.10.3022
35. Chaussabel D, Quinn C, Shen J, et al. A modular analysis framework for blood genomics studies: application to systemic lupus erythematosus. Immunity 2008;29(1):150–164. doi:10.1016/j.immuni.2008.05.012
36. Kennedy WP, Maciuca R, Wolslegel K, et al. Association of the interferon signature metric with serological disease manifestations but not global activity scores in multiple cohorts of patients with SLE. Lupus Sci Med 2015;2(1):e000080. doi:10.1136/lupus-2014-000080
37. Morand EF, Furie RA, Bruce IN, et al. Efficacy of anifrolumab across organ domains in patients with moderate-to-severe systemic lupus erythematosus: a post-hoc analysis of pooled data from the TULIP-1 and TULIP-2 trials. Lancet Rheumatol 2022;4(4):e282–e292. doi:10.1016/S2665-9913(21)00317-9
38. Korkmaz B, Horwitz MS, Jenne DE, et al. Neutrophil elastase, proteinase 3, and cathepsin G as therapeutic targets in human diseases. Pharmacol Rev 2010;62(4):726–759. doi:10.1124/pr.110.002733
39. Soehnlein O, Lindbom L. Neutrophil-derived azurocidin alarms the immune system. J Leukoc Biol 2009;85(3):344–351. doi:10.1189/jlb.0808495
40. Wu Z, Sawamura T, Kurdowska AK, et al. LOX-1 deletion improves neutrophil responses, enhances bacterial clearance, and reduces lung injury in a murine polymicrobial sepsis model. Infect Immun 2011;79(7):2865–2870. doi:10.1128/IAI.01317-10
41. Murty MS, Sharma UK, Pandey VB, et al. Serum cystatin C as a marker of renal function in detection of early acute kidney injury. Indian J Nephrol 2013;23(3):180–183. doi:10.4103/0971-4065.111840
42. Han WK, Bailly V, Abichandani R, et al. Kidney injury molecule-1 (KIM-1): a novel biomarker for human renal proximal tubule injury. Kidney Int 2002;62(1):237–244. doi:10.1046/j.1523-1755.2002.00433.x
43. Baechler EC, Batliwalla FM, Karypis G, et al. Interferon-inducible gene expression signature in peripheral blood cells of patients with severe lupus. Proc Natl Acad Sci U S A 2003;100(5):2610–2615. doi:10.1073/pnas.0337679100
44. Elera-Fitzcarrald C, Vega K, Gamboa-Cárdenas RV, et al. Discrepant perception of lupus disease activity: a comparison between patients' and physicians' disease activity scores. J Clin Rheumatol 2020;26(7S suppl 2):S165–S169. doi:10.1097/RHU.0000000000001267
45. Mahieu M, Yount S, Ramsey-Goldman R. Patient-reported outcomes in systemic lupus erythematosus. Rheum Dis Clin North Am 2016;42(2):253–263. doi:10.1016/j.rdc.2016.01.001
46. Gupta S, Kaplan MJ. Bite of the wolf: innate immune responses propagate autoimmunity in lupus. J Clin Invest 2021;131(3):e144918. doi:10.1172/JCI144918
47. Yurkovich M, Vostretsova K, Chen W, et al. Overall and cause-specific mortality in patients with systemic lupus erythematosus: a meta-analysis of observational studies. Arthritis Care Res (Hoboken) 2014;66(4):608–616. doi:10.1002/acr.22173
48. Maroz N, Segal MS. Lupus nephritis and end-stage kidney disease. Am J Med Sci 2013;346(4):319–323. doi:10.1097/MAJ.0b013e31827f4ee3
49. Parodis I, Tamirou F, Houssiau FA. Prediction of prognosis and renal outcome in lupus nephritis. Lupus Sci Med 2020;7(1):e000389. doi:10.1136/lupus-2020-000389
50. Nakano M, Ota M, Takeshima Y, et al. Distinct transcriptome architectures underlying lupus establishment and exacerbation. Cell 2022;185(18):3375–3389.e21. doi:10.1016/j.cell.2022.07.021
51. Hudspeth K, Wang S, Wang J, et al; Autoimmunity Molecular Team. Natural killer cell expression of Ki67 is associated with elevated serum IL-15, disease activity and nephritis in systemic lupus erythematosus. Clin Exp Immunol 2019;196(2):226–236. doi:10.1111/cei.13263
52. Cozzani E, Drosera M, Gasparini G, et al. Serology of lupus erythematosus: correlation between immunopathological features and clinical aspects. Autoimmune Dis 2014;2014:321359. doi:10.1155/2014/321359
53. Lande R, Ganguly D, Facchinetti V, et al. Neutrophils activate plasmacytoid dendritic cells by releasing self-DNA-peptide complexes in systemic lupus erythematosus. Sci Transl Med 2011;3(73):73ra19. doi:10.1126/scitranslmed.3001180
54. Lood C, Blanco LP, Purmalek MM, et al. Neutrophil extracellular traps enriched in oxidized mitochondrial DNA are interferogenic and contribute to lupus-like disease. Nat Med 2016;22(2):146–153. doi:10.1038/nm.4027
55. Villanueva E, Yalavarthi S, Berthier CC, et al. Netting neutrophils induce endothelial damage, infiltrate tissues, and expose immunostimulatory molecules in systemic lupus erythematosus. J Immunol 2011;187(1):538–552. doi:10.4049/jimmunol.1100450

Arthritis & Rheumatology
Vol. 78, No. 9, September 2026, pp 1892–1906
DOI 10.1002/art.70110
© 2026 The Author(s). *Arthritis & Rheumatology* published by Wiley Periodicals LLC on behalf of American College of Rheumatology.
This is an open access article under the terms of the Creative Commons Attribution-NonCommercial License, which permits use, distribution and reproduction in any medium, provided the original work is properly cited and is not used for commercial purposes.

American College of Rheumatology
Empowering Rheumatology Professionals

TWEAK/Fn14 Signaling Drives Oxidative Cardiac Injury in Systemic Lupus Erythematosus: Evidence From Patient Biomarker Studies, Lupus Mouse Models, and Cardiomyocyte Assays

Yale Liu, MD, PhD,[1] Zhu Yan, MD,[2] Xueting Peng, MD,[1] Meixuan Li, MD,[1] Juan Wang, MD, PhD,[3] Yan Zhang, PhD,[4] Xiaoqian Hu, MD,[5] Mingzhu Zhou, MD,[6] Kaixuan Ren, MD,[1] Dan Zhang, PhD,[7] Xingyi Guo, PhD,[8] Yumin Xia, MD, PhD,[1] and Huanhuan Huo, MD[3]

Objective. Cardiac involvement is a major cause of morbidity in systemic lupus erythematosus (SLE). Tumor necrosis factor–like weak inducer of apoptosis (TWEAK) is elevated in SLE, but its contribution to lupus-associated cardiac injury is unclear. We investigated the role of TWEAK/fibroblast growth factor–inducible 14 (Fn14) signaling in SLE-related cardiomyopathy and its potential as a biomarker and therapeutic target.

Methods. Serum TWEAK, inflammatory cytokines, autoantibodies, and oxidative stress markers were measured in 242 patients with SLE and 66 age- and sex-matched controls, with correlation to echocardiographic, electrocardiographic, and myocardial enzyme findings. Cardiac pathology and redox signaling were assessed in pristane-induced lupus models using wild-type mice and mice deficient of *Fn14* by histopathology, immunoblotting, immunofluorescence, and quantitative proteomics. Direct effects of TWEAK on mitochondrial oxidative stress, antioxidant signaling, and apoptosis were examined in primary cardiomyocytes isolated from MRL/lpr mice who were lupus prone.

Results. Serum TWEAK levels were significantly elevated in patients with SLE and were highest in those with cardiac abnormalities compared with healthy controls. TWEAK correlated positively with malondialdehyde, 8-hydroxy-2'-deoxyguanosine, disease activity, and inflammatory cytokines and inversely with superoxide dismutase. Elevated baseline TWEAK predicted new cardiac abnormalities during follow-up and declined with clinical improvement. In mice with lupus, *Fn14* deficiency reduced cardiac reactive oxygen species accumulation, restored Nrf2/HO-1 antioxidant signaling, attenuated histopathological injury, and preserved cardiac function. In vitro, TWEAK induced mitochondrial superoxide production, suppressed Nrf2 signaling, and promoted apoptosis in lupus-prone cardiomyocytes.

Conclusion. TWEAK/Fn14 signaling drives oxidative stress–mediated cardiomyocyte injury in SLE and represents a promising biomarker and therapeutic target for lupus-associated cardiac damage.

INTRODUCTION

Systemic lupus erythematosus (SLE) is a chronic autoimmune disease that affects multiple organs, including the heart, brain, and kidneys. Cardiovascular disease is a major cause of morbidity and mortality in SLE, arising from both primary autoimmune myocardial injury and secondary damage driven by inflammation and oxidative stress.[1] Patients with SLE exhibit impaired antioxidant defenses, and elevated oxidative stress markers—such as malondialdehyde (MDA) and 8- hydroxy-

Supported by the National Natural Science Foundation of China (grant 82473522), Innovation Capability Support Plan of Shaanxi Health Commission (grant 2024TD-15), Key Medical Research Plan of Xi'an City (grant 24YXYJ0001), and Special Support Program for High-Level Talents of Shaanxi Province.

[1]Department of Dermatology, The Second Affiliated Hospital of Xi'an Jiaotong University, Xi'an, China; [2]Department of Plastic Surgery, Xijing Hospital, Fourth Military Medical University, Xi'an, China; [3]Department of Ultrasound, The Second Affiliated Hospital of Xi'an Jiaotong University, Xi'an, China; [4]Department of Cardiology, The Second Affiliated Hospital of Xi'an Jiaotong University, Xi'an, China; [5]Department of Dermatology, Northwest University First Hospital, Xi'an, China; [6]Department of Dermatology, Xi'an Gaoxin Hospital, Xi'an, China; [7]Department of Scientific Research, The Second Affiliated Hospital of Xi'an Jiaotong University, Xi'an, China; [8]Division of Epidemiology, Department of Medicine, Vanderbilt-Ingram Cancer Center, Vanderbilt University School of Medicine, Nashville, Tennessee, USA.

Drs Liu, Yan, and Peng contributed equally to this work.

Additional supplementary information cited in this article can be found online in the Supporting Information section (https://acrjournals.onlinelibrary.wiley.com/doi/10.1002/art.70110).

Author disclosures and graphical abstract are available at https://onlinelibrary.wiley.com/doi/10.1002/art.70110.

Address correspondence via email to Yumin Xia, MD, PhD, at yuminxia@mail.xjtu.edu.cn; or Huanhuan Huo, MD, at huanhuanhuo0613@163.com.

Submitted for publication August 28, 2025; accepted in revised form February 2, 2026.

2'-deoxyguanosine (8-OHdG)—are linked to increased cardiovascular risk.[2,3] Antioxidant interventions, including itaconic acid supplementation, can mitigate lupus-associated organ damage in experimental models,[4] underscoring the pathogenic role of redox imbalance.

The tumor necrosis factor–like weak inducer of apoptosis (TWEAK) is a multifunctional proinflammatory cytokine that signals through fibroblast growth factor–inducible 14 (Fn14). Although TWEAK is primarily secreted by infiltrating macrophages, Fn14 expression is up-regulated in resident cells under inflammatory conditions.[5] Engagement of the TWEAK/Fn14 axis has been implicated in lupus-related damage to skin, kidneys, and the central nervous system,[6,7] where it promotes tissue remodeling, microvascular injury, and barrier disruption. Importantly, TWEAK/Fn14 signaling can amplify oxidative stress in endothelial cells and macrophages via activation of NADPH oxidase or AMP-activated protein kinase pathways.[8,9] These oxidative mechanisms are further implicated in other complications in patients with SLE.[10]

Beyond its established roles in inflammation, the TWEAK/Fn14 pathway contributes to cardiovascular pathology. TWEAK colocalizes with NADPH oxidase subunits in atherosclerotic plaques, exacerbates experimental myocarditis, and accelerates heart failure progression.[8] Pharmacologic blockade of TWEAK or genetic deletion of Fn14 protects against cardiac dysfunction, hypertrophy, and maladaptive calcium handling,[11] processes intimately linked to oxidative stress in the failing heart.[12] Despite these associations, the precise role of TWEAK in SLE-related cardiac injury remains undefined. In particular, it is unknown whether TWEAK levels reflect cardiac disease severity, whether the TWEAK/Fn14 pathway mechanistically drives oxidative injury in cardiomyocytes, and whether Fn14 inhibition offers cardioprotection in lupus.

Here, we combined clinical, experimental, and in vitro approaches to address these questions. We measured serum TWEAK in a well-characterized cohort of patients with SLE and correlated it with cardiac abnormalities, inflammatory mediators, and oxidative stress markers. Using a pristane-induced lupus model in wild-type mice and mice deficient of *Fn14*, we evaluated the impact of Fn14 signaling on cardiac injury and oxidative stress. Finally, we tested the direct effects of TWEAK on redox homeostasis and survival in lupus-prone cardiomyocytes. Our findings identify TWEAK as both a biomarker and a potential therapeutic target for lupus-related cardiac disease.

METHODS

Human patients. A total of 242 patients with SLE (14–79 years old; fulfilling the 2019 EULAR/American College of Rheumatology classification criteria)[13] and 66 age- and sex-matched healthy controls were enrolled at the Second Affiliated Hospital of Xi'an Jiaotong University between March 2022 and June 2025. Disease activity was assessed using the SLE Disease Activity Index 2000 (SLEDAI-2K). The study was approved by the Institutional Ethics Committee (XJTUAE2022-1039), and written informed consent was obtained from all participants. Demographic and clinical characteristics are summarized in Supplementary Table S1.

Animal studies. BALB/c mice who were *Fn14* knockout (*Fn14*$^{-/-}$) were generated by CRISPR/Cas9 editing.[14] Eight-week-old female mice who were *Fn14*$^{-/-}$ and wild-type littermates were housed under specific pathogen–free conditions. Lupus-like disease was induced by a single intraperitoneal injection of pristane (0.5 mL; Sigma-Aldrich),[15] whereas control animals received phosphate buffered saline (PBS). After six months, blood and urine samples were collected. Serum anti–double-stranded DNA (dsDNA) and antinuclear antibody (ANA) levels were measured by enzyme-linked immunosorbent assay (ELISA), and myocardial enzymes and urinary albumin-to-creatinine ratio were analyzed using an automated biochemical analyzer. All animal experiments were approved by the Xi'an Jiaotong University Biomedical Ethics Committee (XJTUAE2024-368).

Histopathology. All hearts used for histology were sampled at the mid-ventricular short-axis plane. Mouse hearts were harvested at the mid-ventricular short-axis level, fixed in 4% paraformaldehyde, paraffin embedded, and sectioned (4 μm). Hematoxylin–eosin and Masson's trichrome staining were performed to evaluate myocardial injury and fibrosis (n = 6 per group). Lesions were independently scored by two blinded pathologists using a semiquantitative 0 to 4 scale for inflammation, edema, fibrosis, and calcification.[16]

Serum cytokine and biochemistry analysis. Serum cytokines (TWEAK, interleukin-1β [IL-1β], IL-2R, IL-6, IL-8, IL-10, tumor necrosis factor α [TNF-α]) were quantified by ELISA. ANA titers were assessed by immunofluorescence, erythrocyte sedimentation rate (ESR) by automated analyzer, and complement C3 by nephelometry. Oxidative stress markers (MDA, 8-OHdG, Cu/Zn–superoxide dismutase [SOD]) and myocardial enzymes were measured using commercial kits. Reference ranges for myocardial enzymes were as follows: aspartate transaminase (15–40 IU/L), ischemia-modified albumin (<79.6 IU/mL), lactate dehydrogenase (LDH; 120–250 IU/L), hydroxybutyrate dehydrogenase (26–195 IU/L), creatine kinase (50–310 U/L), and creatine kinase myocardial band (2–30 U/L).

Echocardiography and electrocardiography. Transthoracic echocardiography was performed in patients (EPIQ 7c, Philips) and mice (high-frequency ultrasound) using standard B-mode, M-mode, Doppler, tissue Doppler, and

two-dimensional speckle-tracking analyses to assess cardiac structure and function, including global longitudinal strain (GLS).

A 12-lead electrocardiography was conducted in all participants; individuals with prominent U waves were excluded. Electrocardiogram abnormalities were defined as flattened T waves (T-wave amplitude < 10% of R wave), prolonged corrected QT intervals (QTc = QT/√RR; >460 ms), or fragmented QRS complexes (rSr′ patterns with or without Q waves).[17,18]

Primary cardiomyocyte culture and treatment. Primary cardiomyocytes were isolated from two-day-old neonatal MRL/lpr mice who were lupus prone.[19] Cells were cultured in Dulbecco's modified Eagle's medium supplemented with 10% fetal bovine serum and treated with recombinant mouse TWEAK (200 ng/mL) for 0 to 48 hours. *Fn14* knockdown was achieved using specific small interfering RNA (siRNA) transfection for 48 hours. Where indicated, cells were pretreated with the mitochondrial antioxidant MitoTEMPO (0.1 μM, two hours) before TWEAK stimulation.[11,20] For *Fn14* knockdown, cells were transfected with 50 nM of mouse *Fn14*-specific siRNA (Gemira Gene, sense sequence 5′-UCGACAAGUGCAUGGACUGTT-3′, antisense sequence 5′-CAGUCCAUGCACUUGUCGATT-3′) or a nontargeting scramble siRNA using Lipofectamine RNAiMAX Transfection Reagent, according to the manufacturer's protocol.

Immunofluorescence and TUNEL assay. Cardiomyocytes or heart sections were fixed and incubated with primary antibodies against α-actin, NRF2, 8-OHdG, inducible nitric oxide synthase (iNOS), TOMM20, SOD2, PGC-1α, NRF1, TFAM, or Ki67, followed by fluorescent secondary antibodies and DAPI counterstaining. Images were acquired by confocal microscopy and quantified using ImageJ. Apoptosis was assessed by fluorescence-based TUNEL staining.

Quantitative reverse transcriptase–polymerase chain reaction and Western blot. Total RNA was extracted using TRIzol, reverse transcribed, and quantified by quantitative reverse transcriptase–polymerase chain reaction using SYBR Green chemistry. Relative gene expression was calculated by the $2^{-}\Delta Ct$ method. Protein expression was analyzed by sodium dodecyl sulfate–polyacrylamide gel electrophoresis and immunoblotting, with densitometric quantification using ImageJ. Primer sequences and antibody details are listed in Supplementary Tables S2 and S3.

Proteomics analysis. Mouse cardiac tissues were subjected to data-independent acquisition (DIA)-based quantitative proteomics following in-gel tryptic digestion and liquid chromatography mass spectrometry/mass spectrometry analysis. Differentially expressed proteins were annotated using Gene Ontology (GO) analysis via Metascape. For transcriptomics, primary cardiomyocytes treated with TWEAK or PBS were analyzed by RNA sequencing, with data processed on the OE Biotech Cloud Platform and Metascape.[21]

MitoTEMPO pretreatment. Cells were preincubated with the mitochondria-targeted antioxidant MitoTEMPO (MedChemExpress, catalog HY-112879, 0.1 μM) for two hours based on previous studies.[22] The pretreatment medium was then removed, and cells were washed once with fresh culture medium before being exposed to TWEAK or vehicle control.

Reactive oxygen species measurement and mitochondrial analyses. Reactive oxygen species (ROS) in heart cryosections were detected using dihydroethidium staining. Intracellular and mitochondrial ROS in cardiomyocytes were quantified using dichlorodihydrofluorescein diacetate and MitoSOX assays. Mitochondrial ultrastructure was examined by transmission electron microscopy. Mitochondrial respiration was assessed using Seahorse XF extracellular flux analysis, and Cu/Zn-SOD and Mn-SOD activities were measured using a WST-8–based assay.

Statistical analysis. Data are presented as mean ± SEM. Among-group comparisons were made using unpaired or paired Student's *t*-tests, or one-way analysis of variance when appropriate using GraphPad Prism 8.01 (GraphPad Prism Software). TWEAK levels across different creatine kinase-MB (CK-MB) and echocardiogram groups were analyzed using the chi-square test. $P < 0.05$ was considered statistically significant. Transcriptomics *P* values were adjusted for false discovery rate (FDR) multiple hypothesis testing with FDR correction ($p_adj_val < 0.05$).

Patients and/or the public were not involved in the design, or conduct, or reporting, or dissemination plans of this research. The study was reviewed and approved by the Xi'an Jiaotong University Health Science Center Biomedical Ethics Committee (XJTUAE2023-1304) and the Ethics Committee of Second Affiliated Hospital of Xi'an Jiaotong University (2023499). It was conducted with a commitment to upholding ethical considerations. All participants in this study provided written informed consent. The data sets used and/or analyzed during the study are available from the corresponding author upon reasonable request.

RESULTS

Serum TWEAK levels are elevated in patients with SLE with cardiac abnormalities. To investigate the role of TWEAK in patients with SLE, we first measured the serum levels of TWEAK. The results showed serum TWEAK levels were markedly higher in patients with SLE than in healthy controls (758.07 ± 15.25 ng/mL vs 21.44 ± 2.28 ng/mL; $P < 0.0001$; Figure 1A) and correlated positively with SLEDAI-2K scores ($R = 0.484$, $P < 0.0001$; Figure 1B). Patients with echocardiographic,

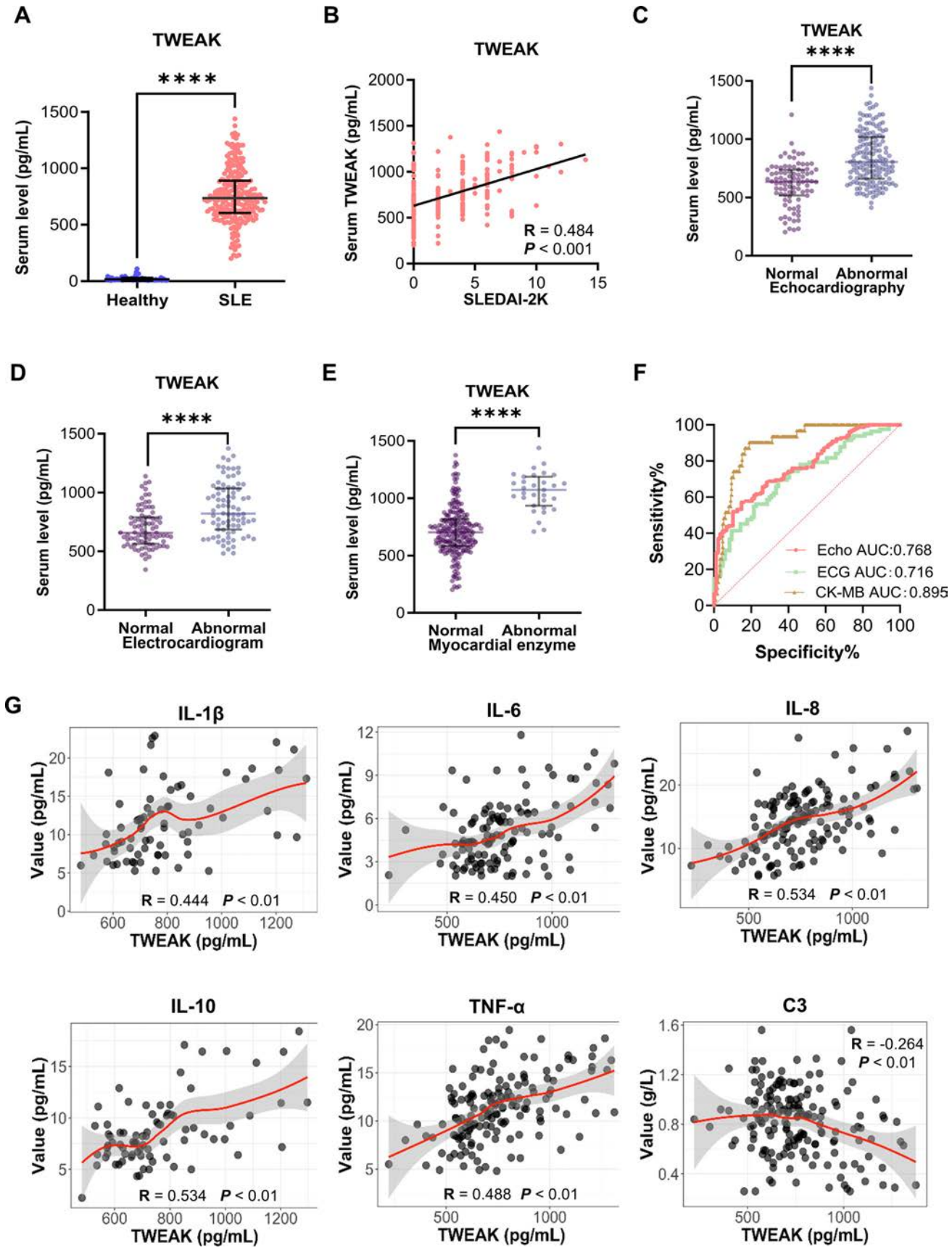

Figure 1. Legend on next page.

electrocardiographic, or myocardial enzyme abnormalities exhibited significantly higher TWEAK levels than those without (Figure 1C–E). Multivariable analysis excluding age and sex as confounders confirmed TWEAK as an independent correlate of cardiac abnormalities (Supplementary Figure S1A–C).

To further evaluate the diagnostic utility of serum TWEAK for cardiac involvement in SLE, receiver operating characteristic (ROC) curve analyses were performed. TWEAK showed good discriminatory ability for echocardiographic abnormalities (area under the curve [AUC] 0.768, 95% confidence interval [CI] 0.709–0.827), electrocardiographic abnormalities (AUC 0.716, 95% CI 0.639–0.794), and elevated CK-MB levels (AUC 0.895, 95% CI 0.846–0.944; Figure 1F). Optimal cutoff values determined by Youden's index yielded sensitivities of 57.14%, 69.51%, and 69.51% and specificities of 85.23%, 65.48%, and 65.48% for these endpoints, respectively. These findings indicate that serum TWEAK may serve as a noninvasive biomarker to aid in the detection of structural, electrical, and biochemical evidence of cardiac injury in SLE.

Serum TWEAK associates with inflammation and oxidative stress. Cardiac disease in SLE has also been linked to circulating autoantibodies, complement components, and proinflammatory cytokines such as IL-1β and TNF-α.[23] To explore the relationship between TWEAK and these mediators, we analyzed sera from patients with SLE. Serum TWEAK levels increased in parallel with ANA titers (Supplementary Figure S1D) and showed positive correlations with IL-1β, IL-6, IL-8, IL-10, and TNF-α but not IL-2R (Figure 1G; Supplementary Figure S1E). In contrast, TWEAK was inversely associated with C3 concentrations (Figure 1G) and positively associated with ESR (Supplementary Figure S1F). These findings suggest that serum TWEAK fluctuates in concert with autoantibody load, complement activation, and proinflammatory cytokines, factors known to increase the risk of cardiac disease in SLE.

Given these associations, we next examined TWEAK in relation to oxidative stress markers. TWEAK levels correlated positively with the lipid peroxidation marker MDA and the DNA damage marker 8-OHdG while showing an inverse correlation with the antioxidant enzyme SOD1 (Figure 2A–C). Taken together, these findings indicate that serum TWEAK reflects both inflammatory activation and oxidative imbalance in SLE, supporting its role as a biomarker that integrates key pathogenic processes underlying lupus-associated cardiac injury.

Serum TWEAK associates with echocardiographic abnormalities. Because echocardiography is a standard noninvasive method for detecting both structural and functional cardiac involvement in SLE, we next investigated the relationship between serum TWEAK levels and echocardiographic abnormalities. Echocardiographic evaluation revealed that 63.64% of patients with SLE exhibited cardiac abnormalities (65.02% of female patients and 47.37% of male patients; Figure 2D). The most common findings were valvular involvement (28.10%), pulmonary hypertension (14.46%), myocardial involvement (13.64%), and left ventricular (LV) diastolic dysfunction (7.02%), typically manifesting as valvular thickening/regurgitation, ventricular dilatation, or impaired systolic function (Figure 2E; Supplementary Table S4). Representative images are shown in Supplementary Figures S2 and S3.

When stratified by echocardiographic subtype, serum TWEAK concentrations were significantly higher in patients with myocardial involvement, pulmonary hypertension, or LV diastolic dysfunction but not in those with isolated valvular lesions, compared with patients with normal echocardiograms (Figure 2F). Moreover, patients with abnormally reduced LV-GLS (>–17%) showed slightly higher TWEAK levels than those with preserved LV-GLS (≤–17%), although the difference was not statistically significant (Figure 2G). In patients whose echocardiographic abnormalities or elevated myocardial enzymes normalized after treatment with steroids alone or in combination with immunosuppressive agents, TWEAK levels declined significantly at follow-up (Figure 2H). Furthermore, patients with high baseline TWEAK were more likely to develop new echocardiographic or electrocardiographic abnormalities during six-month follow-up (Figure 2I). These findings indicate that serum TWEAK not only mirrors the type and severity of echocardiographic abnormalities but also tracks disease dynamics over time, supporting its potential use as a biomarker to complement imaging in the assessment and monitoring of SLE-related cardiac involvement.

Fn14 deficiency protects mice with lupus from cardiac injuries. Given the pathogenic role of TWEAK in SLE-associated cardiac involvement, we next examined the impact of

Figure 1. Elevated serum TWEAK levels in patients with systemic lupus erythematosus (SLE) with cardiac abnormalities and inflammation. (A) Serum TWEAK concentrations in patients with SLE (n = 242) compared with healthy controls (n = 66). ****$P < 0.0001$. (B) Positive correlation between serum TWEAK levels and SLE Disease Activity Index 2000 scores (linear regression; with R and P values derived from Pearson correlation analysis). ****$P < 0.0001$. (C–E) Serum TWEAK levels in patients with SLE stratified by (C) echocardiography, (D) electrocardiography, and (E) myocardial enzyme assay results. ****$P < 0.0001$. (F) Receiver operating characteristic curve analysis showing the diagnostic sensitivity (in percentage) and specificity (in percentage) of TWEAK for detecting abnormalities on echocardiography, electrocardiography, and myocardial enzyme testing. (G) Serum TWEAK levels correlated positively with interleukin-1β (IL-1β), IL-6, IL-8, IL-10, and tumor necrosis factor-α (TNF-α) and inversely with C3. Locally estimated scatterplot smoothing curves are shown, with R and P values derived from Pearson correlation analysis. AUC, area under the curve; CK-MB, creatine kinase-MB; ECG, electrocardiogram.

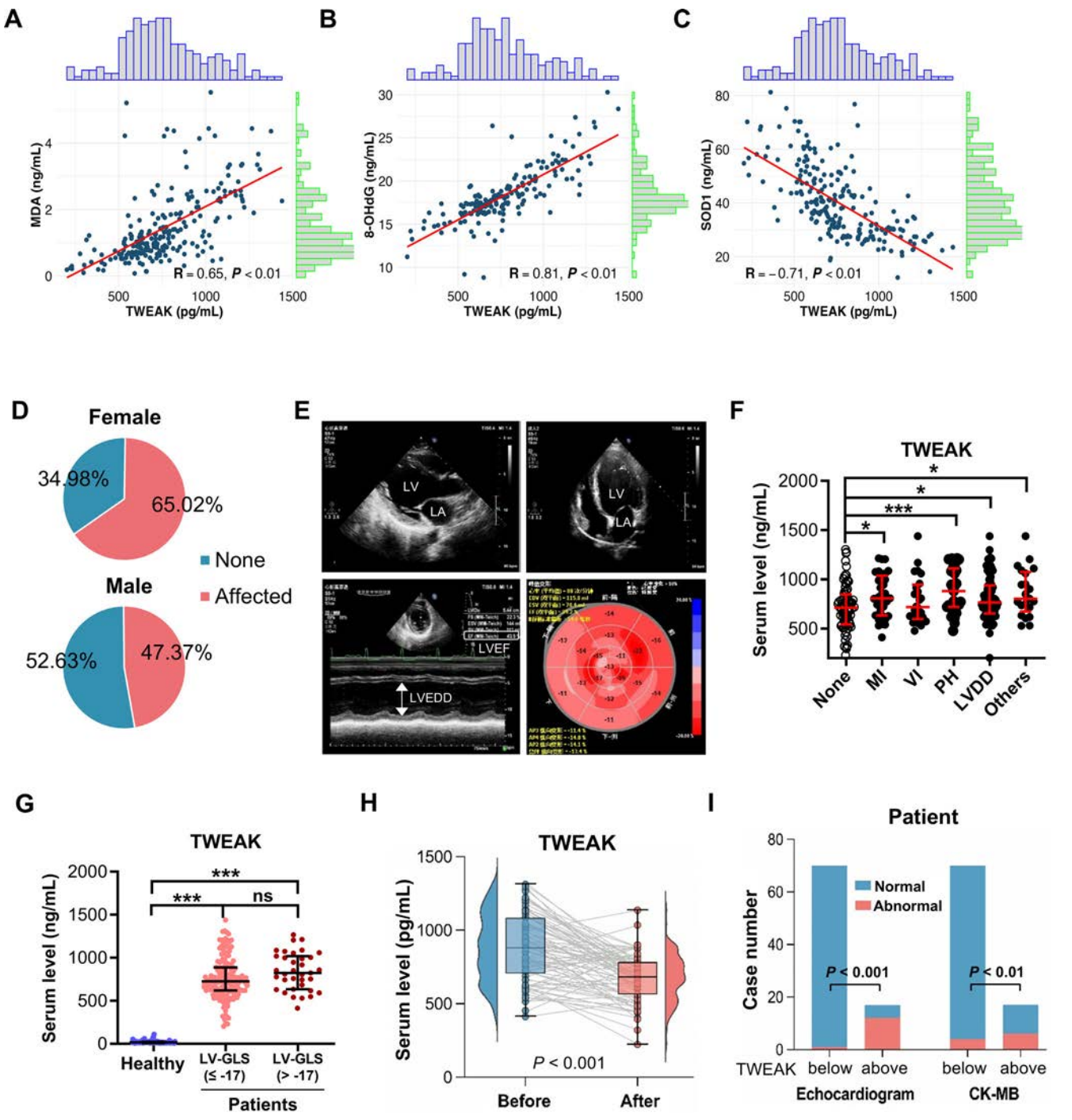

Figure 2. Association of serum TWEAK with oxidative stress and echocardiographic abnormalities. (A–C) TWEAK correlated positively with malondialdehyde (MDA) and 8-hydroxy-2'-deoxyguanosine (8-OHdG) and negatively with superoxide dismutase 1 (SOD1; R and *P* values from Pearson correlation analysis). (D) Prevalence of echocardiographic abnormalities by gender. (E) Representative patient (42-year-old female patient) with dilated left atrium (LA) and left ventricle (LV), increased LV end-diastolic dimension (LVEDD), reduced LV ejection fraction (LVEF), and speckle-tracking echocardiography confirming impaired longitudinal strain in multiple segments. (F) Serum TWEAK levels across five echocardiographic abnormality subtypes and three participant groups. $^{*}P < 0.05$; $^{***}P < 0.001$. (G) Serum TWEAK levels in patients with preserved versus reduced LV global longitudinal strain (LV-GLS). $^{***}P < 0.001$. (H) Serum TWEAK levels before and after resolution of echocardiographic or myocardial enzyme abnormalities following therapy (paired boxplots with *P* values). (I) Prospective analysis among patients with systemic lupus erythematosus without baseline cardiac damage; those with high baseline serum TWEAK (above mean) developed significantly newer echocardiographic or myocardial enzyme abnormalities at six-month follow-up. CK-MB, creatine kinase–MB; MI, myocardial involvement; VI, valvular involvement; PH, pulmonary hypertension; LVDD, left ventricular diastolic dysfunction; ns, not significant.

its receptor, Fn14, on cardiac pathology. Pristane-induced lupus models were established in both wild-type mice and mice deficient of *Fn14*. After six months, serum anti-dsDNA, ANAs, and urinary albumin-to-creatinine ratio were elevated by pristane in wild-type mice, whereas *Fn14* deletion significantly lowered them (Supplementary Figure S4A–C). Concurrently, serum levels of CK, CK-MB, LDH, and LDH-1 rose markedly after pristane challenge and were reduced in mice deficient of *Fn14* (Supplementary Figure S4D–G).

We performed echocardiography in mice to evaluate the long-term protective effect of *Fn14* deletion on cardiac dysfunction. In wild-type mice, pristane injection led to LV enlargement and thinning of the interventricular septum (Figure 3A). Parameters assessed included interventricular septal thickness in diastole (IVSd), LV internal diameter in diastole (LVIDd), LV ejection fraction (LVEF), and LV internal diameter in systole (LVIDs). Pristane injection significantly reduced IVSd and increased LVIDd in wild-type mice, whereas these changes were markedly attenuated in mice deficient of *Fn14* (Figure 3B). LVEF and LVIDs were not significantly altered by pristane treatment, although baseline differences were observed between the two strains (Figure 3B). These findings demonstrate that deleting *Fn14* simultaneously restrains systemic lupus activity and prevents cardiac injury in mice who were lupus prone.

***Fn14* deficiency reduces cardiac oxidative stress and histopathological lesions in mice with lupus.** To investigate the role of Fn14 in lupus-associated cardiac injury, we analyzed heart tissues from pristane-induced lupus models in wild-type mice and mice deficient of *Fn14*. Histologic examination of whole-heart sections revealed mild edema, focal calcium deposition, fibrous connective tissue proliferation, scattered lymphocytes, and occasional mast cells in the epicardium of mice induced with pristane (Figure 4A; Supplementary Figure S5). Inflammation and edema scores did not differ among pristane-induced groups, whereas fibrosis and calcification scores were significantly lower in mice deficient of Fn14, reducing the composite cardiac pathology score (Figure 4B; Supplementary Figure S6A). Masson trichrome staining and quantitative analysis confirmed the attenuated fibrosis (Supplementary Figure S6B and C).

Given that cardiovascular complications in SLE are partly driven by excessive oxidative stress,[2,24] we next assessed ROS production and the expression of oxidative stress–related proteins in cardiac myocardium. Wild-type mice primed with pristane exhibited significantly elevated ROS levels in cardiomyocytes, whereas *Fn14* deficiency suppressed ROS accumulation (Figure 4C and D). Immunofluorescence staining for oxidative damage markers 8-OHdG and iNOS confirmed this pattern (Supplementary Figure S7). Consistent with these findings, Western blot analysis revealed that the proapoptotic protein Diablo was increased in wild-type hearts following pristane injection but attenuated in mice deficient of *Fn14*. Conversely, antioxidant pathway proteins NRF2 and HO-1 were down-regulated in wild-type hearts after pristane exposure but markedly up-regulated in mice deficient of *Fn14* (Figure 4E and F). These data suggest that *Fn14* deficiency restores redox balance by inhibiting ROS accumulation and reactivating NRF2-mediated antioxidant signaling, thereby mitigating oxidative injury in lupus cardiac tissue.

To comprehensively characterize the impact of Fn14 on cardiac injury and oxidative stress, we performed DIA quantitative proteomics on cardiac tissues. Comparative proteomic analysis identified numerous differentially expressed proteins in response to pristane and *Fn14* deficiency (Supplementary Figure S8A). Venn diagram analysis highlighted 30 proteins up-regulated by pristane but normalized by *Fn14* deficiency, and 29 proteins with the opposite trend. Volcano plots emphasized several proteins central to oxidative stress pathways (Supplementary Figure S8B and C). KEGG enrichment revealed significant overrepresentation in pathways linked to SLE or oxidative stress, including ascorbate and aldarate metabolism, HIF-1 signaling, glutathione metabolism, peroxisome, chemical carcinogenesis–ROS, and oxidative phosphorylation (Supplementary Figure S9).

To functionally profile the reversed proteins, we mined their GO terms for oxidative stress response, oxidoreductase regulation, and other pathways and displayed their relative abundances in a heat map (Figure 4G). Mgst1, for example, possesses glutathione-transferase and glutathione-peroxidase activities that protect cells against oxidative injury. The heat map shows that Mgst1 is down-regulated after pristane but up-regulated when *Fn14* is deleted, mirroring the rise in NRF2 and HO-1 and supporting the idea that loss of Fn14 boosts antioxidant defenses. In summary, pristane administration markedly exacerbates cardiac oxidative stress in mice who were lupus prone, whereas Fn14 functions as a critical regulator of this injury. *Fn14* deficiency effectively attenuates these pathologic processes by suppressing ROS accumulation and restoring antioxidant defenses, highlighting Fn14 as a potential therapeutic target for lupus-associated cardiovascular complications.

TWEAK/Fn14 signaling disrupts mitochondrial antioxidant defense, biogenesis programs, and respiratory function. To determine whether Fn14 signaling directly contributes to cardiomyocyte injury in lupus, we isolated primary cardiomyocytes from neonatal MRL/lpr mice who were lupus prone and stimulated them with recombinant TWEAK (200 ng/mL, 24 hours; Supplementary Figure S10A). Transcriptome sequencing revealed that TWEAK treatment significantly up-regulated genes associated with oxidative stress and DNA damage (Figure 5A). Consistently, KEGG pathway analysis indicated activation of nitric oxide synthase–related pathways and inflammatory cytokine signaling (Supplementary Figure S10B).

At the protein level, TWEAK stimulation increased Fn14 and iNOS expression while markedly reducing NRF2, a master

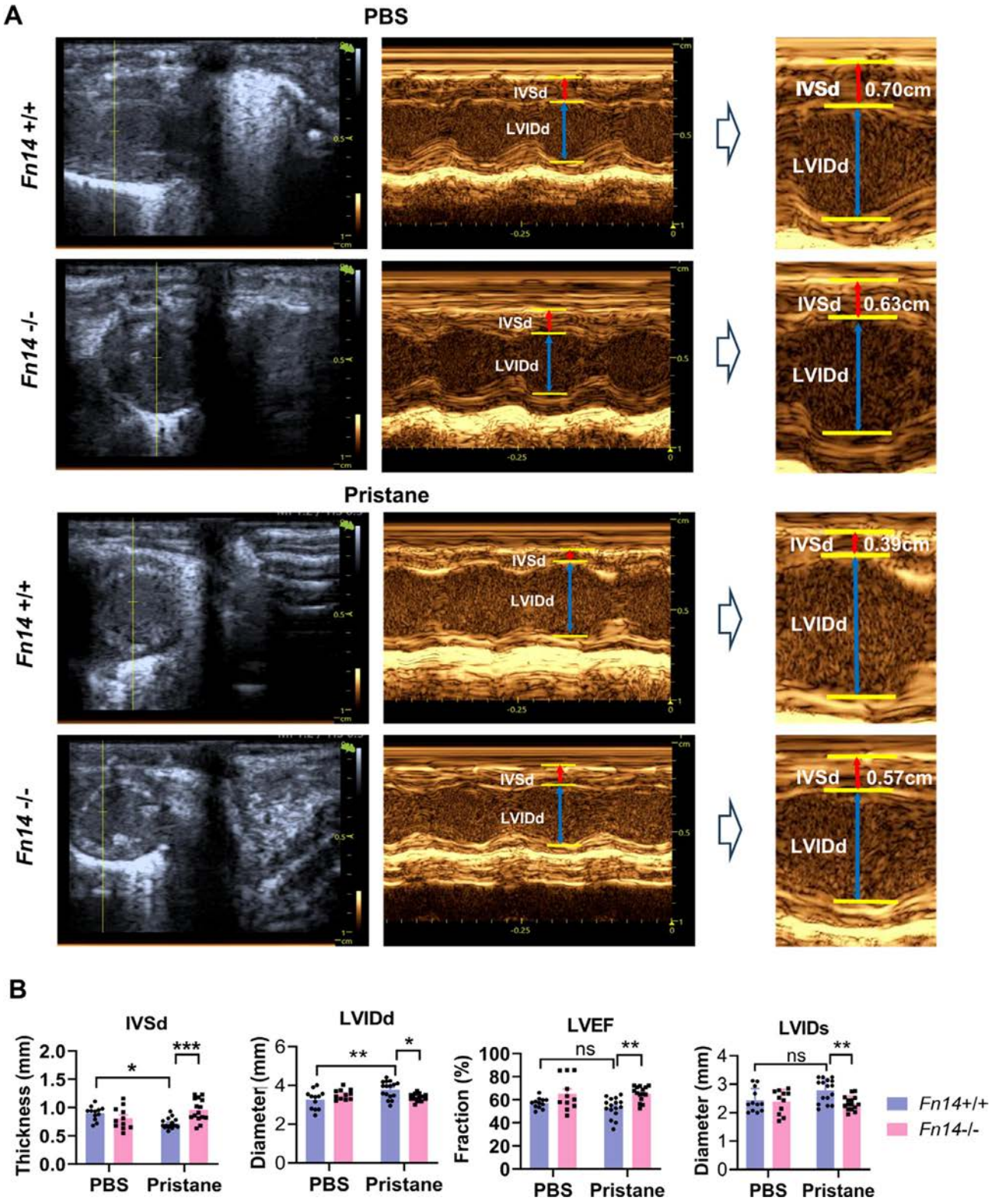

Figure 3. TWEAK receptor deficiency protects mice with lupus from cardiac injuries. Two-dimensional echocardiography was performed in wild-type mice and mice deficient of fibroblast growth factor–inducible 14 (*Fn14*). (A) Representative images showing cardiac abnormalities. Red arrows indicate interventricular septal thickness in diastole (IVSd); blue arrows indicate left ventricular internal diameter in diastole (LVIDd); yellow lines mark LV internal diameter at end systole. Exact IVSd values are shown. (B) Quantification of IVSd, LVIDd, LV ejection fraction (LVEF), and LV internal diameter in systole (LVIDs) in four groups (n = 15 per group). $^{*}P < 0.05$; $^{**}P < 0.01$; $^{***}P < 0.001$. ns, not significant; PBS, phosphate buffered saline.

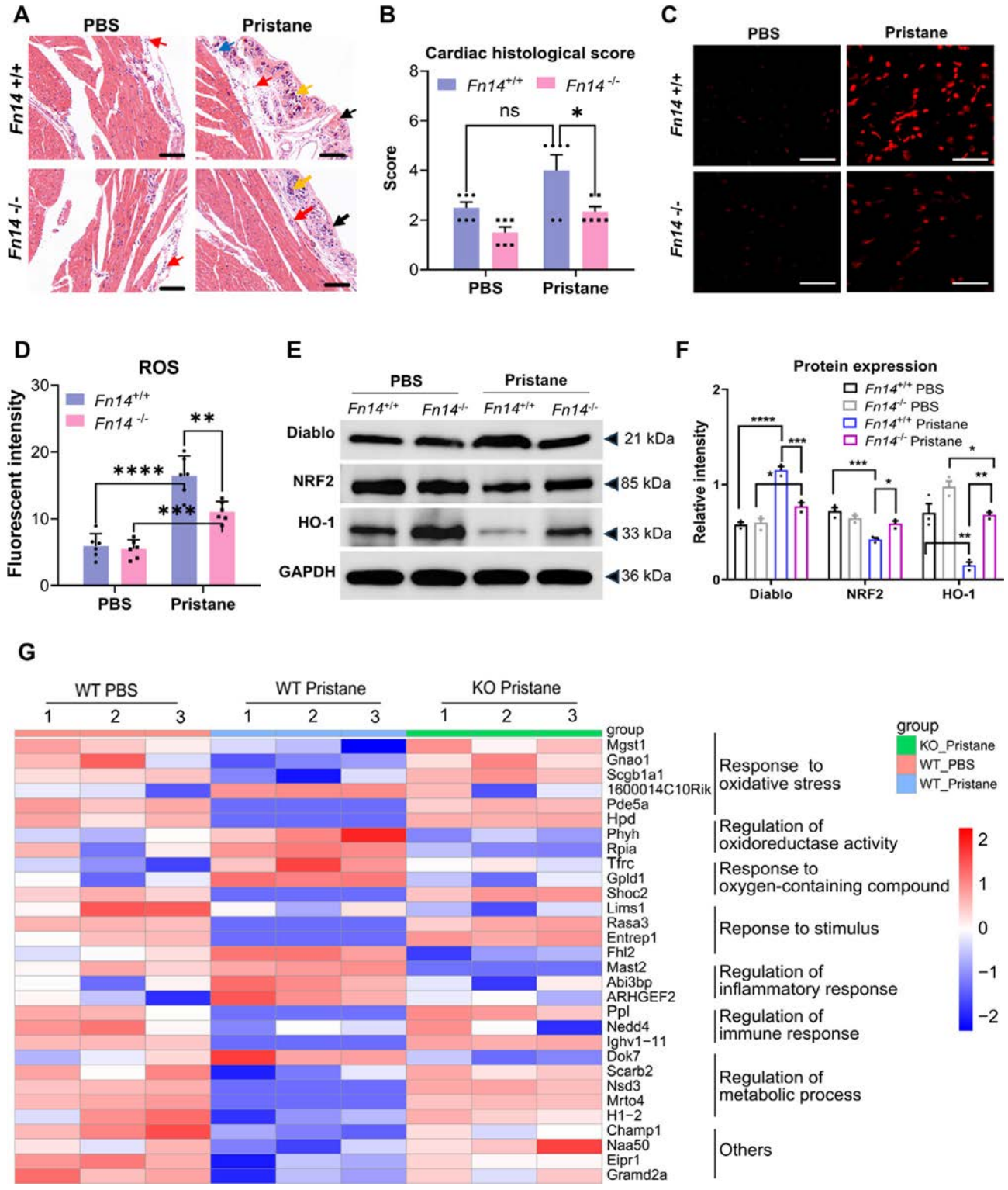

Figure 4. Oxidative stress mediates the TWEAK-induced cardiac injuries in mice with lupus. (A) Hematoxylin and eosin staining showing epicardial foci of calcium deposition (orange arrows), mild fibrous connective tissue proliferation (black arrows), scattered lymphocytic infiltrates (red arrows), and occasional mast cells (blue arrow). Scale, 100 μm. (B) Histopathological scores of cardiac tissues (n = 6 per group). *$P < 0.05$. (C and D) Cardiac reactive oxygen species (ROS) detection by dihydroethidium staining (scale, 50 μm) and quantitative analysis (n = 6 per group). **$P < 0.01$; ***$P < 0.001$; ****$P < 0.0001$. (E) Western blot analysis of Diablo, NRF2, and HO-1 protein expression. (F) The bar plot shows relative expression levels of Diablo, NRF2, and HO-1 normalized to GAPDH (n = 3 per group). *$P < 0.05$; **$P < 0.01$; ***$P < 0.001$; ****$P < 0.0001$. (G) Proteomic heat map of proteins reversed by fibroblast growth factor–inducible 14 (*Fn14*) deletion, with functional classification based on their Gene Ontology terms (knockout [KO] and wild type [WT]). PBS, phosphate buffered saline.

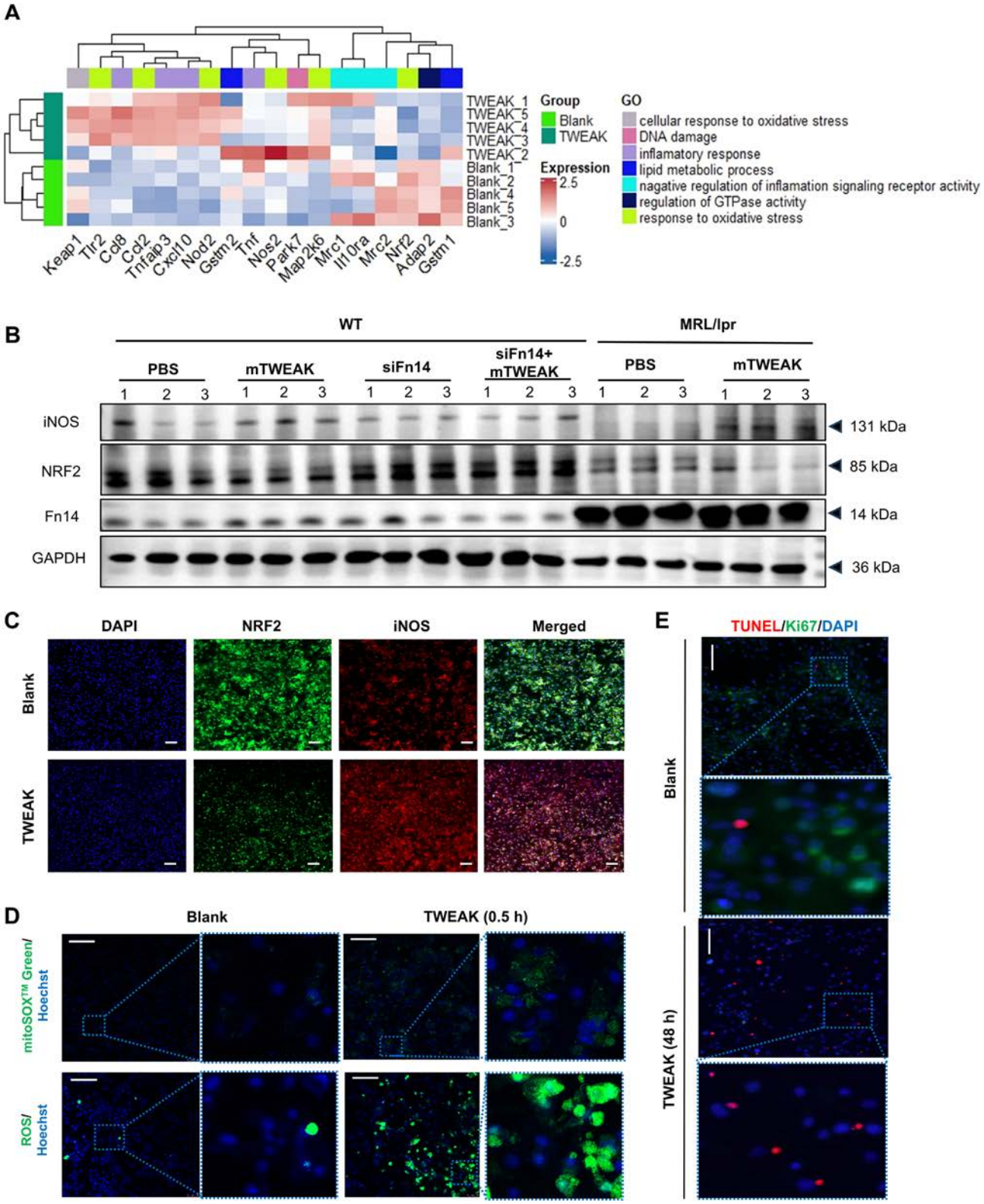

Figure 5. TWEAK modulates oxidative stress–related molecules in cardiomyocytes. Primary cardiomyocytes isolated from neonatal MRL/lpr mice were stimulated with recombinant TWEAK (200 ng/mL) for 48 hours (h). (A) Heatmap showing differential expression of oxidative stress–related and inflammation-related genes identified by bulk RNA sequencing. (B) Western blot analysis of inducible nitric oxide synthase (iNOS), NRF2, and fibroblast growth factor–inducible 14 (Fn14) protein expression. (C) Representative immunofluorescence images and quantification of iNOS and NRF2 expression (scale, 100 μm). (D) Quantification of mitochondrial superoxide and total intracellular reactive oxygen species (ROS) levels in live cardiomyocytes at 48 h. (E) Quantification of apoptosis and proliferation at 48 h, assessed by TUNEL and Ki67 staining (scale, 100 μm). GO, Gene Ontology; mTWEAK, mouse TNF-like weak inducer of apoptosis; PBS, phosphate buffered saline; siFn14, small interfering Fn14; WT, wild type.

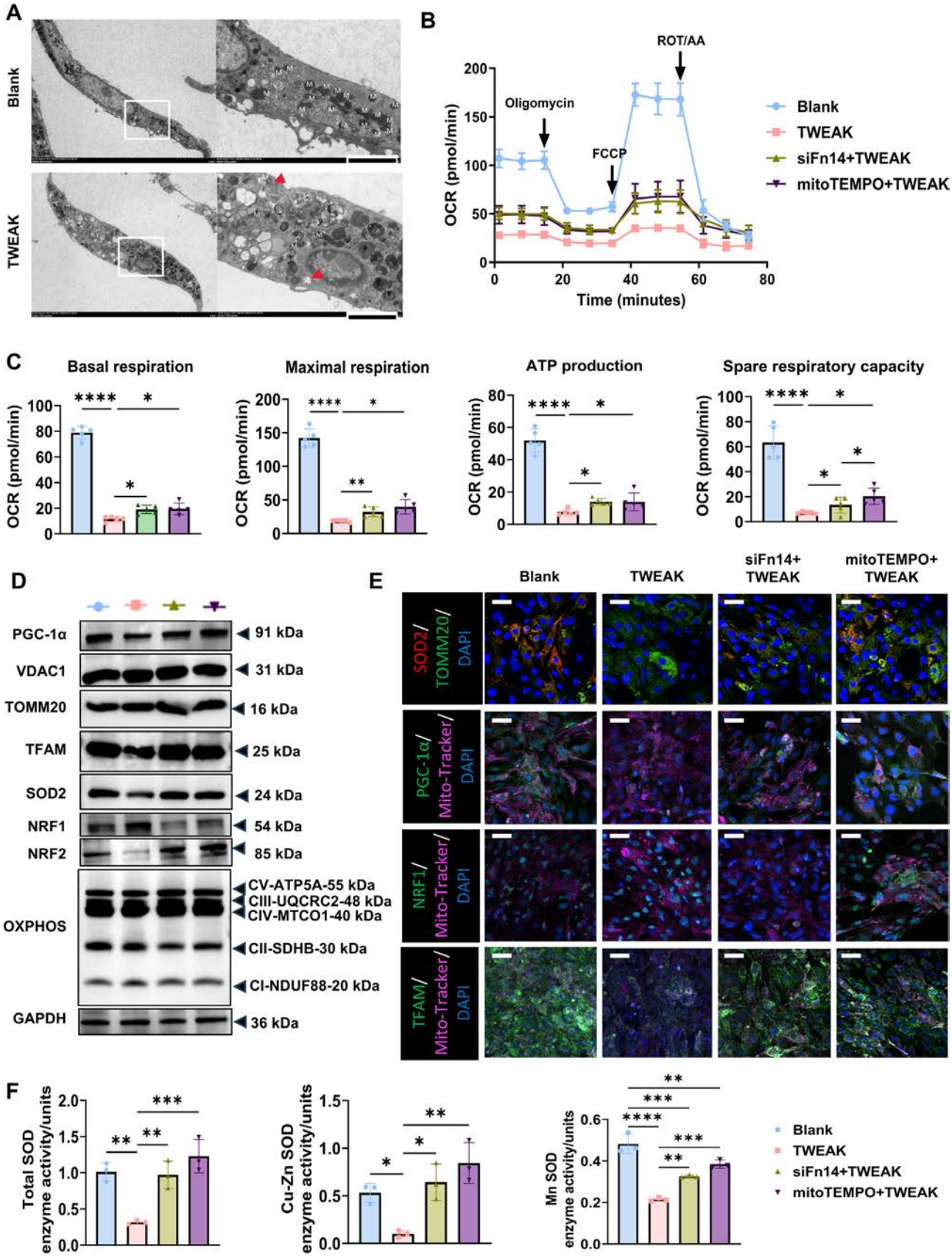

Figure 6. Legend on next page.

transcription factor governing antioxidant responses[25] (Figure 5B; Supplementary Figure S10C). Immunofluorescence analyses corroborated these findings, demonstrating intracellular accumulation of iNOS and diminished NRF2 staining following TWEAK exposure (Figure 5C; Supplementary Figure S10D). Together, these data indicate that TWEAK disrupts the intracellular balance between pro-oxidant and antioxidant pathways.

Because mitochondria are a major source of cellular ROS, we next quantified total ROS and mitochondrial superoxide using ROS-sensitive probes and MitoSOX, respectively.[26] Time-course analyses revealed a rapid and significant increase in both total ROS and mitochondrial superoxide as early as 30 minutes after TWEAK stimulation (Figure 5D; Supplementary Figure S10E and F). To assess the functional consequences of this redox imbalance, we examined cardiomyocyte proliferation and apoptosis. After 48 hours of TWEAK exposure, cardiomyocytes exhibited reduced Ki67 staining and a marked increase in TUNEL-positive apoptotic cells (Figure 5E; Supplementary Figure S10G). Collectively, these results demonstrate that TWEAK/Fn14 signaling directly disrupts redox homeostasis in lupus cardiomyocytes by enhancing pro-oxidant pathways (iNOS induction) while suppressing antioxidant defenses (NRF2 down-regulation), leading to impaired proliferative capacity and increased apoptosis.

TWEAK disrupts mitochondrial structure and bioenergetic function via Fn14 and oxidative stress. Given the central role of mitochondria in oxidative stress regulation,[27] we examined whether TWEAK alters mitochondrial integrity and bioenergetics in MRL/lpr cardiomyocytes. Transmission electron microscopy revealed marked mitochondrial abnormalities following TWEAK treatment, including reduced mitochondrial number, swelling, matrix rarefaction, cristae disruption, and vacuolization (Figure 6A; Supplementary Figure S11A and B). Consistent with these ultrastructural changes, TWEAK (200 ng/mL, 24 hours) significantly reduced basal and maximal oxygen consumption rates (OCRs), indicating impaired mitochondrial respiratory capacity (Figure 6B–D). These defects were attenuated by Fn14 silencing, implicating Fn14 as a key mediator of TWEAK-induced mitochondrial dysfunction. Similarly, pretreatment with the mitochondria-targeted antioxidant MitoTEMPO partially restored OCRs, particularly maximal respiration and spare respiratory capacity, highlighting a critical role for mitochondrial ROS.

At the molecular level, TWEAK markedly down-regulated PGC-1α and TFAM, key regulators of mitochondrial biogenesis and mitochondrial DNA maintenance[28,29] (Figure 6D and E; Supplementary Figures S11C and D and S12), whereas expression of VDAC1 and TOMM20 remained unchanged, suggesting functional impairment precedes overt structural loss[30,31] (Figure 6D; Supplementary Figure S11D). In parallel, TWEAK suppressed SOD2 and NRF2, central components of mitochondrial antioxidant defense,[32] whereas NRF1 expression was increased, possibly reflecting an insufficient compensatory response[33] (Figure 6D and E; Supplementary Figure S11C and D). Moreover, TWEAK selectively increased oxidative phosphorylation complex I without coordinated up-regulation of downstream complexes, indicating respiratory chain imbalance (Figure 6D; Supplementary Figure S11D). Consistently, enzymatic assays demonstrated reduced total SOD, Cu/Zn-SOD, and Mn-SOD activities, which were largely rescued by *Fn14* silencing or MitoTEMPO treatment (Figure 6F). Together, these data indicate that TWEAK impairs cardiomyocyte metabolic capacity and stress resilience by suppressing mitochondrial biogenesis and antioxidant defenses while promoting mitochondrial oxidative stress and respiratory dysfunction, establishing mitochondrial impairment as a central mechanism of TWEAK/Fn14-mediated cardiac injury in lupus.

DISCUSSION

This study identifies serum TWEAK as both a clinically relevant biomarker and a mechanistic driver of cardiac injury in SLE. We demonstrate that circulating TWEAK levels are significantly elevated in patients with SLE, highest in those with cardiac abnormalities, and closely correlated with oxidative stress markers, inflammatory cytokines, and overall disease activity. Importantly, elevated baseline TWEAK predicted subsequent cardiac abnormalities while levels declined in parallel with clinical improvement, underscoring its dynamic association with disease status.

Figure 6. TWEAK disrupts mitochondrial structure and oxidative respiratory function in cardiomyocytes. Transmission electron microscopy (TEM) was performed on cardiomyocytes isolated from MRL/lpr mice following 24 hours of TWEAK treatment. (A) Representative TEM images showing mitochondrial ultrastructural alterations. Red arrows indicate vacuolated mitochondria (M). Boxed regions are shown at higher magnification in the insets. Scale, 10 μm. (B and C) Seahorse ATP rate and mitochondrial respiration analyses in MRL/lpr cardiomyocytes following 24 hours of TWEAK stimulation under the indicated pretreatment conditions. *$P < 0.05$; **$P < 0.01$; ****$P < 0.0001$. (B) Quantification of basal respiration, maximal respiration, ATP production, and spare respiratory capacity. (D) Western blot analysis of mitochondrial biogenesis, structural, and antioxidant proteins, including PGC-1α, VDAC1, TOMM20, superoxide dismutase 2 (SOD2), NRF1, NRF2, TFAM, and oxidative phosphorylation (OXPHOS) complexes. (E) Representative immunofluorescence images and quantification of SOD2, TOMM20, PGC-1α, NRF1, and TFAM expression (scale, 50 μm). (F) Quantification of total SOD activity, Cu/Zn-SOD activity, and Mn-SOD activity in cardiomyocytes from MRL/lpr mice. *$P < 0.05$; **$P < 0.01$; ***$P < 0.001$; ****$P < 0.0001$. FCCP, carbonyl cyanide-*p*-trifluoromethoxyphenylhydrazone; mitoTEMPO, mitochondria-targeted 2,2,6,6-tetramethylpiperidine-1-oxyl; OCR, oxygen consumption rate; ROT/AA, rotenone/antimycin A; siFn14, small interfering fibroblast growth factor–inducible 14.

Complementing these clinical observations, genetic deletion of the TWEAK receptor *Fn14* in mice who were lupus prone preserved cardiac structure, attenuated oxidative stress, and restored antioxidant defenses. Together, our data position TWEAK/Fn14 signaling at the intersection of systemic inflammation, redox imbalance, and cardiac injury in SLE.

Cardiovascular complications remain a leading cause of morbidity and mortality in SLE, driven by the convergence of chronic immune activation and oxidative stress–mediated tissue damage.[2,34] Prior studies have implicated autoantibodies, complement consumption, and proinflammatory cytokines in lupus-associated cardiac risk. Our findings extend this paradigm by identifying TWEAK as a molecular integrator of these inflammatory cues that aligns closely with cardiac phenotypes.[2,35] Although TWEAK/Fn14 signaling has been extensively studied in lupus nephritis and neuropsychiatric lupus, its contribution to SLE-associated cardiac injury has not been systematically examined. By combining patient-level biomarker analyses with in vivo genetic models and mechanistic in vitro studies, our work fills this important knowledge gap.

Oxidative stress is a central driver of SLE pathogenesis and organ damage.[36] Clinically, we found that serum TWEAK positively correlated with markers of lipid peroxidation (MDA) and DNA oxidative damage (8-OHdG) while inversely correlating with antioxidant capacity (SOD1), reflecting a profound redox imbalance. In lupus mouse hearts, TWEAK/Fn14 signaling amplified oxidative injury, as evidenced by increased ROS accumulation and proapoptotic signaling alongside suppression of NRF2 and its downstream antioxidant targets. Fn14 deficiency reversed these abnormalities, supporting a causal, upstream role for TWEAK in redox dysregulation. Importantly, in isolated lupus-prone cardiomyocytes, TWEAK rapidly induced both cytosolic and mitochondrial ROS, suppressed antioxidant defenses, and reduced cell viability, demonstrating a direct, cell-intrinsic effect independent of systemic inflammation.

Our study further reveals that mitochondrial dysfunction is a key mechanistic link between TWEAK/Fn14 signaling and cardiomyocyte injury. TWEAK profoundly disrupted mitochondrial integrity and bioenergetics, inducing ultrastructural abnormalities and suppressing oxidative phosphorylation capacity. Mechanistically, TWEAK concurrently inhibited mitochondrial biogenesis programs through down-regulation of PGC-1α and TFAM while weakening mitochondrial antioxidant defenses via suppression of NRF2 and SOD2. Notably, these deleterious effects were accompanied by an apparent maladaptive response characterized by increased NRF1 expression and selective up-regulation of respiratory chain complex I without coordinated induction of downstream complexes. This imbalance likely exacerbates electron leakage and ROS generation rather than restoring mitochondrial function. Rescue of mitochondrial respiration and antioxidant enzyme activity by *Fn14* silencing or the mitochondrial-targeted antioxidant MitoTEMPO underscores the central role of mitochondrial oxidative stress in TWEAK-mediated cardiotoxicity.

From a clinical perspective, echocardiographic abnormalities in SLE span a broad spectrum of structural and functional changes, often preceding overt symptoms.[37] In our cohort, abnormal LV-GLS was a sensitive measure for early myocardial dysfunction[38] and was associated with significantly higher serum TWEAK levels. TWEAK was elevated across multiple cardiac abnormality subtypes and demonstrated moderate to high diagnostic accuracy for detecting echocardiographic and electrocardiographic abnormalities, as well as myocardial injury markers. ROC analyses confirmed its discriminatory capacity, and elevated baseline TWEAK predicted incident cardiac events. These findings highlight TWEAK as a noninvasive adjunct to cardiac evaluation, with complementary diagnostic and prognostic value, particularly in screening patients who were asymptomatic or in settings with limited imaging resources.

Beyond oxidative injury, TWEAK has been implicated in additional cardiopathogenic processes, including maladaptive calcium handling, hypertrophic signaling, and adverse remodeling following myocardial injury.[11,20,23,39,40] Consistent with these reports, we observed that sustained TWEAK exposure impaired cardiomyocyte proliferative capacity and promoted apoptosis, hallmarks of oxidative stress–driven myocardial injury. Although our DIA proteomic analyses provided a systems-level overview of TWEAK/Fn14-regulated oxidative pathways, further validation of specific downstream effectors will be important to fully delineate the signaling network linking immune activation to mitochondrial dysfunction.

Several limitations should be acknowledged. First, most clinical analyses were cross-sectional, and prospective longitudinal studies are required to definitively establish TWEAK as a predictive biomarker for cardiac outcomes in SLE. Second, due to technical constraints, our mechanistic studies relied on neonatal lupus-prone cardiomyocytes. Although this system is widely used and enabled detailed mechanistic interrogation, cardiomyocytes from adult mice treated with pristane or adult MRL/lpr mice may exhibit maturation- and metabolism-dependent responses that are not fully captured here. Future studies employing adult cardiomyocytes or in vivo metabolic flux analyses will be essential to validate and extend our findings. Third, the recombinant TWEAK concentration used in vitro exceeds circulating levels observed in patients and may amplify downstream signaling; dose–response studies within physiologic ranges will be important for translational relevance. Finally, we did not explicitly account for chronic glucocorticoid exposure, a known contributor to cardiovascular risk in SLE. In conclusion, our study establishes serum TWEAK as a robust indicator of cardiac involvement and oxidative stress in SLE, while uncovering a direct mechanistic role for TWEAK/Fn14 signaling in driving mitochondrial dysfunction, redox imbalance, and cardiomyocyte injury. These findings highlight TWEAK not only as a biomarker but also as a promising therapeutic target for preventing and mitigating lupus-associated cardiac disease.

ACKNOWLEDGMENT

We sincerely thank the healthy volunteers for kindly providing the heart ultrasound and serum samples.

AUTHOR CONTRIBUTIONS

All authors contributed to at least one of the following manuscript preparation roles: conceptualization AND/OR methodology, software, investigation, formal analysis, data curation, visualization, and validation AND drafting or reviewing/editing the final draft. As corresponding authors, Drs Xia and Huo confirm that all authors have provided the final approval of the version to be published, and take responsibility for the affirmations regarding article submission (eg, not under consideration by another journal), the integrity of the data presented, and the statements regarding compliance with institutional review board/Declaration of Helsinki requirements. All authors contributed to the investigation, formal analysis of the data, and writing, reviewing, and editing of the manuscript.

REFERENCES

1. Fleischer S, Nash TR, Tamargo MA, et al. An engineered human cardiac tissue model reveals contributions of systemic lupus erythematosus autoantibodies to myocardial injury. Nat Cardiovasc Res 2024;3(9):1123–1139. doi:https://doi.org/10.1038/s44161-024-00525-w
2. Patiño-Trives AM, Pérez-Sánchez C, Pérez-Sánchez L, et al. Anti-dsDNA antibodies increase the cardiovascular risk in systemic lupus erythematosus promoting a distinctive immune and vascular activation. Arterioscler Thromb Vasc Biol 2021;41(9):2417–2430. doi:https://doi.org/10.1161/ATVBAHA.121.315928
3. Kim SY, Yu M, Morin EE, et al. High-density lipoprotein in lupus: disease biomarkers and potential therapeutic strategy. Arthritis Rheumatol 2020;72(1):20–30. doi:https://doi.org/10.1002/art.41059
4. Blanco LP, Patino-Martinez E, Nakabo S, et al. Modulation of the itaconate pathway attenuates murine lupus. Arthritis Rheumatol 2022;74(12):1971–1983. doi:https://doi.org/10.1002/art.42284
5. Zhang Y, Zeng W, Xia Y. TWEAK/Fn14 axis is an important player in fibrosis. J Cell Physiol 2021;236(5):3304–3316. doi:https://doi.org/10.1002/jcp.30089
6. Xia Y, Herlitz LC, Gindea S, et al. Deficiency of fibroblast growth factor-inducible 14 (Fn14) preserves the filtration barrier and ameliorates lupus nephritis. J Am Soc Nephrol 2015;26(5):1053–1070. doi:https://doi.org/10.1681/ASN.2014030233
7. Wen J, Xia Y, Stock A, et al. Neuropsychiatric disease in murine lupus is dependent on the TWEAK/Fn14 pathway. J Autoimmun 2013;43:44–54. doi:https://doi.org/10.1016/j.jaut.2013.03.002
8. Madrigal-Matute J, Fernandez-Laso V, Sastre C, et al. TWEAK/Fn14 interaction promotes oxidative stress through NADPH oxidase activation in macrophages. Cardiovasc Res 2015;108(1):139–147. doi:https://doi.org/10.1093/cvr/cvv204
9. Shimada K, Fujii T, Tsujikawa K, et al. ALKBH3 contributes to survival and angiogenesis of human urothelial carcinoma cells through NADPH oxidase and tweak/Fn14/VEGF signals. Clin Cancer Res 2012;18(19):5247–5255. doi:https://doi.org/10.1158/1078-0432.CCR-12-0955
10. Yi T, Zhang W, Hua Y, et al. Rutin alleviates lupus nephritis by inhibiting T cell oxidative stress through PPARγ. Chem Biol Interact 2024;394:110972. doi:https://doi.org/10.1016/j.cbi.2024.110972
11. Poveda J, González-Lafuente L, Vázquez-Sánchez S, et al. Targeting the TWEAK-Fn14 pathway prevents dysfunction in cardiac calcium handling after acute kidney injury. J Pathol 2023;261(4):427–441. doi:https://doi.org/10.1002/path.6200
12. Dridi H, Santulli G, Bahlouli L, et al. Mitochondrial calcium overload plays a causal role in oxidative stress in the failing heart. Biomolecules 2023;13(9):1409. doi:https://doi.org/10.3390/biom13091409
13. Aringer M, Costenbader K, Daikh D, et al. 2019 European league against rheumatism/American College of Rheumatology classification criteria for systemic lupus erythematosus. Arthritis Rheumatol 2019;71(9):1400–1412.
14. Luo M, Liu M, Liu W, et al. Inhibition of fibroblast growth factor-inducible 14 attenuates experimental tubulointerstitial fibrosis and profibrotic factor expression of proximal tubular epithelial cells. Inflamm Res 2021;70(5):553–568. doi:https://doi.org/10.1007/s00011-021-01455-0
15. Toumi E, Bestion E, Militello M, et al. GNS561 (ezurpimtrostat), a small basic lipophilic molecule, prevents lupus phenotype in a pristane-induced lupus mouse model. Br J Pharmacol 2025;182(16):3786–3799. doi:https://doi.org/10.1111/bph.70058
16. Jokinen MP, Lieuallen WG, Johnson CL, et al. Characterization of spontaneous and chemically induced cardiac lesions in rodent model systems: the national toxicology program experience. Cardiovasc Toxicol 2005;5(2):227–244. doi:https://doi.org/10.1385/CT:5:2:227
17. Dahlberg P, Diamant U-B, Gilljam T, et al. QT correction using Bazett's formula remains preferable in long QT syndrome type 1 and 2. Ann Noninvasive Electrocardiol 2021;26(1):e12804. doi:https://doi.org/10.1111/anec.12804
18. Yan G-X, Antzelevitch C. Cellular basis for the normal T wave and the electrocardiographic manifestations of the long-QT syndrome. Circulation 1998;98(18):1928–1936. doi:https://doi.org/10.1161/01.CIR.98.18.1928
19. Wang Y, Yao F, Wang L, et al. Single-cell analysis of murine fibroblasts identifies neonatal to adult switching that regulates cardiomyocyte maturation. Nat Commun 2020;11(1):2585. doi:https://doi.org/10.1038/s41467-020-16204-w
20. Hao L, Ren M, Rong B, et al. TWEAK/Fn14 mediates atrial-derived HL-1 myocytes hypertrophy via JAK2/STAT3 signalling pathway. J Cell Mol Med 2018;22(9):4344–4353. doi:https://doi.org/10.1111/jcmm.13724
21. Zhou Y, Zhou B, Pache L, et al. Metascape provides a biologist-oriented resource for the analysis of systems-level datasets. Nat Commun 2019;10(1):1523. doi:https://doi.org/10.1038/s41467-019-09234-6
22. Olgar Y, Billur D, Tuncay E, et al. MitoTEMPO provides an antiarrhythmic effect in aged-rats through attenuation of mitochondrial reactive oxygen species. Exp Gerontol 2020;136:110961. doi:https://doi.org/10.1016/j.exger.2020.110961
23. Henein MY, Vancheri S, Longo G, et al. The role of inflammation in cardiovascular disease. Int J Mol Sci 2022;23(21):12906. doi:https://doi.org/10.3390/ijms232112906
24. Danieli MG, Antonelli E, Longhi E, et al. The role of microbiota and oxidative stress axis and the impact of intravenous immunoglobulin in systemic lupus erythematosus. Autoimmun Rev 2024;23(9):103607. doi:https://doi.org/10.1016/j.autrev.2024.103607
25. Navarro E, Esteras N. Multitarget effects of Nrf2 signalling in the brain: common and specific functions in different cell types. Antioxidants 2024;13(12):1502. doi:https://doi.org/10.3390/antiox13121502
26. Song X, Hao X, Zhu BT. Role of mitochondrial reactive oxygen species in chemically-induced ferroptosis. Free Radic Biol Med 2024;223:473–492. doi:https://doi.org/10.1016/j.freeradbiomed.2024.07.006
27. Jomova K, Alomar SY, Alwasel SH, et al. Several lines of antioxidant defense against oxidative stress: antioxidant enzymes, nanomaterials with multiple enzyme-mimicking activities, and low-molecular-weight antioxidants. Arch Toxicol 2024;98(5):1323–1367. doi:https://doi.org/10.1007/s00204-024-03696-4
28. Oller J, Gabandé-Rodríguez E, Ruiz-Rodríguez MJ, et al. Extracellular tuning of mitochondrial respiration leads to aortic aneurysm.

Circulation 2021;143(21):2091–2109. doi:https://doi.org/10.1161/CIRCULATIONAHA.120.051171

29. Fontecha-Barriuso M, Martin-Sanchez D, Martinez-Moreno JM, et al. The role of PGC-1α and mitochondrial biogenesis in kidney diseases. Biomolecules 2020;10(2):347. doi:https://doi.org/10.3390/biom10020347
30. Fu Z-J, Wang Z-Y, Xu L, et al. HIF-1α-BNIP3-mediated mitophagy in tubular cells protects against renal ischemia/reperfusion injury. Redox Biol 2020;36:101671. doi:https://doi.org/10.1016/j.redox.2020.101671
31. Shoshan-Barmatz V, Krelin Y, Shteinfer-Kuzmine A, et al. Voltage-dependent anion channel 1 as an emerging drug target for novel anti-cancer therapeutics. Front Oncol 2017;7:154. doi:https://doi.org/10.3389/fonc.2017.00154
32. Dosunmu-Ogunbi AM, Wood KC, Novelli EM, et al. Decoding the role of SOD2 in sickle cell disease. Blood Adv 2019;3(17):2679–2687. doi:https://doi.org/10.1182/bloodadvances.2019000527
33. Deng X, He J, Deng W, et al. Celastrol ameliorates lipopolysaccharide (LPS)-induced acute lung injury by improving mitochondrial function through AMPK/PGC-1α/Nrf1-dependent mechanism. Free Radic Biol Med 2025;227:210–220. doi:https://doi.org/10.1016/j.freeradbiomed.2024.12.017
34. Atzeni F, Rodríguez-Pintó I, Cervera R. Cardiovascular disease risk in systemic lupus erythematous: certainties and controversies. Autoimmun Rev 2024;23(10):103646. doi:https://doi.org/10.1016/j.autrev.2024.103646
35. Kostopoulou M, Nikolopoulos D, Parodis I, et al. Cardiovascular disease in systemic lupus erythematosus: recent data on epidemiology, risk factors and prevention. Curr Vasc Pharmacol 2020;18(6):549–565. doi:https://doi.org/10.2174/1570161118666191227101636
36. Shah D, Mahajan N, Sah S, et al. Oxidative stress and its biomarkers in systemic lupus erythematosus. J Biomed Sci 2014;21(1):23. doi:https://doi.org/10.1186/1423-0127-21-23
37. Lai L-P, Wang L-Q, Li S-P. Predictive value of Doppler echocardiography parameters for cardiovascular events in patients with systemic lupus erythematosus. Lupus 2024;33(10):1059–1068. doi:https://doi.org/10.1177/09612033241266083
38. Huang L, Wang X, Yuan Y, et al. Evaluation of subclinical myocardial involvement in systemic lupus erythematosus using multiparametric cardiac magnetic resonance imaging. BMC Cardiovasc Disord 2025;25(1):597. doi:https://doi.org/10.1186/s12872-025-05033-8
39. Çelikkol A, Demirkıran A, Aydın C. The usefulness of tumor necrosis factor-like weak inducer of apoptosis in patients with acute ST-elevation myocardial infarction. Eur Rev Med Pharmacol Sci 2023;27(16):7637–7643.
40. Ren K, Peng X, Duan X, et al. Synergistic effects of LCN2 and TWEAK on the progression of psoriasis. Cell Mol Immunol 2025;22(7):760–775. doi:https://doi.org/10.1038/s41423-025-01292-9

Arthritis & Rheumatology
Vol. 78, No. 9, September 2026, pp 1907–1919
DOI 10.1002/art.70116
© 2026 The Author(s). *Arthritis & Rheumatology* published by Wiley Periodicals LLC on behalf of American College of Rheumatology.
This is an open access article under the terms of the Creative Commons Attribution License, which permits use, distribution and reproduction in any medium, provided the original work is properly cited.

American College of Rheumatology
Empowering Rheumatology Professionals

Single-Cell Level Characterization of B Cell Depletion and Repopulation Following Rituximab in Systemic Lupus Erythematosus

Haerin Jang, MSc,[1] Norzawani Buang, PhD,[2] Catherine Sutherland, PhD,[1] Wanseon Lee, PhD,[1] Lauren Overend, DPhil,[3] Tarran S. Rupall, MSc,[1] Katie L. Burnham, DPhil,[1] Matthew C. Pickering, MD, PhD,[2] Marina Botto, MD,[2] and Emma E. Davenport, DPhil[1]

Objective. Rituximab, a CD20$^+$ B cell depletion therapy, is frequently used to treat systemic lupus erythematosus (SLE). However, variability in patient response highlights the need for a deeper understanding of the underlying immune cell dynamics of B cell depletion and repopulation.

Methods. We conducted longitudinal single-cell profiling of nine patients with SLE treated with rituximab from pre-treatment to up to 15 months post-treatment. These were compared with eight healthy controls. We profiled 169,513 immune cells via single-cell RNA, surface protein, B cell receptor (BCR), and T cell receptor sequencing, and bulk BCR repertoire sequencing.

Results. Significant depletion of naïve, memory, and age-associated B cells was observed early post-treatment, followed by later repopulation of mainly transitional B cells. A fraction of antigen-experienced B cells, particularly in nonresponders, persisted through the depletion. BCR repertoire analysis revealed reduced diversity and persistent clones in antigen-experienced cells at early post-treatment, but these effects were not long-lasting. Repopulated naïve B cells in rituximab responders exhibited reduced NF-κB pathway activation, aligning with lower B cell activating factor receptor (BAFF-R) surface protein levels. In non-B cells, we identified 27 differentially expressed genes across seven immune cell subtypes post-rituximab, with regulatory CD4 T cells and double negative (DN) T cells showing the most changes. Responders specifically had increased expression of genes related to cytotoxicity, major histocompatibility complex class II antigen presentation, and T cell activation in CD4 T central memory and DN T cells.

Conclusion. Our longitudinal profiling provides single-cell resolution of the shifts in immune cell dynamics following B cell depletion.

INTRODUCTION

Systemic lupus erythematosus (SLE) is a chronic autoimmune disease characterized by widespread inflammation and tissue damage in multiple organs, including the skin, kidneys, joints, and central nervous system. Dysregulated immune responses, notably aberrant B cell activity producing autoantibodies, drive disease.[1] Historically, treatment relied on broad immunosuppressants that often carried significant side effects. However, advances in our understanding of SLE pathophysiology have enabled targeted biologic therapies including anti-BAFF, anti-CD20, and anti-interferon (IFN)-α receptor antibodies.[2] By focusing on specific molecular pathways and cell types involved in disease manifestation, these therapies offer targeted and

Supported by the National Institute for Health and Care Research (NIHR) Imperial Biomedical Research Centre. The views expressed are those of the authors and not necessarily those of the NIHR or the Department of Health and Social Care. This research was funded in part by the Wellcome Trust [220540/Z/20/A]. Dr Sutherland received salary support from the Lupus Research Alliance Global Team Science award.

[1]Wellcome Sanger Institute, Wellcome Genome Campus, Hinxton, United Kingdom; [2]Department of Immunology and Inflammation, Imperial College London, London, United Kingdom; [3]Centre for Human Genetics, University of Oxford, Oxford, United Kingdom.

Ms Jang and Dr Buang are co-first authors and contributed equally to this work. Drs Botto and Davenport are co-senior authors and contributed equally to this work.

Additional supplementary information cited in this article can be found online in the Supporting Information section (https://acrjournals.onlinelibrary.wiley.com/doi/10.1002/art.70116).

Author disclosures and graphical abstract are available at https://onlinelibrary.wiley.com/doi/10.1002/art.70116.

Address correspondence via email to Marina Botto, MD, at m.botto@imperial.ac.uk; or to Emma E. Davenport, DPhil, at ed5@sanger.ac.uk.

Submitted for publication May 23, 2025; accepted in revised form February 5, 2026.

potentially safer options and reduce reliance on immunosuppressants. However, our incomplete understanding of treatment mechanisms has limited success in clinical trials.

Rituximab, an anti-CD20 monoclonal antibody, is frequently prescribed off-label for SLE[3] despite failing to meet endpoints in clinical trials.[4,5] It depletes circulating $CD20^+$ B cells, which is followed by gradual repopulation over months. By removing B cells, rituximab likely reduces autoantibody production and proinflammatory cytokines,[6] although its precise mechanisms are not completely understood, particularly because long-lived plasma cells and tissue-resident B cells are spared,[7] yet clinical improvement is often observed. Similarly, it is unclear what underpins variability in patient response.[3] With emerging B cell depletion therapies, such as anti-CD19 CAR-T therapy and obinutuzumab,[8] understanding changes in the immune response following these treatments is increasingly important.

Previous studies have examined B cell subpopulations following rituximab using flow cytometry[9,10] and bulk transcriptomics,[11] but molecular changes using single-cell technologies remain unexplored. Single-cell RNA-seq (scRNA-seq) reveals cell-type–specific transcriptome changes as well as cell abundance. This approach is particularly advantageous for studying immune cells, for which gene function is highly cell-type–specific. Studying B cell depletion therapy with scRNA-seq offers insights into dynamic changes in not only B cell subtypes but also non-B cells, which helps for understanding the broader immune response and potential off-target effects. For example, a single-cell study on CD19 CAR-T cell mediated B cell depletion in SLE found reduced Type I interferon-induced gene expression in monocytes and T cells but not B cells.[12]

Here, we characterized B cell depletion and repopulation following rituximab in nine patients with SLE at the single-cell level. Using a multimodal approach comprising gene expression (scRNA-seq), surface protein levels (cellular indexing of transcriptomes and epitopes by sequencing [CITE-seq]), and B cell receptor (BCR) and T cell receptor (TCR) repertoire data, we analyzed changes in immune cells. Combined with bulk BCR data, we observed dynamic shifts in B cell subtypes after depletion and repopulation, whereas the BCR repertoire remained largely unchanged long-term. By stratifying the patients into responders and nonresponders to rituximab, we found that repopulated naïve B cells in responders are transcriptionally distinct from pretreatment and observed an increase in cytotoxicity and activation related genes in central memory CD4 T cells (CD4 TCM) and double negative (DN) T cells. Our findings offer a detailed view of immune cell dynamics in patients with SLE receiving rituximab.

MATERIALS AND METHODS

Sample collection and sequencing. Blood samples were collected from patients with SLE who were aged at least 18 years old and receiving rituximab at the Imperial Lupus Centre, Imperial College Healthcare NHS Trust in the United Kingdom. Patients were rituximab-naïve, except for one who received rituximab more than five years before this study. "Early post-treatment" samples were collected 1 to 6 months after treatment, and "late post-treatment" were collected 7 to 15 months post-treatment to capture broad phases of B cell depletion and repopulation. Response was determined at 12 months post-treatment following the criteria outlined in the Supplementary Methods. Healthy controls were also sampled. Participant ancestry was self-reported from fixed categories. Samples were obtained from the Imperial College Healthcare Tissue and Biobank (ICHTB). ICHTB is supported by the National Institute for Health Research Biomedical Research Centre based at the Imperial College Healthcare NHS Trust and Imperial College London. ICHTB is approved by Wales REC3 to release human material for research (22/WA/0214), and the samples for this project (Ref: R13010-3A) were issued from subcollection reference number IMM_MB_15_027 and IMM_MB_13_001. Written informed consent was obtained from all participants.

From all collected blood samples, single-cell gene expression, surface proteins (n = 137), TCR, and BCR were sequenced. Peripheral blood mononuclear cells (PBMCs) were isolated and cryopreserved. Sequencing libraries were generated using the 10× Chromium platform and sequenced on Illumina NovaSeq6000. Bulk BCR sequencing followed the protocol from Bashford-Rogers et al.[13] Details on sequencing are in the Supplementary Methods. Flow cytometry was used to quantify B cell frequencies ($CD19^+$ B cell percentage out of live $CD45^+$ cells) (Supplementary Methods) for comparison with single-cell data.

Data preprocessing. Cell Ranger multi v7.0.0 (10× Genomics) yielded 256,696 cell-containing droplets. Post quality control, 169,513 cells remained (Supplementary Methods and Supplementary Figure 1). Filtered BCR and TCR contigs from Cell Ranger were processed using Immcantation[14] and IgBLAST[15] (v1.21.0), resulting in 13,981 BCR and 67,062 TCR sequences for analysis.

Multimodal integration between scRNA-seq and CITE-seq data was performed with totalVI.[16] The resulting low-dimensional latent representations were used for neighborhood construction (k = 15) and uniform manifold approximation and projection (UMAP) generation. Unsupervised clustering used the Leiden algorithm.[17] Cell types were annotated using canonical RNA and surface protein markers, with B cell annotation informed by isotype usage and mutation frequency (Supplementary Figures 2 and 3). Normalized CITE-seq values from totalVI were used for surface protein level analyses, including CD20 and B cell activating factor receptor (BAFF-R). Details on preprocessing are in the Supplementary Methods.

Bulk BCR sequencing data were processed using Immcantation and IgBLAST v1.21.0 (Supplementary Methods) resulting in 1,028,624 unique sequences. Because of technical issues,

IGHV4 sequences were either not amplified or removed during post-processing.

Differential abundance analysis. Differentially abundant cell populations between time points were identified using MiloR (v.2.0)[18] with a mixed effect model adjusting for individual patients. B cell subtype analyses used B cell-only neighborhoods. Spatial false discovery rate (FDR) <0.1 was used to determine significance. Analysis methods are detailed in the Supplementary Methods.

BCR and TCR repertoire analysis. Optimized Likelihood estimate of immunoGlobulin Amino-acid sequences[19] was used to calculate the generation probability of CDR3 sequences. Repertoire diversity was assessed via Shannon entropy on size-matched samples using the *dit* Python package[20] (Supplementary Methods). Heavy chain single-cell and bulk BCR data were combined to identify clonal lineages across time points. Clustering of sequences into clonal groups was conducted using Change-O.[21] Clones present at pretreatment and one post-treatment time point were considered persistent, whereas pretreatment-only clones were nonpersistent. To account for varying numbers of antibody secreting cells, bulk BCR sequences were not weighted by unique molecular identifier counts.

Differential gene expression analysis and pathway analysis. We used a pseudobulk approach, aggregating raw counts by sample and cell type, to identify differentially expressed genes (DEGs). Trimmed mean of M values (TMM) normalization was followed by a quasi-likelihood approach from edgeR[22] with model covariates as patient and cellular detection rate (the fraction of detected genes per cell to adjust for sequencing depth as described in Soneson et al[23]). FDR <0.05 defined significance.

Only cell types with more than 10 cells per sample were analyzed to ensure that the pseudobulk expression accurately represented the gene expression profile. For non-B cells, we compared pretreatment with early post-treatment. To further investigate changes in interferon-stimulated genes, we scored cells using "scanpy.tl.score_genes" from Scanpy (v1.10.1[24]) with "Interferon signaling" pathway genes from Reactome (R-HSA-913531).

To identify differences in depleted and repopulated B cells, we conducted a differential gene expression analysis in naïve B cells from responders at pretreatment and late post-treatment. Gene set enrichment analysis was performed with Reactome (ReactomePA v1.48.0, reactome.db_1.88.0[25]) using log FC-ranked gene lists (including up- and down- regulated genes). We assessed the direction and magnitude of NF-κB pathway activation in naïve B cells using the PROGENy.[26] Pathway activation scores were calculated using decoupleR (v.2.8.0).[27]

To identify genes in non-B cells where response status altered expression changes, we implemented the approach detailed in the edgeR User's Guide (Section 3.5). This identifies genes where changes in expression between time points differ depending on response. To confirm these results were robust, a permutation analysis was conducted. Detailed methods are available in the Supplementary Methods.

Data availability statement. Raw single-cell RNA-seq, CITE-seq, and repertoire sequencing data have been deposited in the European Genome-phenome Archive under accession EGAS00001006798. Processed single-cell data have been deposited in Zenodo (https://zenodo.org/records/17868028). Data will be released and publicly accessible at the time of publication.

RESULTS

Longitudinal single-cell profiling of rituximab response in SLE. We conducted longitudinal single-cell profiling in nine patients with SLE treated with rituximab to characterize immune cell dynamics following B cell depletion (Figure 1A). PBMC were collected at pretreatment and at multiple time points up to 15 months post-treatment to capture initial B cell depletion and later repopulation. Samples were also collected from eight healthy controls to provide a reference. Participant demographics are outlined in Supplementary Table 1, and the clinical information at each time point, including the number of days from rituximab, is detailed in Supplementary Table 2.

A total of 169,513 immune cells were profiled with single-cell RNA, surface protein, BCR, and TCR sequencing. After clustering, we annotated 31 immune cell subtypes using canonical markers (Figure 1B, Supplementary Figure 2). B cell subtype annotation was additionally informed by BCR isotype usage and mutation frequency (Supplementary Figure 3).

To assess B cell depletion following rituximab, we conducted differential cell abundance analysis between early post-treatment and pretreatment (n = 9 vs 9) (Figure 1C). Most cell neighborhoods within naïve B cells (500 of 588 neighborhoods), non-switched memory B cells (23 of 25 neighborhoods), switched memory B cells (54 of 72 neighborhoods) and age-associated B cells (ABCs) (defined as CD11c^{+}, Tbet^{+}, CD21^{low}, CD27^{low}, 53 of 59 neighborhoods) were significantly less abundant at early post-treatment (spatial FDR <0.1). Other cell types remained largely unchanged, including plasma cells and plasmablasts, aligning with their low CD20 surface protein levels (Supplementary Figure 4). Transitional B cells, despite high CD20 expression, were not less abundant at early post-treatment. Among 156 transitional B cell neighborhoods, only 4 decreased in abundance, suggesting rapid repopulation of this cell type, given the rapid turnover and limited lifespan of this cell type[28] or, less likely, survival of these cells despite rituximab. Comparing late post-treatment with early post-treatment (n = 9 vs 6) (Figure 1D), neighborhoods within transitional, naïve, non-switched memory, and ABCs increased, suggesting that repopulation of B cells has begun in patients at these time points.

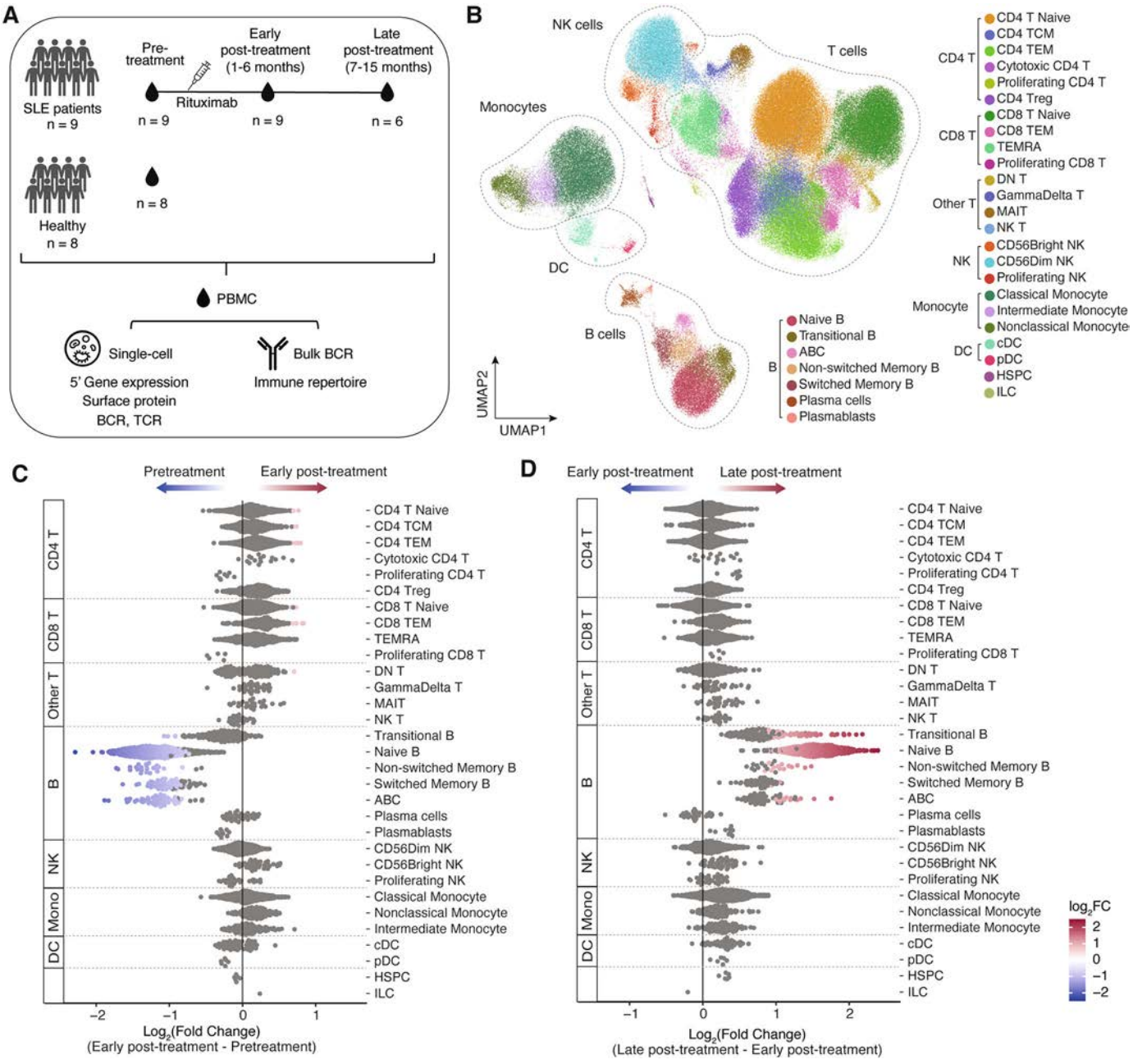

Figure 1. Longitudinal single-cell profiling of response to rituximab in SLE. (A) Overview of study design. PBMCs were collected from nine patients with SLE and eight healthy controls at three time points: pretreatment, early post-treatment, and late post-treatment. scRNA-seq, CITE-seq (surface protein profiling), single-cell BCR/TCR sequencing, and bulk BCR sequencing were performed. Pretreatment bulk BCR repertoire data were available for eight of nine patients with SLE. (B) UMAP of 169,513 cells, annotated into 31 immune cell types. Differential cell abundance between (C) pretreatment and early post-treatment (n = 9 vs 9) and (D) early post-treatment and late post-treatment (n = 9 vs 6). Each point represents a cell neighborhood, where most cells belong to the annotated subtype. Neighborhoods with significantly different cell abundances between time points are colored according to their $\log_2$FC. BCR, B cell receptor; CITE-seq, cellular indexing of transcriptomes and epitopes by sequencing; PBMCs, peripheral blood mononuclear cells; scRNA-seq, single-cell RNA sequencing; SLE, systemic lupus erythematosus; TCR, T cell receptor; UMAP, uniform manifold approximation and projection.

Perturbation of the BCR repertoire after rituximab. We performed both single-cell V(D)J enrichment and bulk heavy chain BCR sequencing to profile the immune receptor repertoire pre- and post-rituximab. A total of 13,981 paired BCR and 1,028,618 unique heavy chain sequences were identified. To explore repertoire characteristics, we calculated Shannon entropy, which is a measure of diversity; generation probability, which is the likelihood of a sequence being generated by random chance; and somatic hypermutation frequency (Figure 2A–C). At pretreatment, these metrics were similar across patients. At early

post-treatment, diversity and generation probability decreased in most patients, whereas mutation frequency increased. Patients with poor B cell depletion generally maintained a more diverse repertoire (Supplementary Figure 5A). By late post-treatment, these metrics returned toward pretreatment levels. Isotype usage also varied across time points, with increased class-switched sequences at early post-treatment and a reduction at late post-treatment. This is consistent with the reduction and subsequent repopulation of naïve B cells (Figure 2D).

BCR clones spanning multiple time points were observed in all patients, although the degree of overlap varied (Supplementary Figure 5B). Persistent clones were found in both responders and nonresponders, and there was minimal sharing of persistent clones between individuals. These persistent clones were enriched for switched memory B cells, plasmablasts, and plasma cells (Figure 2E and Supplementary Figure 5C). Persistent clones had higher mean mutation frequency (paired *t*-test, $P = 4.0 \times 10^{-7}$) (Figure 2F). Together, this suggests the depletion of less mature B cells and persistence of antigen-experienced cells.

As transitional and naïve B cells are preferentially depleted and subsequently repopulated, we examined the BCRs expressed by these cells. Patients with SLE had shorter CDR3 lengths in both transitional and naïve B cells compared with controls, and this was consistent at pretreatment and late post-treatment (Kruskal-Wallis with Dunn's test, adjusted $P = 0.03$) (Figure 2G and H). Patients with SLE also showed biased IGHJ gene usage, particularly in IGHJ3 and IGHJ6 in naïve B cells (Supplementary Figure 5D). Similar signatures were observed in IgM^+/IgD^+ SHM^- sequences from bulk data (Supplementary Figure 5E and F).

Single-cell TCR data showed no consistent differences in repertoire characteristics after rituximab (Supplementary Figure 6).

Transcriptomic changes in non-B cells after rituximab. Given that rituximab may lead to change in other immune cells, we analyzed transcriptional changes following rituximab in non-B cells. We performed differential gene expression analysis in non-B cell subtypes with more than 10 cells in all patients at each time point and compared pretreatment with early post-treatment cells to identify early changes after rituximab. A total of 27 genes (26 unique) were identified across 7 of 10 immune cell subtypes (Figure 3A and B). Regulatory CD4 T (Treg) cells and DN T cells had the most DEGs with nine and eight genes, respectively.

Given the known role of interferon signaling in inflammation, autoantibody production, and disease prognosis in SLE,[29] we focused on transcriptomic changes in interferon-related genes. Out of 26 DEGs, 8 genes were within the "interferon signaling" pathway (Reactome pathway R-HSA-913531): IFI35, XAF1, and IRF7 in Treg cells; IFI44 in effector memory CD8 T cells; USP18 in naïve CD8 T cells; IFIT1 in CD56Dim NK cells; and ISG15 and MX1 in DN T cells. For most, expression decreased following treatment (Supplementary Figure 7A). To assess overall pathway activity, we calculated a score for each cell using "interferon signaling pathway" genes from Reactome (R-HSA-913531) (see "Methods" section). No consistent changes in interferon pathway scores were observed in non-B cells globally or at the cell-type level (Figure 3C and D, Supplementary Figure 7B).

B cell depletion and repopulation in rituximab responders and nonresponders. To assess potential cell-type–level differences based on the clinical response, we examined cell-type abundance over time in rituximab responders and nonresponders separately (Figure 4A). Response was assessed 12 months post-treatment (Supplementary Methods), with five of nine patients responding to rituximab.

To quantify overall B cell depletion, we first calculated the proportion of B cells in single-cell PBMC data pre- and post-treatment (Figure 4B). These proportions correlated well with matched flow cytometry data (Supplementary Figure 8A and B) (Pearson R = 0.98, *P* value $<2.2 \times 10^{-16}$). The B cell proportion was higher in patients with SLE than in healthy controls at pretreatment (Wilcoxon test *P* value = 0.0037), but no difference existed between responders and nonresponders (Wilcoxon test *P* value >0.05). All patients showed reduced B cell proportions after treatment, but incomplete depletion (>1% B cells at early post-treatment) was observed in three of four nonresponders, with an average of 8.4% of PBMCs remaining as B cells. This incomplete depletion was not due to differences in CD20 surface protein levels at pretreatment (*t*-test *P* value >0.05) (Figure 4C and Supplementary Figure 8C). By late post-treatment, B cell proportions were not significantly different from pretreatment (repeated measures analysis of variance *P* value >0.05) (Figure 4B).

To determine the difference between responders and nonresponders in B cell depletion, we performed differential cell abundance analysis between pretreatment and early post-treatment within each group (Figure 4D). This revealed significant depletion in ABCs and switched memory B cells in responders that was not found in nonresponders, suggesting a difference in the effectiveness of depletion in these cells. Naïve B cells and non-switched memory B cells depleted similarly, whereas nonresponders showed a slight increase in plasma cells.

We then compared late post-treatment with pretreatment to understand B cell repopulation (Figure 4E). Responders maintained low ABC and switched memory B cell levels, whereas transitional B cells rapidly repopulated. Consistent with these changes, BCR data showed IgM usage predominating at late post-treatment (Supplementary Figure 9A). There were no consistent differences in Shannon entropy, probability of generation, or mean mutation frequency between responders and nonresponders across time points (Supplementary Figure 9B–D). In nonresponders, no significant differences in abundance were observed between pretreatment and late post-treatment.

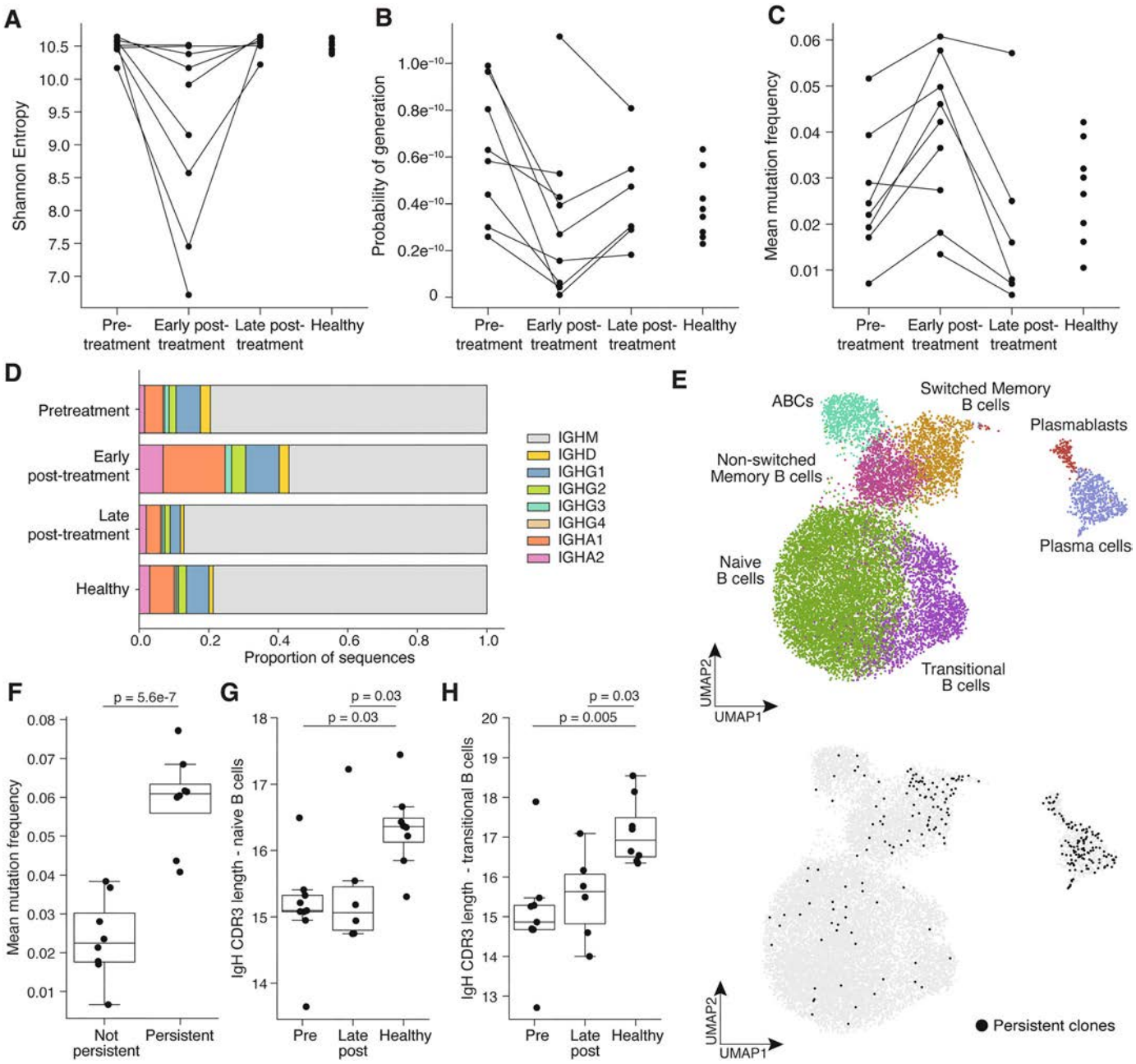

Figure 2. Perturbation of the BCR repertoire after rituximab. (A) Shannon entropy of bulk BCR repertoire samples across time points. Higher values indicate greater diversity. All samples were subset to 1,616 UMIs across 1,000 iterations and a mean was calculated. (B) Mean generation probability of bulk BCR repertoire samples across time points, calculated by OLGA on nucleotide CDR3 sequence. Higher generation probability indicates a sequence that is more likely to occur by chance. (C) Mean mutation frequency of bulk BCR repertoire samples across time points. (D) Isotype usage in total B cells at each time point from single-cell data. (E) B cell UMAP highlighting cells with sequences belonging to persistent clones. Clones were considered persistent if they contained sequences from both pretreatment and one post-treatment time point. (F) Mean mutation frequency of sequences belonging to persistent or nonpersistent clones. Paired *t*-test. Mean IgH CDR3 length at pretreatment, late post-treatment, and in healthy controls in (G) transitional B cells and (H) naïve B cells. FDR adjusted *P* value, Kruskal-Wallis followed by Dunn's test. BCR, B cell receptor; CDR3, complementarity-determining region 3; FDR, false discovery rate; OLGA, Optimized Likelihood estimate of immunoGlobulin Amino-acid sequences; UMI, unique molecular identifier; UMAP, uniform manifold approximation and projection. Color figure can be viewed in the online issue, which is available at http://onlinelibrary.wiley.com/doi/10.1002/art.70116/abstract.

However, there was a trend toward enrichment of IgA and increased persistent IgA clones, suggesting the survival of antigen-experienced cells (Supplementary Figure 9E).

Transcriptomic changes in repopulated naïve B cells in responders. Following rituximab, substantial turnover in B cell populations occurred in responders. To investigate

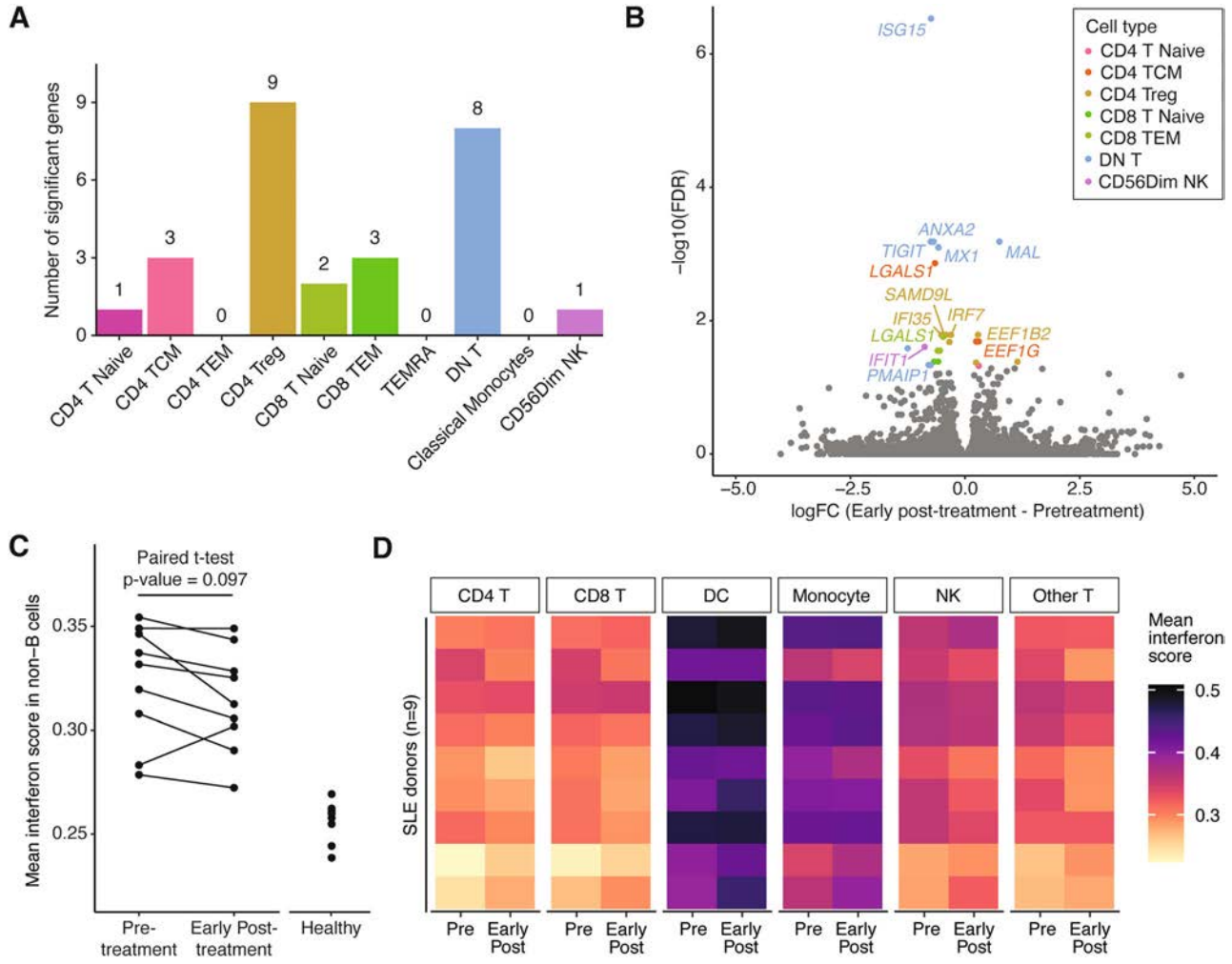

Figure 3. Gene expression changes in non-B cells following rituximab. (A) Number of significant DEGs in non-B cells between pretreatment and early post-treatment (FDR < 0.05, n = 9 vs 9). Only cell types with at least 10 cells in all patients at both time points were included in the analysis. (B) DEGs between early post-treatment and pretreatment. Statistically significant results are colored by cell type. (C) Mean interferon score of non-B cells at pretreatment and early post-treatment to rituximab. Interferon score was calculated using genes from the Reactome gene set "Interferon signaling" (R-HSA-913531). Healthy control scores are shown as reference. (D) Mean interferon score of each non-B cell subtype at pretreatment and early post-treatment by patient. DEG, differentially expressed gene; FDR, false discovery rate. Color figure can be viewed in the online issue, which is available at http://onlinelibrary.wiley.com/doi/10.1002/art.70116/abstract.

transcriptomic differences between depleted and repopulated B cells, we performed differential gene expression analysis between pretreatment and late post-treatment in responders. We focused specifically on naïve B cells because these were completely depleted at early post-treatment (Supplementary Figure 10), and all patients had at least 10 cells at both time points. Other B cell subtypes had insufficient cell numbers and were therefore excluded.

A total of 171 genes (60 up-regulated and 111 down-regulated) showed significant changes (FDR <0.05) (Figure 5A and Supplementary Table 3). Many genes, including *SOCS1*, *SOCS3*, *PTGER4*, *CD83*, *PRDM1*, and *AIF1*, were related to the regulation of immune processes and have previously been reported in SLE genome-wide association studies (GWAS Catalog[30]: trait "systemic lupus erythematosus"). Pathway analysis further highlighted NF-κB pathway and G protein-coupled receptor signaling (Figure 5B).

Given the central role of NF-κB signaling in immune regulation, we sought to quantify its activity at the single-cell level. We calculated the NF-κB pathway activation level of individual cells (Supplementary Methods). In all responders, the level of NF-κB pathway activation was significantly lower in late post-treatment naïve B cells compared with pretreatment (Wilcoxon rank-sum test *P* value <0.05), resembling levels in healthy controls (Figure 5C). Nonresponders had higher activation levels at late post-treatment. A similar pattern was also observed in memory B cell subtypes, including ABCs (Supplementary Figure 11A).

BAFF-R, when in contact with BAFF, activates the NF-κB pathway.[31] Hence, BAFF-R surface protein levels on naïve B cells were investigated to assess whether changes in receptor expression could be linked to altered NF-κB pathway activity (Figure 5D). BAFF-R levels were significantly lower at late post-treatment compared with pretreatment in three of four responders

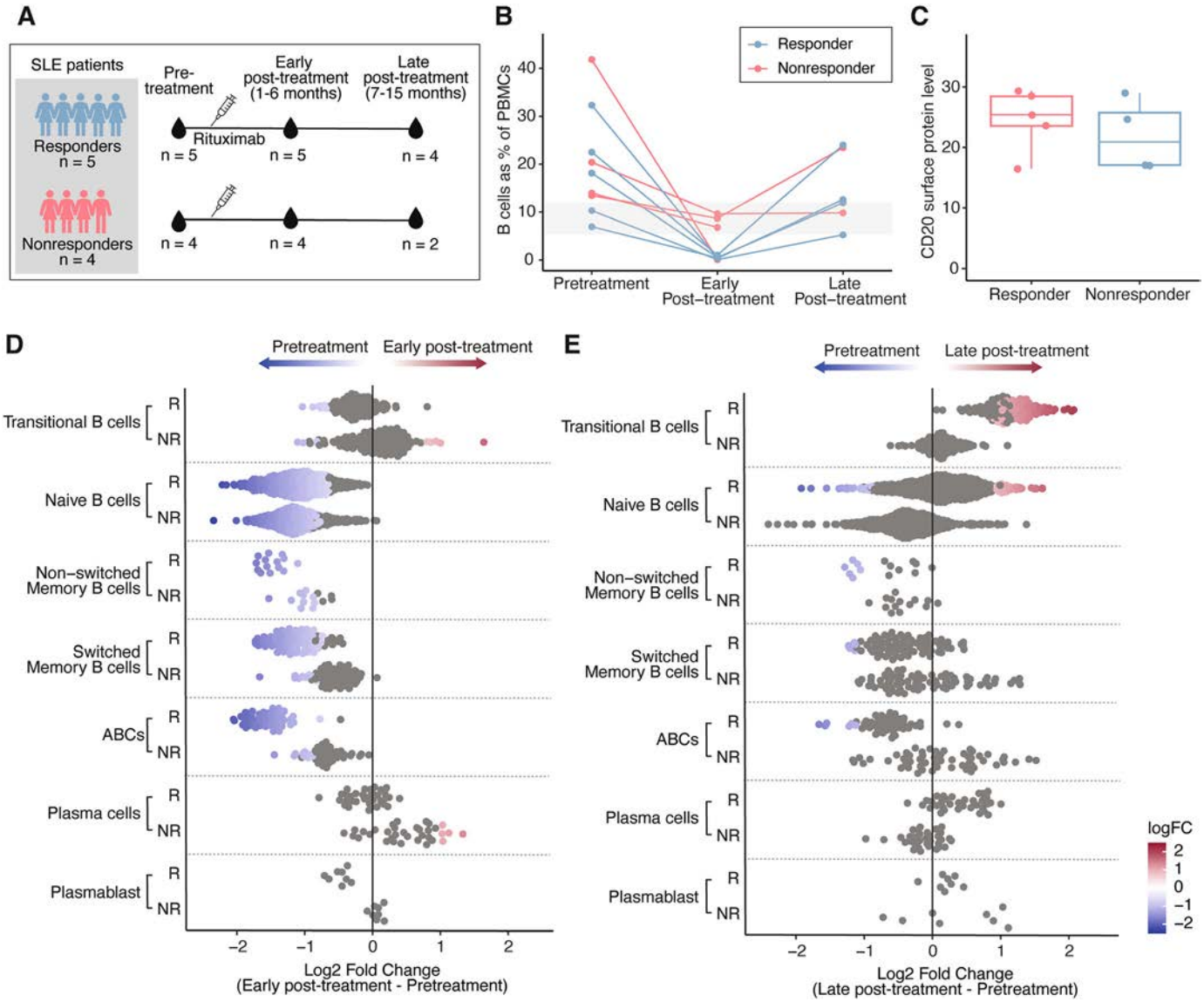

Figure 4. B cell depletion and repopulation in rituximab responders and nonresponders. (A) Patients with SLE stratified into responders (n = 5) and nonresponders (n = 4) based on clinical response to rituximab. Early post-treatment samples were collected for all patients, whereas late post-treatment samples were available for four of five responders and two of four nonresponders. (B) Proportion of B cells among total PBMCs at pretreatment, early post-treatment, and late post-treatment, as measured by single-cell sequencing. The shaded region represents the range observed in healthy controls (n = 8). (C) Average CD20 surface protein expression in B cells from rituximab responders and nonresponders at pretreatment. (D) and (E) Differential B cell abundance in rituximab responders (R) and nonresponders (NR). (D) Comparison between pretreatment and early post-treatment; (E) comparison between pretreatment and late post-treatment. Each point represents a cell neighborhood predominantly composed of the annotated B cell subtype. Neighborhoods with significant changes in abundance between time points within each response group are colored by the log_2FC. Gray points indicate neighborhoods without significant change. PBMCs, peripheral blood mononuclear cells; SLE, systemic lupus erythematosus. Color figure can be viewed in the online issue, which is available at http://onlinelibrary.wiley.com/doi/10.1002/art.70116/abstract.

(Wilcoxon rank-sum test *P* value <0.001) (Supplementary Figure 11B), aligning with the change in NF-κB pathway activation.

Gene expression changes interacting with rituximab response in non-B cells. Broader immune responses may differ between responders and nonresponders following rituximab. To investigate this, we analyzed gene expression changes in non-B cells by comparing response-specific effects from pretreatment with early post-treatment (see "Methods" section). For instance, this approach identifies genes that increase in expression in responders but decrease in nonresponders.

A total of 99 genes (72 unique) in nine immune cell subtypes showed differential expression changes based on rituximab

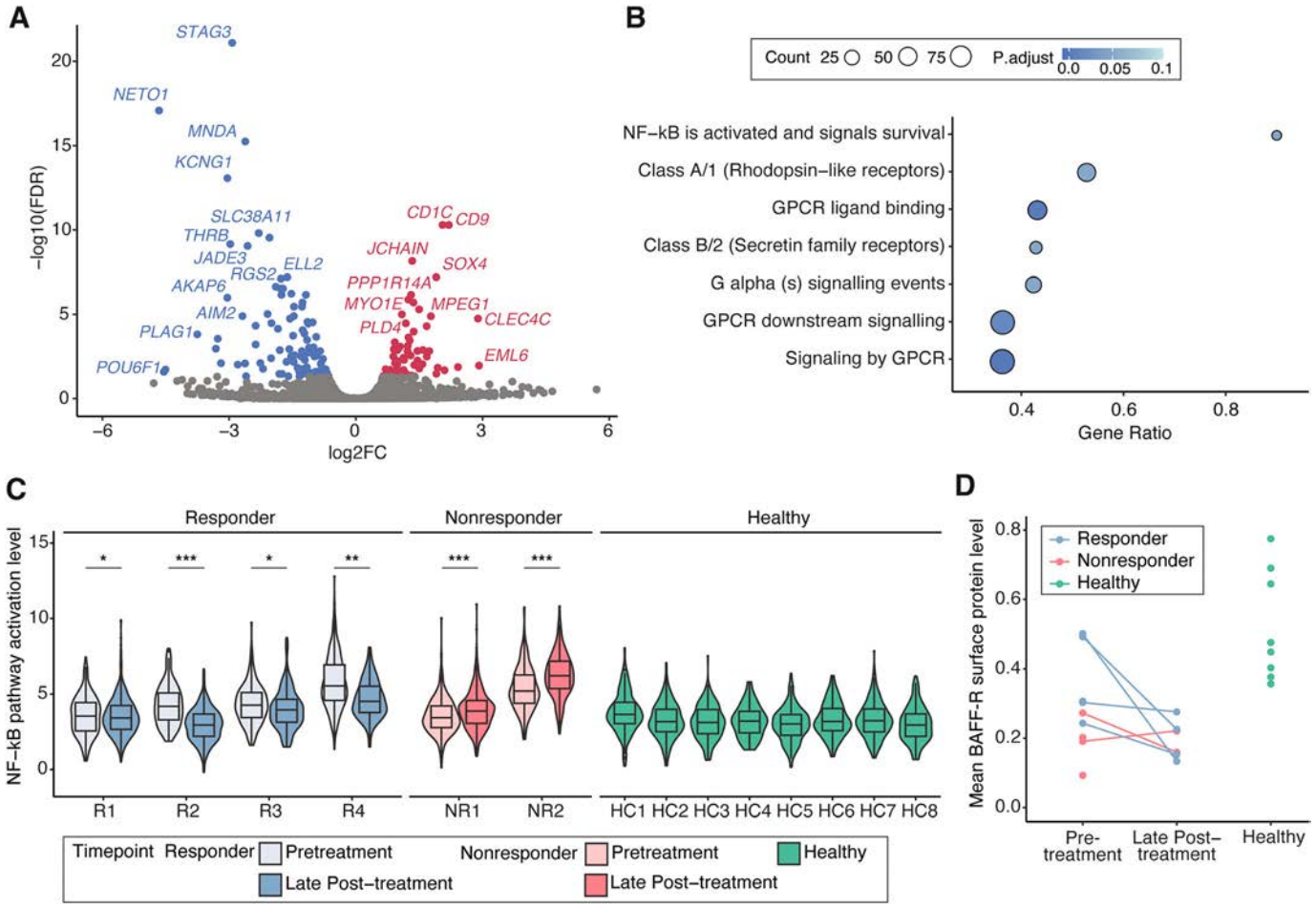

Figure 5. The transcriptomic profile of repopulated B cells in rituximab responders. (A) Volcano plot showing DEGs (n = 171, FDR < 0.05) in naïve B cells from rituximab responders, comparing pretreatment with late post-treatment. Each point represents a gene, with significance and $\log_2$FC plotted on the *y*- and *x*-axes, respectively. (B) Top Reactome pathways enriched among DEGs in responder naïve B cells between pretreatment and late post-treatment. Gene ratio indicates the proportion of core enrichment genes relative to the total number of genes within each pathway. (C) NF-κB pathway activation scores in naïve B cells from individual patients at pretreatment and late post-treatment. Violin plots show the distribution of activation scores across cells, whereas box plots indicate the IQR (box), median (center line), and minimum/maximum values excluding outliers (whiskers). Differences in pathway activation between time points were assessed per patient using the Wilcoxon rank-sum test. Adjusted *P* values: * < 0.05; ** < 0.01; *** < 0.001. (D) Mean BAFF-R cell surface protein levels on naïve B cells from healthy controls and patients with SLE at pretreatment and late post-treatment, measured by CITE-seq using antibody-derived tags. BAFF-R, B cell activating factor receptor; CITE-seq, cellular indexing of transcriptomes and epitopes by sequencing; DEG, differentially expressed gene; FDR, false discovery rate; NF-κB, nuclear factor kappa-light-chain-enhancer of activated B cells; SLE, systemic lupus erythematosus. Color figure can be viewed in the online issue, which is available at http://onlinelibrary.wiley.com/doi/10.1002/art.70116/abstract.

response (FDR <0.05) (Figure 6A and Supplementary Table 4). Among these, CD4 TCMs and DN T cells had the highest number of significant genes, with 29 and 15, respectively. From permutation analysis, this is greater than expected by chance (empirical *P* value <0.05) (Supplementary Figure 12).

Of the 99 genes, 63 showed a greater, positive effect size in responders, whereas nonresponders showed smaller, negative changes (Figure 6B). Many DEGs were involved in cell cytotoxicity (*PRF1*, *GZMA*, *GZMK*), major histocompatibility complex class II antigen presentation (*HLA-DRA*, *HLA-DPB1*, *HLA-DPA1*), and T cell activation (*LGALS1*, *IL7R*, *CD74*, *CD70*, *CCL4*, *IRF1*, *IL2RA*, *ICOS*, *ANXA1*). Most of these genes had increased expression and a higher proportion of expressing cells in responders (Figure 6C). This suggested distinct transcriptomic changes in non-B cells depending on clinical response.

DISCUSSION

Through single-cell profiling, our longitudinal cohort revealed changes in immune cell dynamics following rituximab treatment in SLE. Rituximab led to significant early depletion of naïve and memory B cells while partially sparing antigen-experienced cells, especially in nonresponders. This was followed by repopulation by naïve and transitional B cells.

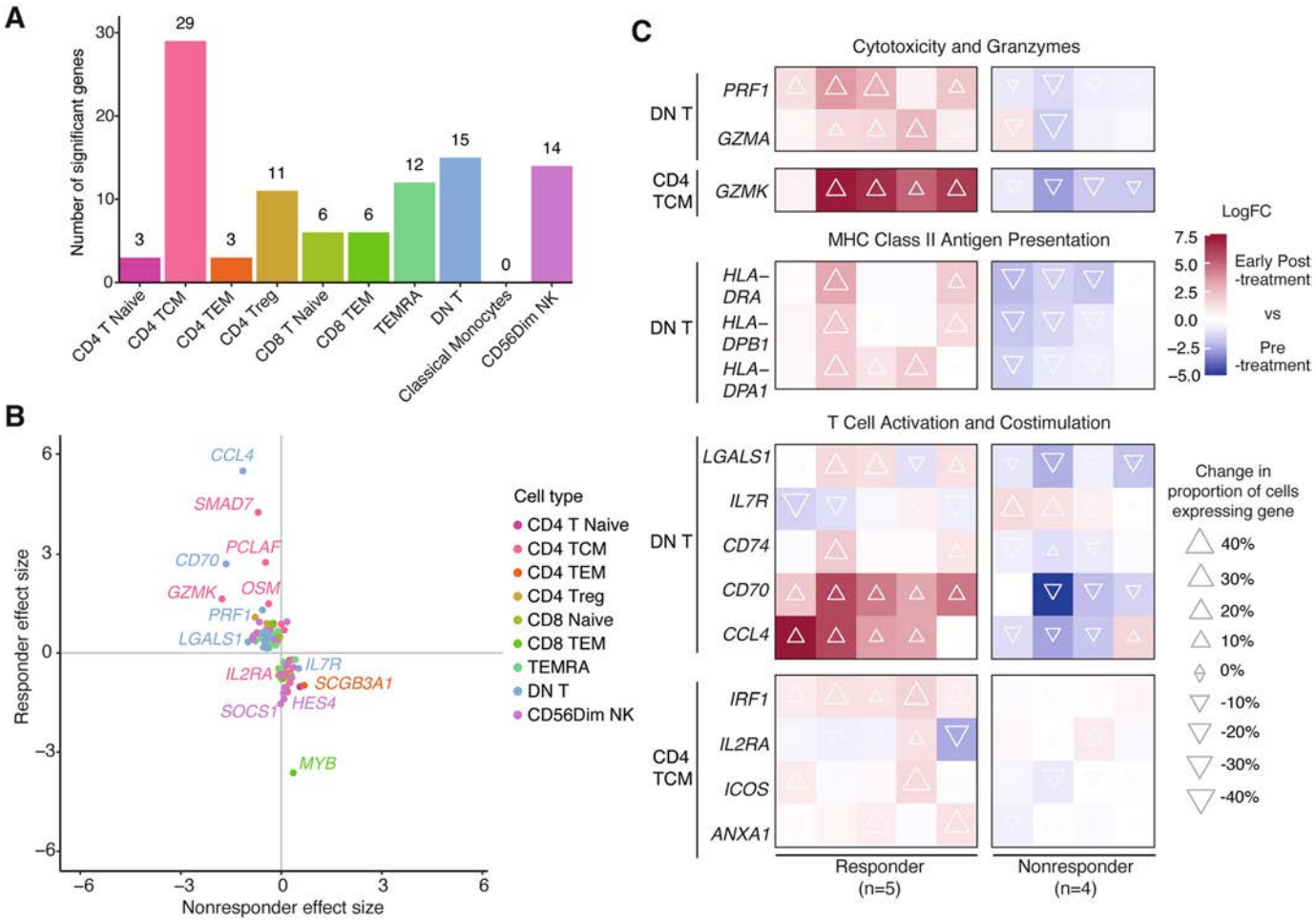

Figure 6. Gene expression changes interacting with rituximab response in non-B cells. (A) The number of significant genes in non-B cell subtypes where rituximab response status alters gene expression changes between pretreatment and early post-treatment (FDR < 0.05). Only cell types with at least 10 cells in all patients at both time points were analyzed. (B) Effect sizes of significant genes where response status modifies gene expression changes between pretreatment and early post-treatment. The *x*-axis shows the effect size in nonresponders, and the *y*-axis shows the effect size in responders. Each point represents a gene and is colored by the immune cell subtype in which it was significantly altered. (C) Significant genes in DN T cells and CD4 TCM cells that function in "cytotoxicity and granzymes", "MHC class II antigen presentation", and "T cell activation and costimulation." The fold changes in expression are shown as color, and changes in the proportion of cells expressing the gene are shown in triangle size and direction. Log_2FC was calculated from TMM normalized expression levels. Expression values were not adjusted for covariates that were included in the model for testing differential gene expression (patient and cellular detection rate). Gene function annotation was informed by Gene Ontology. DN, double negative; FDR, false discovery rate; MHC, major histocompatibility complex; TCM, CD4 T central memory; TMM, trimmed mean of M values. Color figure can be viewed in the online issue, which is available at http://onlinelibrary.wiley.com/doi/10.1002/art.70116/abstract.

This aligns with the changes previously reported by flow cytometry in Iwata et al.[32,33]

Rituximab also affected the BCR repertoire, with sequences at early post-treatment being more mutated, class-switched, and clonally expanded and with lower generation probabilities, as previously reported.[13,34] This contrasts with changes in the repertoire observed after CD19 CAR-T cell therapy, in which IgG and IgA expressing cells are almost completely depleted, and sequences post-treatment have higher generation probabilities.[12] The proportion of naïve B cells increased following CD19 CAR-T cell therapy[35] but decreased after rituximab treatment in both studies, which may explain some differences. Persistent B cell clones were also identified, which were enriched for mature memory and antibody secreting cells. This expands on previous findings in patients with SLE treated with rituximab,[13] and these clones share similar features to persistent clones identified in patients with myasthenia gravis receiving rituximab.[36] Such persistent clones could be a target for future studies to understand their association with treatment response, clinical manifestations, and autoantibody profiles.

The repertoire perturbations we observed are primarily driven by depletion and subsequent repopulation of transitional and naïve B cells, which represent the largest fraction of B cells. Their loss immediately after rituximab enriches for mutated, class-

switched sequences among the surviving antibody-producing cells, whereas their later repopulation restores repertoire diversity and generation probability toward baseline. In contrast, changes in smaller subsets such as ABCs and switched memory B cells may not be fully reflected in repertoire-wide diversity metrics. Overall, changes in the repertoire were not sustained over time, returning to baseline by late post-treatment.

We observed differences in IGHJ usage and CDR3 length between pretreatment patients with SLE and healthy controls that were specific to naïve and transitional cells (Figure 4F and G). Biased V(D)J usage, including for IGHJ genes, has been previously reported in SLE.[37] Certain V genes, including IGHV4-34, have also been implicated in SLE pathology,[38] but we found no significant differences in these genes. Both longer and shorter CDR3 lengths have also been reported in SLE.[13,39,40] Long CDR3 regions are associated with autoreactivity and are normally selected against during development.[41] These conflicting findings may be because of the cell populations sampled, with shorter CDR3 being reported in total B cells or naïve B cells, as in this study.

A small number of genes exhibited differential expression in non-B cells post-rituximab. Certain interferon pathway genes decreased in Treg, naïve CD8 T, effector memory CD8 T, DN T, and CD56Dim NK cells, but not globally. This contrasts with the broad decrease in interferon pathway genes in non-B cells after CAR-T cell mediated B cell depletion.[12] This may reflect differences in target cells ($CD20^+$ vs $CD19^+$) because antibody secreting cells ($CD20^-CD19^+$ plasma cells and plasmablasts) remaining after rituximab could activate the interferon pathway in non-B cells. Furthermore, CAR-T therapy may lead to B cell depletion in lymphoid organs, thus affecting a broader range of immune cells. It has also been associated with a greater down-regulation of Type I and II interferon responses across all PBMCs than that observed in whole blood following standard pharmacotherapy, including rituximab.[35]

The modest gene expression changes observed in non-B cells may also reflect divergent changes between responders and nonresponders, which could mask underlying effects in the pooled analysis. Indeed, our response-interaction analysis revealed more DEGs (99 vs 27 genes), suggesting that many transcriptional changes in non-B cells are response-associated rather than universal. Finally, the use of a conservative pseudobulk framework and stringent significance thresholds may have reduced sensitivity to subtle effects, particularly given the cohort size.

Using single-cell data, we were able to explore specific memory B cell subtypes, especially those that partially persisted through depletion, including ABCs. ABCs can contribute to autoimmune diseases by developing through TLR7/9 stimulation and producing autoantibodies and inflammatory cytokines.[42,43] In SLE, ABC frequency correlates with disease activity,[42,44] and their deletion in MRL.lpr lupus-prone mice suppresses disease.[45] A previous study demonstrated a significant reduction of ABCs ($CD11c^+CD21^-$) following rituximab.[46] In our study, ABCs were fully depleted in responders and remained lowly abundant for an extended period even when overall B cell abundance returned to pretreatment levels. In nonresponders, we saw incomplete depletion in two of four patients. This indicates that a fraction of antigen-experienced cells can persist despite rituximab, reflecting differences in localization or accessibility of B cell subsets. As a disease-relevant cell type, further studies will be needed to clarify how the dynamics of ABC depletion contribute to response to rituximab in SLE.

In our study, patients who responded to rituximab showed increased abundance of transitional B cells at late post-treatment, whereas the memory B cell compartment remained lowly abundant. This finding aligns with previous research characterizing B cell repopulation after rituximab, in which patients achieving full depletion had delayed repopulation and a B cell compartment primarily consisting of transitional B cells at 55 weeks.[47] Transitional B cells are immature precursors of naïve B cells and may play a regulatory role through the production of interleukin (IL)-10 and other cytokines.[48] Therefore, this alteration in the balance between transitional B cells and memory B cells may reflect the response to rituximab. However, transitional B cells producing high levels of proinflammatory cytokines, such as IL-6,[49] have been associated with disease activity in SLE and could potentially contribute to relapse.

In non-B cell populations, several genes showed response-dependent transcriptional changes following rituximab. Genes associated with T cell activation and cytotoxicity were up-regulated in responder CD4 CTMs and DN T cells. In SLE, DN T cells are known to be expanded and contribute to disease pathology by promoting autoantibody production, secreting cytokines such as IL-4, IL-17, and IFN-γ, and infiltrating target organs like the kidney.[50,51] DN T cells have also been reported to regulate B cell apoptosis and inhibit B cell proliferation and plasma cell differentiation.[52] Our analysis identified increased expression of *LGALS1* in responder DN T cells and decreased expression in nonresponders. This gene regulates B cell apoptosis and is linked to rituximab resistance in non-Hodgkin lymphoma.[53] These suggest that DN T cells may contribute to B cell apoptosis during rituximab-induced depletion.

Limitations to our study include the sample size and time points. A larger cohort would enable more comprehensive comparisons between responders and nonresponders at each time point, including cell type proportions and gene expression, while further adjusting for demographic and clinical heterogeneity. Additional time points would provide insight into specific response trajectories.

By conducting longitudinal single-cell sequencing, our study provides valuable insights into cellular changes from rituximab-induced B cell depletion and highlights the role of various immune cells in SLE pathogenesis.

ACKNOWLEDGMENTS

We thank James E. Peters for his valuable clinical insights and feedback, Rachael Bashford-Rogers for her assistance with BCR/TCR library preparation optimization, and Niek de Klein for his input on data quality control. We also acknowledge the use of ChatGPT (OpenAI) for writing support (rephrasing, improving grammar and clarity) during the preparation of this manuscript. We thank the patients and healthy volunteers who participated in the study and the support of the Community Partners of the Immunology Theme of the National Institute for Health and Care Research (NIHR) Imperial Biomedical Research Centre. We acknowledge the support of the health professionals in the Imperial Lupus Centre, Imperial College Healthcare NHS Trust. This research was supported by the NIHR Imperial Biomedical Research Centre. The views expressed are those of the authors and not necessarily those of the NIHR or the Department of Health and Social Care. For the purpose of Open Access, the author has applied a CC BY public copyright license to any Author Accepted Manuscript version arising from this submission.

AUTHOR CONTRIBUTIONS

All authors contributed to at least one of the following manuscript preparation roles: conceptualization AND/OR methodology, software, investigation, formal analysis, data curation, visualization, and validation AND drafting or reviewing/editing the final draft. As corresponding author, Drs Botto and Davenport confirm that all authors have provided the final approval of the version to be published and take responsibility for the affirmations regarding article submission (eg, not under consideration by another journal), the integrity of the data presented, and the statements regarding compliance with institutional review board/Declaration of Helsinki requirements.

REFERENCES

1. Dörner T, Giesecke C, Lipsky PE. Mechanisms of B cell autoimmunity in SLE. Arthritis Res Ther 2011;13(5):243. doi:https://doi.org/10.1186/ar3433
2. Zavaleta-Monestel E, Arrieta-Vega D, Rojas-Chinchilla C, et al. Advances in systemic lupus erythematosus treatment with monoclonal antibodies: a mini-review. Cureus 2024;16(7):e64090. doi:https://doi.org/10.7759/cureus.64090
3. Rydén-Aulin M, Boumpas D, Bultink I, et al. Off-label use of rituximab for systemic lupus erythematosus in Europe. Lupus Sci Med 2016;3(1):e000163. doi:https://doi.org/10.1136/lupus-2016-000163
4. Merrill JT, Neuwelt CM, Wallace DJ, et al. Efficacy and safety of rituximab in moderately-to-severely active systemic lupus erythematosus: the randomized, double-blind, phase II/III systemic lupus erythematosus evaluation of rituximab trial. Arthritis Rheum 2010;62(1):222–233. doi:https://doi.org/10.1002/art.27233
5. Rovin BH, Furie R, Latinis K, et al; LUNAR Investigator Group. Efficacy and safety of rituximab in patients with active proliferative lupus nephritis: the Lupus Nephritis Assessment with Rituximab study. Arthritis Rheum 2012;64(4):1215–1226. doi:https://doi.org/10.1002/art.34359
6. Thatayatikom A, White AJ. Rituximab: a promising therapy in systemic lupus erythematosus. Autoimmun Rev 2006;5(1):18–24. doi:https://doi.org/10.1016/j.autrev.2005.05.006
7. Tur C, Eckstein M, Velden J, et al. CD19-CAR T-cell therapy induces deep tissue depletion of B cells. Ann Rheum Dis 2025;84(1):106–114. doi:https://doi.org/10.1136/ard-2024-226142
8. Furie RA, Aroca G, Cascino MD, et al. B-cell depletion with obinutuzumab for the treatment of proliferative lupus nephritis: a randomised, double-blind, placebo-controlled trial. Ann Rheum Dis 2022;81(1):100–107. doi:https://doi.org/10.1136/annrheumdis-2021-220920
9. Reddy V, Martinez L, Isenberg DA, et al. Pragmatic treatment of patients with systemic lupus erythematosus with rituximab: long-term effects on serum immunoglobulins. Arthritis Care Res (Hoboken) 2017;69(6):857–866. doi:https://doi.org/10.1002/acr.22993
10. Robinson JI, Md Yusof MY, Davies V, et al; MATURA Consortia; MASTERPLANS Consortia. Comprehensive genetic and functional analyses of Fc gamma receptors influence on response to rituximab therapy for autoimmunity. EBioMedicine 2022;86:104343. doi:https://doi.org/10.1016/j.ebiom.2022.104343
11. Carter LM, Alase A, Wigston Z, et al; MASTERPLANS Consortium. Gene expression and autoantibody analysis revealing distinct ancestry-specific profiles associated with response to rituximab in refractory systemic lupus erythematosus. Arthritis Rheumatol 2023;75(5):697–710. doi:https://doi.org/10.1002/art.42404
12. Wilhelm A, Chambers D, Müller F, et al. Selective CAR T cell–mediated B cell depletion suppresses IFN signature in SLE. JCI Insight 2024;9(12):e179433. doi:https://doi.org/10.1172/jci.insight.179433
13. Bashford-Rogers RJM, Bergamaschi L, McKinney EF, et al. Analysis of the B cell receptor repertoire in six immune-mediated diseases. Nature 2019;574(7776):122–126. doi:https://doi.org/10.1038/s41586-019-1595-3
14. Vander Heiden JA, Yaari G, Uduman M, et al. pRESTO: a toolkit for processing high-throughput sequencing raw reads of lymphocyte receptor repertoires. Bioinformatics 2014;30(13):1930–1932. doi:https://doi.org/10.1093/bioinformatics/btu138
15. Ye J, Ma N, Madden TL, et al. IgBLAST: an immunoglobulin variable domain sequence analysis tool. Nucleic Acids Res 2013;41(Web Server issue):W34–W40. doi:https://doi.org/10.1093/nar/gkt382
16. Gayoso A, Steier Z, Lopez R, et al. Joint probabilistic modeling of single-cell multi-omic data with totalVI. Nat Methods 2021;18(3):272–282. doi:https://doi.org/10.1038/s41592-020-01050-x
17. Traag VA, Waltman L, van Eck NJ. From Louvain to Leiden: guaranteeing well-connected communities. Sci Rep 2019;9(1):5233. doi:https://doi.org/10.1038/s41598-019-41695-z
18. Dann E, Henderson NC, Teichmann SA, et al. Differential abundance testing on single-cell data using k-nearest neighbor graphs. Nat Biotechnol 2022;40(2):245–253. doi:https://doi.org/10.1038/s41587-021-01033-z
19. Sethna Z, Elhanati Y, Callan CG Jr, et al. OLGA: fast computation of generation probabilities of B- and T-cell receptor amino acid sequences and motifs. Bioinformatics 2019;35(17):2974–2981. doi:https://doi.org/10.1093/bioinformatics/btz035
20. James G. R., J. Ellison, C. & P. Crutchfield, J. dit: a Python package for discrete information theory. J Open Source Softw 2018;3:738. doi:https://doi.org/10.21105/joss.00738
21. Gupta NT, Vander Heiden JA, Uduman M, et al. Change-O: a toolkit for analyzing large-scale B cell immunoglobulin repertoire sequencing data. Bioinformatics 2015;31(20):3356–3358. doi:https://doi.org/10.1093/bioinformatics/btv359
22. Robinson MD, McCarthy DJ, Smyth GK. edgeR: a Bioconductor package for differential expression analysis of digital gene expression data. Bioinformatics 2010;26(1):139–140. doi:https://doi.org/10.1093/bioinformatics/btp616
23. Soneson C, Robinson MD. Bias, robustness and scalability in single-cell differential expression analysis. Nat Methods 2018;15(4):255–261. doi:https://doi.org/10.1038/nmeth.4612
24. Wolf FA, Angerer P, Theis FJ. SCANPY: large-scale single-cell gene expression data analysis. Genome Biol 2018;19(1):15. doi:https://doi.org/10.1186/s13059-017-1382-0
25. Milacic M, Beavers D, Conley P, et al. The Reactome Pathway Knowledgebase 2024. Nucleic Acids Res 2024;52(D1):D672–D678. doi:https://doi.org/10.1093/nar/gkad1025

26. Schubert M, Klinger B, Klünemann M, et al. Perturbation-response genes reveal signaling footprints in cancer gene expression. Nat Commun 2018;9(1):20. doi:https://doi.org/10.1038/s41467-017-02391-6
27. Badia-I-Mompel P, Vélez Santiago J, Braunger J, et al. decoupleR: ensemble of computational methods to infer biological activities from omics data. Bioinform Adv 2022;2(1):vbac016. doi:https://doi.org/10.1093/bioadv/vbac016
28. Sims GP, Ettinger R, Shirota Y, et al. Identification and characterization of circulating human transitional B cells. Blood 2005;105(11):4390–4398. doi:https://doi.org/10.1182/blood-2004-11-4284
29. Rönnblom L, Leonard D. Interferon pathway in SLE: one key to unlocking the mystery of the disease. Lupus Sci Med 2019;6(1):e000270. doi:https://doi.org/10.1136/lupus-2018-000270
30. Sollis E, Mosaku A, Abid A, et al. The NHGRI-EBI GWAS Catalog: knowledgebase and deposition resource. Nucleic Acids Res 2023;51(D1):D977–D985. doi:https://doi.org/10.1093/nar/gkac1010
31. Gardam S, Brink R. Non-canonical NF-κB signaling initiated by BAFF influences B cell biology at multiple junctures. Front Immunol 2014;4:509. doi:https://doi.org/10.3389/fimmu.2013.00509
32. Iwata S, Saito K, Tokunaga M, et al. Phenotypic changes of lymphocytes in patients with systemic lupus erythematosus who are in long-term remission after B cell depletion therapy with rituximab. J Rheumatol 2011;38(4):633–641. doi:https://doi.org/10.3899/jrheum.100729
33. Iwata S, Saito K, Tokunaga M, et al. B cell or T cell-dominant recurrence after rituximab therapy in patients with SLE. Ann Rheum Dis 2012;71(10):1749–1750. doi:https://doi.org/10.1136/annrheumdis-2012-201317
34. Rouzière A-S, Kneitz C, Palanichamy A, et al. Regeneration of the immunoglobulin heavy-chain repertoire after transient B-cell depletion with an anti-CD20 antibody. Arthritis Res Ther 2005;7(4):R714–R724. doi:https://doi.org/10.1186/ar1731
35. Garantziotis P, Beretta L, Lindblom J, et al. Differential molecular signatures in response to CD19-CAR T cell therapy compared with conventional pharmacotherapy in systemic lupus erythematosus. Ann Rheum Dis 2026;85(1):153–163. doi:https://doi.org/10.1136/ard.2025.06.2132
36. Jiang R, Fichtner ML, Hoehn KB, et al. Single-cell repertoire tracing identifies rituximab-resistant B cells during myasthenia gravis relapses. JCI Insight 2020;5(14):5. doi:https://doi.org/10.1172/jci.insight.136471
37. Ota M, Nakano M, Nagafuchi Y, et al. Multimodal repertoire analysis unveils B cell biology in immune-mediated diseases. Ann Rheum Dis 2023;82(11):1455–1463. doi:https://doi.org/10.1136/ard-2023-224421
38. Richardson C, Chida AS, Adlowitz D, et al. Molecular basis of 9G4 B cell autoreactivity in human systemic lupus erythematosus. J Immunol 2013;191(10):4926–4939. doi:https://doi.org/10.4049/jimmunol.1202263
39. Liu S, Hou XL, Sui WG, et al. Direct measurement of B-cell receptor repertoire's composition and variation in systemic lupus erythematosus. Genes Immun 2017;18(1):22–27. doi:https://doi.org/10.1038/gene.2016.45
40. Yurasov S, Wardemann H, Hammersen J, et al. Defective B cell tolerance checkpoints in systemic lupus erythematosus. J Exp Med 2005;201(5):703–711. doi:https://doi.org/10.1084/jem.20042251
41. Meffre E, Milili M, Blanco-Betancourt C, et al. Immunoglobulin heavy chain expression shapes the B cell receptor repertoire in human B cell development. J Clin Invest 2001;108(6):879–886. doi:https://doi.org/10.1172/JCI13051
42. Jenks SA, Cashman KS, Zumaquero E, et al. Distinct effector B cells induced by unregulated toll-like receptor 7 contribute to pathogenic responses in systemic lupus erythematosus. Immunity 2018;49(4):725–739.e6. doi:https://doi.org/10.1016/j.immuni.2018.08.015
43. Mouat IC, Goldberg E, Horwitz MS. Age-associated B cells in autoimmune diseases. Cell Mol Life Sci 2022;79(8):402. doi:https://doi.org/10.1007/s00018-022-04433-9
44. Jacobi AM, Reiter K, Mackay M, et al. Activated memory B cell subsets correlate with disease activity in systemic lupus erythematosus: delineation by expression of CD27, IgD, and CD95. Arthritis Rheum 2008;58(6):1762–1773. doi:https://doi.org/10.1002/art.23498
45. Nickerson KM, Smita S, Hoehn KB, et al. Age-associated B cells are heterogeneous and dynamic drivers of autoimmunity in mice. J Exp Med 2023;220(5):220. doi:https://doi.org/10.1084/jem.20221346
46. Faustini F, Sippl N, Ståhlesen R, et al. Rituximab in systemic lupus erythematosus: transient effects on autoimmunity associated lymphocyte phenotypes and implications for immunogenicity. Front Immunol 2022;13:826152. doi:https://doi.org/10.3389/fimmu.2022.826152
47. Sutter JA, Kwan-Morley J, Dunham J, et al. A longitudinal analysis of SLE patients treated with rituximab (anti-CD20): factors associated with B lymphocyte recovery. Clin Immunol 2008;126(3):282–290. doi:https://doi.org/10.1016/j.clim.2007.11.012
48. Nova-Lamperti E, Fanelli G, Becker PD, et al. IL-10-produced by human transitional B-cells down-regulates CD86 expression on B-cells leading to inhibition of CD4+T-cell responses. Sci Rep 2016;6(1):20044. doi:https://doi.org/10.1038/srep20044
49. Liu M, Guo Q, Wu C, et al. Type I interferons promote the survival and proinflammatory properties of transitional B cells in systemic lupus erythematosus patients. Cell Mol Immunol 2019;16(4):367–379. doi:https://doi.org/10.1038/s41423-018-0010-6
50. Crispín JC, Oukka M, Bayliss G, et al. Expanded double negative T cells in patients with systemic lupus erythematosus produce IL-17 and infiltrate the kidneys. J Immunol 2008;181(12):8761–8766. doi:https://doi.org/10.4049/jimmunol.181.12.8761
51. Poddighe D, Dossybayeva K, Kozhakhmetov S, et al. Double-negative T (DNT) cells in patients with systemic lupus erythematosus. Biomedicines 2024;12(1):12. doi:https://doi.org/10.3390/biomedicines12010166
52. Hu S-H, Zhang LH, Gao J, et al. NKG2D enhances double-negative T cell regulation of B cells. Front Immunol 2021;12:650788. doi:https://doi.org/10.3389/fimmu.2021.650788
53. Lykken JM, Horikawa M, Minard-Colin V, et al. Galectin-1 drives lymphoma CD20 immunotherapy resistance: validation of a preclinical system to identify resistance mechanisms. Blood 2016;127(15):1886–1895. doi:https://doi.org/10.1182/blood-2015-11-681130

American College of Rheumatology
Empowering Rheumatology Professionals

Arthritis & Rheumatology
Vol. 78, No. 9, September 2026, pp 1920–1928
DOI 10.1002/art.70101
© 2026 American College of Rheumatology

Prognosis and Long-Term Outcome of Stenotic Large Vessel Involvement in Giant Cell Arteritis

Georgina Maalouf, MD, MPH,[1] Bérangère Arnould, MD,[2] Olivier Espitia, MD, PhD,[3] Hubert Deboysson, MD, PhD,[4] Maxime Samson, MD, PhD,[5] Arnaud Hot, MD, PhD,[6] Eric Liozon, MD,[7] Simon Parreau, MD,[8] Christian Lavigne, MD,[9] Valentin Lacombe, MD, PhD,[9] Jean-Francois Alexandra, MD,[10] Thomas Thibault, MD,[5] Laurent Chiche, MD, PhD,[11] Julien Gaudric, MD, PhD,[11] Alban Redheuil, MD, PhD,[12] Matheus Vieira, MD, PhD,[1] Matthieu Groh, MD,[13] Cécile-Audrey Durel, MD,[6] Thibaud Chazal, MD,[14] Chloé Comarmond, MD, PhD,[15] Nadine Magy-Bertrand, MD, PhD,[16] Stéphane Vinzio, MD,[17] Lionel Martzolff, MD,[18] Pierre Lozac'h, MD,[19] Rodérau Outh, MD, PhD,[20] Jérémy Clément, MD,[21] Pierre Duffau, MD,[22] Anael Dumont, MD,[4] Sebastien Humbert, MD,[23] Constance Guillaud, MD,[24] Azeddine Dellal, MD,[25] Grégory Pugnet, MD, PhD,[26] Valérie Devauchelle-Pensec, MD, PhD,[27] Patrice Cacoub, MD, MsC,[1] Lucie Biard, MD, PhD,[28] and David Saadoun, MD, PhD,[1] on behalf of the GEFA (French Study Group for Large Vessel Vasculitis)

Objective. Large vessel-vasculitis (LVV) accounts for up to 70% of patients with giant cell arteritis (GCA). Stenotic involvement in GCA-LVV remains largely unknown. The purpose of this study was to assess the long-term outcome and prognosis of GCA with stenotic LVV.

Methods. This was a retrospective multicenter study of 3,149 patients with GCA, including 198 (6.3%) with stenotic LVV. Hierarchical clustering on principal components was performed on baseline arterial localizations and logistic regression assessed factors associated with vascular complications.

Results. Stenotic LVV affected mostly the subclavian artery (63%), the carotid artery (58%), vertebral artery (37%), and axillary artery (33%), followed by the femoral artery (30%) and mesenteric arteries (13%). Stroke (31%) was the main complication, followed by limb ischemia (21%), myocardial infarction (4%), and mesenteric ischemia (2%). Cumulative incidence of vascular complications was 13.1% (95% confidence interval [CI] 8.9–18.3), 17.3% (95% CI 12.3–22.9), and 19.5% (95% CI 14.3–25.4), at 1, 5, and 10 years, respectively. Hierarchical clustering analysis identified three clusters among which cluster 1 (n = 123; 62%) included older patients with more arteritic anterior ischemic optic neuropathy ($P = 0.04$), vertebral artery stenosis, and a higher mortality rate ($P < 0.044$). In multivariate analysis, age at diagnosis (hazard ratio [HR] 1.06, 95% CI 1.03–1.10; $P = 0.0004$) and vertebral involvement (HR 1.87, 95% CI 1.03–3.40; $P = 0.039$) were significantly associated with higher risk of vascular complication.

Conclusion. Stenotic LVV accounts for less than 10% of GCA and is associated with poor vascular prognosis.

INTRODUCTION

Giant cell arteritis (GCA) is the most common vasculitis, affecting large sized vessels, including the aorta and its branches.[1] Large vessel-vasculitis (LVV) is described in 30% to 83% of patients with GCA.[2–4] The inflammatory involvement of the aorta and its branches in patients with GCA was detected in necropsies during late 1930s and early 1940s.[5] The clinical

[1]Sorbonne Universités AP-HP, Groupe Hospitalier Pitié-Salpêtrière, Département de Médecine Interne et Immunologie Clinique, F-75013, and Centre National de Références Maladies Autoimmunes Systémiques Rares, Centre National de Références Maladies Autoinflammatoires et Amylose Inflammatoire (CEREMAIA), Inflammation-Immunopathology-Biotherapy Department (DMU 3iD), CIC Biotherapy, INSERM 959, Groupe Hospitalier Pitié Salpetriere, AP-HP, Paris, France; [2]Department of Internal Medicine, CHU Rouen, Rouen, France; [3]Department of Vascular Medicine, CHU Nantes, Nantes, France; [4]Department of Internal Medicine, CHU Caen, Caen, France; [5]Internal Medicine and Systemic Disease Unit, CHU Dijon, Dijon, Burgundy, France; [6]Department of Internal Medicine, Hôpital Edouard-Herriot, Lyon, France; [7]Department of Internal Medicine, CHU Limoges, Limoges, France; [8]Department of Internal Medicine, Hôpital Dupuytren, Limoges, France; [9]Médecine interne et polyvalente, CH du Haut-Anjou, Chateau-Gontier; Médecine interne, CHU d'Angers; [10]Department de Médecine Interne-Immunologie Clinique, CHU d'Angers, Angers, France, Centre National de Référence Maladies Autoimmunes Systémiques Rares CeRAINOM-Angers; [11]Department of Vascular Surgery, Groupe Hospitalier Pitié-Salpêtrière, Assistance Publique-Hôpitaux de Paris, Paris, France; [12]Department of Vascular and Interventional Radiology, Groupe Hospitalier Pitié-Salpêtrière, Assistance Publique-Hôpitaux de Paris, Paris, France; [13]Department of Internal Medicine, Hôpital Foch, Suresnes, France; [14]Department of Internal Medicine, Hôpital Fondation Adolphe-de-Rothschild, Paris, France; [15]Department of Internal Medicine, Hôpital Lariboisière, Assistance Publique-Hôpitaux de Paris, Paris, France;

relevance and consequences of this aortic inflammation were first recognized by Evans et al,[6] who reported that patients with GCA were 2.4 and 17.3 times more likely to develop abdominal and thoracic aortic aneurysms than the general population, respectively. Aortic artery branch involvement is asymptomatic unless vascular remodeling leads to marked stenosis with significant reduction in blood flow.[7–9] Reported symptoms occur in around 3% to 13% of patients with GCA and range from stroke, limb claudication, transient distal ischemia resembling Raynaud phenomenon, and limb, renal, mesenteric and/or coronary ischemia.[7,9]

Stenotic involvement of the aortic arch and superior branches, such as the subclavian axillary and carotid and vertebral arteries, predominates in patients with GCA,[10] but it may also involve mesenteric, renal, and coronary vessels and the lower limbs, although this is less well-described.[11,12] Estimates of the incidence of large-artery stenosis in GCA have ranged from 18% to 21% for arm arteries, to 9% to 14% for any large-artery complication, to 7% for cerebrovascular ischemia.[9,13] Stenotic lesions resulting in vascular complications, such as stroke and limb ischemia, may expose patients to vascular procedures.[14] LVV in GCA is associated with higher mortality, a potentially greater risk of relapse, and a higher cumulative dose of glucocorticoids.[15] Data on stenotic involvement in GCA-LVV are scarce, and the long-term evolution of these patients is poorly defined. In this French nationwide retrospective study, we aimed to report on the long-term outcome and prognostic factors of patients with GCA with stenotic LVV.

PATIENTS AND METHODS

Ethical approval. In accordance with French public health law (Articles L1121–1-1 and L1121–1-2), written consent from the patient was not required for this type of retrospective study.

Study population. We conducted a retrospective multicenter study in tertiary centers from the GEFA (French Study Group for Large Vessel Vasculitis) and made a nationwide call for observations. We identified 3,149 patients with GCA diagnosed between January 1999 and December 2023. Patients were included if they satisfied the following criteria: 1) a diagnosis of GCA according to the American College of Rheumatology (ACR)/EULAR 2022 criteria[16] with a minimum score of six points; 2) stenosis (≥50% of arterial stenosis with circumferential wall thickening) of the aorta or of its branches, supra-aortic trunks, or lower limbs arteries; 3) follow-up of at least six months.

We identified 198 (6.3%) patients with GCA with stenotic LVV from a database of 3,149 patients with GCA (Figure 1). Baseline arterial localization was described as follows: supra-aortic trunks (subclavian, vertebral, axillary, carotid, and brachiocephalic arteries), aorta, mesenteric, and lower limbs (iliac and femoral arteries), and degree of stenosis (50–70%, >70% and occluded).

We reviewed the electronic medical records of all patients. Baseline characteristics (including age at diagnosis of LVV, sex, cardiovascular risk factors, constitutional symptoms, symptoms of stenotic LVV, and topography of arterial lesions), biologic markers of inflammation (C-reactive protein level at diagnosis and follow-up), imaging features (computed tomography angiography, magnetic resonance angiography, and/or fluorodeoxyglucose positron emission tomography [FDG-PET]) at baseline and during follow-up, treatments (glucocorticoids, conventional and biologic disease-modifying antirheumatic drugs, antiplatelet therapy, statins), and outcomes (vascular complications, vascular revascularization, and death) were collected retrospectively.

Definition of study endpoints. Vascular complications related to stenotic involvement in GCA-LVV were defined as the occurrence of at least one of the following events: occurrence of stroke/transitory ischemia attack, coronary syndrome, limb ischemia, and renal or mesenteric ischemia. Revascularization was defined as the occurrence of aortic, carotid, vertebral subclavian, renal, coronary mesenteric, or limb artery vascular surgery or endovascular procedure in these arteries for stenotic involvement related to GCA-LVV. Relapses were defined according to the 2018 update of the EULAR recommendation for the management of large vessel vasculitis.[17] Major relapses were defined as the recurrence of active disease with either of the following: clinical features of ischemia (including visual symptoms, visual loss attributable to GCA, scalp necrosis, stroke, limb claudication, jaw claudication), evidence of active aortic inflammation resulting in progressive aortic or large vessel dilatation, stenosis, or dissection. Minor relapses were defined as the recurrence of active disease not fulfilling the criteria for a major relapse.

[16]Department of Internal Medicine, CHRU Jean-Minjoz, Besançon, France; [17]Department of Internal Medicine, Groupe Hospitalier Mutualiste de Grenoble, Grenoble, France; [18]Department of Internal Medicine, Groupe Hospitalier Région Mulhouse et Sud Alsace, Hôpital Emile-Muller, Mulhouse, France; [19]Department of Internal Medicine, CH Le Mans, Le Mans, France; [20]Department of Internal Medicine, CHU Grabiel-Montpied, Clermont-Ferrand, France; [21]Department of Internal Medicine, CH de Blois, Blois, France; [22]Department of Internal Medicine, CHU de Bordeaux, Bordeaux, France; [23]Department of Internal medicine, Centre Hospitalier Louis Pasteur, Dole, France; [24]Department of Internal Medicine, Hôpital Henri-Mondor, Créteil, France; [25]Department of Rheumatology, GHJ Le Raincy-Montfermeil, Montfermeil, France; [26]Department of Internal Medicine and Clinical Immunology, CHU Rangueil, Toulouse, France; [27]Department of Rheumatology, Hôpital de La Cavale-Blanche, Brest, France; [28]Department of Biostatistics, Hôpital Saint Louis, Paris.

Drs Maalouf and Arnould are co-first authors and contributed equally to this work.

Author disclosures and graphical abstract are available at https://onlinelibrary.wiley.com/doi/10.1002/art.70101.

Address correspondence via email to David Saadoun, MD, PhD, at david.saadoun@aphp.fr.

Submitted for publication October 20, 2025; accepted in revised form February 2, 2026.

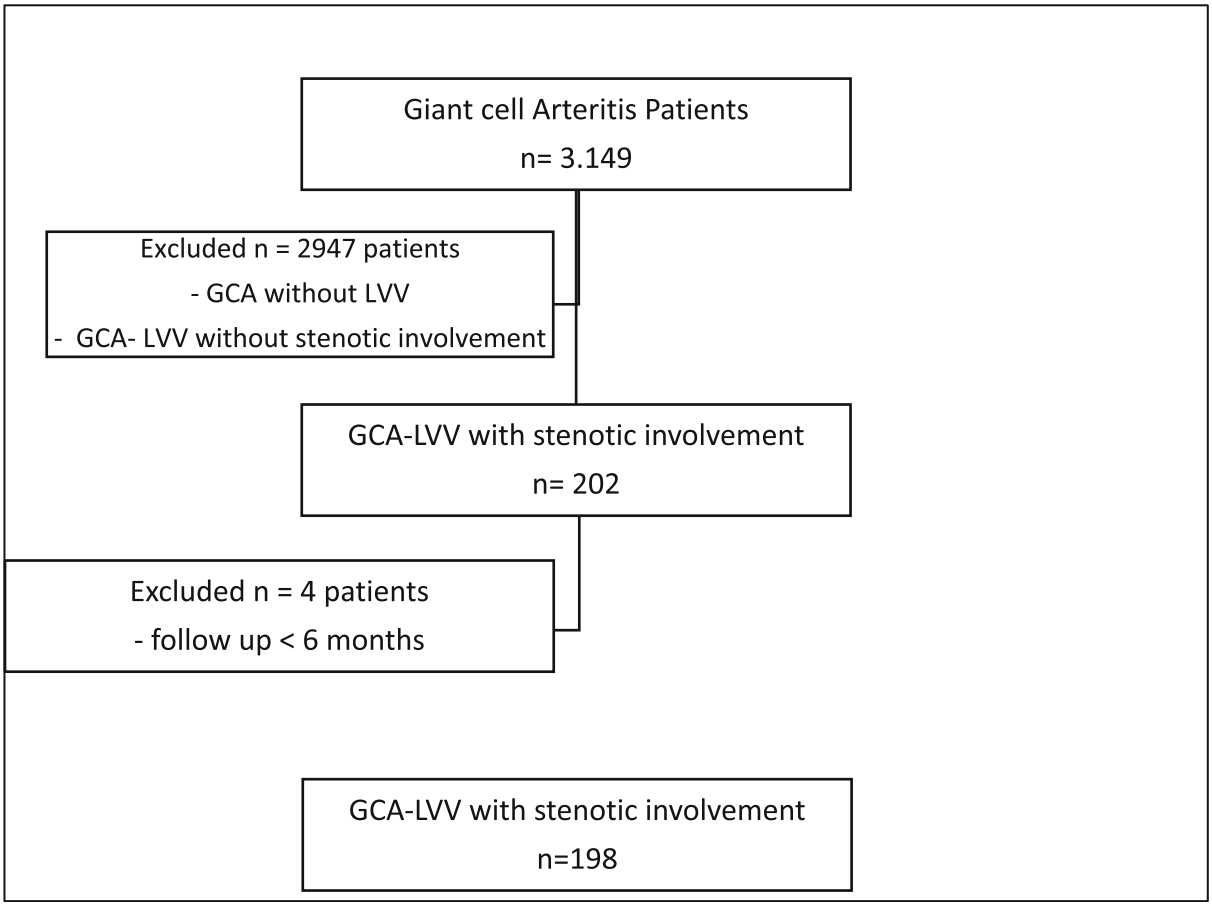

Figure 1. Study flow chart. GCA, giant cell arteritis; LVV, large vessel-vasculitis.

Statistical analysis. Categorical variables are described with n (%) and quantitative variables with median (IQR). Vascular-complication time-to-event endpoints were defined from the date of vasculitis diagnosis to the date of each complication (separate endpoint) or the date of the first complication (composite endpoint). The vascular-procedure time-to-event endpoint was defined from the date of vasculitis diagnosis to the date of the first procedure. For complication and procedure time-to-event endpoints, observations were censored at the end of follow-up when there was no event; death without the studied event was considered a competing event. Cumulative incidences of vascular outcomes were computed using standard methodology.[18] Overall survival was computed using the time from the date of vasculitis diagnosis to the date of death or last follow-up while living, using the Kaplan-Meier estimator. For time to vascular complication and time to any relapse, an adjusted multivariable model was selected based on a *P* value lower than 0.05 in univariate analysis. Clusters were identified using a hierarchical tree clustering approach on a multiple correspondence analysis of baseline arterial localizations (cluster partition criterion: relative loss of inertia). Analyses were performed on R statistical platform, version 4.4.2. The data that support the findings of this study are available from the corresponding author on request.

RESULTS

Characteristics of the study population. The main clinical and demographic characteristics of the 198 patients with stenotic LVV are presented in Table 1. The median age at diagnosis was 72 years (IQR 65–78), and 142 patients were women (72%). More than a third of the patients presented at least one cardiovascular risk factor, such as hypertension (53%), dyslipidemia (30%), and smoking (32%). The median ACR/EULAR 2022 classification criteria[16] score was 12 points (IQR 10–15). Cranial manifestations, such as a new temporal headache or abnormal temporal artery examination, were present in 55% and 13% of the patients, respectively. Ischemic clinical manifestations at diagnosis included 62 (31%) patients presenting a stroke, 64 (32%) with limb claudication, 26 (13%) with arteritic anterior ischemic optic neuropathy, 10 (5%) with central retinal artery occlusion, 9 (5%) with thoracic angina, and 3 (2%) with mesenteric angina (Table 1). Most patients (97%) had biologic inflammation with

Table 1. Main characteristics of the 198 patients and different clusters at diagnosis*

Baseline characteristics	All patients (N = 198)	Cluster 1 (N = 123)	Cluster 2 (N = 54)	Cluster 3 (N = 21)	*P* value
Age at diagnosis, median (IQR)	72 (65–78)	73 (67–79)	67 (62–76)	68 (65–76)	0.028
Female, n (%)	142 (72)	85 (69)	41 (76)	16 (76)	0.63
Cardiovascular risk factors					
Smoking, n (%)	63 (32)	37 (30)	20 (37)	6 (29)	0.61
Hypertension, n (%)	104 (53)	73 (59)	23 (43)	8 (38)	0.046
Dyslipidemia, n (%)	59 (30)	41 (33)	14 (26)	4 (19)	0.35
Median BMI, median (IQR)	23 (21–26)	23 (21–26)	23 (21–26)	25 (19–28)	0.94
Ischemic manifestations, n (%)					
Stroke/TIA	62 (31)	47 (38)	11 (20)	4 (19)	0.03
Limb claudication	64 (32)	33 (27)	22 (41)	9 (43)	0.1
Sudden visual loss	56 (28)	44 (36)	5 (9)	7 (33)	0.0006
Arteritic anterior ischemic optic neuropathy	26 (13)	22 (18)	3 (6)	1 (5)	0.04
Thoracic angina	9 (5)	4 (3)	2 (4)	3 (14)	0.1
Mesenteric angina	3 (2)	2 (2)	0 (0)	1 (5)	0.31
Cephalic manifestations, n (%)					
Jaw or tongue claudication	46 (23)	37 (30)	7 (13)	2 (10)	0.21
New temporal headache	108 (55)	73 (59)	25 (46)	10 (48)	0.23
Scalp tenderness	40 (20)	30 (24)	8 (15)	2 (10)	0.015
Systemic manifestations, n (%)					
Asthenia	108 (55)	63 (51)	28 (52)	17 (81)	0.036
Night sweats	18 (9)	7 (6)	5 (9)	10 (48)	0.23
Weight loss	84 (42)	53 (43)	21 (39)	3 (14)	0.85
Fever	24 (12)	14 (11)	7 (13)	6 (29)	0.009
Polymyalgia rheumatica, n (%)	79 (40)	55 (45)	19 (35)	5 (24)	0.14
ESR > 50 mm/h or CRP > 10 mg/L, n (%)	170 (97)	111 (99)	42 (93)	17 (89)	0.03
FDG-PET activity throughout aorta,[a] n (%)	65 (34)	15 (12)	38 (70)	12 (60)	<0.001
Positive temporal artery biopsy or halo sign on ultrasound, n (%)	119 (88)	82 (88)	24 (86)	13 (93)	0.84
Topography of vascular inflammatory lesions, n (%)					
Supra-aortic trunks					
Subclavian artery	125 (63)	58 (47)	47 (87)	20 (95)	<0.0001
Carotid artery	114 (58)	55 (45)	43 (80)	16 (76)	<0.0001
Vertebral artery	73 (37)	51 (41)	17 (31)	5 (24)	0.2
Axillary artery	66 (33)	26 (21)	26 (48)	14 (67)	<0.0001
Brachiocephalic artery	50 (25)	10 (8)	29 (54)	11 (52)	<0.0001
Aorta, n (%)					
Ascending aorta	57 (29)	5 (4)	41 (76)	11 (52)	<0.0001
Aortic arch	51 (26)	1 (1)	38 (70)	12 (57)	<0.0001
Descending aorta	72 (36)	10 (8)	43 (80)	19 (90)	<0.0001
Abdominal aorta	58 (29)	8 (7)	33 (61)	17 (81)	<0.0001
Renal arteries, n (%)	16 (8)	3 (2)	0 (0)	13 (62)	<0.0001
Celiac trunk, n (%)	23 (12)	5 (4)	1 (2)	17 (81)	<0.0001
Iliac arteries, n (%)	34 (17)	8 (7)	15 (28)	11 (52)	<0.0001
Femoral arteries, n (%)	59 (30)	28 (23)	20 (37)	11 (52)	0.009

* BMI, body mass index; CRP, C-reactive protein; ESR, erythrocyte sedimentation rate; IQR, interquartile range; FDG-PET, fluorodeoxyglucose positron emission tomography; TIA, transient ischemic attack.
[a] PET scan results were positive when ^{18}F-Fluorodeoxyglucose uptake was grade 2 or greater in any large vessel.

elevated C-reactive protein or erythrocyte sedimentation rate levels at diagnosis.

Stenotic lesions at diagnosis were predominantly located on the supra-aortic trunks (84%) (subclavian artery [63%], carotid artery [58%], vertebral artery [37%], axillary artery [33%], and brachiocephalic artery [25%]) followed by lower limbs (26%) and mesenteric arteries (13%). More than half of the stenotic arteries were occluded. Medical treatments of stenotic aortitis included glucocorticoids for most patients (n = 189; 95%). Among them, 52 patients (26%) received intravenous boluses, and 57 patients (29%) received immunosuppressive therapies such as methotrexate (n = 17; 9%) and tocilizumab (n = 35; 18%).

Hierarchical clustering analysis on baseline arterial localizations. Using a hierarchical tree clustering approach based on multiple correspondence analysis on baseline arterial

localizations, three different clusters were identified in our cohort (Figure 2 and Tables 1 and 2).

Patients in cluster 1 (n = 123; 62%) were older, with a median age of 73 years (IQR 67–79; $P = 0.028$). They showed a higher prevalence of stroke at diagnosis (38%, $P = 0.03$), visual loss with amaurosis (36%, $P = 0.0006$), arteritic anterior ischemic optic neuropathy (AAION) (18%, $P = 0.040$), and elevated markers of inflammation (99%, $P = 0.030$) compared with the other clusters (Table 1). Vascular lesions found in this cluster were less frequent than the other two clusters across all anatomic locations, except for the vertebral artery (41%, $P = 0.2$).

In contrast, cluster 2 (n = 54; 27%) comprised patients with pan-aortic involvement. FDG-PET activity throughout the aorta was significantly more frequent in this cluster (70%, $P < 0.0001$).

Finally, cluster 3 (n = 21; 11%) included patients with a more heterogeneous distribution of vascular lesions. These patients presented more systemic symptoms, such as asthenia (81%; $P = 0.036$) and night sweats (29%, $P = 0.009$). Bilateral axillary artery involvement (67%, $P < 0.0001$) and aneurysm (19%, $P = 0.026$) were more prevalent in this group. Vascular involvement included the supra-aortic trunks and branches of the abdominal aorta (67%, $P < 0.0001$) as well as lower limb arteries.

Clusters prognosis. Median follow-up was 4.3 years (IQR 1.7–7.5). Overall survival, vascular complications, and prognosis were compared in the three clusters (Table 2). Cluster 1 presented a higher mortality rate compared with the other clusters ($P = 0.044$). Vascular complications during follow-up between the three clusters were not statistically different; however, stroke seemed more common in clusters 1 and 2, and limb ischemia was more prevalent in cluster 3. The rate and type of vascular procedures were not different between the three clusters.

Vascular complications. During follow-up, 52 patients (26%) presented at least one vascular complication. Stroke (31%) was the main complication followed by limb ischemia (21%), myocardial infarction (4%), and mesenteric ischemia (2%). Cumulative incidences of vascular complications were 13.1% (95% confidence interval [CI] 8.9–18.3), 15.2% (95% CI 10.6–20.6), 17.3% (95% CI 12.3–22.9), and 19.5% (95% CI 14.3–25.4), at 1, 3, 5, and 10 years, respectively. Cumulative

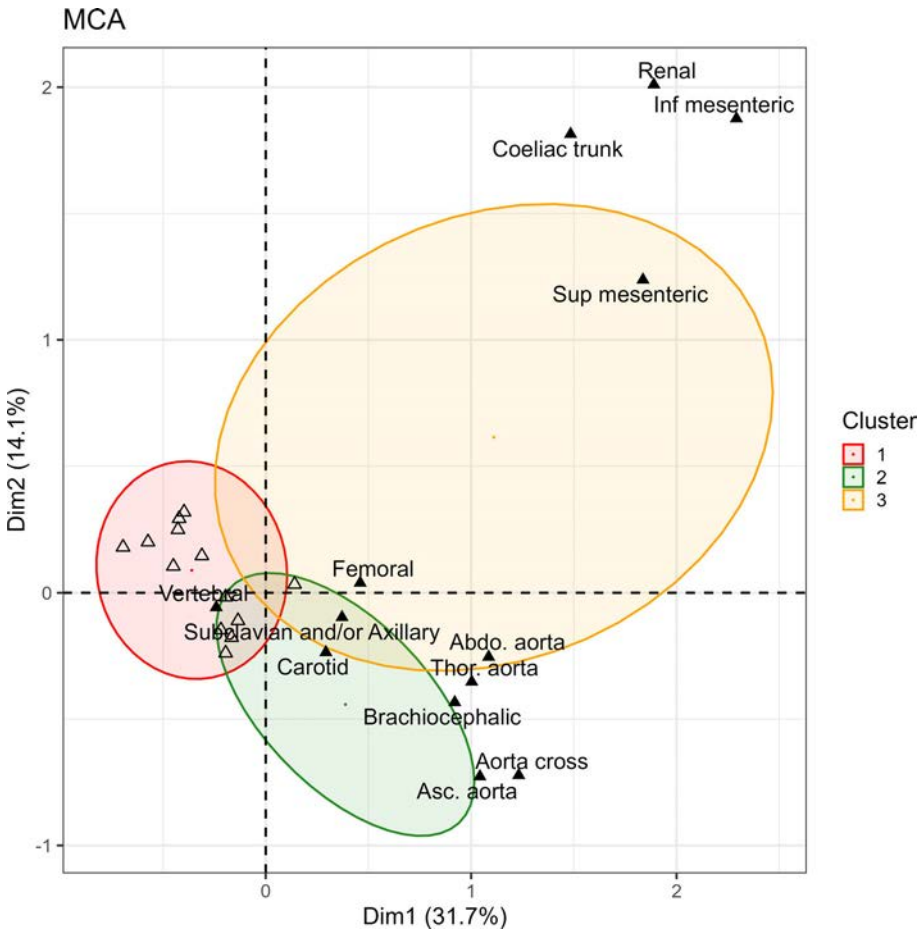

Figure 2. MCA with arterial localizations—hierarchical clustering. Black triangles represent the contribution of the involvement of arterial localizations whereas empty triangles represent the absence of involvement. MCA, multiple correspondence analysis.

Table 2. Outcomes of GCA-LVV with stenotic involvement and according to the different clusters*

Outcomes	Total (N = 198)	Cluster 1 (N = 123)	Cluster 2 (N = 54)	Cluster 3 (N = 21)	*P* value
Vascular complications, n (%)					0.39
Stroke	40 (77)	30 (83)	9 (82)	1 (20)	
Limb ischemia	9 (17)	6 (17)	2 (18)	3 (60)	
Myocardial infarction	2 (4)	1 (3)	0 (0)	1 (20)	
Mesenteric ischemia	1 (2)	0 (0)	1 (9)	0 (0)	
Relapses, n (%)					0.83
Major	48 (49)	29 (48)	13 (48)	6 (60)	
Minor	49 (51)	31 (52)	14 (52)	4 (40)	
Death	18 (34)	16 (13)	1 (1)	1 (4)	0.044

* GCA, giant cell arteritis; LVV, large vessel-vasculitis.

incidences of the different vascular complications from diagnosis are represented in Figure 3. Univariate analysis of vascular complications is presented in Table 3. In multivariable analysis, age at diagnosis (hazard ratio [HR] 1.06, 95% CI 1.03–1.10; P = 0.0004) and vertebral involvement (HR 1.87, 95% CI 1.03–3.40; P = 0.039) were significantly associated with higher risk of vascular complication.

Vascular procedures. During follow-up, 40 (20%) patients had at least one vascular procedure. Among 71 procedures, 53 (75%) were endovascular and 18 (25%) were open surgeries. Vascular interventions involved the lower limbs (n = 40; 57%), upper limbs (n = 11; 15%), subclavian arteries (n = 8; 11%), carotid arteries (n = 7; 10%), aorta (n = 4; 5.6%), and the celiac trunk (n = 1; 1.4%). The cumulative incidence of vascular procedures at 1, 5, and 10 years were 1% (95% CI 0.2–3.4), 3.7% (95% CI 1.6–7.1) and 6.7% (95% CI 3.6–11), respectively. Univariate analysis of time to first vascular procedure was performed using the patient's demographics and baseline vascular localization of stenotic lesions. Stenosis of the upper limbs (HR 2.79, 95% CI 1.36–5.72; P = 0.005) and lower limbs (HR 3.41, 95% CI 1.32–8.79; P = 0.011), celiac trunk (HR 4.99, 95% CI 2.56–9.73; P < 0.0001), renal arteries (HR 3.23, 95% CI 1.48–7.05; P = 0.003), and subclavian or axillary arteries (HR 2.22, 95% CI 1.02–4.84; P = 0.044) were associated with a higher risk of vascular procedures, whereas stenosis of the vertebral arteries was associated with a lower risk (HR 0.31, 95% CI 0.12–0.79; P = 0.014).

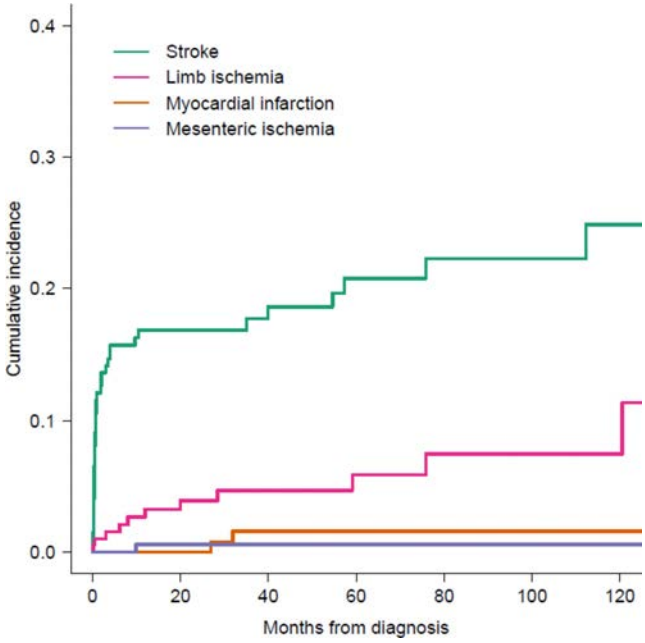

Figure 3. Cumulative incidence of vascular complications during follow-up. The *x*-axis represents time in months from diagnosis, and the *y*-axis represents the cumulative incidence of vascular complications.

Relapses. A total of 97 relapses were recorded, comprising 48 major and 49 minor events. In univariable analysis, dyslipidemia was associated with an increased risk of relapse (HR 1.57, 95% CI 1.03–2.39; P = 0.036), whereas vertebral artery involvement was linked to a reduced risk (HR 0.52, 95% CI 0.32–0.84; P = 0.008). These associations remained significant in multivariable analysis, with dyslipidemia showing a higher risk of relapse (HR 1.64, 95% CI 1.079–2.51; P = 0.023), and vertebral artery involvement being protective (HR 0.50, 95% CI 0.31–0.81; P = 0.005).

Death. After 10 years of follow-up, 18 (9%) of the patients died. Causes of death were mostly stroke (36%), sepsis (24%), heart failure (18%), lower limb ischemia (6%), and sigmoid perforation (6%). In univariable analysis of overall survival, older age was associated with an increased risk of death (HR 1.10, 95% CI 1.04–1.17; P = 0.0008), as was the use of glucocorticoid pulses at diagnosis (HR 2.83, 95% CI 1.05–7.63; P = 0.04). The cumulative incidence of death was 0% (95% CI 0–0), 1% (95% CI 0.2 –3.4), 2.1% (95% CI 0.7–4.9), and 4.3% (95% CI 2.0–8.0), at 1, 3, 5, and 10 years, respectively.

Table 3. Factors associated with vascular complications*

Baseline characteristics	Vascular complications				
	Events, no./ total no.	Univariate analysis		Multivariable analysis	
		HR (95% CI)	*P* value	HR (95% CI)	*P* value
Male	21/56	2.01 (1.15–3.51)	0.014	1.49 (0.84–2.64)	0.17
Age at diagnosis	NA	1.07 (1.04–1.11)	<0.0001	1.06 (1.03–1.10)	0.0004
Smoker	16/63	0.95 (0.53–1.71)	0.86	–	–
Hypertension	32/104	1.48 (0.85–2.59)	0.17	–	–
Dyslipidemia	22/59	1.87 (1.08–3.24)	0.027	–	–
Clinical manifestations					
Sudden visual loss	16/56	1.08 (0.89–1.31)	0.45	–	–
Jaw or tongue claudication	11/46	0.96 (0.69–1.34)	0.80	–	–
New temporal headache	33/108	1.21 (0.91–1.60)	0.19	–	–
Scalp tenderness	12/40	1.16 (0.84–1.60)	0.38	–	–
Bilateral axillary involvement	11/66	0.68 (0.49–0.95)	0.026	–	–
FDG-PET activity throughout aorta	13/65	0.7 (0.57–1.07)	0.13	–	–
Positive temporal artery biopsy or halo sign on ultrasound	38/119	1.97 (0.87–1.31)	0.53	–	–
Topography of the vascular involvement					
Subclavian or axillary	30/129	0.65 (0.37–1.12)	0.12	–	–
Carotid	34/114	1.62 (0.91–2.88)	0.10	–	–
Vertebral artery	26/73	2.73 (1.54–4.82)	0.0005	1.87 (1.03–3.40)	0.039
Brachiocephalic artery	12/50	0.88 (0.46–1.68)	0.69	–	–
Upper limbs	4/21	0.62 (0.22–1.73)	0.37	–	–
Ascending aorta	13/57	0.79 (0.42–1.49)	0.47	–	–
Aortic cross	8/51	0.47 (0.22–1.00)	0.049	0.57 (0.27–1.22)	0.15
Descending aorta	12/58	0.68 (0.35–1.29)	0.24	–	–
Celiac trunk	6/23	0.93 (0.40–2.19)	0.87	–	–
Lower limbs	2/11	0.74 (0.18–3.06)	0.68	–	–
Baseline clustering					
Cluster 1	36/123	1	0.19	–	–
Clusters 2 and 3	16/75	0.67 (0.37–1.22)	0.19	–	–

* CI, confidence interval; FDG-PET, fluorodeoxyglucose positron emission tomography; HR, hazard ratio; NA, no answer.

DISCUSSION

We report here the largest series of stenotic LVV in GCA. Stenotic LVV is a rare subtype of patients with GCA, accounting for 6.25% of our GCA population. Nuenninghoff et al[9] reported large-artery stenosis in their population-based study that was developed in one of every eight patients (13%). Our study identifies three distinct clusters of patients with GCA with different prognoses based on baseline arterial localization. The cluster 1 mainly involves vertebral artery stenosis, supra-aortic trunks, and femoral artery stenosis. It presents a two-fold increased risk of stroke and higher rates of both AAION and mortality at 10 years.

Previous studies have attempted to classify patients with GCA based primarily on clinical presentation. Estrada et al identified three subsets of GCA: cranial, extracranial, and occult. The cranial subset, characterized by headaches and visual symptoms, was associated with a higher risk of severe ischemic complications.[19] The extracranial subset, presenting with limb claudication, showed a stronger link to large vessel involvement. The occult subset, often diagnosed late because of nonspecific symptoms, exhibited a trend toward increased mortality. Similarly, Guédon et al[20] proposed a "vascular relapsing profile" that included younger patients with frequent relapses and a high risk of cardiovascular events, particularly thoracic aortic aneurysms; a "typical GCA profile" defined by classic cranial symptoms and frequent association with polymyalgia rheumatica; and an "ophthalmologic elderly profile" including the oldest patients, who had a higher prevalence of visual loss and the highest mortality rate. Our findings expand these previous classifications by incorporating arterial localization, further refining the understanding of prognosis in a patient with GCA with LVV.

The most frequently affected stenotic lesions in LVV-GCA were subclavian, carotid, and vertebral arteries. Nuenninghoff et al reported that large-artery stenosis predominantly affected the cervical arteries in most patients.[9] Kermani et al, in a longitudinal study on arterial lesions in GCA, found that the subclavian artery (42%), axillary artery (32%), and thoracic aorta (20%) were the most frequently affected.[21] However, their study included all

types of arterial involvement, which explains the difference with our cohort because we specifically focused on stenotic LVV-GCA. Additionally, Lambeck et al,[22] who focused on vertebral artery involvement in GCA, found that 33% of patients with cranial GCA had vertebral artery lesions, with 13% exhibiting severe stenosis or occlusion and 20% having low to medium grade stenosis.

Ischemic complications occurred in 26% of patients in our cohort, with stroke being the most prevalent complication at diagnosis. Ischemic stroke is a well-known complication of GCA, with an incidence rate ranging between 2.8% and 7%,[13,23,24] primarily due to vertebrobasilar involvement. It often occurs early in the disease course, with 73% of cases presenting at diagnosis.[25] Vertebral involvement increased by two times the odds of vascular complication in our study. In a French cohort of 271 patients with GCA, 14 (5.2%) experienced GCA-related cerebrovascular ischemic events, including 8 patients in the vertebrobasilar territory, 5 patients in the carotid territory, and 1 patient with multifocal ischemic and hemorrhagic strokes related to intracranial vasculitis.[26] A meta-analysis involving 3,553 patients reported a pooled prevalence of GCA-related cerebrovascular ischemic events of 4% (95% CI 3–6; $I^2 = 68\%$). Overall, the higher incidence of stroke observed in our cohort emphasizes the need for early recognition and targeted management of this specific GCA patient profile.

Other ischemic complications encountered in our cohort included limb ischemia (21%), myocardial infarction (4%), and mesenteric ischemia (2%). Limb ischemia at diagnosis is a well-described but often underappreciated manifestation of large-vessel GCA. Studies have reported upper limb claudication and decreased pulses due to subclavian and axillary artery involvement, which can precede or accompany classical symptoms of GCA. In some cases, critical limb ischemia requiring revascularization has seldom been reported, particularly in patients with delayed diagnosis. On the other hand, myocardial and mesenteric ischemia remain rare but potentially severe complications, likely resulting from a combination of both arterial inflammation and accelerated atherosclerosis. Finally, age has consistently been associated with an increased risk of ischemic complications in patients with GCA, as demonstrated in multiple retrospective studies and large cohorts.[27,28] This association was similarly observed in our cohort.

Death occurred in 18 patients (9%) during the 10-year follow-up, primarily due to stroke, sepsis, and heart failure. Previous studies have reported varied long-term mortality rates, with 10-year survival ranging from 48% to 81%, depending on the population and study design.[10,15,28] The most commonly reported causes of death in the literature are cardiovascular events and infections. In our cohort, stroke played a particularly significant role in disease-related deaths, highlighting the importance of recognizing and treating patients with stenotic GCA-LVV.

The retrospective nature of data collection is our main limitation. Because of the risk of bias of missing information, this study was not designed to assess treatment strategy, and treatment justification was not recorded. Thus, we could not define the evolution of stenosis aortitis under treatment.

In conclusion, our study describes a specific subgroup of patients with GCA with stenotic LVV accounting for less than 10% of all patients with GCA. We identify three different clusters of patients with different vascular involvement, vascular complications, and prognosis. Close monitoring and extended follow-up are warranted in GCA because of the high risk of vascular complications.

AUTHOR CONTRIBUTIONS

All authors contributed to at least one of the following manuscript preparation roles: conceptualization AND/OR methodology, software, investigation, formal analysis, data curation, visualization, and validation AND drafting or reviewing/editing the final draft. As corresponding author, Dr Saadoun confirms that all authors have provided the final approval of the version to be published and takes responsibility for the affirmations regarding article submission (eg, not under consideration by another journal), the integrity of the data presented, and the statements regarding compliance with institutional review board/Declaration of Helsinki requirements.

REFERENCES

1. Jennette JC, Falk RJ, Bacon PA, et al. 2012 revised International Chapel Hill Consensus Conference nomenclature of vasculitides. Arthritis Rheum 2013;65(1):1–11. doi:https://doi.org/10.1002/art.37715
2. de Boysson H, Liozon E, Espitia O, et al. Different patterns and specific outcomes of large-vessel involvements in giant cell arteritis. J Autoimmun 2019;103:102283. doi:https://doi.org/10.1016/j.jaut.2019.05.011
3. Dejaco C, Duftner C, Buttgereit F, Matteson EL, Dasgupta B. The spectrum of giant cell arteritis and polymyalgia rheumatica: revisiting the concept of the disease. Rheumatology (Oxford) 2017;56(4):506–515. doi:https://doi.org/10.1093/rheumatology/kew273
4. Klein RG, Hunder GG, Stanson AW, et al. Large artery involvement in giant cell (temporal) arteritis. Ann Intern Med 1975;83(6):806–812. doi:https://doi.org/10.7326/0003-4819-83-6-806
5. Hunder GG. The early history of giant cell arteritis and polymyalgia rheumatica: first descriptions to 1970. Mayo Clin Proc 2006;81(8):1071–1083. doi:https://doi.org/10.4065/81.8.1071
6. Evans JM, O'Fallon WM, Hunder GG. Increased incidence of aortic aneurysm and dissection in giant cell (temporal) arteritis. A population-based study. Ann Intern Med 1995;122(7):502–507. doi:https://doi.org/10.7326/0003-4819-122-7-199504010-00004
7. Bongartz T, Matteson EL. Large-vessel involvement in giant cell arteritis. Curr Opin Rheumatol 2006;18(1):10–17. doi:https://doi.org/10.1097/01.bor.0000197996.04709.4e
8. Vautier M, Dupont A, de Boysson H, et al. Prognosis of large vessel involvement in large vessel vasculitis. J Autoimmun 2020;108:102419. doi:https://doi.org/10.1016/j.jaut.2020.102419
9. Nuenninghoff DM, Hunder GG, Christianson TJH, et al. Incidence and predictors of large-artery complication (aortic aneurysm, aortic dissection, and/or large-artery stenosis) in patients with giant cell arteritis: a population-based study over 50 years. Arthritis Rheum 2003;48(12):3522–3531. doi:https://doi.org/10.1002/art.11353
10. Muratore F, Kermani TA, Crowson CS, et al. Large-vessel giant cell arteritis: a cohort study. Rheumatology (Oxford) 2015;54(3):463–470. doi:https://doi.org/10.1093/rheumatology/keu329

11. Assie C, Janvresse A, Plissonnier D, et al. Long-term follow-up of upper and lower extremity vasculitis related to giant cell arteritis: a series of 36 patients. Medicine (Baltimore) 2011;90(1):40–51. doi: https://doi.org/10.1097/MD.0b013e318206af16
12. Kermani TA, Matteson EL, Hunder GG, et al. Symptomatic lower extremity vasculitis in giant cell arteritis: a case series. J Rheumatol 2009;36(10):2277–2283. doi:https://doi.org/10.3899/jrheum.090269
13. Caselli RJ, Hunder GG, Whisnant JP. Neurologic disease in biopsy-proven giant cell (temporal) arteritis. Neurology 1988;38(3):352–359. doi:https://doi.org/10.1212/WNL.38.3.352
14. Sailler L, Paricaud K. Republication de : complications ischémiques de l'artérite à cellules géantes. J Eur Urgences Reanim 2020;32(1):37–44. doi:https://doi.org/10.1016/j.jeurea.2020.02.009
15. Nuenninghoff DM, Hunder GG, Christianson TJH, et al. Mortality of large-artery complication (aortic aneurysm, aortic dissection, and/or large-artery stenosis) in patients with giant cell arteritis: a population-based study over 50 years. Arthritis Rheum 2003;48(12):3532–3537. doi:https://doi.org/10.1002/art.11480
16. Ponte C, Grayson PC, Robson JC, et al. 2022 American College of Rheumatology/EULAR classification criteria for giant cell arteritis. Arthritis Rheumatol 2022;74(12):1881–1889. doi:https://doi.org/10.1002/art.42325.
17. Hellmich B, Agueda A, Monti S, et al. 2018 Update of the EULAR recommendations for the management of large vessel vasculitis. Ann Rheum Dis 2020;79(1):19–30. doi:https://doi.org/10.1136/annrheumdis-2019-215672
18. Kalbfleisch JD, Prentice RL. The Statistical Analysis of Failure Time Data. New York, NY: John Wiley & Sons; 1980:13–14.
19. Estrada P, Narváez J, Moya P, et al. Clinical phenotypes of giant cell arteritis: insights into complications and survival outcomes. Eur J Rheumatol 2024;11(2):33–38. doi:https://doi.org/10.5152/eurjrheum.2024.23065.
20. Guédon AF, Froger C, Agard C, et al. Identifying giant cell arteritis patients with higher risk of relapse and vascular events: a cluster analysis. QJM 2024;117(11):769–776. doi:https://doi.org/10.1093/qjmed/hcae105
21. Kermani TA, Diab S, Sreih AG, et al; Vasculitis Clinical Research Consortium. Arterial lesions in giant cell arteritis: a longitudinal study. Semin Arthritis Rheum 2019;48(4):707–713. doi:https://doi.org/10.1016/j.semarthrit.2018.05.002
22. Lambeck J, Schläger A, Venhoff N, et al. Vertebral artery involvement in giant cell arteritis: symptoms, treatment and outcome. J Stroke Cerebrovasc Dis 2025;34(4):108260. doi:https://doi.org/10.1016/j.jstrokecerebrovasdis.2025.108260
23. Samson M, Jacquin A, Audia S, et al. Stroke associated with giant cell arteritis: a population-based study. J Neurol Neurosurg Psychiatry 2015;86(2):216–221. doi:https://doi.org/10.1136/jnnp-2014-307614
24. de Boysson H, Liozon E, Larivière D, et al. Giant cell arteritis-related stroke: a retrospective multicenter case-control study. J Rheumatol 2017;44(3):297–303. doi:https://doi.org/10.3899/jrheum.161033
25. Oerding C, Uhlmann F, Wollmann J, et al. Carotid artery stenosis and ischemic strokes in patients with giant cell arteritis: a characteristic pattern-literature review and case report. TH Open 2021;6(1):e40–e49. doi:https://doi.org/10.1055/a-1704-0741
26. Penet T, Lambert M, Baillet C, et al. Giant cell arteritis-related cerebrovascular ischemic events: a French retrospective study of 271 patients, systematic review of the literature and meta-analysis. Arthritis Res Ther 2023;25(1):116. doi:https://doi.org/10.1186/s13075-023-03091-x
27. Chaddock NJM, Harden CJ, Sorensen L, et al; UK GCA Consortium. Age, anticoagulants, hypertension and cardiovascular genetic traits predict cranial ischaemic complications in patients with giant cell arteritis. Ann Rheum Dis 2025;84(2):329–340. doi:https://doi.org/10.1136/ard-2024-225515
28. Pugh D, Karabayas M, Basu N, et al. Large-vessel vasculitis. Nat Rev Dis Primers 2022;7(1):93. doi:https://doi.org/10.1038/s41572-021-00327-5

Arthritis & Rheumatology
Vol. 78, No. 9, September 2026, pp 1929–1941
DOI 10.1002/art.70104
© 2026 The Author(s). *Arthritis & Rheumatology* published by Wiley Periodicals LLC on behalf of American College of Rheumatology.
This is an open access article under the terms of the Creative Commons Attribution License, which permits use, distribution and reproduction in any medium, provided the original work is properly cited.

American College of Rheumatology
Empowering Rheumatology Professionals

Long Noncoding RNA *H19* Mediates STAT3-Dependent Activation of Keratinocytes and Fibroblasts in Systemic Sclerosis Skin

Begoña Caballero-Ruiz, PhD,[1] Christopher W. Wasson, PhD,[1] Rebecca L. Ross, PhD,[1,2] and Francesco Del Galdo, MD[1,2]

Objective. Dermal systemic sclerosis (SSc) fibroblasts and their exosomes can activate keratinocytes in SSc, with long noncoding RNA (lncRNA) *H19* highlighted as the most up-regulated RNA in their cargo compared with healthy controls (HCs). The role of *H19* in SSc pathogenesis has never been investigated. Here we determine *H19*'s role in the profibrotic activation of dermal fibroblasts and in their crosstalk with keratinocytes.

Methods. Skin biopsies were obtained from the forearms of patients with diffuse SSc (n = 20) or HCs (n = 8), and dermal fibroblasts were explanted. In situ hybridization was used to determine *H19* expression in the skin, paired with immunohistochemistry of STAT3 and Collagen1. *H19* and STAT3 expression were modulated by retroviral transduction and small interfering RNA. Gel contraction and Transwell coculture were employed for functional studies.

Results. In SSc, high *H19* expression in skin and explanted dermal fibroblasts compared with HCs showed moderate correlation to well-described profibrotic markers. Knockdown of *H19* in SSc fibroblasts decreased profibrotic gene expression and cell contraction ability. *H19* overexpression was sufficient to induce a profibrotic phenotype in HC fibroblasts. Mechanistically, transforming growth factor-β, interleukin-6, and interleukin-11 significantly increased *H19* expression in HC fibroblasts (2.2-, 1.4-, and 3.5-fold, respectively) through activation of STAT3. Additionally, the STAT3 and STAT1 activation of keratinocytes induced by coculture with SSc fibroblasts was suppressed by *H19* knockdown.

Conclusion. This study shows that lncRNA *H19* is a key mediator of STAT3-induced changes in fibrotic activation of fibroblast and keratinocytes in SSc skin and could be considered a promising therapeutic target in tissue fibrosis.

INTRODUCTION

Systemic sclerosis (SSc) is an autoimmune disease characterized by impaired angiogenesis and fibrosis of the skin and internal organs.[1] Specific treatments for fibrosis in SSc, and other fibrotic diseases, are limited. Fibroblast to myofibroblast differentiation is well characterized as a key cellular event in tissue fibrosis. The transforming growth factor-β (TGF-β) pathway is one of the main signaling pathways known to induce myofibroblast activation through targeting transcriptional changes.[2] However, beyond fibroblast activation there is a complex and dysregulated interplay of immune cells, endothelial cells, and epithelial cells that contribute to fibrosis. In the skin, keratinocytes are known to participate in tissue homeostasis via crosstalk with fibroblast and immune cells, which is found dysregulated in SSc.[3] Intercellular communication is a crucial element of tissue homeostasis, and it is orchestrated both by soluble factors and extracellular vesicles better known as exosomes. The role of specific exosome cargoes in the aberrant crosstalk associated with tissue fibrosis in SSc is poorly characterized. Recently, we have shown that fibroblast exosomes can directly influence the pro-inflammatory activation of keratinocytes and play a role in the innate immune activation observed in SSc skin.[4] The analysis of SSc fibroblast exosome contents revealed long noncoding RNA

Supported by the Susan Cheney endowment for Scleroderma Research and the National Institute for Health and Care Research (NIHR) Leeds Biomedical Research Centre (BRC) (NIHR213331). The views expressed are those of the author(s) and not necessarily those of the NIHR or the Department of Health and Social Care.

[1]Leeds Institute of Rheumatic and Musculoskeletal Medicine, University of Leeds, Leeds, United Kingdom; [2]NIHR Leeds Biomedical Research Centre, Leeds Teaching Hospitals, NHS Trust, Chapel Allerton Hospital, Leeds, United Kingdom.

Additional supplementary information cited in this article can be found online in the Supporting Information section (https://acrjournals.onlinelibrary.wiley.com/doi/10.1002/art.70104).

Author disclosures are available at https://onlinelibrary.wiley.com/doi/10.1002/art.70104.

Address correspondence to Francesco Del Galdo, MD, at f.delgaldo@leeds.ac.uk.

Submitted for publication June 26, 2025; accepted in revised form February 5, 2026.

(lncRNA) *H19* as one of the most significant differentially expressed genes in SSc dermal fibroblast derived exosomes compared with healthy controls (HCs).[4]

LncRNAs are defined as RNAs longer than 200 nucleotides that do not code for proteins.[5] LncRNAs have been shown to have roles in modulating gene expression with aberrant expression linked to cancer and fibrosis. In SSc, some lncRNAs are known to be involved in the profibrotic activation of fibroblasts, including *HOTAIR* and MIR503, also known as *H19* located on the X chromosome.[6–11]

An alternative lncRNA known as *H19*, an imprinted and maternally expressed 2.3-kb lncRNA located on chromosome 11, is expressed in many tissues during embryo development and nearly completely down-regulated in all tissues after birth, apart from the skeletal muscle.[12] Recently, numerous studies showed *H19* to be involved in tumorigenesis and as a potential novel therapeutic target for fibrosis of the heart, liver, lungs, and kidney.[12–15] In addition, high levels of *H19* have been found in serum from patients with SSc[16]; however its role in regulating skin fibrosis in SSc is still unknown.

Here we show for the first time that *H19* levels are elevated in SSc skin and dermal fibroblasts ex vivo. Through gain and loss of function approaches we characterize the function of *H19* in dermal fibroblasts and its role in keratinocyte/fibroblast cell-to-cell communication.

MATERIALS AND METHODS

Patient enrollment, clinical characterization, and skin biopsies. Skin biopsies were obtained from the forearms of adult patients with diffuse SSc (n = 20) or HCs (n = 8) as control. All patients were male or female aged 22 to 78 years inclusive at screening with documented diagnosis of SSc, as defined using the 2013 American College of Rheumatology/EULAR criteria.[17] All patients had the diffuse cutaneous form of SSc according to LeRoy and Medsger's criteria[18]; disease duration ≤3 years from the first non-Raynaud phenomenon manifestation; a modified Rodnan skin score of 15 to 45 units at screening; and clinical skin involvement proximal and distal to the elbows, knees, or both or any truncal involvement, with or without face involvement. All participants provided written informed consent according to a protocol approved by the Medicine and Health Regulatory agency (NRES-011NE to FDG, IRAS 15/NE/0211). Fibroblasts were isolated and established as previously described.[19] Primary parental fibroblasts were immortalized using human telomerase reverse transcriptase (hTERT) to produce hTERT parental HC and diffuse SSc fibroblasts as previously described.[19,20] The demographic and clinical features of patients with diffuse SSc are summarized in Supplementary Table 1.

Cell culture. Primary fibroblasts and human immortalized epidermal keratinocytes (HaCaTs; ATCC) were maintained in Dulbecco's modified Eagle medium (DMEM; Gibco) supplemented with 10% fetal bovine serum (FBS; Sigma) and penicillin-streptomycin (Sigma) in a humidified incubator at 37°C and 5% CO_2. For hTERT fibroblasts (HC n = 3; SSc n = 3), 250 μg/mL Geneticin (Thermo Fisher Scientific) was added into the medium. For assays, hTERT fibroblasts were cultured in medium without geneticin and used before passage 10. Primary fibroblasts were used before passage 4. Cells were routinely checked for mycoplasma.

Morphogen stimulation. Cells were serum starved for 24 hours in DMEM containing 0.5% FBS prior treatment with SD208 inhibitor (1 μM, Sigma), cryptotanshinone (CTS; 5 μM, MedChemExpress), or DMSO as control for the time indicated in the figures. When specified, inhibitor cells were stimulated with 10 ng/mL TGF-β (R&D Systems), 50 ng/mL interleukin (IL) 6 (PeproTech) or 50 ng/mL IL-11 (PeproTech) in a humidified incubator at 37°C and 5% CO_2.

Quantitative polymerase chain reaction. Total RNA was isolated using commercial RNA extraction kits (Zymo Research) and quantified by A260nm/A280nm in a Nanodrop. Synthesis of complementary DNA (cDNA) was performed using 500-ng RNA with cDNA synthesis kits (Thermo Fisher). Real-time quantitative polymerase chain reaction (PCR) was performed using 1 μL of 10 ng/μL cDNA and target-specific primers *H19* (forward: 5′-TCAAGCCTGGGCCTTTGAAT; reverse: 5′-GGCTGATGAGGTCTGGTTCC), *STAT3* (forward: 5′-TCTGTGTGACACCAACGACC; reverse: 5′-TCCTCACATGGGGGAGGTAG), *Collagen type 1A1* (*Col1A1*; forward: 5′- CCTCCAGGGCTCCAACGAG; reverse: 5′- TCTATCACTGTCTTGCCCCA), α-*ACTA2* (forward: 5′-TGTATGTGGCTATCCAGGCG; reverse:5′- AGAGTCCAGCACGATGCCAG), *CCN2* (forward: 5′-CTTGCGAAGCTGACCTGGAAGA; reverse: 5′-CCGTCGGTACATACTCCACAGA), and *GAPDH* (forward: 5′- ACCCACTCCTCCACCTTTGA; reverse: 5′-CTGTTGCTGTAGCCAAATTCGT). A SyBr Green PCR kit with a CFX Connect Real-Time PCR Detection System (Bio-Rad) thermocycler was used. Amplification was quantified and expressed following the ΔΔCt method using *GAPDH* as a housekeeping gene.

Western blotting. Total protein was extracted in a radioimmunoprecipitation assay buffer with proteinase and phosphatase inhibitors (Sigma) and resolved by sodium dodecyl sulfate-polyacrylamide gel electrophoresis, transferred onto nitrocellulose membranes (Amersham Biosciences), and probed with antibodies specific for GAPDH (Proteintech, HRP-60004), pSTAT3 Tyr 705 (Cell Signaling, 9131), STAT3 (Abcam, 119352), connective tissue growth factor (CTGF/CCN2; Abcam, ab209780), pSMAD3 (Abcam, ab52903), SMAD3 (Cell Signaling, 9523), pSTAT1 (Cell Signaling, 9167), and STAT1 Tyr 701 (Cell Signaling, 9172). Immunoblots were visualized with species-specific HRP-conjugated secondary antibodies (Sigma) and

Supersignal West Pico PLUS Chemiluminescent Substrate (Thermo Fisher, Cat. No. 34577) on a Bio-Rad chemiDoc imaging system using the Image Lab software (Bio-Rad) according to the manufacturer's instructions. Signal intensity was quantified by ImageJ (Fiji) and normalized to the loading control indicated in the text.

RNAscope and costaining. For in situ hybridization of *H19* in skin biopsies we used the RNAscope probe designed by Biotechnne (Cat. No. 1152841-C1) together with the RNAscope 2.5HD Detection kit RED (Cat. No. 322360) following the manufacturer's instructions. The probe was hybridized for 2 hours at 40°C using the HybEZ Oven provided. Signal detection was obtained using the Fast RED A/B solution provided in the kit. We used 50% Hematoxylin Gill NO.1 (Sigma) to counterstain the slides before mounting.

For codetection of *H19* with Collagen1 (1:100, Abcam 6308) or STAT3 (1:100, Abcam 119352) we used the RNA-Protein codetection Ancillary kit from Biotechnne (Cat. No. 323180), which enables combination of RNAscope with immunohistochemistry-compatible antibodies. Primary antibody was applied overnight (ON) at 4°C. The day after, 10% neutral buffered formalin was added for 30 minutes at room temperature for postprimary fixation. Then we applied the corresponding RNAscope protease for 30 minutes at 40°C. Final detection was performed using 3, 3 -diaminobenzidine (Vector Laboratories) and counterstaining with 50% Hematoxylin Gill NO.1 (Sigma). Slides were scanned using a Leica Biosystems AT2 digital slide scanner at 20× resolution and Zeiss AxioImager.Z1 microscope using 40× resolution.

RNAscope and costaining quantification was performed using ImageJ and represented as the percentage of the probe per area (μm^2) on the indicated samples per group. Four images per sample were used for quantification in the epidermis and subepidermal regions.

Small RNA interference transfections. Two gene-specific 27mer small interfering RNA (siRNA) duplexes specific for *H19* (siRNA 1 and siRNA2) or a scramble (SCR) negative control siRNA duplex from Origene (Cat.No. SR319206) were transfected into SSc hTERT fibroblasts using siTrans 2.0 (Cat. No. TT320001) in complete medium (10% FBS). After 5 hours, fresh medium was added. Fibroblasts were incubated for the indicated times in complete or starved media (0.5% FBS) before harvesting.

A unique siRNA specific for *STAT3* or SCR negative control sequence from Qiagen (Cat. No. SI00048363) was transfected into fibroblasts using Lipofectamine 2000 (Thermo Fisher). After 24 hours, we medium-changed the cells with complete or starved media for the indicated times before harvesting.

Micro-RNA29a transfection. Fibroblasts were transfected in antibiotic-free media with 10 nM of micro-RNA 29a (miRNA29a or miR29a) miRIDIAN miRNA mimic or negative control miRNA (Horizon) using the DharmaFECT4 (Horizon, Cat. No. T-2004-02) transfection reagent. Fibroblasts were then incubated for 48 hours before harvesting.

Retroviral transduction. *H19* expression was induced by transduction with retroviruses carrying pBabepuro vector containing the human *H19* sequence (NR_002196.3) or SCR sequence as control (Dundee University, UK). For this purpose, hTERT healthy dermal fibroblasts were seeded 50% confluence and infected with retroviral particles in full media ON. The day after cells were medium-changed with full media before a second retroviral transduction ON. Transduced fibroblasts were maintained in full media for 48 hours then selected with 1.0 μg/mL Puromycin (Gibco) for another 48 hours. Cells were maintained in 0.5 μg/mL Puromycin and 250 μg/mL Geneticin (Thermo Fisher Scientific).

Gel contraction. On the day of the assay hTERT fibroblasts were trypsinized and seeded at 200,000 cells on gel/cell mixture per well of a 24-well plate. Briefly, the Collagen Gel Working Solution (Cambridge Biosiences, Cat.No. CBA-201) was prepared according to the manufacturer's instructions in a cold sterile tube. The desired number of cells was resuspended in low-glucose DMEM 1% FBS and 1% penicillin-streptomycin in the volume needed to prepare one part of cell mixture and four parts of cold Collagen Gel Working Solution. A total of 0.5 mL of cell collagen mixture was added per well and incubated 1 hour at 37°C in an incubator without CO_2. After collagen polymerization, 1 mL of 1% FBS culture medium was added on top of each collagen gel and incubated ON at 37°C and 5% CO_2. The next day, the sides of the cell collagen gels were detached using sterile spatulas ensuring that the gels were circular. Pictures of the gels were taken at the indicated time points and weight at the last time point. For analysis, the scale was set using the known distance of the bottom of a 24 well plate, and the area of each gel was measured at various time points using ImageJ (Fiji).

Chromatin immunoprecipitation analysis. Chromatin immunoprecipitation (ChIP) was performed according to the protocol published by Thermo Fisher with some modifications. Briefly, cells were harvested and resuspended in 1% paraformaldehyde for 15 minutes to induce crosslinking. Formaldehyde was quenched with 1.25 M glycine. Then, the cells were lyzed in a two-step process with cellular (50 mM Tris-HCl pH 7.5, 1 mM EDTA pH 8.0, 140 mM NaCl, and 1% NP-40) and nuclear lysis buffer (50 mM Tris-HCl pH 7.5, 2 mM EDTA pH 8.0, 0.5% sodium deoxycholate, and 1% sodium dodecyl sulfate [SDS]). The DNA was sheared by sonication (2 × 30 seconds 50 mHz). The sheared chromatin was incubated with pSTAT3 Tyr 705 (Cell Signaling, 9131) or IgG (Thermo Fisher, Cat No. 86199) control antibody for 2 hours at room temperature. Then, Dynabeads Protein

G (Thermo Fisher, Cat No. 10004D) were added to the mixture ON at 4°C. The beads were then washed in low-salt (20 mM Tris-HCl pH 8.0, 2 mM EDTA pH 8.0, 0.1% SDS, 1% Triton X-100, and 150 mM NaCl) and high-salt (20 mM Tris-HCl pH 8.0, 2 mM EDTA pH 8.0, 0.1% SDS, 1% Triton X-100, and 500 mM NaCl) wash buffers, and then the DNA was eluted with elution buffer (1% SDS, 100mM $NaHCO_3$). Crosslinking was reversed with 5 M NaCl for 3 hours at 65°C. The DNA was treated with RNase (Thermo Fisher) and then Proteinase K (Macherey-Nagel). DNA was then purified using a DNA clean-up kit (Qiagen, Cat No. 28104). Co-immunoprecipitated DNA was detected by quantitative PCR using primers to *H19* promoter (forward: 5′-ATGTGGCTCCCATGAATGTC; reverse: 5′-GGCTCTTGCATAGCACATGA) and primers to β-catenin promoter as positive control (forward: 5′-AATTGGAGGCTGCTTAATCG; reverse: 5′-TTCCATTTTTATCTGGTTCCAC). The data were normalized according to the percent input method.

Transwell assay. For coculturing assays, on day 1, 90% HC and/or SSc hTERT fibroblasts were seeded per well in six-well plates, and 90% HaCaTs were seeded separately per 0.40-μm pore translucent high-density polyethylene terephthalate membrane (Corning) in full media. For assays with knockdown cells, on day 2, SSc hTERT dermal fibroblasts were transfected with *H19* siRNA as previously described. On day 3, cells reached 100% confluency and insert and wells were washed with phosphate-buffered serum. The inserts containing HaCaTs were added on top of each well containing fibroblasts, and serum-free media was added. After 48 hours, cells were harvested for RNA and protein.

Statistical analysis. GraphPad Prism 10 was used for statistical analysis and for the generation of graphs. Results were presented as mean and SEM. One-way analysis of variance parametric test or Student's *t*-test were performed for experiments, with $P < 0.05$ considered significant. All data used in this research are already included in the article or the Supplementary Materials. Further information is available from the corresponding author upon reasonable request.

RESULTS

LncRNA *H19* is up-regulated in SSc skin and explanted dermal fibroblasts and correlates with key markers of fibrosis. Dermal SSc fibroblasts have been shown to have increased *H19* in their secreted exosomes compared with HCs,[4] thus we wanted to assess whether differences in *H19* levels could be observed within the whole skin. RNAscope (RNA in situ hybridization) targeting *H19* in skin samples indicated higher *H19* levels in SSc skin (n = 4) compared with HCs (n = 4) (18.2-fold change in the percentage of *H19* probe per area [μm^2]; $P < 0.05$), with increased levels of *H19* being detectable in the epidermal layer as well as within the dermis and the adipose tissue of SSc skin (Figure 1A and B; Supplementary Figure 1A).

Ex vivo, SSc explanted dermal fibroblasts showed markedly increased expression of *H19* (59.6-fold change; $P < 0.001$) compared with fibroblasts isolated from HC skin (reverse transcription–quantitative PCR [RT-qPCR] analysis; SSc n = 20; HC n = 8) (Figure 1C). Similar to the results in skin biopsies, we observed high variability of *H19* expression within SSc fibroblast lines, which also was maintained in vitro following hTERT-mediated immortalization (Supplementary Figure 1B).

Immunohistochemistry studies paired with in situ hybridization revealed that the heterogeneity in *H19* expression aligns with the amount of Collagen 1 (COL-1) profibrotic marker expressed in SSc skin. Despite the small size number, SSc skin tissue with the highest *H19* expression showed the highest collagen staining and vice versa (Figure 1D and Supplementary Figure 1C represent skin levels of *H19* [pink] and COL-1 within the dermis [brown]; Figure 1E represents the percentage of *H19* and COL-1 per sample, n = 3). Consistent with this observation, RT-qPCR studies of explanted SSc fibroblasts in vitro showed a moderate, albeit significant, correlation between *H19* levels and messenger RNA (mRNA) levels of *Col1A1* ($R = 0.54$, $P = 0.007$), α-smooth muscle actin (encoded by *ACTA2*) ($R = 0.38$, $P = 0.049$), and *CTGF* (also known as *CCN2*) ($R = 0.45$, $P = 0.022$) (Figure 1F). Altogether, these findings supported a role of *H19* in the context of profibrotic activation of dermal fibroblasts in SSc.

***H19* expression regulates profibrotic activation of dermal fibroblasts in vitro.** Next, we established loss and gain of function models to determine whether the increased expression of *H19* could play a direct role in profibrotic activation of dermal fibroblasts in SSc. To knockdown the expression of *H19* we employed two siRNAs, which achieved 88% and 74% knockdown (siRNAs H19 1 and 2, respectively) versus scrambled RNA (SCR) after 48 hours. RT-qPCR analysis showed that knockdown of *H19* decreased the gene expression of profibrotic markers *Col1A1* (0.70-fold, $P < 0.05$ and 0.68-fold, $P < 0.05$), *ACTA2* (0.74-fold, $P < 0.01$ and 0.62-fold, $P < 0.05$), *CCN2* (0.66-fold, $P < 0.01$ and 0.62-fold, $P < 0.05$), and *STAT3* (0.78-fold, $P < 0.05$ and 0.69-fold, $P < 0.01$) relative to SCR SSc fibroblasts (Figure 2A). Western blot analysis showed that the knockdown of *H19* using siRNA1 partially suppressed protein levels of pSTAT3 (Tyr-705) and CCN2 (Figure 2B).

SSc fibroblasts have previously been shown to have a higher ability to contract collagen gel compared with HC.[19] SSc fibroblasts with reduced expression of *H19* using siRNA H19 1 showed a 3.1-fold reduction in collagen gel contraction (7% vs 22% from SCR) after 48 hours (Figure 2C; Supplementary Figure 2A). On the other hand, siRNA H19 2 showed a 1.4-fold reduction in collagen gel contraction (16% contraction vs 22% from SCR) (Supplementary Figure 2B). The difference in performance was associated with a similar difference in efficiency of

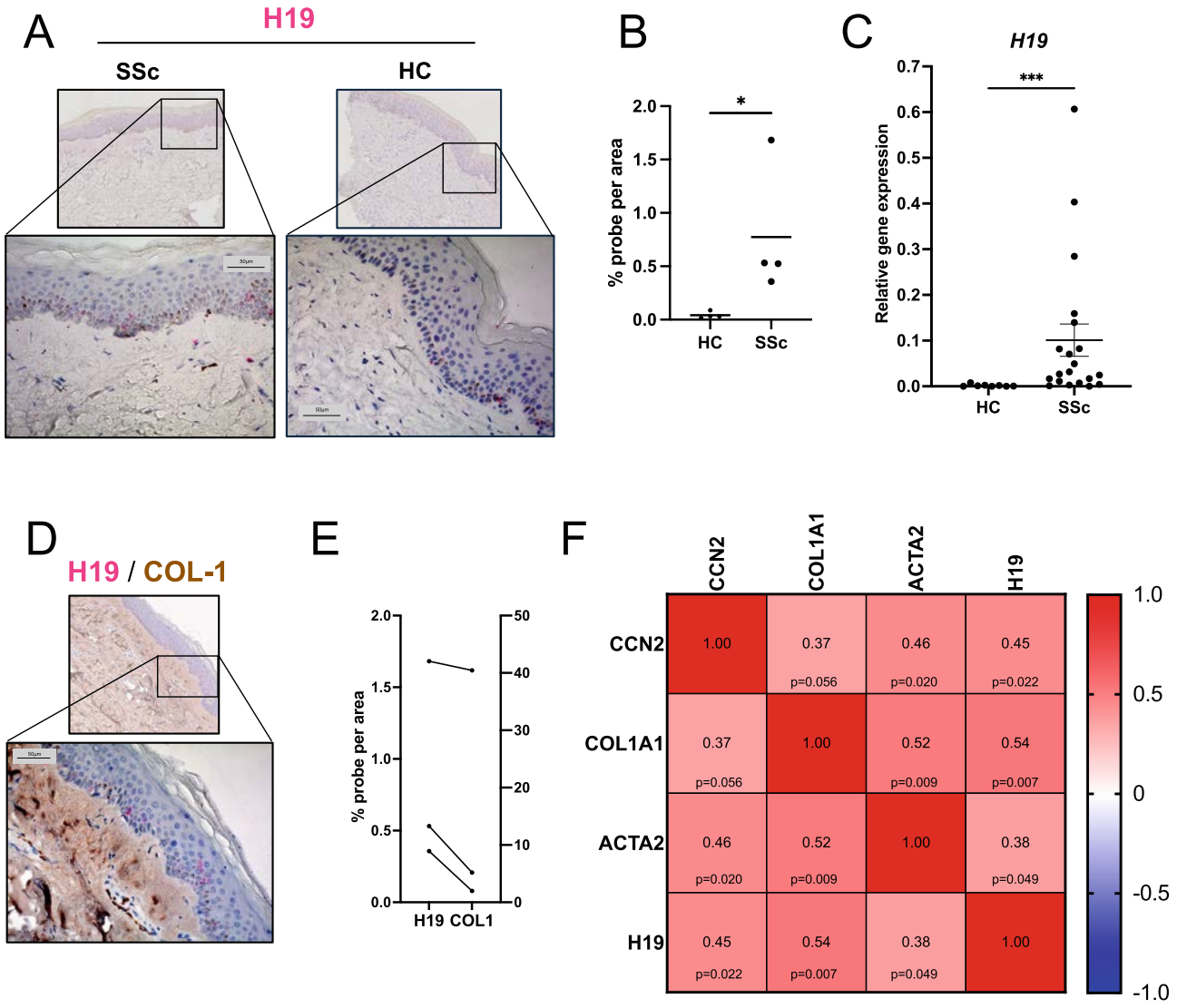

Figure 1. Increased *H19* in SSc skin and explanted dermal fibroblast correlates to profibrotic markers. (A) RNAscope of *H19* (pink) in skin samples. Representative images of one HC and one SSc are shown. Top image represents low-resolution insert and the bottom the high resolution of the selected area. Scale bar = 50 µm. (B) Graph represents the percentage of *H19* probe per area (µm^2) (n = 4 per group). (C) mRNA transcript levels of *H19* normalized to *GAPDH* mRNA levels in primary HC (n = 8) and SSc fibroblast (n = 20). Data show mean ± SEM, unpaired *t*-test ($P < 0.001$). (D) RNAScope of *H19* (pink) co-stained with COL-1 (brown) in representative SSc skin sample with high *H19* levels. Scale bar = 50 µm. (E) The graph represents the percentage of *H19* and COL1 costaining per sample (n = 3). (F) Correlation matrix of *H19* with mRNA levels of the indicated profibrotic markers in 20 SSc primary fibroblast. Values represent Spearman *r* correlation coefficient. Red represents increased expression, and blue represents decreased expression. *$P < 0.05$; ***$P < 0.001$. COL-1, Collagen 1; HC, healthy control; mRNA, messenger RNA; SSc, systemic sclerosis.

maintaining reduced *H19* levels over time (Supplementary Figure 2C). Consistently, gel weight was significantly increased by 38% after 48 hours when in *H19*-siRNA 1 fibroblasts ($P < 0.05$), supporting the observation of a lesser contraction of the matrix (Figure 2D).

In a complementary approach, we established *H19* overexpressed (H19OE) healthy dermal fibroblast (Figure 2E). Overexpression of *H19* induced an increase in gene expression of *Col1A1* (1.43-fold, $P < 0.01$), *ACTA2* (1.47-fold, $P < 0.05$), *CCN2* (1.66-fold, $P < 0.001$), and *STAT3* (1.2-fold, $P < 0.001$) relative to HC fibroblast (Figure 2F). Consistent with these findings, protein analysis showed a slight increase in STAT3 as well as an increase in CCN2 protein levels (Figure 2G). Functionally, *H19* overexpression significantly increased gel contraction ability of HC fibroblast by 1.7-fold after 24 hours ($P < 0.0001$) (20.47% contraction vs 11.8% from HC) (Figure 2H; Supplementary Figure 2D).

H19 is known to sponge miRNAs as one of its most studied regulatory mechanisms.[8] Previously, *H19* has been described to sponge miR29a,[21,22] and miR29a is a key regulator of COL-1 in

SSc.[23,24] Interestingly, in cancer cells, miR29a has been shown to also target STAT3.[25,26] To better understand the regulation of these markers by *H19*, we transfected our H19OE and HC fibroblast with mimic miR29a and its relative negative control. Introduction of miR29a was able to reverse the ability of *H19* to induced *Col1A1* ($P < 0.05$) and *STAT3* ($P < 0.05$) levels

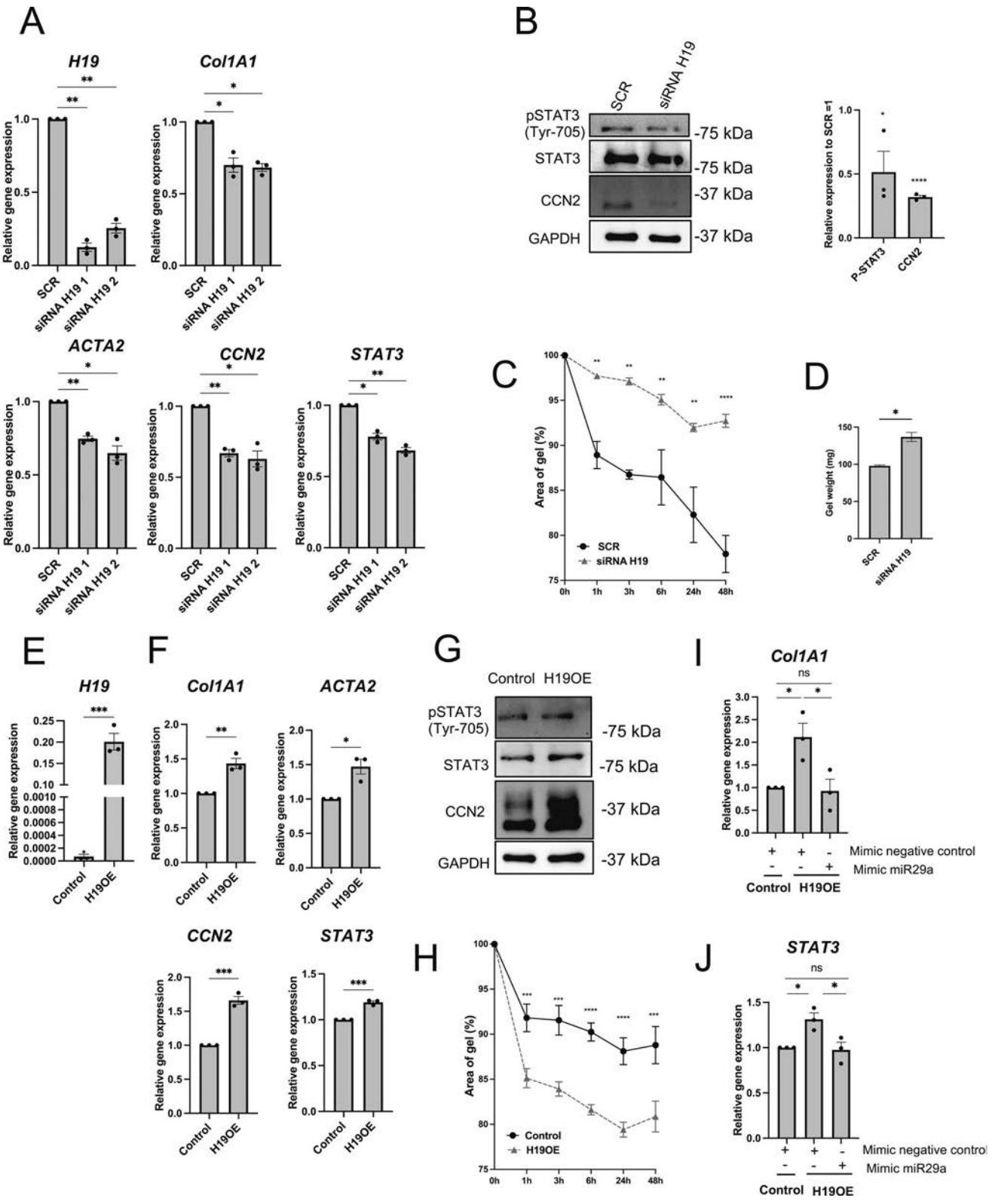

Figure 2. Legend on next page.

(Figure 2I and J). Taken together, these results indicate that *H19* can have a direct role in the profibrotic phenotype of SSc fibroblasts, and inducing *H19* is sufficient to activate a strong profibrotic phenotype in HC fibroblasts.

LncRNA *H19* is regulated by STAT3 in dermal fibroblasts. The regulation of *H19* has been explored in other cellular models, where previously it has been described downstream of SMADs and of STAT3.[27,28] Consistent with these models, Li et al have shown that TGF-β can significantly induce *H19* levels in hepatic stellate cells in the context of profibrotic activation.[5] The TGF-β canonical signaling pathway signals via TGF-β receptor type 1 mediating SMAD proteins. On the other hand, STAT3 is activated by several inflammatory cytokines, as IL-6, and phosphorylated at Tyr-705 by kinases such as JAK, SRC, and JNK, also mediators of the TGF-β noncanonical pathways.[29]

To explore the regulation of *H19* expression in dermal fibroblasts, our first approach was to stimulate HC fibroblast with TGF-β and in combination with the TGF-βR inhibitor (SD208) or STAT3 dimerization inhibitor (CTS) (Figure 3A). Protein analysis showed that TGF-β induced phosphorylation of SMAD3 and STAT3 (Tyr-705), which was suppressed by SD208, as expected. Treatment with CTS decreased total STAT3 levels and prevented its phosphorylation (Tyr-705) while leaving SMAD3 phosphorylation levels unaffected (Figure 3B). In this experimental setting, TGF-β stimulation significantly increased *H19* gene expression by 2.2-fold in HC fibroblasts ($P < 0.0001$), which was reduced by SD208. On the contrary, prevention of STAT3 dimerization led to a significant decrease (71%; $P < 0.0001$) in *H19* levels (Figure 3C).

In a complementary approach, we induced *H19* expression in HC fibroblasts with TGF-β and directly targeted STAT3 with specific siRNA (siSTAT3). STAT3 knockdown was assessed by mRNA levels (Figure 3D). Consistent with our previous findings, siRNA targeting of STAT3 significantly suppressed TGF-β–mediated *H19* induction ($P < 0.001$) (Figure 3E). These results suggested that the effects of TGF-β on *H19* are directly mediated by STAT3.

To explore the effect of other sources of STAT3 activation on *H19* levels, we treated HC fibroblast with human recombinant IL-6. Six hours of IL-6 stimulation induced a significant (46-fold) phosphorylation of STAT3 (Tyr-705) as well as an increase in *STAT3* mRNA levels by 1.7-fold, as expected (Figure 3F and G). In this experimental setting, *H19* expression was induced by 1.7-fold ($P < 0.001$), which was entirely suppressed by siRNA knockdown of STAT3 despite a limited efficiency (42%) (Figure 3H). RNA-sequencing of primary human dermal fibroblast revealed that the IL-11 receptor α subunit is one of the most highly expressed receptors part of the IL-6 family.[30] Consistently, 6 hours of IL-11 stimulation also induced a significant phosphorylation of STAT3 (Tyr-705) and *STAT3* mRNA levels by 4.8-fold ($P < 0.05$) (Figure 3I and J). *H19* expression was induced by 3.5-fold ($P < 0.05$), which was partially suppressed by siRNA knockdown of STAT3 (Figure 3K).

STAT3 activation is consistently reported to be increased in SSc skin and fibroblasts.[29] Furthermore, a previous study showed that pSTAT3 can access the promoter of *H19* in pancreatic cancer cells.[31] Here, using ChIP analysis, we showed that pSTAT3 binds to the *H19* promoter in SSc dermal fibroblasts. pSTAT3 was enriched five-fold at the *H19* promoter compared with the IgG control (Figure 3L). This suggests a role for STAT3 in the regulation of *H19* expression in SSc dermal fibroblasts. This was confirmed when we knocked down STAT3 in SSc dermal fibroblasts, given their known increased STAT3 activation.[29] Silencing of STAT3 in SSc dermal fibroblasts led to a significant suppression of baseline *H19* expression ($P < 0.01$) (Figure 3M and N). Taken together, these data suggest *H19* expression in fibroblasts is regulated by STAT3 both in HC fibroblasts following TGF-β or IL-6/IL-11 stimulation and in SSc dermal fibroblasts.

LncRNA *H19* dermal fibroblast expression can modulate cell-cell communication and induction of STAT3 activation in epidermal cells. We previously observed *H19* expression in the epidermis (Figure 1A) and STAT3 being both upstream and downstream of *H19* regulation in dermal fibroblasts (Figures 2 and 3). This is of interest as STAT3 signaling has been reported to regulate keratinocyte differentiation and skin homeostasis, which is disrupted in SSc.[32,33] We next wanted to assess the effect of *H19* in keratinocyte STAT3 activation. Costaining for *H19* and STAT3 in SSc skin suggested that

Figure 2. *H19* knockdown decreased profibrotic activation of SSc fibroblasts, in vitro. On the contrary, overexpression of *H19* induced profibrotic activation of HC dermal fibroblasts. (A) mRNA expression in SSc SCR and *H19* knockdown fibroblast using siRNA1 and 2 at 48 hours in serum-starved media. Normalized to *GAPDH* mRNA levels, fold change to SCR. (B) Left: Western blot of the indicated markers in SSc fibroblast transfected with SCR and *H19* siRNA1 at 48 hours in serum-starved media. Right: densitometry of indicated markers relative to SCR (SCR = 1). (C) Area of collagen gel in percentage over time of SSc SCR (black) and *H19* knockdown fibroblast using siRNA1 (gray). (D) Gel weight in milligrams after 48 hours of the gel conditions shown in panel C. (E) *H19* mRNA expression normalized to *GAPDH* mRNA levels in HC fibroblast H19OE and control. (F) mRNA expression in HC fibroblast H19OE and control. Normalized to *GAPDH* mRNA levels, fold change to control. (G) Western blot of the indicated markers in HC H19OE and control. (H) Area of collagen gel in percentage over time of healthy fibroblast H19OE (gray) and control (black). (I) *Col1A1* mRNA expression in control and H19OE transfected with mimic negative control or mimic miR29a for 48 hours. Normalized to *GAPDH* mRNA levels, fold change to control. (J) *STAT3* mRNA expression from panel I. Data show mean ± SEM. *$P < 0.05$; **$P < 0.01$; ***$P < 0.001$; ****$P < 0.0001$. HC, healthy control; mRNA, messenger RNA; ns, not significant; SCR, scramble; siRNA, small interfering RNA; SSc, systemic sclerosis.

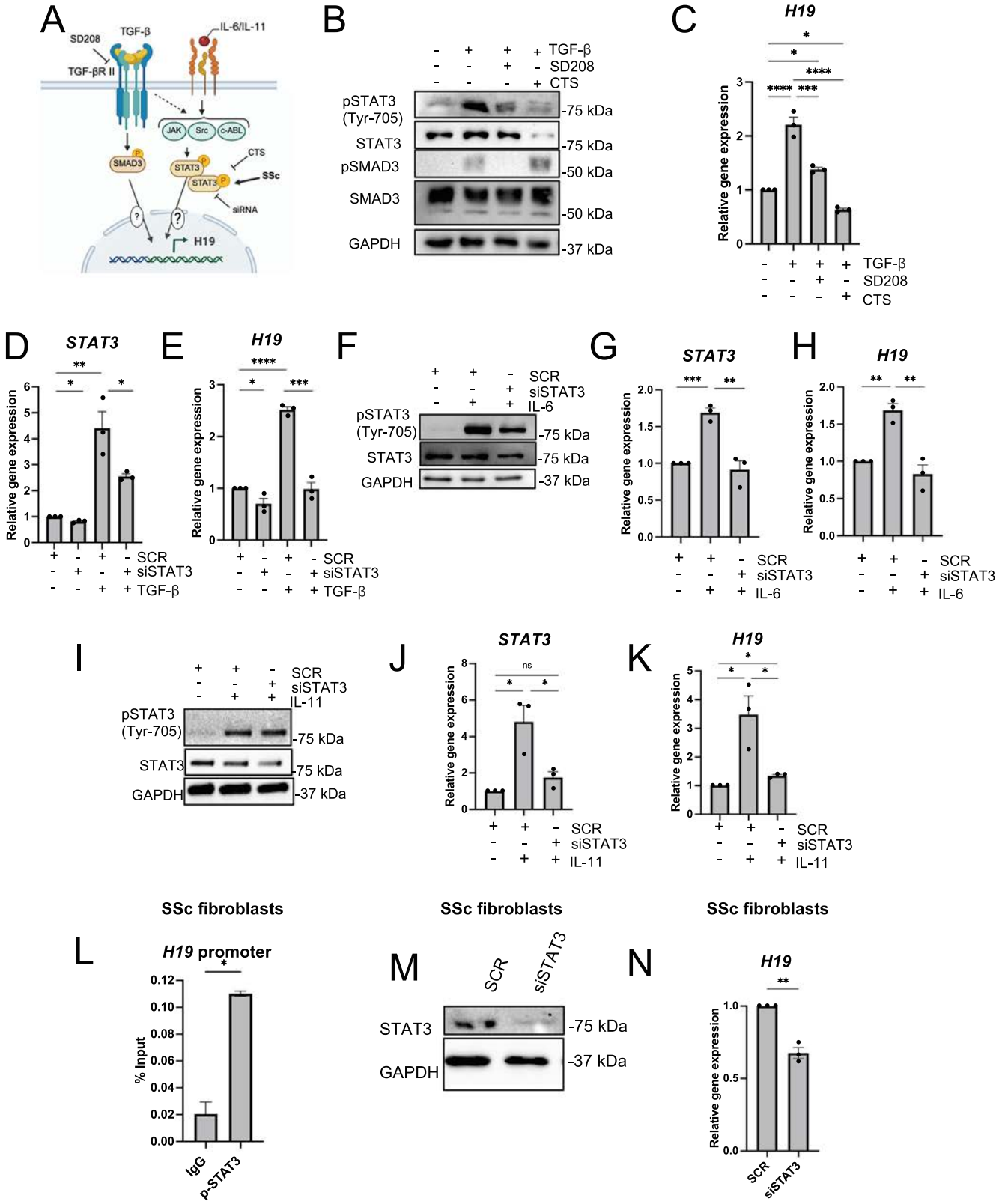

Figure 3. Legend on next page.

higher levels of *H19* align to high STAT3 protein levels, colocalizing within the lower base of the epidermis and fibroblasts (representative images are shown in Figure 4A; Figure 4B shows the quantification of the percentage of STAT3 and *H19* per area). Because fibroblast to keratinocyte communication, partially via exosomes, is known to be key in skin homeostasis,[4] we hypothesized that higher *H19* levels in SSc fibroblasts could play a key role in keratinocyte STAT3 activation. To investigate this, we first cocultured SSc and HC fibroblast with HaCaTs in which we assessed STAT3 levels after 48 hours (Figure 4C). SSc fibroblasts significantly induced phosphorylation of STAT3 (Tyr-705) by 1.4-fold ($P < 0.05$) in HaCaTs compared with HC fibroblast (Figure 4D and E). Next, we cocultured HaCaTs with SSc fibroblast with *H19* knockdown (siRNA1; Figure 4F). Importantly, knockdown of *H19* in SSc fibroblasts prevented keratinocyte activation as assessed by the total and phosphorylation protein levels of STAT3 (Figure 4G and H). Previously, our group showed that SSc fibroblasts can induce phosphorylation of STAT1 in keratinocytes when cocultured in vitro[34] and through exosomes.[4] Interestingly, *H19* knockdown in fibroblasts also prevented phosphorylation of STAT1 in HaCaTs (Figure 4I and J). All together, we conclude that *H19* expression in dermal fibroblasts can regulate STAT3 and STAT1 activation in epidermal cells.

DISCUSSION

The importance of fibroblasts to keratinocyte crosstalk maintaining skin homeostasis in SSc has recently been shown, where SSc exosomes induced an innate immune activation of keratinocytes, similar to that observed in SSc skin. RNA-sequencing of exosome cargo highlighted lncRNA *H19* as a potential mediator of cell-to-cell communication in SSc.[4] In the present study we confirm *H19* expression in SSc skin and show that specific manipulation of its expression can impact inflammatory, as well as fibrotic, phenotypes in skin. Specifically, we show for the first time that *H19* is up-regulated in SSc skin and explanted dermal fibroblast compared with HCs. Importantly, we show that despite being variable, *H19* expression shows a moderate, albeit significant, positive correlation to well-described profibrotic markers in SSc explanted dermal fibroblasts. In addition, despite the limited sample size, we observe an alignment between expression of *H19* and COL-1, as well as STAT3, in SSc skin. This observation may offer a molecular basis to the known heterogeneity of skin fibrosis severity in SSc.[26,27]

We identified *H19* as an epigenetic factor important for fibroblast activation. In vitro, knockdown of *H19* in SSc fibroblasts and overexpression of *H19* in healthy fibroblasts modulated profibrotic markers and the cell contraction ability of these cells. There are different regulatory mechanisms described downstream of *H19*, including sponging miRNA.[8,35] *H19* can bind different miRNAs such as miRNA17, miR29a, or miR196a.[22,36–38] Previous studies have shown downregulation of miR29a in SSc skin and fibroblast compared with HCs.[23,24] Moreover, reintroduction of miR29a in SSc fibroblast significantly reduced COL-1 transcript levels.[24] In addition, miR29a has been implicated in the regulation of STAT3 in cancer cells.[25,26] Because of our interest in understanding the role of *H19* in regulating profibrotic markers and hypothesizing a regulatory loop between STAT3 and *H19*, we further investigated the effect of miR29a in restoring *STAT3* and *Col1A1* levels in fibroblast overexpressing *H19*. Although this approach allowed us to better understand the regulatory role of *H19* in dermal fibroblast, it is important to consider that for the purpose of this study we did not analyze the basal levels of miRNAs in our *H19* overexpressing model. Moreover, the regulatory role of *H19* is complex and involves multiple mechanisms that could be explored in future studies.

Our study highlights that IL-6, IL-11, and TGF-β, very well-described factors in SSc, regulate *H19* expression mainly via the STAT3 signaling pathway (Figure 5), which has been shown to be instrumental for fibroblast to myofibroblast transition.[29] In this context, additional studies to decipher the role of other imputed

Figure 3. *H19* is regulated by STAT3 in dermal fibroblast. (A) Schematic design of the canonical and noncanonical TGF-β pathway, IL-6/IL-11 pathways, and the different inhibitors used (created with BioRender.com). (B) Western blot of the indicated markers in HC fibroblast serum starved ON, followed by SD208 or CTS for 24 hours and another 24 hours of TGF-β or the corresponding control. (C) *H19* mRNA levels normalized to *GAPDH* from panel B. (D) *STAT3* mRNA levels normalized to *GAPDH* in HC fibroblast transfected with siSTAT3 or SCR, 24-hour later cells were serum starved ON and 24-hour TGF-β induced or corresponding control. (E) *H19* mRNA levels normalized to *GAPDH* from panel D. (F) Western blot of the indicated markers in HC fibroblast transfected with siSTAT3 or SCR, 24-hour later cells were serum starved ON and 6-hour IL-6 or corresponding control. (G) *STAT3* mRNA levels normalized to *GAPDH* from panel F. (H) *H19* mRNA levels normalized to *GAPDH* from panel F. (I) Western blot of the indicated markers in HC fibroblast transfected with siRNA STAT3 or SCR, 24-hour later cells were serum starved ON and 6-hour IL-11 or corresponding control. (J) *STAT3* mRNA levels normalized to *GAPDH* from panel I. (K) *H19* mRNA levels normalized to *GAPDH* from panel I. (L) Chromatin immunoprecipitation assay performed using p-STAT3 antibody and IgG control, followed by reverse transcription–quantitative polymerase chain reaction using primers specific for *H19* promoter. The data were normalized according to the percentage input method. (M) Western blot of STAT3 and GAPDH in SSc fibroblast transfected with siSTAT3 for 24 hours and then serum-starved media for another 48 hours. (N) *H19* mRNA levels normalized to *GAPDH* from panel M. Data shows mean ± SEM. $^{*}P < 0.05$; $^{**}P < 0.01$; $^{***}P < 0.001$; $^{****}P < 0.0001$. CTS, cryptotanshinone; HC, healthy control; IL, interleukin; mRNA, messenger RNA; ns, not significant; ON, overnight; SCR, scramble; siRNA, small interfering RNA; siSTAT3, STAT3 with specific siRNA; SSc, systemic sclerosis; TGF-β, transforming growth factor-β. Color figure can be viewed in the online issue, which is available at http://onlinelibrary.wiley.com/doi/10.1002/art.70104/abstract.

soluble mediators of profibrotic activation in SSc (such as Shh, NOTCH, and WNT) in the regulation of *H19* are warranted.

Our work supports the idea that aberrant *H19* expression in SSc dermal fibroblasts induces STAT3 and STAT1 activation in the adjacent keratinocytes (Figure 4). We propose that SSc fibroblasts secrete *H19* in exosomes as shown in our recent work.[4] Although exosome analyses were beyond the scope of this study, our data showed that *H19* downregulation affects several signaling pathways. We therefore speculate that, alongside *H19*, other factors may play key roles in exosomal cargo

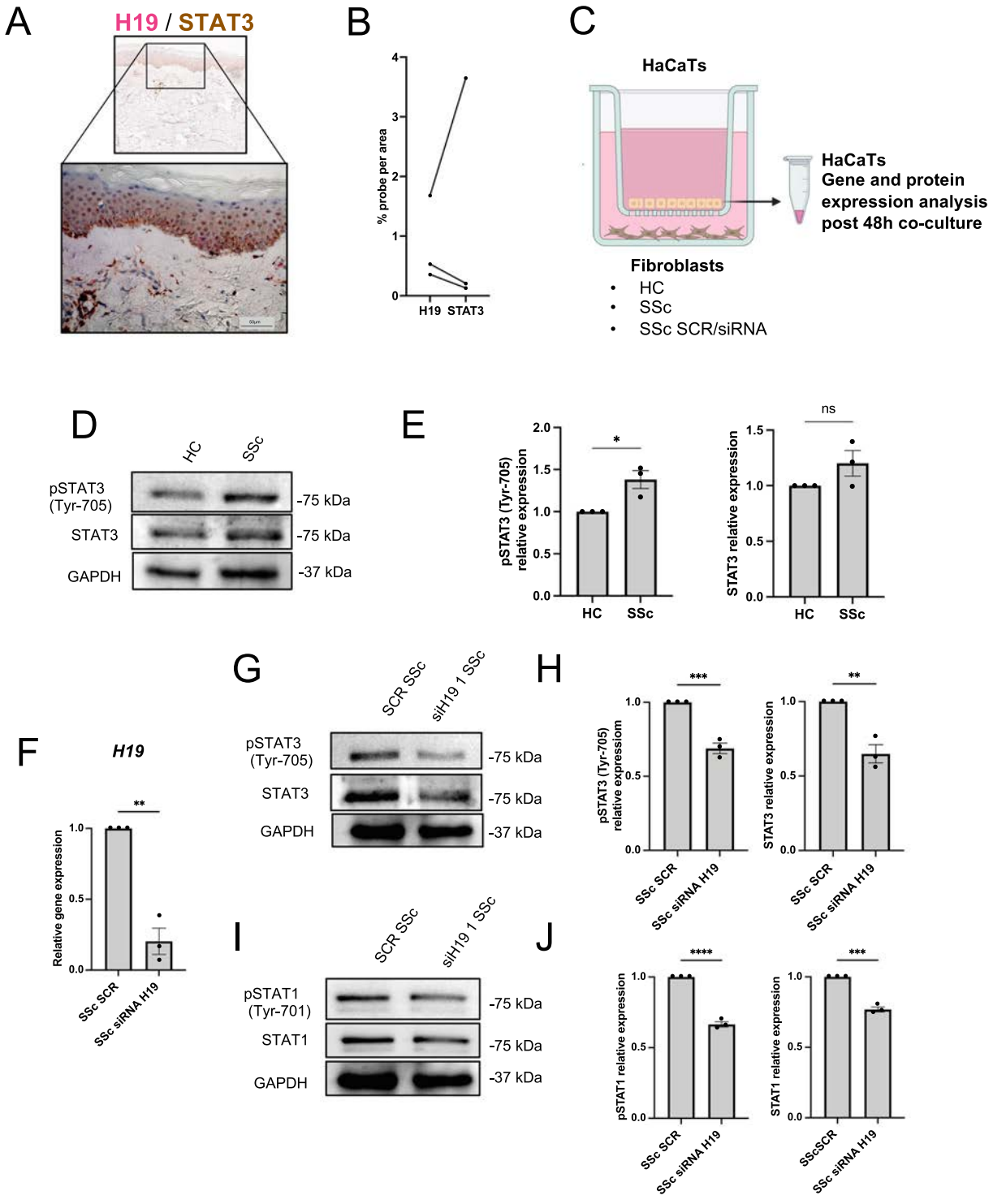

Figure 4. Legend on next page.

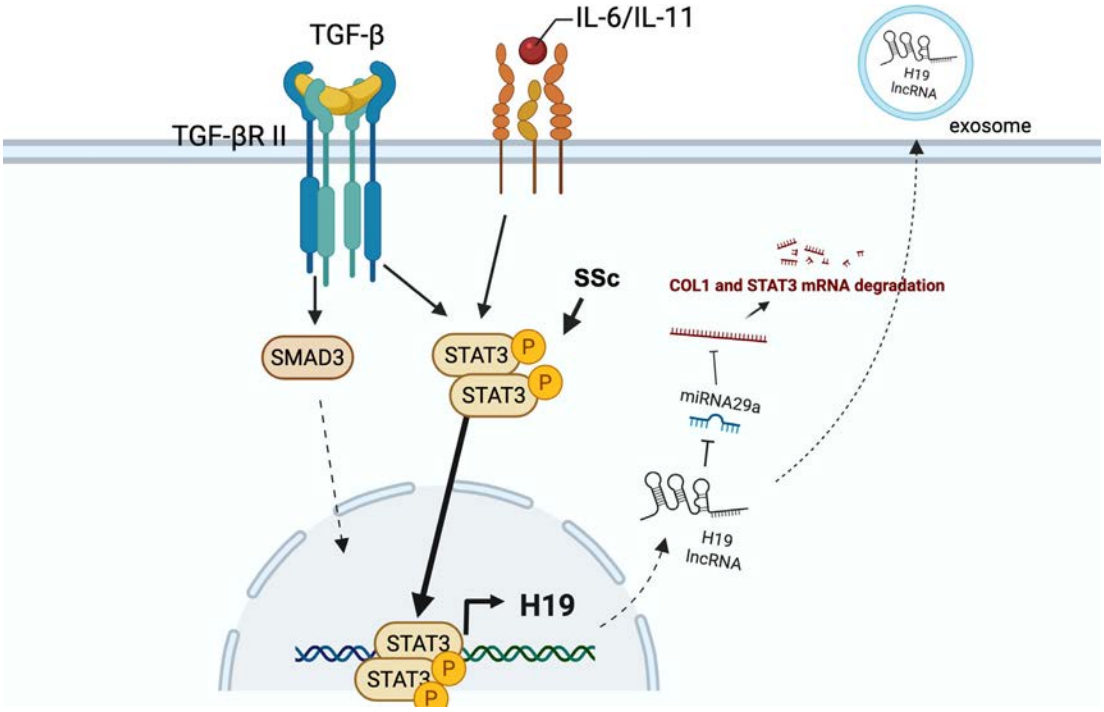

Figure 5. *H19* regulatory mechanisms in SSc fibroblast. TGF-β and IL-6/IL-11, via SMAD3 and mainly STAT3 downstream signaling pathways, known to be increased in SSc, induce *H19* expression in dermal fibroblast. *H19* regulates profibrotic markers by sponging miRNA29a among other mechanisms described in the literature. We propose that *H19* is secreted into exosomes important in cell-to-cell communication. Created with BioRender.com. IL, interleukin; lncRNA, long noncoding RNA; miRNA29a, micro-RNA 29a; mRNA, messenger RNA; SSc, systemic sclerosis; TGF-β, transforming growth factor-β. Color figure can be viewed in the online issue, which is available at http://onlinelibrary.wiley.com/doi/10.1002/art.70104/abstract.

composition and intercellular communication. It should be noted that exosomal *H19* may originate not only from fibroblasts but also from other cell types, including adipose mesenchymal stem cells and macrophages.[39,40]

Although a complete characterization of inflammatory pathways fell outside the scope of this study, we found this particularly interesting as dysregulation of the type I interferon pathway and STAT3 have been implicated in the pathogenesis of SSc.[4,29,41] Furthermore, a number of studies link *H19* to inflammatory pathways as NF-κB, p38/MAPK/mammalian target of rapamycin, toll-like receptor, and tumor necrosis factor-α while this is context dependent and still unclear.[42] One study suggested *H19* recruiting STAT1 into the nucleus to enhance the transcriptional expression of sorting nexin 10, promoting proliferation, invasion, and tube formation of fibroblast-like synoviocytes in rheumatoid arthritis.[43] Thus, a more detailed characterization of keratinocytes by transcriptomic analysis would be key to extend our analysis of *H19*'s role in skin inflammation in SSc. Interestingly, STAT3 can induce epithelial to mesenchymal transition (EMT), which supports a potential role of *H19* in the observed EMT in SSc skin. Inconsistencies about the role of *H19* and EMT are found in the literature showing either induction or reversion of EMT independently of EMT inducers.[42] Further studies will be required to address this question.

Overall, our data shed new light into the complex pathogenesis of SSc and, together with previous works from our group,

Figure 4. SSc fibroblast-induced STAT3 and STAT1 activation in epidermal cells is dependent on *H19*. (A) RNAScope of *H19* (pink) co-stained with STAT3 (brown) in representative SSc skin. Scale bar = 50 μm. (B) Graph represents the percentage of *H19* and STAT3 costaining per sample (n = 3). (C) Schematic design of the fibroblast and HaCaTs coculture. (D) Western blot of the indicated markers in HaCaTs cocultured with HC or SSc fibroblast for 48 hours. (E) Densitometry of pSTAT3 (Tyr-705) protein expression (left) and total STAT3 (right) normalized to GAPDH from panel D. Represented as fold change to HC. (F) mRNA transcript levels of *H19* in SSc SCR or *H19* knockdowned after 48 hours of coculture and 72 hours after transfection. (G) Western blot of the indicated markers in HaCaTs cocultured for 48 hours with SSc SCR and *H19* knockdowned fibroblasts. (H) Densitometry of pSTAT3 (Tyr-705) protein expression (left) and total STAT3 (right) normalized to GAPDH from panel G. Represented as fold change to SCR SSc. (I) Western blot of the indicated markers in HaCaTs cocultured for 48 hours with SSc SCR and *H19* knockdowned fibroblasts. (J) Densitometry of pSTAT1 protein expression (left) and total STAT1 (right) normalized to GAPDH from panel H. Represented as fold change to SCR SSc. Data show mean ± SEM. $^{*}P < 0.05$; $^{**}P < 0.01$; $^{***}P < 0.001$; $^{****}P < 0.0001$. HaCaT, human immortalized epidermal keratinocyte; HC, healthy control; mRNA, messenger RNA; ns, not significant; SCR, scramble; siRNA, small interfering RNA; SSc, systemic sclerosis. Color figure can be viewed in the online issue, which is available at http://onlinelibrary.wiley.com/doi/10.1002/art.70104/abstract.

supports the notion of lncRNAs playing a key part in epigenetic regulation of SSc. Collectively, our study indicates that *H19* lncRNA is a key mediator of STAT3-induced changes in SSc skin and could be considered a promising therapeutic target in tissue fibrosis.

AUTHOR CONTRIBUTIONS

All authors contributed to at least one of the following manuscript preparation roles: conceptualization AND/OR methodology, software, investigation, formal analysis, data curation, visualization, and validation AND drafting or reviewing/editing the final draft. As corresponding author, Dr Del Galdo confirms that all authors have provided the final approval of the version to be published and takes responsibility for the affirmations regarding article submission (eg, not under consideration by another journal), the integrity of the data presented, and the statements regarding compliance with institutional review board/Declaration of Helsinki requirements.

REFERENCES

1. Denton CP, Khanna D. Systemic sclerosis. Lancet 2017;390(10103):1685–1699. doi:10.1016/S0140-6736(17)30933-9
2. Piek E, Ju WJ, Heyer J, et al. Functional characterization of transforming growth factor β signaling in Smad2- and Smad3-deficient fibroblasts. J Biol Chem 2001;276(23):19945–19953. doi:10.1074/jbc.M102382200
3. Truchetet ME, Brembilla NC, Chizzolini C. Current concepts on the pathogenesis of systemic sclerosis. Clin Rev Allergy Immunol 2023;64(3):262–283. doi:10.1007/s12016-021-08889-8
4. Bryon J, Wasson CW, Koeppen K, et al. Systemic sclerosis dermal fibroblast exosomes trigger type 1 interferon responses in keratinocytes via a TBK/JAK/STAT signaling axis. Arthritis Rheumatol 2025;77(3):322–334. doi:10.1002/art.43029
5. Li XJY, Zhou F, Li YJ, et al. LncRNA H19-EZH2 interaction promotes liver fibrosis via reprogramming H3K27me3 profiles. Acta Pharmacol Sin 2023;44(12):2479–2491. doi:10.1038/s41401-023-01145-z
6. Wasson CW, Ross RL, Wells R, et al. Long non-coding RNA HOTAIR induces GLI2 expression through Notch signalling in systemic sclerosis dermal fibroblasts. Arthritis Res Ther 2020;22(1):286. doi:10.1186/s13075-020-02376-9
7. Wasson CW, Abignano G, Hermes H, et al. Long non-coding RNA HOTAIR drives EZH2-dependent myofibroblast activation in systemic sclerosis through miRNA 34a-dependent activation of NOTCH. Ann Rheum Dis 2020;79(4):507–517. doi:10.1136/annrheumdis-2019-216542
8. Ghafouri-Fard S, Esmaeili M, Taheri M. H19 lncRNA: roles in tumorigenesis. Biomed Pharmacother 2020;123:109774. doi:10.1016/j.biopha.2019.109774
9. Li J, Cao LT, Liu HH, et al. Long non coding RNA H19: an emerging therapeutic target in fibrosing diseases. Autoimmunity 2020;53(1):1–7. doi:10.1080/08916934.2019.1681983
10. Pachera E, Assassi S, Salazar GA, et al. Long noncoding RNA H19X is a key mediator of TGF-β-driven fibrosis. J Clin Invest 2020;130(9):4888–4905. doi:10.1172/JCI135439
11. Wasson CW, Perez Barreiro E, Del Galdo F, et al. Lysine demethylase 1 has demethylase-dependent and non-canonical functions in myofibroblast activation in systemic sclerosis. Cells 2025;14(6):433. doi:10.3390/cells14060433
12. Jiang X, Ning Q. The mechanism of lncRNA H19 in fibrosis and its potential as novel therapeutic target. Mech Ageing Dev 2020;188:111243. doi:10.1016/j.mad.2020.111243
13. Tang Y, He R, An J, et al. The effect of H19-miR-29b interaction on bleomycin-induced mouse model of idiopathic pulmonary fibrosis. Biochem Biophys Res Commun 2016;479(3):417–423. doi:10.1016/j.bbrc.2016.09.028
14. Liu R, Li X, Zhu W, et al. Cholangiocyte-derived exosomal long noncoding RNA H19 promotes hepatic stellate cell activation and cholestatic liver fibrosis. Hepatology 2019;70(4):1317–1335. doi:10.1002/hep.30662
15. Creemers EE, van Rooij E. Function and therapeutic potential of noncoding RNAs in cardiac fibrosis. Circ Res 2016;118(1):108–118. doi:10.1161/CIRCRESAHA.115.305242
16. Khedr AM, Shaker OG, El-Komy MH, et al. miRNA-133 and lncRNA-H19 expressions and their relation to serum levels of PKM2 and TGF-β in patients with systemic sclerosis. Noncoding RNA Res 2023;9(1):253–261. doi:10.1016/j.ncrna.2023.12.003
17. Van den Hoogen F, Khanna D, Fransen J, et al. Classification criteria for systemic sclerosis: an American college of rheumatology/European league against rheumatism collaborative initiative. Ann Rheum Dis 2013;72(11):1747–1755. doi:10.1136/annrheumdis-2013-204424
18. LeRoy EC, Medsger TA. Criteria for the classification of early systemic sclerosis. J Rheumatol 2001;28(7):1573–1576.
19. Ross RL, Caballero-Ruiz B, Clarke EL, et al. Biological hallmarks of systemic sclerosis are present in the skin and serum of patients with very early diagnosis of systemic sclerosis (VEDOSS). Rheumatology (Oxford) 2025;64(6):3606–3617. doi:10.1093/rheumatology/keae698
20. Gillespie J, Ross RL, Corinaldesi C, et al. Transforming growth factor β activation primes canonical Wnt signaling through down-regulation of axin-2. Arthritis Rheumatol 2018;70(6):932–942. doi:10.1002/art.40437
21. Shi S, Song L, Yu H, et al. Knockdown of LncRNA-H19 ameliorates kidney fibrosis in diabetic mice by suppressing miR-29a-mediated EndMT. Front Pharmacol 2020;11:586895. doi:10.3389/fphar.2020.586895
22. Wang Z, Feng C, Song K, et al. lncRNA-H19/miR-29a axis affected the viability and apoptosis of keloid fibroblasts through acting upon COL1A1 signaling. J Cell Biochem 2020;121(11):4364–4376. doi:10.1002/jcb.29649
23. Jafarinejad-Farsangi S, Gharibdoost F, Farazmand A, et al. MicroRNA-21 and microRNA-29a modulate the expression of collagen in dermal fibroblasts of patients with systemic sclerosis. Autoimmunity 2019;52(3):108–116. doi:10.1080/08916934.2019.1621856
24. Maurer B, Stanczyk J, Jüngel A, et al. MicroRNA-29, a key regulator of collagen expression in systemic sclerosis. Arthritis Rheum 2010;62(6):1733–1743. doi:10.1002/art.27443
25. Liu S, Zhang X, Hu C, et al. miR-29a inhibits human retinoblastoma progression by targeting STAT3. Oncol Rep 2018;39(2):739–746. doi:10.3892/or.2017.6144
26. Gao J, Shao Z, Yan M, et al. Targeted regulation of STAT3 by miR-29a in mediating taxol resistance of nasopharyngeal carcinoma cell line CNE-1. Cancer Biomark 2018;22(4):641–648. doi:10.3233/CBM-170964
27. Bergström R, Savary K, Morén A, et al. Transforming growth factor β promotes complexes between Smad proteins and the CCCTC-binding factor on the H19 imprinting control region chromatin. J Biol Chem 2010;285(26):19727–19737. doi:10.1074/jbc.M109.088385
28. Li L, Wei J, Hei J, et al. Long non-coding RNA H19 regulates proliferation of ovarian granulosa cells via STAT3 in polycystic ovarian syndrome. Arch Med Sci 2019;17(3):785–791. doi:10.5114/aoms.2019.89254
29. Chakraborty D, Šumová B, Mallano T, et al. Activation of STAT3 integrates common profibrotic pathways to promote fibroblast activation

and tissue fibrosis. Nat Commun 2017;8(1):1130. doi:10.1038/s41467-017-01236-6

30. Adami E, Viswanathan S, Widjaja AA, et al. IL11 is elevated in systemic sclerosis and IL11-dependent ERK signalling underlies TGFβ-mediated activation of dermal fibroblasts. Rheumatology (Oxford) 2021;60(12):5820–5826. doi:10.1093/rheumatology/keab168
31. Sasaki N, Hirano K, Shichi Y, et al. Gp130-mediated STAT3 activation contributes to the aggressiveness of pancreatic cancer through *H19* long non-coding RNA expression. Cancers (Basel) 2022;14(9):2055. doi:10.3390/cancers14092055
32. Miyauchi K, Ki S, Ukai M, et al. Essential role of STAT3 signaling in hair follicle homeostasis. Front Immunol 2021;12:663177. doi:10.3389/fimmu.2021.663177
33. Nikitorowicz-Buniak J, Shiwen X, Denton CP, et al. Abnormally differentiating keratinocytes in the epidermis of systemic sclerosis patients show enhanced secretion of CCN2 and S100A9. J Invest Dermatol 2014;134(11):2693–2702. doi:10.1038/jid.2014.253
34. Wasson CW, Dibb SL, Caballero-Ruiz B, et al. Transforming growth factor beta (TGF-β) induces type 1 interferon signalling in systemic sclerosis keratinocytes through the chloride intracellular channel 4 (CLIC4). Arthritis Res Ther 2025;27(1):173. doi:10.1186/s13075-025-03632-6
35. Mattick JS, Amaral PP, Carninci P, et al. Long non-coding RNAs: definitions, functions, challenges and recommendations. Nat Rev Mol Cell Biol 2023;24(6):430–447. doi:10.1038/s41580-022-00566-8
36. Huang Z, Lei W, Hu HB, et al. H19 promotes non-small-cell lung cancer (NSCLC) development through STAT3 signaling via sponging miR-17. J Cell Physiol 2018;233(10):6768–6776. doi:10.1002/jcp.26530
37. Liu L, Liu L, Lu S. lncRNA H19 promotes viability and epithelial-mesenchymal transition of lung adenocarcinoma cells by targeting miR-29b-3p and modifying STAT3. Int J Oncol 2019;54(3):929–941. doi:10.3892/ijo.2019.4695
38. Lu Q, Guo Z, Xie W, et al. The lncRNA H19 mediates pulmonary fibrosis by regulating the miR-196a/COL1A1 axis. Inflammation 2018;41(3):896–903. doi:10.1007/s10753-018-0744-4
39. Zhang Y, Hong L, Li X, et al. M1 macrophage-derived exosomes promote autoimmune liver injury by transferring long noncoding RNA H19 to hepatocytes. MedComm 2023;4(4):e303. doi:10.1002/mco2.303
40. Qian L, Pi L, Fang BR, et al. Adipose mesenchymal stem cell-derived exosomes accelerate skin wound healing via the lncRNA H19/miR-19b/SOX9 axis. Lab Invest 2021;101(9):1254–1266. doi:10.1038/s41374-021-00611-8
41. Kakkar V, Assassi S, Allanore Y, et al. Type 1 interferon activation in systemic sclerosis: a biomarker, a target or the culprit. Curr Opin Rheumatol 2022;34(6):357–364. doi:10.1097/BOR.0000000000000907
42. Wang B, Suen CW, Ma H, et al. The roles of H19 in regulating inflammation and aging. Front Immunol 2020;11:579687. doi:10.3389/fimmu.2020.579687
43. Sun Y, Guo Y, Chang L, et al. Long noncoding RNA H19 synergizes with STAT1 to regulate SNX10 in rheumatoid arthritis. Mol Immunol 2023;153:106–118. doi:10.1016/j.molimm.2022.11.018

Arthritis & Rheumatology
Vol. 78, No. 9, September 2026, pp 1942–1951
DOI 10.1002/art.70096
© 2026 The Author(s). *Arthritis & Rheumatology* published by Wiley Periodicals LLC on behalf of American College of Rheumatology.
This is an open access article under the terms of the Creative Commons Attribution-NonCommercial License, which permits use, distribution and reproduction in any medium, provided the original work is properly cited and is not used for commercial purposes.

American College of Rheumatology
Empowering Rheumatology Professionals

Investigating the Role of Type I Interferon Signaling on Muscle Disease Using Mouse Models

Rita Spathis, MS,[1] Sabrina Narvesen, BS,[1] Deeva Robles Kuriplach, BS,[1] Karen Huang, BS,[1] Teja Sundar, MS,[1] Elizabeth Bagley, BS,[1] Joanna Parkes, PhD,[1] Xinyu Jia, PharmD,[1] Nandhana Sudhan,[2] Alfredo Guzman, MA,[1] Kanneboyina Nagaraju, PhD, DVM,[1] and Melissa Morales, PhD[1]

Objective. Dysregulated type I interferon (IFN) signaling contributes to autoimmune myositis pathogenesis. We investigated the therapeutic effects of JAK inhibitors in two mouse models. We also examined how type I IFNs affect muscle vasculature.

Methods. Myositis was induced in major histocompatibility complex class I double transgenic ([TRE-H-2K^b (H mice)/MCK-tTA (T mice)] (HT)) female mice at day 21. Mice were randomized into four groups (n = 10–11/group): baricitinib (10 mg/kg), tofacitinib (20 mg/kg), vehicle, and healthy controls. Outcomes included survival, weight, muscle strength, histopathology, and IFN-stimulated gene expression. To model IFNβ overexpression, C57BL/6 mice received AAV9-triple muscle-specific creatine kinase (tMCK)-IFNβ and were treated with vehicle or tofacitinib (40 mg/kg/day) for 10 weeks (n = 8–13/group).

Results. Tofacitinib—but not baricitinib—significantly reduced IFN scores in mice with severe myositis ($P < 0.05$). Survival differed across groups (overall log-rank $P < 0.01$), with untreated- and baricitinib-treated HT mice showing shorter survival than BL/6 controls, whereas tofacitinib-treated mice did not differ from controls. IFNβ overexpression induced muscle inflammation ($P < 0.01$), reduced grip strength ($P < 0.0001$), and increased the IFN score ($P < 0.0001$) and H2Kb ($P < 0.0001$) expression.

Conclusion. Tofacitinib reduced the IFN signature, and survival in this group did not differ significantly from healthy controls, whereas untreated and baricitinib-treated HT mice showed shorter survival; functional improvement was not observed. Our results also show that type I IFN signaling contributes to muscle inflammation and weakness, making it a key driver of muscle damage and thereby reinforcing its potential as a therapeutic target.

INTRODUCTION

Idiopathic inflammatory myopathies (myositis) are a rare and heterogeneous group of autoimmune diseases characterized by chronic muscle inflammation, progressive muscle weakness, and fatigue. The disease's rarity and variability in clinical presentation, including involvement of other organs, have made the development of standardized treatment guidelines difficult. Current therapeutic management primarily involves broad immunosuppressives, with glucocorticoids being the first-line treatment, often in combination with a steroid-sparing immunosuppressive agent.[1,2] However, the significant side effects of long-term glucocorticoids and the fact that many patients remain refractory to treatment highlight the need for more targeted therapeutic approaches.[3,4]

A major advancement in understanding myositis pathophysiology is the identification of type I interferon (IFN) dysregulation. An IFN "signature," characterized by elevated expression of type I IFN(α/β)-inducible genes, has been identified in both blood and muscle tissue, particularly in patients with dermatomyositis (DM).[5–8] Moreover, the degree of IFN signature is associated with IFNβ expression and correlates with disease activity.[9–13] Functional studies have provided mechanistic insight into the pathogenic role of type I IFNs in myositis. In vitro, type I IFNs have been shown to impair myotube formation and disrupt vascular network organization,[14] whereas in vivo studies demonstrate that IFN signaling leads to muscle impairment in mice.[15] Collectively,

Supported by The Myositis Association and Cure JM Foundation.
[1]Department of Pharmaceutical Sciences, School of Pharmacy and Pharmaceutical Sciences, Binghamton University, Binghamton, New York; [2]Vestal High School, Vestal, New York.
Author disclosures and graphical abstract are available at https://onlinelibrary.wiley.com/doi/10.1002/art.70096.

Address correspondence via email to Melissa Morales, PhD, at mmorales@binghamton.edu.
Submitted for publication June 16, 2025; accepted in revised form February 5, 2026.

these findings highlight type I IFN as a key contributor to myositis pathogenesis and provide support for therapeutic strategies targeting IFN signaling, such as JAK/STAT inhibitors. Given the dysregulation of type I IFN signaling in myositis, JAK inhibitors have been investigated as a potential treatment for patients with DM.[16–18] Notably, patients with myositis have demonstrated significant clinical improvement following treatment with US Food and Drug Administration (FDA)–approved JAK inhibitors, including baricitinib, tofacitinib, and ruxolitinib.[14,19–21]

To better understand disease mechanisms and evaluate potential therapies, several mouse models of myositis have been developed.[22] One widely used mouse model involves overexpressing major histocompatibility complex (MHC) class I, an early feature observed in myositis.[23–25] In these transgenic mice, MHC class I overexpression in skeletal muscle recapitulates key aspects of human myositis, including upregulation of IFN-stimulated genes (ISGs).[26,27] Although both baricitinib and tofacitinib target JAK1, baricitinib also inhibits JAK2, whereas tofacitinib also inhibits JAK3, mediating different cytokine signaling pathways.[28] Therefore, we sought to directly compare the effects of these two JAK inhibitors on disease progression in the MHC class I transgenic mouse model. Furthermore, to directly assess the impact of IFNβ on muscle function, we developed a novel mouse model with targeted IFNβ expression in skeletal muscle.

MATERIALS AND METHODS

Animal studies. All mouse experimental procedures were performed under approved Institutional Animal Care and Use Committee (IACUC) protocols and in accordance with guidelines at Binghamton University. Mice were housed at Binghamton University's animal facility under a 12-hour light/dark cycle and fed a standard mouse chow diet.

MHC class I model of myositis. Generation of conditional MHC class I transgenic mice was described previously.[26] Briefly, these transgenic mice contain the tetracycline-responsive element–H-2Kb (H mice) in the germ line, and when bred with mice stably expressing tetracycline-controlled transactivator by a muscle-specific creatine kinase (MCK) promotor (T mice), produce double transgenic myositis (HT) mice, resulting in inducible H-2Kb expression. H-2Kb expression is suppressed by including doxycycline in the drinking water of the HT mice. In this study, HT breeders were maintained on drinking water containing doxycycline hydrochloride (200 μg/mL; Sigma) dissolved in 2% sucrose. At weaning (postnatal day 21), doxycycline water was replaced with regular drinking water to induce H-2Kb expression at a young age.[29] MHC class I mice were classified as mild HT (HT-M) or severe HT (HT-S) based on the level of MHC class I expression (see results). Previously, it was shown that higher MHC class I expression drives a self-amplifying inflammatory loop involving NF-κB and type I IFN signaling, leading to greater muscle inflammation, dystrophin loss, and functional impairment.[27] Female mice were housed with same-sex littermates and randomly assigned to the following four experimental groups: group 1, BL/6 (single transgenic) with vehicle (n = 10); group 2, HT with vehicle (n = 11); group 3, HT with baricitinib (HT+B; n = 11); and group 4, HT with tofacitinib (HT+T; n = 11). Baricitinib and tofacitinib (Advanced ChemBlocks, Inc) were administered as an oral suspension in 10% DMSO/cherry syrup (HUMCO) at 10 mg/kg and 20 mg/kg, respectively. Baricitinib and tofacitinib doses were selected based on preclinical pharmacokinetic and toxicology studies as well as efficacy studies in mouse models of inflammatory and autoimmune diseases.[30–36] BL/6 and HT untreated mice received vehicle only (10% DMSO/cherry syrup). Mice were treated in the same order daily with baricitinib, tofacitinib, or vehicle for six weeks.

IFNβ1-overexpressing mouse model. Five-week-old female C57BL/6 mice were purchased from The Jackson Laboratory. All mice were acclimated to the animal facility for one week before any manipulation. Six-week-old mice were randomly assigned to the following four experimental groups: group 1, BL/6 with vehicle (n = 8); group 2, AAV9-IFNβ1 with vehicle (n = 12); group 3, AAV9-IFNβ1 with tofacitinib, 40 mg/kg (n = 13); and group 4, AAV9-eGFP (n = 2). AAV9-tMCK-m-IFNβ1-WPRE and AAV9-tMCK-eGFP-WPRE (Vector Biolabs) were administered via retro-orbital injection at a dose of 1.6×10^{12} vg/mouse. Tofacitinib was administered in the same order daily as an oral suspension in 10% DMSO/cherry syrup, and vehicle-treated mice received cherry syrup (10% DMSO/cherry syrup) alone for 10 weeks.

Grip strength test. Grip strength was measured using a grip strength meter consisting of horizontal forelimb mesh and force gauge (Columbus Instruments) as previously described.[37] Briefly, all mice were acclimatized to the apparatus for five consecutive days one week before actual data collection. For forelimb strength assessment, the animal was allowed to hold the horizontal mesh with the forelimb paws and then was gently pulled back until its grip was broken. This was repeated five times during each session within a two-minute timeframe. The maximum values for each day over a five-day period were used for subsequent analysis. All grip strength measurements were performed in a anonymized manner and at the same time of day. Data are expressed as normalized forelimb strength in kilogram-force per kilogram.

Tissue collection. Mice were euthanized according to approved IACUC protocols and American Veterinary Medical Association Guidelines on Euthanasia using carbon dioxide inhalation. Skeletal muscles (tibialis anterior, triceps, quadricep) were collected, weighed, and either fixed in 4% paraformaldehyde or flash-frozen in liquid nitrogen–chilled isopentane, then stored at

–80°C until analysis. HT mice reaching their humane endpoint (≥20% body weight loss, hunched posture, or reduced activity) were euthanized early; all others were euthanized at week 6 (MHC class I model) or week 10 (IFNβ1-overexpressing model).

RNA extraction and reverse transcription–polymerase chain reaction. Frozen quadricep muscles were pulverized using a liquid nitrogen–cooled mortar and pestle. Total RNA was extracted from ground tissue by homogenization in TRIzol (Life Technologies) using a handheld pestle to lyse the tissue. RNA was extracted from whole blood using the GeneJET RNA purification kit (ThermoFisher Scientific). After isolation, RNA was quantified on a Nanodrop N1000 spectrophotometer and 1-μg reverse transcribed using qScript cDNA SuperMix (Quantabio). Quantitative reverse transcription–polymerase chain reaction was conducted using TaqMan Fast Advanced Master Mix (Applied Biosystems) and Taqman gene expression assays (ThermoFisher Scientific). *Gapdh* was used as an internal control, and fold change was calculated using the ΔΔCt method. The following TaqMan Assays were used: *H2Kb* (APMF600), *Mx1* (Mm00487796_m1), *Isg15* (Mm01705338_s1), *Irf7* (Mm00516793_g1), *Ifit1* (Mm00515153_m1), and *Gapdh* (Mm99999915_g1).

Histologic evaluation of inflammation. Slides were prepared and stained by Histoserv, Inc. Digital images from each animal were acquired in 20× using an Olympus VS120 slide scanner microscope. One entire transverse quadricep muscle section was analyzed per animal in a anonymized manner. Inflammation foci (group of ≥10 inflammatory cell nuclei) were counted and normalized to the entire tissue section (in squared millimeters).

Immunofluorescence staining. Isopentane frozen quadricep muscles were sectioned at 8 to 10-μm thickness and fixed with acetone for 10 minutes at –20°C. After washing in phosphate buffered saline (PBS), nonspecific binding was blocked with a blocking buffer containing 5% normal goat serum and 0.3% Triton-X100 in PBS. Sections were incubated with a rat monoclonal antibody against CD31 (5 ng/mL; 14-0311-82; ThermoFisher Scientific) overnight at 4°C. After washing in PBS, tissues were incubated for one hour at room temperature with fluorescein isothiocyanate–labeled goat anti-rat IgG2a (0.8 μg/mL; Fisher Scientific) and DAPI (2 μg/mL; Fisher Scientific) for nuclear counterstain. Tissues were washed in PBS containing 0.1% Tween 20, briefly rinsed in deionized water, and coverslipped with ProLong Gold Antifade Mountant (Thermofisher Scientific). Digital images were acquired in 20× using an Olympus VS120 slide

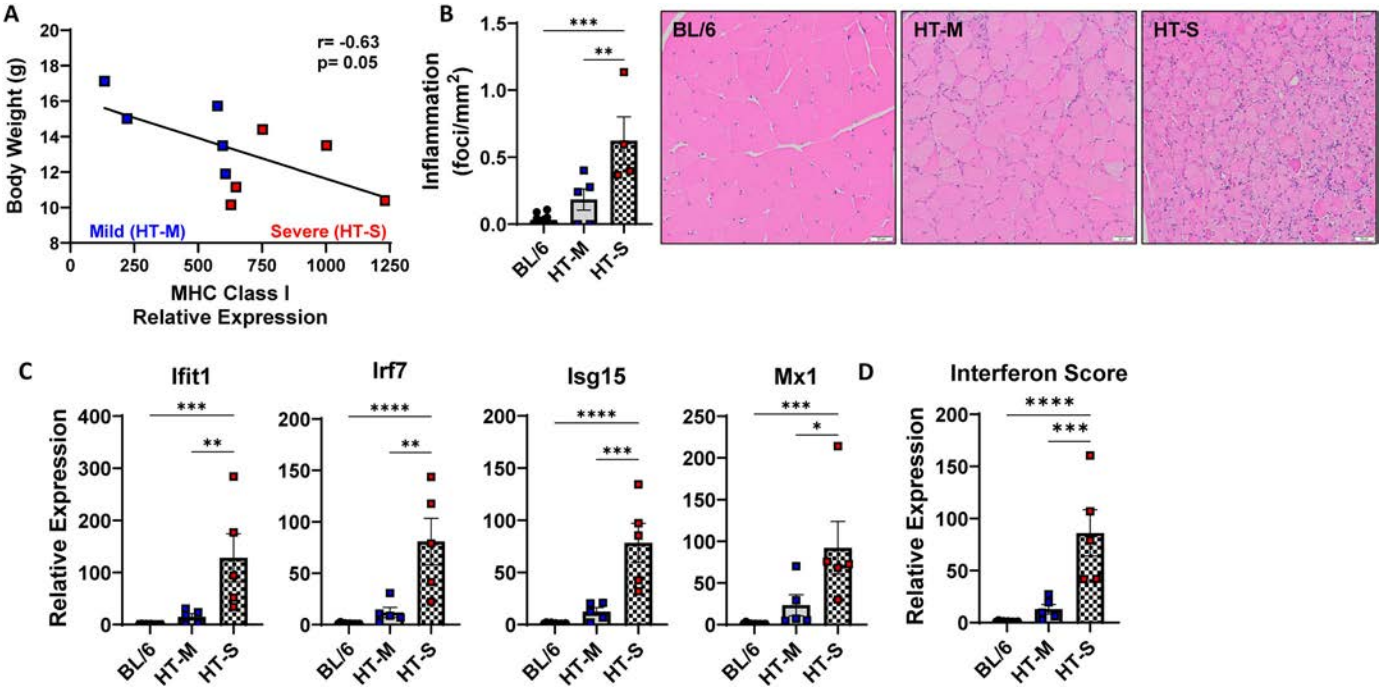

Figure 1. Variable disease expression in untreated myositis mice. (A) Mice were classified based on the median fold change in major histocompatibility complex (MHC) class I gene expression (607-median fold change relative to BL/6 mice; n = 10) as mild (HT-M; n = 5) or severe (HT-S; n = 5) myositis. Correlation was performed using Spearman's correlation coefficient. (B) Inflammation quantification and representative images of hematoxylin and eosin staining in the quadricep muscle of BL/6 (n = 10), HT-M (n = 5), and HT-S (n = 4) mice. $^{**}P < 0.01$; $^{***}P < 0.001$; by analysis of variance (ANOVA), presented as mean ± SEM. (C) Type I interferon-stimulated gene (ISG) levels (interferon-induced protein with tetratricopeptide repeats 1 [Ifit1], interferon regulatory factor 7 [Irf7], ISG15 [Isg15], and interferon-induced GTP-binding protein Mx1 [Mx1]). $^{*}P < 0.05$; $^{**}P < 0.01$; $^{***}P < 0.001$; $^{****}P < 0.0001$ by ANOVA, presented as mean ± SEM. (D) Interferon score (median relative expression of the four ISGs) in the muscle of HT-M (n = 5) and HT-S (n = 5). $^{***}P < 0.001$; $^{****}P < 0.0001$ by ANOVA, presented as mean ± SEM.

scanner microscope. The ratio of $CD31^+$ per total muscle fibers for each section was evaluated in a anonymized manner using ImageJ software. On average, 1,500 muscle fibers per section were measured.

Statistical analysis. Data with two or more groups were analyzed via Student's *t*-test or one-way analysis of variance, respectively. Survival data were analyzed via log-rank (Mantel–Cox) analysis of survival curves. Outliers were removed before data analysis as determined by the Robust regression and Outlier removal (ROUT) method. Data are presented as mean ± SEM, and significance was set as a *P* value <0.05. All data were analyzed using Prism software (GraphPad).

RESULTS

MHC class I mouse model of myositis. *Disease severity in myositis mice is related to MHC class I expression.* Kinder et al[27] previously reported variable disease progression that was related to MHC class I levels in skeletal muscle of adult HT mice. We therefore investigated whether similar variability exists with earlier disease onset. As shown in Figure 1A, higher MHC class I expression at euthanasia negatively correlated with body weight (r_s = –0.63, *P* = 0.05). Using the method employed by Kinder et al,[27] mice were classified as HT-M or HT-S based on MHC class I expression (cutoff: 607-median fold relative to BL/6). Histologic evaluation of the quadricep muscle revealed significantly more inflammation in HT-S versus HT-M ($P < 0.01$) and BL/6 ($P < 0.001$), along with other signs of muscle damage, including greater fiber size variation and regeneration (Figure 1B). The increased nuclei in the muscle likely reflect inflammatory infiltrates, which have previously been shown to be composed predominantly of macrophages/monocytes with little T or B cell involvement.[26,29]

Type 1 IFN score in myositis mice. To evaluate type 1 IFN expression, we measured four ISGs in the quadricep muscle of untreated myositis mice. Expression of all four ISGs—IFN-induced protein with tetratricopeptide repeats 1 (*Ifit1*), IFN regulatory factor 7 (*Irf7*), ISG15 (*Isg15*), and IFN-induced GTP-binding protein Mx1 (*Mx1*)—were not significantly different between HT-M and BL/6 (Figure 1C). However, HT-S mice had significantly elevated levels of all ISGs relative to BL/6 and HT-M mice (Figure 1C). The IFN score—determined by calculating the median relative expression of the four ISGs—was significantly elevated in HT-S compared to BL/6 ($P < 0.0001$) and HT-M mice ($P < 0.001$; Figure 1D).

Effect of JAK/STAT inhibition in mice with myositis. We next evaluated the effect of JAK inhibitors in mice with myositis treated

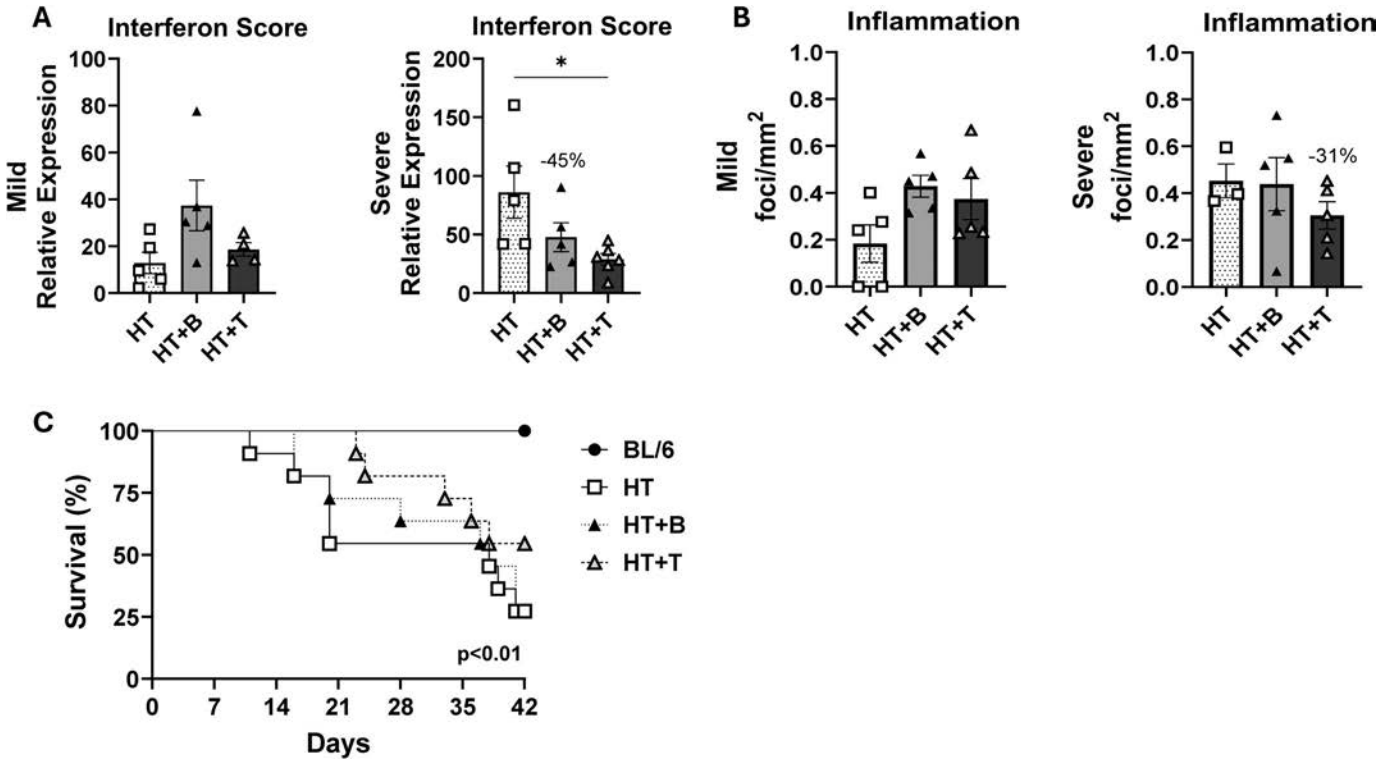

Figure 2. Effect of baricitinib and tofacitinib in myositis mice. (A) Interferon score (median relative expression of the four interferon-stimulated genes) in untreated HT mice (mild HT [HT-M], n = 5; severe HT [HT-S], n = 5), baricitinib-treated HT mice (mild HT with baricitinib [HT+B], n = 5; severe HT+B, n = 5), and tofacitinib-treated HT mice (mild HT with tofacitinib [HT+T], n = 4; severe HT+T, n = 6). *$P < 0.05$ by analysis of variance, presented as mean ± SEM. (B) Inflammation quantification in HT-M (n = 5) and HT-S (n = 3); mild HT+B (n = 5) and severe HT+B (n = 5); and mild HT+T (n = 5) and severe HT+T (n = 5) myositis mice. (C) Survival curves in BL/6 (n = 10), untreated (n = 11), HT+B (n = 11), and HT+T (n = 11) mice analyzed by log-rank (Mantel–Cox) test.

daily for six weeks with baricitinib (10 mg/kg) or tofacitinib (20 mg/kg). Tofacitinib administration resulted in a significant reduction in the IFN score in HT-S but not HT-M mice, whereas baricitinib had no significant effect (Figure 2A). Skeletal muscle inflammation followed a similar pattern (Figure 2B). Tofacitinib reduced inflammation in HT-S mice by 31%, although this did not reach statistical significance. The log-rank analysis of survival curves (Figure 2C) was significant ($P < 0.01$). After adjusting for multiple testing, HT and HT+B mice exhibited shorter survival compared to BL/6, whereas HT+T did not differ from BL/6 mice. Neither drug improved muscle function (grip strength or torque; data not shown).

CD31 immunofluorescence in HT mice. Microvascular pathology is often observed in patients with DM. We therefore quantified the capillary-to-muscle fiber ratio ($CD31^+$ immunofluorescence staining) in myositis mice. HT mice had a significantly reduced $CD31^+$-to-muscle fiber ratio compared to BL/6 mice ($P < 0.0001$; Figure 3A and B). Despite fewer capillaries, those remaining in HT mice appeared enlarged (Figure 3B, white arrows).

IFNβ1-overexpressing mouse model. *Overexpression of IFNβ1 impairs muscle function in normal mice.* To evaluate the role of IFNβ1 in skeletal muscle, we overexpressed IFNβ1 in six-week-old female C57BL/6 mice using an AAV9-tMCK-m-IFNb1-WPRE vector. Histologic analysis revealed significantly increased muscle inflammation in AAV9-IFNβ1–injected mice compared to BL/6 controls ($P < 0.01$) and AAV9-eGFP–injected mice ($P < 0.05$; Figure 4A). Although body weight did not differ between groups (Figure 4B), grip strength was significantly reduced in the AAV9-IFNβ1–injected mice ($P < 0.0001$; Figure 4C). We measured ISG expression in blood two weeks after AAV9-IFNβ1 injection, and as expected, IFNβ1 overexpression significantly increased the IFN score compared to both BL/6 and AAV9-eGFP–injected mice ($P < 0.0001$ and $P < 0.01$, respectively), indicating that the IFN signature is not due to a general immune response to AAV9 injection (Figure 4D). H2Kb expression was also significantly increased in the skeletal muscle of AAV9-IFNβ1–injected mice relative to BL/6 controls and AAV9-eGFP–injected mice ($P < 0.0001$ and $P < 0.05$, respectively; Figure 4E).

Effect of tofacitinib in IFNβ1-overexpressing mice. Given that tofacitinib significantly reduced the IFN score in HT-S mice and normalized survival in myositis mice, we next evaluated whether a higher tofacitinib dose (40 mg/kg) in IFNβ1-overexpressing mice would result in stronger JAK inhibition, thereby further suppressing IFN-driven pathology and improving muscle function. Tofacitinib treatment did not significantly improve grip strength compared to untreated AAV9-IFNβ1–overexpressing mice (Figure 5A). In skeletal

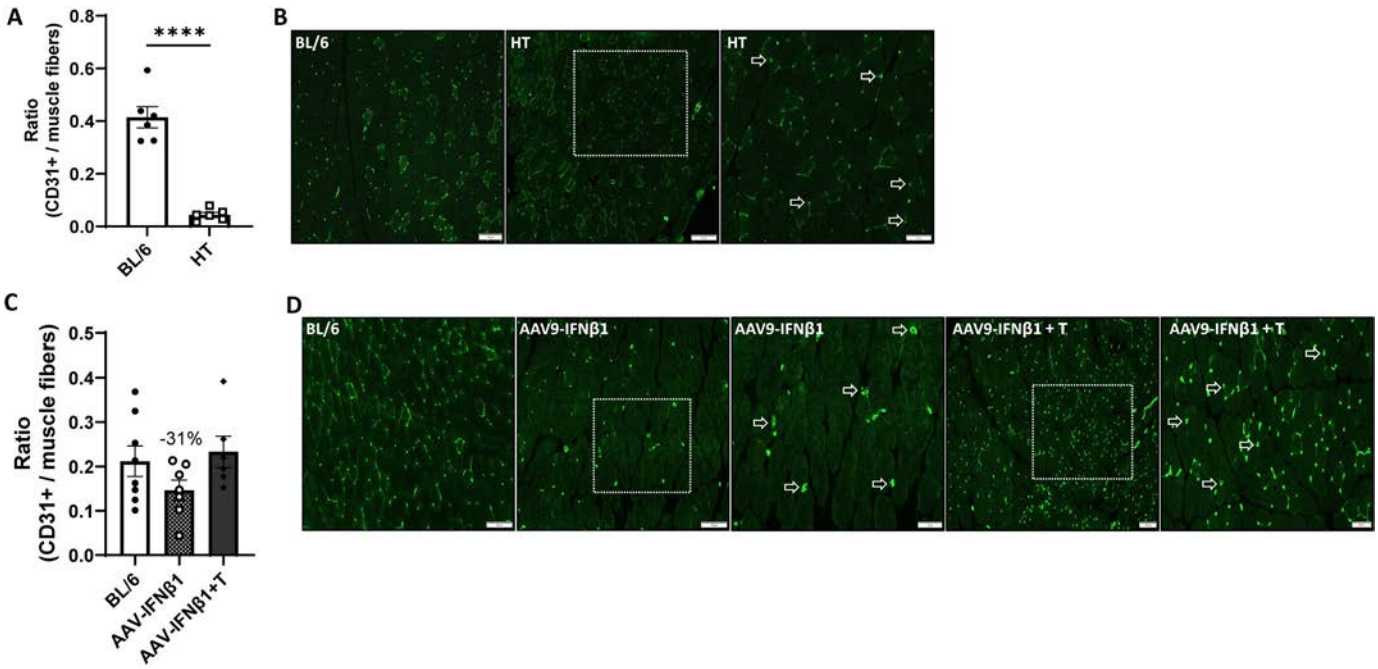

Figure 3. Analysis of endothelial density by CD31 immunofluorescent staining in the quadricep muscle of myositis and interferon (IFN) β1–expressing mice. (A) Endothelial density was measured by quantifying CD31 immunofluorescence per muscle fiber area ($CD31^+$-to-muscle fiber ratio) in BL/6 (n = 6) and untreated myositis mice (HT; n = 6). ****$P < 0.0001$ by Student's *t*-test, presented as mean ± SEM. (B) Representative images of $CD31^+$ staining. (C) $CD31^+$-to-muscle fiber ratio quantification in BL/6 (n = 8), AAV9-IFNβ1 (n = 7), and tofacitinib-treated AAV9-IFNβ1 mice (AAV9-IFNβ1+T; n = 6). (D) Representative images of CD31 staining. $CD31^+$ staining (green) was performed for all groups (scale, 100 μm). The dotted box represents magnified area selected from labeled group. White arrows show enlarged capillaries from magnified area (50 μm). Color figure can be viewed in the online issue, which is available at http://onlinelibrary.wiley.com/doi/10.1002/art.70096/abstract.

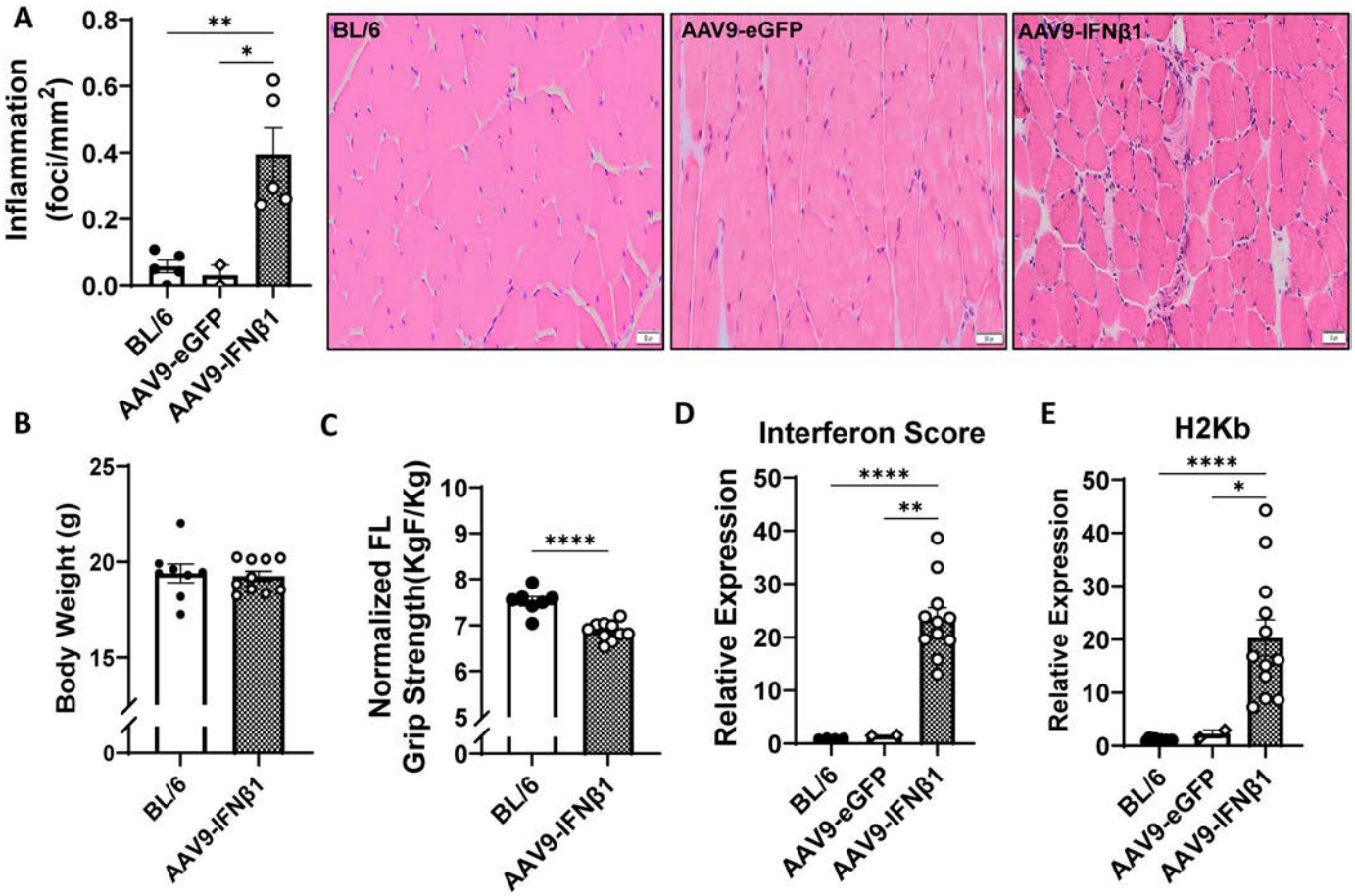

Figure 4. Effect of interferon (IFN) β1 overexpression in normal mice. AAV9-tMCK-m-IFNβ1-WPRE or AAV9-tMCK-eGFP-WPRE were administered to six-week-old female C57BL/6 mice via retro-orbital injection at a dose of 1.6×10^{12} vg/mouse. (A) Inflammation quantification and representative images of hematoxylin and eosin staining in the quadricep muscle of BL/6 (n = 5), AAV9-eGFP–injected (n = 2), and AAV9-IFNβ1–injected mice (n = 5). *$P < 0.05$; **$P < 0.01$; ****$P < 0.0001$ by analysis of variance (ANOVA), presented as mean ± SEM. (B) Body weight (in grams) of BL/6 (n = 8) and AAV9-IFNβ1–injected mice (n = 10) at end of study (10 weeks after injection). (C) Forelimb (FL) grip strength was measured at the end of study and normalized to body weight (in kilogram-force per kilogram) for BL/6 (n = 7) and AAV9-IFNβ1–injected mice (n = 10). ****$P < 0.0001$ by ANOVA, presented as mean ± SEM. (D) IFN score (median relative expression of the four IFN-stimulated genes) in the blood of noninjected (BL/6, n = 4), AAV9-eGFP–injected (n = 2), and AAV9-IFNβ1–injected mice (n = 11). Blood was collected from mice two weeks after eGFP or IFNβ1 injection. **$P < 0.01$; ****$P < 0.0001$ by ANOVA, presented as mean ± SEM. (E) H2Kb levels in the muscle of BL/6 (n = 10), AAV9-eGFP–injected (n = 2), and AAV9-IFNβ1–injected mice (n = 12). *$P < 0.05$; ****$P < 0.0001$ by ANOVA, presented as mean ± SEM. Color figure can be viewed in the online issue, which is available at http://onlinelibrary.wiley.com/doi/10.1002/art.70096/abstract.

muscle, tofacitinib treatment reduced expression of all four ISGs tested and was statistically significant for *Ifit1* and *Mx1*, and the IFN score was reduced by 41% (although not statistically significant; Figure 5B).

CD31 immunofluorescence in IFNβ1-overexpressing mice. To assess the impact of IFNβ1 overexpression on muscle microvasculature, we quantified the capillary-to-muscle fiber ratio (CD31 immunofluorescence staining). AAV9-IFNβ1–injected mice showed a 31% reduction in the $CD31^+$-to-muscle fiber ratio compared to BL/6 mice, although this was not statistically significant (Figure 3C). Tofacitinib treatment restored the $CD31^+$-to-muscle fiber ratio to control levels (Figure 3C). Representative images for BL/6, AAV9-IFNβ1, and AAV9-IFNβ1 with tofacitinib-treated mice are shown in Figure 3D. Capillaries in IFNβ1-injected mice appeared enlarged, regardless of tofacitinib treatment (Figure 3D, white arrows).

All data used in this research are already included in the article. Further inquiries can be directed to the corresponding author.

DISCUSSION

Results from our current study, using two complementary mouse models, provide additional evidence supporting a pathogenic role for type I IFN signaling in autoimmune myositis. Consistent with prior studies in the MHC class I–overexpressing model of myositis, we found that higher levels of MHC class I in the skeletal muscle correlate with disease severity, including histologic

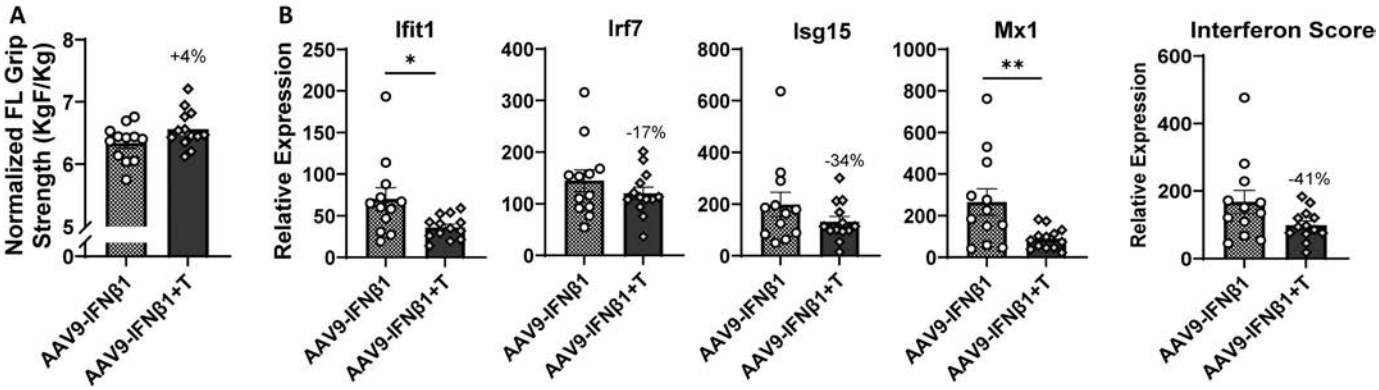

Figure 5. Tofacitinib treatment partially improved muscle function and decreased the interferon (IFN) score in normal mice overexpressing IFNβ1. AAV9-tMCK-m-IFNβ1-WPRE was administered to six-week-old female C57BL/6 mice via retro-orbital injection at a dose of 1.6×10^{12} vg/mouse. Tofacitinib was administered daily at 40 mg/kg. (A) Forelimb (FL) grip strength was measured at the end of study and normalized to body weight (in kilogram-force per kilogram) in BL/6 (n = 12) and AAV9-IFNβ1 mice (n = 13). (B) Type I IFN-stimulated gene (ISG) levels (IFN-induced protein with tetratricopeptide repeats 1 [Ifit1], IFN regulatory factor 7 [Irf7], ISG15 [Isg15], and IFN-induced GTP-binding protein Mx1 [Mx1]) and the IFN score (median relative expression of the four ISGs) in muscle of untreated (AAV9-IFNβ1; n = 12) and tofacitinib-treated AAV9-IFNβ1 mice (AAV9-IFNβ1+T; n = 13). *$P < 0.05$; **$P < 0.01$ by analysis of variance, presented as mean ± SEM.

features of muscle damage.[27] In juvenile DM (JDM) and DM, MHC class I is aberrantly expressed in muscle fibers and is a characteristic histopathological feature of muscle biopsies from patients with myositis.[24,38,39] By stratifying mice based on MHC class I expression, we identified a subset of HT-S mice with significantly elevated expression of ISGs and muscle damage, supporting a molecular link between type I IFN signaling and myositis disease severity. Type I IFN signatures have been detected in muscle and blood primarily from patients with DM and JDM, with higher IFN scores associated with disease severity and activity.[7–9,40] Our findings that ISG expression was significantly elevated in HT-S mice—but not HT-M mice—support these clinical observations. Additionally, these findings support a pathogenic mechanism of MHC class I–type I IFN signaling, which is also consistent with previous observations.

To assess the effect of blocking type I IFN signaling on disease progression, we tested two JAK inhibitors—baricitinib and tofacitinib—that act by inhibiting JAK-dependent STAT phosphorylation. Treatment with tofacitinib, but not baricitinib, significantly reduced the IFN score in HT-S mice. Tofacitinib also modestly reduced inflammation, although it did not significantly improve muscle strength. Survival differed across groups, with untreated and baricitinib-treated mice showing shorter survival than controls, whereas tofacitinib-treated mice did not differ from controls. These results are consistent with recent studies in patients with DM, in which JAK inhibitors led to clinical improvement and reductions in type I IFN levels.[14,16,20,41,42] The greater efficacy of tofacitinib compared to baricitinib in reducing IFN scores and normalizing survival may reflect differences in their JAK inhibition profiles. Although both drugs inhibit JAK1, tofacitinib also targets JAK3, which is critical for signaling downstream of the common γ-chain cytokines (eg, interleukin [IL]-2, IL-4, IL-7, IL-9, IL-15, and IL-21) that regulate T cell and natural killer cell activation. In contrast, baricitinib primarily inhibits JAK1 and JAK2, affecting cytokines like granulocyte–macrophage colony-stimulating factor, erythropoietin, and thrombopoietin that are more relevant for myeloid and erythroid cell activation.[43,44] Given the immune cell involvement and prominent IFN signature in myositis, tofacitinib's inhibition of both JAK1 and JAK3 may more effectively blunt proinflammatory signaling pathways relevant to disease pathogenesis. Tofacitinib did not improve muscle strength; however, it reduced the IFN score, inflammation, and IFN-associated microvascular pathology, and survival in this group was not significantly different from healthy controls. These results suggest that tofacitinib exerts protective effects independent of direct improvements in muscle strength.

In contrast, baricitinib treatment was associated with a nonsignificant increase in ISG expression and inflammation in mice with mild myositis, revealing a disease-severity–dependent response to JAK inhibition. In this low-inflammation setting, neither drug was protective, and baricitinib trended toward exacerbating inflammatory measures, possibly due to a signaling imbalance from selective JAK1/2 inhibition. In severe myositis mice, tofacitinib (JAK1/3) provided clear benefit by significantly reducing the IFN signature and through nonsignificantly lowering inflammatory foci. However, baricitinib (JAK1/2) was ineffective, suggesting that JAK3 inhibition may be critical for anti-inflammatory efficacy in established disease. The absence of functional improvement in either treatment group indicates that type I IFN is only one component of a broader pathogenic network. Additional mechanisms such as the NF-kB inflammatory response, endoplasmic reticulum (ER) stress, and mitochondrial dysfunction may contribute either independently or synergistically to disease progression,[15,45–50] suggesting that combining JAK inhibitors with therapies targeting these mechanisms could enhance clinical outcomes. Although dose-escalation

experiments were not performed, it is also possible that the relatively high baricitinib dose may have contributed to the paradoxical increase in inflammatory measures in mild disease. Future dose–response studies will be important to determine whether lower doses are efficacious.

The role of type I IFN as a contributor to muscle damage was further validated in our AAV9-IFNβ1–overexpression model. Overexpression of IFNβ1 in skeletal muscle induced a robust IFN signature, increased muscle inflammation, and significantly reduced grip strength in otherwise healthy mice. These findings underscore the key role of type I IFN signaling in initiating and sustaining muscle inflammation and functional impairment. Tofacitinib treatment led to reduced ISG expression, with significant reductions in *Ifit1* and *Mx1* and consistent downward trends across other ISGs, although the overall reduction in ISG score did not reach statistical significance (41% reduction). Additionally, tofacitinib produced a trend toward improved muscle strength ($P = 0.07$). This limited therapeutic response may be due to suboptimal dosing or treatment duration.

CD31/PECAM-1 is a well-established marker of endothelial cells and plays a critical role in leukocyte transmigration during inflammation. Several studies demonstrated a pattern of microvascular damage, including reduced capillary density, visualized by reduced CD31 immunoreactivity in patients with myositis.[51–53] Some studies also reported enlarged capillaries in DM muscle, likely as a compensatory response to increased blood flow through fewer vessels.[54] Microvascular pathology in DM muscle, such as capillary loss, may impair oxygen and nutrient delivery to muscle cells, contributing to muscle fiber damage, fatigue, and weakness. In both the MHC class I and IFNβ1-overexpression mouse models, we observed reduced capillary density and enlarged capillaries in skeletal muscle, resembling the microvascular pathology observed in patients with DM. Tofacitinib treatment partially restored capillary density in the IFNβ1 model, but abnormal vessel morphology persisted. These findings identify IFNβ1 as a novel contributor of vascular pathology in muscle damage and show that JAK inhibition can provide partial capillary protection.

Although the present study advances the understanding of IFN-driven mechanisms in muscle damage and myositis, it has several limitations. The small sample size may reduce statistical power and limit our ability to detect significant differences between groups. For baricitinib and tofacitinib treatment studies, a single dose was used, which may not accurately reflect the full therapeutic potential of JAK inhibitors. Although these doses (10 mg/kg baricitinib and 20 mg/kg tofacitinib) are higher than those used clinically, they are consistent with prior preclinical studies in mice. Additionally, all mice were euthanized at a single time point, preventing a time course evaluation of inflammation and tissue repair. Future studies exploring dose–response relationships and longitudinal assessments would provide a more comprehensive understanding of disease progression and therapeutic response in myositis.

In summary, our findings provide evidence that type I IFN signaling contributes to muscle damage and weakness in mice and that JAK inhibitors, particularly tofacitinib, provide some benefit. Although the magnitude of IFN suppression and functional improvement after JAK inhibition varied between models, these differences likely reflect distinct disease severity and additional pathogenic factors beyond IFN signaling. Future studies should explore combination therapies that target other identified pathogenic mechanisms, such as ER stress and mitochondrial dysfunction. Together, these findings support a model in which type I IFN is a central driver of muscle damage, offering additional support for targeting IFN signaling in managing diseases like autoimmune myositis.

AUTHOR CONTRIBUTIONS

All authors contributed to at least one of the following manuscript preparation roles: conceptualization AND/OR methodology, software, investigation, formal analysis, data curation, visualization, and validation AND drafting or reviewing/editing the final draft. As corresponding author, Dr Morales confirms that all authors have provided the final approval of the version to be published, and takes responsibility for the affirmations regarding article submission (eg, not under consideration by another journal), the integrity of the data presented, and the statements regarding compliance with institutional review board/Declaration of Helsinki requirements.

REFERENCES

1. Oldroyd A, Dixon W, Chinoy H, et al. Patient insights on living with idiopathic inflammatory myopathy and the limitations of disease activity measurement methods - a qualitative study. BMC Rheumatol 2020; 4(1):47. doi:https://doi.org/10.1186/s41927-020-00146-3
2. Barsotti S, Lundberg IE. Current treatment for myositis. Curr Treatm Opt Rheumatol 2018;4(4):299–315. doi:https://doi.org/10.1007/s40674-018-0106-2
3. Yasir M, Goyal A, Sonthalia S. Corticosteroid adverse effects. In: StatPearls. StatPearls Publishing; 2025.
4. Lundberg IE. Expert Perspective: Management of Refractory Inflammatory Myopathy. Arthritis Rheumatol 2021;73(8):1394–1407. doi: https://doi.org/10.1002/art.41762
5. Pinal-Fernandez I, Casal-Dominguez M, Derfoul A, et al. Identification of distinctive interferon gene signatures in different types of myositis. Neurology 2019;93(12):e1193–e1204. doi:https://doi.org/10.1212/WNL.0000000000008128
6. Greenberg SA. Type 1 interferons and myositis. Arthritis Res Ther 2010;12(3):198–203. doi:https://doi.org/10.1186/ar2885
7. Walsh RJ, Kong SW, Yao Y, et al. Type I interferon-inducible gene expression in blood is present and reflects disease activity in dermatomyositis and polymyositis. Arthritis Rheum 2007;56(11):3784–3792. doi:https://doi.org/10.1002/art.22928
8. Baechler EC, Bauer JW, Slattery CA, et al. An interferon signature in the peripheral blood of dermatomyositis patients is associated with disease activity. Mol Med 2007;13(1–2):59–68. doi:https://doi.org/10.2119/2006-00085.Baechler
9. Moneta GM, Pires Marafon D, Marasco E, et al. Muscle expression of type I and type II interferons is increased in juvenile dermatomyositis and related to clinical and histologic features. Arthritis Rheumatol 2019;71(6):1011–1021. doi:https://doi.org/10.1002/art.40800

10. O'Connor KA, Abbott KA, Sabin B, et al. MxA gene expression in juvenile dermatomyositis peripheral blood mononuclear cells: association with muscle involvement. Clin Immunol 2006;120(3):319–325. doi:https://doi.org/10.1016/j.clim.2006.05.011
11. Greenberg SA, Higgs BW, Morehouse C, et al. Relationship between disease activity and type 1 interferon- and other cytokine-inducible gene expression in blood in dermatomyositis and polymyositis. Genes Immun 2012;13(3):207–213. doi:https://doi.org/10.1038/gene.2011.61
12. Bilgic H, Ytterberg SR, Amin S, et al. Interleukin-6 and type I interferon-regulated genes and chemokines mark disease activity in dermatomyositis. Arthritis Rheum 2009;60(11):3436–3446. doi:https://doi.org/10.1002/art.24936
13. Liao AP, Salajegheh M, Nazareno R, et al. Interferon β is associated with type 1 interferon-inducible gene expression in dermatomyositis. Ann Rheum Dis 2011;70(5):831–836. doi:https://doi.org/10.1136/ard.2010.139949
14. Ladislau L, Suárez-Calvet X, Toquet S, et al. JAK inhibitor improves type I interferon induced damage: proof of concept in dermatomyositis. Brain 2018;141(6):1609–1621. doi:https://doi.org/10.1093/brain/awy105
15. Meyer A, Laverny G, Allenbach Y, et al. IFN-β-induced reactive oxygen species and mitochondrial damage contribute to muscle impairment and inflammation maintenance in dermatomyositis. Acta Neuropathol 2017;134(4):655–666. doi:https://doi.org/10.1007/s00401-017-1731-9
16. Paik JJ, Lubin G, Gromatzky A, et al. Use of Janus kinase inhibitors in dermatomyositis: a systematic literature review. Clin Exp Rheumatol 2023;41(2):348–358. doi:https://doi.org/10.55563/clinexprheumatol/hxin6o
17. LI Wilkinson MG, Deakin CT, Papadopoulou C, et al. JAK inhibitors: a potential treatment for JDM in the context of the role of interferon-driven pathology. Pediatr Rheumatol Online J 2021;19(1):146. doi:https://doi.org/10.1186/s12969-021-00637-8
18. Kim H. Updates on interferon in juvenile dermatomyositis: pathogenesis and therapy. Curr Opin Rheumatol 2021;33(5):371–377. doi:https://doi.org/10.1097/BOR.0000000000000816
19. Hornung T, Janzen V, Heidgen F-J, et al. Remission of recalcitrant dermatomyositis treated with ruxolitinib. N Engl J Med 2014;371(26):2537–2538. doi:https://doi.org/10.1056/NEJMc1412997
20. Paik JJ, Christopher-Stine L. A case of refractory dermatomyositis responsive to tofacitinib. Semin Arthritis Rheum 2017;46(4):e19. doi:https://doi.org/10.1016/j.semarthrit.2016.08.009
21. Moghadam-Kia S, Charlton D, Aggarwal R, et al. Management of refractory cutaneous dermatomyositis: potential role of Janus kinase inhibition with tofacitinib. Rheumatology (Oxford) 2019;58(6):1011–1015. doi:https://doi.org/10.1093/rheumatology/key366
22. Konishi R, Ichimura Y, Okiyama N. Murine models of idiopathic inflammatory myopathy. Immunol Med 2023;46(1):9–14. doi:https://doi.org/10.1080/25785826.2022.2137968
23. Kurdi M, Alshareef A, Bamaga AK, et al. The assessment of major histocompatibility complex (MHC) class-I expression in different neuromuscular diseases. Degener Neurol Neuromuscul Dis 2021;11:61–68. doi:https://doi.org/10.2147/DNND.S340117
24. Milisenda JC, Pinal-Fernandez I, Lloyd TE, et al. The pattern of MHC class I expression in muscle biopsies from patients with myositis and other neuromuscular disorders. Rheumatology (Oxford) 2023;62(9):3156–3160. doi:https://doi.org/10.1093/rheumatology/kead052
25. van der Pas J, Hengstman GJD, ter Laak HJ, et al. Diagnostic value of MHC class I staining in idiopathic inflammatory myopathies. J Neurol Neurosurg Psychiatry 2004;75(1):136–139.
26. Nagaraju K, Raben N, Loeffler L, et al. Conditional up-regulation of MHC class I in skeletal muscle leads to self-sustaining autoimmune myositis and myositis-specific autoantibodies. Proc Natl Acad Sci U S A 2000;97(16):9209–9214. doi:https://doi.org/10.1073/pnas.97.16.9209
27. Kinder TB, Heier CR, Tully CB, et al. Muscle weakness in myositis: microRNA-mediated dystrophin reduction in a myositis mouse model and human muscle biopsies. Arthritis Rheumatol 2020;72(7):1170–1183. doi:https://doi.org/10.1002/art.41215
28. Clark JD, Flanagan ME, Telliez J-B. Discovery and development of Janus kinase (JAK) inhibitors for inflammatory diseases. J Med Chem 2014;57(12):5023–5038. doi:https://doi.org/10.1021/jm401490p
29. Li CK, Knopp P, Moncrieffe H, et al. Overexpression of MHC class I heavy chain protein in young skeletal muscle leads to severe myositis: implications for juvenile myositis. Am J Pathol 2009;175(3):1030–1040. doi:https://doi.org/10.2353/ajpath.2009.090196
30. Makabe K, Okada H, Tachibana N, et al. Baricitinib ameliorates inflammatory and neuropathic pain in collagen antibody-induced arthritis mice by modulating the IL-6/JAK/STAT3 pathway and CSF-1 expression in dorsal root ganglion neurons. Arthritis Res Ther 2024;26(1):121. doi:https://doi.org/10.1186/s13075-024-03354-1
31. Lee J, Park Y, Jang SG, et al. Baricitinib attenuates autoimmune phenotype and podocyte injury in a murine model of systemic lupus erythematosus. Front Immunol 2021;12:704526. doi:https://doi.org/10.3389/fimmu.2021.704526
32. Collotta D, Hull W, Mastrocola R, et al. Baricitinib counteracts metaflammation, thus protecting against diet-induced metabolic abnormalities in mice. Mol Metab 2020;39:101009. doi:https://doi.org/10.1016/j.molmet.2020.101009
33. Aung WW, Wang C, Xibei J, et al. Immunomodulating role of the JAKs inhibitor tofacitinib in a mouse model of bleomycin-induced scleroderma. J Dermatol Sci 2021;101(3):174–184. doi:https://doi.org/10.1016/j.jdermsci.2020.12.007
34. Yokoyama S, Perera P-Y, Terawaki S, et al. Janus kinase inhibitor tofacitinib shows potent efficacy in a mouse model of autoimmune lymphoproliferative syndrome (ALPS). J Clin Immunol 2015;35(7):661–667. doi:https://doi.org/10.1007/s10875-015-0203-z
35. Carfagna M, Cannady E, Ryan T, et al. Carcinogenicity assessment of baricitinib in Tg.rasH2 mice and Sprague-Dawley (Crl:CD) rats. Regul Toxicol Pharmacol 2018;92:458–471. doi:https://doi.org/10.1016/j.yrtph.2017.11.020
36. Figueroa-Romero C, Monteagudo A, Murdock BJ, et al. Tofacitinib suppresses natural killer cells in vitro and in vivo: implications for amyotrophic lateral sclerosis. Front Immunol 2022;13:773288. doi:https://doi.org/10.3389/fimmu.2022.773288
37. Spathis R, Kuriplach DR, Narvesen S, et al. Corrigendum: enhancing AAV-microdystrophin gene therapy after repeat dosing by blocking phagocytosis. Front Immunol 2025;16:1593193. doi:10.3389/fimmu.2025.1593193 Erratum in: Front Immunol 2025;16:1527840.
38. Shinjo SK, Sallum AME, Silva CA, et al. Skeletal muscle major histocompatibility complex class I and II expression differences in adult and juvenile dermatomyositis. Clinics (Sao Paulo) 2012;67(8):885–890. doi:https://doi.org/10.6061/clinics/2012(08)05
39. Sallum AME, Kiss MHB, Silva CA, et al. MHC class I and II expression in juvenile dermatomyositis skeletal muscle. Clin Exp Rheumatol 2009;27(3):519–526.
40. Raupov R, Suspitsin E, Preobrazhenskaya EV, et al. Interferon type I signature associated with skin disease in juvenile dermatomyositis. Front Med (Lausanne) 2024;11:1214920. doi:https://doi.org/10.3389/fmed.2024.1214920
41. Zhang J, Sun L, Shi X, et al. Janus kinase inhibitor, tofacitinib, in refractory juvenile dermatomyositis: a retrospective multi-central study in China. Arthritis Res Ther 2023;25(1):204. doi:https://doi.org/10.1186/s13075-023-03170-z

42. Corbella-Bagot L, Bosch-Amate X, Gimeno-Ribes E, et al. JAK inhibitors in refractory dermatomyositis: a case series. Australas J Dermatol 2024;65(7):588–592. doi:https://doi.org/10.1111/ajd.14335
43. Schwartz DM, Bonelli M, Gadina M, et al. Type I/II cytokines, JAKs, and new strategies for treating autoimmune diseases. Nat Rev Rheumatol 2016;12(1):25–36. doi:https://doi.org/10.1038/nrrheum.2015.167
44. Banerjee S, Biehl A, Gadina M, et al. JAK-STAT signaling as a target for inflammatory and autoimmune diseases: current and future prospects. Drugs 2017;77(5):521–546. doi:10.1007/s40265-017-0701-9 Erratum in: *Drugs* 2017;77:939; Drugs 2017;77:1261.
45. Hedberg-Oldfors C, Lindgren U, Visuttijai K, et al. Respiratory chain dysfunction in perifascicular muscle fibres in patients with dermatomyositis is associated with mitochondrial DNA depletion. Neuropathol Appl Neurobiol 2022;48(7):e12841. doi:https://doi.org/10.1111/nan.12841
46. Gonzalez-Chapa JA, Macêdo MB, Lood C. The emerging role of mitochondrial dysfunction in the pathogenesis of idiopathic inflammatory myopathies. Rambam Maimonides Med J 2023;14(2):e0006. doi:https://doi.org/10.5041/RMMJ.10493
47. Nagaraju K, Casciola-Rosen L, Lundberg I, et al. Activation of the endoplasmic reticulum stress response in autoimmune myositis: potential role in muscle fiber damage and dysfunction. Arthritis Rheum 2005;52(6):1824–1835. doi:https://doi.org/10.1002/art.21103
48. Henriques-Pons A, Nagaraju K. Nonimmune mechanisms of muscle damage in myositis: role of the endoplasmic reticulum stress response and autophagy in the disease pathogenesis. Curr Opin Rheumatol 2009;21(6):581–587. doi:https://doi.org/10.1097/BOR.0b013e3283319265
49. Ma X, Gao H-J, Zhang Q, et al. Endoplasmic reticulum stress is involved in muscular pathogenesis in idiopathic inflammatory myopathies. Front Cell Dev Biol 2022;10:791986. doi:https://doi.org/10.3389/fcell.2022.791986
50. Duvvuri B, Pachman LM, Hermanson P, et al. Role of mitochondria in the myopathy of juvenile dermatomyositis and implications for skeletal muscle calcinosis. J Autoimmun 2023;138:103061. doi:https://doi.org/10.1016/j.jaut.2023.103061
51. Lemmer D, Schmidt J, Kummer K, et al. Impairment of muscular endothelial cell regeneration in dermatomyositis. Front Neurol 2022;13:952699. doi:https://doi.org/10.3389/fneur.2022.952699
52. Emslie-Smith AM, Engel AG. Microvascular changes in early and advanced dermatomyositis: a quantitative study. Ann Neurol 1990;27(4):343–356. doi:https://doi.org/10.1002/ana.410270402
53. Buckley AF, Bossen EH. Skeletal muscle microvasculature in the diagnosis of neuromuscular disease. J Neuropathol Exp Neurol 2013;72(10):906–918. doi:https://doi.org/10.1097/NEN.0b013e3182a7f0b8
54. Jerusalem F, Rakusa M, Engel AG, et al. Morphometric analysis of skeletal muscle capillary ultrastructure in inflammatory myopathies. J Neurol Sci 1974;23(3):391–402. doi:https://doi.org/10.1016/0022-510X(74)90157-9

Arthritis & Rheumatology
Vol. 78, No. 9, September 2026, pp 1952–1960
DOI 10.1002/art.70103
© 2026 The Author(s). *Arthritis & Rheumatology* published by Wiley Periodicals LLC on behalf of American College of Rheumatology.
This article has been contributed to by U.S. Government employees and their work is in the public domain in the USA.
This is an open access article under the terms of the Creative Commons Attribution-NonCommercial License, which permits use, distribution and reproduction in any medium, provided the original work is properly cited and is not used for commercial purposes.

Improved Detection of Myositis-Specific Autoantibodies Using Luciferase Immunoprecipitation Systems Assay: Comparison With Line Blot and Conventional Immunoprecipitation

Peter D. Burbelo, PhD,[1] Iago Pinal-Fernandez, MD, PhD,[2] Maria Casal-Dominguez, MD, PhD,[2] Xin Tian, PhD,[3] Shijinqiu Gao, MS,[3] Neha Gupta, BS,[4] Eric W. Robbins, MD,[5] John A. Chiorini, PhD,[1] Christopher A. Mecoli, MD, MHS,[6] Lisa Christopher-Stine, MD, MPH,[6] Livia Casciola-Rosen, PhD,[6] Andrew L. Mammen, MD, PhD,[2] Sonye K. Danoff, MD, PhD,[7] Anthony F. Suffredini, MD,[4] and Julio A. Huapaya, MD, MHS[4]

Objective. Myositis-specific autoantibodies guide the diagnosis and classification of idiopathic inflammatory myopathies, but current immunoassays vary in accuracy, particularly for autoantibodies associated with interstitial lung disease. To compare the performance of the luciferase immunoprecipitation systems (LIPS) assay with line blot and immunoprecipitation (IP) and to evaluate whether antibody-specific thresholds modify line blot concordance.

Methods. We analyzed 279 sera with line blot results from the Johns Hopkins Myositis Center. LIPS was performed for anti–Jo-1, anti–PL-7, anti–PL-12, anti–MDA-5, anti-EJ, and anti-Ro52 autoantibodies. Line blot results were evaluated using standard thresholds (≥36 and ≥71 arbitrary units [AU]). Assay performance was evaluated against IP (n = 141). In patients without IP (n = 138), clinical diagnoses were examined.

Results. LIPS showed excellent agreement with IP (κ = 0.90, area under the receiver operating characteristic curve 0.935), outperforming line blot. Line blot cutoffs influenced performance: ≥36 AU increased sensitivity (92.9%) but reduced specificity (73.8%), whereas ≥71 AU improved specificity (92.9%) but lowered sensitivity (82.8%). Antibody-specific thresholds modified concordance but remained quantitatively inferior to LIPS. In patients without IP, concordance between LIPS and line blot was 89% at ≥36 AU and 83% at ≥71 AU. LIPS-positive cases were enriched for antisynthetase syndrome and dermatomyositis. Among discordant cases (line blot positive and LIPS negative), most were clinically classified as inclusion body myositis (5 of 11). For anti-Ro52, discrepancies were most frequent at titers <36 AU.

Conclusion. LIPS provides quantitative discrimination, strong concordance with IP, and improved performance compared with line blot, particularly at low to intermediate titers. By reducing misclassification and complementing antibody-specific thresholds, LIPS has the potential to enhance clinical stratification in patients with myositis.

INTRODUCTION

Myositis-specific autoantibodies (MSAs) play a critical role in the diagnosis and classification of idiopathic inflammatory myopathies (IIM).[1,2] These antibodies define clinical subgroups with distinct clinical trajectories, including interstitial lung disease (ILD), which remains a major driver of morbidity and mortality.[3] In clinical practice, immunoassays such as enzyme-linked immunosorbent assays (ELISA) and immunoblots are widely used, with the line blot being one of the most common tests.[4] However,

The contributions of the NIH authors are considered works of the US Government. The findings and conclusions presented in this paper are those of the authors and do not necessarily reflect the views of the NIH or the US Department of Health and Human Services.

Supported in part by the Intramural Research Program of the NIH, a Mentored Research Fellowship from The Myositis Association, and the Bench-to-Bedside and Back Program of the NIH. The Rheumatic Diseases Research Core Center at Johns Hopkins University, where line blot antibody assays were performed on sera from the Johns Hopkins Myositis Center, is supported by the National Institute of Arthritis and Musculoskeletal and Skin Diseases (NIAMS), NIH (grant P30AR070254).

[1]Adeno-Associated Virus Biology Section, National Institute of Dental and Craniofacial Research, NIH, Bethesda, Maryland; [2]Muscle Disease Section, National Institute of Arthritis and Musculoskeletal and Skin Diseases, NIH, Bethesda, Maryland; [3]Office of Biostatistics Research, National Heart, Lung, and Blood Institute (NHLBI), NIH, Bethesda, Maryland; [4]Critical Care Medicine Department, NHLBI, NIH, Bethesda, Maryland; [5]NHLBI, NIH, Bethesda, Maryland; [6]Department of Medicine, Division of Rheumatology, Johns Hopkins University School of Medicine, Baltimore, Maryland; [7]Pulmonary and Critical Care Medicine Department, Johns Hopkins University School of Medicine, Baltimore, Maryland.

these assays often report qualitative results and are prone to variability in sensitivity and specificity, particularly for non–Jo-1 autoantibodies.[5] This limitation is most apparent at low or moderate autoantibody titers, in which the clinical significance is uncertain, and both false positives and false negatives are frequent, leading to potential underdiagnosis or overdiagnosis.[4–9]

Luciferase immunoprecipitation systems (LIPS) is a highly quantitative assay with a wide dynamic range, using *Renilla* luciferase–tagged antigens to measure autoantibodies.[10] It has demonstrated excellent performance in multiple autoimmune and infectious diseases, providing greater sensitivity and a broader dynamic range than conventional immunoassays.[11–13] We recently showed that LIPS can accurately detect and quantify broad levels of antisynthetase and anti–MDA-5 autoantibodies, highlighting how autoantibody levels may serve as biomarkers for treatment response in patients with autoimmune ILD.[14] Here, we extend these findings in a larger, clinically well-characterized cohort by directly comparing LIPS, line blot, and immunoprecipitation (IP) assays to assess whether LIPS improves diagnostic accuracy, particularly in the clinically ambiguous low to moderate titer range in which conventional assays have limitations.[15,16]

MATERIALS AND METHODS

An analysis of archived serum samples was conducted from patients with suspected IIM enrolled in a natural history study at the Johns Hopkins Myositis Center. Line blot testing (EUROLINE Autoimmune Inflammatory Myopathies 16 Ag IgG, Euroimmun, Lubeck, Germany) was performed for research purposes, with titers classified as low positive (≥15 arbitrary units [AU], 1+), moderate positive (≥36 AU, 2+), and strong positive (≥71 AU, 3+). Patients with borderline titers (8–14 AU) for MSAs were excluded. Patients were assigned to a specific autoantibody group if line blot assay was positive for an MSA by line blot (≥15 AU). LIPS testing was performed for the corresponding MSAs. LIPS testing was performed as previously described using *Renilla* luciferase–tagged antigens, with predefined antigen-specific thresholds.[10–13] Antibody binding is detected via luminescence light units (LU), with signal intensity proportional to the levels of antibodies. In an exploratory manner, a myositis-associated autoantibody (anti-Ro52) was also analyzed and compared to titers from the line blot. Data from IP, the reference standard for the measurement of MSAs, were included for comparison to the line blot and LIPS assays. IP testing was performed using the Oklahoma Medical Research Foundation (OMRF) myositis panel, which incorporates IP along with complementary confirmatory methods for antibody designation. Additional confirmatory IP testing for selected cases was performed at Johns Hopkins University using an in-house assay. Discrepancies in results, potentially related to differences in the timing of sample acquisition, are reported. Other assays were incorporated when available through chart review. These included a commercial line blot myositis panel ordered through Quest Diagnostics (Secaucus, New Jersey), a laboratory-developed ELISA performed at Johns Hopkins Hospital. Results from outside laboratories for which the specific assay methodology could not be determined were categorized as unspecified. Patients with co-positivity by line blot for other autoantibodies were classified as "undefined" and reviewed separately.

To assess diagnostic agreement, the performance of LIPS and line blot assays was compared with IP as the gold standard. The LIPS assay was analyzed as a binary result (positive vs negative) based on previously published thresholds.[14] Line blot was evaluated using established cutoffs for defining positive results (≥36 and ≥71). Agreement metrics included sensitivity, specificity, accuracy, Cohen's κ-coefficient, and the area under the receiver operating characteristic (ROC) curve (AUC). ROC curves were generated for LIPS, with line blot operating points (≥36, ≥71, and antibody specific) overlaid as discrete markers. AUC was estimated nonparametrically. To compare the performance of two diagnostic tests, McNemar's test was used to assess differences in sensitivity, specificity, and accuracy, DeLong's test was applied to compare AUCs, and Hotelling's T^2 test was used to compare κ-coefficients.[17,18] For patients without IP data, ILD status and clinical diagnoses were summarized by LIPS positivity and compared with line blot titers at thresholds of ≥36 and ≥71 to illustrate the effect of thresholding on classification. Importantly, clinical diagnoses had been previously established through multidisciplinary clinical evaluation and retrospective chart review and were not based solely on antibody test results. Statistical analyses were performed using R software (version 4.5, R Foundation for Statistical Computing) and the R packages pROC, multiagree, and DTComPair.

Ethics approval. This retrospective study used de-identified samples and was deemed exempt from review by the institutional review board (IRB00455938).

RESULTS

We analyzed 279 samples from patients with suspected IIM who had line blot titers of ≥15. These included 136 anti–Jo-1, 56 anti–MDA-5, 49 anti–PL-7, 31 anti–PL-12, and 7 anti-EJ

Additional supplementary information cited in this article can be found online in the Supporting Information section (https://acrjournals.onlinelibrary.wiley.com/doi/10.1002/art.70103).

Author disclosures are available at https://onlinelibrary.wiley.com/doi/10.1002/art.70103.

Address correspondence via email to Julio A. Huapaya, MD, MHS, at julio.huapayacarrera@nih.gov.

Submitted for publication November 21, 2025; accepted in revised form February 5, 2026.

Table 1. Agreement of line blot and luciferase immunoprecipitation systems assays with immunoprecipitation across standard cutoffs*

Method	TP	TN	FP	FN	Sensitivity (95% CI)	Specificity (95% CI)	Accuracy (95% CI)	κ coefficient (95% CI)	AUC (95% CI)
Line blot ≥36	92	31	11	7	0.929 (0.879–0.980)	0.738 (0.605–0.871)	0.872 (0.789–0.911)	0.686 (0.552–0.820)	0.834 (0.762–0.906)
Line blot ≥71	82	39	3	17	0.828 (0.754–0.903)	0.929 (0.851–1.000)	0.858 (0.789–0.911)	0.691 (0.568–0.813)	0.878 (0.824–0.933)
Line blot, antibody-specific[a]	92	36	6	7	0.929 (0.879–0.980)	0.857 (0.751–0.963)	0.908 (0.847–0.950)	0.781 (0.668–0.894)	0.893 (0.834–0.953)
LIPS	98	37	5[b]	1[c]	0.990 (0.970–1.000)	0.881 (0.783–0.979)	0.957 (0.910–0.984)	0.895 (0.814–0.977)	0.935 (0.885–0.986)

* N = 141 samples. Accuracy is defined as the proportion of correctly classified (true positive and true negative). AUC, area under the receiver operating characteristic curve; CI, confidence interval; FN, false negative; FP, false positive; LIPS, luciferase immunoprecipitation systems; TN, true negative; TP, true positive.
[a] ≥36 for Jo-1/MDA-5; ≥71 for PL-7, PL-12, EJ.
[b] Of the five discordant luciferase immunoprecipitation systems (+)/immunoprecipitation (–) cases, four occurred in anti–Jo-1 and one in anti–MDA-5. Among the Jo-1 cases, three were clinically consistent with antisynthetase syndrome and one with polymyositis overlap; all had positive results by another contemporaneous assay. In three of these patients, immunoprecipitation had been performed 8 to 15 years before luciferase immunoprecipitation systems. In the fourth, same-day immunoprecipitation was positive for PL-12, which luciferase immunoprecipitation systems also detected, suggesting dual positivity. The single anti–MDA-5 discordance occurred in a patient with finger ulcers suggestive of an anti–MDA-5 phenotype; in this case, the immunoprecipitation method did not specifically include anti–MDA-5 testing.
[c] Immunoprecipitation performed three months before line blot and luciferase immunoprecipitation systems testing.

samples. Table 1 summarizes the diagnostic performance of LIPS and line blot compared with IP. Heatmaps of different antibody-specific assays and ILD per subgroup are shown in the Supplementary Material (e-Figure 1). Among healthy controls, the mean ± SD values for LIPS ranged from 4,795 ± 855 to 10,099 ± 2,323 across antigens.

Agreement between LIPS and IP with clinical context of discordant cases. Across all autoantibodies with concomitant IP data (n = 141, 99 positive and 42 negative), LIPS demonstrated the highest agreement with IP (κ = 0.90, accuracy 95.7%, AUC 0.935), correctly classifying 135 of 141 cases (98 true positives, 37 true negatives, 5 false positives, and 1 false negative) (Table 1). In contrast, line blot performance was more threshold dependent than LIPS; at a threshold of ≥36, sensitivity was high (92.9%) and specificity was moderate (73.8%), reducing its accuracy (87.2%, κ = 0.686) compared to IP. Using a threshold of ≥71, specificity improved (92.9%) but sensitivity declined (82.8%), yielding similar accuracy (85.8%, κ = 0.691) yet remaining quantitatively inferior to LIPS across sensitivity-specificity balance, κ coefficient, and AUC. Using antibody-specific cutoffs (≥36 for Jo-1/MDA-5; ≥71 for PL-7/PL-12/EJ) modestly improved line blot agreement (κ = 0.781) but still remained inferior to LIPS. Overall, LIPS performance was significantly superior compared to line blot results (Table 1; Figure 1A). ROC analysis confirmed these trade-offs, with LIPS achieving a greater AUC (0.935) compared to line blot results (0.834–0.893; Figure 1B). Detailed per-antibody results are provided in Supplementary e-Table 1. Comparisons of sensitivity, specificity, positive predictive values, and negative predictive values are presented in Supplementary e-Table 2 and Supplementary e-Figure 2.

Most apparent discordances between LIPS and IP were attributable to differences in sample timing rather than assay performance. The median interval between LIPS testing and IP was one day (interquartile range 0–819). When analyses were restricted to samples collected within 30 days of IP testing, only one LIPS-IP discordant result remained; when restricted to samples collected within 90 days, two LIPS-IP discordant results remained. Four Jo-1 cases were LIPS positive but IP negative; in three of these, IP had been performed 8 to 13 years earlier, and all had ELISA or commercial line blot results at other time points consistent with Jo-1 positivity. Another case was positive for Jo-1 by both LIPS and ELISA, positive for PL-12 by LIPS, and positive only for PL-12 by IP, suggesting true dual antibody positivity. For anti–MDA-5, one case was LIPS positive and IP negative but clinically consistent with anti–MDA-5, again favoring the LIPS result. After these considerations, only a single unexplained discordance remained, underscoring the robustness of LIPS concordance with IP.

Agreement between LIPS and line blot in patients without IP results. Among patients without IP results (n = 138), 87 tested positive and 51 negative by LIPS. Applying the stricter line blot thresholds described above, 83 patients had titers ≥36 and 69 had titers ≥71. Among patients who were LIPS negative, 40 had line blot titers <36 and 46 had titers <71. At the ≥36 cutoff, LIPS and line blot were concordant in 89% of cases (11% discordant), whereas at the ≥71 cutoff, concordance fell to 83%. In essentially all LIPS-positive cases, a clinically plausible corresponding diagnosis was present (antisynthetase syndrome [AS], dermatomyositis [DM], and overlap syndromes), with no misclassification of inclusion body myositis (IBM). By contrast, among discordant cases (line blot positive but LIPS negative), 5 of 11 patients were clinically diagnosed with IBM. These diagnostic distributions, summarized in Table 2, reinforce the clinical specificity of LIPS and illustrate how antibody-specific

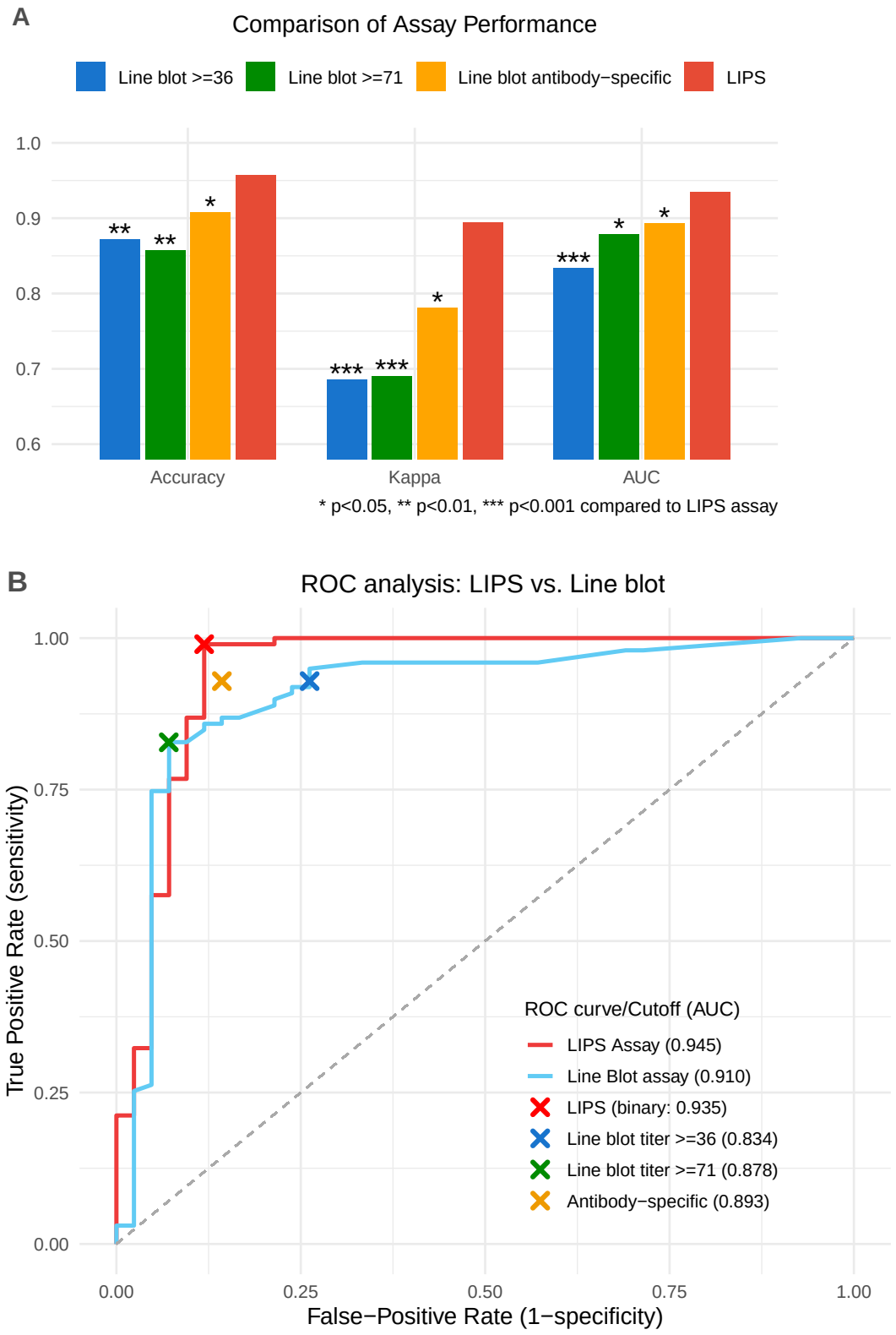

Figure 1. Legend on next page.

thresholds modify interpretation of line blot results by shifting sensitivity-specificity trade-offs; however, these effects are antibody dependent and do not uniformly improve performance across antibodies, with persistent misclassification for some specificities. Patient-level patterns of discordance between LIPS and line blot across both thresholds are presented in Supplementary e-Table 3.

Anti–Jo-1. Of 136 line blot–positive samples, 123 (90%) were LIPS positive (range 42,000–11 million LU), whereas 13 (10%) were LIPS negative (9,000–24,000 LU). Among the patients who were LIPS positive, 117 were confirmed by another method (56 by IP, 9 by commercial line blot, and 70 by ELISA). Four samples were discordant between LIPS and IP, although the time between testing was highly variable (Table 1). In patients categorized as "undefined" by line blot but positive by LIPS (n = 15), 11 had DM, 4 had polymyositis (PM), 11 had ILD, and 5 were IP confirmed.

Among the 13 LIPS-negative cases, IP testing was available for 2, with 1 discordant result (Table 1). In a subset of patients, ELISA results showed partial concordance (Supplementary e-Figure 1). Line blot titers in this group were generally low (15–30), except for one patient with a high titer of 120. From a clinical perspective, this group included four patients with IBM, four patients with myositis overlap syndromes, two patients with AS, two patients with DM, and one patient with PM. Of note, 10 of these patients were categorized as "undefined" by line blot.

Anti–MDA-5. Of 56 line blot–positive samples, 37 (66%) were LIPS positive (range 500,000–7,000,000 LU) and 19 (34%) were LIPS negative (<25,000 LU). Among patients who were LIPS positive, 28 had IP data, with 27 positive for anti–MDA-5. One discordant sample was LIPS positive but IP negative; however, the IP panel did not specifically include MDA-5, and the patient was clinically consistent with anti–MDA-5. Notably, 13 patients who were LIPS positive had low to moderate line blot titers (16–70), 10 of whom had ILD. Among 13 patients categorized as "undefined" by line blot but positive by LIPS, 12 had DM (one amyopathic), 1 had lupus overlap, 10 had ILD, and 4 were IP confirmed.

Among 19 patients who were LIPS negative, 15 had confirmation by another method (10 IP and 5 commercial line blot). Three of these had line blot titers between 36 to 64, including one with ILD (anti–Jo-1+ by OMRF). Clinically, this group included three patients with IBM, four patients with overlap syndromes, one patient with necrotizing myopathy, eight patients with DM, two patients with AS, and one patient with undifferentiated myopathy; only seven patients had ILD. Eleven patients in this group were categorized as "undefined" by line blot.

Anti–PL-7. Of 49 line blot–positive samples, 13 (27%) were LIPS positive (range 1–4 million LU) and 36 (73%) were LIPS negative (4,000–50,000 LU). All patients who were LIPS positive had confirmation by at least one additional method, with some undergoing multiple confirmatory assays (7 IP, 4 commercial line blot, 1 ELISA, and 2 unspecified). One patient had a low line blot titer of 18 and was correctly identified by LIPS; this patient had PM without ILD, showing that LIPS can detect true positives even when the line blot is weak. Only one patient who was LIPS positive was categorized as "undefined" by line blot, and this case was confirmed as positive by IP.

Among 36 patients who were LIPS negative, 18 had confirmation by another method (15 IP, 4 commercial line blot, and 1 unspecified). Four patients in this group had moderate to strong line blot titers (67–175), three did not have ILD, and two had additional negative confirmatory testing, indicating that even strong line blot titers can be false positives. Clinically, this group included 12 patients with DM (1 amyopathic), 14 patients with IBM, 5 patients with PM, 1 patient with polymyalgia rheumatica, 1 patient with statin-induced necrotizing myopathy, 1 patient with undifferentiated myopathy, 4 patients had ILD. Fifteen were IP negative. Except for one patient with negative results, all were categorized as "undefined" by line blot.

Anti–PL-12. Of the 31 line blot–positive samples, 14 (44%) were LIPS positive (150,000–2.2 million LU) and 17 were LIPS negative (3,000–22,000 LU). All patients who were LIPS positive had confirmation by at least one additional method, with some undergoing multiple confirmatory assays (11 IP, 6 commercial line blot, and 1 unspecified). One patient with a low line blot titer of 16 was confirmed positive by both LIPS and IP and had ILD, demonstrating that LIPS can detect clinically meaningful positives even at weak line blot titers. No patients who were LIPS positive were categorized as "undefined" by line blot.

Among patients who were LIPS negative, 12 had confirmation (9 IP, 1 commercial line blot, and 2 unspecified). Three patients had high line blot PL-12 titers (66–87 AU). One of these patients had ILD but was also negative for anti–PL-12 by IP. A

Figure 1. Performance of LIPS and line blot compared with immunoprecipitation. (A) Comparison of assay performance between LIPS and line blot at different cutoffs: titer ≥36 (blue), titer ≥71 (green), and antibody-specific thresholds (orange). Accuracy, Cohen's κ, and AUC values were calculated using immunoprecipitation as the reference standard. Statistical significance is shown relative to the LIPS assay (*$P < 0.05$, **$P < 0.01$, ***$P < 0.001$). (B) ROC curves for LIPS (blue) and line blot (red) in comparison with immunoprecipitation as the gold standard. LIPS demonstrated a higher area under the curve (AUC = 0.935) compared to line blot (AUC = 0.893). The (x) points indicate the binary (yes/no) LIPS result, line blot cutoffs at ≥36, ≥71, and antibody-specific cutoff, illustrating the trade-off between sensitivity and specificity. AUC, area under the receiver operating characteristic curve; LIPS, luciferase immunoprecipitation systems; ROC, receiver operating characteristic.

Table 2. Diagnostic patterns and concordance between LIPS and line blot at ≥36 and ≥71 cutoffs in patients without immunoprecipitation*

Antibody	N	Line blot ≥36	Line blot ≥71	ILD+	ILD–	Diagnoses	Discordant results ≥36	Clinical diagnosis ≥36	Discordant results ≥71	Clinical diagnosis ≥71
LIPS(+) patients by antibody subtype (n = 87)										
Jo-1	67	65	52	60	7	60 AS; 3 overlap; 2 DM; 2 PM	2	1 AS; 1 PM	15	13 AS; 1 overlap; 1 PM
MDA-5	9	8	7	9	0	7 DM; 1 PM; 1 overlap	1	1 DM	2	1 DM; 1 overlap
PL-7	6	5	5	5	1	5 AS; 1 PM	1	1 PM	1	1 PM
EJ	2	2	2	2	0	2 AS	0		0	
PL-12	3	3	3	3	0	3 AS	0		0	
All	87	83	69	79	8		4		18	
LIPS(−) patients by antibody subtype (n = 51)										
Jo-1	11	1	1	4	7	3 AS; 3 IBM; 2 overlap; 2 DM; 1 PM	1	1 IBM	1	1 IBM
MDA-5	9	2	0	2	7	3 IBM; 3 DM; 2 AS; 1 overlap	2	1 IBM; 1 overlap	0	
PL-7	21	6	2	3	18	13 IBM; 4 other; 2 PM; 1 DM; 1 AS	6	3 IBM; 1 other; 1 PM; 1 DM	2	1 PM; 1 DM
EJ	2	0	0	0	2	2 IBM	0		0	
PL-12	8	2	2	3	5	4 IBM; 3 other; 1 DM	2	1 DM; 1 other	2	1 DM; 1 other
All	51	11	5	12	39		11		5	

* AS, antisynthetase syndrome; DM, dermatomyositis; IBM, inclusion body myositis; ILD, interstitial lung disease; LIPS, luciferase immunoprecipitation systems; PM, polymyositis.

second patient had mild ILD and was negative for PL-12 by another line blot test. The third patient did not have ILD, was negative by another line blot, and was clinically diagnosed with overlap syndrome. These cases were therefore classified as false positives by line blot, although lung-limited or early AS cannot be definitively excluded in patients with ILD who lacked IP confirmation. Clinically, this group included four patients with DM, six patients with IBM, two patients with PM, one patient who was amyloid, two patients with overlap syndromes, one patient with necrotizing myopathy, one patient without myopathy, and four patients had ILD. All patients in this group were categorized as "undefined" by line blot.

Anti-EJ. Of seven line blot–positive samples, three (43%) were LIPS positive (2–7 million LU) and four (57%) were LIPS negative (17,000–31,000 LU). All patients who were LIPS positive had confirmation by another method (1 IP and 2 unspecified). Line blot titers in this group were strongly positive (135–194). No patients who were LIPS positive were categorized as "undefined" by line blot.

Among the patients who were LIPS negative, IP confirmation was available for two cases, both concordant. Line blot titers ranged from 15 to 27. Clinically, this group included two patients with IBM and two patients with overlap syndromes, and all were categorized as "undefined" by line blot. Despite the small sample size, LIPS results were concordant with IP where available, supporting its reliability for this rare autoantibody.

Anti-Ro52. When comparing LIPS anti-Ro52 levels with line blot titers, discrepancies were concentrated at low and borderline values (Figure 2). Of note, in contrast to MSAs, no IP-based gold standard exists for anti-Ro52. Among 118 patients with line blot–negative results (<8 AU), the majority were also negative by LIPS, although six had high LIPS levels (110,000–2,000,000 LU). Of the eight patients with borderline titers (8–14 AU), only one demonstrated a high LIPS level (1.3 million LU). In the low-positive range (15–35 AU; n = 15), LIPS confirmed eight patients as positive, most with very high levels (125,000–3 million LU), whereas the remainder were negative. By contrast, 24 of 28 patients with moderate positives (36–70 AU) were confirmed by LIPS, and among 106 patients with strong positives (≥71 AU), nearly all were concordant, with only 3 discrepant negatives (line blot titers of 80, 119, and 169). Overall, LIPS would have reclassified 21 patients (14 to positive, and 7 to negative). These findings suggest that although line blot is generally reliable at moderate to high titers (≥36 AU), results below this range are more uncertain, and LIPS may provide additional clarity in such cases.

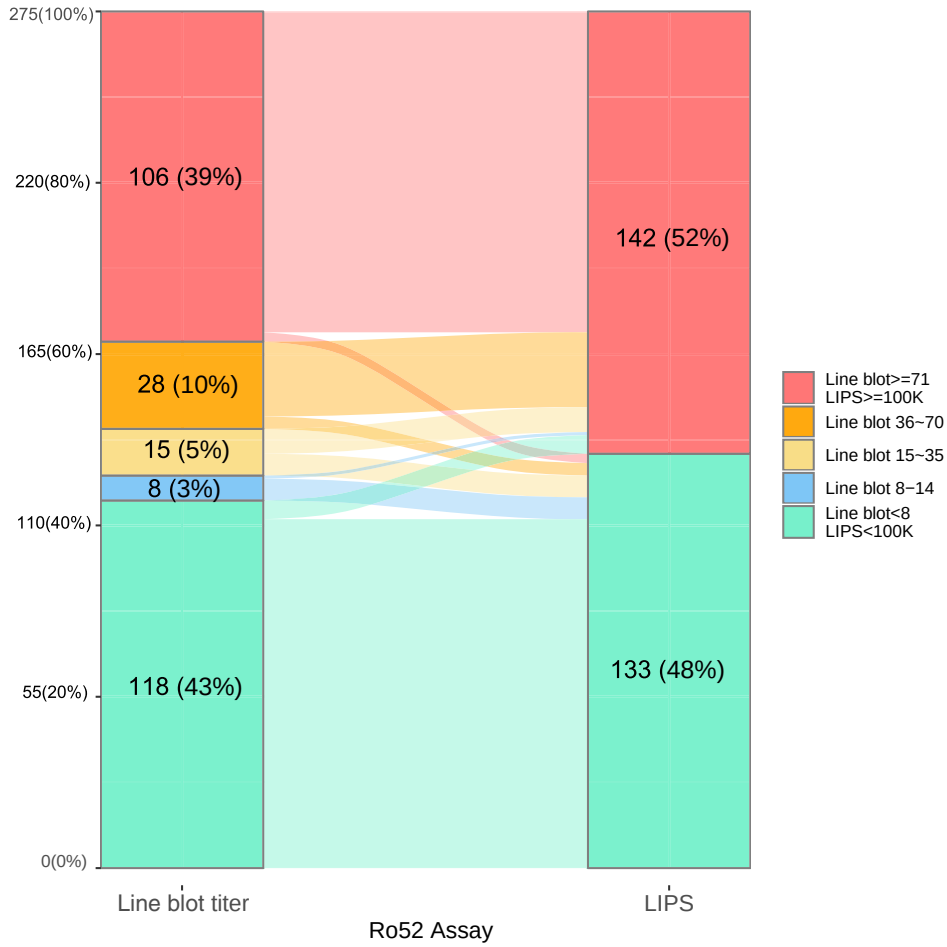

Figure 2. Comparison of LIPS anti-Ro52 levels with line blot titers. Sankey plot illustrating the relationship between line blot titers and LIPS anti-Ro52 levels. The left column shows anti-Ro52 line blot titers categorized into ranges: ≥71 (positive, red), 36 to 70 (orange), 15 to 35 (yellow), 8 to 14 (blue), and <8 (negative, teal). The right column depicts corresponding LIPS results, with ≥100,000 considered positive (red) and <100,000 considered negative (teal). Width of the flows represents the number of patients in each category, and percentages are shown within boxes. LIPS, luciferase immunoprecipitation systems. Color figure can be viewed in the online issue, which is available at http://onlinelibrary.wiley.com/doi/10.1002/art.70103/abstract.

DISCUSSION

Our study demonstrates strong concordance between the diagnostic performance of LIPS and IP (κ = 0.90) across testing for anti–Jo-1, anti–PL-7, anti–PL-12, anti–MDA-5, and anti-EJ autoantibodies. Importantly, LIPS showed superior performance compared to line blot, particularly in the low to intermediate autoantibody titer range, in which misclassification was most common. LIPS identified autoantibodies in patients with IIM who would have been missed by line blot at low titers and would have excluded false positives at higher titers, especially for anti–PL-7 and anti–PL-12, many of whom did not have ILD. In light of these findings, LIPS could help decrease both underdiagnosis and false positives of clinically relevant autoantibodies associated with ILD. Although line blot titers of cutoff values ≥71 were generally more reliable, false positives still occurred, underscoring the limitations of fixed thresholds. Analysis of patients without IP further supported these findings. In this cohort, patients who were LIPS positive were enriched for AS, DM, and overlap syndromes with frequent ILD, whereas patients who were LIPS negative were primarily IBM. These diagnostic patterns highlight the greater clinical specificity of LIPS and illustrate that although antibody-specific cutoffs (≥36 for Jo-1 and MDA-5; ≥71 for PL-7, PL-12, and EJ) modify line blot interpretation, potential misclassification remains. Overall, LIPS provided the most consistent alignment with IP and clinical phenotype, reinforcing its value for accurate classification and patient stratification. Of note, the quantitative nature of LIPS for detecting MSAs may facilitate earlier recognition of pulmonary involvement, particularly in patients with low-level autoantibody positivity. In addition, LIPS may help refine diagnostic classification in clinically ambiguous cases and support longitudinal monitoring in therapeutic trials or in the assessment of treatment response.[14]

Our analysis of anti-Ro52 further illustrates these threshold-dependent challenges. Discrepancies with LIPS were most frequent at line blot titers <36 AU. Although no gold standard exists for anti-Ro52 antibody detection, the broader dynamic range and quantitative output of LIPS support is its greater interpretive value,[14,19] especially at low to borderline titers (<36 AU), in which line blot appears prone to misclassification. The quantitative resolution of LIPS clarified interpretation in 21 cases and highlighted that line blot is most reliable at titers >36 AU. These findings suggest that although line blot adequately captures Ro52 at moderate to high titers, LIPS may provide useful information in cases with low to moderate titers.

These findings build upon prior studies that have highlighted variability in myositis autoantibody testing across platforms.[4–9,20] Shinoda et al[16] reported poor specificity for line blot (κ = 0.23), compared to RNA-IP, which improved (κ = 0.75) with stricter thresholds (going from 1 to 2+). In our study, we demonstrate that even 2+ (titer ≥36) can be poorly discriminative for some autoantibodies, particularly non–Jo-1 autoantibodies. Mecoli et al also found that antibody-specific thresholds improved agreement with IP (≥15 for anti–Jo-1, ≥36 for anti–PL-12/EJ, and ≥71 for anti–PL-7), but discordance persisted; only a fraction (n = 5 of 19) of discordant cases fit clinical AS.[21] Espinosa-Ortega et al observed good agreement between line blot and IP for anti–Jo-1 (κ = 0.69) but only moderate agreement for a small number of patients with anti–MDA-5 (κ = 0.49).[15] Loganathan et al showed high concordance between ELISA and IP across multiple autoantibodies but reported reduced sensitivity for anti–MDA-5.[22] Another study on myositis-specific antibodies in neurologic disorders also identified false-positive results in more than 1 of 10 patients with nonmyositis diseases when the standard low (≥15) thresholds were used.[23] Our work confirms and extends these observations in a larger, clinically well-characterized cohort, establishing LIPS as a reliable alternative for autoantibody detection in IIM-ILD.

These data have important clinical implications. Patients classified as "undefined" by line blot may have a clear antibody positivity by LIPS, with clinical features consistent with AS. LIPS may therefore refine diagnostic classification when results are ambiguous. For clinicians, line blot titers in the 15 to 70 range or multiple antibody positivity should prompt confirmatory testing with another method such as IP. Although some undefined cases may represent true dual positivity, without contemporaneous IP, this remains uncertain, underscoring the need for future work to distinguish true seropositivity from artifactual multiple reactivity.

Our study has several strengths. It represents one of the largest head-to-head evaluations of LIPS, line blot, and IP across multiple clinically relevant myositis autoantibodies. We included both patients with IP data and those without, enabling assessment of assay concordance as well as clinical enrichment patterns in the non-IP cohort. The limitations include its retrospective design, variability in assay timing, and small numbers for rarer antibodies such as EJ. Further, the anti–Jo-1 analysis was characterized by extreme prevalence imbalance, with very few true negative samples, a setting in which Cohen's κ-coefficient may substantially underestimate agreement despite high observed concordance (overall agreement 91.4%). Accordingly, κ values should be interpreted in the context of sensitivity and specificity, particularly in antigen groups with marked prevalence imbalance. Discordant results may reflect long gaps between collections or true longitudinal changes in autoantibody levels. Additionally, this referral-center cohort was enriched for antibody-positive cases, and availability of IP may have been influenced by clinical and logistical constraints, which should be considered when interpreting concordance metrics. This limits generalizability to unselected screening populations. Finally, as LIPS was performed in 2025 on sera stored since 2016, our findings also highlight the stability of autoantibodies over time. Future work should evaluate LIPS prospectively in multicenter cohorts, incorporate longitudinal sampling, and test whether integration of LIPS into diagnostic workflows improves clinical outcomes. In particular, linking LIPS-based classification to ILD progression, treatment response, and survival will be critical to determine its clinical use. Such studies could inform future diagnostic algorithms and guidelines, in which reflex testing with LIPS may provide a more accurate and clinically meaningful assessment of myositis autoantibody status.

LIPS demonstrated strong concordance with IP across multiple myositis autoantibodies and provided clearer discrimination than line blot at low to intermediate titers, in which misclassification was most common. Antibody-specific thresholds (≥36 for Jo-1 and MDA-5; ≥71 for PL-7, PL-12, and EJ) modified line blot interpretation by shifting sensitivity-specificity trade-offs and may improve clinical interpretability in practice; however, residual false positives persisted, particularly among non–Jo-1 antibodies. By offering quantitative, high–dynamic-range output, LIPS complements existing assays, reduces diagnostic uncertainty, and has the potential to enhance patient stratification and ILD risk recognition in IIM as it becomes more broadly available.

ACKNOWLEDGMENTS

We thank all the members of the Johns Hopkins Myositis Center and the patients who generously contributed to this study. We also acknowledge the Johns Hopkins Myositis Center Biobank team for their essential contributions in processing, storing, and managing patient samples. Finally, we thank Kelly Byrne for her assistance with the submission process.

AUTHOR CONTRIBUTIONS

All authors contributed to at least one of the following manuscript preparation roles: conceptualization AND/OR methodology, software, investigation, formal analysis, data curation, visualization, and validation AND drafting or reviewing/editing the final draft. As corresponding author, Dr Huapaya confirms that all authors have provided the final approval of the version to be published and takes responsibility for the affirmations regarding article submission (eg, not under consideration

by another journal), the integrity of the data presented, and the statements regarding compliance with institutional review board/Declaration of Helsinki requirements.

REFERENCES

1. Pinal-Fernandez I, Casal-Dominguez M, Huapaya JA, et al. A longitudinal cohort study of the anti-synthetase syndrome: increased severity of interstitial lung disease in black patients and patients with anti-PL7 and anti-PL12 autoantibodies. Rheumatology (Oxford) 2017;56(6):999–1007. doi:https://doi.org/10.1093/rheumatology/kex021
2. Pinal-Fernandez I, Mecoli CA, Casal-Dominguez M, et al. More prominent muscle involvement in patients with dermatomyositis with anti-Mi2 autoantibodies. Neurology 2019;93(19):e1768–e1777. doi:https://doi.org/10.1212/WNL.0000000000008443
3. Sehgal S, Patel A, Chatterjee S, et al. Idiopathic inflammatory myopathies related lung disease in adults. Lancet Respir Med 2025;13(3):272–288. doi:https://doi.org/10.1016/S2213-2600(24)00267-4
4. Tansley SL, Snowball J, Pauling JD, et al; International Myositis Assessment and Clinical Studies (IMACS) Group Myositis Autoantibody Scientific Interest Group. The promise, perceptions, and pitfalls of immunoassays for autoantibody testing in myositis. Arthritis Res Ther 2020;22(1):117. doi:https://doi.org/10.1186/s13075-020-02210-2
5. Loganathan A, Zanframundo G, Yoshida A, et al; CLASS Project. Agreement between local and central anti-synthetase antibodies detection: results from the Classification Criteria of Anti-Synthetase Syndrome project biobank. Clin Exp Rheumatol 2024;42(2):277–287. doi:https://doi.org/10.55563/clinexprheumatol/s14zq8
6. Kerola AM, Pietikäinen A, Barantseva J, et al. Predictive value of myositis antibodies: role of semiquantitative classification and positivity for more than one autoantibody. RMD Open 2025;11(1):e005007. doi:https://doi.org/10.1136/rmdopen-2024-005007
7. Anderson HT, O'Donnell JL, Tustin P, et al. Diagnosis and subtyping of idiopathic inflammatory myopathies: caution required in the use of myositis autoantibodies. Intern Med J 2024;54(4):682–686. doi:https://doi.org/10.1111/imj.16350
8. Lackner A, Tiefenthaler V, Mirzayeva J, et al. The use and diagnostic value of testing myositis-specific and myositis-associated autoantibodies by line immunoassay: a retrospective study. Ther Adv Musculoskelet Dis 2020;12:1759720X20975907.
9. Chang YC, Yang L, Budhram A. Positive predictive value of myositis antibody line blot testing in patients with suspected idiopathic inflammatory myopathy. Muscle Nerve 2024;69(5):626–630. doi:https://doi.org/10.1002/mus.28050
10. Burbelo PD, Ching KH, Klimavicz CM, et al. Antibody profiling by luciferase immunoprecipitation systems (LIPS). J Vis Exp 2009;(32):1549. doi:https://doi.org/10.3791/1549
11. Burbelo PD, Joshi M, Chaturvedi A, et al. Detection of PLA2R autoantibodies before the diagnosis of membranous nephropathy. J Am Soc Nephrol 2020;31(1):208–217. doi:https://doi.org/10.1681/ASN.2019050538
12. Burbelo PD, Lebovitz EE, Notkins AL. Luciferase immunoprecipitation systems for measuring antibodies in autoimmune and infectious diseases. Transl Res 2015;165(2):325–335. doi:https://doi.org/10.1016/j.trsl.2014.08.006
13. Ching KH, Burbelo PD, Gonzalez-Begne M, et al. Salivary anti-Ro60 and anti-Ro52 antibody profiles to diagnose Sjogren's Syndrome. J Dent Res 2011;90(4):445–449. doi:https://doi.org/10.1177/0022034510390811
14. Burbelo PD, Huapaya JA, Khavandgar Z, et al. Quantification of autoantibodies using a luminescent profiling method in autoimmune interstitial lung disease. Front Immunol 2024;15:1462242. doi:https://doi.org/10.3389/fimmu.2024.1462242
15. Espinosa-Ortega F, Holmqvist M, Alexanderson H, et al. Comparison of autoantibody specificities tested by a line blot assay and immunoprecipitation-based algorithm in patients with idiopathic inflammatory myopathies. Ann Rheum Dis 2019;78(6):858–860. doi:https://doi.org/10.1136/annrheumdis-2018-214690
16. Shinoda K, Okumura M, Yamaguchi S, et al. Comparison of line blots, enzyme-linked immunosorbent, and RNA-immunoprecipitation assays of antisynthetase antibodies in serum samples from 44 patients. Intern Med 2022;61(3):313–322. doi:https://doi.org/10.2169/internalmedicine.7824-21
17. Fleiss JL. Statistical methods for rates and proportions. 2nd ed. Wiley; 1981.
18. Vanbelle S. Comparing dependent kappa coefficients obtained on multilevel data. Biom J 2017;59(5):1016–1034. doi:https://doi.org/10.1002/bimj.201600093
19. Burbelo PD, Teos LY, Herche JL, et al. Autoantibodies against the immunoglobulin-binding region of Ro52 link its autoantigenicity with pathogen neutralization. Sci Rep 2018;8(1):3345. doi:https://doi.org/10.1038/s41598-018-21522-7
20. Oldroyd AGS, Lilleker JB, Amin T, et al; British Society for Rheumatology Standards, Audit and Guidelines Working Group. British Society for Rheumatology guideline on management of paediatric, adolescent and adult patients with idiopathic inflammatory myopathy. Rheumatology (Oxford) 2022;61(5):1760–1768. doi:https://doi.org/10.1093/rheumatology/keac115
21. Mecoli CA, Albayda J, Tiniakou E, et al. Myositis autoantibodies: a comparison of results from the Oklahoma Medical Research Foundation myositis panel to the Euroimmun research line blot. Arthritis Rheumatol 2020;72(1):192–194. doi:https://doi.org/10.1002/art.41088
22. Loganathan A, McMorrow F, Lu H, et al. The use of ELISA is comparable to immunoprecipitation in the detection of selected myositis-specific autoantibodies in a European population. Front Immunol 2022;13:975939. doi:https://doi.org/10.3389/fimmu.2022.975939
23. Kleiser B, Hoffmann D, Kowarik MC, et al. Myositis -specific and -associated antibodies in neurological disorders - a retrospective study of 727 patients. J Neurol Sci 2024;466:123213. doi:https://doi.org/10.1016/j.jns.2024.123213

Arthritis & Rheumatology
Vol. 78, No. 9, September 2026, pp 1961–1974
DOI 10.1002/art.70102
© 2026 The Author(s). *Arthritis & Rheumatology* published by Wiley Periodicals LLC on behalf of American College of Rheumatology.
This is an open access article under the terms of the Creative Commons Attribution-NonCommercial License, which permits use, distribution and reproduction in any medium, provided the original work is properly cited and is not used for commercial purposes.

American College of Rheumatology
Empowering Rheumatology Professionals

A Multifaceted Interplay Among Hemophagocytosis, Interleukin-18, and Type I Interferon Distinguishes Still Disease From Other Autoinflammatory Diseases

Yvonne M. Mueller, PhD,[1] Charlotte Girard, MD, PhD,[2] Harmen J. G. van de Werken, PhD,[1] Stefan J. Erkeland, PhD,[1] Dwin G. B. Grashof, MSc,[1] Laurie Vaillant, PhD,[2] Renske J. H. den Dekker, MSc,[1] Iris van Zuijen, MSc,[1] Sharon Veenbergen, PhD,[1] Fanny Coffin, PhD,[3] Eric Bindels, PhD,[4] Yvan Jamilloux, MD,[5] Katerina Laskari, MD,[6] Vassili Soumelis, MD, PhD,[7] Bruno Fautrel, MD, PhD,[8] Cem Gabay, MD, PhD,[2] and Peter D. Katsikis, MD, PhD[1]

Objective. The unknown pathophysiology and the lack of specific features for systemic juvenile idiopathic arthritis and adult-onset Still disease (collectively known as Still disease; SD) delay diagnosis and appropriate treatment. The goal of this study was to identify features and mechanisms that distinguish SD from other systemic autoinflammatory diseases (SAID).

Methods. Using the SomaScan assay and RNA sequencing (RNA-Seq), we determined the plasma proteomes and immune cell microRNA (miRNA) and RNA transcriptomes of 372 patients with SAID, respectively. Proteomic findings were validated by enzyme-linked immunosorbent assays. SD (n = 72) and non-SD SAIDs (n = 300) were compared to identify distinguishing features of SD. We performed integrated and unbiased analyses of all data sets using weighted gene correlation network analysis to identify feature modules that characterize SD and stratify patients.

Results. Elevated plasma heme oxygenase 1 (HO-1) and interleukin-18 (IL-18) strongly correlate and characterize SD but do not associate with general inflammation. SD was characterized by ferroptosis in plasma, type I interferon (IFN) signaling in monocyte transcriptomes, and elevated natural killer cell miRNA-146a-5p, which is an IL-18 induced miRNA. Finally, we identified feature modules that distinguish SD from other SAIDs and stratified patients with SD into two distinct subgroups not attributable to disease activity or inflammation but hemophagocytosis.

Conclusion. This unprecedented large omics data set of SAIDs revealed that complex interactions among hemophagocytosis, IL-18, and type I IFN signaling characterize SD. Furthermore, two distinct subgroups in patients with SD were distinguished by the degree of hemophagocytic activity. Finally, the large proteomics and RNA-Seq data sets generated in this study can serve as an invaluable resource for the further investigation of SD and other SAIDs.

INTRODUCTION

Still disease (SD) is a systemic autoinflammatory disease (SAID), a heterogeneous group of rare and debilitating diseases in which patients suffer from recurrent episodes of inflammation usually without evidence of autoimmunity.[1] SD affects children (systemic juvenile idiopathic arthritis [sJIA]) and adults (adult-onset Still disease [AOSD])[1] with a prevalence that ranges from 1 patient per 10,000 children for sJIA to 0.15 to 1.5 patients per 1,000,000 adults for AOSD.[2–4] Although the genetic cause of

Supported by the ImmunAID project funded by a European Union's Horizon 2020 research and innovation program (grant agreement #779295).

[1]Department of Immunology, Erasmus University Medical Center, Rotterdam, the Netherlands; [2]Department of Internal Medicine, University of Geneva, Geneva, Switzerland; [3]Institut Curie, Paris, France, Research University, Paris, France, Mines Paris Tech, Fontainebleau, France; [4]Department of Hematology, Erasmus University Medical Center, Rotterdam, the Netherlands; [5]Department of Internal Medicine, University Hospital Croix-Rousse, Hospices Civils de Lyon, University of Lyon, Lyon, France, Centre International de Recherche en Infectiologie (CIRI), Inserm U1111, ENS/CNRS UMR5308, Lyon, France, Lyon Immunopathology FEderation (LIFE), Lyon, France, CEREMAIA, Lyon, France; [6]Rheumatology Unit, First Department of Propaedeutic Internal Medicine, Joint Academic Rheumatology Program, University of Athens, Medical School, Athens, Greece; [7]Department of Immunology, Université de Paris, Paris, France; [8]Sorbonne University – Assistance Publique Hôpitaux de Paris, Rheumatology Department, IMIDIATE Clinical Research Network, Pitié Salpêtrière Hospital, Paris, France, CEREMAIA Reference Center, Paris, France, INSERM UMRS 1136, Paris, France.

Additional supplementary information cited in this article can be found online in the Supporting Information section (https://acrjournals.onlinelibrary.wiley.com/doi/10.1002/art.70102).

Author disclosures and graphical abstract are available at https://onlinelibrary.wiley.com/doi/10.1002/art.70102.

Address correspondence via email to Peter D. Katsikis, MD, PhD, at p.katsikis@erasmusmc.nl.

Submitted for publication July 30, 2025; accepted in revised form February 2, 2026.

some SAIDs has been identified,[5] 60% to 70% of patients with SAIDs lack a genetic cause.[5] Because of SD rarity and the nonspecific nature of its symptoms, patients with AOSD go undiagnosed on average for more than seven years[5] and often undergo rounds of ineffective treatments. A serious complication of SD is macrophage activation syndrome (MAS)/hemophagocytic lymphohistiocytosis (HLH), a life-threatening syndrome characterized by hemophagocytosis and cytokine storm.[1]

The overlapping markers of inflammation and symptoms between SD and other SAIDs has hampered efforts to discover SD-specific diagnostic biomarkers and uncover its poorly understood pathophysiologic mechanisms. Despite progress in identifying biomarkers for SD,[6] for example the use of hyperferritinemia and acute phase proteins such as C-reactive protein (CRP) as biomarkers of SD and very high ferritin as a predictor of MAS development,[6,7] these are not sufficient to discriminate SD from other SAIDs, and more specific biomarkers are needed. Interleukin 18 (IL-18) has been associated with SD[8] and recently recommended as a SD biomarker, although IL-18 testing is not always available.[9] SD has been difficult to distinguish on the basis of inflammatory cytokines, even from unrelated non-autoinflammatory conditions such as sepsis, which explains why CRP is not a specific marker for SD.[10] Other biomarkers may be more subgroup-specific, such as myeloid-related protein 8/14 (MRP8/14) in sJIA[11] and S100 calcium-binding protein A12 (S100A12) and S100A8/A9 in JIA.[12] IL-18, however, is a cytokine that does seem to provide some discrimination between SD and sepsis.[13,14] In SD, IL-18 and ferritin are elevated,[15,16] and IL-18 levels associates with MAS[17,18] and remission.[19] This has led to the suggestion that IL-18 may be a good biomarker for SD, especially for those patients at risk to develop MAS.[20] Overall, the most common biomarkers recommended for AOSD and sJIA are ferritin, S100 proteins, and IL-18.[9] In addition to ferritin, heme oxygenase-1 (HO-1) has also been associated with SD. Plasma HO-1 was suggested to be increased in SD by earlier studies, but the low numbers of patients with SD and the lack of comparison with other SAIDs made it unclear how specific HO-1 is for SD.[21–24] Currently, however, it remains unclear how IL-18, HO-1, and ferritin associate in SD and if these can serve to differentiate SD from other SAIDs.

In this report, we examine 372 patients with SAIDs assembled by the European Union–funded Immunome project consortium for AutoInflammatory Disorders (ImmunAID). We directly compared the plasma proteome, plasma cytokines, and blood monocyte transcriptome of SD with other SAIDs, described potential biomarkers for SD, and uncovered active molecular pathways that could inform better treatment for these patients.

MATERIALS AND METHODS

A detailed description of all materials and methods is provided in the Supplementary Materials and Methods. The following SAIDs were included: AOSD, sJIA, Behçet disease, Cryopyrin-associated periodic syndrome, chronic nonbacterial osteomyelitis, Familial Mediterranean fever, hyperimmunoglobulin D syndrome, inflammation of unknown origin (IUO), Kawasaki disease, pediatric inflammatory multisystem syndrome, Pyoderma gangrenosum, recurrent pericarditis, Schnitzler syndrome, Sweet syndrome, Takayasu arteritis, and tumor necrosis factor (TNF) receptor associated periodic syndrome (Supplementary Tables 1–3). Healthy controls (HC) were also included. The ImmunAID study was approved by the ethical committees of the included clinical centers and by the Geneva ethical committee. ImmunAID consortium members are listed in Appendix A. All participants signed an informed consent form.

RESULTS

Proteomics discovery analysis

To identify differentially abundant plasma proteins, we performed a proteomics discovery analysis using the SomaScan 7K assay that queries 6,596 unique plasma protein targets. We analyzed 372 patients with SAIDs with active disease collected by the ImmunAID consortium (Supplementary Table 1). Comparing SD (n = 72; n = 19 sJIA, n = 53 AOSD) with all other SAIDs (non-SD SAIDs: 14 diseases, n = 300) revealed that the top differentially increased proteins were heme oxygenase 1 (HO-1) (increased 3.8-fold in SD), ferritin heavy chain (increased 3.2-fold in SD), and ferritin light chain (increased 3.2-fold in SD) (Figure 1A and Supplementary Table 4A). Other proteins increased in SD plasma included apolipoprotein L3 (2.2-fold), phospholipase A2 (NPS-PLA2) (2.1-fold), and serum amyloid A-1 protein (SAA) (1.9-fold). The most reduced plasma proteins in SD were chondroadherin (0.63-fold), collagen alpha-2(XI) chain (0.67-fold), leucine-rich repeat-containing protein 15 (0.67-fold), and carbonic anhydrase 6 (0.67-fold).

When comparing SD with HC (n = 65) the most increased plasma proteins were associated with inflammation and included SAA (7.0-fold), NPS-PLA2 (4.4-fold), SAA2 (4.3-fold), and CRP (3.1-fold) (Figure 1B, Supplementary Table 4B). The proteins that differed the most between SD and non-SD SAIDs were also increased in SD compared with HC (HO-1: 3.7-fold; ferritin heavy chain: 4.1-fold; ferritin light chain: 4.2-fold) (Figure 1B, Supplementary Table 4B). Overall, 66 and 194 proteins were differentially abundant (adjusted *P* value [Padj] <0.05 and absolute $\log_2$ fold change ≥0.5) in SD compared with non-SD SAIDs and HC, respectively. From these proteomic data it is apparent that as a result of general inflammation, acute phase proteins are upregulated in SD, but heme signaling and metabolism most strongly distinguishes SD from non-SD SAIDs.

HO-1 and IL-18 are highly increased in SD but do not correlate with general inflammation

We confirmed increased levels of plasma HO-1 and ferritin in SD using enzyme-linked immunosorbent assay (ELISA) for HO-1

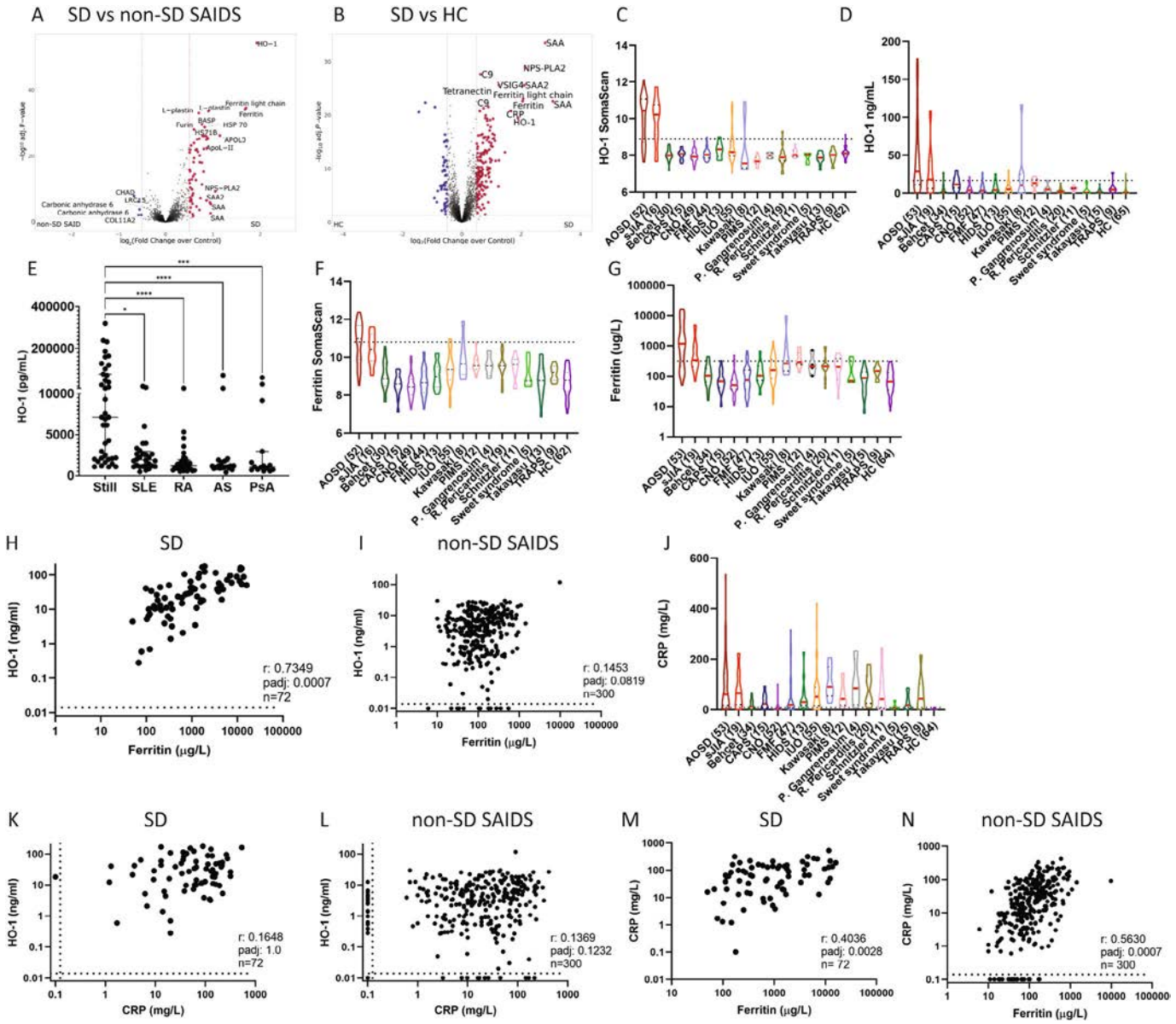

Figure 1. Plasma proteomics reveals a distinct profile for patients with SD and elevated HO-1 levels that do not correlate with general inflammation. Differentially detected plasma proteins by SomaScan proteomics for SD versus non-SD SAID (A) and SD versus HC comparison (B) (red increased and blue decreased in SD); SomaScan (C) and ELISA (D) HO-1 levels in patients with SAID and HC; (E) ELISA HO-1 plasma levels in Geneva cohort (SD, SLE, RA, AS, PsA); SomaScan (F) and ECLIA (G) ferritin levels in patients with SAID and HC; HO-1 correlation with ferritin in SD (H) and non-SD SAIDs (I); (J) CRP levels in SAID patients and HC; HO-1 correlation with CRP in SD (K) and non-SD SAIDs (L); CRP correlation with ferritin in SD (M) and non-SD SAIDs (N). HO-1, ferritin, and CRP statistical differences and % above cutoffs shown in Supplementary Tables 5 and 6. Significance in panel (E) was calculated using a Kruskal-Wallis test with Dunn's multiple comparison test. Correlations coefficients in panels (H), (I), (K), (L), (M) and (N) were calculated using a Spearman's rank correlation test with a Bonferroni correction for multiple comparison. AOSD, adult-onset Still disease; AS, ankylosing spondylitis; CAPS, cryopyrin-associated periodic syndrome; CNO, chronic non-bacterial osteomyelitis; CRP, C-reactive protein; ECLIA, electrochemiluminescence immunoassay; ELISA, enzyme-linked immunosorbent assay; FMF, Familial Mediterranean fever; HC, healthy control; HIDS, hyperimmunoglobulin D syndrome; HO-1, heme oxygenase 1; IUO, inflammation of unknown origin; PIMS, pediatric inflammatory multisystem syndrome; PsA, psoriatic arthritis; RA, rheumatoid arthritis; SAID, systemic autoinflammatory disease; SD, Still disease; sJIA, systemic juvenile idiopathic arthritis; SLE, systemic lupus erythematosus; TRAPS, TNF receptor associated periodic syndrome.

and electrochemiluminescence immunoassay for ferritin; both strongly correlated with SomaScan measurements in SD (r = 0.87 and r = 0.88, respectively) (Supplementary Figure 1A and B). HO-1 was increased in both AOSD and sJIA (Figure 1C and D; Supplementary Table 5), with 66% of AOSD and 53% of sJIA being above cutoff. Kawasaki disease was 50% above cutoff. Only 7.2% of patients with IUO were above HO-1 cutoff despite high CRP (Figure 1D, Supplementary Table 6). The

increased HO-1 levels in SD were further confirmed in an independent second cohort of patients comparing active SD (Geneva cohort) (Figure 1E).

Serum hyperferritinemia, although not specific, has aided AOSD diagnosis.[25] Ferritin was elevated in patients with AOSD and sJIA (Figure 1F and 1G, Supplementary Table 5), and 74% of patients with AOSD and 53% of those with sJIA were above cutoff, respectively (Figure 1G, Supplementary Table 6). Ferritin correlated with HO-1 in SD but not in non-SD SAIDs (r = 0.73 and r = 0.15, respectively) (Figure 1H and I). Because CRP is often used in the diagnosis of SD, we investigated its relationship to HO-1. CRP was frequently elevated in all patient groups with SAIDs (Figure 1J). CRP did not correlate with HO-1 in SD (r = 0.16) (Figure 1K) and non-SD SAIDs (r = 0.14) (Figure 1L). In contrast, ferritin correlated with CRP in both SD and non-SD SAIDs (r = 0.42 and r = 0.56, respectively) (Figure 1M and N). These results suggest that plasma ferritin in SD and non-SD SAIDs is in part due to inflammatory cytokines or reactive oxygen species and not only the result of hemophagocytosis.[26]

To further explore the relationship between inflammation and HO-1 in SD, we measured plasma inflammatory cytokines. IL-6 was not higher in AOSD and sJIA compared with most other non-SD SAIDs (Figure 2A, Supplementary Table 5), whereas TNF, IL-10, and IFNγ differed the most (Supplementary Figure 1C, Supplementary Table 5). IL-12 was not detectable (data not shown). In contrast, IL-18 was markedly elevated in patients with AOSD and sJIA (Figure 2B, Supplementary Table 5). IL-18 strongly correlated with HO-1 in patients with SD (r = 0.91) but weakly in non-SD SAIDs (r = 0.21) (Figure 2C), whereas IL-6 did not correlate with HO-1 in either patient group (Figure 2D). IL-18 in patients with SD did not correlate with CRP (r = 0.07) but correlated moderately in non-SD SAIDs (r = 0.33; Figure 2E). As expected, IL-6 correlated strongly with CRP in non-SD SAIDs (r = 0.59) and less so in SD (r = 0.34) (Figure 2F). In agreement with these results, the correlation between IL-18 and HO-1 was confirmed in another cohort of SD where total and free IL-18 also strongly correlated with HO-1, further reinforcing the functional association between bioactive IL-18 and plasma HO-1 (Figure 2G). HO-1 and total IL-18 did not correlate in non-SD rheumatic diseases (Figure 2G). The strong correlation between IL-18 and HO-1, and their dissociation from CRP or IL-6 levels, indicate that HO-1 and IL-18 increases in SD are not a measure of general inflammation but reflect yet-to-be-defined SD-specific inflammatory mechanisms.

Blood monocytes are not the source of HO-1 and IL-18 in SD

We next sorted peripheral blood monocytes from SD and non-SD SAIDs from the same patients and time points as mentioned previously and performed RNA-Seq to investigate HO-1 production and activated signaling pathways (for RNA-Seq sample numbers, see Supplementary Table 1). Differential gene expression between SD and non-SD SAIDs revealed that 112 genes were up-regulated and 71 genes were down-regulated in SD. Unsupervised clustering of gene expression in SD and non-SD SAIDs revealed distinct gene modules differentially expressed in SD when compared with non-SD SAIDs (Figure 3A and B). We found that monocyte HO-1, ferritin light chain, and ferritin heavy chain and IL-18 messenger RNA (mRNA) did not differ between SD, non-SD SAID, and HC (Supplementary Table 7A–C) indicating that blood monocytes are not the source of these in plasma. SD monocytes had both haptoglobin and CD163 up-regulated compared with non-SD SAIDs (up-regulated 1.99-fold and 1.53-fold, respectively), and this may suggest a propensity to uptake hemoglobin in SD (Supplementary Table 7A).

Pro-inflammatory cytokine IL-6 mRNA in SD was increased by 1.4-fold compared with HC but did not differ from non-SD SAIDs (Supplementary Table 7A–C). TNF and IFNγ did not differ between SD and non-SD SAIDs nor with HC, whereas IL-10 was increased in SD compared with non-SD SAIDs and with HC (1.4-fold and 1.8-fold, respectively). The most up-regulated gene in SD was the IL-1 decoy receptor IL-1R2,[27,28] which was increased in SD by 1.8-fold compared with non-SD SAIDs and 15.2-fold compared with HC (Supplementary Table 7A and B). In contrast, IL-1R1 and IL-1α did not differ in SD, whereas IL-1β was only increased by 1.2-fold. As previously reported, Placenta Associated 8[29] was increased in SD compared with non-SD SAIDs and HC by 1.75- and 2.46-fold, respectively. These RNA data suggest that blood monocytes may not be the source of plasma HO-1 and IL-18 in patients with SD.

MicroRNA transcriptome in SD

Because microRNAs (miRNAs) regulate gene expression but also respond to inflammatory signals, we analyzed the miRNA transcriptome of fluorescence-activated cell sorted peripheral blood monocytes, natural killer (NK) cells, B cells, and dendritic cells (DC). In keeping with the known distinct cell-type specific expression patterns of miRNAs,[30] we find that clustering in t-distributed stochastic neighbor embedding plots was dominated by the cell type (Figure 3D) but not disease type (Figure 3E and data not shown). Differential expression of miRNA between SD and non-SD SAIDs revealed specific miRNA differences (Figure 3F and Supplementary Tables 8–11). NK cells had the most changes in the miRNAome compared with monocytes, B cells, and DC. The most increased miRNAs in SD compared with non-SD SAIDs was miR-146a-5p, an IL-18 responsive miRNA,[31] in NK cells (increased 2.9-fold), followed by miR-151a-5p in monocytes (increased 1.2-fold), miR-92b-3p in B cells (increased 1.9-fold), and miR-1268b in DC (increased 2.6-fold) (Figure 3F and Supplementary Tables 8A–C). Most decreased miRNA were miR181a-2-3p in NK cells (decreased 1.4-fold), miR-365b-5p in

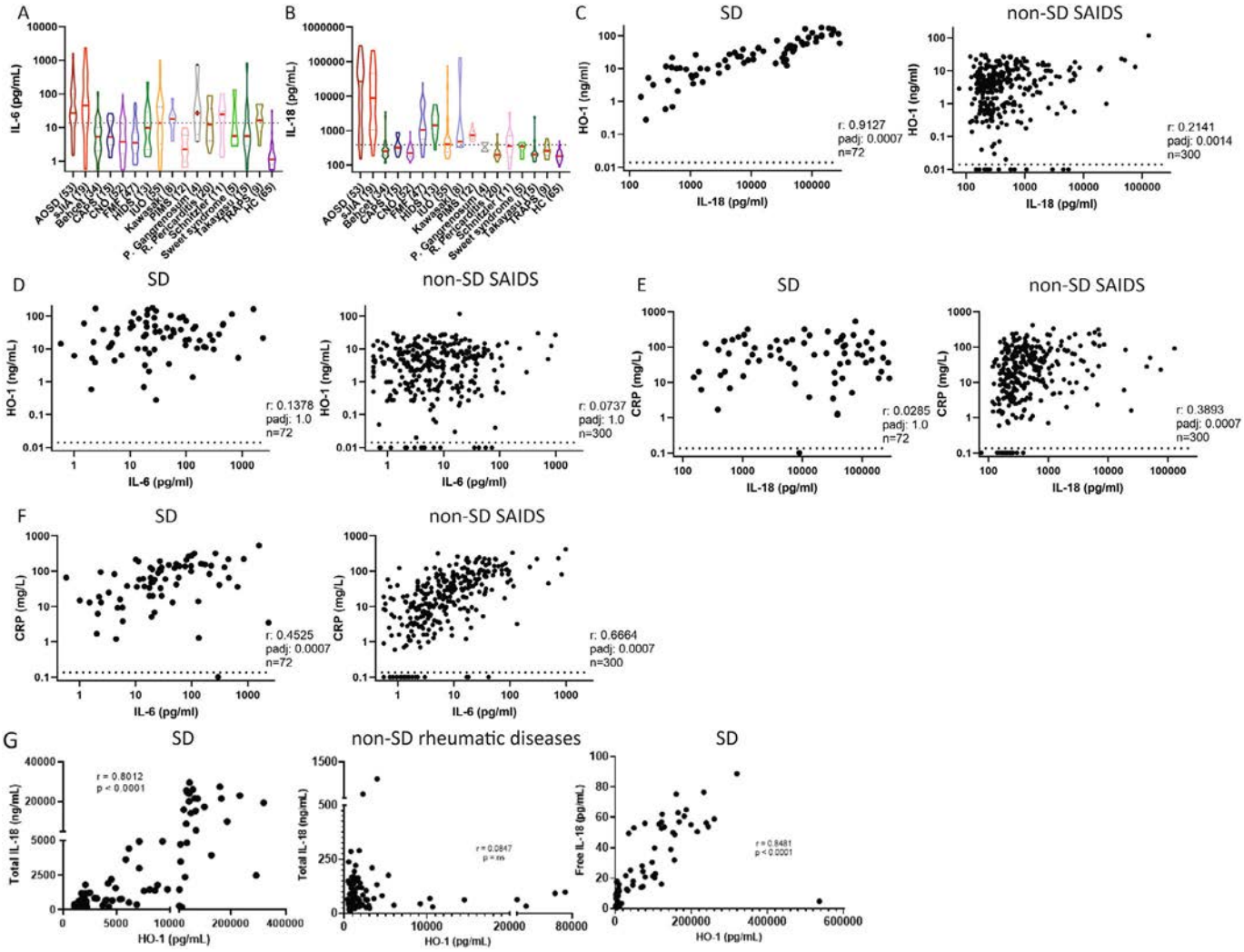

Figure 2. Elevated HO-1 and IL-18 in patients with SD strongly correlate with each other but not with general inflammation. IL-6 (A) and IL-18 (B) levels in patients with SAID and HC; HO-1 correlation with IL-18 (C) and IL-6 (D) in SD and non-SD SAIDs; CRP correlation with IL-18 (E) and IL-6 (F) in SD and non-SD SAIDs; IL-6 and IL-18 statistical differences and % above cutoffs for patient group comparisons are reported in Tables 4 and 5; (G) Geneva cohort: HO-1 (ELISA) correlation with IL-18 in SD (left) and non-SD rheumatic diseases (SLE, RA, AS, and PsA) (middle), and HO-1 (ELISA) correlation with free IL-18 in SD (right). In all figures, IL-18 measurements depict total IL-18 unless otherwise indicated. Correlations coefficients in panels (C)–(G) were calculated using a Spearman's rank correlation test with a Bonferroni correction for multiple comparison. AOSD, adult-onset Still disease; AS, ankylosing spondylitis; CAPS, cryopyrin-associated periodic syndrome; CNO, chronic non-bacterial osteomyelitis; CRP, C-reactive protein; ELISA, enzyme-linked immunosorbent assay; FMF, Familial Mediterranean fever; HC, healthy control; HIDS, hyperimmunoglobulin D syndrome; IL, interleukin; HO-1, heme oxygenase 1; IUO, inflammation of unknown origin; PIMS, pediatric inflammatory multisystem syndrome; PsA, psoriatic arthritis; RA, rheumatoid arthritis; SAID, systemic autoinflammatory disease; SD, Still disease; sJIA, systemic juvenile idiopathic arthritis; SLE, systemic lupus erythematosus; TRAPS, TNF receptor associated periodic syndrome.

monocytes (decreased 1.2-fold), and miR-223-3p in B cells (decreased 1.3-fold) (Figure 3F and Supplementary Tables 8–11). No miRNA was significantly decreased in DC. These findings demonstrate that SD exhibits distinct miRNA changes in specific immune populations.

Ferroptosis and Type I IFN signaling in SD

To identify discreet pathophysiologic mechanisms in SD, we performed pathway analysis on our proteomics (Figure 3G) and monocyte RNA-Seq data (Figure 3H, Supplementary Figure 2A and B, Supplementary Table 7A). Pathway analysis of differentially abundant plasma proteins between SD and non-SD SAIDs identified ferroptosis as the pathway with the highest normalized enrichment (NES) score (Figure 3G). In SD, 43 plasma proteins were increased whereas only one was less abundant compared with non-SD SAIDs (Figure 3G). Interferon αβ (IFNαβ) signaling was the top up-regulated pathway (as determined by NES) in differentially expressed genes (DEGs) in SD monocytes compared with non-SD SAIDs (Figure 3H). Other top pathways in SD were

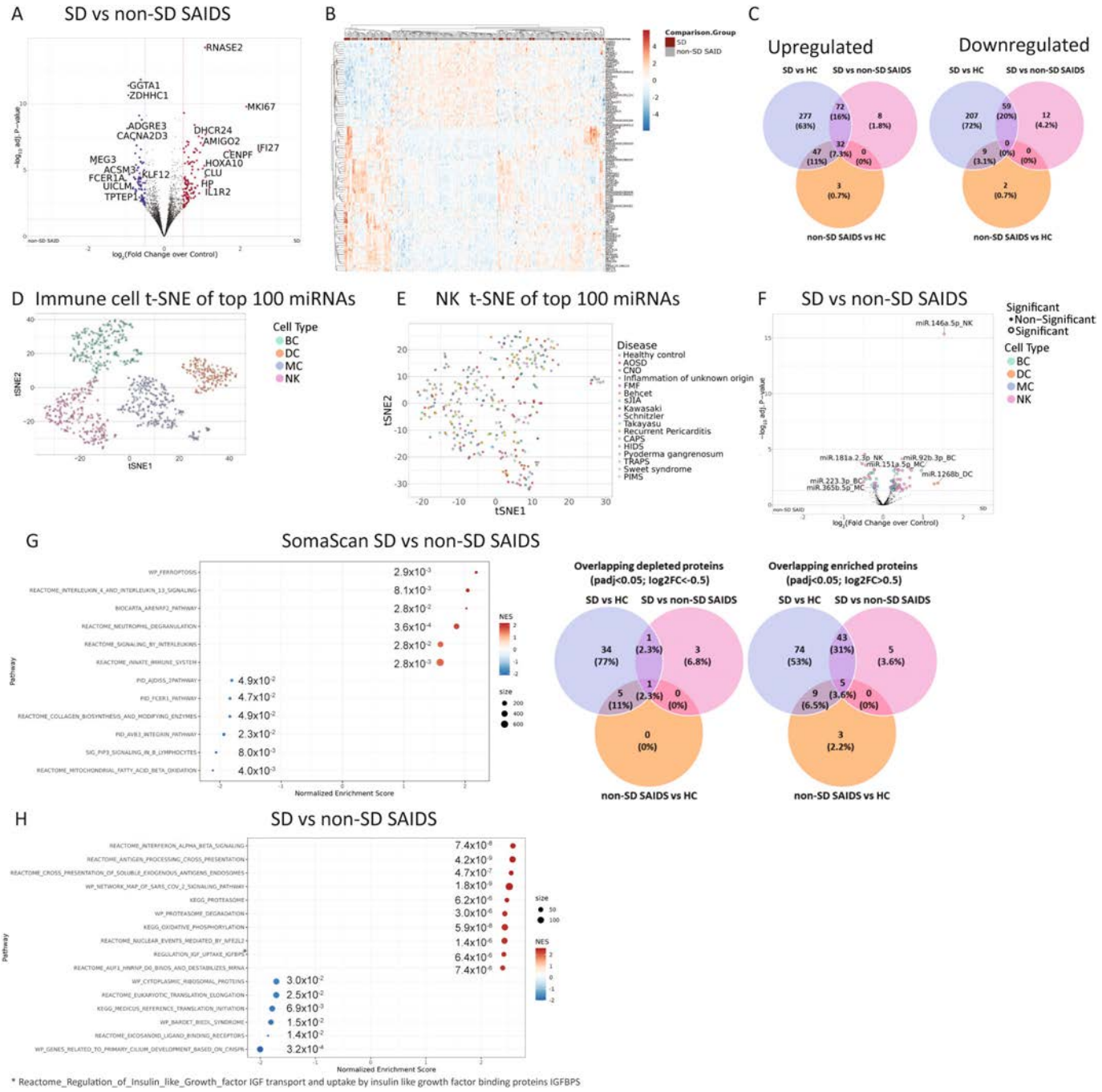

Figure 3. Patients with SD have distinct RNA and miRNA transcriptomes and exhibit activated type I IFN signaling and ferroptosis. (A) Volcano plot showing DEGs in SD compared with non-SD. Patients with SAID (red: increased; blue: reduced expression in SD); (B) Heat map of top 100 DEGs in monocytes, SD versus non-SD SAID comparison; (C) Venn diagram showing numbers of up-regulated (left) and down-regulated (right) genes; pairwise comparisons SD, non-SD SAID, and HC. Number of genes and % DEGs shown. (A), (B), and (C): Padj <0.05, CPM > 1, Log2Fold change < –0.5 or >0.5. (D) t-SNE plots of miRNA expression (n = 1,140) for monocytes, NK cells, B cells, and DC. (E) NK cell miRNA t-SNE plot for individual diseases (n = 311 miRNA); (F) Volcano plot of differentially expressed miRNA in monocytes, NK cells, B cells, and DC comparing patients with SD and non-SD with SAID; (G) pathway analysis of differentially expressed plasma proteins (left) and Venn diagrams (right) showing numbers of depleted and enriched plasma proteins; pairwise comparisons SD, non-SD SAID, and HC. Number of proteins and % differentially abundant proteins shown. (H) Pathway analysis of genes differentially expressed in monocytes between patients with SD and non-SD with SAID. Top pathways most enriched in SD (red) and top pathways most enriched in non-SD SAIDs (blue) shown. Individual pathways with normalized enrichment score (NES) and adjusted *P* values depicted. Size indicates number of genes in pathway. AOSD, adult-onset Still disease; CAPS, cryopyrin-associated periodic syndrome; CNO, chronic non-bacterial osteomyelitis; CPM, counts per million; DC, dendritic cell; DEGs, differentially expressed genes; FMF, Familial Mediterranean fever; HC, healthy control; HIDS, hyperimmunoglobulin D syndrome; IFN, interferon; miRNA, microRNA; NES, normalized enrichment score; NK, natural killer; Padj, adjusted P value; PIMS, pediatric inflammatory multisystem syndrome; SAID, systemic autoinflammatory disease; SD, Still disease; sJIA, systemic juvenile idiopathic arthritis; TRAPS, TNF receptor associated periodic syndrome; t-SNE, t-distributed stochastic neighbor embedding.

antigen-processing and cross presentation as well as SARS-CoV-2 signaling (Figure 3H), both of which are responsive to type I IFN. Several IFN inducible genes, including *IFI27* (5.7-fold) and *SIGLEC-1* (1.73-fold) were up-regulated in SD compared with non-SD SAIDs (Supplementary Table 7A). IFNαβ signaling was the fourth most up-regulated pathway in SD when compared with HC, with inflammatory cytokine pathways also up-regulated, as expected (Supplementary Figure 2A). IFNαβ signaling was not up-regulated in non-SD SAIDs compared with HC (Supplementary Figure 2B), suggesting that type I IFN signaling is specific for SD and not a general feature of SAIDs.

The pathway nuclear events associated with nuclear factor erythroid-derived 2-like 2 Nrf2 (*NFE2L2*), a pathway that regulates HO-1 production,[32] was up-regulated in SD (Figure 3H). Despite the pathway being activated, *NFE2L2* and *HMOX1* were not up-regulated (Supplementary Table 7A).

Hemophagocytosis induces HO-1 in macrophages and synergizes with type I IFN to induce inflammation

The remarkable association between HO-1 and IL-18 in SD led us to investigate whether IL-18 induces HO-1. Red blood cells (RBC) and heme are known inducers of HO-1 in macrophages,[33] and we find that RBC potently induced HO-1 protein and mRNA in monocyte-derived macrophages (Figure 4A). HO-1 protein was detectable in cell lysates but not supernatants. Despite IL-18's strong correlation with HO-1, IL-18 alone or in combination with IL-12 or IFNγ failed to augment HO-1 production by RBC in macrophages (data not shown).

Because the type I IFN pathway was enriched in SD, we examined whether IFNβ affected HO-1 or IL-18 production. IFNβ in vitro inhibited HO-1 production when added to RBC treated macrophages (Figure 4B) but did not induce IL-18 (data not shown). IFNβ greatly augmented both protein and mRNA IL-6 production in RBC exposed macrophages (Figure 4C). IFNβ does not induce HO-1 in mice, but HO-1 is required for toll-like receptor (TLR) 3 and 4 induced IFNβ production.[34,35] Therefore, we examined RBC treatment alone or in combination with IL-12 or IL-18 but found no induction of IFNβ in macrophages (data not shown).

We tested whether hemophagocytosis can induce IL-18 as it did for HO-1 because this could explain their strong correlation in plasma. However, IL-18 protein and mRNA were not induced by RBC in monocytes or macrophages (data not shown). We next examined patients with SD (n = 3) treated with Tadekinig alfa (r-hIL-18BP, an IL-18 inhibitor) and despite the rapid decline of plasma free IL-18, HO-1 decreased with delayed kinetics (Figure 4D) but only in patients responding to Tadekinig alfa. A patient with no clinical response showed no effect of Tadekinig alfa on HO-1.

These results indicate that IL-18 and HO-1 do not directly regulate each other, but the delayed kinetics of HO-1 decrease after r-hIL-18BP treatment suggests IL-18 indirectly affects plasma HO-1 levels. Type I IFN, on the other hand, synergizes with hemophagocytosis to potently induce IL-6 and contribute to inflammation in SD.

Biomarkers for SD diagnosis

To identify biomarkers that distinguish SD from non-SD SAIDs, we generated receiver operating characteristic (ROC) curves for SD elevated markers. IL-18, HO-1, and ferritin ROC curves (area under the curve [AUC]: 0.881, 0.851, and 0.841, respectively) outperformed IL-6 (AUC: 0.745) and CRP (AUC: 0.674) in distinguishing SD from non-SD SAIDs (Figure 5A). Combinations of these analytes did not improve further the ROC curves (data not shown). In a separate cohort (Geneva cohort), HO-1 distinguished SD from other rheumatic diseases (AUC: 0.826) (Figure 5B). Plasma HO-1 and IL-18 were significantly elevated in SD compared with acute lymphoblastic leukemia (ALL) and acute COVID-19 infection, which are both conditions that may require differential diagnosis from SD (Figure 5C). HO-1 and IL-18 levels decreased after treatment of patients with SAID (Supplementary Figure 2C).

Given the type I IFN pathway enrichment in SD (Figure 3H), we investigated whether IFN signatures in blood monocyte RNA could serve as a biomarker. We tested two IFN signatures, a 6-gene score (*ISG15*, *RSAD2*, *IFIT1*, *IFI27*, *IFI44L*, and *SIGLEC1*, called IFN6) associated with type I interferon-mediated autoinflammation,[36,37] and a 3-gene IFN score (IFN3) that we devised based on genes *SIGLEC1*, *CD163*, and *IL1R2* that are induced by type I IFN but inhibited by IFNγ.[38–42] IFN6 and IFN3 scores were up-regulated in SD compared with non-SD SAIDs (Figure 5D), but only the IFN6 and not the IFN3 score correlated with plasma IFNγ (r = 0.71 and r = 0.19, respectively) (Figure 5E), suggesting IFN3 score is not dependent on IFNγ and its inducer IL-18. The IFN3 score ROC curves outperformed the IFN6 score (AUC: 0.740 and 0.545, respectively) (Figure 5F) in predicting SD. Overall, our analysis suggests that HO-1, IL-18, and ferritin are better biomarkers of SD compared with IL-6 and CRP, whereas a 3-gene type I IFN-specific score outperformed a routinely used 6-gene IFN score.

Patient stratification by data integration

Finally, we took an unbiased approach to discover clusters of features that associate with SD. For this we integrated by weighted gene co-expression network analysis (WGCNA) our large data sets to identify modules that distinguish SD from non-SD SAIDs but to also stratify patients with SD into distinct groups (Figure 6A). The feature module that was most associated with SD was Yellowgreen (R = 0.59, $P = 2e^{-43}$), while also having a clear negative association with non-SD SAIDs (R = −0.29, $P = 5e^{-10}$) (Figure 6A). This association was more prominent in

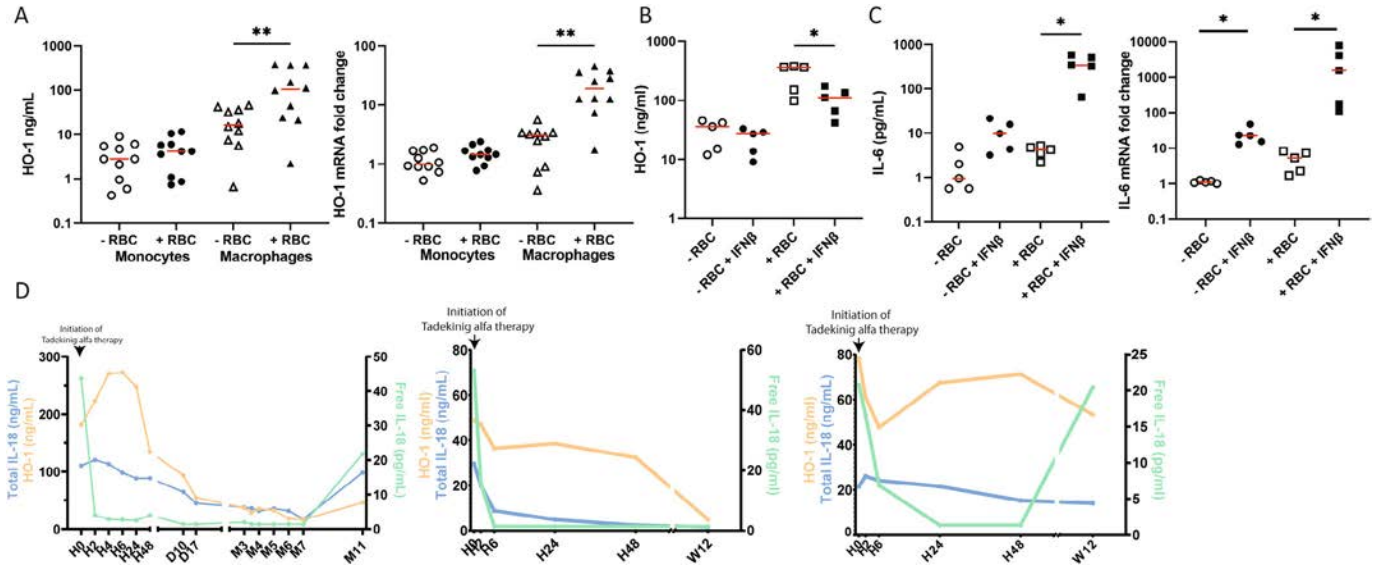

Figure 4. IFNβ synergizes with RBC to induce IL-6 but inhibits HO-1 in macrophages. (A) HO-1 protein and mRNA levels induced by RBC in monocytes and macrophages; (B) HO-1 protein induction by RBC in macrophages is inhibited by IFNβ; (C) IL-6 protein and mRNA are potently induced in macrophages exposed to IFNβ and RBC. Each symbol is an individual healthy donor (n = 5–10). (D) Kinetics of HO-1, total IL-18, and free IL-18 in Tadekinig alpha treated patients with SD. Clinical responders (left and middle) and a nonresponder (right) shown. On *x*-axis: H = hours, D = days, W = weeks. Statistical analysis was performed using Wilcoxon matched-pairs signed rank test (A), Paired *t*-test (B) and Friedman test with Dunn's multiple comparisons test (C). DC, dendritic cell; HC, healthy control; HO-1, heme oxygenase 1; IFNβ, interferon-β; IL, interleukin; mRNA, messenger RNA; NK, natural killer; RBC, red blood cells; SD, Still disease.

patients with AOSD than with sJIA (Figure 6A). These modules comprised the following features: IL-18; HO-1; ferritin; IL-10 from ELISA; CYP27A1 and RTN1 from monocyte RNA-Seq; miR-146a-5p, let-7i-5p, miR-21-5p, miR-1843, miR-7-5p and miR-95-3p in NK cells; miR1271-5p, miR-200b-3p and miR-128-3p in B cells; miR-3650 in DC miRNA; and 80 additional plasma proteins from proteomics (Figure 6B). This module within SD revealed two distinct signatures indicating two SD subgroups (Figure 6C). These signatures did not correlate with disease activity, as measured either by the Auto-Inflammatory Diseases Activity Index (AIDAI)—a general, non-SD-specific activity score—or by plasma CRP levels, an indicator of systemic inflammation (Figure 6D). These signatures also associated with hemophagocytic syndrome (HLH or MAS) as indicated by the HScore[43] (Figure 6D). These two signatures that have arisen from a wealth of data may indicate SD disease subtypes with different pathophysiologies and treatment responses.

DISCUSSION

The ImmunAID consortium has amassed an unprecedented set of data for SAIDs, and in this report we queried for SD-specific biomarkers but also possible pathophysiologic pathways that distinguish SD from other SAIDs that often share overlapping clinical and laboratory features. We find that HO-1, IL-18, and ferritin outperformed IL-6 and CRP in distinguishing SD and confirmed this in a second cohort. Currently, CRP and ferritin, although not specific for SD, are commonly used for diagnosing sJIA and AOSD[15] and are predictive of MAS development.[7,24] Recently, recommendations for SD diagnosis included, in addition to ferritin, S100 proteins and IL-18.[9] Previously, plasma HO-1 was suggested to be increased in SD, but low patient numbers and the lack of other SAIDs made it unclear how specific HO-1 is for SD.[22,23] We show that HO-1 is clearly higher in patients with SD compared with other SAIDs and does not correlate with general inflammation as indicated by CRP levels. In contrast, ferritin correlated in SD and non-SD SAIDs with CRP, suggesting that inflammatory cytokines[26] contribute to ferritin's elevation in SAIDs. Elevated HO-1 in SD may indicate a continuum from mild SD disease to MAS where hyperferritinemia and hemophagocytosis are very high. In our cohort, some patients with SD had very high levels of HO-1, and it would be important to investigate if this associates with MAS development.

Although proinflammatory cytokines and CRP did not distinguish SD from other SAIDs, IL-18 was highly increased and predicted SD. SD is associated with extremely elevated levels of IL-18 and hyperferritinemia,[15,16] high IL-18 levels associate with MAS,[17,18] and IL-18 serves as an indicator for disease activity in sJIA[44] and to diagnose remission.[19] IL-18 has therefore been proposed as a good biomarker for SD, especially for those patients at risk to develop MAS.[20] The challenge, however, remains in distinguishing SD from other autoinflammatory diseases, viral infection, or hematologic malignancies that need to be excluded during differential diagnosis. We report here that IL-

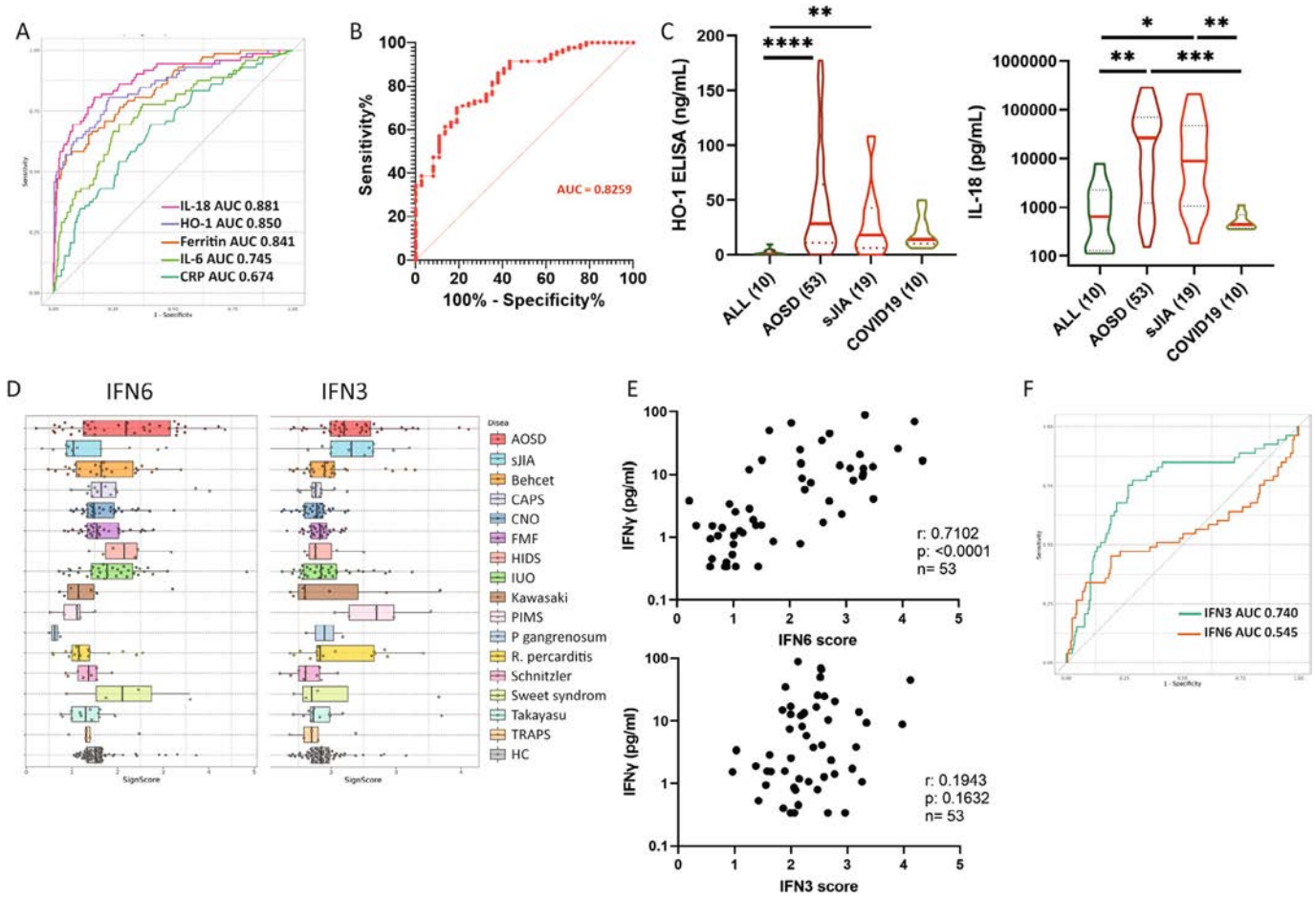

Figure 5. IL-18 and HO-1 are predictors of SD and a type I IFN-specific IFN3 outperforms an IFNγ-related IFN6 score. (A) ROC curves for HO-1, IL-18, ferritin, IL-6, and CRP for SD classification within all patients with SAID. (B) Geneva cohort ROC curves for HO-1 SD classification from autoimmune patients. (C) HO-1 levels and IL-18 levels in ALL, AOSD, sJIA, and acute COVID-19 infection. (D) IFN6 score (ISG15, RSAD2, IFIT1, IFI27, IFI44L, and SIGLEC1) and IFN3 score (SIGLEC1, CD163, and IL1R2) in PB monocytes of patients with SAID. (E) IFN6 and IFN3 score correlation with plasma IFNγ in patients with SD. (F) IFN3 score outperforms IFN6 in ROC curves for SD classification within all patients with SAID. Statistical analysis was performed using Kruskal-Wallis test with Dunn's multiple comparisons test (C), and a Spearman's rank correlation test (E). ALL, acute lymphoblastic leukemia; AOSD, adult-onset Still disease; AUC, area under the curve; CAPS, cryopyrin-associated periodic syndrome; CNO, chronic non-bacterial osteomyelitis; CRP, C-reactive protein; DC, dendritic cell; ELISA, enzyme linked immunosorbent assay; FMF, Familial Mediterranean fever; HIDS, hyperimmunoglobulin D syndrome; HO-1, heme oxygenase 1; IFN, interferon; IL, interleukin; IUO, inflammation of unknown origin; PB, peripheral blood; PIMS, pediatric inflammatory multisystem syndrome; RA, rheumatoid arthritis; ROC, receiver operating characteristic; SAID, systemic autoinflammatory disease; SD, Still disease; sJIA, systemic juvenile idiopathic arthritis; TRAPS, TNF receptor associated periodic syndrome.

18 together with HO-1 are both elevated in SD compared with leukemia (ALL) and an acute viral infection (COVID-19 infection). Larger cohorts, however, are needed to confirm the utility of IL-18 and HO-1 in the differential diagnosis of SD from leukemias and acute viral infections.

Our findings from RNA-Seq of blood monocytes in SD are comparable to previous studies. The top pathways identified by Huang et al[45] when comparing MAS with HC or MAS with SD were IFNγ and type I IFN. Although we did not include patients with MAS in our cohort, both of these pathways were the top pathways in our patients with SD. Schulert et al[46] compared monocytes of high and low ferritin patients with sJIA. Their top 20 DEGs were also DEGs in our data when we compared SD with controls. Our analysis suggests potential pathophysiologic pathways active in SD that differ from most other patients with SAIDs. Based on our RNA data, a pattern emerges of type I IFN signaling but also of heme inducing Nrf2 signaling[32] and hemoglobin capture and signaling pathways that discriminate between SD and non-SD SAIDs. Previous work comparing patients with sJIA with systemic lupus erythematosus and HC found IL-1 but not type I IFN signatures in peripheral blood mononuclear cell,[47] whereas a small study reported IFN type I and II signatures in blood monocytes only in patients with SD with MAS.[45] Our data, comparing 72 patients with SD with 300 non-SD SAIDs and 65 HC, find a clear type I IFN signature in SD blood monocytes, and this is further confirmed by the IFN3 score, a type I IFN-specific score we

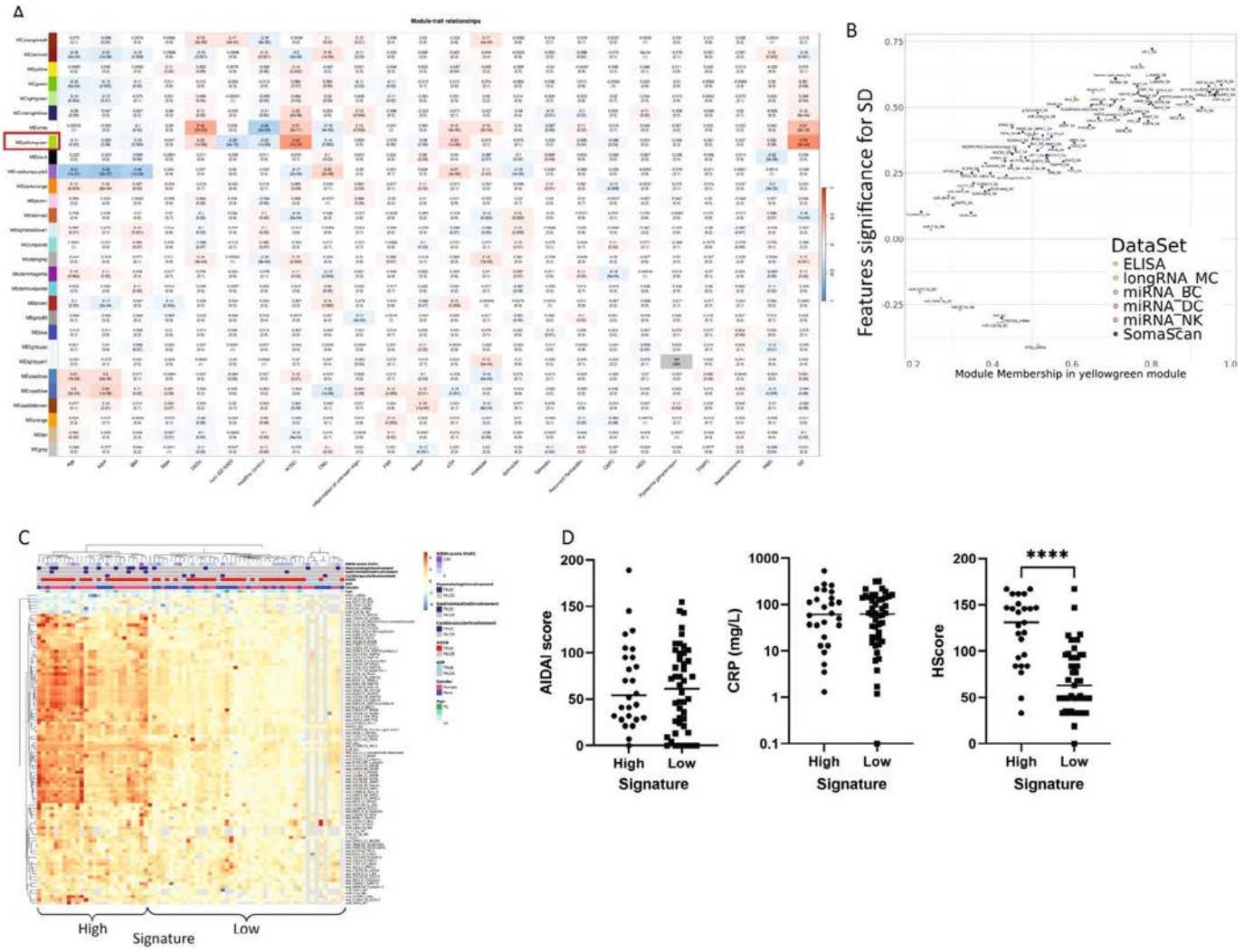

Figure 6. Unbiased feature clustering reveals feature modules that associate with SD and two distinct SD patient signatures. (A) WGCNA analysis of all data (clinical data, serum measurements, proteomics, miRNA transcriptome, and RNA transcriptome) identified modules of features that associate with SD. Module-trait relationships shown. *y*-axis: individual ME vectors color coded. *x*-axis: Traits (age, adult, BMI, male, and individual SAIDs. Still includes both AOSD and sJIA). MEyellowgreen module (in red box) associates with SD. Filled red and blue boxes indicate positive and negative associations. Correlation coefficient and *P* value are shown in boxes. (B) Features (n = 96) included in MEyellowgreen module shown. *y*-axis: feature significance for SD and *x*-axis: MEyellowgreen module membership correlation coefficient for individual features. (C) Heatmap of 96 features of MEyellowgreen module shown for patients with SD. Right label: individual features. Top bars: clinical traits and patients with AOSD or sJIA. Bottom label: patients with SD with high and low signature based of MEyellowgreen module. (D) AIDAI clinical scores (left), plasma CRP (center), and HScore (right) for high and low signature patients with SD shown. Statistical analysis was performed using Kruskal-Wallis test with Dunn's multiple comparisons test (D). AIDAI, Autoinflammatory Disease Activity Index; AOSD, adult-onset Still disease; BMI, body mass index; CRP, C-reactive protein; DC, dendritic cell; HScore, hemophagocytic syndrome score; IL, interleukin; ME, module eigengene; SAID, systemic autoinflammatory disease; SD, Still disease; sJIA, systemic juvenile idiopathic arthritis; WGCNA, weighted gene co-expression network analysis.

propose that comprises genes *SIGLEC1*, *CD163*, and *IL1R2*, which are all induced by IFNα/β but negatively impacted by IFNγ.[38–40,42] The high levels of IL-18, a potent inducer of IFNγ, in patients with SD complicates the interpretation of IFN signatures, but the role and origin of type I IFN signaling and the possible distinct role from IFNγ in SD merits further investigation. In mice, CpG-induced MAS is completely TLR9 dependent,[48] but IFNγ does not mediate hemophagocytosis and hyperferritinemia,[48,49] and in our data, IFNγ does not affect in vitro HO-1 production. In addition, inflammatory hemophagocytes are induced by TLR7 and TLR9 signaling but not IFNγ.[50] In contrast, in the mouse MAS model, disruption of type I IFN signaling abrogates anemia and hemophagocytosis,[49] indicating that type I and II IFN contribute distinctly to pathophysiology. Because HO-1 is not secreted, elevated HO-1 in plasma in SD could indicate ferroptosis, also suggested by our proteomics pathway analysis. Therefore, it is possible that the IFN I and II may contribute distinctly to splenic macrophage death, something mouse models could address.

The importance of IL-18 in patients with SD is highlighted by their successful treatment with r-hIL-18BP.[51] The question arises of what is the link among IL-18, HO-1, and type I IFN? The remarkable correlation, we find, between plasma IL-18 and HO-1, and the observation that r-hIL-18BP treatment associates, albeit with delayed kinetics, with a reduction of plasma HO-1 levels in SD, suggest that IL-18 acts indirectly to increase hemophagocytosis, HO-1 protein induction, or ferroptosis and HO-1 release into the blood. This mediator could be IFNγ, however, because in vitro IL-18 and IFNγ did not affect RBC-induced HO-1 by macrophages, and IFNγ does not promote hemophagocytosis in the CpG MAS model,[48,49] this favors the hypothesis that IL-18 and downstream IFNγ promote the release of HO-1 possibly via macrophage death. Plasma proteomics suggested ferroptosis as the most active pathway in SD, showed that HO-1 itself accelerates ferroptosis,[52] and demonstrated that the ferroptosis-associated zrt-/irt-like protein 8 (encoded by SLC39A8)[53] was increased in SD (1.92- and 2.78-fold increases compared with non-SD SAIDs and HC, respectively). Such ferroptosis could further contribute to the inflammation of SD by releasing DAMPs and alarmins.[54]

The origin of high IL-18 in SD is unknown, but type I IFN may contribute. Although not effective on its own, type I IFN can prime monocytes to produce IL-18 via TLR activation, and in CpG-induced MAS in mice, a JAK1/2 inhibitor reduces IL-18 production.[55,56] In bacterial and viral infections of mice, type I IFN is required for absent in melanoma 2 inflammasome complex activation, which induces, in an IRF3-dependent manner, IL-18.[57,58] HO-1, on the other hand, is produced by monocytes in response to various stresses and cytokines[59] and inhibits pro-inflammatory responses, in part, by inducing IL-10.[60] HO-1, however, can also regulate IFNβ production and ameliorates autoimmune animal models.[34] HO-1-deficient macrophages exhibit reduced IFNβ production, which is due to HO-1 being required for IRF3 activation after TLR3/TLR4 stimulation or viral infection.[34] Thus, HO-1 overproduction in SD could also contribute to excessive type I IFN signaling, which in turn drives IL-18 production. As mentioned, in the CpG-induced MAS mouse model, type I IFN signaling, but not IFNγ, contributes to hemophagocytosis, anemia, and hyperferritinemia.[48,49] This would suggest that in SD, type I IFNs may contribute to HO-1 production via hemophagocytosis and IL-18 production. Conversely, HO-1 can facilitate type I IFN production and thus a fast forward loop is set up that amplifies type I IFN and IL-18 production via hemophagocytosis by red-pulp macrophages in the spleen. We also found, unexpectedly, that type I IFN synergizes with hemophagocytosis to potently induce IL-6 and inflammation. Thus, type I IFN in SD could be a common driver of both general inflammation, IL-18, and hemophagocytosis, and could therefore be a potential therapeutic upstream target. It should be stressed, however, that despite the increases of IL-18 and HO-1 in plasma, the tissue of origin for these in SD remains to be established. Although mRNA for IL-18 was not increased in the blood monocytes of SD, these cells could still be the source of IL-18 because its production is primarily regulated at the protein level and cleavage by caspase-1, –4 or –5.[61] IL-18 is known to be produced by Kupffer cells and liver-resident macrophages but also barrier epithelia cells.[8] HO-1 mRNA was not increased in SD blood monocytes, making them an unlikely source. High levels of HO-1 can be produced by erythrophagocytic macrophages, such as splenic red-pulp macrophages and liver Kupffer cells and monocyte-derived macrophages.[60] During inflammation, HO-1 can be also produced by intestinal epithelial cells and endothelial cells.[60] Identifying the source of IL-18 and HO-1 in SD therefore may provide insight into the pathophysiology of the disease.

Finally, the stratification of patients with SD may lead to better tailored therapies[62] because therapies blocking IL-1, IL-6, or IL-18 may be affected by patient heterogeneity.[63] IL-18:IL-6 ratios have been used to classify patients with SD as MAS or arthritis dominated.[64] However, in our study, IL-18:IL-6 ratios did not identify separate patient subgroups, and we believe this was because we did not include patients with MAS/HLH in our cohort (data not shown). Using WGCNA analysis of our extensive data sets, we could identify two subtypes of SD that did not associate with disease activity or general inflammation, as indicated by disease activity score and CRP levels, but associated instead with hemophagocytosis. These signatures may predict progression to MAS or response to therapy.

In conclusion, the ImmunAID consortium has amassed an unprecedented data set from one of the largest cohorts of patients with SAIDs ever assembled, and we report here distinct features that distinguish SD from other patients with SAIDs. We further report that integrated and unbiased analysis of these data sets can help stratify patients with SD into two distinct groups that do not associate with disease activity or general inflammation but with the levels of hemophagocytic activity. Our findings on SD advance our understanding of this complex autoinflammatory disease and indicate that IL-18, hemophagocytosis, ferroptosis, and type I IFN signaling are involved in SD disease. Finally, with this report, we provide an invaluable and deep omic resource for the study of SD and other SAIDs that are included in the ImmunAID cohort.

ACKNOWLEDGMENTS

We would like to thank Vincent van der Velden (Erasmus MC) and Bart Rijnders (Erasmus MC) for providing plasma from patients with ALL and SARS-CoV-2, respectively. The graphical abstract was created in BioRender https://BioRender.com/qqjit0a.

AUTHOR CONTRIBUTIONS

All authors contributed to at least one of the following manuscript preparation roles: conceptualization AND/OR methodology, software, investigation, formal analysis, data curation, visualization, and validation AND drafting or reviewing/editing the final draft. As corresponding

author, Dr Katsikis confirms that all authors have provided the final approval of the version to be published and takes responsibility for the affirmations regarding article submission (eg, not under consideration by another journal), the integrity of the data presented, and the statements regarding compliance with institutional review board/Declaration of Helsinki requirements.

REFERENCES

1. Ruscitti P, Cantarini L, Nigrovic PA, et al. Recent advances and evolving concepts in Still's disease. Nat Rev Rheumatol 2024;20(2):116–132. doi:https://doi.org/10.1038/s41584-023-01065-6
2. Ciccarelli F, De Martinis M, Ginaldi L. An update on autoinflammatory diseases. Curr Med Chem 2014;21(3):261–269. doi:https://doi.org/10.2174/09298673113206660303
3. Cimaz R. Systemic-onset juvenile idiopathic arthritis. Autoimmun Rev 2016;15(9):931–934. doi:https://doi.org/10.1016/j.autrev.2016.07.004
4. Feist E, Mitrovic S, Fautrel B. Mechanisms, biomarkers and targets for adult-onset Still's disease. Nat Rev Rheumatol 2018;14(10):603–618. doi:https://doi.org/10.1038/s41584-018-0081-x
5. Krainer J, Siebenhandl S, Weinhäusel A. Systemic autoinflammatory diseases. J Autoimmun 2020;109:102421. doi:https://doi.org/10.1016/j.jaut.2020.102421
6. Fautrel B, Mitrovic S, De Matteis A, et al. EULAR/PReS recommendations for the diagnosis and management of Still's disease, comprising systemic juvenile idiopathic arthritis and adult-onset Still's disease. Ann Rheum Dis 2024;83(12):1614–1627. doi:https://doi.org/10.1136/ard-2024-225851
7. Di Benedetto P, Cipriani P, Iacono D, et al. Ferritin and C-reactive protein are predictive biomarkers of mortality and macrophage activation syndrome in adult onset Still's disease. Analysis of the multicentre Gruppo Italiano di Ricerca in Reumatologia Clinica e Sperimentale (GIRRCS) cohort. PLoS One 2020;15(7):e0235326. doi:https://doi.org/10.1371/journal.pone.0235326
8. Landy E, Carol H, Ring A, et al. Biological and clinical roles of IL-18 in inflammatory diseases. Nat Rev Rheumatol 2024;20(1):33–47. doi:https://doi.org/10.1038/s41584-023-01053-w
9. De Matteis A, Bindoli S, De Benedetti F, et al. Systemic juvenile idiopathic arthritis and adult-onset Still's disease are the same disease: evidence from systematic reviews and meta-analyses informing the 2023 EULAR/PReS recommendations for the diagnosis and management of Still's disease. Ann Rheum Dis 2024;83(12):1748–1761. doi:https://doi.org/10.1136/ard-2024-225853
10. Rau M, Schiller M, Krienke S, et al. Clinical manifestations but not cytokine profiles differentiate adult-onset Still's disease and sepsis. J Rheumatol 2010;37(11):2369–2376. doi:https://doi.org/10.3899/jrheum.100247
11. Park C, Miranda-Garcia M, Berendes R, et al. MRP8/14 serum levels as diagnostic markers for systemic juvenile idiopathic arthritis in children with prolonged fever. Rheumatology (Oxford) 2022;61(7):3082–3092. doi:https://doi.org/10.1093/rheumatology/keab729
12. Gohar F, Kessel C, Lavric M, et al. Review of biomarkers in systemic juvenile idiopathic arthritis: helpful tools or just playing tricks? Arthritis Res Ther 2016;18(1):163. doi:https://doi.org/10.1186/s13075-016-1069-z
13. Priori R, Colafrancesco S, Alessandri C, et al. Interleukin 18: a biomarker for differential diagnosis between adult-onset Still's disease and sepsis. J Rheumatol 2014;41(6):1118–1123. doi:https://doi.org/10.3899/jrheum.130575
14. Koga T, Sumiyoshi R, Furukawa K, et al. Interleukin-18 and fibroblast growth factor 2 in combination is a useful diagnostic biomarker to distinguish adult-onset Still's disease from sepsis. Arthritis Res Ther 2020;22(1):108. doi:https://doi.org/10.1186/s13075-020-02200-4
15. Mitrovic S, Fautrel B. New markers for adult-onset Still's disease. Joint Bone Spine 2018;85(3):285–293. doi:https://doi.org/10.1016/j.jbspin.2017.05.011
16. Girard-Guyonvarc'h C, Rodriguez E, Mueller YM, et al; ImmunAID consortium. Elevated serum levels of interleukin-18 discriminate Still's disease from other autoinflammatory conditions: results from the European ImmunAID cohort. RMD Open 2025;11(2):e005388. doi:https://doi.org/10.1136/rmdopen-2024-005388
17. Shimizu M, Nakagishi Y, Inoue N, et al. Interleukin-18 for predicting the development of macrophage activation syndrome in systemic juvenile idiopathic arthritis. Clin Immunol 2015;160(2):277–281. doi:https://doi.org/10.1016/j.clim.2015.06.005
18. Weiss ES, Girard-Guyonvarc'h C, Holzinger D, et al. Interleukin-18 diagnostically distinguishes and pathogenically promotes human and murine macrophage activation syndrome. Blood 2018;131(13):1442–1455. doi:https://doi.org/10.1182/blood-2017-12-820852
19. Shimizu M, Nakagishi Y, Yoshida A, et al. Serum interleukin 18 as a diagnostic remission criterion in systemic juvenile idiopathic arthritis. J Rheumatol 2014;41(11):2328–2330. doi:https://doi.org/10.3899/jrheum.140025
20. Shimizu M, Takei S, Mori M, et al. Pathogenic roles and diagnostic utility of interleukin-18 in autoinflammatory diseases. Front Immunol 2022;13:951535. doi:https://doi.org/10.3389/fimmu.2022.951535
21. Kirino Y, Takeno M, Iwasaki M, et al. Increased serum HO-1 in hemophagocytic syndrome and adult-onset Still's disease: use in the differential diagnosis of hyperferritinemia. Arthritis Res Ther 2005;7(3):R616–R624. doi:https://doi.org/10.1186/ar1721
22. Miyazaki T, Kirino Y, Takeno M, et al. Serum HO-1 is useful to make differential diagnosis of secondary hemophagocytic syndrome from other similar hematological conditions. Int J Hematol 2010;91(2):229–237. doi:https://doi.org/10.1007/s12185-010-0495-y
23. Shimizu M, Yachie A. Compensated inflammation in systemic juvenile idiopathic arthritis: role of alternatively activated macrophages. Cytokine 2012;60(1):226–232. doi:https://doi.org/10.1016/j.cyto.2012.05.003
24. Grom AA, Mellins ED. Macrophage activation syndrome: advances towards understanding pathogenesis. Curr Opin Rheumatol 2010;22(5):561–566. doi:https://doi.org/10.1097/01.bor.0000381996.69261.71
25. Mehta B, Efthimiou P. Ferritin in adult-onset Still's disease: just a useful innocent bystander? Int J Inflamm 2012;2012:298405.
26. Kernan KF, Carcillo JA. Hyperferritinemia and inflammation. Int Immunol 2017;29(9):401–409. doi:https://doi.org/10.1093/intimm/dxx031
27. Kaneko N, Kurata M, Yamamoto T, et al. The role of interleukin-1 in general pathology. Inflamm Regen 2019;39(1):12. doi:https://doi.org/10.1186/s41232-019-0101-5
28. Peters VA, Joesting JJ, Freund GG. IL-1 receptor 2 (IL-1R2) and its role in immune regulation. Brain Behav Immun 2013;32:1–8. doi:https://doi.org/10.1016/j.bbi.2012.11.006
29. Segawa S, Kondo Y, Nakai Y, et al. Placenta specific 8 Suppresses IL-18 production through regulation of autophagy and is associated with adult Still disease. J Immunol 2018;201(12):3534–3545. doi:https://doi.org/10.4049/jimmunol.1800667
30. Bartel DP. MicroRNAs: genomics, biogenesis, mechanism, and function. Cell 2004;116(2):281–297. doi:https://doi.org/10.1016/S0092-8674(04)00045-5
31. Wang H, Zhang Y, Wu X, et al. Regulation of human natural killer cell IFN-γ production by microRNA-146a *via* targeting the NF-κB signaling pathway. Front Immunol 2018;9:293. doi:https://doi.org/10.3389/fimmu.2018.00293

32. Kasai S, Mimura J, Ozaki T, et al. Emerging regulatory role of Nrf2 in iron, heme, and hemoglobin metabolism in physiology and disease. Front Vet Sci 2018;5:242. doi:https://doi.org/10.3389/fvets.2018.00242
33. Alam MZ, Devalaraja S, Haldar M. The heme connection: linking erythrocytes and macrophage biology. Front Immunol 2017;8:33. doi:https://doi.org/10.3389/fimmu.2017.00033
34. Tzima S, Victoratos P, Kranidioti K, et al. Myeloid heme oxygenase-1 regulates innate immunity and autoimmunity by modulating IFN-beta production. J Exp Med 2009;206(5):1167–1179. doi:https://doi.org/10.1084/jem.20081582
35. Camhi SL, Alam J, Wiegand GW, et al. Transcriptional activation of the HO-1 gene by lipopolysaccharide is mediated by 5′ distal enhancers: role of reactive oxygen intermediates and AP-1. Am J Respir Cell Mol Biol 1998;18(2):226–234. doi:https://doi.org/10.1165/ajrcmb.18.2.2910
36. Rodero MP, Tesser A, Bartok E, et al. Type I interferon-mediated autoinflammation due to DNase II deficiency. Nat Commun 2017;8(1):2176. doi:https://doi.org/10.1038/s41467-017-01932-3
37. Zhang X, Bogunovic D, Payelle-Brogard B, et al. Human intracellular ISG15 prevents interferon-α/β over-amplification and auto-inflammation. Nature 2015;517(7532):89–93. doi:https://doi.org/10.1038/nature13801
38. Buechler C, Ritter M, Orsó E, et al. Regulation of scavenger receptor CD163 expression in human monocytes and macrophages by pro- and antiinflammatory stimuli. J Leukoc Biol 2000;67(1):97–103. doi:https://doi.org/10.1002/jlb.67.1.97
39. Mantovani A, Locati M, Vecchi A, et al. Decoy receptors: a strategy to regulate inflammatory cytokines and chemokines. Trends Immunol 2001;22(6):328–336. doi:https://doi.org/10.1016/S1471-4906(01)01941-X
40. Weaver LK, Pioli PA, Wardwell K, et al. Up-regulation of human monocyte CD163 upon activation of cell-surface Toll-like receptors. J Leukoc Biol 2007;81(3):663–671. doi:https://doi.org/10.1189/jlb.0706428
41. Rizzo MD, Crawford RB, Henriquez JE, et al. HIV-infected cannabis users have lower circulating CD16+ monocytes and IFN-γ-inducible protein 10 levels compared with nonusing HIV patients. AIDS 2018;32(4):419–429. doi:https://doi.org/10.1097/QAD.0000000000001704
42. Bourgoin P, Biéchelé G, Ait Belkacem I, et al. Role of the interferons in CD64 and CD169 expressions in whole blood: relevance in the balance between viral- or bacterial-oriented immune responses. Immun Inflamm Dis 2020;8(1):106–123. doi:https://doi.org/10.1002/iid3.289
43. Fardet L, Galicier L, Lambotte O, et al. Development and validation of the HScore, a score for the diagnosis of reactive hemophagocytic syndrome. Arthritis Rheumatol 2014;66(9):2613–2620. doi:https://doi.org/10.1002/art.38690
44. Shimizu M, Yokoyama T, Yamada K, et al. Distinct cytokine profiles of systemic-onset juvenile idiopathic arthritis-associated macrophage activation syndrome with particular emphasis on the role of interleukin-18 in its pathogenesis. Rheumatology (Oxford) 2010;49(9):1645–1653. doi:https://doi.org/10.1093/rheumatology/keq133
45. Huang Z, Brodeur KE, Chen L, et al. Type I interferon signature and cycling lymphocytes in macrophage activation syndrome. J Clin Invest 2023;133(22):e165616. doi:https://doi.org/10.1172/JCI165616
46. Schulert GS, Pickering AV, Do T, et al. Monocyte and bone marrow macrophage transcriptional phenotypes in systemic juvenile idiopathic arthritis reveal TRIM8 as a mediator of IFN-γ hyperresponsiveness and risk for macrophage activation syndrome. Ann Rheum Dis 2021;80(5):617–625. doi:https://doi.org/10.1136/annrheumdis-2020-217470
47. Pascual V, Allantaz F, Patel P, et al. How the study of children with rheumatic diseases identified interferon-alpha and interleukin-1 as novel therapeutic targets. Immunol Rev 2008;223(1):39–59. doi:https://doi.org/10.1111/j.1600-065X.2008.00643.x
48. Behrens EM, Canna SW, Slade K, et al. Repeated TLR9 stimulation results in macrophage activation syndrome-like disease in mice. J Clin Invest 2011;121(6):2264–2277. doi:https://doi.org/10.1172/JCI43157
49. Canna SW, Wrobel J, Chu N, et al. Interferon-γ mediates anemia but is dispensable for fulminant toll-like receptor 9-induced macrophage activation syndrome and hemophagocytosis in mice. Arthritis Rheum 2013;65(7):1764–1775. doi:https://doi.org/10.1002/art.37958
50. Akilesh HM, Buechler MB, Duggan JM, et al. Chronic TLR7 and TLR9 signaling drives anemia via differentiation of specialized hemophagocytes. Science 2019;363(6423):eaao5213. doi:https://doi.org/10.1126/science.aao5213
51. Gabay C, Fautrel B, Rech J, et al. Open-label, multicentre, dose-escalating phase II clinical trial on the safety and efficacy of tadekinig alfa (IL-18BP) in adult-onset Still's disease. Ann Rheum Dis 2018;77(6):840–847. doi:https://doi.org/10.1136/annrheumdis-2017-212608
52. Kwon MY, Park E, Lee SJ, et al. Heme oxygenase-1 accelerates erastin-induced ferroptotic cell death. Oncotarget 2015;6(27):24393–24403. doi:https://doi.org/10.18632/oncotarget.5162
53. Zhang T, Wang S, Hua D, et al. Identification of ZIP8-induced ferroptosis as a major type of cell death in monocytes under sepsis conditions. Redox Biol 2024;69:102985. doi:https://doi.org/10.1016/j.redox.2023.102985
54. Sun Y, Chen P, Zhai B, et al. The emerging role of ferroptosis in inflammation. Biomed Pharmacother 2020;127:110108. doi:https://doi.org/10.1016/j.biopha.2020.110108
55. Verweyen E, Holzinger D, Weinhage T, et al. Synergistic signaling of TLR and IFNα/β facilitates escape of IL-18 expression from endotoxin tolerance. Am J Respir Crit Care Med 2020;201(5):526–539. doi:https://doi.org/10.1164/rccm.201903-0659OC
56. Zhu Q, Kanneganti TD. Cutting edge: distinct regulatory mechanisms control proinflammatory cytokines IL-18 and IL-1β. J Immunol 2017;198(11):4210–4215. doi:https://doi.org/10.4049/jimmunol.1700352
57. Fernandes-Alnemri T, Yu JW, Juliana C, et al. The AIM2 inflammasome is critical for innate immunity to Francisella tularensis. Nat Immunol 2010;11(5):385–393. doi:https://doi.org/10.1038/ni.1859
58. Lee AJ, Chen B, Chew MV, et al. Inflammatory monocytes require type I interferon receptor signaling to activate NK cells via IL-18 during a mucosal viral infection. J Exp Med 2017;214(4):1153–1167. doi:https://doi.org/10.1084/jem.20160880
59. Ryter SW, Alam J, Choi AM. Heme oxygenase-1/carbon monoxide: from basic science to therapeutic applications. Physiol Rev 2006;86(2):583–650. doi:https://doi.org/10.1152/physrev.00011.2005
60. Campbell NK, Fitzgerald HK, Dunne A. Regulation of inflammation by the antioxidant haem oxygenase 1. Nat Rev Immunol 2021;21(7):411–425. doi:https://doi.org/10.1038/s41577-020-00491-x
61. Shi X, Sun Q, Hou Y, et al. Recognition and maturation of IL-18 by caspase-4 noncanonical inflammasome. Nature 2023;624(7991):442–450. doi:https://doi.org/10.1038/s41586-023-06742-w
62. Ruscitti P, Allanore Y, Baldini C, et al. Tailoring the treatment of inflammatory rheumatic diseases by a better stratification and characterization of the clinical patient heterogeneity. Findings from a systematic literature review and experts' consensus. Autoimmun Rev 2024;23(7-8):103581. doi:https://doi.org/10.1016/j.autrev.2024.103581
63. Fautrel B, Patterson J, Bowe C, et al. Systematic review on the use of biologics in adult-onset Still's disease. Semin Arthritis Rheum 2023;58:152139. doi:https://doi.org/10.1016/j.semarthrit.2022.152139
64. Shimizu M, Nakagishi Y, Yachie A. Distinct subsets of patients with systemic juvenile idiopathic arthritis based on their cytokine profiles. Cytokine 2013;61(2):345–348. doi:https://doi.org/10.1016/j.cyto.2012.11.025

APPENDIX A: IMMUNAID CONSORTIUM MEMBERS

The ImmunAID Consortium Members are as follows: Serge Amselem,[1] Jordi Anton,[2] Tadej Avcin,[3] Alexandre Belot,[4] Violeta Bittermann,[2] Anne Boland,[5] Alina Boteanu,[6] Jean-David Bouaziz,[7] Søren Brunak,[8] Sonia Caccia,[9] Luca Cantarini,[10] Sabrina Carpentier,[11] Arturo Hernandez Cervantes,[12] Emna Chabaane,[13] Fanny Coffin,[14] Dominique de Seny,[15] Henri de Soyres,[14] Jean-François Deleuze,[5] Marc Dubourdeau,[16] Perrine Dusser,[17] Emanuele Bizzi,[18] Stefan J Erkeland,[19] Evangelos Andreakos,[20] Bruno Fautrel,[21] Dirk Foell,[22] Dimitrios I. Fotiadis,[23] Cem Gabay,[24] Apolline Gallois,[14] Sara Garcia,[8] Sophie Georgin-Lavialle,[25] Charlotte Girard,[24] Irina Giurgea,[1] Mieke Gouwy,[26] Eric Hachulla,[27] Haner Direskeneli,[28] Gilles Hayem,[29] Thomas Henry,[4] Michael Hofer,[30] Stephanie Humblet-Baron,[31] Philippe Hupé,[14] Antonella Insalaco,[32] Yvan Jamilloux,[33] Isabella Friis Jørgensen,[8] Sonia Karabina,[1] Peter D Katsikis,[19] Andres Jimenez Kaufmann,[8] Christoph Kessel,[22] Isabelle Koné-Paut,[17] Keshia Koutekissa,[25] Karoline Krause,[34] Helen Lachmann,[35] Katerina Laskari,[36] Adrian Liston,[37] Thibault Mahevas,[7] Thierry Martin,[38] Nasima Matsa,[17] Patrick Matthys,[26] Michael F. McDermott,[39] Stephane Mitrovic,[21] Aura Moreno Vega,[11] Yvonne M Mueller,[19] Marco Francesco Natale,[32] Antoine Néel,[40] Maria Papadaki,[20] Costas Papaloukas,[41] Christophe Poulet,[15] Nicolas Poursac,[42] Sebastian Proost,[26] Paul Proost,[26] Pierre Quartier,[43] Jeroen Raes,[26] Julien Roméjon,[21] David Saadoun,[44] Sarhan Yaiche,[45] Léa Savey,[33] Sinisa Savic,[39] Savvas Savvides,[46] Seza Ozen,[47] Paolo Sfriso,[48] Vassili Soumelis,[12] Sigrid Swagemakers,[49] Marie-Elise Truchetet,[42] Umut Kalyoncu,[50] Paul Van Daele,[19,51] Harmen J. G. van de Werken,[19] Peter van der Spek,[49] Rogier van Wijck,[49] Steven Vanderschueren,[52] Clementien Vermont,[53] Matheus Vieira,[44] Carine Wouters[54]

[1]Childhood Genetic Diseases, Hôpital Trousseau, Sorbonne Université, Paris, France; [2]Pediatric Rheumatology, Hospital Sant Joan de Déu, Institut de Recerca Sant Joan de Déu, Universitat de Barcelona, Spain; [3]Department of Allergology, Rheumatology and Clinical Immunology, University Children's Hospital, University Medical Centre Ljubljana, Ljubljana, Slovenia; [4]Centre International de Recherche en Infectiologie (CIRI), Univ Lyon, Lyon, France; [5]Commissariat À L'énergie Atomique Et Aux Énergies Alternatives (CEA), Centre National de Recherche en Génomique Humaine (CNRGH), Université Paris-Saclay, Evry, France; [6]Department of Rheumatology, University Hospital Ramón y Cajal, Madrid, Spain; [7]APHP, Saint Louis Hospital, Paris Cité University, Paris, France; [8]Novo Nordisk Foundation Center for Protein Research, University of Copenhagen, Copenhagen, Denmark; [9]Department of biomedical and clinical sciences, University of Milano, Italy; [10]Rheumatology Unit Department of Medical Sciences, Surgery and Neurosciences, University of Siena, Siena, Italy; [11]OWKIN France, Paris, France; [12]Department of Immunology, Université de Paris, Paris, France; [13]Department Recherche Clinique et Innovation, Hôpital de La Pitié Salpêtrière, Paris, France; [14]Institut Curie, Paris, France; PSL Research University, Paris, France; Mines Paris Tech, Fontainebleau, France; [15]Laboratory of Rheumatology, GIGA-Research, CHU Liège, University of Liège, Liège, Belgium; [16]AMBIOTIS SAS, Toulouse, France; [17]Pediatric rheumatology department and CEREMAIA, Bicêtre hospital APHP, University of Paris Saclay, France; [18]Internal Medicine Ospedale Fatebenefratelli, Milano, Italy; [19]Department of Immunology, Erasmus University Medical Center, Rotterdam, the Netherlands; [20]Laboratory of Immunobiology, Center for Clinical, Experimental Surgery and Translational Research, Biomedical Research Foundation of the Academy of Athens, Athens, Greece; [21]Department of Rheumatology, Pitie Salpetriere University Hospital, Sorbonne Université, UPMC, Paris, France; [22]Department of Pediatric Rheumatology and Immunology, University of Muenster, Muenster, Germany; [23]Unit of Medical Technology and Intelligent Information Systems, Department of Materials Science and Engineering, University of Ioannina, Greece; [24]Department of Internal Medicine, University of Geneva, Geneva, Switzerland; [25]Internal medicine department, Tenon hospital, Sorbonne University, Paris, France; [26]Department of Microbiology, Immunology and Transplantation, Rega Institute for Medical Research, KU Leuven, Leuven, Belgium; [27]Département de Médecine Interne et Immunologie Clinique, University of Lille, Lille, France; [28]Department of Internal Medicine, Division of Rheumatology, Marmara University, School of Medicine, Istanbul, Turkey; [29]Rheumatology Department. Groupe Hospitalier Paris Saint-Joseph, Paris, France; [30]Pediatric immuno-rheumatology, Dept Pediatrics, CHUV, University Hospital of Lausanne, Lausanne, Switzerland; [31]Laboratory of Adaptive Immunology, Department of Microbiology, Immunology and Transplantation, KU Leuven, Leuven, Belgium; [32]Division of Rheumatology, Bambino Gesù Children's Hospital, IRCCS, Roma, Italy; [33]Department of Internal Medicine, Hospices Civils de Lyon, University of Lyon, Lyon, France; [34]Institute of Allergology, Charité - Universitätsmedizin Berlin, Berlin, Germany; [35]National Amyloidosis Centre, Royal Free London NHS Foundation Trust and University College London, London, UK; [36]Rheumatology Unit, 1st Department of Propaedeutic Internal Medicine, University of Athens, Medical School, Athens, Greece; [37]Department of Pathology, University of Cambridge, Cambridge, United Kingdom; [38]Clinical Immunology department, Strasbourg University Hospital, Strasbourg France; [39]Leeds Institute of Rheumatic and Musculoskeletal Medicine, St James's University Hospital, University of Leeds, Leeds, UK; [40]Internal Medicine Department, Nantes Université, Nantes, France; [41]Department of Biological Applications and Technology, University of Ioannina, Greece; [42]Rheumatology Department, Bordeaux University Hospital and Bordeaux University, Bordeaux, France; [43]Paris-Cité University and Pediatric Hematology-Immunology and Rheumatology Department, APHP, Necker University Hospital, Paris, France; [44]Department of Internal Medicine and Clinical Immunology, Pitie Salpetriere University Hospital, Sorbonne Université, UPMC, Paris, France; [45]European Clinical Research Infrastructure Network (ECRIN), Paris, France; [46]VIB Center for Inflammation Research (IRC), Ghent, Belgium; [47]Department of Pediatrics, Division of Rheumatology, Hacettepe University Faculty of Medicine, Ankara, Turkey; [48]Rheumatology Unit, Department of Medicine, University of Padova, Italy; [49]Department of Pathology & Clinical Bioinformatics, Erasmus MC, Rotterdam, The Netherlands; [50]Division of Rheumatology, Department of Internal Medicine, Hacettepe University Faculty of Medicine, Ankara, Turkey; [51]Department of Internal Medicine, Erasmus MC, Rotterdam, The Netherlands; [52]Department of General Internal Medicine, UZ Leuven & Department of Microbiology, Immunology, and Transplantation, KU Leuven, Leuven, Belgium; [53]Department of Pediatric Immunology and Infectious Diseases, Erasmus MC, Rotterdam, The Netherlands; [54]Department of Pediatrics, University Hospitals Leuven, Leuven, Belgium.

Arthritis & Rheumatology
Vol. 78, No. 9, September 2026, pp 1975–1988
DOI 10.1002/art.70126
© 2026 American College of Rheumatology

American College of Rheumatology
Empowering Rheumatology Professionals

Landscape of Somatic Mutations in a Large Cohort of Chinese Patients With Immune Dysregulations

Jinjian Fu, BS,[1,2,3] Qiong Fu, MD,[4,5] Jun Wang, PhD,[2,3] Qintao Wang, PhD,[2,3] Liang Zhang, MD,[6] Huihui Chi, MD,[7] Lei Zhang, MS,[8] Li Sun, MD,[9] Ying Huang, MD,[10] Tingyan He, MD,[11] Yuhao Yao, BS,[1,2,3] Xu Han, PhD,[2,3,12] Shuangyue Ma, BS,[2,3] Chenlu Liu, BS,[1,2,3] Lin Liu, MD,[1,2,3,13] Xiang Chen, PhD,[2,3,14] Shihao Wang, PhD,[2,3,15] Hong Jiang, MD,[16] Wenjie Zheng, MD,[17] Shaoling Zheng, MD,[18] Qiao Ye, MD,[19] Yue Du, MD,[20] Li Guo, MD,[21] Jing Zhu, MS,[22] Guomin Li, MD,[9] Changming Zhang, MD,[23] Zhimiao Lin, MD,[24] Xiuli Ju, MD,[25] Yongmei Han, MD,[2,3] Weiqian Chen, MD,[26] Jin Lin, MD,[26] Jing Xue, MD,[27] Hao Cheng, MD,[28] Caiqing Xu, MD,[29] Lin Huang, MD,[30] Longyan Qin, MS,[31] Jiashun Zeng, MD,[31] Yifang Mei, MD,[32] Tingting Yan, MS,[19] Qianying Lv, MD,[9] Yaoyao Shangguan, BS,[17] Cuifang Zheng, MD,[10] Xiaoliang He, MS,[33] Hongfei Liu, MD,[34] Xiaoli Chen, MD,[35] Hua Xie, MD,[35] Xue Li, MD,[25] Ying Jin, MD,[23] Jiahui Peng, MD,[2,3] Bo Lin, MD,[13] Yao Huang, MS,[36] Xiuli Wang, MD,[20] Xiaoxi Yang, MD,[37,38,39,40] Nan Jiang, MD,[37,38,39,40] Wei Wang, MS,[41] Tong Wu, MS,[22] Dongze Wu, MD,[22] Yun Zhu, MD,[42] Yakai Fu, MD,[4] Jie Chen, MD,[4] Ran Wang, MD,[4] Xiaojun Liu, MS,[8] Dongbin Jiang, MS,[8] Huijie Xiao, MS,[43] Baige Su, MD,[43] Benshan Zhang, MS,[44] Fengqi Wu, MD,[45] Qiongyi Hu, MD,[7] Chengde Yang, MD,[7] Meiping Lu, MD,[21] Shuang Ye, MD,[4] Min Shen, MD,[46,47] Hongmei Song, MD,[41] Jianghua Chen, MD,[16] Jun Yang, MS,[11] Zhihong Liu, MD,[23] Xiaomin Yu, PhD,[1,2,3] and Qing Zhou, PhD[1,2,3]

Objective. This study aims to characterize pathogenic somatic mutations in patients with autoinflammatory or autoimmune diseases lacking disease-causing germline mutations, explore their contribution to disease pathogenesis and progression, and evaluate their implications for diagnosis and targeted therapy.

Methods. We performed a systematic analysis of somatic mutations in a selected panel of 185 immune-related genes in 2,912 patients with autoinflammatory or autoimmune diseases, recruited from 41 medical centers across China, who were previously negative for germline mutations based on whole-exome sequencing.

Results. We identified both previously reported and novel somatic mutations in genes such as *UBA1*, *KRAS*, and *NLRP3*. Pathogenic somatic mutations in *TNFAIP3* were discovered first in patients with autoinflammatory diseases. The pathogenic somatic mutation detection rate was 1.35% in adults and 0.97% in children, emphasizing the importance of genetic diagnosis and novel gene discovery for somatic mutations. In addition, somatic mutations in Ras-related genes were identified in seven patients, and 39 clonal hematopoiesis–associated mutations were identified in 36 adult patients. Moreover, myeloid cells harboring somatic mutations expanded during disease flare and reduced during remission. Disregarding the dynamic elevation of the variant allele fraction during disease progression led to therapeutic failure.

Conclusion. This study delineated the genetic landscape of pathogenic somatic mutations underlying autoinflammatory and autoimmune diseases, offering valuable insights for genetic diagnosis and targeted therapies.

INTRODUCTION

Somatic mutations are genetic alterations that occur at the cellular level in somatic tissues after fertilization, which can arise throughout one's lifetime either early in development or later in life.[1] Although the important roles of somatic mutations in the pathogenesis of cancer have been comprehensively studied,[2] their role as causes of monogenic disorders remain

Dr Zhou's work was supported by the National Natural Science Foundation of China (grants 82225022, 32141004, and 32321002), the XPLORER PRIZE from New Cornerstone Science Foundation, the National Key Research and Development Program of China (grant 2024YFC2511002), and the Clinical Research Project for the Summit Program of Children's Hospital of Chongqing Medical University (grant CHCMU-2024-XKDF-1001). Dr Song's work was supported by the National Key Research and Development Program of China (grant 2021YFC2702000). Dr Yu's work was supported by the National Natural Science Foundation of China (grants 82394420, 82394424, and 82471844), the Hundred-Talent Program of Zhejiang University, the Leading Innovative and Entrepreneur Team Introduction Program of Zhejiang (grant 2021R01012), and the Key Technology Breakthrough Program of Ningbo

underrecognized and have not been systematically investigated.

Currently, genetic diagnosis mainly focuses on germline mutations including single-nucleotide polymorphisms and copy number variations.[3] Analysis of somatic mutations in monogenic disorders have not been routinely performed in genetic diagnosis because detecting somatic variants in whole-exome sequencing (WES) data is challenging.[4] Although there are multiple somatic variant–calling software tools,[5] most are designed for detecting somatic variants in cancer, typically requiring a tumor sample along with a matched normal sample to distinguish them from germline variants. Detecting somatic variants for monogenic disorders without a matched normal sample usually results in a high false-positive rate. Additionally, variant detection software usually requires high read depth through next-generation sequencing (NGS),[4] often necessitating the detection of somatic variants using targeted sequencing separately. Detecting low variant allele fraction (VAF) somatic variants that are lower than 10% is particularly challenging, as they are difficult to distinguish from false positives caused by low read quality at specific sites. Moreover, the genetic diagnosis yield for somatic mutations has yet to be established in a large cohort study. Although genetic variants that cause rare disorders may remain elusive even after WES and/or genome sequencing, the benefit of analyzing somatic mutations in these negative cases remains unclear.

Autoinflammatory and autoimmune diseases are both immune dysregulation disorders caused by the activation of myeloid cells or lymphocytes, which affect approximately 5% to 10% of the global population.[6,7] Pathogenic somatic mutations in genes such as *UBA1, NLRP3, NLRC4, NRAS*, and *NOD2* have been reported to cause autoinflammatory or autoimmune diseases in both early-onset and late-onset conditions.[1,8–20] However, the landscape of pathogenic somatic mutations in autoinflammatory and autoimmune diseases remains unknown. In addition, the signaling pathways implicated in these diseases

Sci-Tech Innovation YONGJIANG 2035 (grant 2024Z221). Dr J. Wang's work was supported by the National Natural Science Foundation of China (grants 82394420, 82394423, and 82402121) and the China Postdoctoral Science Foundation (grant 2023M733104). Dr S. Wang's work was supported by the National Natural Science Foundation of China (grant 82402118).

[1]Life Sciences Institute, Zhejiang University, Department of Rheumatology, The Second Affiliated Hospital, Zhejiang University School of Medicine, Hangzhou, China; [2]Liangzhu Laboratory of Zhejiang University, Hangzhou, China; [3]Department of Rheumatology, Sir Run Run Shaw Hospital, Zhejiang University School of Medicine, Hangzhou, China; [4]Department of Rheumatology, Renji Hospital, Shanghai Jiao Tong University School of Medicine, Shanghai, China; [5]Shanghai Immune Therapy Institute, Shanghai, China; [6]The Affiliated Children's Hospital of Xiangya School of Medicine, Central South University (Hunan Children's Hospital), Changsha, China; [7]Department of Rheumatology and Immunology, Ruijin Hospital, Shanghai Jiao Tong University School of Medicine, Shanghai, China; [8]Department of Rheumatology, The First Affiliated Hospital of Zhengzhou University, Zhengzhou, China; [9]Department of Rheumatology, Children's Hospital of Fudan University, National Children's Medical Center, Shanghai, China; [10]Department of Gastroenterology, Children's Hospital of Fudan University, National Children's Medical Center, Shanghai, China; [11]Department of Rheumatology and Immunology, Shenzhen Children's Hospital, Shenzhen, China; [12]Hangzhou Institute of Medicine Chinese Academy of Sciences, Hangzhou, China; [13]Urology & Nephrology Center, Department of Nephrology, Zhejiang Provincial People's Hospital (Affiliated People's Hospital, Hangzhou Medical College), Hangzhou, China; [14]Yangtze Delta Region Institute (Quzhou), University of Electronic Science and Technology of China, Quzhou, China; [15]Cell and Molecular Biology Laboratory, Affiliated Zhoushan Hospital of Wenzhou Medical University, Zhoushan, China; [16]Kidney Disease Center, The First Affiliated Hospital, Zhejiang University School of Medicine, Hangzhou, China; [17]Department of Pediatric Rheumatology, The Second Affiliated Hospital and Yuying Children's Hospital of Wenzhou Medical University, Wenzhou, China; [18]Department of Rheumatology and Immunology, Guangdong Second Provincial General Hospital, Guangzhou, China; [19]Department of Rheumatology, The Second Affiliated Hospital of Jiaxing University, Jiaxing, China; [20]Department of Pediatrics, Shengjing Hospital of China Medical University, Shenyang, China; [21]Department of Rheumatology Immunology and Allergy, Children's Hospital, Zhejiang University School of Medicine, Hangzhou, China; [22]Department of Rheumatology and Immunology, Sichuan Provincial People's Hospital, University of Electronic Science and Technology of China, Chengdu, China; [23]National Clinical Research Center of Kidney Diseases, Jinling Hospital, Affiliated Hospital of Medical School, Nanjing University, Nanjing, China; [24]Dermatology Hospital, Southern Medical University, Guangzhou, China; [25]Pediatric Department, Qilu Hospital of Shandong University, Jinan, China; [26]Division of Rheumatology, The First Affiliated Hospital, Zhejiang University School of Medicine, Hangzhou, China; [27]Department of Rheumatology, The Second Affiliated Hospital, Zhejiang University School of Medicine, Hangzhou, China; [28]Department of Dermatology and Venereology, Sir Run Run Shaw Hospital, Zhejiang University School of Medicine, Hangzhou, China; [29]Yiwu Hospital Affiliated to Hangzhou Medical College, Jinhua, China; [30]School of Basic Medical Sciences, Zhejiang Chinese Medical University, Hangzhou, China; [31]Department of Rheumatology and Immunology, The Affiliated Hospital of Guizhou Medical University, Guiyang, China; [32]The Second Affiliated Hospital of Southern University of Science and Technology, Shenzhen, China; [33]Department of Rheumatology, Children's Hospital of Anhui Province, Hefei, China; [34]He Bei Yanda Hospital, Langfang, China; [35]Department of Medical Genetics, Capital Institute of Pediatrics, Beijing, China; [36]Department of Nephrology, Zhejiang Provincial People's Hospital Bijie Hospital, Bijie, China; [37]State Key Laboratory of Complex Severe and Rare Diseases, Peking Union Medical College Hospital, Beijing, China; [38]Department of Rheumatology and Clinical Immunology, Peking Union Medical College Hospital, Chinese Academy of Medical Sciences, Peking Union Medical College, Beijing, China; [39]National Clinical Research Center for Dermatologic and Immunologic Diseases (NCRC-DID), Ministry of Science & Technology, Beijing, China; [40]Key Laboratory of Rheumatology and Clinical Immunology, Ministry of Education, Beijing, China; [41]Department of Pediatrics, State Key Laboratory of Complex Severe and Rare Diseases, Peking Union Medical College Hospital, Chinese Academy of Medical Sciences & Peking Union Medical College, Beijing, China; [42]Department of Rheumatology and Immunology, Nanjing Drum Tower Hospital, Affiliated Hospital of Medical School, Nanjing University, Nanjing, China; [43]Department of Pediatrics, Peking University First Hospital, Beijing, China; [44]Department of Hematology, Hunan Children's Hospital, Changsha, China; [45]Children's Hospital, Capital Institute of Pediatrics, Beijing, China; [46]Department of Rare Diseases, Peking Union Medical College Hospital, Chinese Academy of Medical Sciences & Peking Union Medical College, Beijing, China; [47]State Key Laboratory of Complex Severe and Rare Diseases, Peking Union Medical College Hospital, Beijing, China.

Mr J. Fu, Dr Q. Fu, Dr J. Wang, Dr Q. Wang, Dr Liang Zhang, and Dr Chi contributed equally to this work. Dr Zhou, Dr Yu, Dr Z. Liu, Mr J. Yang, Dr Jianghua Chen, and Dr Song jointly supervised the work.

Additional supplementary information cited in this article can be found online in the Supporting Information section (https://acrjournals.onlinelibrary.wiley.com/doi/10.1002/art.70126).

Author disclosures are available at https://onlinelibrary.wiley.com/doi/10.1002/art.70126.

Address correspondence via email to Qing Zhou, PhD, at zhouqingnwu@gmail.com; to Xiaomin Yu, PhD, at yuxiaomin@zju.edu.cn; to Zhihong Liu, MD, at liuzhihong@nju.edu.cn; to Jun Yang, MS, at rogasansz@163.com; to Jianghua Chen, MD, at chenjianghua@zju.edu.cn; or to Hongmei Song, MD, at songhm1021@126.com

Submitted for publication September 18, 2025; accepted in revised form February 2, 2026.

and the expansion of somatic mutations throughout the disease course remain poorly defined.

In this study, we conducted the cohort study of patients with autoinflammatory and autoimmune diseases and systematically explored the genetic landscape of pathogenic somatic mutations by analyzing 185 immune-related genes, which could improve diagnosis and provide precision medicine for these two types of diseases.

METHODS

Study design and participants. Patients clinically diagnosed with autoinflammatory or autoimmune diseases were recruited from 41 medical centers across China (Supplementary Table S1). We performed WES on DNA extracted from the patients' peripheral blood. Patients carrying germline mutations classified as pathogenic or likely pathogenic in the ClinVar database and consistent with known pathogenic inheritance patterns were excluded. A total of 2,912 patients were enrolled in the present study, including 1,136 children (aged <18 years) and 1,776 adults (aged ≥18 years) (Supplementary Table S2).

All patients with somatic mutations enrolled in the study were evaluated under a protocol approved by the institutional review boards of Sir Run Run Shaw Hospital, Zhejiang University School of Medicine (2023–935-03); Children's Hospital, Zhejiang University School of Medicine (2021-IRB-0172-Y-01); Jinling Hospital, Affiliated Hospital of Medical School, Nanjing University (2025DZKY-012-01); Peking Union Medical College Hospital (I-24PJ2288); and Ruijin Hospital, Shanghai Jiao Tong University School of Medicine (2023–346). Informed consent was obtained from patients.

Procedures. WES data were reanalyzed to identify somatic mutations using GATK Mutect2 and HaplotypeCaller. Genes with autosomal dominant or X-linked inheritance are more likely to cause disease through somatic mutations.[21] Accordingly, we assembled a panel of 185 candidate genes relevant to immune dysregulation for somatic mutation analysis. Among these genes, 157 were directly implicated in immune-related disorders, including 20 genes in which somatic pathogenic mutations have been reported to cause monogenic immune dysregulation disorders, 134 inborn errors of immunity (IEI) genes listed in the 2024 International Union of Immunological Societies Expert Committee that follow autosomal dominant or X-linked modes of inheritance, and 3 genes reported to cause immune-mediated diseases but not yet incorporated into the current IEI framework. Given that mutations in Ras-related genes can contribute to immune dysregulation phenotypes in some patients,[22,23] we additionally included 16 Ras-associated candidate genes. Furthermore, considering the established association between clonal hematopoiesis and immune dysregulation,[1] we incorporated the 11 frequently reported genes related to clonal hematopoiesis into our candidate list.[24,25] Supplementary Table S3 provides detailed information on this gene list, including the literature sources for each gene.

The pathogenicity of variants was manually evaluated based on American College of Medical Genetics and Genomics guidelines.[26] Variants classified as pathogenic or likely pathogenic in the ClinVar database, based on criteria from multiple submitters without conflicts or reviewed by an expert panel, were also considered for inclusion. Variants previously classified as pathogenic in the ClinVar database or reported as pathogenic in published studies were categorized as "reported variants." Variants and genes identified for the first time as disease-causing in this study were categorized as "novel somatic variants" and "novel somatic genes," respectively.

Targeted sequencing was then performed to validate these candidate variants. Variants confirmed by targeted sequencing with a VAF <44.1% on autosomes were classified as true somatic mutations. For male patients, variants on the X chromosome with a VAF <100% were also classified as somatic. Variants undetectable by targeted sequencing were considered false positives, whereas those with a VAF ≥44.1% on autosomes or 100% on the X chromosome in male patients were classified as germline. False positives and germline variants were excluded from analysis. Detailed descriptions of sequencing, the candidate genes list, and analysis methods are provided in Supplementary Methods S1. No unique code was generated during this study. All other relevant data are available from the corresponding author on reasonable request.

RESULTS

Calling somatic mutations in a large cohort. We included patients with autoinflammatory or autoimmune diseases who underwent WES with negative diagnostic results. The cohort for somatic variant analysis included 2,912 patients from 41 medical centers across China, including 1,136 children (aged <18 years) and 1,776 adults (aged ≥18 years) (Figure 1; Supplementary Table S2). We analyzed somatic variants using our in-house pipeline, and the identified variants were confirmed through targeted sequencing (Supplementary Methods S1).

Calling somatic variants from WES data remains a technical challenge for existing somatic callers, especially in reducing false-positive calls and accurately detecting low-VAF variants (<10%) with high sensitivity. To address this challenge, we developed an in-house pipeline that incorporates GATK HaplotypeCaller and Mutect2 for improved somatic variant detection (Supplementary Methods S1). The average sequencing depth of the cohort was 98.73×, enabling the detection of low-frequency somatic mutations.[5,27] A total of 1,106,072 variants were identified through the in-house pipeline, with an average of 379 variants per sample (Supplementary Table S4 and Figure S1).

Pathogenic somatic mutations in genetic diagnosis negative cases. In this study, we identified nine genes with pathogenic somatic mutations in patients, including *UBA1,*

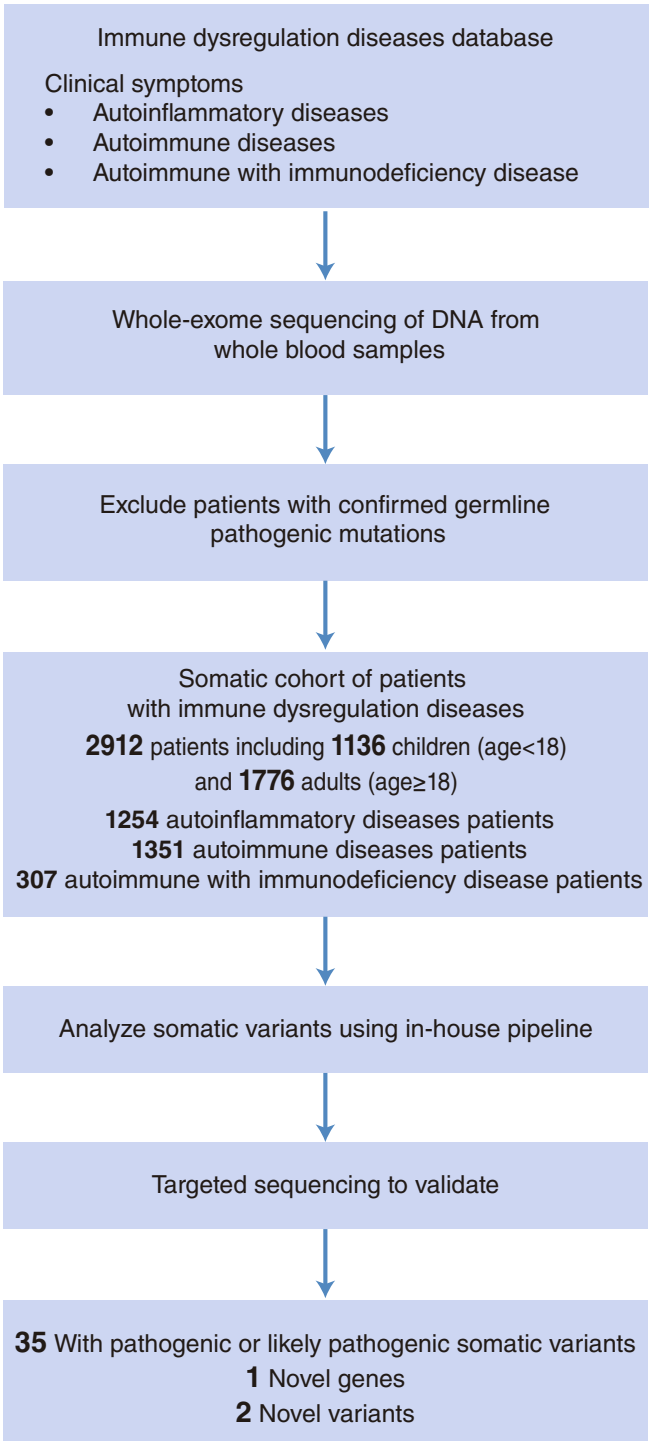

Figure 1. Overview of the study design. Somatic mutations were analyzed in 2,912 patients who were previously negative for germline mutations based on whole-exome sequencing and validated using targeted sequencing. Variant pathogenicity assessed using American College of Medical Genetics and Genomics guidelines or ClinVar (https://www.ncbi.nlm.nih.gov/clinvar/).

KRAS, TNFAIP3, NRAS, NLRP3, CARD14, NFKBIA, NLRC4, and *STING1* (Figure 2A and B; Table 1 and Figure S2). *UBA1* and *KRAS* are the most common genes with pathogenic somatic mutations, accounting for 34.3% (12 of 35) and 28.6% (10 of 35) of the total number of the identified pathogenic somatic mutations. In addition, we identified new somatic mutations in *NFKBIA* (c.95G>A, p.S32N) and *STING1* (c.852G>T, p.R284S). For example, the germline gain-of-function (GOF) *NFKBIA* S32N mutation has been reported in patients with ectodermal dysplasia with immunodeficiency.[28] *NFKBIA* encodes IkBα, an inhibitor of NF-κB. The mutation enhances the inhibitory activity of IkBα by preventing its phosphorylation on serine 32 and its subsequent degradation. The patient with somatic *NFKBIA* S32N mutation presented with lupus nephritis (Table 1). Despite its association with immunodeficiency in the germline setting, partial attenuation of NF-κB signaling may paradoxically promote autoimmunity by triggering activation of alternative inflammatory pathways, particularly type I interferon (IFN) signaling, in nonmutant cells.[29,30] GOF mutations in *STING1* cause STING-associated vasculopathy with onset in infancy manifesting with systemic inflammation, skin lesions, and interstitial lung disease.[20] The *STING1* R284S germline mutation has been reported to result in constitutive activation in the absence of cyclic dinucleotides.[31] The patient with *STING1* somatic R284S mutation manifested with skin rashes and thrombocytopenia (Table 1). Moreover, we identified somatic mutations in *TNFAIP3* that have not been previously reported to carry pathogenic somatic mutations in patients with immune dysregulations, suggesting the identification of novel genes with somatic mutation. These novel variants were not found in the Chinese population databases HuaBiao, ChinaMAP, or CHN100K (Supplementary Table S5).

For the two most frequently diagnosed disorders, vacuoles, E1 enzyme, X-linked, autoinflammatory, somatic (VEXAS) and RAS-associated autoimmune leukoproliferative disorder (RALD), we summarized their detailed clinical phenotypes (Supplementary Figure S3 and Table S6). For VEXAS, our analysis revealed a correlation between VAF and disease severity. Specifically, the P4 with the lowest VAF had the mildest presentation, limited to chondritis. In contrast, patients with higher VAFs (P6, P7, and P8) exhibited more extensive clinical involvement, which was associated with more severe phenotypes. Moreover, fever, macrocytic anemia, vacuoles, and chondritis were identified as the most common features of VEXAS, providing valuable insights for clinical diagnosis (Supplementary Figure S3). For RALD, 8 of 12 patients exhibited elevated serum IgG levels, and 11 of 12 patients were positive for autoantibodies. Autoimmune cytopenia was diagnosed in all nine patients tested, with hemolytic anemia and thrombocytopenia being the most common presentations (Supplementary Table S6). These findings are consistent with previously reported cases of RALD,[32] suggesting that these are representative clinical manifestations of the disease.

The VAF of somatic mutations ranged from 1.32% to 41.40%, except for *UBA1*, which ranged from 3.63% to 93.67% (Figure 2B; Table 1). Mutations on chromosome X are identified only in the *UBA1* gene, whereas mutations in the remaining genes

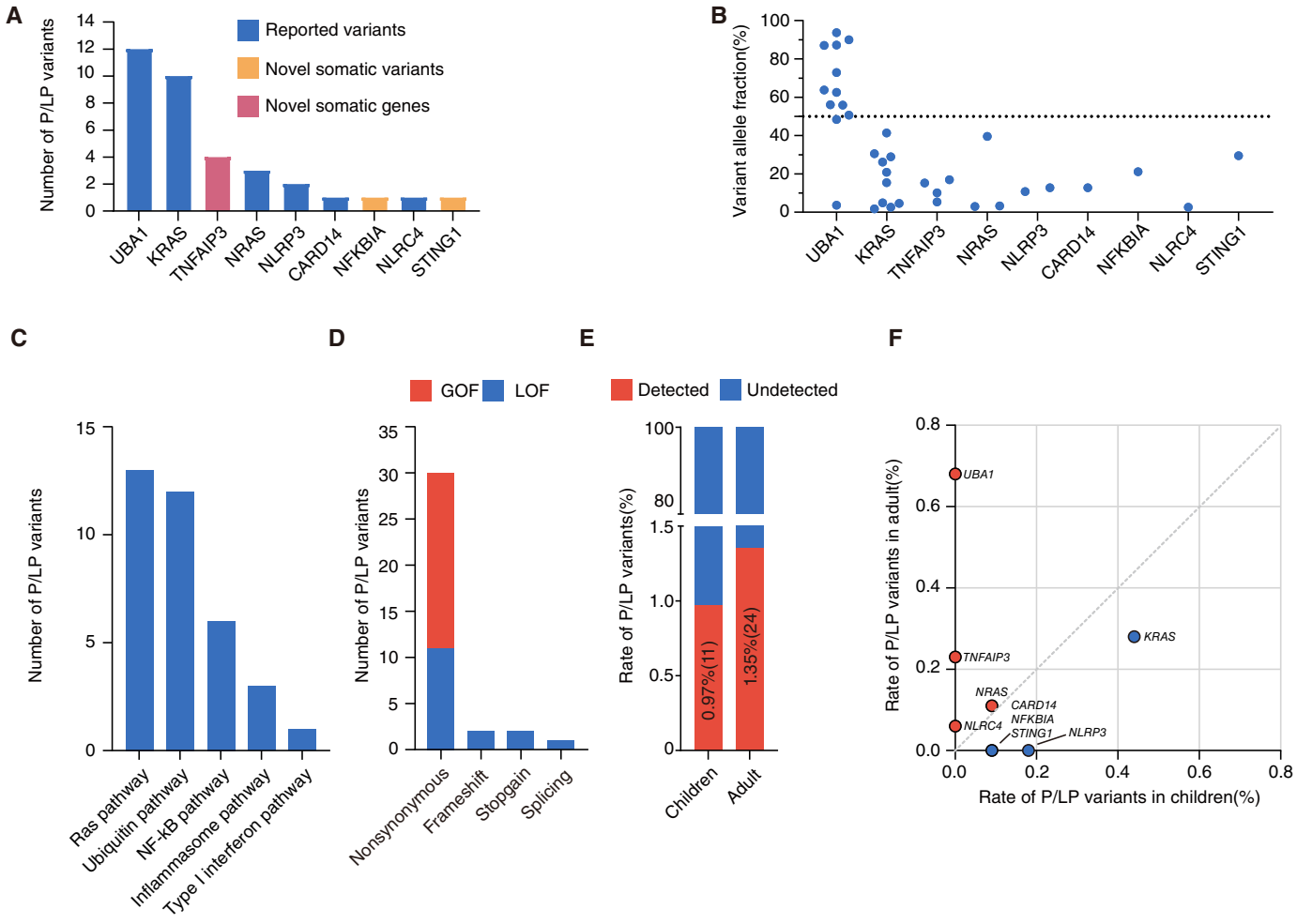

Figure 2. Overview of P/LP somatic mutations identified in autoinflammatory and autoimmune diseases cohort. (A) P/LP somatic mutations were identified in 35 patients across nine genes, including two previously unreported somatic mutation genes and one novel somatic mutation gene. Reported variants refer to mutations identified as pathogenic in ClinVar or previously published studies. Novel somatic genes refer to genes with somatic mutations that are reported for the first time in this study to cause diseases. Novel somatic variants refer to variants with somatic that are reported for the first time in this study to cause diseases. (B) Distribution of variant allele fraction for P/LP somatic mutations. The dashed line indicates a variant allele fraction of 50%. (C) Proportional distribution of P/LP somatic mutation genes in signaling pathways. (D) Types of P/LP somatic mutations and their impact on protein function. (E) Diagnostic rate of P/LP somatic mutations in pediatric and adult patients. (F) Distribution of diagnostic rates for P/LP somatic mutation genes in pediatric and adult patients. GOF, gain-of-function; LOF, loss-of-function; P/LP, pathogenic/likely pathogenic. Color figure can be viewed in the online issue, which is available at http://onlinelibrary.wiley.com/doi/10.1002/art.70126/abstract.

are located on autosomes. Overall, genes with somatic mutations are most commonly involved in the Ras pathway followed by the ubiquitin, NF-κB, inflammasome, and type I IFN pathways (Figure 2C).

The most common pathogenic somatic mutations are nonsynonymous variants followed by frameshift, stop-gain, and splicing variants (Figure 2D). Regarding the functional effect of the somatic mutations, these somatic mutations can result in either GOF mutations, which lead to constitutive activation of kinases, inflammasomes, or downstream inflammatory signaling (such as *KRAS, NRAS, NLRP3, NLRC4*, and *STING1*), or loss-of-function (LOF) mutations, which result in insufficient inhibitory effect in the inflammatory pathways (such as *TNFAIP3*). Nonsynonymous variants can be either GOF or LOF mutations (Figure 2D).

Among the 1,136 pediatric patients, the detection rate for somatic mutations was 0.97% (11 of 1,136), and the detection rate in adult patients was 1.35% (24 of 1,776) (Figure 2E), which is a higher frequency than that in pediatric patients. The results suggest that although pediatric patients often have a higher frequency of carrying germline mutations, somatic mutations occur more commonly in adult patients with autoinflammatory or autoimmune diseases. Somatic mutations in *UBA1, TNFAIP3*, and *NLRC4* were detected in adult patients, whereas *CARD14, STING1*, and *NLRP3* somatic mutations were identified in pediatric patients (Figure 2F), indicating an age bias for certain genes with somatic mutations.

Table 1. Information of pathogenic or likely pathogenic somatic variants in 35 patients*

Patient ID	Age at sampling, y	Clinical symptoms	Sex	Gene	Mutation	WES VAF, %; reads n/N	Targeted seq VAF, %; reads n/N	CADD	gnomAD v4.1.0	Classification
P1	65	Chondritis and arthritis	Male	*UBA1*	NM_003334.4: c.118-1G>C	46.85; 67/143	48.42; 2,156,849/4,454,572	34	0	Reported variant
P2	66	Fever, skin involvement, and arthritis	Male	*UBA1*	NM_003334.4: c.121A>C; p.M41L	53.39; 63/118	56.04; 1,335,433/2,383,063	22.9	8.25e-7	Reported variant
P3	63	Fever, chondritis, skin involvement, pulmonary infiltrates, and recurrent oral ulcer	Male	*UBA1*	NM_003334.4: c.121A>C; p.M41L	66.67; 62/93	55.91; 2,484,905/4,444,165	22.9	8.25e-7	Reported variant
P4	45	Ear redness and swelling	Male	*UBA1*	NM_003334.4: c.121A>C; p.M41L	3.64; 2/55	3.63; 47,699/1,314,248	22.9	8.25e-7	Reported variant
P5	57	Pain and swelling in ears and multiple joints and painless red rash	Male	*UBA1*	NM_003334.4: c.121A>C; p.M41L	51.14; 90/176	50.68; 193,239/381,328	22.9	8.25e-7	Reported variant
P6	51	Pain and swelling in ears, polychondritis, anemia, and thrombocytopenia	Male	*UBA1*	NM_003334.4: c.121A>G; p.M41V	89.31; 142/159	93.67; 5,072,244/5,415,165	19.96	0	Reported variant
P7	68	Ear chondritis, periorbital swelling, anemia, and thrombocytopenia	Male	*UBA1*	NM_003334.4: c.121A>G; p.M41V	89.57; 103/115	90.01; 710,244/789,045	19.96	0	Reported variant
P8	68	Fever, skin involvement, arthritis, periorbital edema, pulmonary infiltrates, and conjunctivitis	Male	*UBA1*	NM_003334.4: c.121A>G; p.M41V	83.76; 98/117	87.07; 3,770,229/4,330,281	19.96	0	Reported variant
P9	71	Recurring fever, skin rash, anemia, and thrombocytopenia	Male	*UBA1*	NM_003334.4: c.122 T>C; p.M41T	66.27; 110/166	63.81; 631,727/989,969	21.3	1.65e-6	Reported variant
P10	63	Redness and pain on the feet and fingers, erythema nodosum, and vasculitis	Male	*UBA1*	NM_003334.4: c.122 T>C; p.M41T	90.32; 56/62	87.23; 1,082,901/1,241,369	21.3	1.65e-6	Reported variant
P11	71	Ear chondritis, skin rash, anemia, and pleural effusion	Male	*UBA1*	NM_003334.4: c.122 T>C; p.M41T	76.25; 61/80	72.91; 721,365/989,348	21.3	1.65e-6	Reported variant
P12	66	Fever, skin involvement, and arthritis	Male	*UBA1*	NM_003334.4: c.122 T>C; p.M41T	59.2; 74/125	62.54; 1,478,867/2,364,708	21.3	1.65e-6	Reported variant
P13	9	Evans's syndrome, pancytopenia, thrombocytopenia, and anemia	Female	*KRAS*	NM_004985.5: c.37G>T; p.G13C	17.47; 87/498	15.45; 227,334/1,471,846	28	0	Reported variant
P14	4	Thrombocytopenia, anemia, and autoimmune leukoproliferative disorder	Male	*KRAS*	NM_004985.5: c.38G>A; p.G13D	13.33; 4/30	4.86; 243,374/5,009,444	23.8	3.10e-6	Reported variant

(Continued)

Table 1. (*Cont'd*)

Patient ID	Age at sampling, y	Clinical symptoms	Sex	Gene	Mutation	WES VAF, %; reads n/N	Targeted seq VAF, %; reads n/N	CADD	gnomAD v4.1.0	Classification
P15	31	Fever, rash, arthralgia, and lupus nephritis	Male	*KRAS*	NM_004985.5: c.38G>A; p.G13D	10.71; 3/28	2.58; 13,293/515,256	23.8	3.10e-6	Reported variant
P16	7 mos	Upper respiratory tract infection, thrombocytopenia, moderate anemia, and neutropenia	Male	*KRAS*	NM_004985.5: c.38G>A; p.G13D	27.97; 99/354	41.4; 1,134,471/2,740,323	23.8	3.10e-6	Reported variant
P17	12	Fever, purpura of both lower limbs, and thrombocytopenia	Female	*KRAS*	NM_004985.5: c.182A>G: p.Q61R	23.26; 10/43	28.91; 168,566/583,101	22.9	0	Reported variant
P18	47	Fever, hemophagocytic, and lymphohistiocytosis	Female	*KRAS*	NM_004985.5: c.436G>A; p.A146T	26.32; 10/38	30.53; 428,312/1,402,852	27.2	1.86e-6	Reported variant
P19	26	Fever and HLH	Female	*KRAS*	NM_004985.5: c.436G>A; p.A146T	18.18; 8/44	1.32/26.16/7.6; 22,043/1,671,838; 25,633/97,979; 259,612/3,417,015	27.2	1.86e-6	Reported variant
P20	12	Hair loss, oral ulcer, lupus encephalopathy, and lupus pneumonitis	Female	*KRAS*	NM_004985.5: c.436G>A; p.A146T	3.36; 11/327	1.73; 11,481/663,283	27.2	1.86e-6	Reported variant
P21	31	Autoimmune leukoproliferative disorder, and antinuclear antibody positive	Male	*KRAS*	NM_004985.5: c.437C>T; p.A146V	19.68; 49/249	20.84; 1,156,967/5,550,748	31	3.10e-6	Reported variant
P22	23	Purpuric rash, thrombocytopenia, and lupus nephritis	Male	*KRAS*	NM_004985.5: c.437C>T; p.A146V	4.92; 3/61	4.62; 118,446/2,566,304	31	3.10e-6	Reported variant
P23	27	Frequent diarrhea	Male	*TNFAIP3*	NM_001270508.2: c.130_137del: p.R45Tfs*53	13.22; 23/174	10.14; 534,952/5,273,163	NA	0	Novel somatic gene
P24	35	Recurrent oral ulcers	Male	*TNFAIP3*	NM_001270508.2: c.577G>T; E193*	16.78; 24/143	15.26; 432,323/2,833,198	40	0	Novel somatic gene
P25	33	Recurrent oral ulcers	Female	*TNFAIP3*	NM_001270508.2: c.820delC; p.P274Hfs*13	9.86; 14/142	5.39; 140,884/2,614,902	NA	0	Novel somatic gene
P26	40	Severe oral ulcers three or four times once a year	Female	*TNFAIP3*	NM_001270508.2: c.1156A>T; K386*	15.79; 30/190	16.98; 696,194/4,100,191	37	0	Novel somatic gene
P27	31	Lupus nephritis (type III) with ballistic sclerosis	Female	*NRAS*	NM_002524.5: c.35G>T; p.G12V	41.91; 57/136	39.55; 806,518/2,039,188	26.5	6.20e-7	Reported variant
P28	21	Lupus nephritis (type V)	Female	*NRAS*	NM_002524.5: c.37G>T; p.G13C	4.05; 13/321	2.96; 28,452/960,479	31	6.20e-7	Reported variant
P29	8	Immune vasculitis and lupus nephritis	Male	*NRAS*	NM_002524.5: c.38G>A; p.G13D	7.50; 12/160	3.25; 146,148/4,491,716	24.5	6.20e-7	Reported variant
P30	13	Recurring fever and skin rash	Male	*NLRP3*	NM_001243133.2: c.1305G>T; p.K435N	13.90; 77/554	12.75; 139,519/1,094,135	23.5	0	Reported variant

(Continued)

Table 1. (*Cont'd*)

Patient ID	Age at sampling, y	Clinical symptoms	Sex	Gene	Mutation	WES VAF, %; reads n/N	Targeted seq VAF, %; reads n/N	CADD	gnomAD v4.1.0	Classification
P31	8	Recurring fever and juvenile idiopathic arthritis	Male	*NLRP3*	NM_001243133.2: c.1699G>A; p.E567K	10.31; 20/194	10.81; 59,387/549,524	20.2	0	Reported variant
P32	2	Red rash all over the body with a scaly surface	Female	*CARD14*	NM_001366385.1: c.412A>G; p.E138K	8.42; 8/95	12.75; 257,265/2,017,565	26.2	0	Reported variant
P33	2	Lupus nephritis	Female	*NFKBIA*	NM_020529.3: c.95G>A; p.S32N	35.29; 24/68	21.11; 156,909/743,154	26.7	0	Novel somatic variant
P34	69	Recurrent rash and long-lasting fever episodes	Female	*NLRC4*	NM_001199138.2: c.1329C>G; p.H443Q	2.61; 3/115	1.73/19.49; 409,224/2,099,514	17.75	0	Reported variant
P35	2	Skin rash and thrombocytopenia	Female	*STING1*	NM_198282.4: c.G852T; p.R284S	28.42; 83/292	29.49; 115,030/390,041	22.5	0	Novel somatic variant

* CADD, Combined Annotation Dependent Depletion; HLH, hemophagocytic lymphohistiocytosis; seq, sequencing; VAF, variant allele fraction; WES, whole-exome sequencing.

Novel pathogenic somatic mutation genes. Haploinsufficiency of A20 (HA20) was first reported as a monogenic autoinflammatory disease caused by heterozygous LOF mutations in the *TNFAIP3* gene.[33] The clinical characteristics of HA20 are diverse, including symptoms such as arthralgia/arthritis, oral and genital ulcers, ocular inflammation, inflammatory bowel disease, and positivity for autoantibodies in some cases, indicating a combined autoinflammatory and autoimmune disorder.[34,35] Although somatic mutations in *TNFAIP3* have been reported in lymphomas,[36] their role in causing autoinflammatory and autoimmune diseases has not yet been reported. It remains unclear whether somatic *TNFAIP3* mutation that causes mosaicism of A20 haploinsufficiency is sufficient to trigger inflammation. We first identified somatic *TNFAIP3* mutations in four families, with gonosomal mosaicism transmitted to affected children in three of these families (Figure 3A). Targeted sequencing confirmed that the VAF of mutant *TNFAIP3* allele ranges from 5% to 20% in different types of cells and tissues, such as whole blood, B cells, T cells, neutrophils, monocytes, sperm, hair follicle, nail, and urine from the probands (Figure 3B–D). Three patients presented with oral ulcers, and one patient experienced recurrent diarrhea. None of the four patients showed evidence of lymphoma (Table 1).

Secondary findings identified in the cohort. We classified somatic mutations in Ras-related genes, clonal hematopoiesis genes, and variants of uncertain significance as secondary findings. Seven patients in the cohort were found to harbor somatic variants in Ras-related genes (Supplementary Table S7 and Figure S4). Among them, four carried *NF1* variants, all of which are annotated as pathogenic in ClinVar. One patient carried a somatic *CBL* R420P variant, and substitutions at the same residue (R420L and R420Q) are classified as pathogenic in ClinVar, suggesting that R420P is a likely pathogenic variant. Another patient carried a somatic *LZTR1* G248R variant. *LZTR1* is a regulator of Ras ubiquitination.[37,38] Germline mutations in *LZTR1* including G248R cause Noonan syndrome because of dysregulation of Ras.[39] The patient with the somatic *LZTR1* G248R variant presented with systemic lupus erythematosus (Supplementary Table S7). The *LZTR1* somatic G248R mutation was detected by WES with VAF of 2.87% and confirmed by targeted sequencing with a VAF of 3.15% (Supplementary Figure S4).

Somatic variants associated with clonal hematopoiesis have been closely linked to immune dysregulation and aging.[1,24,25] In our cohort, 39 clonal hematopoiesis–related somatic variants were identified in 36 patients, all of whom were adults (Supplementary Table S8). Notably, 72.2% of these patients (26 of 36) presented with autoinflammatory diseases and 27.8% (10 of 36) presented with autoimmune diseases, suggesting a potential predisposition toward late-onset autoinflammatory diseases in individuals with clonal hematopoiesis. We collected data from 179 previously reported cases of clonal hematopoiesis in individuals with nonimmune dysregulation carrying variants

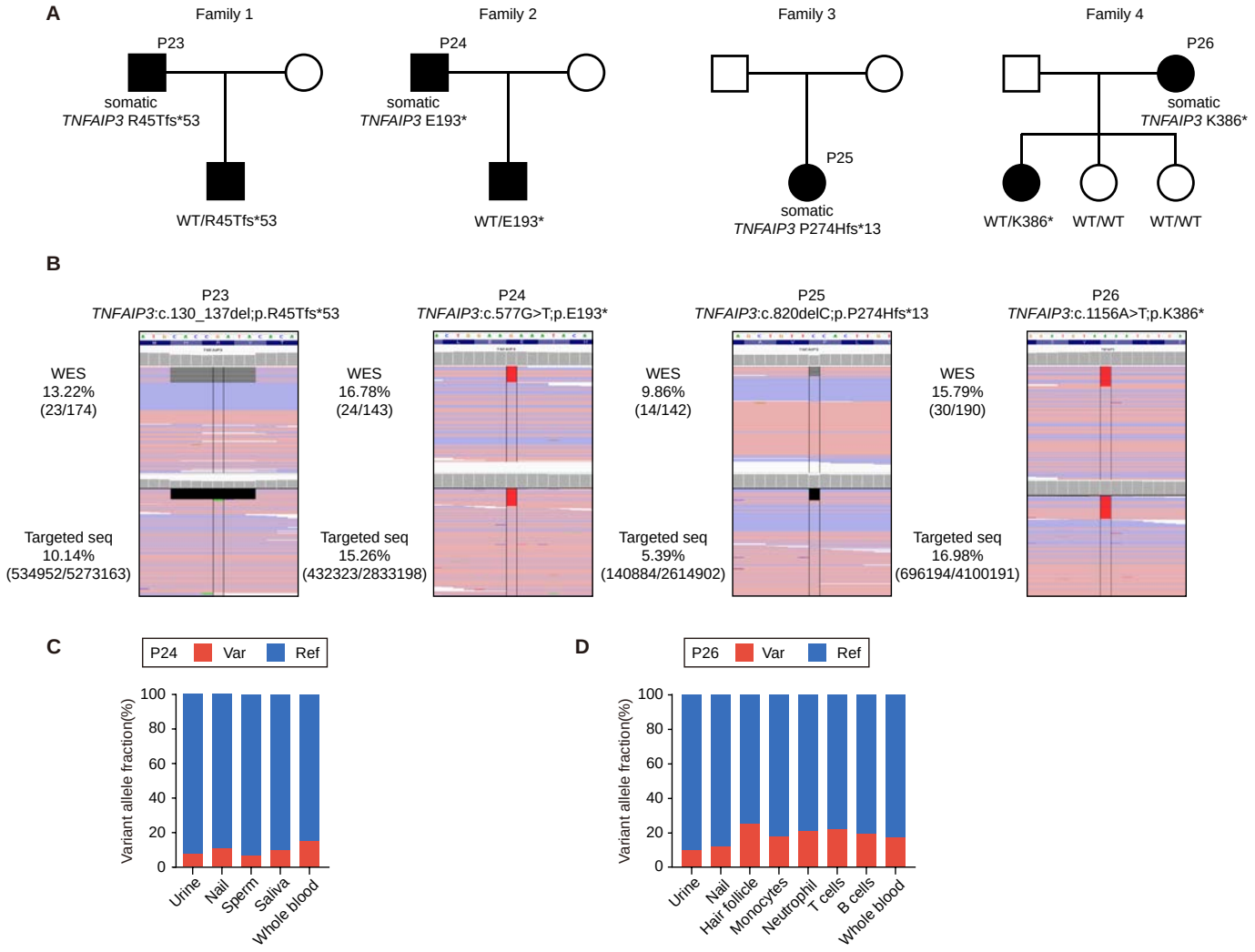

Figure 3. Genetic identification of *TNFAIP3* somatic mutations. (A) Pedigrees of four families with four patients carrying *TNFAIP3* somatic mutations. (B) WES and targeted seq results of *TNFAIP3* somatic mutations. (C) Proportions of *TNFAIP3* somatic mutations in different sources of samples of P24 measured by targeted seq, including urine, nail, sperm, saliva, and whole blood. (D) Proportions of *TNFAIP3* somatic mutations in different sources of samples of P26 measured by targeted seq, including urine, nail, hair follicle, monocytes, neutrophil, T cells, B cells, and whole blood. Red indicates variants, and blue represents WT sequences consistent with the reference genome. Ref, reference; seq, sequencing; Var, variant; WES, whole-exome sequencing; WT, wild-type. Color figure can be viewed in the online issue, which is available at http://onlinelibrary.wiley.com/doi/10.1002/art.70126/abstract.

in genes from our candidate list, with available information on age, VAF, and affected genes,[24,40] and we found that patients with immune dysregulation disorders carrying clonal hematopoiesis–related somatic mutations in our cohort were significantly younger than those in the nonimmune dysregulation group, with a mean age of 60.46 years compared with 70.73 years in controls, indicating that the onset of clonal hematopoiesis in immune dysregulation disorders occurs approximately a decade earlier (Supplementary Figure S5).

Dynamic expansion and reduction of somatic mutations in relation to disease states. We investigated the correlation between the VAF of somatic mutations and disease status (Figure 4A and B). Interestingly, the VAF showed dynamic changes corresponding to disease activity. In a patient (P19) with the *KRAS* somatic mutation, the somatic mosaicism VAF was 26.16% when the disease was active and flared. However, the VAF dramatically decreased to 1.32% in peripheral blood mononuclear cells (PBMCs) during a nonflare period. The VAF of the mutation during another nonflare period in this patient was also at a relatively low level, at 7.6% (Figure 4A and Supplementary Table S9). These results demonstrated that somatic mutations are responsible for monogenic disorders, undergoing dynamic expansion and reduction. Furthermore, there is a strong correlation between disease activity and the fraction of somatic mutations.

We further studied the disease progression and VAF change during the disease course in a patient (P34) with *NLRC4* somatic mutation (Figure 4B). At the diagnosis in 2020, the VAF was

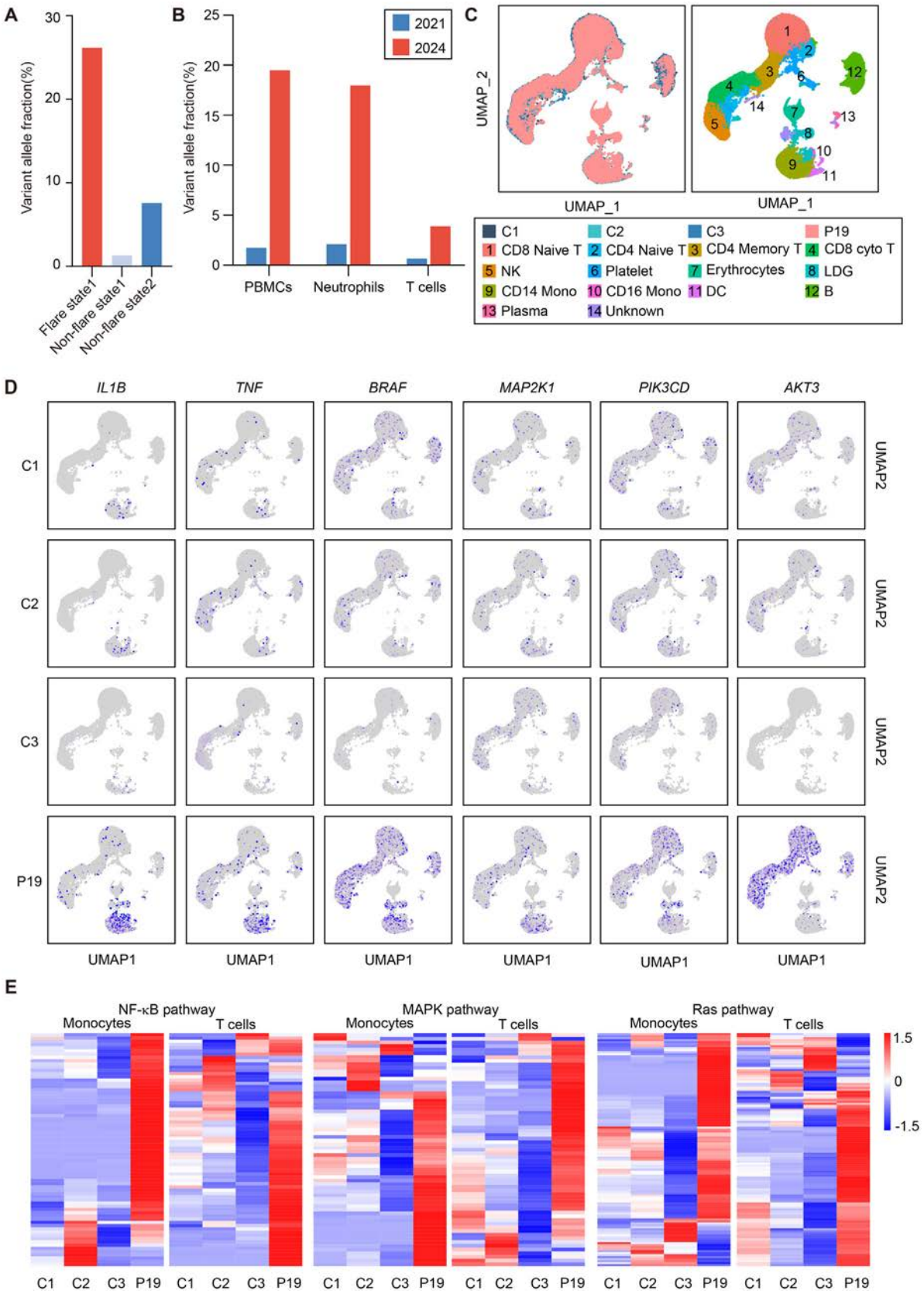

Figure 4. Legend on next page.

1.73% in PBMCs, 2.1% in neutrophils, and 0.66% in T cells.[15] The patient initially responded well to the interleukin (IL)-6 inhibitor tocilizumab from 2020 to 2022 and subsequently showed a favorable response to the IL-1 inhibitor canakinumab in 2022 (Supplementary Figure S6). However, after 2 years, the patient's response to canakinumab diminished (Supplementary Figure S6). We performed targeted sequencing of the somatic mutation in the patient's PBMC and immune cell subsets. The sequencing results revealed that the VAF had increased to 19.49% in PBMCs, 17.97% in neutrophils, and 3.9% in T cells (Figure 4B). The increased proportion of cells carrying the somatic mutation led to an elevated secretion of inflammatory factors, rendering the original drug dosage insufficient to suppress the heightened inflammatory response. These findings highlight that disregarding changes in the VAF of somatic mutations may result in the failure of targeted therapies.

Somatic mutations resulted in the activation of inflammatory pathways and targeted therapies. To investigate the impact of somatic mutations on inflammatory pathways at the single-cell level, we performed single-cell RNA sequencing on a patient (P19) with a *KRAS* somatic mutation (Figure 4C). Gene set enrichment analysis indicated that the increased gene expression is enriched in the tumor necrosis factor (TNF) signaling pathway, IL6-STAT3 signaling pathway, inflammatory responses, and the KRAS signaling pathway (Supplementary Figure S7). The transcriptional levels of proinflammatory cytokines such as *IL1B* and *TNF* and inflammatory mediators such as *NFKB1* and *TNFAIP3* are more predominantly increased in the patient's monocytes and T cells compared with healthy controls (Figure 4D; Supplementary Figure S7). Genes involved in the MAPK pathway and Ras pathway, such as *BRAF, MAP2K1, PIK3CD*, and *AKT3*, also showed elevated expression in monocytes or T cells (Figure 4D). Overall, the patient's data revealed activation of the NF-κB, MAPK, and Ras pathways in monocytes and T cells (Figure 4E and Supplementary Table S10). These findings demonstrate that although the patient only carries a somatic mutation, it is sufficient to trigger inflammatory responses, especially in myeloid and T cells.

DISCUSSION

This is the first study to systematically analyze pathogenic somatic mutations in autoinflammatory and autoimmune diseases, revealing a diagnostic rate of approximately 1.2% owing to pathogenic somatic mutations in previously genetic diagnosis negative cases. NGS has demonstrated unparalleled advantages and significant progress in medical genetics since its introduction into genetic diagnostics. Diagnostic rates have gradually improved not only because of advances in sequencing technology, such as the production of long reads, but also through reanalysis as new disease genes are identified. However, many patients with suspected genetic disorders remain undiagnosed. Although somatic mutations have been reported in nonneoplastic diseases sporadically,[41] they have not been widely appreciated and systematically evaluated. Our results suggested that cases negative for pathogenic germline mutations should be reanalyzed for somatic mutations, not only in patients with adult-onset diseases but also in those with early-onset diseases.

Adult-onset diseases have a higher incidence of somatic mutations compared with early-onset diseases, likely because certain somatic mutations occur in adulthood. Our previous studies have demonstrated that for adult-onset autoinflammatory diseases, some mutations are restricted to myeloid cells, which resulted in the overproduction of proinflammatory cytokines.[11] Moreover, the somatic mosaicism VAF can be below 5%; even at such low levels, GOF mutations with constitutive activation of Ras (*NRAS* or *KRAS*) or inflammasomes (*NLRP3* or *NLRC4*) are sufficient to trigger strong inflammatory responses.[15,42] Compared with patients with pathogenic germline mutations, the clinical manifestations of patients with somatic mutations can vary significantly depending on the somatic mutations that occur in the early embryo stage or later stages of life with various VAFs.

It is well known that somatic mutations in cancer can expand and evolve.[2,41] Our study for the first time demonstrated that somatic mutations in monogenic disorders may not only expand but also reduce over time, which correlated with disease flares and remission. A *TET2*-driver variant has been reported to be responsible for the clonal expansion of *NLRC4* mutation in an adult autoinflammatory patient[43]; we did not identify driver variants in our patients to explain the expansion of somatic mutations. Therefore, the factors and mechanisms that drive the expansion and reduction of cells with somatic mutation require more investigation. Moreover, our study revealed that somatic mutations can expand during disease progression, potentially resulting in a failure of targeted therapy regardless of the somatic mutations dynamic changes. Hence, patients with

Figure 4. Dynamic change of somatic mutations and activation of inflammatory signaling pathways. (A) Targeted sequencing results of somatic mutations in P19 were analyzed across three stages: flare state (sampled on May 2019), nonflare state 1 (sampled on October 2022), and nonflare state 2 (sampled on April 2024). (B) Targeted sequencing results of somatic mutations in P34 during the disease progression stage. The 2021 diagnostic findings were reported previously,[15] and samples from the progression stage were collected in June 2024. (C) UMAP visualization and marker-based annotation of P19 and three unaffected controls (C1, C2, and C3). (D) UMAP plot showing the expression of *IL1B, TNF, BRAF*, *MAP2K1*, *PI3KCD*, and *AKT3* (colored single cells) in PBMCs from P19 and three unaffected controls (C1, C2, and C3). (E) Comparison of the NF-κB pathway, MAPK pathway, and Ras pathway in monocytes and T cell subsets from P19 and unaffected controls determined by single-cell RNA sequencing. DC, dendritic cell; LDG, low-density granulocyte; NK, natural killer; PBMC, peripheral blood mononuclear cell; UMAP, Uniform Manifold Approximation and Projection. Color figure can be viewed in the online issue, which is available at http://onlinelibrary.wiley.com/doi/10.1002/art.70126/abstract.

somatic mutations may require tailored adjustments in therapy based on changes in VAF.

We reported the first four patients with HA20 with somatic *TNFAIP3* mutations. We identified that *TNFAIP3* somatic mutation can lead to autoinflammatory disease rather than lymphoma. Specifically, we found that *TNFAIP3* somatic mutations can not only cause autoinflammatory disease in affected individuals but also be transmitted to offspring in the form of gonosomal mosaicism. The condition of patients with somatic mutations was less severe than children with germline mutation. Because somatic *TNFAIP3* mutations have been reported in a healthy individual with no symptoms,[44] the somatic HA20 cases provided a good example to explore the severity of HA20 and the effect of gene dosage. The presence of somatic mutations in various cells derived from different germ layers suggested that the mutational event probably occurred early in embryogenesis. However, a late occurrence of somatic *TNFAIP3* mutations occurring mainly in myeloid cells or lymphoid cells may also have clinical manifestations, which require the identification of more patients with somatic HA20.

Germline mutations in *NF1*, *CBL*, and *LZTR1* are known to cause Noonan syndrome,[22,23,38] and somatic mutations in *NF1* and *CBL* have been implicated in leukemia.[45,46] Unlike somatic mutations in *NRAS* and *KRAS*, somatic variants in *NF1*, *CBL*, and *LZTR1* have not been previously reported to cause autoimmune or autoinflammatory diseases. Because of the lack of functional studies, we classified these findings as secondary findings. Clonal hematopoiesis–associated mutations have previously been described in adults without immune dysregulation.[24,25] *DNMT3A* and *TET2* are primarily myeloid-specific driving clonal expansion that favors myeloid differentiation. Previous studies have shown that inflammatory environments can confer a cell-intrinsic survival advantage to clones harboring *DNMT3A* or *TET2* mutations, and the expansion of these mutant clones can further promote and perpetuate inflammatory responses.[47] This bidirectional relationship between clonal hematopoiesis and inflammation may help explain why patients carrying clonal hematopoiesis–associated mutations are predominantly affected by autoinflammatory diseases. Our results indicate a potential association between clonal hematopoiesis and susceptibility to late-onset autoinflammatory diseases, although the mutations identified are not regarded as direct causative factors.

In our previous study on genetic testing for adult lupus nephritis, the diagnostic yield of pathogenic germline mutations was approximately 4%.[48] In the present cohort, we identified pathogenic somatic mutations in 1.2% of patients with immune dysregulation who tested negative for germline pathogenic variants. A greater sequencing depth would not only increase the probability of detecting low-VAF somatic variants but also improve the stability of variant-calling algorithms. Moreover, the use of a single algorithm may introduce detection bias. Considering that our WES depth was only 100×, that we detected somatic mutations solely using GATK-based algorithms, and that the analysis was limited to a predefined gene list, we speculate that the actual number of somatic mutations is likely higher. These findings highlight the clinical significance of somatic mutations as an important and often overlooked category in genetic diagnosis.

Detection of somatic mutations requires cross-validation using multiple sequencing approaches. WES enables relatively unbiased detection of variants in coding regions; however, technical limitations may introduce false positives, and its sensitivity for detecting non-coding and structural variants is relatively low. Sanger sequencing is cost-effective and convenient but has limited sensitivity for low-VAF somatic variants, which may lead to false negatives. Targeted sequencing offers high sensitivity for detecting extremely low-VAF somatic variants but is restricted to predefined genomic regions and therefore lacks unbiased coverage. Furthermore, conventional single-cell sequencing cannot simultaneously detect somatic mutations, and the sequencing read depth of full-length complementary DNA single-cell sequencing is also insufficient to detect somatic mutations. Consequently, identifying and validating somatic mutations necessitates integration and cross-validation of multiple sequencing methods. In addition, as awareness of somatic mutations in patients increases, more novel pathogenic somatic mutations are likely to be identified. It is expected that the mechanisms of pathogenicity underlying other autoinflammatory and autoimmune diseases caused by GOF mutations,[49] such as those in *RIPK1*, *PLCG1*, *PLCG2*, *IL1R1*, *ALPK1*, *CDC42*, *LYN*, and *PSTPIP1*, may also involve somatic mutations.

The identification of somatic mutations may provide valuable insights for targeted therapies (Supplementary Figure S8). The identified genes with somatic mutations are involved in the NF-κB pathway, such as *TNFAIP3* and *CARD14*, and TNF inhibitors or IL-6 inhibitors are effective therapies for these patients with somatic mutations activating the NF-κB pathway. Somatic GOF mutations in *STING1*, resulting in the activation of the type I IFN pathway, can be treated with JAK inhibitors. Somatic mutations in *NRAS* and *KRAS* activate the Ras pathway, making these cases responsive to mammalian target of rapamycin inhibitors. *NLRP3* and *NLRC4* somatic mutations result in increased activation of inflammasomes, leading to increased cleavage of caspase1, which processes more pro–IL-1β and pro–IL-18 into their active forms and drives the overproduction of proinflammatory cytokines IL-1β and IL-18. Therefore, IL-1 inhibitors are effective.[49] Thus, identifying somatic mutations is very critical for precision medicine.

In conclusion, our findings suggest that 1.2% of patients with autoinflammatory or autoimmune diseases may be misdiagnosed because of underrecognized somatic mutations. Neglecting the temporal dynamics of somatic mutation burden may compromise the efficacy of targeted therapies. Our study highlights the importance of incorporating somatic mutation analysis into genetic diagnosis and provided critical evidence that somatic mutations may account for a proportion of autoinflammatory and autoimmune diseases with undetermined genetic explanations.

ACKNOWLEDGMENTS

We thank the patients and their families for their support during this research study.

AUTHOR CONTRIBUTIONS

All authors contributed to at least one of the following manuscript preparation roles: conceptualization AND/OR methodology, software, investigation, formal analysis, data curation, visualization, and validation AND drafting or reviewing/editing the final draft. As corresponding authors, Dr Zhou, Dr Yu, Dr Z. Liu, Mr J. Yang, Dr Jianghua Chen, and Dr Song confirm that all authors have provided the final approval of the version to be published and takes responsibility for the affirmations regarding article submission (eg, not under consideration by another journal), the integrity of the data presented, and the statements regarding compliance with institutional review board/Declaration of Helsinki requirements.

REFERENCES

1. Torreggiani S, Castellan FS, Aksentijevich I, et al. Somatic mutations in autoinflammatory and autoimmune disease. Nat Rev Rheumatol 2024; 20(11):683–698. doi:https://doi.org/10.1038/s41584-024-01168-8
2. Stratton MR, Campbell PJ, Futreal PA. The cancer genome. Nature 2009;458(7239):719–724. doi:https://doi.org/10.1038/nature07943
3. Wojcik MH, Lemire G, Berger E, et al. Genome sequencing for diagnosing rare diseases. N Engl J Med 2024;390(21):1985–1997. doi: https://doi.org/10.1056/NEJMoa2314761
4. Dou Y, Gold HD, Luquette LJ, et al. Detecting somatic mutations in normal cells. Trends Genet 2018;34(7):545–557. doi:https://doi.org/10.1016/j.tig.2018.04.003
5. Cibulskis K, Lawrence MS, Carter SL, et al. Sensitive detection of somatic point mutations in impure and heterogeneous cancer samples. Nat Biotechnol 2013;31(3):213–219. doi:https://doi.org/10.1038/nbt.2514
6. Zitoun NM, Demirkaya E, Goldbach-Mansky R, et al. Time for a new approach to drug development for rare systemic autoinflammatory diseases. Nat Rev Rheumatol 2024;20(6):317–318. doi:https://doi.org/10.1038/s41584-024-01108-6
7. Conrad N, Misra S, Verbakel JY, et al. Incidence, prevalence, and co-occurrence of autoimmune disorders over time and by age, sex, and socioeconomic status: a population-based cohort study of 22 million individuals in the UK. Lancet 2023;401(10391):1878–1890. doi: https://doi.org/10.1016/S0140-6736(23)00457-9
8. Mensa-Vilaró A, Bravo García-Morato M, de la Calle-Martin O, et al. Unexpected relevant role of gene mosaicism in patients with primary immunodeficiency diseases. J Allergy Clin Immunol 2019;143(1): 359–368. doi:https://doi.org/10.1016/j.jaci.2018.09.009
9. Beck DB, Ferrada MA, Sikora KA, et al. Somatic mutations in *UBA1* and severe adult-onset autoinflammatory disease. N Engl J Med 2020; 383(27):2628–2638. doi:https://doi.org/10.1056/NEJMoa2026834
10. Tanaka N, Izawa K, Saito MK, et al. High incidence of NLRP3 somatic mosaicism in patients with chronic infantile neurologic, cutaneous, articular syndrome: results of an International Multicenter Collaborative Study. Arthritis Rheum 2011;63(11):3625–3632. doi:https://doi.org/10.1002/art.30512
11. Zhou Q, Aksentijevich I, Wood GM, et al. Brief report: cryopyrin-associated periodic syndrome caused by a myeloid-restricted somatic NLRP3 mutation. Arthritis Rheumatol 2015;67(9):2482–2486. doi:https://doi.org/10.1002/art.39190
12. Rowczenio DM, Gomes SM, Aróstegui JI, et al. Late-onset cryopyrin-associated periodic syndromes caused by somatic NLRP3 mosaicism-UK single center experience. Front Immunol 2017;8: 1410. doi:https://doi.org/10.3389/fimmu.2017.01410
13. Kawasaki Y, Oda H, Ito J, et al. Identification of a high-frequency somatic NLRC4 mutation as a cause of autoinflammation by pluripotent cell-based phenotype dissection. Arthritis Rheumatol 2017; 69(2):447–459. doi:https://doi.org/10.1002/art.39960
14. Ionescu D, Peñín-Franch A, Mensa-Vilaró A, et al. First description of late-onset autoinflammatory disease due to somatic NLRC4 mosaicism. Arthritis Rheumatol 2022;74(4):692–699. doi:https://doi.org/10.1002/art.41999
15. Wang J, Ye Q, Zheng W, et al. Low-ratio somatic NLRC4 mutation causes late-onset autoinflammatory disease. Ann Rheum Dis 2022; 81(8):1173–1178. doi:https://doi.org/10.1136/annrheumdis-2021-221708
16. Oliveira JB, Bidère N, Niemela JE, et al. NRAS mutation causes a human autoimmune lymphoproliferative syndrome. Proc Natl Acad Sci U S A 2007;104(21):8953–8958. doi:https://doi.org/10.1073/pnas.0702975104
17. Niemela JE, Lu L, Fleisher TA, et al. Somatic KRAS mutations associated with a human nonmalignant syndrome of autoimmunity and abnormal leukocyte homeostasis. Blood 2011;117(10):2883–2886. doi:https://doi.org/10.1182/blood-2010-07-295501
18. de Inocencio J, Mensa-Vilaro A, Tejada-Palacios P, et al. Somatic NOD2 mosaicism in Blau syndrome. J Allergy Clin Immunol 2015; 136(2):484–487.e2. doi:https://doi.org/10.1016/j.jaci.2014.12.1941
19. Janssen R, van Wengen A, Hoeve MA, et al. The same IkappaBalpha mutation in two related individuals leads to completely different clinical syndromes. J Exp Med 2004;200(5):559–568. doi:https://doi.org/10.1084/jem.20040773
20. Liu Y, Jesus AA, Marrero B, et al. Activated STING in a vascular and pulmonary syndrome. N Engl J Med 2014;371(6):507–518. doi: https://doi.org/10.1056/NEJMoa1312625
21. Schmitz EG, Griffith M, Griffith OL, et al. Identifying genetic errors of immunity due to mosaicism. J Exp Med 2025;222(5):e20241045. doi:https://doi.org/10.1084/jem.20241045
22. Romano AA, Allanson JE, Dahlgren J, et al. Noonan syndrome: clinical features, diagnosis, and management guidelines. Pediatrics 2010;126(4):746–759. doi:https://doi.org/10.1542/peds.2009-3207
23. Zenker M, Edouard T, Blair JC, et al. Noonan syndrome: improving recognition and diagnosis. Arch Dis Child 2022;107(12):1073–1078. doi:https://doi.org/10.1136/archdischild-2021-322858
24. Xie M, Lu C, Wang J, et al. Age-related mutations associated with clonal hematopoietic expansion and malignancies. Nat Med 2014; 20(12):1472–1478. doi:https://doi.org/10.1038/nm.3733
25. Jaiswal S, Fontanillas P, Flannick J, et al. Age-related clonal hematopoiesis associated with adverse outcomes. N Engl J Med 2014; 371(26):2488–2498. doi:https://doi.org/10.1056/NEJMoa1408617
26. Richards S, Aziz N, Bale S, et al; ACMG Laboratory Quality Assurance Committee. Standards and guidelines for the interpretation of sequence variants: a joint consensus recommendation of the American College of Medical Genetics and Genomics and the Association for Molecular Pathology. Genet Med 2015;17(5):405–424. doi: https://doi.org/10.1038/gim.2015.30
27. Dou Y, Kwon M, Rodin RE, et al. Accurate detection of mosaic variants in sequencing data without matched controls. Nat Biotechnol 2020; 38(3):314–319. doi:https://doi.org/10.1038/s41587-019-0368-8
28. Moriya K, Sasahara Y, Ohnishi H, et al. IKBA S32 mutations underlie ectodermal dysplasia with immunodeficiency and severe noninfectious systemic inflammation. J Clin Immunol 2018;38(5):543–545. doi:https://doi.org/10.1007/s10875-018-0522-y
29. Fei Y, Liu L, Ma S, et al. IRAK2 deficiency causes a new immune dysregulation disorder. medRxiv. Preprint posted online October 22, 2024. doi:https://doi.org/10.1101/2024.10.21.24315796

30. Moriya K, Nakano T, Honda Y, et al. Human RELA dominant-negative mutations underlie type I interferonopathy with autoinflammation and autoimmunity. J Exp Med 2023;220(9):e20212276. doi:https://doi.org/10.1084/jem.20212276
31. Konno H, Chinn IK, Hong D, et al. Pro-inflammation associated with a gain-of-function mutation (R284S) in the innate immune sensor STING. Cell Rep 2018;23(4):1112–1123. doi:https://doi.org/10.1016/j.celrep.2018.03.115
32. Neven Q, Boulanger C, Bruwier A, et al. Clinical spectrum of Ras-associated autoimmune leukoproliferative disorder (RALD). J Clin Immunol 2021;41(1):51–58. doi:https://doi.org/10.1007/s10875-020-00883-7
33. Zhou Q, Wang H, Schwartz DM, et al. Loss-of-function mutations in TNFAIP3 leading to A20 haploinsufficiency cause an early-onset autoinflammatory disease. Nat Genet 2016;48(1):67–73. doi:https://doi.org/10.1038/ng.3459
34. Yu MP, Xu XS, Zhou Q, et al. Haploinsufficiency of A20 (HA20): updates on the genetics, phenotype, pathogenesis and treatment. World J Pediatr 2020;16(6):575–584. doi:https://doi.org/10.1007/s12519-019-00288-6
35. Karri U, Harasimowicz M, Carpio Tumba M, et al. The complexity of being A20: from biological functions to genetic associations. J Clin Immunol 2024;44(3):76. doi:https://doi.org/10.1007/s10875-024-01681-1
36. Ma A, Malynn BA. A20: linking a complex regulator of ubiquitylation to immunity and human disease. Nat Rev Immunol 2012;12(11):774–785. doi:https://doi.org/10.1038/nri3313
37. Bigenzahn JW, Collu GM, Kartnig F, et al. LZTR1 is a regulator of RAS ubiquitination and signaling. Science 2018;362(6419):1171–1177. doi:https://doi.org/10.1126/science.aap8210
38. Steklov M, Pandolfi S, Baietti MF, et al. Mutations in LZTR1 drive human disease by dysregulating RAS ubiquitination. Science 2018;362(6419):1177–1182. doi:https://doi.org/10.1126/science.aap7607
39. Yamamoto GL, Aguena M, Gos M, et al. Rare variants in SOS2 and LZTR1 are associated with Noonan syndrome. J Med Genet 2015;52(6):413–421. doi:https://doi.org/10.1136/jmedgenet-2015-103018
40. Abelson S, Collord G, Ng SWK, et al. Prediction of acute myeloid leukaemia risk in healthy individuals. Nature 2018;559(7714):400–404. doi:https://doi.org/10.1038/s41586-018-0317-6
41. Mustjoki S, Young NS. Somatic mutations in "benign" disease. N Engl J Med 2021;384(21):2039–2052. doi:https://doi.org/10.1056/NEJMra2101920
42. Pesqué D, Mensa-Vilaró A, García-Herrera A, et al. Low-level NLRP3 somatic mosaicism in adult-onset cryopyrin-associated periodic syndrome misdiagnosed as chronic urticaria. J Allergy Clin Immunol Pract 2024;12(8):2205–2207.e2. doi:https://doi.org/10.1016/j.jaip.2024.04.049
43. De Langhe E, Van Loo S, Malengier-Devlies B, et al. *TET2*-driver and *NLRC4*-passenger variants in adult-onset autoinflammation. N Engl J Med 2023;388(17):1626–1629. doi:https://doi.org/10.1056/NEJMc2212928
44. Kadowaki T, Ohnishi H, Kawamoto N, et al. Haploinsufficiency of A20 causes autoinflammatory and autoimmune disorders. J Allergy Clin Immunol 2018;141(4):1485–1488.e11. doi:https://doi.org/10.1016/j.jaci.2017.10.039
45. Eisfeld AK, Kohlschmidt J, Mrózek K, et al. NF1 mutations are recurrent in adult acute myeloid leukemia and confer poor outcome. Leukemia 2018;32(12):2536–2545. doi:https://doi.org/10.1038/s41375-018-0147-4
46. Leardini D, Messelodi D, Muratore E, et al. Role of CBL mutations in cancer and non-malignant phenotype. Cancers (Basel) 2022;14(3):839. doi:https://doi.org/10.3390/cancers14030839
47. Gutierrez-Rodrigues F, Kusne Y, Fernandez J, et al. Spectrum of clonal hematopoiesis in VEXAS syndrome. Blood 2023;142(3):244–259. doi:https://doi.org/10.1182/blood.2022018774
48. Zhang C, Han X, Jin Y, et al. Pathogenic gene spectrum and clinical implication in Chinese patients with lupus nephritis. Clin J Am Soc Nephrol 2023;18(7):869–880. doi:https://doi.org/10.2215/CJN.0000000000000185
49. Zhang J, Lee PY, Aksentijevich I, et al. How to build a fire: the genetics of autoinflammatory diseases. Annu Rev Genet 2023;57(1):245–274. doi:https://doi.org/10.1146/annurev-genet-030123-084224

Arthritis & Rheumatology
Vol. 78, No. 9, September 2026, pp 1989–1999
DOI 10.1002/art.70097
© 2026 The Author(s). *Arthritis & Rheumatology* published by Wiley Periodicals LLC on behalf of American College of Rheumatology.
This is an open access article under the terms of the Creative Commons Attribution License, which permits use, distribution and reproduction in any medium, provided the original work is properly cited.

American College of Rheumatology
Empowering Rheumatology Professionals

Inosine-Triphosphate-Pyrophosphatase Activity as a Potential Predictor of Methotrexate Remission in Juvenile Idiopathic Arthritis

Sofia Sindici Forgiarini, MSc,[1] Marianna Lucafò, PhD,[2] Debora Curci, PhD,[3] Davide Selvestrel, PhD,[4] Valentina Moressa, MD,[3] Sofia Pagarin, PhD,[1] Barbara Bellich, PhD,[3] Martina Franzin, PhD,[3] Alberto Tommasini, MD, PhD,[1,3] Mara L. Becker, MD, MSCE,[5] Laura B. Ramsey, PhD,[6,7] Susan D. Thompson, PhD,[8] Carl D. Langefeld, PhD,[9] Federica Corba, MSc,[2] Edoardo Marrani, MD,[10] Gabriele Simonini, MD,[10] Gabriele Stocco, PhD, PharmD,[1,3] Giuliana Decorti, MD,[1] Andrea Taddio, MD,[1,3] and Serena Pastore, MD[3]

Objective. Methotrexate (MTX) is the first-line therapy for juvenile idiopathic arthritis (JIA), but up to 40% of patients do not respond to it. Low inosine triphosphate pyrophosphatase (ITPA) activity has been associated with reduced clinical remission. We investigated the role and underlying mechanisms of ITPA in vitro.

Methods. ITPA enzymatic activity was measured by high-performance liquid chromatography with ultraviolet detection in erythrocyte lysates from patients with JIA (enrolled in Trieste, Italy; Florence, Italy; and Kansas City, Missouri) receiving weekly MTX (10–15 mg/m^2) for at least 12 months. Remission was evaluated by Wallace et al criteria. *ITPA* rs1127354, which reduces enzyme activity, was genotyped. Immortalized human hepatocytes were transfected with either an *ITPA*-containing or empty plasmid to evaluate cytotoxicity (MTT), ADORA$_{2A}$ expression (quantitative polymerase chain reaction), intracellular cyclic AMP (cAMP) (enzyme-linked immunosorbent assay), PKA-Cα expression (immunoblot), and extracellular adenosine metabolites (liquid chromatography–tandem mass spectrometry).

Results. A total of 195 patients with JIA (mean age: 8 years, range: 0–22 years, 74% female participants) were enrolled. Patients reaching remission (48%) had higher ITPA activity than nonresponders during therapy and at treatment onset (meta-analysis: $P = 0.0004$ and $P = 0.007$, respectively). Predictive cutoffs for overall and onset measurements were identified: 181.9 and 177.8 nmol of inosine monophosphate per hour. None of the patients with variant *ITPA* rs1127354 achieved remission (Fisher's exact test $P = 0.0063$); however, 48% of wild-type patients failed to respond. ITPA-overexpressing cells showed elevated MTX sensitivity, cAMP levels, PKA-Cα expression, and hypoxanthine (all $P < 0.05$, two-way analysis of variance).

Conclusion. ITPA activity is a promising predictive biomarker for MTX response in JIA, outperforming *ITPA* rs1127354 genotyping. Its predictive value is evident at treatment initiation, supporting its use for personalized treatment. Mechanistically, higher enzyme activity may enhance MTX efficacy through the adenosine/inosine-ADORA$_{2A}$ pathway.

INTRODUCTION

Juvenile idiopathic arthritis (JIA) is the most common chronic rheumatic disease in childhood and is characterized predominantly by immune-mediated inflammatory arthritis with a heterogenous clinical presentation.[1,2] Low-dose methotrexate (MTX), which is highly effective both as monotherapy and in combination with biologic drugs, is a first-line therapy in JIA.[3] As a folate analog, MTX

Supported by the Italian Ministry of Health through the contribution provided to the Institute for Maternal and Child Health IRCCS Burlo Garofolo, Trieste, Italy (RC 03/12).

[1]Department of Medicine, Surgery and Health Sciences, University of Trieste, Trieste, Italy; [2]Department of Life Sciences, University of Trieste, Trieste, Italy; [3]Institute for Maternal and Child Health IRCCS Burlo Garofolo, Trieste, Italy; [4]International Centre for Genetic Engineering and Biotechnology, Trieste, Italy; [5]Department of Pediatrics, Duke University School of Medicine, Durham, North Carolina; [6]Department of Pediatrics, Children's Mercy Kansas City, Kansas City, Missouri; [7]Department of Pediatrics, University of Missouri-Kansas City; [8]Department of Pediatrics, University of Cincinnati College of Medicine, Division of Human Genetics, Cincinnati Children's Hospital Medical Center, Cincinnati, Ohio; [9]Department of Biostatistics and Data Science, Wake Forest School of Medicine, Winston-Salem, North Carolina; [10]Pediatric Rheumatology Unit Meyer Children's Hospital IRCCS, Florence, Italy.

Additional supplementary information cited in this article can be found online in the Supporting Information section (https://acrjournals.onlinelibrary.wiley.com/doi/10.1002/art.70097).

Author disclosures and graphical abstract are available at https://onlinelibrary.wiley.com/doi/10.1002/art.70097.

Address correspondence via email to Gabriele Stocco, PhD, PharmD, at stoccog@units.it.

Submitted for publication September 23, 2025; accepted in revised form February 2, 2026.

modulates pathways that involve folates, including the de novo synthesis of purines and pyrimidines by inhibition of the activities of dihydrofolate reductase (DHFR) and thymidylate synthetase.[4] However, folic acid administration does not interrupt the anti-inflammatory effect of MTX, suggesting additional mechanisms behind its action in JIA.[3]

The most widely accepted mechanism for MTX's therapeutic response in JIA is the accumulation of adenosine, mainly caused by 5-aminoimidazole-4-carboxamide ribonucleotide transformylase inhibition.[3] Extracellular adenosine subsequently binds its receptors, the ADORAs, and the consequent downstream signaling of $ADORA_{2A}$ stimulation inhibits nuclear factor κB (NF-κB), a key regulator of inflammatory responses.[3,5–7] Indeed, the administration of two adenosine receptor antagonists, caffeine and theophylline, nullifies the MTX effect in the rat adjuvant arthritis model of rheumatoid arthritis (RA).[8] Moreover, patients with RA who consume large quantities of caffeine have been shown to have reduced responsiveness to MTX.[9]

Despite MTX safety, effectiveness, and low cost, up to 40% of patients do not respond to therapy, which leads to disease progression and permanent joint damage.[10] Therefore, identifying biomarkers of MTX response is crucial to direct patients toward the optimal therapeutic option.[3] Inosine triphosphate pyrophosphatase (ITPA) activity measured during therapy is correlated with MTX response, evaluated as remission[11]: patients with low ITPA activity presented lower remission probability.[11] ITPA is an essential enzyme that preserves nucleotide homeostasis by hydrolyzing noncanonical triphosphate purine nucleotides, such as (deoxy)inosine triphosphate (ITP) and (deoxy)xantosine triphosphate, into their monophosphate derivatives.[12] Inosine monophosphate (IMP) can be converted to AMP, which can then be further converted to adenosine.[11] Therefore, the aim of this study was to evaluate the correlation of ITPA activity, measured both at the onset of MTX therapy and during treatment, with the probability of remission, expanding the previous cohort of patients.[11] Additionally, we aimed to investigate in vitro molecular mechanisms linking ITPA activity with MTX response.

MATERIALS AND METHODS

Patients and study design. Children meeting International League of Associations for Rheumatology criteria for JIA, receiving or about to start MTX for active arthritis, were enrolled from three major pediatric rheumatology hospitals (IRCCS Burlo Garofolo Children's Hospital and Meyer Children's Hospital IRCCS in Italy and Children's Mercy Hospital of Kansas City in Missouri). Eligible patients were either treatment-naïve or had not received MTX for at least 10 months before enrollment. Patients with systemic JIA or receiving concomitant biologic therapy were excluded. The study was conducted according to the Declaration of Helsinki and approved by the Regional Ethics Committee of Friuli Venezia Giulia (CEUR-2018-Em-137-BURLO, September 5th, 2018). Fully informed parental consent and child assent, when appropriate, were obtained. Demographic and clinical data, as well as venous blood samples, were collected at baseline (up to 4 weeks before treatment), at 6 months, and then every 3 months, with a minimum follow-up of 12 months. The timing of sample collection was standardized across all study participants; however, not all time points were available for every patient. Analyses using the mean of all time points were performed on available samples. For the analyses at therapy onset, patients without samples and clinical data collected before MTX initiation were excluded to minimize potential bias. Therapy onset was defined as the visit when MTX was prescribed. Weekly MTX (10–15 mg/m^2) was administered orally or subcutaneously. Clinical remission was defined according to Wallace et al criteria[13] as a continuous six-month period of clinically inactive disease (CID) while on MTX therapy, beginning within one year of starting therapy. CID was defined as absence of joints with active disease, systemic symptoms, and uveitis; erythrocyte sedimentation rate and/or C-reactive protein within normal range (if both were tested); physician's global assessment at the best score; and morning stiffness less than 15 minutes. During this period, patients received no other drugs (biologics, nonsteroidal anti-inflammatory drugs, oral or intra-articular steroids). Race information was obtained from medical records or self-reported using standard categories.

Measurement of ITPA activity. ITPA activity was measured in erythrocyte lysates by quantifying IMP, the ITP hydrolysis product, using high-performance liquid chromatography (HPLC) with ultraviolet (UV) detection (Agilent 1200 HPLC with UV detector, Agilent Technologies, Milan, Italy), as previously reported.[14] The detailed protocol is in the Supplementary Material.

Genotyping of *ITPA* rs1127354. Total genomic DNA was extracted from peripheral blood by a commercial kit (Sigma-Aldrich, Milan, Italy) and stored at –20°C. Genotyping used a TaqMan assay (identification: C_16218146_10, Applied Biosystems, Foster City, California).[11,14]

Immortalized cell lines and cell culture. The immortalized human hepatic IHH cell line was stably transfected with pCMV6 plasmid vectors, empty (IHH MOCK) or containing the *ITPA* complementary DNA (cDNA) sequence (IHH ITPA).[15] IHH cell lines were maintained as described in the Supplementary Material.

MTT cytotoxicity test. To evaluate the cytotoxicity of MTX on cell lines, the 3-(4,5-dimethylthiazol-2-yl)-2,5-diphenyltetrazolium bromide (MTT) assay was performed. IHH MOCK and ITPA cells were seeded at 5 × 10^3 cells/well in 96-well plates and exposed to six MTX concentrations (3.125 nM, 25 nM, 200 nM, 600 nM, and 200 μM) in DMEM-HG for 72 hours. Details are provided in the Supplementary Material.

Total RNA isolation and reverse transcription. Total RNA was extracted from IHH MOCK and IHH ITPA cell lines using TRIzol reagent (Thermo Scientific, Carlsbad, California) and the PureLink RNA Mini kit (Thermo Fisher Scientific, Milan, Italy). Concentration and purity were determined by NanoDrop 2000 (EuroClone, Milan, Italy). Reverse transcription was conducted with the High-Capacity RNA-to-cDNA Kit (Applied Biosystem, Foster City, California).

Quantitative real-time polymerase chain reaction. $ADORA_{2A}$ expression was evaluated by SYBR green-based real-time polymerase chain reaction (RT-PCR) using the CFX96TM RealTime Detection System-C1000 Thermal Cycler (Bio-Rad Laboratories, Hercules, California). Real-time PCR, performed in triplicate, used KiCqStart SYBR Green qPCR ReadyMix (Sigma-Aldrich, Milan, Italy) and gene-specific forward and reverse primers (Sigma-Aldrich, Milan, Italy). Thermal cycling conditions were set as described in the Supplementary Material.

Intracellular levels of cyclic AMP. Intracellular cyclic AMP (cAMP) levels were assessed with the cyclic AMP enzyme-linked immunosorbent assay kit (Cayman Chemical, Ann Arbor, Michigan). IHH MOCK and IHH ITPA cells, seeded in six-well plates at densities of 7.5×10^5 cells/well for the 24-hour treatment and 4.8×10^5 cells/well for the 48-hour one, were exposed to MTX (25 nM, 200 nM). cAMP concentrations, normalized to total protein content, were expressed as a percentage relative to untreated cells.

Western blot analysis. Cells, seeded in six-well plates at densities of 7.5×10^5, 4.8×10^5, and 3.3×10^5 cells/well for 24-, 48-, and 72-hour treatments, respectively, were exposed to MTX (25 nM, 200 nM). Protocol details, including lysis procedures, are provided in the Supplementary Material.

Quantification of adenosine, inosine, hypoxanthine and uric acid in cell supernatants through LC-MS/MS. Cells, seeded in 24-well plates at a density of 1.6×10^5 cells/well, were treated for 48 hours with 25 and 200 nM of MTX. To preserve adenosine levels at the end of the treatment, a stop solution (see the Supplementary Material) was added 30 minutes before the end of incubation. Cell supernatants were collected, filtered using Amicon Ultra centrifugal filters, MWCO 10 kDa (Millipore, Milan, Italy), and stored at −80°C. Supernatants were thawed immediately before LC-MS/MS analysis and analyzed by Ultra-High-Pressure Liquid Chromatography Vanquish Neo UHPLC instrument (Thermo Fisher Scientific, Milan, Italy) coupled with mass spectrometry Exploris 240 (Thermo Fisher Scientific, Milan, Italy). Chromatographic separation and mass spectrometry acquisition followed the Supplementary Material protocol.

Statistical analysis. Analyses were performed using GraphPad Prism and R (v3.6.1–4.5.0). ITPA activity differences across clinical sites were assessed by the Kruskal-Wallis test with Dunn's post-hoc test (Bonferroni corrected). Sex associations were evaluated by logistic regression (clinical remission) and the Wilcoxon rank-sum test (ITPA activity). Remission–ITPA activity association was tested by logistic regression, adjusting for clinical site via multivariate models and meta-analysis (weighted Z-method). Longitudinal ITPA activity changes were assessed by linear mixed-effects models with random intercepts (patient, site). The role of clinical site on remission was tested via likelihood ratio test. Receiver operating characteristic (ROC) curve analysis (minimum distance to [0,1]) identified ITPA thresholds predictive of remission. ITPA activity was compared across rs1127354 genotypes and between wild-type (WT) patients (remission vs nonremission) using the Wilcoxon test. Genotype–remission association was tested by Fisher's exact test with Haldane–Anscombe correction. In vitro data were analyzed by two-way analysis of variance (ANOVA) with Sidak's test. ITPA activity is expressed as mean ± SD. Data from all other experiments are shown as mean ± SEM; $P < 0.05$ was considered significant. In vitro assays were based on at least three biologic replicates. The data analyzed for the current study are available from the corresponding author on reasonable request.

RESULTS

Patients enrolled and clinical remission. Demographic and clinical data of 195 patients with JIA, treated with MTX between 2000 and 2022, are reported in Table 1. A total of 134 patients were enrolled in Italy (112 in Trieste at IRCCS Burlo Garofolo and 22 in Florence at IRCCS Meyer) and 61 in the United States (in Kansas City, Missouri, at Children's Mercy). Clinical remission was achieved by 48% of patients (93 of 195). Although 74% of patients were female, sex was not significantly associated with either clinical remission (logistic regression: $P = 0.55$) or ITPA activity (Wilcoxon rank-sum test: $P = 0.60$). Racial information was collected for 176 of 195 patients; for the remaining 19 patients this information was not available.

Clinical remission and ITPA activity. The association of ITPA activity with remission was evaluated considering all time points during therapy and only the measurement at therapy onset. The all-time points analysis included all 195 patients, whereas the baseline-only analysis involved 97 patients with JIA (43 from Trieste, 18 from Florence, and 36 from Kansas City) because samples at therapy onset were not available for the remaining patients.

A significant association was observed between ITPA activity and clinical remission when considering all time points (logistic regression: $P = 0.0012$, odds ratio [OR] = 1.01, 95% confidence interval [CI] 1.002–1.009), as well as when ITPA activity was

Table 1. Patients' demographic and clinical data*

Characteristic	Overall	Remission	No remission
Number of cases, N/n (%)	195	93 (48)	102 (52)
Female, n (%)	145 (74)	71	74
Male, n (%)	50 (26)	22	28
White, n (%)	176 (90)		
Unknown, n (%)	19 (10)		
JIA subtypes at the beginning of therapy with MTX, n (%)			
Oligoarticular persistent	97 (50)	53	44
Oligoarticular extended	8 (4)	1	7
Polyarticular RF –	65 (33)	28	37
Polyarticular RF +	8 (4)	2	6
Enthesitis related arthritis	9 (5)	6	3
Psoriatic	7 (4)	2	5
Undifferentiated	1 (0.5)	1	0
Age at the start of MTX, mean and range, y	8, 0–22	6, 0–22	10, 0–21

* JIA, juvenile idiopathic arthritis; MTX, methotrexate; RF, rheumatoid factor.

measured at therapy onset alone (logistic regression: $P = 0.01$, OR = 1.01, 95% CI 1.002–1.011). A likelihood ratio test did not show a significant effect of the clinical site on remission (all time points: $P = 0.57$, therapy onset: $P = 0.25$).

A significant difference in ITPA activity emerged among clinical sites, both when considering all measurements during therapy and only those at therapy onset (all measurements: Kruskal-Wallis test $P = 4.62 \times 10^{-5}$, therapy onset: Kruskal-Wallis test $P = 0.025$). In particular, patients at the IRCCS Burlo Garofolo in Trieste showed lower activity than those from the other hospitals when all time points are considered (Dunn's post test with Bonferroni correction: Trieste vs Florence $P = 2.0 \times 10^{-4}$, Trieste vs Kansas City $P = 3.0 \times 10^{-3}$) (See Supplementary Figure 1). A significant difference was also observed when considering only the measurements at therapy onset (Dunn's post test with Bonferroni correction: Trieste vs Florence $P = 5.4 \times 10^{-3}$, Trieste vs Kansas City $P = 3.1 \times 10^{-3}$) (see Supplementary Figure 2).

Despite these differences, the association between ITPA activity and remission remained significant for overall measurements during treatment after adjustment for clinical site (logistic regression: $P = 0.0006$; meta-analysis: $P = 0.0004$) and was also confirmed for those at therapy onset (logistic regression: $P = 0.003$; meta-analysis: $P = 0.007$). In detail, patients with JIA who reached remission had higher ITPA activity than those who did not, both for all time points (212.1 ± 90.8 vs 169.6 ± 81.5 nmol IMP/h) (Figure 1A) and for the therapy onset (232.4 ± 92.0 vs 183.7 ± 84.3 nmol IMP/h) (Figure 1B). Supplementary Tables 1 and 2 summarize ITPA activity stratified by clinical site, including number of patients per group, mean ITPA activity for remission and nonremission groups, logistic regression P values, OR, and 95% CI.

ITPA activity was not significantly different between therapy onset and subsequent treatment time points (203.3 ± 91.7 vs 193.30 ± 98.5 nmol IMP/h, linear mixed-effects model with random intercepts for patient and clinical site: $P = 0.38$) (Supplementary Figure 3). Considering only those patients who achieved remission, there was no significant difference between ITPA activity at onset and during therapy (229.8 ± 94.8 vs 211.9 ± 106.4 nmol IMP/h, same model: $P = 0.65$) (Supplementary Figure 4).

Potential cutoffs of ITPA activity for remission. ROC curve analysis was used to define a cutoff value of ITPA activity to discriminate between patients achieving remission and those who did not. For all time points, the calculated cutoff was 181.9 nmol IMP/h, yielding a sensitivity of 60% and a specificity of 63% (Figure 1C). Specifically, 60% (56 of 94) of patients above the determined cutoff achieved clinical remission, compared with 37% (37 of 101) of those below the threshold.

For the therapy onset, the calculated cutoff was 177.8 nmol IMP/h, corresponding to a sensitivity of 67% and a specificity of 58% (Figure 1D). Specifically, 55% (28 of 51) of patients above the determined cutoff achieved clinical remission, compared with 30% (14 of 46) of those below the threshold.

Clinical remission and genotyping. *ITPA* rs1127354 was genotyped in 129 patients with JIA. Five patients from the Italian cohort and the American cohort were excluded because of lack of available DNA. In the analyzed cohort, the polymorphism was in the Hardy–Weinberg equilibrium, and its frequency agrees with its distribution in the White population, with minor allele frequency of 3.9%. In detail, 8 of 129 patients with JIA carried the variant. As shown in Figure 1E, ITPA activity was higher in WT patients compared with those carrying the variant (Wilcoxon rank-sum test: $P = 6.2 \times 10^{6}$, 186.0 ± 73.6 vs 58.2 ± 40.1 nmol IMP/h).

None of the patients with the variant reached clinical remission (Fisher's exact test $P = 0.0063$, corrected OR = 18.45, 95% CI 1.04–326.82). In contrast, 63 WT patients (52%) achieved remission. Among WT patients, ITPA activity was still associated with a greater likelihood of achieving remission (Wilcoxon rank-sum test, $P = 0.044$).

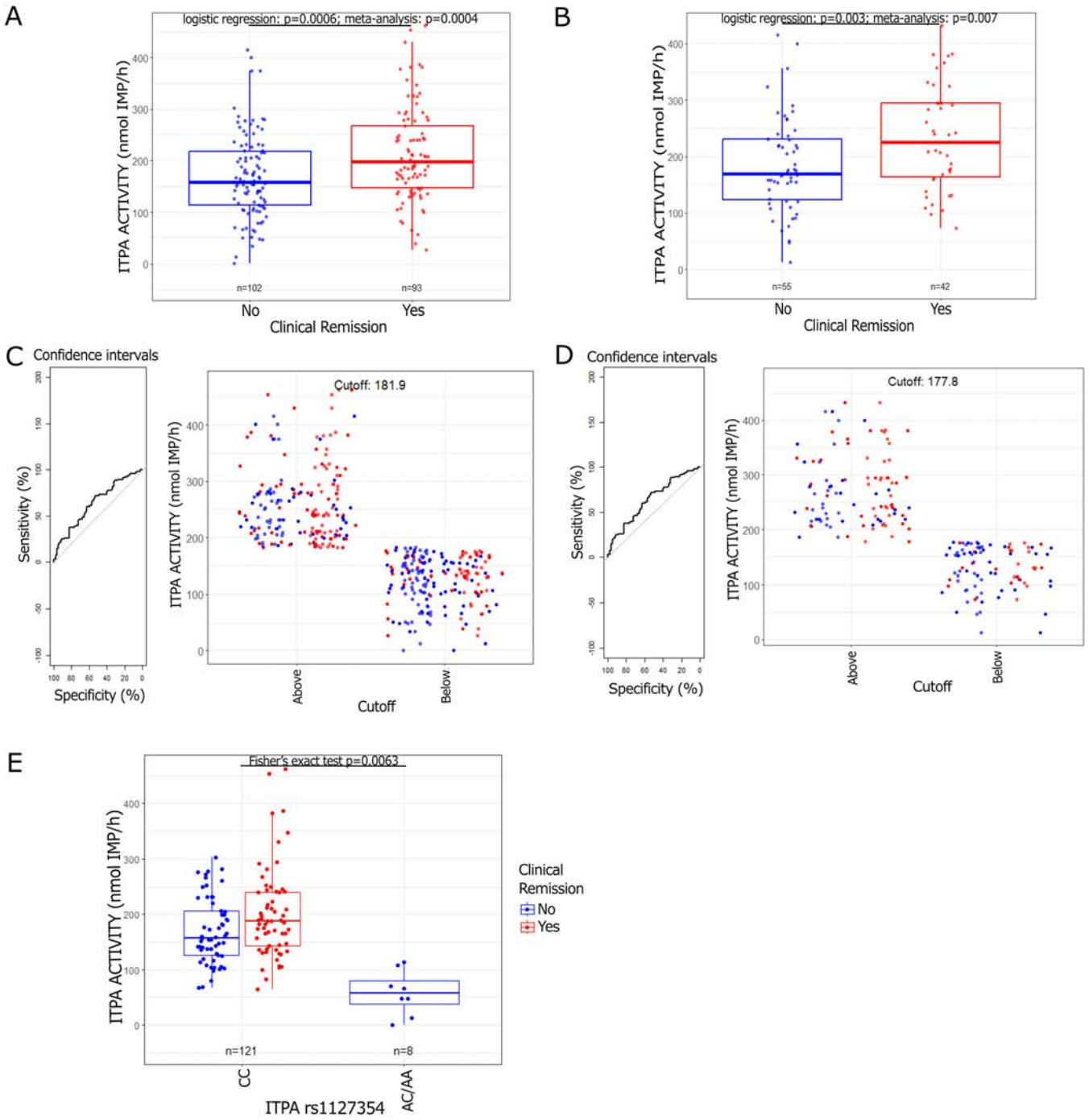

Figure 1. ITPA activity in patients with JIA, considering their clinical remission. (A) Boxplots showing mean ITPA activity at all time points during therapy, comparing patients who did not achieve remission with those who did. (B) Boxplots showing mean ITPA activity at therapy onset, comparing patients who did not achieve remission with those who did. (C) ROC curve and boxplot for ITPA activity measured during therapy. Patients with JIA are stratified by the predictive cutoff of 181.9 nmol IMP/h, displaying their remission status. (D) ROC curve and boxplot for ITPA activity measured at therapy onset. Patients with JIA are stratified by the predictive cutoff of 177.8 nmol IMP/h, displaying their remission status. (E) Boxplot showing ITPA activity during treatment and clinical remission status for rs1127354 genotype (WT vs patients carrying the variant) in patients with JIA. Panels were created using Inkscape. IMP, inosine monophosphate; ITPA, inosine triphosphate pyrophosphatase; JIA, juvenile idiopathic arthritis; ROC, receiver operating characteristic; WT, wild-type.

Role of ITPA overexpression in modulating MTX sensitivity in IHH cells. To investigate the mechanisms underlying the differential response to MTX therapy between patients with JIA with high and low ITPA activity, IHH cells overexpressing ITPA (RE ($2^{-\Delta\Delta Ct}$) ± SEM: 18.94 ± 5.17) and the MOCK control were treated with a range of MTX concentrations, and MTT assay

was performed to compare cytotoxicity in the two cell lines. ITPA activity in IHH ITPA and IHH MOCK cell lines is shown in Supplementary Figure 5. As shown in Figure 2A, after 72 hours of treatment, ITPA-overexpressing cells were more sensitive to MTX (25 nM, 200 nM, 600 nM) than MOCK cells (IC_{50} MOCK ± SEM: 35.6 ± 72.4 nM, IC_{50} ITPA ± SEM: 7.2 ± 5.39 nM).

Elevated intracellular cAMP levels and PKA C-α expression in ITPA-overexpressing cells. MTX concentrations for subsequent experiments were selected among those showing statistical significance in cytotoxicity assay and approximating in vivo patient levels. ITPA, by hydrolyzing ITP into IMP, which is subsequently converted to AMP, could enhance AMP-to-adenosine conversion. Therefore, considering the potential influence of ITPA activity on adenosine levels and subsequent $ADORA_{2A}$-mediated signaling, we first assessed the expression of $ADORA_{2A}$ under basal conditions in both cell lines (IHH ITPA $RE^{-2\Delta Ct}$: 0.0059 ± 0.00044, IHH MOCK $RE^{-2\Delta Ct}$: 0.0056 ± 0.00088, Welch's *t*-test $P = 0.76$). Given that $ADORA_{2A}$ activation increases intracellular cAMP and subsequently activates protein kinase A (PKA), we measured cAMP levels after MTX treatment. Although no differences in cAMP levels were observed after 24 hours of treatment, intracellular cAMP levels were higher in IHH ITPA than in the MOCK cell line at both concentrations of MTX after 48 hours (Figure 2B and C).

Based on elevated intracellular cAMP levels, the expression of the catalytic subunit Cα (PKA-Cα) was measured to evaluate potential modulation of the PKA pathway. As shown in Figure 2D–E, no changes were observed after 24 and 48 hours. However, IHH ITPA exhibited higher PKA-Cα expression after 72-hour treatment with 25 nM and 200 nM MTX (Figure 2F).

Phosphorylated p65 in IHH ITPA and MOCK cell lines. Considering the role of NF-κB in regulating cell proliferation and inflammation, Western blot analyses were performed to assess phosphorylated p65, a subunit of NF-κB, following MTX treatment. After 24 and 48 hours of MTX treatment, no statistically significant differences in phosphorylated p65 were observed at the tested concentrations (Figure 2G–H). Nonetheless, after 72 hours, IHH MOCK cells showed higher levels of phosphorylated p65 compared with IHH ITPA cells treated with the same concentrations of MTX (Figure 2I).

Adenosine, inosine, hypoxanthine, and uric acid quantification in cell supernatant by LC-MS/MS. To quantify adenosine released by the two cell lines, cell supernatants were analyzed through LC-MS/MS. After 48 hours of treatment, analysis showed IHH MOCK cells had higher extracellular adenosine levels than IHH ITPA at 200 nM MTX (Figure 2L).

Because adenosine is rapidly converted into inosine and subsequently degraded to hypoxanthine and then uric acid, these metabolites were also measured. IHH ITPA cells exhibited significantly higher hypoxanthine levels compared with MOCK at all conditions (Figure 2N), whereas no significant differences were observed in inosine and uric acid concentrations (Figure 2M–O).

DISCUSSION

We analyzed data from 195 patients with JIA treated with MTX to further characterize the relationship between ITPA activity and clinical remission. Remission frequency was similar to those reported in literature.[16,17]

Inter-site differences in ITPA activity are consistent with previous multicenter pharmacogenetic studies, in which changes often reflect population stratification and varying genetic backgrounds of the recruited cohorts.[18] To account for this variability, all subsequent analyses were adjusted for study site as a covariate, following established recommendations.[19]

Consistent with literature,[11] patients with JIA with low ITPA activity had a lower probability of reaching clinical remission than those with higher activity. ITPA activity correlates with treatment response even when measured before MTX treatment. To our knowledge, this is the first study demonstrating the clinical use of measuring ITPA activity before MTX start. Based on these findings, we identified thresholds that may help divide responders and nonresponders. Despite moderate sensitivity and specificity, both thresholds support the potential predictive value of ITPA activity. However, integration with other biomarkers or clinical factors may be necessary for clinical usefulness.

To investigate inter-individual differences in ITPA activity, *ITPA* rs1127354 SNP, a nonsynonymous variant previously associated with reduced enzymatic activity, was genotyped.[20,21] Consistent with previous findings,[14] ITPA activity was higher in WT patients with JIA than in those carrying the variant allele. Indeed, P32T mutation alters the enzyme's structure, resulting in a reduced activity.[22] None of the variant allele carriers achieved clinical remission, suggesting a strong association between rs1127354 genotype and remission. Similar findings were reported in a Dutch cohort, in which WT patients showed a better response.[23] However, 48% of WT patients also did not reach remission. Among WT patients, those with higher ITPA activity had a higher probability of remission. These results suggest that both rs1127354 genotype and ITPA activity influence remission likelihood, highlighting ITPA activity as a potentially stronger predictor than genotyping alone.

IHH cells were selected to investigate mechanisms underlying the clinical observations primarily for their nontumoral phenotype and high transfection efficiency. The use of a hepatocyte cell line is consistent with a previous study using HepG2 to investigate the interaction between methylenetetrahydrofolate reductase function and MTX treatment.[24]

The increased cytotoxicity observed in ITPA-overexpressing cells is in line with our hypothesis that enhanced ITP to IMP conversion by ITPA may feed into adenosine synthesis pathways

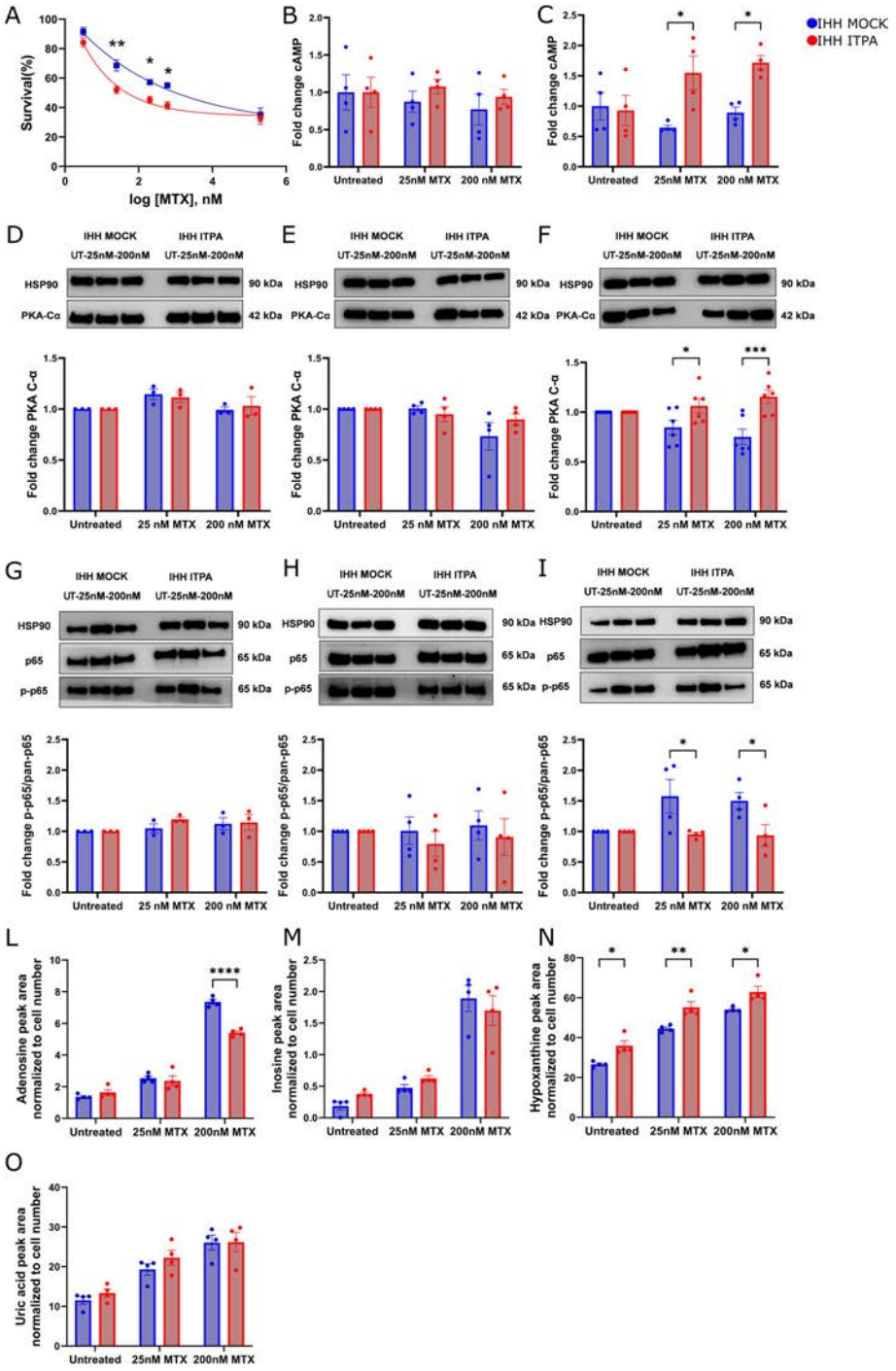

Figure 2. MTX cytotoxic and molecular effects treatment on IHH MOCK and ITPA cell lines. Western blot analyses were normalized to HSP90; fold change was calculated relative to the corresponding untreated condition. Data (mean ± SEM) were analyzed by two-way ANOVA with Sidak's post-test (* = $P < 0.05$, ** = $P < 0.01$, *** = $P < 0.0001$, **** = $P < 0.0001$). (A) Cytotoxic effects of 72-hour MTX treatment (n = 3) (IHH ITPA vs IHH MOCK at 3.125, 25, 200, 600, 200 μM). (B) and (C) cAMP levels after 24 (n = 4) and 48 (n = 4) hours of MTX treatment (25 nM, 200 nM) (IHH ITPA vs IHH MOCK at 0, 25, 200 nM). (D–F) PKA-Cα expression after 24 (n = 3), 48 (n = 4) and 72 (n = 6) hours of treatment in cell lysates from untreated (NT) and MTX-treated (25 nM, 200 nM) cells (IHH ITPA vs IHH MOCK at 0, 25, 200 nM). (G–I) Phosphorylated form of p65-NF-κB after 24 (n = 3), 48 (n = 4), and 72 (n = 3) hours of MTX treatment in cell lysates from untreated (NT) and MTX-treated (25 nM, 200 nM) cells (IHH ITPA vs IHH MOCK at 0, 25, 200 nM) (L–O) LC-MS/MS quantification of adenosine, inosine, hypoxanthine, and uric acid in the supernatant after 48-hour MTX (n = 3) (IHH ITPA vs IHH MOCK at 0, 25, 200 nM). Panels were created using Inkscape. ANOVA, analysis of variance; cAMP, cyclic adenosine monophosphate; HSP90, heat shock protein 90; IHH, immortalized human hepatocyte; ITPA, inosine triphosphate pyrophosphatase; LC-MS/MS, liquid chromatography–tandem mass spectrometry; MOCK, mock-transfected control; MTX, methotrexate; NF-κB, nuclear factor-κB; UT, untreated; p65-NF-κB, p65 subunit of nuclear factor-κB; PKA-Cα, protein kinase A catalytic subunit α. Color figure can be viewed in the online issue, which is available at http://onlinelibrary.wiley.com/doi/10.1002/art.70097/abstract.

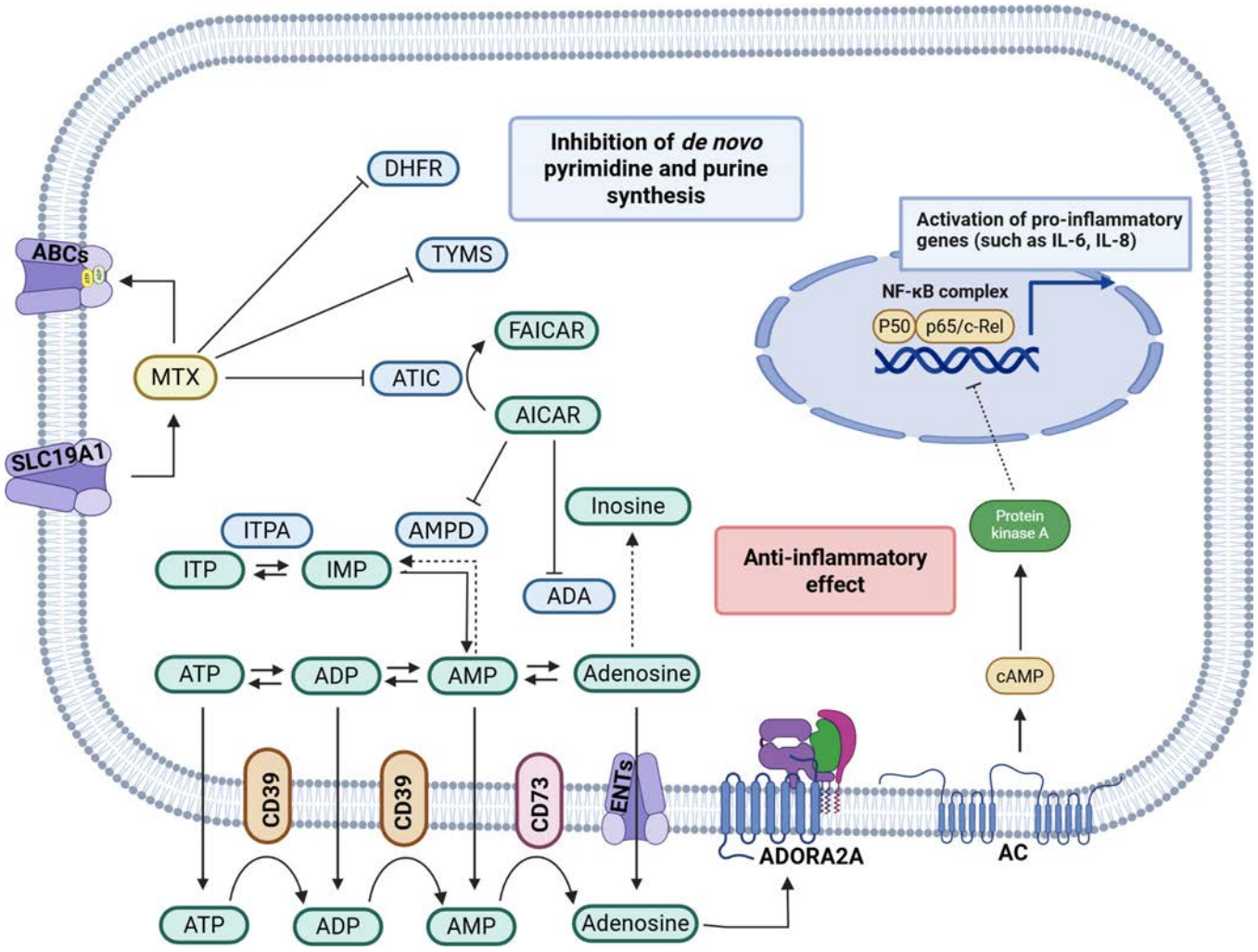

Figure 3. MTX is transported into the intracellular space by SLC19A1, whereas ABCs regulate its efflux. Intracellularly, MTX inhibits DHFR and TYMS, interfering with de novo pyrimidine and purine synthesis, and inhibits ATIC, promoting adenosine release. Specifically, AICAR accumulation, resulting from MTX interference with FAICAR formation, leads to the inhibition of ADA and AMPD. This blocks both adenosine degradation to inosine and AMP conversion to IMP. Moreover, ITPA-mediated conversion of ITP to IMP could enhance AMP formation. AMP is also produced by the dephosphorylation of ATP and ADP, further increasing adenosine levels, which are transported extracellularly by ENTs. Adenosine nucleotides are also transported extracellularly, where they are converted sequentially to adenosine by CD39 and CD73. Extracellular adenosine binds to $ADORA_{2A}$, activating adenylate cyclase, increasing cAMP, and subsequently activating PKA. PKA exerts an inhibitory effect on the nuclear NF-κB complex, preventing the transcription of pro-inflammatory genes (Created with BioRender.com). $ADORA_{2A}$, adenosine A_2A receptor; ABC, ATP-binding cassette transporter; ADA, adenosine deaminase; ADP, adenosine diphosphate; $ADORA_{2A}$, adenosine A_2A receptor; AICAR, 5-aminoimidazole-4-carboxamide ribonucleotide; AMPD, AMP deaminase; ATIC, 5-Aminoimidazole-4-carboxamide ribonucleotide transformylase; CD39, ectonucleoside triphosphate diphosphohydrolase-1; CD73, ecto-5′-nucleotidase; DHFR, dihydrofolate reductase; ENTs, equilibrative nucleoside transporters; FAICAR, 5-formamidoimidazole-4-carboxamide ribonucleotide; IMP, inosine monophosphate; ITP, inosine triphosphate; ITPA, inosine-triphosphate-pyrophosphatase; MTX, methotrexate; NF-κB, nuclear factor-κB; PKA, protein kinase A; SLC19A1, folate transporter 1; TYMS, thymidylate synthase. Color figure can be viewed in the online issue, which is available at http://onlinelibrary.wiley.com/doi/10.1002/art.70097/abstract.

because IMP can be converted to AMP and subsequently to adenosine.[11,25] This could provide a direct molecular link between ITPA enzymatic function and MTX's established anti-inflammatory mechanism through adenosine accumulation. Subsequent experiments used MTX at 25 nM and 200 nM, selected among those that showed significance in the cytotoxicity assay because they better represent levels typically reached in vivo after oral administration.[26,27] These concentrations were selected to represent physiologically relevant exposure ranges observed in vivo rather than to mimic a specific post-dose time point.

After intracellular accumulation, adenosine is transported extracellularly by the equilibrative nucleoside transporters (ENTs) and binds to ADORA receptors, mainly $ADORA_{2A}$, mediating anti-inflammatory effects by increasing cAMP and activating PKA, which modulates NF-κB activity, a key regulator of inflammatory responses (Figure 3).[3–6,28–31] Consistent with previous

studies,[32] the observed increase in intracellular cAMP and PKA-Cα levels in IHH ITPA cells may result from the interaction of adenosine with $ADORA_{2A}$ receptors.

Extracellular adenosine can also be generated via sequential dephosphorylation of ATP, adenosine diphosphate, and AMP by ectoenzymes ectonucleoside triphosphate phosphohydrolase (CD39) and ecto-5′nucleotidase (CD73) at the cell surface. In RA, both enzymes have emerged as key markers of MTX effect. Although CD73 expression is restored by MTX treatment, contributing to its anti-inflammatory action, low CD39 density on Treg cells predicts MTX nonresponse before treatment initiation.[3,33] Although reported primarily in RA, these findings support a shared adenosine-mediated anti-inflammatory mechanism of MTX. In this context, we suggest ITPA activity as an additional intracellular determinant of adenosine availability, potentially acting in parallel with extracellular nucleotide catabolism.

Given the key role of NF-κB in modulating the inflammatory responses,[34] we evaluated total and phosphorylated p65 protein expression. The higher activation of p65 may underlie the reduced MTX cytotoxicity in the IHH MOCK cell line, consistent with the role of NF-κB in apoptosis and cell survival.[34,35] Moreover, these findings align both with previous observations in patients with JIA[11] and in the present cohort, in which higher ITPA activity has been associated with an increased likelihood of achieving clinical remission.

Because phosphorylated p65 is not sufficient to confirm NF-κB activation, investigating the nuclear translocation of the subunit will be essential to obtain a more accurate measurement of the complex activity. Nevertheless, although NF-κB nuclear translocation primarily depends on degradation of the inhibitor of κB, the observed increase in p65 Ser536 phosphorylation, often associated with enhanced transcriptional activity,[36,37] strongly indicates the complex activation.

Although analysis showed increased adenosine levels in IHH MOCK cells supernatant after the highest MTX concentration, hypoxanthine resulted in elevated IHH ITPA under all conditions, including untreated cells. Following MTX-induced intracellular accumulation, adenosine is transported extracellularly via ENTs and rapidly metabolized to inosine by membrane-associated adenosine deaminase (ecto–adenosine deaminase), then to hypoxanthine by purine nucleoside phosphorylase, and further metabolized to uric acid by xanthine oxidase.[3,38–42] Because the stop solution was added 30 minutes before the end of the incubation, the already released adenosine could have been metabolized to inosine and subsequently to hypoxanthine, suggesting a faster and greater release of adenosine by IHH ITPA cells, followed by its degradation.

However, increased hypoxanthine might also result from the conversion of inosine metabolized from IMP, the product of ITP conversion by ITPA, which can be converted to AMP or degraded to inosine.[25,43] Because inosine is an anti-inflammatory in different disease models, it might underlie the differences between the two cell lines. Indeed, a study on a human epithelial cell line demonstrated that inosine suppressed interleukin-8 production, and several studies demonstrated its ability to decrease tumor necrosis factor-α in vitro and in vivo.[44–46] Inosine acts both independently and via ADORA receptors, especially $ADORA_{2A}$.[45,47] Its affinity for $ADORA_{2A}$ may explain the results obtained in IHH ITPA cells because the binding of inosine may activate anti-inflammatory signaling pathways similar to those induced by adenosine.

In a murine pleurisy model, adenosine and inosine at subeffective doses showed a synergistic anti-inflammatory effect, reducing leukocyte migration and neutrophil infiltration, probably through $ADORA_{2A}$ and $ADORA_{2B}$ receptors.[48] Thus, inosine and adenosine might act synergistically in IHH ITPA cells, potentially reflecting what happens in patients with JIA with high ITPA activity.

Beyond the adenosine/inosine-related pathway, other explanations warrant consideration. An alternative hypothesis is that ITPA activity influences MTX response through ITP-MTX competition for folylpolyglutamate synthetase.[49,50] Specifically, low ITPA activity leads to ITP accumulation, potentially interfering with MTX polyglutamate formation, reducing intracellular active MTX metabolites and diminishing therapeutic efficacy. Conversely, high ITPA activity would efficiently clear ITP, removing this competitive inhibition, allowing optimal MTX polyglutamation, enhancing target enzymes inhibition, and improving therapeutic outcomes. This alternative mechanism provides a plausible biochemical explanation for our clinical observations.

Although the findings are promising, there are several limitations that should be considered. These include a relatively small sample size and single ancestry cohort considered to calculate ITPA activity cutoffs, with no replication cohort currently available. Additionally, the lack of racial diversity among patients may limit the generalizability of the findings. Increasing patient numbers in future studies could help find a more reliable cutoff. Despite sensitivity and specificity limitations, this is the first study to define cutoffs for ITPA activity in JIA, representing a crucial step toward translating this biomarker into clinical practice. Moreover, our study did not investigate the correlation between MTX polyglutamate levels and ITPA activity, which represents a limitation in establishing the mechanistic basis for the clinical findings.

In vitro limitations include the limited number of biologic replicates and the use of a hepatocyte cell line, which does not fully represent the cell types involved in the pathophysiology of the disease. The aim was to explore the molecular mechanisms associated with ITPA activity independently of the disease context, and this model provided a controlled system to isolate the effects of the different ITPA activity on MTX response. Repeating these experiments in a disease-representative cell model will help confirm the observed differences and clarify their impact in JIA.

Single-time point adenosine measurement limits the understanding of its dynamic metabolism. Future studies considering

multiple time points would provide a more comprehensive understanding of adenosine and inosine anti-inflammatory effects, as well as treatment with these metabolites to clarify their individual roles in modulating the anti-inflammatory effect. The use of selective antagonists could validate $ADORA_{2A}$ involvement.

In conclusion, the present study proposes ITPA activity as a new therapeutic tool for personalizing JIA treatment. Our findings suggest that patients with low ITPA activity, at baseline or during treatment, may be assigned to a more aggressive therapy, such as the early initiation of biologic drug. This approach could optimize treatment response and reduce the risk of disease progression and permanent joint damage.

ACKNOWLEDGMENTS

We thank Luca Messineo for his valuable support during the early phases of the in vitro experiments. Open access publishing facilitated by Universita degli Studi di Trieste, as part of the Wiley - CRUI-CARE agreement.

AUTHOR CONTRIBUTIONS

All authors contributed to at least one of the following manuscript preparation roles: conceptualization AND/OR methodology, software, investigation, formal analysis, data curation, visualization, and validation AND drafting or reviewing/editing the final draft. As corresponding author, Dr Stocco confirms that all authors have provided the final approval of the version to be published and takes responsibility for the affirmations regarding article submission (eg, not under consideration by another journal), the integrity of the data presented, and the statements regarding compliance with institutional review board/Declaration of Helsinki requirements.

REFERENCES

1. McCurdy D, Parsa MF. Updates in juvenile idiopathic arthritis. Adv Pediatr 2021;68:143–170. doi:https://doi.org/10.1016/j.yapd.2021.05.014
2. Ravelli A, Martini A. Juvenile idiopathic arthritis. Lancet 2007;369(9563):767–778. doi:https://doi.org/10.1016/S0140-6736(07)60363-8
3. Cronstein BN, Aune TM. Methotrexate and its mechanisms of action in inflammatory arthritis. Nat Rev Rheumatol 2020;16(3):145–154. doi:https://doi.org/10.1038/s41584-020-0373-9
4. Brown PM, Pratt AG, Isaacs JD. Mechanism of action of methotrexate in rheumatoid arthritis, and the search for biomarkers. Nat Rev Rheumatol 2016;12(12):731–742. doi:https://doi.org/10.1038/nrrheum.2016.175
5. Vincenzi F, Padovan M, Targa M, et al. A(2A) adenosine receptors are differentially modulated by pharmacological treatments in rheumatoid arthritis patients and their stimulation ameliorates adjuvant-induced arthritis in rats. PLoS One 2013;8(1):e54195. doi:https://doi.org/10.1371/journal.pone.0054195
6. Minguet S, Huber M, Rosenkranz L, et al. Adenosine and cAMP are potent inhibitors of the NF-kappa B pathway downstream of immunoreceptors. Eur J Immunol 2005;35(1):31–41. doi:https://doi.org/10.1002/eji.200425524
7. Csóka B, Haskó G. Adenosine, inflammation pathways and therapeutic challenges. Joint Bone Spine 2011;78(1):4–6. doi:https://doi.org/10.1016/j.jbspin.2010.08.010
8. Montesinos MC, Yap JS, Desai A, et al. Reversal of the antiinflammatory effects of methotrexate by the nonselective adenosine receptor antagonists theophylline and caffeine: evidence that the antiinflammatory effects of methotrexate are mediated via multiple adenosine receptors in rat adjuvant arthritis. Arthritis Rheum 2000;43(3):656–663. doi:https://doi.org/10.1002/1529-0131(200003)43:3<656:AID-ANR23>3.0.CO;2-H
9. Nesher G, Mates M, Zevin S. Effect of caffeine consumption on efficacy of methotrexate in rheumatoid arthritis. Arthritis Rheum 2003;48(2):571–572. doi:https://doi.org/10.1002/art.10766
10. Bava C, Mongelli F, Pistorio A, et al. A prediction rule for lack of achievement of inactive disease with methotrexate as the sole disease-modifying antirheumatic therapy in juvenile idiopathic arthritis. Pediatr Rheumatol Online J 2019;17(1):50. doi:https://doi.org/10.1186/s12969-019-0355-0
11. Pastore S, Stocco G, Moressa V, et al. 5-Aminoimidazole-4-carboxamide ribonucleotide-transformylase and inosine-triphosphate-pyrophosphatase genes variants predict remission rate during methotrexate therapy in patients with juvenile idiopathic arthritis. Rheumatol Int 2015;35(4):619–627. doi:https://doi.org/10.1007/s00296-014-3131-y
12. Zamzami MA. Inosine triphosphate pyrophosphatase (ITPase): functions, mutations, polymorphisms and its impact on cancer therapies. Cells 2022;11(3):384. doi:https://doi.org/10.3390/cells11030384
13. Wallace CA, Ruperto N, Giannini E; Childhood Arthritis and Rheumatology Research Alliance; Pediatric Rheumatology International Trials Organization; Pediatric Rheumatology Collaborative Study Group. Preliminary criteria for clinical remission for select categories of juvenile idiopathic arthritis. J Rheumatol 2004;31(11):2290–2294.
14. Shipkova M, Lorenz K, Oellerich M, et al. Measurement of erythrocyte inosine triphosphate pyrophosphohydrolase (ITPA) activity by HPLC and correlation of ITPA genotype-phenotype in a Caucasian population. Clin Chem 2006;52(2):240–247. doi:https://doi.org/10.1373/clinchem.2005.059501
15. Pelin M, De Iudicibus S, Fusco L, et al. Role of oxidative stress mediated by glutathione-s-transferase in thiopurines' toxic effects. Chem Res Toxicol 2015;28(6):1186–1195. doi:https://doi.org/10.1021/acs.chemrestox.5b00019
16. Bardan I, Fagerli KM, Sexton J, et al. Treatment response to tumor necrosis factor inhibitors and methotrexate monotherapy in adults with juvenile idiopathic arthritis: data from NOR-DMARD. J Rheumatol 2023;50(4):538–547. doi:https://doi.org/10.3899/jrheum.220645
17. Castillo-Vilella M, Giménez N, Tandaipan JL, et al. Clinical remission and subsequent relapse in patients with juvenile idiopathic arthritis: predictive factors according to therapeutic approach. Pediatr Rheumatol Online J 2021;19(1):130. doi:https://doi.org/10.1186/s12969-021-00607-0
18. Zhou Y, Lauschke VM. Population pharmacogenomics: an update on ethnogeographic differences and opportunities for precision public health. Hum Genet 2022;141(6):1113–1136. doi:https://doi.org/10.1007/s00439-021-02385-x
19. Kahan BC, Rushton H, Morris TP, et al. A comparison of methods to adjust for continuous covariates in the analysis of randomised trials. BMC Med Res Methodol 2016;16(1):42. doi:https://doi.org/10.1186/s12874-016-0141-3
20. Sumi S, Marinaki AM, Arenas M, et al. Genetic basis of inosine triphosphate pyrophosphohydrolase deficiency. Hum Genet 2002;111(4-5):360–367. doi:https://doi.org/10.1007/s00439-002-0798-z
21. Arenas M, Duley J, Sumi S, et al. The ITPA c.94C>A and g.IVS2+21A>C sequence variants contribute to missplicing of the ITPA gene. Biochim Biophys Acta 2007;1772(1):96–102. doi:https://doi.org/10.1016/j.bbadis.2006.10.006

22. Stenmark P, Kursula P, Flodin S, et al. Crystal structure of human inosine triphosphatase. Substrate binding and implication of the inosine triphosphatase deficiency mutation P32T. J Biol Chem 2007;282(5):3182–3187. doi:https://doi.org/10.1074/jbc.M609838200
23. Wessels JA, Kooloos WM, De Jonge R, et al. Relationship between genetic variants in the adenosine pathway and outcome of methotrexate treatment in patients with recent-onset rheumatoid arthritis. Arthritis Rheum 2006;54(9):2830–2839. doi:https://doi.org/10.1002/art.22032
24. Wang YC, Wu MT, Tang FY, et al. *MTHFR* C677T polymorphism increases MTX sensitivity via the inhibition of *S*-adenosylmethionine and *de novo* purine synthesis. Clin Sci (Lond) 2019;133(2):253–267. doi:https://doi.org/10.1042/CS20180932
25. Pareek V, Pedley AM, Benkovic SJ. Human de novo purine biosynthesis. Crit Rev Biochem Mol Biol 2021;56(1):1–16. doi:https://doi.org/10.1080/10409238.2020.1832438
26. Carmichael SJ, Beal J, Day RO, et al. Combination therapy with methotrexate and hydroxychloroquine for rheumatoid arthritis increases exposure to methotrexate. J Rheumatol 2002;29(10):2077–2083.
27. Xu K, Cai Y-S, Lu S-M, et al. Autophagy induction contributes to the resistance to methotrexate treatment in rheumatoid arthritis fibroblast-like synovial cells through high mobility group box chromosomal protein 1. Arthritis Res Ther 2015;17(1):374. doi:https://doi.org/10.1186/s13075-015-0892-y
28. Baldwin SA, Beal PR, Yao SYM, et al. The equilibrative nucleoside transporter family, SLC29. Pflugers Arch 2004;447(5):735–743. doi:https://doi.org/10.1007/s00424-003-1103-2
29. da Silva JLG, Passos DF, Bernardes VM, et al. ATP and adenosine: role in the immunopathogenesis of rheumatoid arthritis. Immunol Lett 2019;214:55–64. doi:https://doi.org/10.1016/j.imlet.2019.08.009
30. Fredholm BB, Chern Y, Franco R, et al. Aspects of the general biology of adenosine A2A signaling. Prog Neurobiol 2007;83(5):263–276. doi:https://doi.org/10.1016/j.pneurobio.2007.07.005
31. Dell'Acqua ML, Scott JD. Protein kinase A anchoring. J Biol Chem 1997;272(20):12881–12884. doi:https://doi.org/10.1074/jbc.272.20.12881
32. Mediero A, Perez-Aso M, Cronstein BN. Activation of adenosine A(2A) receptor reduces osteoclast formation via PKA- and ERK1/2--mediated suppression of NFκB nuclear translocation. Br J Pharmacol 2013;169(6):1372–1388. doi:https://doi.org/10.1111/bph.12227
33. Bossennec M, Rodriguez C, Hubert M, et al. Methotrexate restores CD73 expression on Th1.17 in rheumatoid arthritis and psoriatic arthritis patients and may contribute to its anti-inflammatory effect through ado production. J Clin Med 2019, 3;8(11):1859. doi:https://doi.org/10.3390/jcm8111859
34. Liu T, Zhang L, Joo D, et al. NF-κB signaling in inflammation. Signal Transduct Target Ther 2017;2(1):17023. doi:https://doi.org/10.1038/sigtrans.2017.23
35. Verzella D, Pescatore A, Capece D, et al. Life, death, and autophagy in cancer: NF-κB turns up everywhere. Cell Death Dis 2020;11(3):210. doi:https://doi.org/10.1038/s41419-020-2399-y
36. Sasaki CY, Barberi TJ, Ghosh P, et al. Phosphorylation of RelA/p65 on serine 536 defines an IkappaBalpha-independent NF-kappaB pathway. J Biol Chem 2005;280(41):34538–34547. doi:https://doi.org/10.1074/jbc.M504943200
37. Geng B, Chen X, Chi J, et al. Platelet membrane-coated alterbrassicene A nanoparticle inhibits calcification of the aortic valve by suppressing phosphorylation P65 NF-κB. Theranostics 2023;13(11):3781–3793. doi:https://doi.org/10.7150/thno.85323
38. Löfgren L, Pehrsson S, Hägglund G, et al. Accurate measurement of endogenous adenosine in human blood. PLoS One 2018;13(10):e0205707. doi:https://doi.org/10.1371/journal.pone.0205707
39. Allard B, Allard D, Buisseret L, et al. The adenosine pathway in immuno-oncology. Nat Rev Clin Oncol 2020;17(10):611–629. doi:https://doi.org/10.1038/s41571-020-0382-2
40. Zoref-Shani E, Kessler-Icekson G, Sperling O. Pathways of adenine nucleotide catabolism in primary rat cardiomyocyte cultures. J Mol Cell Cardiol 1988;20(1):23–33. doi:https://doi.org/10.1016/S0022-2828(88)80176-7
41. Garcia-Gil M, Camici M, Allegrini S, et al. Metabolic aspects of adenosine functions in the brain. Front Pharmacol 2021;12:672182. doi:https://doi.org/10.3389/fphar.2021.672182
42. Haskó G, Sitkovsky MV, Szabó C. Immunomodulatory and neuroprotective effects of inosine. Trends Pharmacol Sci 2004;25(3):152–157. doi:https://doi.org/10.1016/j.tips.2004.01.006
43. Chen W, Hoerter J, Guéron M. A comparison of AMP degradation in the perfused rat heart during 2-deoxy-D-glucose perfusion and anoxia. Part I: the release of adenosine and inosine. J Mol Cell Cardiol 1996;28(10):2163–2174. doi:https://doi.org/10.1006/jmcc.1996.0208
44. Marton A, Pacher P, Murthy KG, et al. Anti-inflammatory effects of inosine in human monocytes, neutrophils and epithelial cells in vitro. Int J Mol Med 2001;8(6):617–621. doi:https://doi.org/10.3892/ijmm.8.6.617
45. Lovászi M, Németh ZH, Gause WC, et al. Inosine monophosphate and inosine differentially regulate endotoxemia and bacterial sepsis. FASEB J 2021;35(11):e21935. doi:https://doi.org/10.1096/fj.202100862R
46. Gomez G, Sitkovsky MV. Differential requirement for A2a and A3 adenosine receptors for the protective effect of inosine in vivo. Blood 2003;102(13):4472–4478. doi:https://doi.org/10.1182/blood-2002-11-3624
47. Welihinda AA, Kaur M, Raveendran KS, et al. Enhancement of inosine-mediated A_{2A}R signaling through positive allosteric modulation. Cell Signal 2018;42:227–235. doi:https://doi.org/10.1016/j.cellsig.2017.11.002
48. da Rocha Lapa F, da Silva MD, de Almeida Cabrini D, et al. Anti-inflammatory effects of purine nucleosides, adenosine and inosine, in a mouse model of pleurisy: evidence for the role of adenosine A2 receptors. Purinergic Signal 2012;8(4):693–704. doi:https://doi.org/10.1007/s11302-012-9299-2
49. Baram J, Chabner BA, Drake JC, et al. Identification and biochemical properties of 10-formyldihydrofolate, a novel folate found in methotrexate-treated cells. J Biol Chem 1988;263(15):7105–7111. doi:https://doi.org/10.1016/S0021-9258(18)68611-9
50. Allegra CJ, Chabner BA, Drake JC, et al. Enhanced inhibition of thymidylate synthase by methotrexate polyglutamates. J Biol Chem 1985;260(17):9720–9726. doi:https://doi.org/10.1016/S0021-9258(17)39298-0

American College of Rheumatology
Empowering Rheumatology Professionals

Arthritis & Rheumatology
Vol. 78, No. 9, September 2026, pp 2000
© 2026 American College of Rheumatology

DOI 10.1002/art.70088

Clinical Images: Complete Distal Phalanx Resorption in Systemic Sclerosis

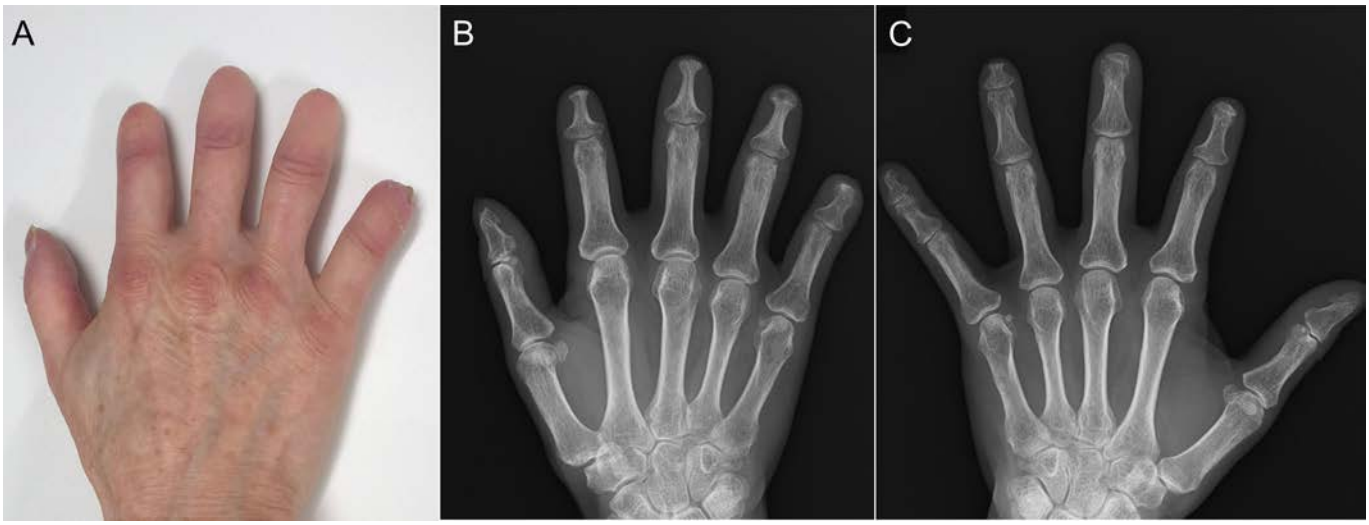

The patient, a 66-year-old woman with a 30-year history of Raynaud phenomenon and recurrent digital ulcers, was observed in our clinic. (A) Examination showed skin thickening extending from the fingers to the dorsum of the hands, multiple fingertip ulcers, marked digital shortening, and complete nail loss of the second through fifth digits of the right hand. Radiographs demonstrated (B) complete resorption of the distal phalanges of the second through fifth digits, with an apple-core–like appearance of the middle phalanges on the right hand, and (C) complete distal phalanx loss of the second and third digits with shortened remnants of the fourth and fifth digits on the left hand. She was diagnosed with limited cutaneous systemic sclerosis 30 years earlier, based on Raynaud phenomenon, digital skin thickening, interstitial lung disease, and anti–topoisomerase I antibody positivity. The most notable complication was acro-osteolysis. Although acro-osteolysis is a recognized feature of systemic sclerosis, it typically manifests as partial distal tuft resorption.[1,2] Severe forms with complete distal phalanx loss are uncommon. The findings are consistent with chronic vascular insufficiency and repeated ischemic injury. Radiographs of both hands illustrate different stages of this irreversible process. Although acro-osteolysis may also occur with polyvinyl chloride exposure, chronic infection, hyperparathyroidism, or other rheumatic diseases,[2] its presence in systemic sclerosis carries particular clinical relevance. Notably, despite the severity of acro-osteolysis, no soft-tissue calcification or radiographic osteopenia was observed, which is atypical for advanced disease. It remains unknown whether early recognition and management of vascular complications, including Raynaud phenomenon and digital ulcers, can prevent progression to severe acro-osteolysis or distal digital tuft resorption. Current recommendations highlight the need for further evidence regarding vascular-targeted and immunosuppressive therapies in systemic sclerosis,[3] and the value of such treatments for this complication also remains uncertain. Written informed consent was obtained directly from the patient. At our institution, ethics committee approval is not required for single-patient case reports when written consent has been obtained from the patient. No additional data are available.

Author disclosures are available at https://onlinelibrary.wiley.com/doi/10.1002/art.70088.

1. Avouac J, Guerini H, Wipff J, et al. Radiological hand involvement in systemic sclerosis. Ann Rheum Dis 2006;65(8):1088–1092. doi: https://doi.org/10.1136/ard.2005.044602
2. Kemp SS, Dalinka MK, Schumacher HR. Acro-osteolysis: etiologic and radiological considerations. JAMA 1986;255(15):2058–2061. doi: https://doi.org/10.1001/jama.1986.03370150100036
3. Del Galdo F, Lescoat A, Conaghan PG, et al. EULAR recommendations for the treatment of systemic sclerosis: 2023 update. Ann Rheum Dis 2025;84(1):29–40. doi:https://doi.org/10.1136/ard-2024-226430

Ken Yoshida, MD, PhD
k.yoshida@jikei.ac.jp
Division of Rheumatology, Department of Internal Medicine
The Jikei University School of Medicine
Tokyo, Japan

Arthritis & Rheumatology
Vol. 78, No. 9, September 2026, pp 2001
© 2026 The Author(s). *Arthritis & Rheumatology* published by Wiley Periodicals LLC on behalf of American College of Rheumatology. This is an open access article under the terms of the Creative Commons Attribution-NonCommercial-NoDerivs License, which permits use and distribution in any medium, provided the original work is properly cited, the use is non-commercial and no modifications or adaptations are made.

DOI 10.1002/art.70148

Clinical Images: Skeletal fluorosis presenting with diffuse periostitis and polyarticular synovitis

The patient, a 33-year-old White male with hypertension, diabetes, hyperlipidemia, and mild hepatomegaly, presented with abrupt-onset, disabling polyarticular pain, swelling, and stiffness (hands, wrists, elbows, shoulders, hips, knees, and ankles); progressive loss of mobility; and wheelchair dependence. Examination showed marked polyarticular synovitis and palpable periarticular bony nodularity at the wrists and shins. Radiographs demonstrated bilaterally symmetrical, diffuse, solid periosteal reaction in small and large tubular bones without effusions or erosions. Lumbar spine dual x-ray absorptiometry Z score was +10.2, far exceeding biologic expectations and likely spuriously elevated by generalized osteosclerosis and degenerative/calcific change in fluorosis rather than true trabecular hypertrophy. Positron emission tomography/computed tomography (CT) showed diffusely increased skeletal radiotracer uptake concordant with periosteal proliferation and no malignancy. Chest CT and CT enterography excluded pulmonary or gastrointestinal drivers of hypertrophic osteoarthropathy. Laboratory testing showed an elevated erythrocyte sedimentation rate/C-reactive protein level, low vitamin D level, elevated parathyroid hormone level, and elevated bone-specific alkaline phosphatase level; rheumatoid factor, cyclic citrullinated peptide, antinuclear antibody, extractable nuclear antigen, and HLA-B27 test results were negative. His serum fluoride level was 1.9 mg/L (reference <0.13 mg/L), supporting fluoride excess as the unifying etiology, although cause of toxicity is unknown at this time. Fluoride toxicity integrates the clinicoradiologic picture: fluoride incorporates into hydroxyapatite (fluorapatite), stimulates osteoblasts, and drives osteosclerosis and periosteal apposition; later, disordered mineralization contributes to elevated alkaline phosphatase and secondary hyperparathyroidism.[1] Radiographic hallmarks include generalized osteosclerosis, diffuse periostitis, entheso/ligamentous ossification, and sacroiliac changes without erosions.[1] Typical exposures include high fluoride groundwater, heavy tea consumption, industrial/inhalational sources (eg, aluminum smelting), and fluorinated medications (voriconazole or difluoroethane inhalant abuse).[2,3] Diagnosis rests on an elevated serum/urinary fluoride level with compatible imaging and exclusion of mimics.[1] This case underscores skeletal fluorosis as a treatable mimic of inflammatory arthropathy; management centers on identifying and removing the fluoride source, vitamin D repletion, and symptomatic control.[1]

Author disclosures are available at https://onlinelibrary.wiley.com/doi/10.1002/art.70148.

1. Sellami M, Riahi H, Maatallah K, et al. Skeletal fluorosis: don't miss the diagnosis! Skeletal Radiol 2020;49(3):345–357. doi:10.1007/s00256-019-03302-0
2. Whyte MP, Totty WG, Lim VT, et al. Skeletal fluorosis from instant tea. J Bone Miner Res 2008;23(5):759–769. doi:10.1359/jbmr.080101
3. Wermers RA, Cooper K, Razonable RR, et al. Fluoride excess and periostitis in transplant patients receiving long-term voriconazole therapy. Clin Infect Dis 2011;52(5):604–611. doi:10.1093/cid/ciq188

Mitali Sen, MD
msen@uabmc.edu
Division of Clinical Immunology and Rheumatology, University of Alabama at Birmingham

American College of Rheumatology
Empowering Rheumatology Professionals

Arthritis & Rheumatology
Vol. 78, No. 9, September 2026, pp 2002–2005
© 2026 American College of Rheumatology

LETTER

DOI 10.1002/art.70197

How do interleukin-33 and neutrophil extracellular traps cooperate to induce epithelial-mesenchymal transition in alveolar epithelial cells?: comment on the article by Yang et al

To the Editor:

We read with great interest the article by Yang et al[1] recently published in *Arthritis & Rheumatology*. This article elucidates, with substantial data, the critical role of interleukin-33 (IL-33) in pulmonary inflammation and fibrosis in idiopathic inflammatory myopathy (IIM)–associated interstitial lung disease (ILD) and suggests the potential of IL-33 as a therapeutic target for IIM-ILD. We agree with the authors' perspective but feel that their elaboration on the mechanism by which IL-33 regulates epithelial-mesenchymal transition (EMT) in alveolar epithelial cells (AECs) is not yet sufficiently clear, and some specific points require clarification.

IL-33 can be released extracellularly during cellular damage, acting as a DAMP. A previous study has reported that IL-33 alone can induce endothelial-to-mesenchymal transition in pulmonary arterial endothelial cells.[2] IL-33 can also function as a transcription factor, entering the nucleus and binding to chromatin to regulate target genes.[3] However, this study by Yang et al[1] did not detect whether the release of IL-33 increases during the process of neutrophil extracellular traps (NETs) inducing EMT in AECs, nor did it investigate whether IL-33 alone can induce EMT in AECs. Consequently, it remains unclear whether NETs induce AEC EMT through the extracellular action of IL-33 or via its intracellular, transcription factor-like role. Furthermore, it is uncertain whether IL-33 plays a primary or merely a synergistic role in NETs-induced AEC EMT.

In this article,[1] the authors repeatedly emphasized the critical role of the IL-33/ERK axis in the inflammation and fibrosis of IIM-ILD and claimed that IL-33 drives AEC EMT in an ERK-dependent manner. We find such statements overly absolute and subjective, for the following reasons. First, the authors demonstrated that application of an ERK inhibitor can suppress inflammation and fibrosis in IIM-ILD. However, this only indicates that the ERK pathway is involved in IIM-ILD, but it does not prove the specific role of the IL-33/ERK axis, because many factors can activate the ERK pathway.[4] Second, the authors confirmed that IL-33 can promote ERK phosphorylation and activate the ERK signaling pathway. However, this does not demonstrate that the IL-33–driven inflammation and fibrosis in IIM-ILD are ERK pathway-dependent. This is because IL-33 can also activate multiple other signaling molecules, such as NF-κB, p38, and JNK.[3] The authors lacked direct evidence to prove that IL-33 drives the inflammation and fibrosis of IIM-ILD in an ERK-dependent manner.

A few figures in this article[1] are somewhat confusing and require clarification. The text mentions that IL-33 expression was detected in lung tissues from three patients with IIM-ILD and three healthy controls, but Figures 1A and B appeared to show three samples each from patients with IIM-ILD-1 or IIM-ILD-2. Additionally, we are unsure about the interpretation of the results shown in Figures 3G and H, as well as Figures 5G and H, likely due to mislabeling.

Author disclosures are available at https://onlinelibrary.wiley.com/doi/10.1002/art.70197.

Jiaxin Cai, MD
Zaixing Yang, PhD
yangzaixingdiyi@163.com
Department of Laboratory Medicine, Taizhou First People's Hospital
Zhejiang, China

1. Yang J, Li W, Zhu J, et al. Interleukin-33 promotes interstitial lung disease in idiopathic inflammatory myopathy via ERK-mediated epithelial-mesenchymal transition: ERK as a potential therapeutic target. Arthritis Rheumatol 2026:78(4):948–960. doi:https://doi.org/10.1002/art.43453
2. Becher C, Groeneveld EJ, Quarck R, et al. BMP9 modulates IL-33 signaling to mitigate EndMT in pulmonary arterial hypertension. Hypertension 2026;83(2):e24916. doi:https://doi.org/10.1161/HYPERTENSIONAHA.125.24916
3. Dwyer GK, D'Cruz LM, Turnquist HR. Emerging functions of IL-33 in homeostasis and immunity. Annu Rev Immunol 2022;40:15–43. doi:https://doi.org/10.1146/annurev-immunol-101320-124243
4. Gagliardi PA, Pertz O. The mitogen-activated protein kinase network, wired to dynamically function at multiple scales. Curr Opin Cell Biol 2024;88:102368. doi:https://doi.org/10.1016/j.ceb.2024.102368

DOI 10.1002/art.70198

Reply

To the Editor:

Regarding the mechanism of interleukin-33 (IL-33) in neutrophil extracellular traps (NETs)–induced epithelial-mesenchymal transition (EMT), we agree that this is a pertinent question. In this study, we primarily observed from a functional

perspective that knockdown of IL-33 significantly inhibits NETs-induced EMT and downstream ERK activation, suggesting that IL-33 may play an important role in this signaling cascade.[1] We fully agree that IL-33, as a multifunctional molecule, warrants further investigation into the significance of its nuclear transcriptional regulation and other roles in alveolar epithelial cells. Our work provides initial clues into this complex mechanism, and future research should further distinguish between its extracellular and intracellular functions—this is also a direction we intend to pursue.

With respect to whether the IL-33/ERK pathway is overemphasized, we fully acknowledge that IL-33 can activate multiple signaling pathways and that the ERK pathway itself is regulated by various factors. In our experimental system, we observed that IL-33 expression positively correlates with phosphorylated ERK levels, downregulation of IL-33 markedly attenuates ERK phosphorylation, and the ERK inhibitor U0126 alleviates IL-33–associated pathologic manifestations. Therefore, we believe that the IL-33/ERK axis plays an important role in the EMT process of idiopathic inflammatory myopathy–associated interstitial lung disease but is not the exclusive pathway. The discussion section of our paper also notes that other signaling pathways may cooperate in this process.

Supported by the National Natural Science Foundation of China (grant 82260325), the Natural Science Foundation of Gansu Province (grants 24JRRA923 and 25YFFA055), and the Cuiying Scientific and Technological Innovation Program of Lanzhou University Second Hospital (grants CY2024-MS-A03 and CY2023-QN-B06).

Author disclosures are available at https://onlinelibrary.wiley.com/doi/10.1002/art.70198.

Jumei Yang, MSc
Jiarui Zhu, MSc
Cuiying Biomedical Research Center, The Second Hospital & Clinical Medical School, Lanzhou University
Lanzhou, China
Wenjun Li, MMed
Xi Cui, MMed
Hui Chai, MMed
Qiyan Su, MMed
Yingyue Feng, MMed
The Second Clinical Medical School, Lanzhou University
Lanzhou, China
Sigong Zhang, PhD
zhangsg@lzu.edu.cn
Department of Rheumatology and Immunology, Lanzhou University Second Hospital and Gansu Provincial Clinical Center for Rheumatology and Immunology
Lanzhou, China

1. Yang J, Li W, Zhu J, et al. Interleukin-33 promotes interstitial lung disease in idiopathic inflammatory myopathy via ERK-mediated epithelial-mesenchymal transition: ERK as a potential therapeutic target. Arthritis Rheumatol 2026:78(4):948–960. doi:https://doi.org/10.1002/art.43453

DOI 10.1002/art.70214

Clarifying the clinical implications of clonal hematopoiesis in late-onset seropositive rheumatoid arthritis: comment on the article by Zhao et al

To the Editor:

We read with great interest the study by Zhao et al, who reported that clonal hematopoiesis (CH) was associated primarily with incident, late-onset seropositive rheumatoid arthritis (SPRA) across three large biobanks.[1] By integrating a harmonized phenotyping strategy with age-scale survival modeling, the authors provide an important contribution to the emerging literature on somatic hematopoietic variation and rheumatic disease. Given the potential clinical and mechanistic implications of these findings, several methodologic issues warrant further clarification.

First, temporal inference remains challenging. Rheumatoid arthritis onset was defined as the date when the first diagnosis code appeared in the medical record.[1] Yet rheumatoid arthritis commonly includes a prolonged preclinical phase marked by autoantibody positivity and evolving immune dysregulation before clinically apparent arthritis.[2,3] Some cases classified as "incident" after blood draw may therefore represent delayed clinical recognition of pre-existing disease biology rather than true post-CH disease onset, which weakens a strong causal interpretation.

Second, selection and information bias may influence the observed associations. Eligibility required substantial health care engagement, including multiple diagnosis codes, laboratory data, medication data, and ascertainable smoking status; participants without smoking questionnaire data were excluded.[1] In the UK Biobank, only about 45% of participants had primary care data available, and follow-up for those without rheumatoid arthritis was truncated in 2016.[1] Although these choices likely improved specificity, they may also have preferentially retained participants with greater health system contact, older age, or higher comorbidity burden.

Third, phenotype interpretation deserves caution. The authors introduced late-onset rheumatoid arthritis using the conventional threshold of onset at age ≥60 years, yet the largest clonal hematopoiesis of indeterminate potential (CHIP)–associated excess appeared concentrated in the 70–80-year subgroup.[1,4] This pattern suggests that the signal may be strongest in a narrower elderly-onset phenotype rather than across the broader late-onset rheumatoid arthritis spectrum. Similarly, the reported excess mortality among patients with SPRA and TET2-CHIP should be interpreted carefully because the mortality models did not account for several clinically relevant factors, including cardiovascular comorbidity, infection burden, glucocorticoid exposure, disease-modifying antirheumatic drug intensity, and disease activity.[1] In addition, genome or exome sequencing–based CHIP detection may underestimate disease associations.[5]

Finally, the complement and chromosomal mosaicism findings would benefit from external validation. The complement interaction analysis relied on genetically predicted protein levels derived from European-ancestry effect estimates, and the mosaic chromosomal alteration/mosaic loss of chromosome Y analyses were confined to the UK Biobank subset.[1] Replication in independent multi-ancestry cohorts would help determine whether theseY associations reflect a generalizable biologic mechanism or, at least in part, ancestry- and biobank-specific structure.[4]

Overall, this study provides important epidemiologic evidence linking CH to SPRA and helps advance current understanding of the interface between aging-related hematopoietic alterations and autoimmune disease. Clarifying issues related to diagnostic timing, selection bias, phenotype definition, and external validity would further strengthen the causal and clinical interpretation of these findings. These considerations are intended not to diminish the value of the study but to help refine the interpretation of this clinically relevant association.

Author disclosures are available at https://onlinelibrary.wiley.com/doi/10.1002/art.70214.

Weiqi Hu, MS
laylarschanbaek@163.com
Xun Zhou, MS
zhouxun077@163.com
Luxue Wang, MS
18203780962@163.com
College of Basic Medical Sciences
Zhejiang Chinese Medical University
Hangzhou, China
Changfeng Hu, PhD
zhudianzhuifeng@163.com
College of Basic Medical Sciences, Zhejiang Chinese Medical University Hangzhou, China
and Jinhua Academy of Zhejiang Chinese Medical University
Jinhua, China

1. Zhao K, Pershad Y, Heimlich JB, et al. Association of clonal hematopoiesis with incident, late-onset, seropositive rheumatoid arthritis. Arthritis Rheumatol Published online March 18, 2026. doi:https://doi.org/10.1002/art.70133
2. Deane KD. Preclinical rheumatoid arthritis (autoantibodies): an updated review. Curr Rheumatol Rep 2014;16(5):419. doi:https://doi.org/10.1007/s11926-014-0419-6
3. Majka DS, Deane KD, Parrish LA, et al. Duration of preclinical rheumatoid arthritis-related autoantibody positivity increases in subjects with older age at time of disease diagnosis. Ann Rheum Dis 2008;67(6):801–807. doi:https://doi.org/10.1136/ard.2007.076679
4. Uchiyama S, Ishikawa Y, Ikari K, et al. Mosaic loss of chromosome Y characterises late-onset rheumatoid arthritis and contrasting associations of polygenic risk score based on age at onset. Ann Rheum Dis 2025;84(8):1313–1323. doi:https://doi.org/10.1016/j.ard.2025.01.034
5. Corty R, Pershad Y, Heimlich JB, et al. Detection of clonal hematopoiesis of indeterminate potential via genome or exome sequencing underestimates disease associations. J Clin Invest 2026;136(5):e198861. doi:https://doi.org/10.1172/JCI198861

DOI 10.1002/art.70204

Reply

To the Editor:

First, Hu et al raise the concern that some research participants who were categorized as incident rheumatoid arthritis (RA) may have had prevalent pre-RA. We agree on the first point—RA is the result of a step-wise progression from health to immune dysregulation without overt disease (pre-RA) to diagnosable RA.[1] They claim that this reality weakens the causal argument that CHIP contributes to RA and raises the competing hypothesis that pre-RA contributes to CHIP. However, the competing hypothesis is unlikely because a well-powered test of association between CHIP and prevalent RA observed no effect.[2]

Second, Hu et al raise the concern that requiring substantial health care engagement as an entry criterion for the study may have biased the cohort toward research participants with older age or higher comorbidity burden. For selection bias to explain the observed findings, it would require that participants with CHIP be more likely to come to a biobank-participatory site for their RA diagnosis than participants without CHIP. To our knowledge, there is no biologically plausible reason for this elaborate form of selection bias.

Third, Hu et al note that the CHIP-associated risk for late-onset seropositive RA is not spread evenly across all people age ≥60 years but rather is concentrated mostly in the 70- to 80-year age range. To maximize interpretability and generalizability, we used an established definition of late-onset RA (≥60 years).[3–5] The statistical test for whether the clonal hematopoiesis of indeterminate potential–seropositive RA (CHIP-SPRA) association is greater among the 70- to 80-year subgroup was underpowered, but we agree that the observed pattern suggests that that subgroup may be at greater risk. Relatedly, we agree with the remark by Hu et al that the observed association likely underestimates the true CHIP-SPRA association, due to attenuation bias in both CHIP detection and phenotype ascertainment.[6]

Finally, Hu et al note that the analyses related to complement proteins and mosaic chromosomal abnormalities were restricted to a single-ancestry group. Unfortunately, at present, large-scale biobank-based genetic prediction models for circulating proteins have been developed primarily in European-ancestry populations.[7] We agree that as new data resources become available, assessing the generalizability of these and other single-ancestry results will be critical.

Supported by the NIH (grants DP5-OD-029586, R01-AG-088657, and R01-AG-083736), the Burroughs Wellcome Fund, the Edward P. Evans Foundation, the RUNX1 Research Program, the Pew Charitable Trusts, a Hevolution/American Federation for Aging Research New Investigator Award, and the Vanderbilt University Medical Center Brock Family Endowment and Young Ambassador Award (to Dr Bick), the Arthritis National Research Foundation and Rheumatology Research Foundation (to Dr Corty), and the NIH (grant F30-AG-099331 to Dr Pershad).

Kun Zhao, PhD
Yash Pershad, BS
Alexander G. Bick, MD, PhD
Division of Genetic Medicine and Clinical Pharmacology, Department of Medicine, Vanderbilt University Medical Center Nashville, Tennessee
Robert W. Corty, MD, PhD
robert.corty@vumc.org
Division of Rheumatology, Department of Medicine Vanderbilt University Medical Center Nashville, Tennessee

1. Gravallese EM, Firestein GS. Rheumatoid arthritis - common origins, divergent mechanisms. N Engl J Med 2023;388(6):529–542. doi:https://doi.org/10.1056/NEJMra2103726
2. Zhao K, Pershad Y, Heimlich JB, et al. Association of clonal hematopoiesis with incident, late-onset, seropositive rheumatoid arthritis. Arthritis Rheumatol Published online March 18, 2026. doi:https://doi.org/10.1002/art.70133
3. Wu AH, Tseng C, Park S-Y, et al. Late-onset rheumatoid arthritis and air pollution in a multiethnic cohort. Arthritis Rheumatol 2026;78(7):1425–1436. doi:https://doi.org/10.1002/art.70054
4. Zimba O, Baimukhamedov C, Kocyigit BF. Late-onset rheumatoid arthritis: clinical features, diagnostic challenges, and treatment approaches. Rheumatol Int 2025;45(6):152. doi:https://doi.org/10.1007/s00296-025-05908-1
5. Sugitani N, Tanaka E, Inoue E, et al. Higher risk of poor functional outcome and unfavourable clinical events for late-onset rheumatoid arthritis: results from the IORRA cohort. Rheumatology (Oxford) 2025;64(5):2541–2549. doi:https://doi.org/10.1093/rheumatology/keae673
6. Corty R, Pershad Y, Heimlich JB, et al. Detection of clonal hematopoiesis of indeterminate potential via genome or exome sequencing underestimates disease associations. J Clin Invest 2026;136(5):e198861. doi:https://doi.org/10.1172/JCI198861
7. Zhao K, Pershad Y, Xue L, et al. Clonal hematopoiesis and risk of stroke: evidence from over 800 000 individuals across 3 cohorts. Stroke Published online April 8, 2026. doi:https://doi.org/10.1161/STROKEAHA.125.054128